

Value Recovery from Waste Electrical and Electronic
Equipment (WEEE):
A potential opportunity towards a circular economy for
end-of-life Mobile Phones

A thesis submitted in fulfilment of the requirements for the degree of Doctor of Philosophy

Moisés Ulises Andrés Gómez Soto

March 2022

Department of Civil and Environmental Engineering

Imperial College London

2022

Statement of originality

I hereby declare that the contents of this thesis are all by my own work, and any work of other, quotation, description, and material presented is explicitly and fully acknowledged.

Copyright declaration

The copyright of this thesis rests with the author. Unless otherwise indicated, its contents are licensed under a Creative Commons Attribution-Non-Commercial 4.0 International Licence (CC BY-NC).

Under this licence, you may copy and redistribute the material in any medium or format. You may also create and distribute modified versions of the work. This is on the condition that: you credit the author and do not use it, or any derivative works, for a commercial purpose.

When reusing or sharing this work, ensure you make the licence terms clear to others by naming the licence and linking to the licence text. Where a work has been adapted, you should indicate that the work has been changed and describe those changes.

Please seek permission from the copyright holder for uses of this work that are not included in this licence or permitted under UK Copyright Law.

Abstract

Waste electrical and electronic equipment (WEEE) is one of the fastest growing solid waste streams worldwide and, if not treated properly, presents serious health and environmental issues as well as extensive loss of strategic metals. The dramatic increase in the consumption of raw materials over recent decades to meet consumer demand has led to an imbalance in supply and demand, and a potential threat to the continued supply of critical metals. WEEE is a resource-rich source with many of the metals embedded in its composition listed as critical by the European Commission; extraction of these metals from WEEE, to mitigate their threat to supply, is imperative.

Using end-of-life mobile phones (EoL-MPs), fast-moving consumer electronics, representative of the value embedded in WEEE, as a case study, a full characterisation of metallic and non-metallic fractions within a mobile phone confirms the presence of up to 71 elements, with many of the strategic and critical metals found in higher concentrations than in their natural ores. Exploiting the unique properties of ionic liquids (ILs), chosen for their selectivity as potential extractants, [Bmim]HSO₄ for copper, Cyphos 101 for gold, Cyphos 101 and Aliquat 336 for indium, and [Hbet][Tf₂N] for REEs, processes were developed using model test systems to determine optimal parameters to achieve recovery. These developed processes were then applied to treat as-received multigenerational EoL-MP components (printed circuit boards, screens, speakers, etc.), with metals of almost 99% purity recovered, for conversion to products of commercial value. Moreover, the benefit of recycling the ILs as extractants multiple times, without impacting their integrity or efficiency, is realised.

This research demonstrates the potential to unlock value from this waste stream that can be exploited in other WEEE streams, as a step towards balancing the criticality of supply and demand of metals that are under threat.

Acknowledgements

I would like to express my sincere gratitude to my supervisors Professor Sue Grimes and Dr Geoff Fowler for their consistent support, guidance, wisdom, and kindness during the running of my thesis, and during the time of uncertainty that the COVID-19 pandemic brought. Professor Grimes continuously provided encouragement and was always willing and enthusiastic to assist me in any way she could throughout my thesis and personal matters. Dr Fowler is a source of unlimited knowledge, and he is a great banter, who made my laboratories days better and gave me novel ideas to approach in my research. I must also thank Professor John Donaldson (R.I.P.), who provided me with insightful questions that improved and stimulated my critical thinking, as a Greek philosopher with the Socratic Method, sharing his wisdom and experience with me. My especial gratitude to Dr Ángel Nievas, a friend now, who with his experience, knowledge and willing to help, several experiments would not have been possible.

My gratitude is extended to all the administration staff in the college and the department, particularly Sarah Willis and Fionnuala Ni Dhonnabhain for their help, friendliness and patience. My warmest thanks to my new friends that I have met at Imperial and in London; Praj, Erika, Ricardo, Boris, Luis, Diegos, Leika, Shayne, Yiannis, Ana, Camila, Martiza, Felipe, Lucille, pepe, Andrew and so many others. All of you have contributed to making this a wonderful experience. Of course thanks to my old friends, which I met every time I was back in Chile. My life has been much more colourful and enriched with all of you!

I would like to thank my great family for their unconditional love and support, I could not be here without them; my mom Silvia, dad Sergio, my brothers Jimmy and Benito, and tía Rosa thank you from the bottom of my heart. Special thanks to Pierre-Henri M. for all his support and care, merci beaucoup.

Finally, I would like to acknowledge CONICYT (Comisión Nacional de Investigación Científica y Tecnológica) for the financial support through these years by the *Becas Chile* Scholarship Doctoral Fellowship program Grant No. 72180123.

Table of Contents

ABSTRACT	II
ACKNOWLEDGEMENTS	III
LIST OF FIGURES	VII
LIST OF TABLES	XIV
GLOSSARY OF TERMS	XVI
1 INTRODUCTION	1
1.1 BACKGROUND	1
1.2 AIMS AND OBJECTIVES	4
1.3 SCOPE OF THESIS	5
2 LITERATURE REVIEW	7
2.1 AN OVERVIEW OF WASTE ELECTRICAL AND ELECTRONIC EQUIPMENT	7
2.1.1 <i>Global WEEE generation and trends</i>	9
2.1.2 <i>An overview of End-of-Life (EoL) mobile phones</i>	12
2.1.3 <i>Composition of WEEE</i>	15
2.1.4 <i>Hazardous substances in WEEE</i>	18
2.2 CIRCULAR ECONOMY, POLICIES, AND LEGISLATION IN THE CONTEXT OF WEEE MANAGEMENT	20
2.2.1 <i>Policies on waste management in Europe and the UK</i>	22
2.2.2 <i>WEEE and RoHS Directives</i>	24
2.3 CRITICALITY OF MATERIALS	28
2.4 METHODS OF RECYCLING WEEE.....	34
2.4.1 <i>Physical/mechanical processes</i>	34
2.4.2 <i>Metallurgical processes</i>	36
2.5 IONIC LIQUIDS	39
2.5.1 <i>Physiochemical properties of ionic liquids</i>	40
2.5.2 <i>Recovery of metals by ionic liquids from WEEE</i>	45
2.6 SUMMARY	46
3 DETAILED CHARACTERISATION OF MULTIGENERATIONAL MOBILE PHONES TO DETERMINE POTENTIAL FOR RECOVERY OF VALUE	47
3.1 INTRODUCTION	47
3.2 MATERIALS AND METHODOLOGY	50
3.2.1 <i>Materials</i>	50
3.2.2 <i>Pre-treatment for Selection of Key Component Fractions for Analysis</i>	54

3.2.3	<i>Analytical Techniques</i>	56
3.3	RESULTS AND DISCUSSION	66
3.3.1	<i>Key Component Fractions of EoL-Mobile Phones</i>	66
3.3.2	<i>Characterisation of the Metallic Fraction</i>	73
3.3.3	<i>Characterisation of the Non-Metallic Fraction</i>	89
3.3.4	<i>Potential Key Value Components for Recycle and Recovery</i>	103
3.4	SUMMARY	111
4	COPPER RECOVERY FROM END-OF-LIFE MOBILE PHONE PRINTED CIRCUIT BOARDS USING IONIC LIQUIDS AND ELECTROLYSIS	113
4.1	INTRODUCTION	113
4.2	METHODOLOGY	115
4.2.1	<i>Materials</i>	115
4.2.2	<i>Analytical Techniques for Characterisation</i>	119
4.2.3	<i>Experimental Procedures</i>	120
4.3	RESULTS AND DISCUSSION	127
4.3.1	<i>Solubility Testing to Determine Optimised Conditions for IL- Leaching of Copper from WPCBs</i> ... 127	
4.3.2	<i>Pre-treatment of As-received WPCBs to Remove Solder and Electronic Components</i>	146
4.3.3	<i>Electrowinning of Copper from Leached Solutions Derived from IL-Treated WPCBs</i>	151
4.3.4	<i>Recovery of the Ionic liquids for Recycle and Reuse</i>	159
4.3.5	<i>Proposed copper recycling process from WPCBs</i>	165
4.4	SUMMARY	168
5	DEVELOPMENT OF A PROCESS FOR GOLD RECOVERY FROM GOLD-RICH E-WASTE COMPONENTS USING IONIC LIQUIDS	170
5.1	INTRODUCTION	170
5.2	METHODOLOGY	173
5.2.1	<i>Materials</i>	173
5.2.2	<i>Analytical Techniques for Characterisation</i>	176
5.2.3	<i>Experimental Procedure</i>	177
5.3	RESULTS AND DISCUSSION	187
5.3.1	<i>Selection of IL for Gold Extraction</i>	187
5.3.2	<i>Optimised Conditions for Gold Extraction and Recovery Using a Model Test System</i>	190
5.3.3	<i>Pre-treatment of As-Received E-Waste Components</i>	223
5.3.4	<i>Application of the Optimised Conditions for Gold Extraction and Recovery from Pre-treated E-Waste Components</i>	231
5.3.5	<i>Proposed Hydrometallurgical Process for Gold Extraction and Recovery from E-Waste Components</i>	242
5.4	SUMMARY	246

6	RECOVERY OF INDIUM FROM EOL MOBILE PHONE LIQUID CRYSTAL DISPLAY SCREENS USING IONIC LIQUIDS	248
6.1	INTRODUCTION	248
6.2	METHODOLOGY	251
6.2.1	<i>Materials</i>	251
6.2.2	<i>Analytical Techniques for Characterisation</i>	252
6.2.3	<i>Experimental Procedures</i>	253
6.3	RESULTS AND DISCUSSION	261
6.3.1	<i>Optimised Conditions for Indium Extraction and Recovery Using a Model Test System</i>	261
6.3.2	<i>Pre-treatment of waste LCD screens</i>	280
6.3.3	<i>Application of the Optimised Conditions for Recovery of Indium from Waste LCD Screens</i>	298
6.3.4	<i>Proposed Hydrometallurgical Process for Indium recovery from LCD Panels (as ITO Glass Substrate Fractions)</i>	308
6.4	SUMMARY	311
7	RECOVERY OF RARE-EARTH ELEMENTS FROM EOL MOBILE PHONE SPEAKERS USING IONIC LIQUIDS .	313
7.1	INTRODUCTION	313
7.2	METHODOLOGY	316
7.2.1	<i>Materials</i>	316
7.2.2	<i>Analytical Techniques for Characterisation</i>	320
7.2.3	<i>Experimental Procedure</i>	321
7.3	RESULTS AND DISCUSSION	330
7.3.1	<i>Optimised Conditions of [Hbet][Tf₂N] for REEs Extraction and Recovery Using a Model Test System</i> 332	
7.3.2	<i>Pre-treatment of As-received Speakers from EoL-MPs</i>	353
7.3.3	<i>REEs recovery from EoL-MP speakers by [Hbet][Tf₂N]:H₂O system</i>	356
7.3.4	<i>Proposed hydrometallurgical process for REOs recovery from EoL speakers</i>	360
7.3.5	<i>Optimised Conditions for REEs Extraction and Recovery Using a Model Test System: Alternative Recovery Method</i>	362
7.4	SUMMARY	370
8	CONCLUSIONS AND RECOMMENDATIONS	372
8.1	CONCLUSIONS	372
8.1.1	<i>Motivation for the Research</i>	372
8.1.2	<i>Research Outcomes</i>	372
8.2	RECOMMENDATIONS FOR FUTURE WORK	374
	REFERENCES.....	376
	APPENDIX: SUPPLEMENTARY INFORMATION OF CHAPTERS	391

List of Figures

FIGURE 1.1: SCHEMATIC DIAGRAM OF THE THESIS STRUCTURE AND RELATIONSHIP BETWEEN THE SECTIONS OF WORK PERFORMED. ...	6
FIGURE 2.1: WEEE GENERATED IN 2019; (A) PER CONTINENT, AND (B) PER CAPITA. DATA OBTAINED FROM THE UNU [5].	10
FIGURE 2.2: SUMMARY OF GLOBAL WEEE GENERATION IN 2019 (KG/PERSON/YEAR) [32].	11
FIGURE 2.3: NUMBER OF MOBILE SUBSCRIPTIONS WORLDWIDE FROM 1993 TO 2017 (IN MILLIONS). DATA OBTAINED FROM STATISTA.	13
FIGURE 2.4: ENERGY CONSUMPTION OF MOBILE PHONES DURING THEIR LIFE CYCLE [44].	14
FIGURE 2.5: LINEAR ECONOMY VS CIRCULAR ECONOMY. DIAGRAM OBTAINED FROM THE ELLEN MACARTHUR FOUNDATION.	21
FIGURE 2.6: ECONOMIC IMPORTANCE AND SUPPLY RISK RESULTS OF RAW MATERIAL. CRITICALITY ASSESSMENT, 2020.	30
FIGURE 2.7: COUNTRIES ACCOUNTING FOR THE LARGEST SHARE OF GLOBAL SUPPLY OF CRMS (2020) [17].	32
FIGURE 2.8: FLOW CHART OF A TYPICAL MECHANICAL PROCESSING AS PRE-TREATMENT AND SEPARATION.	35
FIGURE 2.9: WEEE RECYCLING FLOWSHEET WITH A COMBINATION OF PHYSICAL, CHEMICAL AND METALLURGICAL STEPS [12].	38
FIGURE 2.10: SCHEMATIC OF SOME COMMON CATIONS (BLUE) AND ANIONS (RED) OF ILs [109].	39
FIGURE 2.11: INDUSTRIAL APPLICATION OF IONIC LIQUIDS [108].	40
FIGURE 3.1: POSTER USED FOR THE COLLECTION OF EoL-MPS.	50
FIGURE 3.2: FLOWSHEET OF PROCESSING METHODS AND PRODUCTS OBTAINED.	55
FIGURE 3.3: METHODS USED IN THE CHARACTERISATION OF EoL-MPS.	56
FIGURE 3.4: SCHEMATIC FLOWCHART FOR SAMPLE PREPARATION OF ARD AND LFT METHODS.	59
FIGURE 3.5: PROXIMITY ANALYSIS OF A FEATURE MOBILE PHONE CASING.	61
FIGURE 3.6: MAIN COMPONENTS OF A MOBILE PHONE (NOKIA N70).	67
FIGURE 3.7: AVERAGE MASS FRACTION (WT. %) OF COMPONENTS OF EoL-MPS BY (A) BY GENERATIONS AND (B) ON AVERAGE.	68
FIGURE 3.8: AVERAGE MATERIAL COMPOSITION OF MOBILE PHONES.	69
FIGURE 3.9: PCB SAMPLES OBTAINED AFTER MILLING; (A) ≤ 150 MM, (B) 150-710 MM, (C) 710-2000 MM.	70
FIGURE 3.10: BSE-EDS IMAGES OF COMMINATION FINES AFTER CRYOMILLING (≤ 150 MM); A) PCBs, B) SCREENS, C) CAMERAS AND D) SPEAKERS.	71
FIGURE 3.11: AVERAGE METAL AND METALLOID CONCENTRATIONS PER EoL MOBILE PHONE UNIT.	77
FIGURE 3.12: BSE-EDS IMAGE OF (A) PCB CROSS-SECTION, (B) PBC RECONSTRUCTION OF LAYERS.	78
FIGURE 3.13: MOBILE PHONE SCREEN A) POLYMERIC SET, B) BSE-EDS IMAGES OF A CROSS-SECTION SCREEN, AND C) RECONSTRUCTION OF A CROSS-SECTION OF AN LCD SCREEN.	81
FIGURE 3.14: CAMERA COMPONENTS AND DSE-EDS IMAGE OF A SENSOR INTEGRATED CIRCUIT FOUND IN CAMERAS.	82
FIGURE 3.15: SPEAKER COMPONENTS AND DSE-EDS IMAGE OF A SPEAKER.	83
FIGURE 3.16: HAZARDOUS METALS (SELECTED AS THOSE MOST COMMONLY CITED AS TOXIC IN WEEE) IN EoL MULTIGENERATIONAL MOBILE PHONES AND IN THEIR COMPONENTS: PCBs, SCREENS, CAMERAS, AND SPEAKERS.	88
FIGURE 3.17: FTIR SPECTRUM OF A MILLED SAMPLE OF CASINGS OF FEATURE PHONE, MULTIMEDIA PHONE AND SMARTPHONE.	90
FIGURE 3.18: PRINTED PLASTIC CODE IN EoL-MPS CASINGS.	90

FIGURE 3.19: FTIR SPECTRUM OF A MILLED SAMPLE OF PCBs OF FEATURE PHONE, MULTIMEDIA PHONE AND SMARTPHONE.	91
FIGURE 3.20: FTIR SPECTRUM OF A MILLED SAMPLE OF SCREENS OF FEATURE PHONE, MULTIMEDIA PHONE AND SMARTPHONE.	92
FIGURE 3.21: MAIN COMPONENTS OF LCD SCREENS FROM EoL-MPs.	93
FIGURE 3.22: FTIR SPECTRUM OF (A) DIFFUSER SHEET 1, (B) DIFFUSER SHEET 2, (C) DIFFUSER SHEET 3, (D) DIFFUSER PLATE, (E) REFLECTIVE SHEET, AND (F) PLASTIC FRAME	94
FIGURE 3.23: TGA OF MILLED SAMPLE OF (A) CASINGS (B) PCBs AND (C) SCREENS OF FEATURE PHONE, MULTIMEDIA PHONE AND SMARTPHONE (10 °C/MIN, N ₂ ATMOSPHERE).	99
FIGURE 3.24: AVERAGE CONCENTRATION AND DISTRIBUTION OF METALS AND METALLOIDS IN EoL-MPs.	104
FIGURE 3.25: POLYMERIC COMPOSITION AND POTENTIAL ENERGY RECOVERY PER TON OF EoL-MPs.	110
FIGURE 3.26: PERIODIC TABLE TO SHOW CONCENTRATIONS OF METALS, METALLOIDS AND NON-METALLIC ELEMENTS PRESENT IN EoL MULTIGENERATIONAL MOBILE PHONES.	112
FIGURE 4.1: ANALYTICAL METHODS APPLIED AND MEASURES USED TO DETERMINE THE EFFECTIVENESS OF THE EXTRACTION AND RECOVERY METHODS PROPOSED.	119
FIGURE 4.2: OVERVIEW OF EXPERIMENTAL PROCEDURE.	120
FIGURE 4.3: SCHEME OF THE FLAT-PLATE ELECTROWINNING CELL DEVELOPED AND USED IN THIS WORK.	125
FIGURE 4.4: OVERVIEW OF THE EXPERIMENTAL PROCEDURE IN THE COPPER RECOVERY PROCESS.	126
FIGURE 4.5: STUDY OF DIFFERENT CONDITIONS ON COPPER SOLUBILITY (USING POWDERED COPPER); (A) EFFECT OF TEMPERATURE, (B) EFFECT OF REACTION TIME AND (C) EFFECT OF THE OXIDANT (H ₂ O ₂) DOSAGE.	128
FIGURE 4.6: EFFECT OF THE COPPER FORM ON LEACHING; (A) WITHOUT H ₂ O ₂ , (B) OPTIMAL CONDITION OF H ₂ O ₂ OF EACH IL (50 VOL.% FOR [BMIM]HSO ₄ , [EMIM]Cl AND [BMIM]Cl, 30 VOL.% FOR [HBET]NTF ₂). COPPER LEACHING WERE AT 80 °C, 2 H AND 500 RPM.	129
FIGURE 4.7: LEACHING OF CU, FE AND ZN: (A) FROM SINGLE METAL SOLUTIONS, AND (B) FROM A SIMULATED CU:FE:ZN 1:1:1 MIXED METAL SOLUTION. OPTIMAL CONDITIONS (80°C, 2 H, 50%v/v H ₂ O ₂ , 500RPM).	130
FIGURE 4.8: EFFECT OF THE [BMIM]HSO ₄ CONCENTRATION ON COPPER LEACHING.	132
FIGURE 4.9: EFFECT OF THE SOLID/LIQUID RATIO ON WPCBs LEACHING; (A) LEACHING EFFICIENCY, AND (B) METAL CONCENTRATION.	133
FIGURE 4.10: EFFECT OF THE H ₂ O ₂ DOSAGE ON LEACHING FROM WPCBs; (A) LEACHING EFFICIENCY, AND (B) METAL CONCENTRATION.	134
FIGURE 4.11: EFFECT OF TIME AND TEMPERATURE ON COPPER LEACHING FROM WPCBs.	135
FIGURE 4.12: EFFECT OF TIME AND TEMPERATURE ON THE LEACHING OF MAJOR METALS PRESENT IN WPCBs.	136
FIGURE 4.13: EFFECT OF TIME AND TEMPERATURE ON THE CONCENTRATION OF MAJOR METALS PRESENT IN WPCBs.	137
FIGURE 4.14: METAL LEACHING FROM WPCBs USING OPTIMAL CONDITIONS; (A) METAL CONCENTRATION AND LEACHING EFFICIENCIES, AND (B) METAL PROPORTION IN SOLUTION	138
FIGURE 4.15: SEM-EDS IMAGES OF WPCBs POWDERS (A) AND (B) BEFORE REACTION, (C) AND (D) AFTER REACTION.	139
FIGURE 4.16: XRD PATTERNS OF WPCBs POWDERS BEFORE REACTION AND AFTER REACTION.	139
FIGURE 4.17: MODEL FITTING FOR LEACHING KINETICS OF CU FROM WPCBs BY [BMIM]HSO ₄ ; A) FILM DIFFUSION CONTROL DENSE CONSTANT SIZE SMALL PARTICLES – ALL GEOMETRIES, B) FILM DIFFUSION CONTROL DENSE SHRINKING SPHERES, C) CHEMICAL	

REACTION CONTROL DENSE CONSTANT SIZE CYLINDRICAL PARTICLES, D) CHEMICAL REACTION CONTROL DENSE CONSTANT SIZE AND E) ASH DIFFUSION CONTROL DENSE CONSTANT SIZE-SPHERICAL PARTICLES.....	142
FIGURE 4.18: ARRHENIUS PLOT FOR METAL LEACHING FROM WPCBS.	144
FIGURE 4.19: PROCESS FOR DISMANTLING ECS FROM THE WPCBS USING [BMIM]BF ₄	147
FIGURE 4.20: SEM-EDS IMAGES OF RECOVERED SOLDER FROM WPCBS USING [BMIM]BF ₄	148
FIGURE 4.21: XRD PATTERNS OF WPCBS POWDERS BEFORE REACTION AND AFTER SOLDER AND ECS REMOVING BY [BMIM]BF ₄	150
FIGURE 4.22: EFFECT OF THE Cu:Fe RATIO AND TIME IN THE CEMENTATION OF COPPER FROM COPPER SULPHATE SOLUTIONS.....	152
FIGURE 4.23: CEMENTATION OF Cu BY Fe FROM LEACHED WPCBS; (A) CONCENTRATION AND (B) METAL PERCENTAGE IN SOLUTION.	153
FIGURE 4.24: EFFECT OF ELECTROLYSIS TIME ON COPPER CONCENTRATION, COPPER RECOVERY AND CURRENT EFFICIENCY FROM WPCBS USING DIFFERENT CURRENTS; (A) 10MA, (B) 50MA, (C) 100MA AND (D) 500MA.	155
FIGURE 4.25: SEM IMAGES OBTAINED AT DIFFERENT CURRENT DENSITIES; A) 10 MA, B) 50 MA, C) 100 MA AND D) 500 MA.	156
FIGURE 4.26: FTIR AND TGA OF [BMIM]BF ₄ USED IN 3 CYCLES OF ECS AND SOLDER SEPARATION FROM WPCBS.	159
FIGURE 4.27: LEACHING, ELECTROWINNING, AND OVERALL EFFICIENCY OVER FIVE CYCLES BY [BMIM]HSO ₄	161
FIGURE 4.28: FTIR SPECTRA OF VIRGIN OF [BMIM]HSO ₄ AND RECOVERED [BMIM]HSO ₄ AFTER 5 CYCLES – THE HATCHED BOX INDICATES THE EMERGENCE OF FEATURE LINKED TO C=O STRETCH FREQUENCIES.	163
FIGURE 4.29: THERMOGRAVIMETRIC RESULTS OF VIRGIN [BMIM]HSO ₄ AND RECOVERED [BMIM]HSO ₄ AFTER 5 CYCLES; A) TGA, B) DTG AND C) HEAT FLOW.	164
FIGURE 4.30: FLOWSHEET OF COPPER RECOVERY PROCESS FROM WPCBS.	166
FIGURE 4.31: SCHEMATIC DIAGRAM OF THE EXPERIMENTAL PROCESS FOR THE RECOVERY OF COPPER FROM WPCBS.	167
FIGURE 5.1: CHEMICAL STRUCTURE OF AMBERLITE™ XAD-7 RESIN [210].	175
FIGURE 5.2 ANALYTICAL METHODS APPLIED AND MEASURES USED TO DETERMINE THE EFFECTIVENESS OF THE EXTRACTION AND RECOVERY METHODS PROPOSED.	176
FIGURE 5.3: OVERVIEW OF EXPERIMENTAL PROCEDURE.	177
FIGURE 5.4: OVERVIEW OF THE EXPERIMENTAL PROCEDURE APPLIED IN THE DEVELOPMENT OF AN OPTIMISED PROCESS FOR GOLD RECOVERY.....	186
FIGURE 5.5: LEACHING EFFICIENCY OF IL FROM GOLD AND COPPER.	187
FIGURE 5.6: EXTRACTION EFFICIENCY OF GOLD FROM HCL SOLUTION; (A) EFFECT OF THE TIME AND (B) EFFECT OF THE TEMPERATURE.	188
FIGURE 5.7: EFFECT OF DILUENTS ON GOLD EXTRACTION.	190
FIGURE 5.8: EFFECT OF DIFFERENT CONDITION ON GOLD EXTRACTION: (A) TIME, (B) TEMPERATURE, (C) CYPHOS 101 CONCENTRATION, AND (D) HYDROCHLORIC ACID CONCENTRATION.	192
FIGURE 5.9: EFFECT OF CYPHOS 101 CONCENTRATION ON GOLD EXTRACTION VS; (A) EXTRACTION EFFICIENCY, AND (B) LOG (D). .	194
FIGURE 5.10: EFFECT OF THE GOLD EXTRACTION BY; (A) HCL CONCENTRATION, (B) CHLORIDE CONCENTRATION, AND (C) LOG [Cl ⁻] VS LOG (D).	195
FIGURE 5.11: EFFECT OF THE TEMPERATURE ON GOLD EXTRACTION: (A) EXTRACTION EFFICIENCY, AND (B) 1/T VS LOG(D).	196
FIGURE 5.12: SEM–EDS ANALYSIS (ELEMENT CARTOGRAPHY) OF RAW AMBERLITE™ XAD-7 RESIN (A) AND (C), AND CYPHOS 101 IMPREGNATED RESIN (B) AND (D). RED AND GREEN DOTS DENOTE P AND CL, RESPECTIVELY.....	200

FIGURE 5.13: INFLUENCE OF HCL CONCENTRATION AND IL LOADING ON AU(III) SORPTION EFFICIENCY USING AMBERLITE™ XAD-7 (SD: 3 G/L, 150 RPM, 20 °C, 24 H, C ₀ = 300 MG AU/L)	201
FIGURE 5.14: INFLUENCE OF IL LOADING ON AU(III) SORPTION ISOTHERMS USING AMBERLITE XAD-7 (SD: 2 G/L, 150 RPM, 20 °C, 24 H).	202
FIGURE 5.15: EXPERIMENTAL ADSORPTION ISOTHERMS FITTED WITH FREUNDLICH AND LANGMUIR ISOTHERMS AT DIFFERENT GOLD CONCENTRATIONS.	204
FIGURE 5.16: INFLUENCE OF IL LOADING ON AU(III) SORPTION KINETICS.....	205
FIGURE 5.17: SORPTION MODELS FOR AU(III) ONTO AMBERLITE™ XAD-7/CYPHOS 101 RESINS; (A) PSEUDO-FIRST ORDER MODEL, (B) PSEUDO-SECOND ORDER MODEL, (C) WEBER–MORRIS MODEL, AND (D) BOYD MODEL.	209
FIGURE 5.18: EFFECT OF THE TEMPERATURE ON THE SORPTION EFFICIENCIES.	210
FIGURE 5.19: EFFECT OF THE TEMPERATURE ON THE EQUILIBRIUM THERMODYNAMICS FOR DIFFERENT CYPHOS 101 LOADINGS; (A) RAW AMBERLITE™ XAD-7, (B) 100 MG IL/G RESIN, (C) 300 MG IL/G RESIN, (D) 500 MG IL/G RESIN.....	211
FIGURE 5.20: GOLD ELUTION FROM 0.1 M CYPHOS 101 IN TOLUENE; (A) EFFECT OF THE HCL CONCENTRATION (1M THIOUREA),(B) EFFECT OF THE THIOUREA CONCENTRATION (1M HCL), AND (C) EFFECT OF THE CONTACT TIME.....	216
FIGURE 5.21: GOLD EXTRACTION, ELUTION DESORPTION, AND ORGANIC PHASE (0.1 M CYPHOS IN TOLUENE) REUSABILITY OVER FIVE CYCLES.	217
FIGURE 5.22: FTIR SPECTRA OF THE ORGANIC EXTRACTANT (0.1 M CYPHOS 101 IN TOLUENE) OVER FIVE CYCLES.	218
FIGURE 5.23: GOLD DESORPTION FROM XAD-7 IMPREGNATED WITH CYPHOS 101 (300 MG IL/G); (A) EFFECT OF THE HCL CONCENTRATION (1M THIOUREA),(B) EFFECT OF THE THIOUREA CONCENTRATION (1M HCL), AND (C) EFFECT OF THE CONTACT TIME.....	219
FIGURE 5.24: GOLD SORPTION, DESORPTION, AND RESIN RECYCLABILITY OVER FIVE CYCLES.	220
FIGURE 5.25: BSE IMAGES OF IMPREGNATED AMBERLITE XAD-7: (A) AND (B) BEFORE CYCLES, (C) AND (D) AFTER 5 CYCLES OF SORPTION/DESORPTION.	221
FIGURE 5.26: FIRST LEACHING STAGE WITH NITRIC ACID: (A) AND (B) FOR ECS, (C) AND (D) FOR CPUs, (E) AND (F) FOR WPCBs, (G) AND (H) FOR WPCBs WITH [BMIM]HSO ₄	225
FIGURE 5.27: SECOND LEACHING STAGE WITH AQUA REGIA: (A) AND (B) FOR ECS, (C) AND (D) FOR CPUs, (E) AND (F) FOR WPCBs, (G) AND (H) WPCBs WITH [BMIM]HSO ₄	226
FIGURE 5.28: IMAGES OF THE FIRST AND SECOND LEACHING LIQUORS.	227
FIGURE 5.29: GOLD EXTRACTION FROM ICS LEACHING LIQUOR BY 0.1 M CYPHOS 101: (A) METALS IN THE ORGANIC PHASE, (B) METALS IN THE AQUEOUS PHASE, (C) METAL DISTRIBUTION OF THE EXTRACTED METALS, (D) METAL DISTRIBUTION IN THE ORGANIC AND AQUEOUS PHASES AFTER EXTRACTION. CONDITIONS: O:A=1:1, 150 RPM, 20 °C, 30 MIN.	234
FIGURE 5.30: ELUTION OF LOADED ORGANIC PHASE (0.1 M CYPHOS IN TOLUENE) WITH THIOUREA: (A) CONCENTRATION AND ELUTION EFFICIENCY, AND (B) METAL DISTRIBUTION IN THE ELUTION SOLUTION. CONDITIONS: 0.5 M THIOUREA IN 0.5 M HCL, O:A=1:1, 150 RPM, 20 °C, 2 H.	235
FIGURE 5.31: GOLD SORPTION FROM ICS LEACHING LIQUOR BY SIRs (AMBERLITE™ XAD7-300MG CYPHOS 101): (A) METAL SORPTION, (B) METALS IN THE AQUEOUS PHASE, (C) METAL DISTRIBUTION OF THE EXTRACTED METALS, (D) METAL DISTRIBUTION IN THE ORGANIC AND AQUEOUS PHASES AFTER EXTRACTION. CONDITIONS: SD:25 G/L,150 RPM, 20°C,4H.	237

FIGURE 5.32: DESORPTION OF LOADED SIRS (AMBERLITE™XAD7-300MG CYPHOS 101) WITH THIOUREA: (A) CONCENTRATION AND ELUTION EFFICIENCY, AND (B) METAL DISTRIBUTION IN THE ELUTION SOLUTION. CONDITIONS: 0.5 M THIOUREA IN 0.5 M HCL, SD=25 G/L, 150 RPM, 20 °C, 3 H.	238
FIGURE 5.33: PHOTOGRAPHIC IMAGES OF SIRS: (A) BEFORE SORPTION, (B) AFTER SORPTION, AND (C) AFTER DESORPTION.	239
FIGURE 5.34: SEM-EDS IMAGES OF THE PRECIPITATED GOLD NANOPARTICLES BY NABH ₄ : (A) SEM IMAGE (500 μM), (B) SEM IMAGE (100 μM), (C) EDS (100 μM), AND (D) EDS MAP SUM SPECTRUM.	240
FIGURE 5.35: GOLD RECOVERY PROCESS FROM WEEE (WPCBs, ICs, CPUs) BY LIQUID-LIQUID EXTRACTION.	244
FIGURE 5.36: GOLD RECOVERY PROCESS FROM WEEE (WPCBs, ICs, CPUs) BY SORPTION EXTRACTION.	245
FIGURE 6.1: ANALYTICAL METHODS APPLIED AND MEASURES USED TO DETERMINE THE EFFECTIVENESS OF THE EXTRACTION AND RECOVERY METHODS PROPOSED.	252
FIGURE 6.2: OVERVIEW OF EXPERIMENTAL PROCEDURE.	253
FIGURE 6.3: OVERVIEW OF THE EXPERIMENTAL PROCEDURE APPLIED IN THE DEVELOPMENT OF AN OPTIMISED PROCESS FOR INDIUM RECOVERY.	260
FIGURE 6.4: EFFECT OF DIFFERENT ACIDS IN THE INDIUM EXTRACTION WITH; (A) CYPHOS 101 AND (B) ALIQUAT 336.	262
FIGURE 6.5: EFFECT OF DIFFERENT DILUENTS IN THE INDIUM EXTRACTION.	263
FIGURE 6.6: EFFECT OF THE INDIUM EXTRACTION IN (A) TIME, (B) TEMPERATURE, AND (C) IL CONCENTRATION.	264
FIGURE 6.7: EFFECT OF THE CL ⁻ CONCENTRATION ON INDIUM EXTRACTION.	266
FIGURE 6.8: EFFECT OF THE H ⁺ CONCENTRATION ON INDIUM EXTRACTION.	267
FIGURE 6.9: EFFECT OF THE IL EQUILIBRIUM ON INDIUM EXTRACTION.	268
FIGURE 6.10: EFFECT OF THE TEMPERATURE ON THE THERMODYNAMICS PARAMETERS OF INDIUM EXTRACTION.	270
FIGURE 6.11: INDIUM STRIPPING AT DIFFERENT H ₂ SO ₄ ACID CONCENTRATION	272
FIGURE 6.12: INDIUM STRIPPING FROM SIMULATED SOLUTION; (A) EFFECT OF TIME, AND (B) EFFECT OF STRIPPING SOLUTION VOLUME.	273
FIGURE 6.13: INDIUM RECOVERY FROM 0.1M H ₂ SO ₄ BY CEMENTATION; (A) EFFECT OF TIME, AND (B) EFFECT OF STOICHIOMETRIC EXCESS ZN MOLES/IN MOLES.	274
FIGURE 6.14: INDIUM OXIDE OBTAINED BY PRECIPITATION OF IN BY NaOH; (A) SEM, AND (B) EDS IMAGES.	275
FIGURE 6.15: EFFICIENCIES OF EXTRACTION AND STRIPPING OVER 5 CYCLES: (A) CYPHOS 101, AND (B) ALIQUAT 336.	277
FIGURE 6.16: FTIR SPECTRA OF (A) TOLUENE AND 0.1M IL, VIRGIN ILS AND AFTER 3 CYCLES FOR (B) ALIQUAT 336, AND (C) CYPHOS 101.	279
FIGURE 6.17: EFFECT OF THE TEMPERATURE IN THE INDIUM LEACHING FROM LCD SCREENS WITH DIFFERENT ACIDS.	281
FIGURE 6.18: EFFECT OF (A) TIME, (B) ACID CONCENTRATION, AND (C) SOLID/LIQUID RATIO ON THE INDIUM LEACHING.	282
FIGURE 6.19: METAL LEACHING OF LCD SCREENS UNDER OPTIMAL CONDITIONS (A) AND (B) HCL, (C) AND (D) H ₂ SO ₄	283
FIGURE 6.20: STRUCTURE OF (A) AN EOL-MP SCREEN, (B) EOL-LCD PANEL AND A CROSS-SECTION, AND (C) SEM-EDS IMAGES OF THE INNER GLASS SUBSTRATE.	285
FIGURE 6.21: PHOTOGRAPHS AND SE IMAGES OF THE POLARISERS OBTAINED BY HOT WATER AND ACETONE.	287
FIGURE 6.22: METAL LEACHING OF PRE-TREATED LCD PANELS UNDER OPTIMAL CONDITIONS; (A) METAL CONCENTRATION AND LEACHING EFFICIENCY, AND (B) METAL DISTRIBUTION AFTER LEACHING.	288
FIGURE 6.23: LCD LEACHING AND SEM-EDS IMAGES BEFORE AND AFTER REACTION.	290

FIGURE 6.24: PRE-TREATMENT OF EOL-MP SCREENS AND RECOVERY OF VALUABLE MATERIALS.	291
FIGURE 6.25: INDIUM EXTRACTION FROM LEACH LIQUOR DERIVED FROM PRE-TREATED STRIP LCD PANELS BY 0.1M CYPHOS 101; (A) METALS IN THE ORGANIC PHASE AND EXTRACTION EFFICIENCIES, (B) METALS IN THE AQUEOUS PHASE, (C) METAL DISTRIBUTION OF THE EXTRACTED METALS, AND (D) METAL DISTRIBUTION IN THE ORGANIC AND AQUEOUS PHASES AFTER EXTRACTION.	300
FIGURE 6.26: INDIUM EXTRACTION FROM LEACH LIQUOR DERIVED FROM PRE-TREATED STRIP LCD PANELS BY 0.1M ALIQUAT 336; (A) METALS IN THE ORGANIC PHASE AND EXTRACTION EFFICIENCIES, (B) METALS IN THE AQUEOUS PHASE, (C) METAL DISTRIBUTION OF THE EXTRACTED METALS, AND (D) METAL DISTRIBUTION IN THE ORGANIC AND AQUEOUS PHASES AFTER EXTRACTION.	301
FIGURE 6.27: INDIUM EXTRACTION BY CYPHOS 101; (A) MCCABE-THIELE PLOT FOR IN, AND (B) COUNTER-CURRENT ON THE EXTRACTION OF IN FROM PRE-TREATED STRIP LCD PANELS LEACHED IN HYDROCHLORIC MEDIUM.	303
FIGURE 6.28: INDIUM EXTRACTION BY ALIQUAT 336; (A) MCCABE-THIELE PLOT FOR IN, AND (B) COUNTER-CURRENT ON THE EXTRACTION OF IN FROM PRE-TREATED STRIP LCD PANELS LEACHED IN HYDROCHLORIC MEDIUM.	304
FIGURE 6.29: METAL STRIPPING FROM LOADED 0.1M ILS WITH DIFFERENT H ₂ SO ₄ CONCENTRATIONS; (A) AND (B) CYPHOS 101, (C) AND (D) ALIQUAT 336.	307
FIGURE 6.30: PROCESS DEVELOPED FOR INDIUM RECOVERY FROM ITO GLASS SUBSTRATE.	309
FIGURE 6.31: FLOWSHEET FOR PROCESS DEVELOPED FOR TOTAL INDIUM RECOVERY FROM EOL-MP SCREENS.	310
FIGURE 7.1: SPEAKERS AND CAMERAS FROM EOL MOBILE PHONES UTILISED IN THE RECOVERY OF REEs. GENERATION 1: FEATURE PHONES, GENERATION 2: MULTIMEDIA PHONES, AND GENERATION 3: SMARTPHONES.	319
FIGURE 7.2: ANALYTICAL METHODS AND MEASURES USED TO DETERMINE THE EFFECTIVENESS OF THE EXTRACTION AND RECOVERY METHODS PROPOSED.	320
FIGURE 7.3: OVERVIEW OF EXPERIMENTAL PROCEDURE.	321
FIGURE 7.4: OVERVIEW OF THE EXPERIMENTAL PROCEDURE APPLIED IN THE DEVELOPMENT OF AN OPTIMIZED PROCESS FOR RARE EARTH ELEMENTS RECOVERY.	329
FIGURE 7.5: REEs CONCENTRATION AND DISTRIBUTION IN SPEAKERS (A) AND (B), AND IN CAMERAS (C) AND (D) OF EOL-MPs. ...	330
FIGURE 7.6: TOTAL METAL CONCENTRATION AND DISTRIBUTION; (A) SPEAKERS AND (B) CAMERAS.	331
FIGURE 7.7: SOLUBILITY OF REOs IN 1:1 [HBET][TF ₂ N]:H ₂ O SYSTEM WITH RESPECT TO TIME; (A) EFFECT OF TIME OVER THE DURATION STUDIED, (B) SHOWN IN MORE DETAIL IN THE RANGE UP TO 15 MINS.	333
FIGURE 7.8: EFFECT OF THE TEMPERATURE ON REOs SOLUBILITIES IN [HBET][TF ₂ N]:H ₂ O (1:1) SYSTEM; (A) EXTRACTION CONCENTRATION, (B) EXTRACTION EFFICIENCY.	334
FIGURE 7.9: EFFECT OF THE IL:H ₂ O RATIO IN THE SOLUBILITY AND METAL DISTRIBUTION OF Nd ₂ O ₃ (A) AND (B), AND Pr ₂ O ₃ (C) AND (D).	337
FIGURE 7.10: INFLUENCE OF METAL SALTS (1 M) ON THE DISTRIBUTION RATIO OF Nd AND Pr IONS IN THE 1:1 [HBET][TF ₂ N]:H ₂ O SYSTEM.	338
FIGURE 7.11: EFFECT OF THE TEMPERATURE IN THE SOLUBILITY OF Nd ₂ O ₃ (A) AND (B), AND Pr ₂ O ₃ (C) AND (D).	339
FIGURE 7.12: MODEL FITTING FOR LEACHING KINETICS OF Nd ₂ O ₃ BY [HBET][TF ₂ N]:H ₂ O (1:1); A) FILM DIFFUSION CONTROL DENSE CONSTANT SIZE SMALL PARTICLES – ALL GEOMETRIES, B) FILM DIFFUSION CONTROL DENSE SHRINKING SPHERES, C) CHEMICAL REACTION CONTROL DENSE CONSTANT SIZE CYLINDRICAL PARTICLES, D) CHEMICAL REACTION CONTROL DENSE CONSTANT SIZE AND E) ASH DIFFUSION CONTROL DENSE CONSTANT SIZE-SPHERICAL PARTICLES.	341

FIGURE 7.13: MODEL FITTING FOR LEACHING KINETICS OF Pr_2O_3 BY $[\text{HBET}][\text{TF}_2\text{N}]:\text{H}_2\text{O}$ (1:1); A) FILM DIFFUSION CONTROL DENSE CONSTANT SIZE SMALL PARTICLES – ALL GEOMETRIES, B) FILM DIFFUSION CONTROL DENSE SHRINKING SPHERES, C) CHEMICAL REACTION CONTROL DENSE CONSTANT SIZE CYLINDRICAL PARTICLES, D) CHEMICAL REACTION CONTROL DENSE CONSTANT SIZE AND E) ASH DIFFUSION CONTROL DENSE CONSTANT SIZE-SPHERICAL PARTICLES.....	342
FIGURE 7.14: ARRHENIUS PLOT FOR REOs LEACHING (A) Nd_2O_3 AND (B) Pr_2O_3	344
FIGURE 7.15: EFFECT OF THE Nd_2O_3 : Pr_2O_3 RATIO ON THE LEACHING BY $[\text{HBET}][\text{TF}_2\text{N}]:\text{H}_2\text{O}$ (1:1) SYSTEM.	345
FIGURE 7.16: SOLUBILITY OF Fe_2O_3 OVER (A) TEMPERATURE, AND (B) IL: H_2O RATIO.	346
FIGURE 7.17: EFFECT OF THE Nd_2O_3 : Pr_2O_3 : Fe_2O_3 RATIO ON THE LEACHING BY $[\text{HBET}][\text{TF}_2\text{N}]:\text{H}_2\text{O}$ (1:1) SYSTEM.	347
FIGURE 7.18: TG-DSC CURVES OF REEs OXALATES AT A HEATING RATE OF 20 °C/MI IN AIR.....	349
FIGURE 7.19: Nd_2O_3 LEACHING, STRIPPING, AND $[\text{HBET}][\text{TF}_2\text{N}]$ REUSABILITY OVER FIVE CYCLES.	351
FIGURE 7.20: FTIR SPECTRA OF $[\text{HBET}][\text{TF}_2\text{N}]$ OVER FIVE CYCLES.....	352
FIGURE 7.21: TG-DSC CURVES OF SPEAKER POWDER AT A HEATING RATE OF 20 °C/MIN IN AIR.	354
FIGURE 7.22: METAL DISTRIBUTION AFTER $[\text{HBET}][\text{TF}_2\text{N}]:\text{H}_2\text{O}$ SYSTEM LEACHING/EXTRACTION.	357
FIGURE 7.23: FLOW CHART OF THE RECYCLING OF RARE-EARTH ELEMENTS FROM EOL MOBILE PHONES SPEAKERS.	361
FIGURE 7.24: EFFECT OF THE ILS ($[\text{BMIM}][\text{TF}_2\text{N}]$, $[\text{P}_{6,6,6,14}][\text{TF}_2\text{N}]$ AND $[\text{P}_{6,6,6,14}][\text{Cl}]$) IN THE EXTRACTION OF ND IN HYDROCHLORIC SOLUTION IN FUNCTION OF (A) HCL CONCENTRATION, (B) TEMPERATURE, AND (C) TIME.	364
FIGURE 7.25: EFFECT OF THE ND:PR RATIO ON THE LEACHING BY $[\text{BMIM}][\text{TF}_2\text{N}]$, $[\text{P}_{6,6,6,14}][\text{TF}_2\text{N}]$ AND $[\text{P}_{6,6,6,14}][\text{Cl}]$ WITH RATIOS OF; (A) ND:PR=1:2, (B) ND:PR=1:1, AND (C) ND:PR=2:1.	365
FIGURE 7.26: NEODYMIUM (Nd^{+3}) EXTRACTION, STRIPPING, AND $[\text{BMIM}][\text{TF}_2\text{N}]$ REUSABILITY OVER FIVE CYCLES.....	366
FIGURE 7.27: FTIR SPECTRA OF $[\text{BMIM}][\text{TF}_2\text{N}]$ OVER FIVE CYCLES.....	367
FIGURE 7.28: A PROPOSED FLOW CHART FOR THE RECOVERY OF RARE-EARTH ELEMENTS FROM EOL MOBILE PHONE SPEAKERS USING THE ALTERNATIVE METHOD.	368
FIGURE A.1: MODEL FITTING FOR LEACHING KINETICS OF IRON FROM WPCBS BY $[\text{BMIM}]\text{HSO}_4$	391
FIGURE A.2: MODEL FITTING FOR LEACHING KINETICS OF NICKEL FROM WPCBS BY $[\text{BMIM}]\text{HSO}_4$	392
FIGURE A.3: MODEL FITTING FOR LEACHING KINETICS OF LEAD FROM WPCBS BY $[\text{BMIM}]\text{HSO}_4$	393
FIGURE A.4: MODEL FITTING FOR LEACHING KINETICS OF LEAD FROM WPCBS BY $[\text{BMIM}]\text{HSO}_4$	394
FIGURE A.5: LINEAR FIT OF THE FREUNDLICH MODEL AT DIFFERENT Au(III) EQUILIBRIUM CONCENTRATIONS.	395
FIGURE A.6: LINEAR FIT OF THE LANGMUIR MODEL AT DIFFERENT Au(III) EQUILIBRIUM CONCENTRATIONS.	395
FIGURE A.7: LINEAR FIT OF THE PSEUDO-FIRST ORDER MODEL.	396
FIGURE A.8: LINEAR FIT OF THE PSEUDO-SECOND ORDER MODEL.	396
FIGURE A.9: INDIUM EXTRACTION BY CYPHOS 101 WITHOUT ASCORBIC ACID; (A) MCCABE-THIELE PLOT FOR IN, AND (B) COUNTER-CURRENT ON THE EXTRACTION OF IN FROM LCD PANELS LEACHED IN HYDROCHLORIC MEDIUM.....	397
FIGURE A.10: INDIUM EXTRACTION BY ALIQUAT 336 101 WITHOUT ASCORBIC ACID; (A) MCCABE-THIELE PLOT FOR IN, AND (B) COUNTER-CURRENT ON THE EXTRACTION OF IN FROM LCD PANELS LEACHED IN HYDROCHLORIC MEDIUM.	398

List of Tables

TABLE 2.1: CLASSIFICATION OF WEEE ACCORDING TO THE EUROPEAN WEEE DIRECTIVE (2012/19/EC) [31].	8
TABLE 2.2: GLOBAL GROWTH OF EEE AND WEEE [9].	9
TABLE 2.3: MATERIAL COMPOSITION FOR EACH CATEGORY OF THE WEEE (% w/w) [45].	15
TABLE 2.4: METAL CONCENTRATION IN PCBs OF MOBILE PHONES AND COMPUTERS.	17
TABLE 2.5: HAZARDOUS SUBSTANCES IN WEEE [12].	19
TABLE 2.6: HAZARDOUS SUBSTANCES RESTRICTED IN EEE UNDER THE EU DIRECTIVE 2011/65/EU.	26
TABLE 2.7: CRITICAL RAW MATERIALS BY THE EUROPEAN COMMISSION, 2020 [17].	31
TABLE 2.8: MECHANISMS FOR THE TRANSFER OF METALS FROM AN AQUEOUS PHASE [131].	45
TABLE 3.1: EOL FEATURE PHONES UTILISED IN THIS STUDY.	51
TABLE 3.2: EOL MULTIMEDIA PHONES UTILISED IN THIS STUDY.	52
TABLE 3.3: EOL SMARTPHONES UTILISED IN THIS STUDY.	53
TABLE 3.4: METAL AND METALLOID COMPOSITION OF PCBs, SCREENS, CAMERAS AND SPEAKERS FROM FEATURE, MULTIMEDIA AND SMART PHONES.	74
TABLE 3.5: CONCENTRATION OF METALS IN PCBs REPORTED BY VARIOUS RESEARCHERS IN COMPARISON TO RESULTS FROM THIS STUDY.	86
TABLE 3.6: CHARACTERISATION OF THE POLYMERIC FILMS IN LCD MOBILE PHONE SCREENS.	95
TABLE 3.7: FTIR CHARACTERISATION OF THE POLYMERS IN THE POLYMERIC SET OF LCD SCREENS.	95
TABLE 3.8: ELEMENTAL ANALYSIS OF CASINGS, SCREENS AND PCBs OF MULTIGENERATIONAL EOL-MPS.	96
TABLE 3.9: TEMPERATURES OF POLYMER DEGRADATION ZONES AND RESIDUE MATERIAL FROM TGA-DSC ((10 °C/MIN, N ₂ ATMOSPHERE).	97
TABLE 3.10: PROXIMATE ANALYSIS AND HHV FROM MULTIGENERATIONAL MOBILE PHONES.	100
TABLE 3.11: MAIN METALS USED IN EEE, CONCENTRATION IN PRIMARY ORES, ESTIMATES OF PEAK PRODUCTION, RECYCLING RATES, AND PRICES.	107
TABLE 4.1: PROPERTIES, CHARACTERISATION AND STRUCTURE OF THE IONIC LIQUIDS USED IN THIS STUDY.	117
TABLE 4.2: STANDARD REDUCTION POTENTIALS OF METALS USED IN THIS STUDY (25 °C, 101 kPa, 1 M).	124
TABLE 4.3: LINEAR FITTING PARAMETERS OF ASH DIFFUSION CONTROL DENSE CONSTANT SIZE-SPHERICAL PARTICLES MODEL.	143
TABLE 4.4: METAL CONCENTRATION OF AS-RECEIVED WPCBs AND BARE WPCBs.	149
TABLE 4.5: ADVANTAGES AND DISADVANTAGES OF DIFFERENT ELECTRODES IN THE COPPER EW.	154
TABLE 4.6: ENERGY CONSUMPTION PARAMETERS FROM EW OF COPPER FROM WPBC.	157
TABLE 4.7: LEACHING OF CU AND MAJOR METALS PRESENT IN WPCBs OVER FIVE CYCLES OF LEACHING AND EW.	162
TABLE 5.1: PROPERTIES, CHARACTERISATION AND STRUCTURE OF THE IONIC LIQUIDS USED IN THIS STUDY.	173
TABLE 5.2: PHYSICAL PROPERTIES OF AMBERLITE™ XAD-7 [210].	175
TABLE 5.3: EXPERIMENTAL PARAMETERS FOR DETERMINATION OF OPTIMAL GOLD LIQUID/LIQUID EXTRACTION CONDITIONS, MECHANISM, AND THERMODYNAMICS CYPHOS 101.	179
TABLE 5.4: EXPERIMENTAL PARAMETERS OF SORPTION; AMBERLITE™ XAD-7 IMPREGNATED WITH CYPHOS 101.	182

TABLE 5.5: EXPERIMENTAL PARAMETERS FOR ELUTION & DESORPTION.	183
TABLE 5.6: FREUNDLICH AND LANGMUIR PARAMETERS FOR AU ADSORPTION AT DIFFERENT INITIAL GOLD CONCENTRATIONS.	204
TABLE 5.7: PARAMETERS OF THE KINETICS MODELS FOR Au(III) SORPTION ON AMBERLITE™ XAD-7/CYPHOS 101 RESINS.	208
TABLE 5.8: THERMODYNAMICS PARAMETERS OF GOLD EXTRACTION BY SIRS.	211
TABLE 5.9: METAL CONCENTRATION AND LEACHING EFFICIENCIES OF THE TWO-LEACHING PROCESS.	228
TABLE 6.1: PROPERTIES, CHARACTERISATION AND STRUCTURE OF THE IONIC LIQUIDS USED IN THIS STUDY.	251
TABLE 6.2: EXPERIMENTAL PARAMETERS FOR DETERMINATION OF OPTIMAL EXTRACTION CONDITIONS, MECHANISM, AND THERMODYNAMICS FOR ALIQUAT 336 AND CYPHOS 101.	255
TABLE 6.3: EXPERIMENTAL PARAMETERS FOR DETERMINATION OF OPTIMAL STRIPPING CONDITIONS.	256
TABLE 6.4: EXPERIMENTAL PARAMETERS FOR DETERMINATION OF OPTIMAL LEACHING CONDITIONS.	258
TABLE 6.5: THERMODYNAMICS PARAMETERS OF INDIUM EXTRACTION.	270
TABLE 6.6: EFFECTS OF ACETONE ON POLARISERS THROUGH TIME.	286
TABLE 6.7: METAL LEACHING FROM LCD PANELS (UNTREATED AND TREATED) UNDER OPTIMAL LEACHING CONDITIONS.	289
TABLE 6.8: COMPARATIVE ANALYSIS OF RECYCLING APPROACHES FOR LCD PANELS FOCUSED ON INDIUM LEACHING.	292
TABLE 6.9: COMPARATIVE ANALYSIS OF RECYCLING APPROACHES FOR LCD PANELS FOCUSED ON INDIUM EXTRACTION.	294
TABLE 6.10: METAL CONCENTRATION IN THE ORGANIC AND AQUEOUS PHASES, AND EXTRACTION EFFICIENCIES OF ILS.	299
TABLE 6.11: FINAL METAL COMPOSITION AND CONCENTRATION OF THE STRIPPING SOLUTION BY 0.1M H ₂ SO ₄	306
TABLE 7.1: PROPERTIES, CHARACTERISATION AND STRUCTURE OF THE IONIC LIQUIDS USED IN THIS STUDY.	316
TABLE 7.2: REOs UTILISED IN THIS STUDY AND THEIR PHYSICAL AND CHEMICAL PROPERTIES.	318
TABLE 7.3: EXPERIMENTAL PARAMETERS FOR LEACHING/EXTRACTION BY [HBET][TF ₂ N]:H ₂ O SYSTEM.	323
TABLE 7.4: EXPERIMENTAL PARAMETERS FOR DETERMINATION OF OPTIMAL EXTRACTION CONDITIONS.	327
TABLE 7.5: LINEAR FITTING PARAMETERS OF ASH DIFFUSION CONTROL DENSE CONSTANT SIZE-SPHERICAL PARTICLES MODEL.	343

Glossary of Terms

Acronyms	Definition
ABS	Acrylonitrile butadiene styrene
AHWG-CRM	Ad-Hoc working group on defining critical raw materials
ARD	Aqua regia digestion
BFRs	Brominated flame retardants
BMs	base metals
CE	Conformité Européenné (European conformity)
CPUs	Central processing units
CRMs	Critical raw materials
CTA	Cellulose triacetate
DEHPA	Di-(2-ethylhexyl)phosphoric acid
DOE	U.S. Department of energy
DSC	Differential scanning calorimetry
EAPs	Environmental action programmes
EC	European commission
EC	European commission
ECs	Electric components
EDS	Energy dispersive X-Ray spectroscopy
EEE	Electrical and electronic equipment
EoL	End-of-life
EPA	Environmental Protection Agency
EPR	Extended producer responsibility
EU	European union
EW	Electrowinning
e-waste	Electrical waste
FRs	Flame retardants
FTIR	Fourier transform infrared spectrometry
GDP	Gross domestic product
HHV	High Heating Value
HREEs	Heavy rare earth elements
HSs	hazardous substances
IC	Chromatography

ICP-OES	Inductively coupled plasma optical emission spectroscopy
ILs	Ionic Liquids
ITO	Indium-tin oxides
ITTT	Information and telecommunication technologies
ITU	International telecommunication union's
LCD	Liquid crystal display
LREEs	Light rare earth elements
LTF	Lithium tetraborate fusion
NRC	U.S. National research council
OECD	Organization for economic co-operation and development
OMs	other metals
PBB	Polybrominated biphenyls
PBDE	Polybrominated diphenyl ethers
PBDEs	Polybrominated diphenyl ethers
PC	Polycarbonate
PCBs	Printed circuit boards
PET	Poly(ethylene terephthalate)
PGMs	Platinum group metals
PMMA	Poly(methyl methacrylate)
POPs	Persistent organic pollutants
PVA	Polyvinyl alcohol
REEs	Rare earth elements
RJD	Rivet joint device
RMI	Raw material initiative
RO	Reverse osmosis
RoHS	Restriction of the use of certain hazardous substances
RTILs	Room temperature ionic liquids
SEM	Scanning electron microscopy
SIRs	Solvent impregnated resins
SJD	Joint device
SMD	Surface mounted device
SPD	Socket pedestal device
TBBPA	Tetrabromobisphenol-A
TGA	Thermogravimetric analysis

THD	Through-hole device
TPP	Triphenyl phosphate
TSILs	Task-specific ionic liquids
UNEP	United nations environment programme
UNU	United nation university
UPR	Unsaturated polyester re
VOCs	Volatile organic compounds
WEEE	Waste electrical and electronic equipment
WFD	Waste framework directive
WPCBs	Waste printed circuit boards
XRD	X-ray diffraction

1 Introduction

1.1 Background

Over the three past decades, the production of electrical and electronic equipment (EEE) has been one of the fastest growing markets in the world due to the rapid technological developments, lower prices, and global markets growth [1, 2]. The consumption of EEE was approximately 19.5 Mt in the nineties which almost doubled in 2000 (34 Mt), trebled in 2010 (57.4 Mt) and quadrupled by 2016 (76.1 Mt) [1, 3]; and with the rapid increase in consumption of EEE there is an inevitable increase in waste electrical and electronic equipment (WEEE). In fact, WEEE is one of the fastest growing waste streams throughout the world with an annual growth rate between 3% and 5% [2, 4]. The global WEEE generation estimation in 2014 was 44.4 Mt, increasing up to 53.6 Mt in 2019, and it was estimated to reach 74.7 Mt in 2030, growing at a rate of almost 2 Mt per year [5]. Moreover, WEEE represents a serious problem to human health and the environment; problems that arise because EEE contains a large number of hazardous substances, including heavy metals such as lead, cadmium, arsenic, chromium, and mercury, flame-retardants, dioxin, and furans [6-8], and from poor waste management, handling and disposal of EEE at end of life [9-11]. The impact on human health has been linked to brain and liver damage, cancer, adverse effects on hormonal, immune, reproductive, nervous and endocrine systems [12]. The environmental risks associated with WEEE are due to the liberation of toxic substances, which can contaminate the soil, water, and the atmosphere, mostly through metal leaching [6-10].

WEEE generation has a strong correlation with the gross domestic product (GDP) and therefore, higher income countries generate more WEEE per capita. The exponential increase in WEEE generation is particularly prevalent in countries with developed economies such as the UK, USA, Australia, for example. In the European Union (EU-28), it was estimated that WEEE generation increased 12% between 2013 and 2020. China plays a crucial role in the EEE industry and WEEE generation, with nearly 20% of the total WEEE generated in 2020, which was an increase of 98% of WEEE generation in 2020 compared to 2013. In other developing economies such as India, Brazil and Russia a marked increase in WEEE generation is also projected in the following years [13].

To address this serious and growing problem, the European Union (EU) has produced environmental legislation and policies for each EU member state that sets firm targets for the collection, reuse, and recycling of WEEE, which started with a collection target of 45% in 2016 with an

increase to 65% in 2019. These legislation and policy instruments also restrict the use of certain hazardous substances such as heavy metals, flame-retardants, among other substances in EEE goods [14, 15]. Additionally, material dependence and scarcity has also been identified as a grave problem for the EU, identifying 30 materials as critical by the European Commission (EC) [16, 17], several of these critical materials are found in WEEE.

Apart from the environmental issues with WEEE, another major problem is that WEEE is a complex and heterogeneous combination of materials, and its composition depends largely on the type, manufacturer, and age of the equipment [7, 13]. In general, the major mass fractions of WEEE are metals (40%), plastics (30%), and refractory oxides (30%) [18]. A simple individual item may contain up to 70 elements including trace amounts of strategically/economically important materials such as rare earth elements (REEs), indium, platinum group metals, among others [7, 19]. The majority of metals in WEEE are found at higher concentrations than in their respective ores, making WEEE a potentially significant secondary material resource [20]. It has been reported that the content of metals in printed circuit boards (PCBs) are at least 10 times higher than in their natural ores, which has stimulated the motivation to recycle metals from end-of-life EEE, especially from PCBs which are regarded as the most valuable component in WEEE [12, 20-22]. Taking gold as an example, it is normal to mine approximately 3 grams of gold per tonne of its ore (3 ppm), whilst the concentration of gold in PCBs is found to be between 300 ppm and 1000 ppm, i.e. over 100-300 times higher than in its natural ore [23]. Furthermore a benchmarking study, conducted for aluminium, copper, ferrous, lead, nickel, tin and zinc, applied to the energy requirement and CO_{2e} consumption for the production of primary and secondary metals demonstrated the environmental benefits of recycling with a total annual savings in CO₂ calculated at approximately 500Mt CO₂ [24]. A follow-up study in 2016 using a more detailed and refined methodology that benefitted from industry-acquired data concluded that for just the three metals, aluminium, ferrous and copper, savings in CO₂ emissions are considerably greater at 572Mt CO₂ per annum [25].

In 2019, approximately only 17% of global WEEE was formally collected and recycled [5]. In the EU, around 25-40% of WEEE is treated and the rest is discarded into landfill or exported to low income countries [26]. In these countries, most of the WEEE is handled and treated in the informal recycling system, which results in severe environment problems and material loss. The low rates of recycling are principally due to inefficient collection, technological difficulties and lack of incentives [27]. Recent work by Vaccari and co-workers [28] reported the development of a scenario-based framework - E-Waste Integrated Assessment Scheme (EWIAS) - to improve the management of WEEE

in Agbogbloshie in Ghana. The tool permitted the evaluation of key economic, social, and environmental factors facing workers managing WEEE, and from the results the authors proposed the best solution was the evolution from informal to formal management with the introduction of important measures, including improved personal protective equipment, introduction of refurbishment activities and the sale of components on the second-hand market.

WEEE comprises complex composites containing a heterogeneous mix of materials, is a resource-rich source of valuable metals and materials, and, albeit a major challenge, offers the potential for recovery of some critical and strategic materials. The work described in this thesis therefore seeks to address this challenge and unlock this value through the development of novel, efficient and integrated recycling processes, focussed on end-of-life mobile phones, to recover value, (primarily in the form of strategic metals or their derivatives) and minimise the environmental impacts and health risks through the safe reuse of resources embedded in WEEE.

1.2 Aims and Objectives

The aim of this research is to develop methods to extract key value strategic materials from Waste Electrical and Electronic Equipment (WEEE) using End-of-Life (EoL) mobile phones as a case study example, for conversion to products of commercial value and to minimise the environmental impact of waste through the safe reuse of resources contained in WEEE.

The specific objectives are to:

- Conduct a comprehensive characterisation of EoL mobile phone components to determine the metal and non-metal fractions.
- Identify task-specific ionic liquids as potential extractants that can selectively solubilise target metals.
- Develop optimised methods for recovery of target metals present in the key components of EoL mobile phones using Model Test Systems.
- Develop, where appropriate, optimised pre-treatment methods to facilitate ionic liquid extraction of the target metal from real samples.
- Apply the optimised processes to sample pre-treatment and recovery of target metals from real samples of as-received e-waste, as pure materials, and fractions of commercial value.
- Demonstrate the successful reuse of ionic liquids and reagents through multiple cycles to conserve reagent use and minimise energy consumption.

1.3 Scope of Thesis

Following this brief introduction which sets out the rationale for the research, the overall aim and the specific objectives set to meet this aim, a review of the literature presented in Chapter 2 provides an overview on WEEE, its classifications, with a brief discussion on mobile phones as a fast-moving consumer electronic generating extensive e-waste, and the subject of the current research, legislation and policies, methods of recycle and recovery, including the potential for ionic liquids as greener solvents and a discussion on the target metals for recovery in the context of the EU critical metals list. The main body of the research, illustrated in the schematic Figure 1.1, is set out in five chapters with the first of these (Chapter 3) providing a comprehensive characterisation of the metallic and non-metallic fractions of multigenerational end-of-life mobile phones and the determination of the sources of the key strategic metals within the mobile phone components. The focus of the next four chapters (Chapters 4-7) is then on the development of processes to recover these strategic metals from key components in EoL mobile phones. To develop optimised methods for extraction and recovery of each of the target metal from real mobile phone samples (mobile phone components), process development steps are performed using a Model Test System before applying the optimised conditions for extraction and recovery to real samples derived from EoL mobiles phones and related e-waste components. The methods developed for the recovery of copper from printed circuit boards (PCBs) is described in Chapter 4, and for gold in Chapter 5; the recovery of indium from liquid crystal display screens is reported in Chapter 6 and the recovery of rare earth metals as metal and as oxide from speakers is reported in Chapter 7. Chapter 8 summarises the key findings of the study and recommendations for future work are proposed.

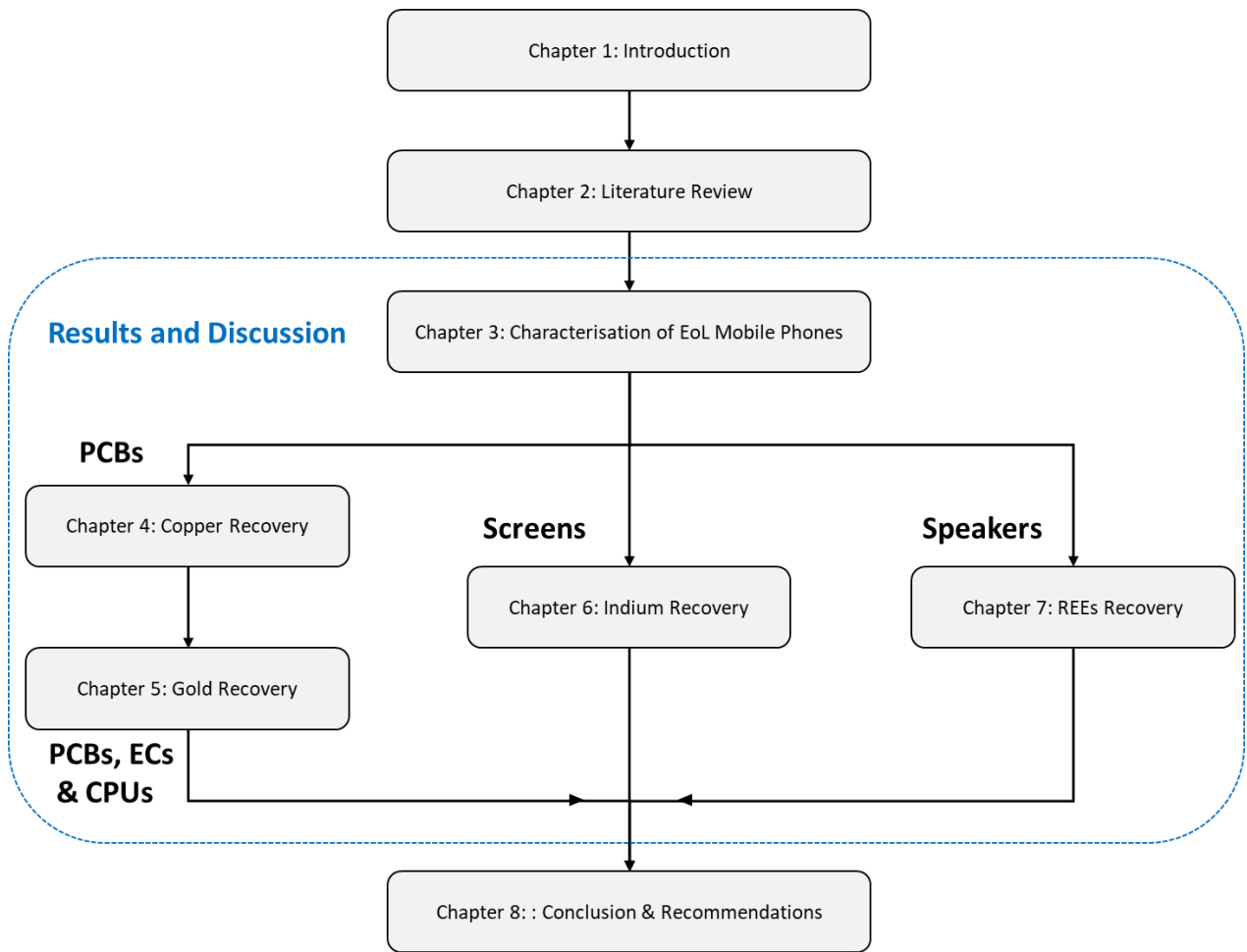


Figure 1.1: Schematic diagram of the thesis structure and relationship between the sections of work performed.

2 Literature Review

A review of the literature presented in this chapter discusses key aspects of relevance to the research presented in this thesis providing an overview of WEEE, its classifications, global trends, its composition, and a brief discussion on end-of-life mobile phones. A summary of the policies and legislative instruments guiding waste management (and related to WEEE) follows. The importance of securing critical raw materials embedded in electronic products, to set the context of the current research is emphasised before describing the methods used for recovery of metals, and the potential for exploiting the unique properties of ionic liquids as extractants is described. At the start of each research chapter there is a literature review to serve as background of relevance to the target metal under study.

2.1 An overview of Waste Electrical and Electronic Equipment

The rapid development and advancement in material science, manufacturing, efficiency processes, among other technologies have created global markets with fast diffusion of technology to consumers. In addition, advancements in information and telecommunication technologies have facilitated the consumption of these technologies globally, making possible the development of novel markets for new products at scales larger than ever seen before. Proliferation of products, distribution to global markets, and market penetration combined with cheaper prices and affordability have generated an escalation of disposable products, creating enormous environmental challenges for managing these streams of waste. This has been also intensified during the last 50 years, where the world population has doubled, and now at approximately 7.8 billion people in 2021. As a result of increasing population, growing urbanization, increasing life expectancy, and economic development over the last decades, the demand for electrical and electronic equipment (EEE) such as mobile phones, computers, TV-sets, sound systems, refrigerators, printers, radios, washing machines, etc. has escalated drastically [8, 29]. The global estimation market of EEE has risen from 19.5 million tons (Mt) in 1990 to 76.1 Mt in 2015 [1, 3], with an average annual growth of 2.5 Mt [5], estimating that approximately 113.6 Mt of EEE will be produced in 2030. This increase in EEE production and consumption generates, at their end-of-life, enormous amounts of waste electrical and electronic equipment (WEEE), which is used interchangeably with the term '*e-waste*', although '*e*' stands for electronic and does not cover electrical; the term, WEEE, however, is mostly used in the UK and Europe. The European Union (EU) classified WEEE in the first WEEE Directive (2002/96/EC) [30] into ten categories and in the later Directive (2012/96/EC) [31], reclassified them to six categories which is a broader classification and is more globally adopted in other countries [32]. The United Nation

University (UNU) further divides EEE into 54 different product-centric categories, using different factors including size and weight, functionality and composition, and refers to this categorisation as the UNU-KEYS, (aligning these to the six EU categories), as reported by Forti et al. [5]. Table 2.1 sets out the WEEE classification defined by the EU under the WEEE Directive (2012/96/EC), a list of six categories which replaced the previous ten. The new six category of WEEE classification became effective on 15 August 2018 [15].

Table 2.1: Classification of WEEE according to the European WEEE Directive (2012/19/EC) [31].

No.	Category	Examples
1	Temperature exchange equipment	Refrigerators, freezers, air conditioning equipment, radiators
2	Screens, monitors, and equipment containing screens having a surface greater than 100 cm ²	Screens, televisions, LCD photo frames, monitors, laptops, notebooks
3	Lamps	Fluorescent lamps, LED lamps, high intensity discharge lamps
4	Large equipment (any external dimension more than 50 cm)	Washing machines, clothes dryers, dish washing machines, cookers, electric stoves
5	Small equipment (no external dimension more than 50 cm)	Vacuum cleaners, luminaires, microwaves, irons, toasters, electric knives, electric kettles
6	Small IT and telecommunication equipment (no external dimension more than 50 cm)	Mobile phones, telephones, GPS, pocket calculators, routers, printers, personal computers

2.1.1 Global WEEE generation and trends

The global WEEE generation has increased rapidly in the last decades, as a consequence of the considerable higher consumption rates of EEE, short life cycles, and few repair options, from 37.3 Mt in 2012 to 50 Mt in 2018 [8, 33], and it was projected to reach 74.7 Mt by 2030 [5], which is an increase of over 50% in less than 20 years. Furthermore, WEEE is the fastest growing solid waste stream throughout the world with an annual growth rate of 3- 5% [7, 19, 34]. An overview of EEE put on the market, WEEE generation, and their estimation in 2020 of some representative low and high-income countries is presented in Table 2.2. It can be observed that the considerable increase in WEEE generation is particularly prevalent in countries with high-income economies, in which EEE markets are saturated. In fact, it has been shown that there is a strong correlation between the gross domestic product (GDP) and WEEE generation, where the economic development of a country is proportional to the amount of WEEE generated per person [13].

Table 2.2: Global growth of EEE and WEEE [9].

Country	EEE put on market in 2012 (Mt)	Estimated WEEE in 2013 (Mt)	Estimated WEEE in 2020 (Mt)	Increase between 2013 and 2020
EU-28	9,800	10,205	11,430	12%
United States	9,350	9,359	10,050	7%
China	12,405	6,033	12,066	98%
Japan	3,300	3,022	3,200	5%
India	3,026	2,751	6,755	145%
Germany	1,752	1,696	1,974	16%
Russia	1,599	1,556	2,000	28%
Brazil	1,850	1,530	1,850	20%
France	1,520	1,224	1,625	32%
Italy	1,124	1,154	1,343	16%
Korea	959	961.3	1,050	9%
Turkey	726	661	800	21%
Netherlands	432	394	421	6%
Romania	217	157	227	44%
Norway	175	127	136	7%

Figure 2.1 shows the WEEE generated by continent in 2019, where Asia generated the highest quantity of WEEE with 24.9 Mt, followed by Americas (13.1 Mt), Europe (12 Mt), Africa (2.9 Mt) and Oceania (0.7 Mt). In terms of WEEE- generated per capita (Figure 2.1b), Europe ranked first with 16.2 Kg per capita, closely followed by Oceania with 16.1 Kg per capita. The Americas, Asia and Africa generated 13.3, 5.6, and 2.5 kg per capita, respectively [5]. A summary of global generation figures per country in 2019 is presented in Figure 2.2. From the list of countries presented, United Kingdom was the country with the highest generation of WEEE per capita in 2019 with 23.9 kg, followed by Switzerland, Australia, U.S.A., and Japan with 23.4 kg, 21.7 kg, 21.0 kg, and 20.4 kg, respectively. The countries with the highest WEEE generation per capita are mostly high-income countries, confirming that the increase in WEEE generation is particularly prevalent in countries with developed economies. WEEE in developed countries makes up to 8% of the municipal waste by weight, with an increasing trend [35]. It is acknowledged that WEEE generation estimates are difficult to determine on a global level as estimates can vary markedly due to the information available from region to region and the diversity of methods used to quantify the volumes generated. Nevertheless, there is a clear and undeniable upward trend in WEEE generation through the years, with a marked increase in the last decades.

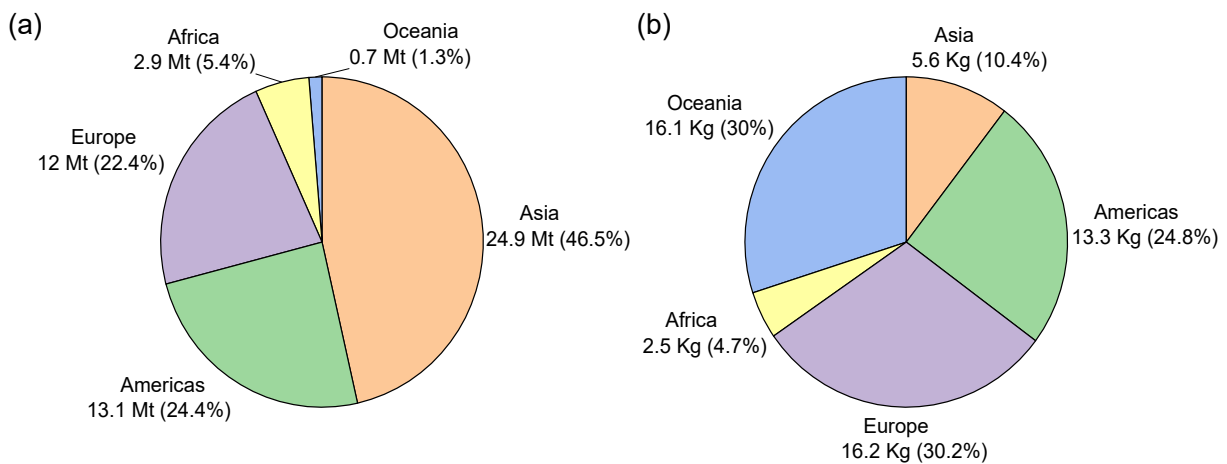


Figure 2.1: WEEE generated in 2019; (a) per continent, and (b) per capita. Data obtained from the UNU [5].

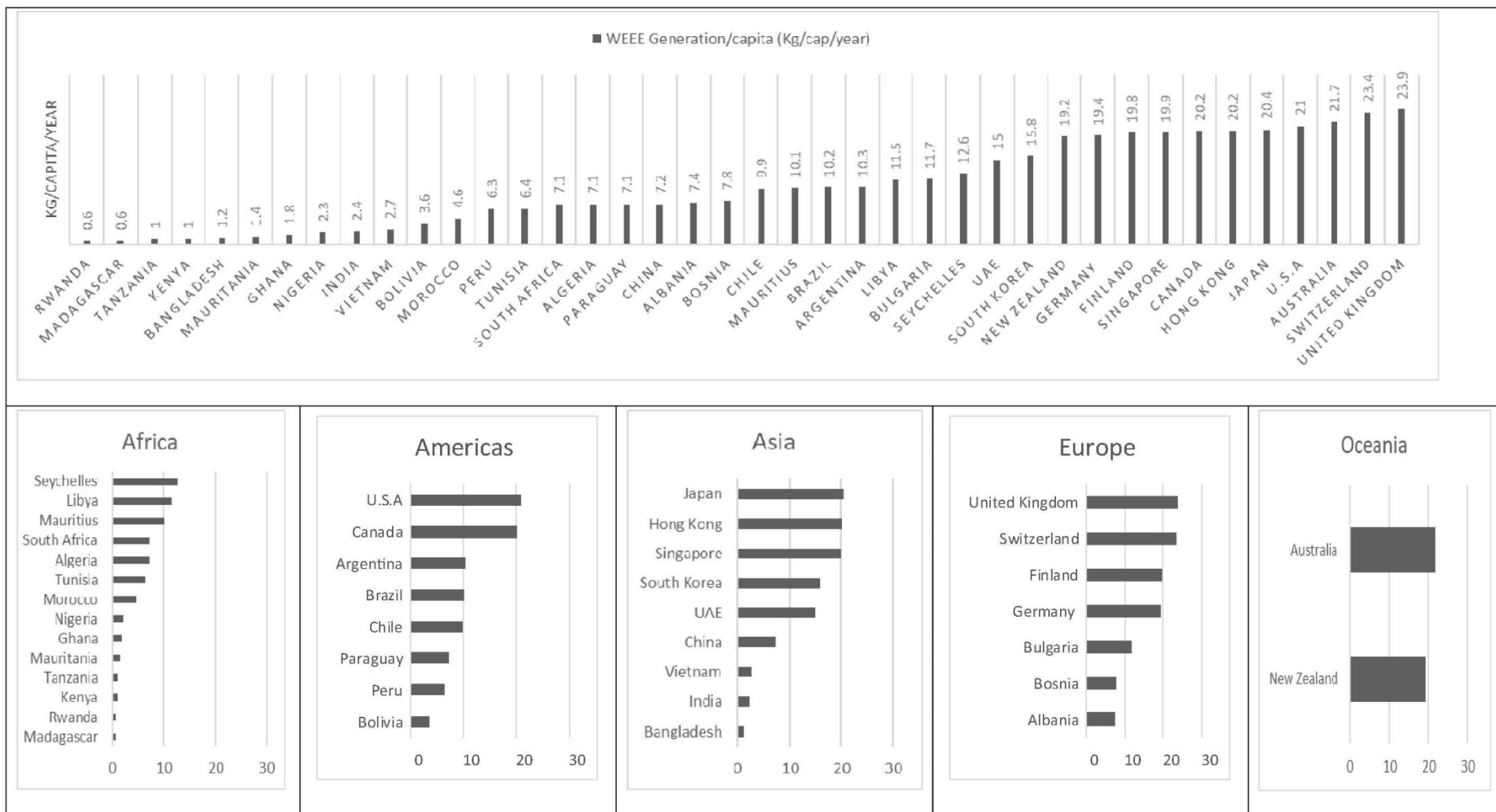


Figure 2.2: Summary of global WEEE generation in 2019 (kg/person/year) [32].

2.1.2 An overview of End-of-Life (EoL) mobile phones

Alexander Graham Bell invented the telephone in 1876 which for first time enabled voice transmission, and from this point developments in telephony led to radio links in handheld radio transceivers during the World War II, and with mobile telephony pioneered by Bell Labs in the late 1940s deployed in phones installed in cars and other vehicles. In 1973 Dr Martin Cooper, a former general manager for the systems division at Motorola, developed the first handheld mobile phone, with advances in mobile telephony, permitting both voice and data transmission, since then progressing through successive generations from 0G to 5G in 2019. DynaTAC 8000x was the first commercially available cellular phone small enough to be easily carried, manufactured by Motorola Inc. This handset with dimensions of 33 x 4.45 x 8.9 cm weighed 0.8 kg, a full charge took roughly 10 hours, and it offered 30 minutes of talk time. Before the DynaTAC 8000x, mobile phones were so large and heavy, usually more than 4 kg, that were usually installed in vehicles [36].

Nowadays, a typical mobile phone weighs approximately 150 grams, is presented in a range of dimensions (depending on its use) and style in response to consumer preferences. The phone is powered by a small battery that can last several hours and can be charged in 2-3 hours [36, 37]. The lifespan of a mobile phone has been drastically reduced from an average of 5 years in the nineties to less than 2-3 years, mostly because of the fast evolution of technology supported by marketing and promotion campaigns [37, 38]. In high-income countries, the lifetime of mobile phones is even shorter. A Statista survey conducted in the United Kingdom in 2017 on mobile phones showed that 36% of mobile phone owners use them for 1-2 years, whereas 27% only use them for 6-12 months, and 19% for less than 6 months. In addition, in the UK, there was a forecast that 16% of households owned a mobile phone in 1996 and in 2017 this percentage increased significantly to 95%. The same survey conducted in the United States showed similar results; 30% of respondents said that they use a mobile phone for 1-2 years, 30% use them for 6-12 months and 19% for less than 6 months [39]. In China, which is the largest producer of mobile phones accounting for about 86% of the global production in 2014, show the lifespans of mobile phones to be 10% less than 1 year, 40% less than 2 years, 30% between 2-3 years and 20% more than 3 years [38]. Therefore, at least 50% of the mobile phone owners use them for less than 2 years, despite the technical lifespan of a mobile phone being almost 10 years [40]. Furthermore, the majority of mobile phone users reject refurbished handset phones mostly as a consequence of a negative trade-off between perceived risks and benefits [41]. It is important to note that as the mobile phone's lifetime is being reduced, this model of consumption creates an unnecessary carbon footprint and hazardous waste, contributing to environmental pollution and global warming as well as the loss of valuable resources. The number of subscriptions of

mobile phones has drastically increased from 34 million in the year 1993 to more than 8 billion worldwide in 2019, as shown in Figure 2.3; a figure reported in 2021 to have reached 8.6 billion [39], which is close to the prediction made by the International Telecommunication Union’s (ITU) in 2015 in estimating that there would be more than 9 billion mobile phone subscriptions globally by the end of 2020, with a population-wise penetration rate of 97% [37]. Statistics on the number of mobile phone users in the world were estimated to exceed 5 billion in 2019. In China and India, alone the value was reported to have reached approximately 1.5 and 1.1 billion mobile connections in 2019, respectively, leading the mobile phone users [39].

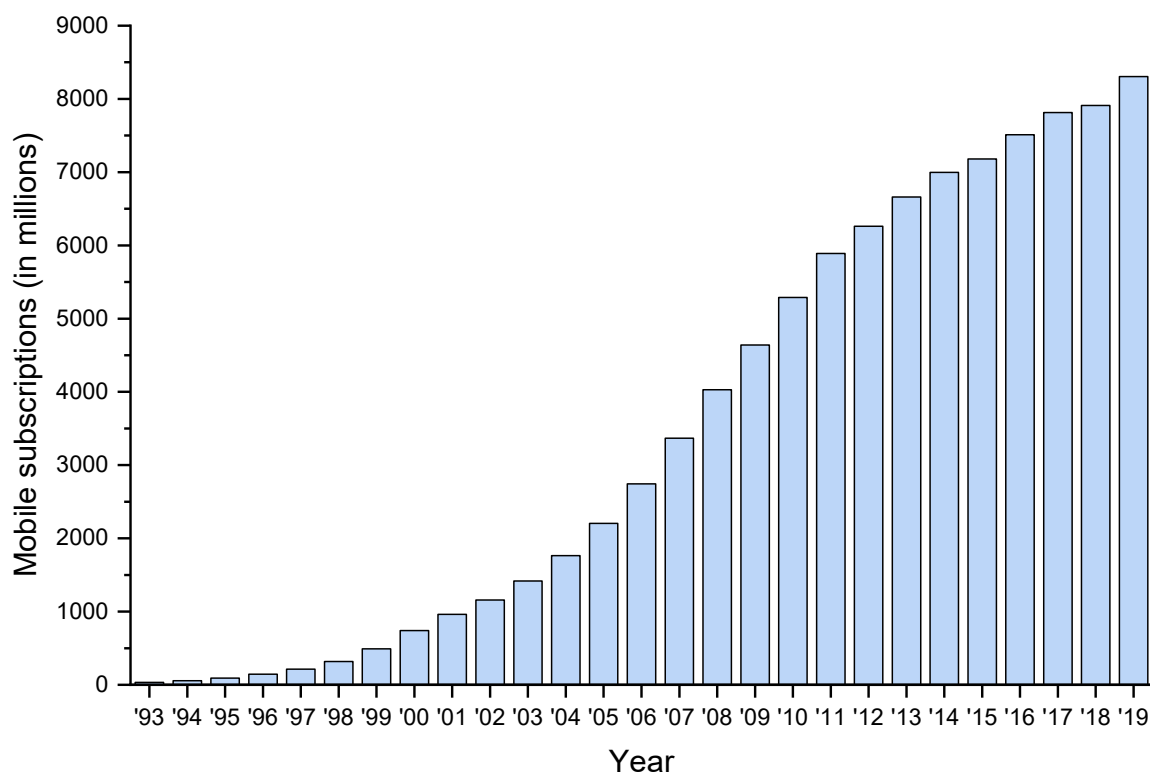


Figure 2.3: Number of mobile subscriptions worldwide from 1993 to 2017 (in millions). Data obtained from Statista.

Despite the benefits of mobile phones enabling communication with family, friends, and business, they also have environmental impacts associated with their use. The production of new mobile phones contributes to climate change by using large amount of virgin materials and energy in their processes, consequently releasing greenhouse gases into the atmosphere. The United Nations Environment Programme (UNEP) estimated that the manufacture of a mobile phone produces about 60 kg of CO_{2e} and that using a mobile phone for a year produces about 122 kg of CO_{2e} on average. The

use of a mobile phone includes base station, administration, transport, etc. [42]. While the carbon footprint of a mobile phone use is largely determined by the extent of use, a year's typical usage of just under 2 minutes per day has a greenhouse gas emission of 47 kg of CO_{2e}, while a year's usage at 1 hour per day is equivalent to 1,250 kg of CO_{2e}. This is due to the high-energy consumption of calls with an average of 0.5 kWh, which is even higher than the consumption of a washing machine (0.43 kWh) [41, 43]. The effect of mobile phones CO_{2e} emissions was estimated to reach 55 million metric tons in 2020 [41].

In terms of energy consumption, it was determined that over a mobile phone life cycle, manufacturing accounts for approximately 50% of the total energy consumption with an overall estimation of 175 MJ/unit. The manufacturing process can be separated in four steps: raw material extraction and processing, component manufacturing, mobile phone assembly, and packaging and transportation. The high demand of energy in the manufacturing process of mobile phones is mostly due to the component manufacturing (120 MJ), following by packaging and transportation (30 MJ), and raw material extraction and processing (23 MJ). Figure 2.4 provides an estimate of the total energy consumption of a mobile phone cycle, where usage (64.8 MJ) and network (66 MJ) represent approximately 37% of the total energy consumption of a mobile phone's life cycle [44]. Both usage and network are based in a lifetime of 2 years. The growth and development of the mobile phone market and network has led to an increase in the demand for energy, with an inevitable impact on the environment.

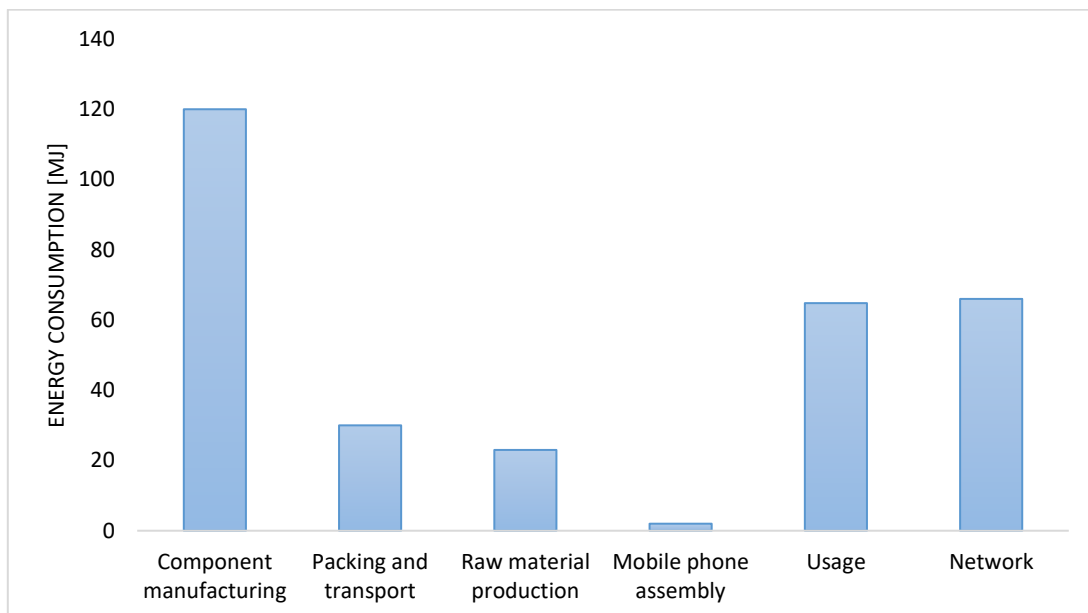


Figure 2.4: Energy consumption of mobile phones during their life cycle [44].

2.1.3 Composition of WEEE

WEEE is a complex and heterogeneous mix of material, and its composition depends largely on the type, manufacturer, and age of the equipment, which can contain many organic and inorganic substances [7, 13]. The major mass fractions are bulk metals (aluminium, copper and ferrous) and plastics (polyethylene, polypropylene, polyesters, and polycarbonates). Table 2.3 presents the material composition for each of the 10 categories of WEEE. Although the categories of WEEE have been refined from 10 to 6 effective 15th August 2018, some equipment is split across one or more of these new categories. To account for the inexact representation of equipment therefore across the categories the most complete characterization of WEEE is that obtained across all 10 categories. The category “11” reported in the table was defined by the authors as detached components, single parts and products which could not fit into the other 10 listed categories [45]. Plastics account for nearly 40% of the total weight of the WEEE, followed by electronic components and ferrous metals with 26 %w/w and 16 %w/w, respectively. This WEEE composition is only a representation since the composition of WEEE can vary due to the category of WEEE, the production year, the producers, the laws at the time of production, among other factors.

Table 2.3: Material composition for each category of the WEEE (% w/w) [45].

Material fraction	EEE Category											
	1	2	3	4	5	6	7	8	9	10	“11”	Average
Ferrous metals	51.60	8.99	25.27	12.04	10.40	13.32	2.50	7.42	0.27	–	27.92	15.97
Non-ferrous metals	2.89	8.22	0.09	1.08	–	2.69	0.23	8.12	–	–	0.70	3.01
Plastics	9.85	40.70	27.49	28.17	24.19	9.18	83.60	29.27	76.62	69.48	34.26	39.35
Rubber	0.05	0.69	0.79	0.54	–	0.21	1.12	3.25	0.22	–	0.43	0.81
Cables	3.00	7.55	3.34	2.80	0.77	7.02	2.26	–	0.46	8.50	6.54	4.22
PWBs*	0.08	0.52	10.17	6.77	–	0.92	3.84	–	22.44	4.33	0.72	5.53
Electronic components	28.16	18.41	4.45	38.48	64.64	66.11	3.92	20.09	–	1.48	13.78	25.95
“Bonded” materials	4.35	11.77	11.09	5.28	–	0.53	0.004	–	–	15.32	7.29	6.95
Various	–	2.53	14.03	3.00	–	0.04	1.91	31.84	–	–	3.33	8.10
Batteries	–	0.49	2.63	1.74	–	–	0.53	–	–	0.33	5.04	1.79
LCDs	–	0.12	0.64	0.08	–	–	0.09	–	–	0.56	–	0.30

* : PWBs stands for printed wiring boards, which in this research printed board circuits (PCBs) is used.

The most valuable component of WEEE is found in the metals fraction, especially in the non-ferrous fraction. A simple individual item may contain up to 60 elements including trace amounts of strategically/economically important materials such as rare earth elements (REEs), indium, precious metals (rhenium, ruthenium, rhodium, iridium, osmium, palladium, gold, and silver), among others [7, 19]. As the focus of the research described in this thesis is on IT and telecommunication equipment, category 3 in the old classification and category 6 in the new WEEE category, Table 2.4 lists the metal content of printed circuit boards of mobile phones and computers. Printed circuit boards (PCBs) are boards that are used as the base in most electronics, which act as a physical support piece and as the wiring area for the surface, where components are mounted and socketed. PCBs are essential for all the IT and telecommunication equipment, and it is here that most of the metal value is found. Table 2.4 shows that the most abundant metal is copper with a range of 29-49 %w/w, followed by the precious metals. In the literature, it has been reported that the content of metals in PCBs is much higher than that in their natural ores, with PCBs being at least 10 times richer in metals [12, 20-22].

Table 2.4: Metal concentration in PCBs of mobile phones and computers.

	D. fontana et al., 2019 ¹ [46]	M.C.Vats & S.K.Singh, 2015 ² [22]	Angela C. Kasper et al., 2011 ¹ [47]	William Hall J. and Paul Williams, 2008 ¹ [48]	Y. JunPark & D. J.Fray, 2008 ² [49]	Anjan Kumari et al., 2015 ² [50]	Jessica Hanafi et al., 2012 ¹ [51]		
Metals/Units	% w/w	% w/w	Brand A % w/w	Brand B % w/w	<600 µm mg/kg	>600 µm mg/kg	% w/w	% w/w	% w/w
Copper	57.47	49.0	39.56	38.33	323,163	333,228	16.0	39.85	29.39
Silver	0.15	1.5	0.06	0.06	4,125	8,118	0.1	-	-
Gold	0.12	0.1	0.06	0.1	28	18	0.03	-	-
Aluminium	0.77	5.5	0.31	0.99	18,333	14,949	5.0	-	40.85
Iron	25.23	11.6	1.42	6.53	5,366	15,089	-	2.58	-
Zinc	4.29	21.8	3.43	0.97	960	1,011	1.0	3.27	-
Nickel	5.10	6.5	3.42	1.67	6,870	13,454	1.0	0.22	-
Lead	0.85	1.9	1.17	1.26	2,495	1,405	2.0	0.05	-
Tin	3.49	1.7	2.09	3.11	-	-	3.0	-	3.99
Indium	-	-	-	-	<5.6	<5.6	-	-	-
Palladium	-	Trace	-	-	<5.6	<5.6	0.01	-	-
Others metals	0.08	-	-	-	-	-	-	-	-

1: Concentration in PCB of mobile phones.

2: Concentration in PCB of computers.

2.1.4 Hazardous substances in WEEE

WEEE contains many hazardous substances, including heavy metals such as mercury, cadmium, lead, among others, flame-retardants (e.g., pentabromophenol, polybrominated diphenyl ethers (PBDEs), tetrabromobisphenol-A (TBBPA), etc.) and other toxic substances. Due to the presence of these substances, WEEE is generally considered as a hazardous waste, which, if improperly managed, may pose significant human health and environmental risks [6-8]. The environmental risks associated with WEEE include pollution of the ground, acidification of soils, generation of toxic fume and gases after burning, fast accumulation in municipal disposal areas, liberation of carcinogenic substances into the air, etc. [6, 12]. Open dumping is the most common form of WEEE disposal in the most developing countries. Burial or landfill disposal allows heavy metals to be leached into the ground water or methane off-gassing. Combustion of organic substances in e-waste by incineration makes hazardous material airborne, generates ashes and heat. Leaching of the ashes may cause water and soil contamination. In addition, WEEE accounts for 40% of lead and 70% of heavy metals in landfills [6, 12, 52]. Table 2.5 lists some hazardous substances present in WEEE along with their possible adverse effects to the human health.

Table 2.5: Hazardous substances in WEEE [12].

Substances	Occurrence in WEEE	Possible adverse effects
Lead (Pb)	CRT screens, batteries, printed circuit boards (PCBs)	Vomiting, diarrhoea, convulsions, coma or even death, appetite loss, abdominal pain, constipation, fatigue, sleeplessness, irritability and headache
Mercury (Hg)	Fluorescent lamps, some alkaline batteries, switches	Brain and liver damage
Chromium VI (Cr ⁶)	Data tapes, floppy-discs	Irritating to eyes, skin and mucous membranes, damages on DNA
Barium (Ba)	Getters in CRT	Brain swelling, muscle weakness, damage to the heart, liver and spleen
Cadmium (Cd)	NiCd batteries, fluorescent layer (CRT screens), printer inks and toners	Symptoms of poisoning (weakness, fever, headache, chills, sweating and muscle pain), lung cancer and kidney damage
Arsenic (As)	Gallium arsenide in light emitting diodes (LED)	Skin diseases, decrease nerve conduction velocity, lung cancer
Americium (Am)	Smoke detectors	Radioactive element
Antimony (Sb)	Flame retardants in plastics	Carcinogenic potential
Chlorofluorocarbon (CFC)	Cooling units, insulation foams	Deleterious effect on the ozone layer, increased incidence of skin cancer and/or genetic damages
Polychlorinated biphenyls (PCB)	Condensers, transformers	Cancer, effects on the immune systems, reproductive system, nervous system, endocrine system and other health effects
PBDEs, PBBs	Flame retardants in plastics	Hormonal effects, under thermal treatment possible formation of dioxins and furans

2.2 Circular Economy, Policies, and Legislation in the Context of WEEE Management

The current socioeconomic system is based on the fundamental characterisation established in the early days of industrialisation: a linear model of resource consumption that follows a *'take-make-dispose'* pattern. Under this concept, material flow in this process is understood as the conceptual logic of value creation in which only virgin material enters at the beginning of the value chain. This linear production model incurs unnecessary resource losses in several ways: raw material, production chain, end-of-life (EoL) waste, excessive energy use, erosion of ecosystems, among other [53, 54]. By contrast, a *'circular economy'* (CE) aims to create a closed loop system where resources are conserved and brought back into the life cycle after being used [53, 55]. CE is concept that has many different definitions across academia, international organisations, businesses and non-government bodies, with the most cited definition of CE in the literature being that provided by Charonis, in line with the Ellen Macarthur Foundation vision, as *"an industrial system that is restorative or regenerative by intention and design"* [56]. The concept and strategies to promote a CE are not new; the concept was first mentioned in 1972, in the book *"The Limits to Growth"*, where the fundamental aspect of industrial ecology principles were developed [57]. The CE system brings the idea of restoration and circularity in order to replace the traditional concept of EoL, shifting towards the use of renewable energy, eliminating the use of toxic substances, and aims for the elimination of waste through a superior design of material, products, systems and business models [53]. The linear and circular economies are illustrated in Figure 2.5. The CE is based in three principles: *designing out of waste*, where products are designed and optimised for a cycle of disassembly and reuse; therefore, waste as a concept does not exist; *building resilience through diversity*, where modularity, versatility, and adaptivity need to be prioritised, aspects inspired by natural ecosystems as models; and *use of renewable energy* to decrease resource dependence and increase system resilience [3, 53, 58]. Another interesting point in the CE is the introduction of the differentiation between the terms, *consumable* and *durable*. Consumables in CE are made of biological ingredients or nutrients that are non-toxic, which can be returned to the biosphere, while durables are made of technical nutrients unsuitable for the biosphere, such as metals and most plastics [53]. The focus of the research presented in this thesis is on the recovery of materials from EoL mobile phones, which aligns with the principles of circular economy.

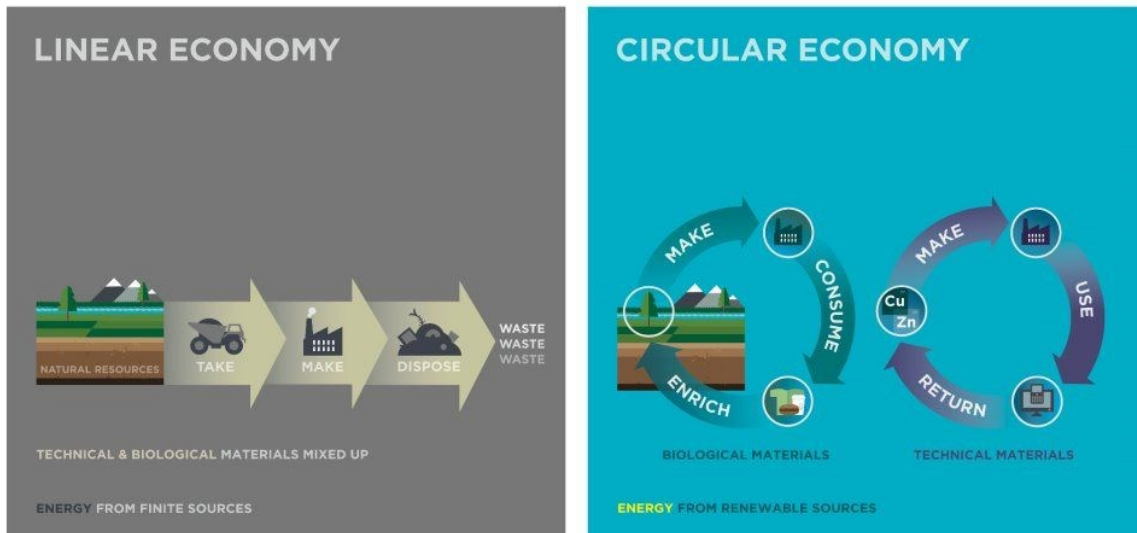


Figure 2.5: Linear economy vs circular economy. Diagram obtained from the Ellen MacArthur foundation.

It has been estimated that eco-design, waste prevention and reuse can bring net savings to EU businesses of up to €600 billion, while at the same time reduce greenhouse gas emissions. Moreover, the additional measures to increase resource productivity by 30% by 2030 could boost the GDP by nearly 1% and create 2 million additional jobs within the EU countries. In the UK, it has been estimated that a circular economy could help generate 50,000 new jobs and €12 billion of investment [59]. McKinsey’s study ‘*Growth within: A circular economy vision for a competitive Europe*’ concurs with this view that adopting circular economy principles could not only benefit Europe environmentally and socially but could also generate a net economic benefit of £1.8 trillion by 2030, a figure which would translate into a GDP increase of as much as seven percentage points [60].

Since prices and volatility are likely remaining high as populations grow and urbanise, resource extraction challenges move to harder-to-reach locations, and the environmental costs associated with the depletion of natural capital increase. In fact, humanity now consumes more than the productivity of Earth’s ecosystems can provide sustainably, and is thus reducing the Earth’s natural capital, not just living off of its productivity [53]. Due to this, the European Union has designated resource-efficiency as one of the flagships of its Europe 2020 strategy [61], and it has implemented legislation and policies to incorporate a CE. Within the UK, with its recent exit from Europe, although much of the European legislation is retained, the UK has introduced a Circular Economy Package policy in July 2020 [62] and more recently in the new Environment Act 2021 embraces the concept of transition to a more circular economy [63]. Germany showed an early interest in CE initiatives; for instance, its “*Closed Substance Cycle and Waste Management Act*” of 1996, which tried to ensure environmentally friendly schemes

of waste disposal. Other countries such as Japan, created and the Basic Law for Establishing the Recycling based Society of 2000 [56]. Australia has regulations that cover WEEE management; the National Waste Policy; Product Stewardship Act, Product Stewardship (for TVs and computers) regulations, and the National Television and Computer Recycling Scheme. Chile introduced a WEEE-specific law in 2016 which provides a legal framework for WEEE management via extended producer responsibility [32]. Several other countries have also been developing WEEE management strategies [13, 32, 56, 64, 65]. Given Europe's role in setting policy and legislative frameworks that underpin the protection of resources and the relevance of these instruments core to the research presented in this thesis, these are now briefly described.

2.2.1 Policies on waste management in Europe and the UK

The majority of legislation covering the control and management of waste, not just WEEE, flows from the European Union (EU), where legislation and policies are then implemented through domestic law in each EU member state [66]. The first environmental policy in the EU (previously known as the European Community) appeared in 1973 which developed and shaped environmental legislation was provided by the first of what was to become a suite of Environmental Action Programmes (EAPs) [58, 66]. This programme set out the principles and priorities that would inform future policy and is based on 11 principles. Since 1973, there have been 8 programmes of work to date and the current programme, EAP8, has been recently adopted in 2021. Among the EAPs, EAP5 titled *'Towards sustainability'* in 1993, began to set long-term objectives and the concept of sustainable development and management of waste were introduced [67]. The seventh Environmental Action Programme, entitled *'Living well, within the limits of our planet'* was adopted by the European Parliament and the Council of the European Union on 20 of November 2013. This programme was intended to help guide EU action on the environment and climate change with a vision of the long-term period towards 2050: *'In 2050, we live well, within the planet's ecological limits. Our prosperity and healthy environment stem from an innovative, circular economy where nothing is wasted and where natural resources are managed sustainably, and biodiversity is protected, valued, and restored in ways that enhance our society's resilience. Our low-carbon growth has long been decoupled from resource use, setting the pace for a safe and sustainable global society'* [68]. The current EAP8, titled *'Turning the Trends Together'* calls for active engagement of all stakeholders at all levels of governance, to ensure that EU climate and environment laws are effectively implemented, reiterating the commitment to the 7th EAP's 2050 vision. This 8th EAP will guide the European environmental policy until 2030. It is important to note that the recommendations of the EAPs are not legally binding, however, they do clearly set out the aspirations of the EU members.

The Waste Framework Directive (WFD) was introduced in 1975 (Directive 75/442/EEC), following the creation of the first EAP. The focus of the Directive's provisions at that stage was on ensuring the safe disposal of waste, and set out a waste management hierarchy with the well-known '3Rs: Reduce, Reuse and Recycling' [66, 69]. This hierarchy is the core of sustainable waste management and has thus been embedded into legislation. The WFD was the subject of substantial amendment in 1991 (Directive 91/156/EEC) [70]. One of the major changes made was to extend the scope of the WFD's objectives and controls from waste disposal to also cover waste recovery – with 'recovery' including recycling, re-use of waste, reclamation, and the use of waste as a source of energy. In addition, the definition of waste was formalised since the original WFD enabled member states to adopt their own national definitions of waste. The next major overhaul of the waste framework directives came in 2008, a new WFD was made (Directive 2008/98/EC) [71] and entered into force on 12 December 2008. This directive reenacted the definition of waste as "*any substance or object which the holder discards or intends or is required to discard*", which remains as the official definition of waste [69].

The WFD 2008 defines the waste management hierarchy which is a set of preferred options for the treatment and handling of waste. The hierarchy as set out in Article 4 of the revised waste framework by the European Commission (Directive 2008/98/EC) [71]. This hierarchy ranks waste management options according to what is best for the environment and it introduces an approach that takes into account the whole life cycle of products and materials and not only the waste phase [12]. Source reduction which seeks to prevent and conserve scarce resources, also includes using less material in design and manufacture and fewer hazardous materials. Reuse supports keeping products in use for longer by checking, cleaning, repairing, and refurbishing whole items or spare parts. Recycling turns the 'waste' material or product at end-of-life into a new substance or product and includes composting if it meets quality protocols. These three actions of reduction, reuse and recycling are the most favoured options and are on top of the waste hierarchy pyramid. Resource recovery includes anaerobic digestion, incineration with energy recovery, gasification and pyrolysis which produce energy (fuels, heat and power), and materials from waste. Incineration without energy recovery followed by landfill, which does not conserve resources, rank lowest in the waste hierarchy, and are viewed as the least favoured options in the waste management pyramid, and they should be avoided.

Within the hierarchy, the priority is given to waste prevention and to promote waste as a secondary resource to deliver best available environmental outcomes. In addition, the Directive introduces the '*polluter pays principle (PPP)*' and the '*extended producer responsibility (EPR)*' [66]. The polluter pays principle is the commonly accepted practice that those who produce pollution should

bear the costs of managing it to prevent damage to human health or the environment. This principle underpins most of the regulation of pollution affecting land, water, and air. Pollution is defined in the UK law as contamination of the land, water, or air by harmful or potentially harmful substances. The EPR principle was implemented by the European Union regarding the treatment of WEEE in 2001 by focusing on the extending producer responsibility beyond the use stage of the products and it is based on the polluter pays principle. The organization for economic co-operation and development (OECD) defines the extended producer responsibility principle as *'a policy approach under which producers are given a significant responsibility – financial and/or physical – for the treatment or disposal of post-consumer products. Assigning such responsibility could in principle provide incentives to prevent wastes at the source, promote product design for the environment and support the achievement of public recycling and materials management goals'* [72]. According to the OECD, the four principal goals of EPR are source reduction (natural resource conservation/materials conservation), waste prevention, design of more environmentally compatible products, and closure of material loops to promote sustainable development. The EPR promotes eco-design of products such as ease of disassembly, lead free product, design for reuse and design for cost effective recycling. The European Commission through a series of circular economy action plans with the first in 2015, adopted an ambitious circular economy package (CEP), which includes revised legislative proposals on waste to stimulate Europe's transition towards a circular economy that will boost global competitiveness, foster sustainable economic growth, and generate new jobs [53, 59].

2.2.2 WEEE and RoHS Directives

The increase of WEEE and its potential risks to the environment and human health has led to the introduction of two pieces of legislation, namely: The Directive on Waste Electrical and Electronic Equipment (WEEE Directive) and the Directive on the Restriction of the Use of certain Hazardous Substances in EEE (RoHS Directive). The first WEEE Directive (Directive 2002/96/EC) entered into force in February 2003 [73]. The Directive set firm targets for the collection, reuse, recycling of WEEE, and with a recovery of a minimum rate of 4 kilograms per head of population per annum recovered for recycling by 2009. The collection, treatment, recovery, and disposal of WEEE, which households have taken back to the collection, have to be financed by the producers and do not have to be shared with the purchasers (this applied to all products put on market after August 2005).

The WEEE Directive defines WEEE as: *'any electrical or electronic equipment, designed for use with a voltage rating not exceeding 1000 Volt for alternating current and 1500 Volt for direct current, which is waste, including all components, subassemblies and consumables which are part of the*

product at the time of discarding' [73]. In addition, it categorised the electrical and electronic equipment in 10 categories, categories which applied from 2012 to 2018; this categorization was replaced by a list of 6 categories on 15th August of 2018 [15], and the current list is shown in Table 2.1.

The WEEE Directive (Directive 2002/96/EC) also requires that the rate of recovery shall be increased to a minimum of 70% by an average weight per appliance. In addition, component, material and substance reuse and recycling shall be increased to a minimum of 50 % by an average weight per appliance by 31st December 2006 (for the categories 1, 3, 4 and 10 these percentages are higher). Despite member states being required to implement the WEEE Directive by August 2004, only Greece and the Netherlands were positioned to do so. It took until the start of 2008 for all member states to implement the directive. Magalini and Huisman attributed the differences in timing for the member states to implement the directive to the differences in the pre-existing infrastructure, technology, and the complexity of the legislation itself as well as financing issues [74]. In December 2008, the European Commission proposed to revise the Directive to tackle technical, legal, and administrative problems as well as to address the concerns relating to the rapid increase in growth of the WEEE stream. The new WEEE Directive (2012/19/EU) [15] entered into force on 13th August 2012 and became effective on 14th February 2014. The key elements of the WEEE Directive were set as follows (from 15th August 2018)[14, 15]:

- New elements in EEE were included; photovoltaic panels, equipment containing ozone-depleting substances and fluorescent lamps containing mercury.
- A collection target of 45% of electronic equipment sold that applied from 2016 and, as a second step from 2019, a target of 65% of equipment sold, or 85% of WEEE generated.
- The new collection targets agreed should ensure that around 10 million tonnes or roughly 20 kg per capita, should be separately collected from 2019 onwards.
- Consumers should be allowed to return, for free, any electrical good, without needing to buy a new product. Furthermore, it was required retail shops with an EEE sales area of at least 400 m² to offer free take-back of very small WEEE.
- Producers continued to contribute towards the financial costs of meeting processing targets.
- Tighter controls on illegal shipments of WEEE to prevent it from being processed in countries where practice is less rigorous than set out by the EU.

The Restriction of Hazardous Substances (RoHS Directive 2002/95/EC) is a companion legislative instrument to the WEEE Directive [75]. The objectives of this Directive are to protect human/animal health and ensure the environmentally sound recovery and disposal of WEEE. This legislation restricting the use of hazardous substances in EEE entered into force in February 2003. The

legislation requires heavy metals such as lead, mercury, cadmium, and hexavalent chromium and flame retardants such as polybrominated biphenyls (PBB), polybrominated diphenyl ethers (PBDE), among others to be substituted by safer alternatives. In December 2008, the European Commission proposed to revise the Directive at the same time as the WEEE Directive to promote harmonized and coherent legislation [14]. The RoHS recast Directive (2011/65/EU) [76] became effective on 3rd January 2013. It addresses the same substances as the original Directive (2002/95/EC) while improving regulatory conditions and legal clarity, with periodic re-evaluations that facilitate gradual broadening of its requirements to cover additional electronic and electrical equipment, cables, and spare parts. Similar to the WEEE Directive, this Directive has had a history of amendments and was recast by the EU (Directive (EU) 2015/863) as part of its overall commitment for a better regulatory environment [77]. In this recast, four new restricted substances were included (which have been restricted from 22nd July 2019). Table 2.6 lists the ten hazardous substances restricted in EEEs under the current EU Directive 2011/65/EU.

Table 2.6: Hazardous substances restricted in EEE under the EU Directive 2011/65/EU.

Restricted hazardous substance	Restricted limit (%)*	Added year
Cadmium (Cd)	0.01	2003
Mercury (Hg)	0.1	2003
Lead (Pb)	0.1	2003
Hexavalent chromium (Cr ⁶⁺)	0.1	2003
Polybrominated biphenyls (PBB). Flame retardant.	0.1	2003
Polybrominated diphenyl ethers (PBDE). Flame retardant.	0.1	2003
Bis(2-Ethylhexyl) phthalate (DEHP)	0.1	2015
Benzyl butyl phthalate (BBP)	0.1	2015
Dibutyl phthalate (DBP)	0.1	2015
Di-isobutyl phthalate (DIBP)	0.1	2015

*: Maximum concentration values tolerated by weight in homogeneous materials.

It is noted that the above maximum concentration values apply to each homogeneous material rather than to a product or component. A homogeneous material refers to a material of uniform composition throughout that cannot be mechanically separated into different materials [76]. In addition, new substances are being considered for restrictions in the next few years including phthalates, brominated flame retardants (BFRs), chlorinated flame retardants (CFRs), and PVC. To inform users that producers are complying with the requirements of the Directives, the producers of EEEs have the obligation to mark their products with a crossed-out wheelie bin symbol [73]. The black

line indicates that goods have been placed on the market after August 2005 (when the Directive came into force). In addition, a CE mark is placed on the products by the manufacturer to demonstrate that the product complies with all the relevant requirements of an EU Directive (health, safety, and environmental protection standards) [76]. The CE stands for '*Conformité Européenne*', which means European conformity. The WEEE and RoHS Directives are stimulating change in the next generation of green electronics. This is exemplified in the design and development of products, utilising greener materials, such as printed circuit boards (PCBs) where industry is using less brominated flame retardants and less traditional tin/lead solder alloys [14]. Other countries, such as USA, China, Japan, and South Korea have followed the EU example and brought in similar legislation [14].

2.3 Criticality of materials

With the development of society, the acceleration of technological innovation requires more and more resources, while globalisation makes it possible to have access to more materials around the world. Nevertheless, the supply and demand of those materials is not always in balance. Due to a variety of reasons, demand for one material may increase significantly in a short time and far exceed the supply available at that time. The supply may be severely reduced or even temporarily unavailable. At the same time, these materials (and most especially their applications) may be important or irreplaceable to certain companies, countries, or areas. Examples of imbalance linked to criticality of materials include the cobalt crisis at the end of 20th century and the rare earth elements (REEs) dispute around 2010-2013 [16, 78-80]. Elsewhere Graedel and co-workers considered the imbalance between metal supply and demand and developed a methodology to evaluate the metal criticality of 62 metals and metalloids taking account of supply risk, environmental implications and vulnerability to supply restriction, and showed in particular the limitations of many metals of significance in emerging technologies [81].

The dependence on metals and minerals to sustain businesses and the economy is particularly true for the EU, where about 30 million jobs are directly reliant on access to metals and minerals [16]. It is noted that although there are several definitions for critical materials, there is not an accepted worldwide definition. The definition proposed by the European Commission (EC), U.S. Department of Energy (DOE) or U.S. National Research Council (NRC) are the most commonly cited and used [78]. In the context of the current research the definition of critical materials considered of most relevance and adopted is from the EC: *'materials which display a particularly high supply risk shortage in the next 10 years and which are particularly important for the value chain, in other words economic importance to the EU'* [82]. Vulnerable to supply disruption means that their supply is associated with a high risk of not being adequate to meet EU industry demand. This risk could be due to the demographic trends, infrastructure needs, governance performance, globalised markets, trade restrictions and agreements, climate changes, among others [53]. On the other hand, high economic importance means that the material is of fundamental importance to industry sectors that create added value and jobs, which could be lost in case of inadequate supply and if adequate substitutes cannot be found [65, 78]. It should be noted that criticality, in this context, is a dynamic property since products will utilise more and more elements from the periodic table and the demand for these products will continue to increase, which raises competition between sectors for the same materials and therefore, this will shift their criticality status. Furthermore, replacement or substitution of some materials could lower the criticality of some elements [55, 81].

The EU criticality methodology, based on the economic importance (EI) and supply risk (SR), was developed between 2009 and 2010 with the support of the European Commission, Ad-Hoc working group on defining critical raw materials (AHWG-CRM) within the raw material initiative (RMI) in close cooperation with EU member states and stakeholders [65]. This methodology has already been applied four times; creating the first list of 14 critical raw materials (CRMs) in 2011, an updated list of 20 CRMs in 2014, 26 CRMs in 2017, and 30 CRMs in 2020, where a total of 83 individual materials were evaluated [17]. Figure 2.6 maps the results of the 2020 criticality assessment prepared by the EC on the *'supply risk'* and *'economic importance'* dimensions.

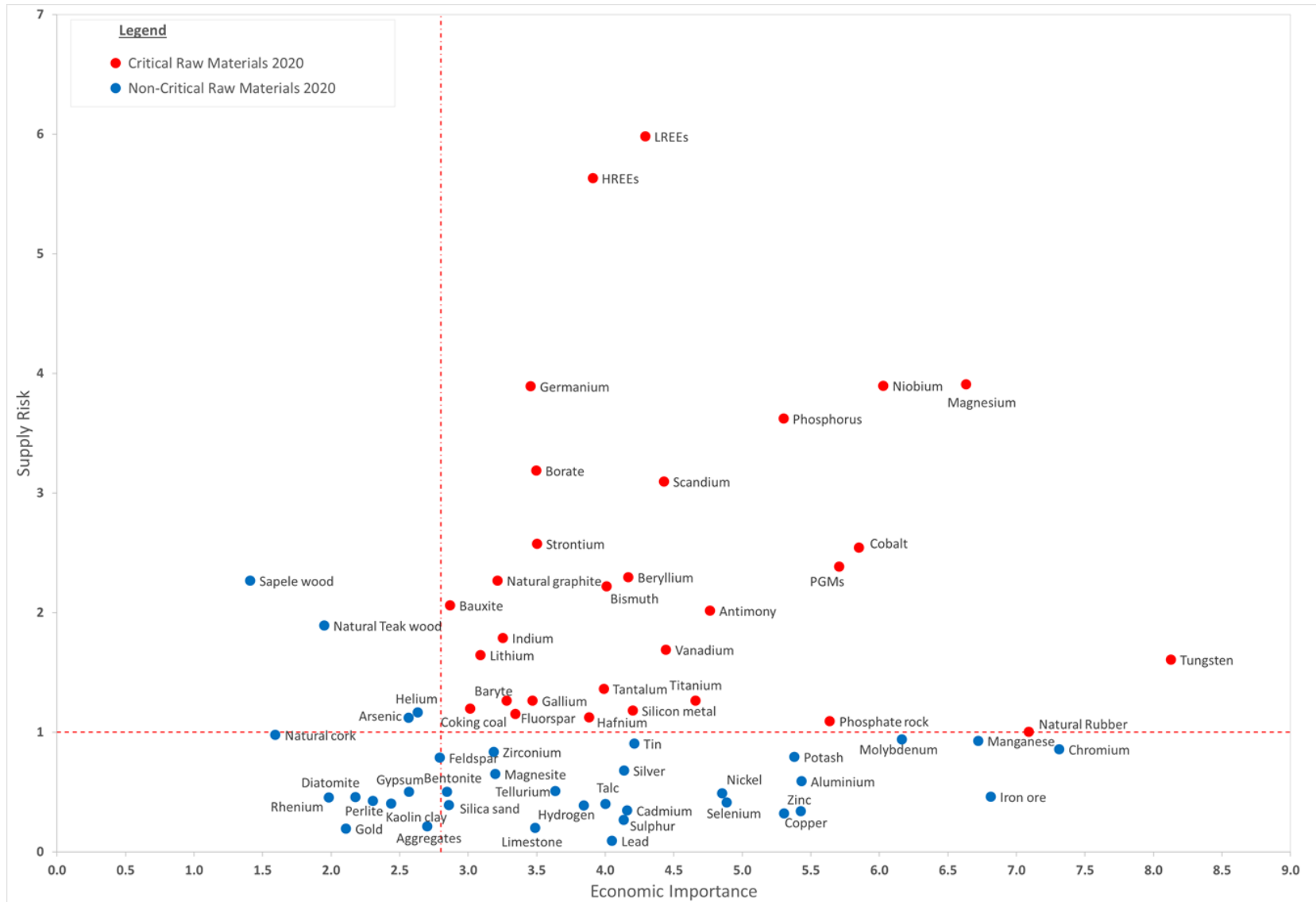


Figure 2.6: Economic importance and supply risk results of raw material. Criticality assessment, 2020.

Table 2.7 lists the CRMs of 2020. Amongst those listed are three groups of metals, namely: platinum group metals (PGMs, which include Ru, Rh, Pd, Os, Ir, and Pt), heavy rare earth elements (HREEs, which include Y, Gd, Tb, Dy, Ho, Er, Tm, Yb, and Lu), and light rare earth elements (LREEs, including Sc, La, Ce, Pr, Nd, Pm, Sm, and Eu). These metal groups comprise metals that have similar properties and are frequently used in related fields.

Table 2.7: Critical raw materials by the European Commission, 2020 [17].

Critical Raw Materials (30)			
Antimony	Fluorspar	Magnesium	Silicon Metal
Baryte	Gallium	Natural Graphite	Tantalum
Bauxite	Germanium	Natural Rubber	Titanium
Beryllium	Hafnium	Niobium	Vanadium
Bismuth	HREEs	PGMs	Tungsten
Borates	Indium	Phosphate rock	Strontium
Cobalt	Lithium	Phosphorus	
Coking Coal	LREEs	Scandium	

In the list of CRMs, rare earth elements (REEs) are considered as the most critical raw materials for the European Commission, with the highest supply risk. In addition, the U.S. DoE also has REEs listed in their medium-term criticality matrix [78]. REEs are a group of 17 elements comprising the 15 lanthanides, scandium, and yttrium; the latter two being included in the group because of their similar chemical and physical properties to the other elements of that group. Although in terms of inherent abundance in the earth's crust, REEs are not rare, they are termed rare because they are generally not concentrated in commercially viable quantities and so are difficult to mine, furthermore they usually co-exist with other metals so there is the added difficulty in terms of separation.

Raw materials are not only essential for production of a range of goods and services used in everyday life, but also for the development of emerging innovations, which are notably necessary for the development of more eco-efficient technologies and globally competitive products. REEs play a crucial role in the transition to a low-carbon and green economy. For instance, REEs are key components in almost all technology products, ranging from smartphones and flat screen TVs to all sorts of electric motors, nickel-metal hydride batteries, high performance metal alloys, compact fluorescent lamps, automotive catalysts, hybrid and electric cars, permanent magnets, optics and lasers, catalysts, wind and solar energy conversion, rechargeable batteries and other green economy applications, which is causing an increase in their demand and price [26, 27, 83]. Figure 2.7 is a map of those countries worldwide accounting for the largest share of global supply of CRMs. China is the major global supplier as well as consumer of REEs, with >85% of the global production of REEs.

Furthermore, China is also the major global supplier of 66% of the individual CRMs, evaluated by the EC, such as magnesium, tungsten, antimony, gallium, and germanium among others. Other countries that are also important global suppliers of specific materials include Russia and South Africa for PGMs, the USA for beryllium and helium and Brazil for niobium [16, 83, 84]. Due to large and increasing domestic demands and concerns for environment effects, China restricted its REEs through quotas, licenses, and taxes, decreasing from 50,145 tons in 2009 to only 31,130 tons in 2012. Although after losing the world trade organization case on exports of REEs in 2015, China eased export controls and the production tends to be stable, it has been estimated that over the next 25 years, the demand for REEs will increase sharply. For instance, it is projected that the demand for neodymium and dysprosium will rise by 700% and 2600%, respectively [16, 26, 27]. As the EU economy is severely dependent on imported supplies of several minerals and metals needed by industry, securing its access has become a major challenge.

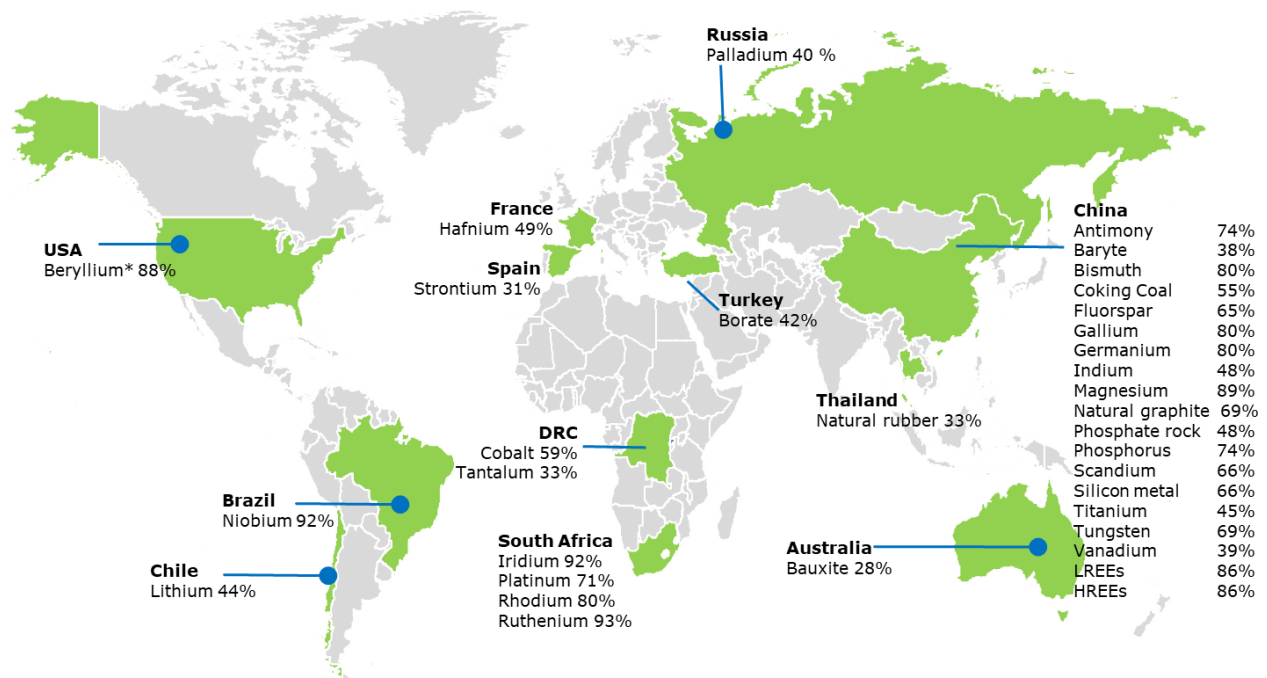


Figure 2.7: Countries accounting for the largest share of global supply of CRMs (2020) [17].

This scenario of scarcity of CRMs is critical with zero or almost negligible recycling of materials. In 2014, only about 15% of global WEEE was formally collected and treated, and although it was increased to 17.4% in 2019, recycling is still low globally, especially in low income countries [5]. Furthermore, in the EU, only around 25-40% of WEEE is treated, and the rest is discarded into landfill or exported to developing countries [26, 32]. In developing countries, most WEEE treated is handled

in the informal recycling system. This can lead to severe environmental problems and materials loss, where treatment processes are not well developed. For instance, in India about 98% of total WEEE is recycled by informal recycling sector [12, 13, 26]. In the case of the REEs, the recycling is extremely low with less than 1%. This is principally due to inefficient collection, technological difficulties, and a lack of incentives [27, 85]. Therefore, a drastic improvement in recycling rates for CRMs, especially for REEs, is needed, even more so in the EU, where countries have zero to few REEs' deposits. In December 2021, China had established a merger between 3 leading rare earth mining companies to further strengthen its hold on the global supply of REEs [86]. The UK and the US are pushing back on China's dominance in the provision of rare earth elements, with a £125M minerals processing plant currently under construction in the Port of Hull, Yorkshire, England, and the US senators proposing a law to increase domestic supply of rare earth metals by building a strategic reserve of minerals by 2025 [87], but to address the materials' scarcity problem, the most practical and reasonable method for the EU is to increase the recycling of secondary resources from WEEE. This recycling process is known as '*urban mining*'. Regarding the recycling of critical metals there are two distinct approaches: *pre-consumer recycling* which refers to the recycling of production scrap of manufacturing processes ('*new scrap*'), and *post-consumer recycling*, which refers to recycling end-of-life (EoL) products. Of the two, *new scrap* recycling is much easier compared to the recycling of EoL WEEE since the *new scrap* exists in higher metal concentrations, is derived from a well-known and defined source of waste, is in continuous supply, and very often in high volumes which makes recycling economically more profitable [80]. At present *new scrap* is the main source for recycling critical metals; indium, for example, is mainly recycled from waste indium-tin oxides (ITO) [88-90], but when it comes to the recycling of WEEE, the situation is not so optimistic as it is for '*new scrap*' [26]. WEEE is a complex combination of materials, where its composition depends essentially on the type, manufacturer, and age of equipment, therefore recycling WEEE is a significant challenge. WEEE, contain a large variety of elements, which makes it an excellent secondary source of materials, especially for metals and CRMs [7, 12, 13, 35]. As an example, a typical circuit board can contain a spectrum of metals such as copper, tin, cobalt, gold, silver, indium, palladium, platinum, neodymium, etc. [13, 20, 22, 50, 51, 91]. Therefore, although WEEE is a complex and challenging source of materials, it offers a huge potential opportunity for recovery of several valuable and critical metals through development of novel, efficient, and integrated recycling processes. Recycling CRMs from WEEE is imperative to make efficient use of natural resources and to improve and ensure the supply of these essential materials for the economy. Moreover, recycling of WEEE will also contribute to mitigation of environmental pollution and human health risk. In the next section a discussion on the current methods for recycling of WEEE is given.

2.4 Methods of Recycling WEEE

The aim of this section is to give an introductory overview of the typical processes for metal recovery, with further detail provided and discussed elsewhere in the relevant chapters of this thesis. These include the main physical/mechanical and metallurgical processes used in metal recovery and the metallurgical processes are of three types: pyrometallurgical, hydrometallurgical and biohydrometallurgical. Each is defined and its advantages and disadvantages are discussed.

2.4.1 Physical/mechanical processes

Physical or mechanical processes for recycling of WEEE are usually employed during the upgrading stage to separate, liberate, and concentrate the valuable metallic fraction from the non-metallic fraction by disassembly, shredding and crushing processes. The separation of the metallic and non-metallic fraction is achieved using their physical properties such as density, conductivity, and magnetic properties. The mechanical recycling techniques include a crusher, pulveriser, classifier, and separator. The separation and enrichment methods include sieving, gravity separation, magnetic separation, electrostatic separation, eddy current sorting, etc. [12, 88, 92, 93]. Figure 2.8 illustrates a typical mechanical separation process for WEEE. Dismantling, through manual, automated and semi-automated methods, removes components and/or group of parts from WEEE, which are used to selectively remove, unlock, and separate valuable materials for further recovery processes. Dismantling is a not energy intensive and can also be used to remove hazardous components prior to treatment processes. Comminution of WEEE by shredding/crushing is used to reduce the size of the material through cutting, tearing, and extruding, and it is essential to achieve effective liberation of the metallic fraction from the non-metallic fraction (plastics and ceramics). Comminution of WEEE and highly effective liberation of the metal fraction is a prerequisite for the separation steps that follow to achieve better metal recovery. The vibration screen is used to ensure a desirable particle size; where the desired size is largely dependent on the subsequent metallurgical processes deployed. Typically, hydrometallurgical processes require finer particles (between 500 μm and 2 mm) to achieve high leaching efficiencies and recovery rates, whilst pyrometallurgical processes can deal with coarser feed particles ($\leq 4 \times 4 \text{ cm}^2$). Magnetic, eddy current, density and other separation methods are used to selectively separate the ferrous and non-ferrous particles and the metallic fraction from the non-metallic particles [12, 92, 93]. Magnetic and eddy current processes separate metallic particles based on their different electrical conductivities, whilst density separation exploits the large differences between plastic ($< 2.0 \text{ g/cm}^3$) and metal (light metals $\geq 2.7 \text{ g/cm}^3$ and heavy metals $\geq 7.0 \text{ g/cm}^3$) densities [12].

The advantages of physical recycling methods are that the processing is relatively simple and requires low energy consumption, low capital, and operating costs, has minimal impact on the environment, and can be applied to diverse WEEE types. Nevertheless, there are still challenges in the physical separation methods. Generally, a significant amount of dust is generated in the processes, metals are not completely liberated from the non-metallic fraction, producing metal loss. It has been estimated that dust generation and incomplete metal liberation can lead to a high loss of precious metals of up to 40% [94]. Furthermore, in the shredding and separation processes, hazardous metal fines and dust containing BFRs, and dioxins can be liberated, putting workers' health at risk, and polluting the environment [12, 93, 94].

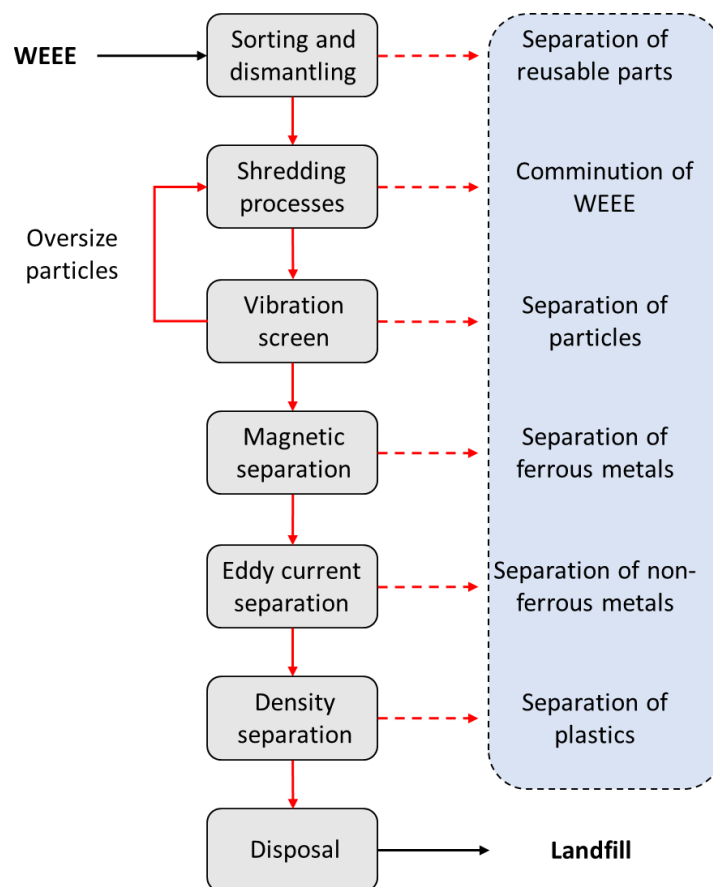


Figure 2.8: Flow chart of a typical mechanical processing as pre-treatment and separation.

2.4.2 Metallurgical processes

Physical and mechanical processing techniques are useful for the preliminary separation, concentration, and classification of valuable materials; however, the output obtained by these methods are still a combination of metals and alloys, which generally require further separation and recovery processes. Typically, metallurgical processes are carried out to refine and purify specific metals from the concentrated metal mixture, using either pyrometallurgical, hydrometallurgical or biohydrometallurgical processes.

Pyrometallurgical processes are conventional methods that used high temperature treatment to recover metals. These processes include incineration, melting, smelting, calcination, combustion, roasting and pyrolysis. In these processes, crushed WEEE scrap is burned to eliminate the organic components whilst leaving non-volatile metals and minerals for further recovery processes. The advantages of pyrometallurgical process are that any form of WEEE scrap can be used as feedstock, no pre-treatment is required (except perhaps a previous shredding step which will depend on the size of the reactor), and processing is relatively straightforward [12, 88, 92, 93].

The hydrometallurgical process is an extractive metallurgical technique used for the obtaining metal from their ores and has been widely used for the recovery of metals from WEEE. This process involves the use of aqueous solutions, normally acids such as mineral acids including hydrochloric acid (HCl), nitric acid (HNO₃), sulphuric acid (H₂SO₄), and aqua regia (a mixture of H₂SO₄ +3HCl). The aqueous solutions act as leaching or extracting agents, the selective extraction of metals. Hydrometallurgical processes are generally divided into three main functions: leaching, concentration and purification, and metal recovery. The advantages of hydrometallurgical process are their fast reaction kinetics, relatively clean methods, flexibility in operation, low capital requirement and low energy demand [12, 19, 50]. In recent years, biohydrometallurgy processes have been successfully applied for the recovery of metals [12]. Biohydrometallurgy technique is a subfield of hydrometallurgy processes, which used biological agents, mostly bacteria, to selectively dissolve and leach metals. Normally, biohydrometallurgy has the advantages of being the most environmental friendly process, requires low cost of investment and has high selectivity of metals [12].

In the recovery of metals from WEEE, several physical and metallurgical processes have been developed and applied for metal recycling, including mechanical separation such as multi-steps crushing, grinding, magnetic separation, electrostatic separation, gravity separation and density-based separation [12, 92, 95, 96], pyrometallurgical processes such as smelting, calcinations, roasting and pyrolysis [18, 97-99], hydrometallurgical processes [12, 96, 100], biohydrometallurgical methods [96, 101], use of supercritical fluids [102], vacuum metallurgical technology [103], chelation and hybrid

technologies [104]. Kaya and co-workers [12] produced a detailed flowsheet (illustrated here for reference in Figure 2.9) summarising the physical and metallurgical processes required for metal recovery from WEEE, much of which has been covered in the discussion here but the processes do have constraints associated with them. Mechanical separation methods present a high material loss of mainly precious metals, and dust sources can contain HFRs and dioxins, and dangerous metal fines such as lead, chromium, cadmium, are also present [96, 103, 104]. Pyrometallurgical methods are energy intensive with high operational costs and may liberate toxic gases to the atmosphere [12, 104]. Although hydrometallurgical processes have milder conditions, require lower capital cost, energy and have less environmental impact than pyrometallurgical methods, they consume a substantial amount of toxic, corrosive, and flammable reagents, generating a large volume of wastewater that has to be treated [12, 91, 104]. Biohydrometallurgical leaching is environment-friendly, requires low cost of investment and has high selectivity of metals, however, toxic influence of ingredients on the growth of micro-organisms, longer reaction time and the sensitivity of the microorganisms to pH and temperature are the major drawbacks [12, 101, 104]. Therefore, novel, and greener technologies for metal recovery from WEEE are of great significance to overcome the limitations associated with conventional technologies. A more environment-friendly method that has been emerging as very promising in recent years is the use of ionic liquids (ILs) as a leaching agent, which are discussed in the following section.

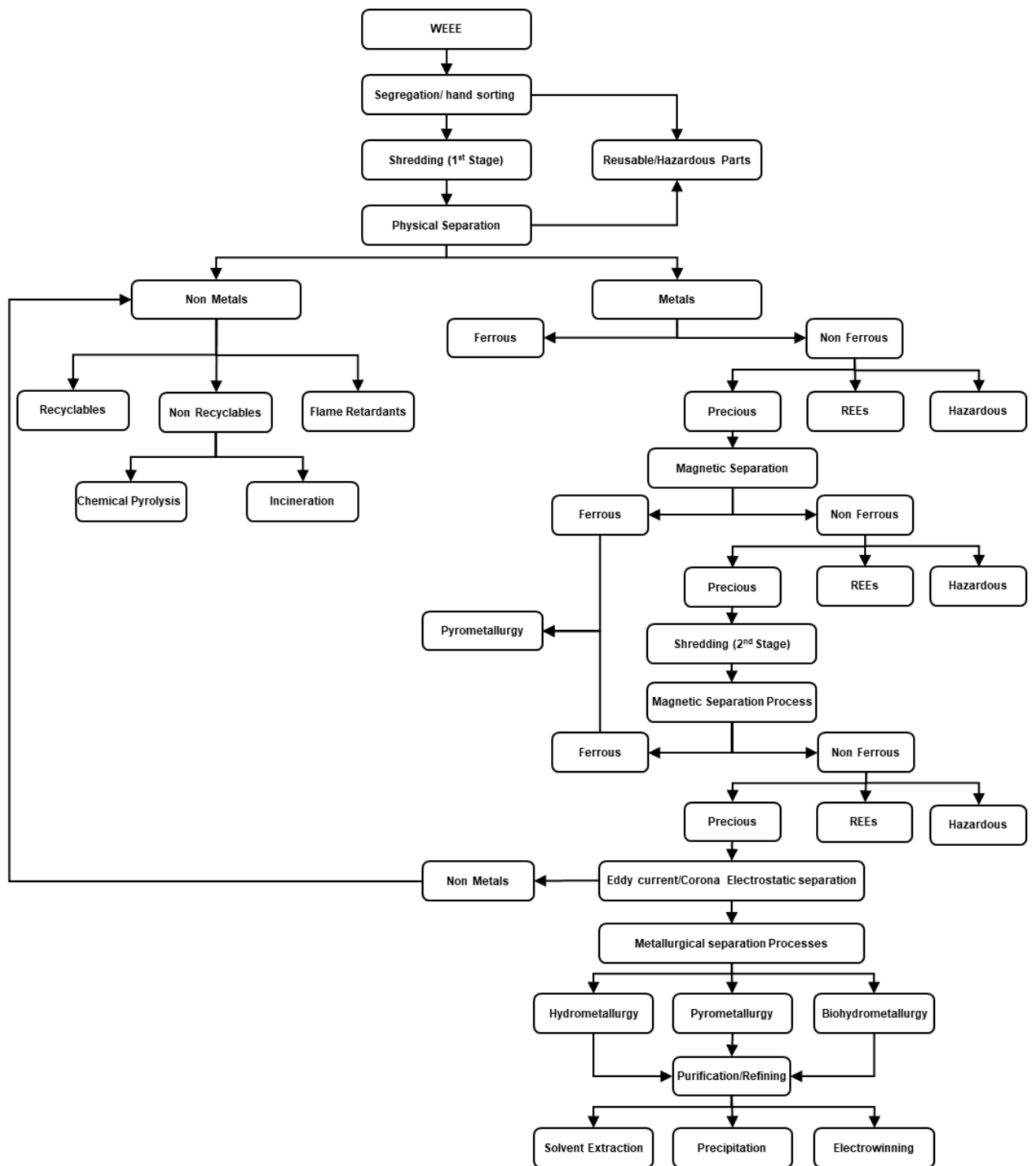


Figure 2.9: WEEE recycling flowsheet with a combination of physical, chemical and metallurgical steps [12].

2.5 Ionic Liquids

Ionic liquids (ILs) are entirely ionic in nature and typically consist of a large asymmetrical organic cation associated with a polyatomic anion that may be either inorganic or organic. Figure 2.10 illustrates some common cations and anions present in ILs. Ionic liquids are also known as room temperature ionic liquids (RTILs) because of their melting points typically below 100 °C, thereby making them liquids at ambient temperatures. Ionic liquids are solvents with remarkable properties; wide liquid range (from room temperature to above 300 °C), negligible vapour pressure, excellent thermal, chemical, and electrochemical stability, relatively low viscosity, and high recyclability [104, 105]. An interesting characteristic of ILs is that their properties such as density, viscosity, polarity, melting point, water miscibility, etc. can be tailored through different combinations of cations, anions, and side chain substituents [106, 107]. Due to these unique properties, ILs can be designed for specific purposes, and as such are referred to as task-specific ionic liquids (TSILs). ILs have generated considerable scientific and industrial interest and technological processes making use of them are currently underway. ILs have been utilised in a vast number of industrial applications including as well as solvents, catalysis, additives, chemistry, analysis, batteries, and electrochemistry [108], as illustrated in Figure 2.11. In this thesis, ILs are used as leaching and extraction solvents for the recovery of key strategic metals; their importance in this research warrants some further discussion on their properties which is set out in the subsections below.

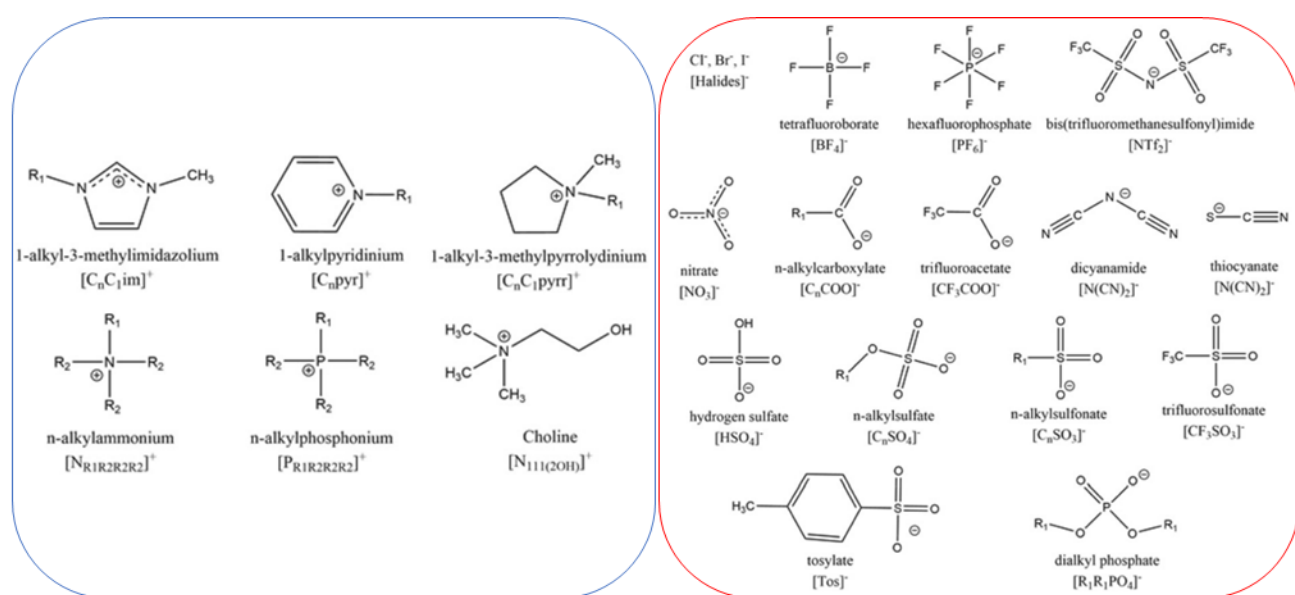


Figure 2.10: Schematic of some common cations (blue) and anions (red) of ILs [109].

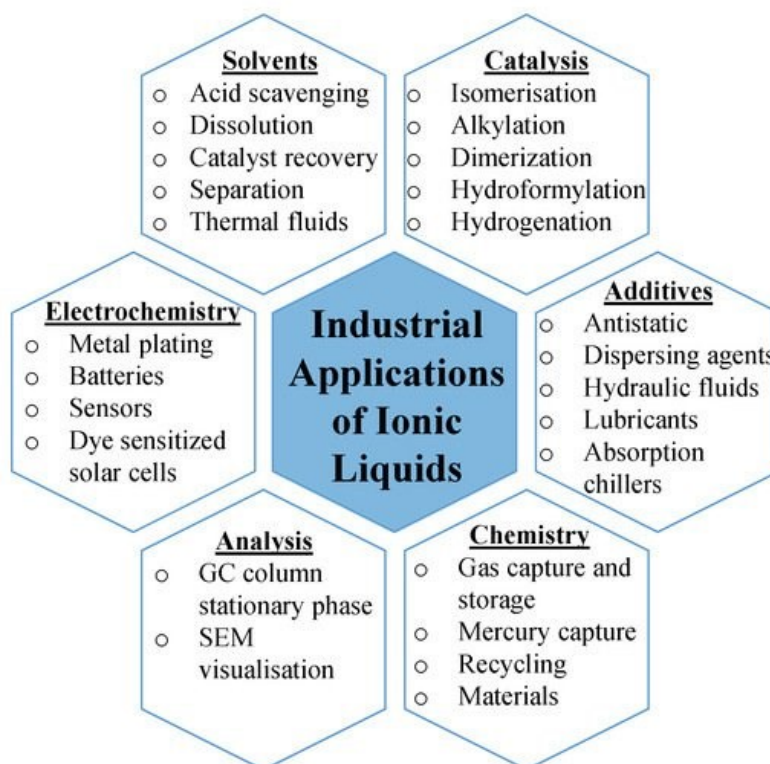


Figure 2.11: Industrial application of ionic liquids [108].

2.5.1 Physicochemical properties of ionic liquids

In this sub-section, the physicochemical properties of ionic liquids are described; properties that are likely to have significance where ILs are used as solvents applied to the recovery of metals from WEEE. The selected properties of importance are briefly introduced, but detail on these and other properties have been explained and reviewed elsewhere [106, 107, 110-120]. Whilst prediction of the physicochemical properties of ILs may be difficult there are some properties that show a pattern of behaviour that offers insight as to how ILs might perform.

2.5.1.1 Viscosity

Ionic liquids are organic solvents with typical viscosity values between 100 and 1000 centipoise (cP). The viscosity of an IL is critical as it plays a crucial role in the mass transfer efficiency in IL-based leaching and extraction processes. Generally, as the cation molecules are usually large organic molecules, the geometry and the extension of the cations can modify the viscosity. Larger ring structures increase the viscosity compared to aliphatic hydrocarbons. Thus, maintaining the same anion, the trend follows as six-membered rings > five-membered rings, aromatic rings (five-membered) > aliphatic hydrocarbons. The length of the alkyl chains also increases the viscosity due to

stronger van der Waals forces between cations [121]. On the other hand, keeping the same cation and changing the anion, the viscosity is enhanced as the anion volume increases since it induces greater van der Waals forces [122]. As an example, retaining the same cation, the viscosity follows $[\text{C}_8\text{SO}_3]^- > [\text{C}_5\text{SO}_3]^-$, $[\text{NfO}]^- > [\text{TfO}]^-$ as the anion volume is increased. These rules are generalised and several exceptions are found. For instance, in the ILs with the presence of $[\text{BF}_4]^-$, the viscosity follows $[\text{BF}_4]^- > [\text{CF}_3\text{BF}_3]^- > [\text{C}_2\text{F}_5\text{BF}_3]^-$, due to the small size of $[\text{BF}_4]^-$ and the limited hydrogen bonding capacity [123]. Imidazolium-based ILs have been widely utilised in comparison with other ILs. In this case, the viscosity of imidazolium-based IL increases as the alkyl chain on the cation is lengthened due to the increased van der Waals interactions.

2.5.1.2 Density

The density of ILs depends on several factors, it is mainly governed, however, by the elemental composition, the molar mass of the anions and the alkyl chain lengths of the cations. In the elemental composition, it has been found that the greater the number of fluorine atoms, the higher the density. The mass of the anions refers to the larger the molar mass of anions, the higher the density. In the case of cations, the increase in the alkyl chain length generally decreases the density. In addition, if the anions and cations remain chemically identical, asymmetric cations do not pack efficiently, reducing their density. The density of the imidazolium ILs is reported to decrease slightly as the cation alkyl chains are lengthened [112, 121].

2.5.1.3 Volatility

ILs are non-volatile substances and their vapour pressure is normally negligible at ambient temperatures and under low pressure, which makes them an excellent substitute for the harmful and volatile organic compounds (VOCs) [107, 112, 113]. It has been reported that most of the ILs show no sign of volatility before reaching their thermal decomposition temperature (300-450 °C). The negligible volatility of ILs is due to a strong interaction between the anions and cations. It has been reported that the enthalpy of evaporation in ILs is approximately an order of magnitude greater compared to that of a normal molecular liquids [124]. ILs with symmetrical anions are also found to present higher enthalpy of evaporation than the asymmetrical anions. For instance, keeping the same cations, anions such as $[\text{BF}_4]^-$ and $[\text{PF}_6]^-$ have higher enthalpy of evaporation than asymmetrical anions such as $[\text{NTf}_2]^-$ [125]. In terms of cations, it has been found that longer alkyl chains are usually associated with higher enthalpy of evaporation, which is a product of stronger van der Waals interaction between the cations and anions of the IL [126]. It is noted that although it is widely accepted that a defining characteristic of ILs is that they exert no measurable vapour pressure, and hence cannot be distilled, this is not completely true. It has been reported that some selected families

of commonly used aprotic ionic liquids such as [C₆mim][NTf₂], [C₂mim]Cl, among others can be distilled at 200–300 °C and with low pressure [124]. Nevertheless, at normal pressure and standard working temperatures, the vapour pressure of ILs remains negligible.

2.5.1.4 Thermal stability

Another characteristic property of ILs is their significant thermal stability. ILs can be used across a large temperature range, below their decomposition temperatures, without loss of their properties. Only at high temperatures can the decomposition of ILs take place and it is most likely due to an anionic attack towards the cations. The thermal stability of ILs can be improved by the hydrophobicity of anion, thus the higher hydrophobicity, the higher the thermal stability. With the same cation, a linear increase in the thermal stability of ILs is observed by changing the hydrophobicity of anions, which follows the sequence [PF₆]⁻ > [NTf₂]⁻ ≈ [BF₄]⁻ > [AsF₆]⁻ > I⁻, Br⁻, Cl⁻ [127]. The thermal stability of the imidazolium ILs has been found to improve with the increase in linear alkyl chains. Furthermore, the presence of fluoride can also potentially increase the decomposition onset temperature [128]. On the other hand, the presence of nitrogen atoms, as substituents on the alkyl chains in the cation, can potentially decrease the thermal stability due to the facile elimination of the stabilised alkyl cations [127].

2.5.1.5 Flammability

The non-flammability of IL under standard conditions is also characteristic of ILs and one of the advantages over VOCs. This characteristic of non-flammability does not mean, however, that they do not present a risk near fire and/or heat sources. Smiglak et al. concluded that several ILs, including many commercial ILs, are combustible due to the nature of their positive heats of formation, oxygen content, and decomposition products [129]. In addition, they reported that certain elements such as F, Cl, P, S, among other, can provide high energy and combustibility in ammonium, imidazolium, pyridinium, pyrrolidinium, tetrazolium, and aminotetrazole ILs-based because of the presence of these elements in the anions in the form of [NO₃]⁻, [CH₃CO₂]⁻, [N(CN)₂]⁻, [C(CN)₃]⁻, [PF₆]⁻, [NTf₂]⁻ and [N(NO₂)₂]⁻.

2.5.1.6 Water miscibility

ILs, depending on their miscibility with water, can be either hydrophilic or hydrophobic. In some cases, ILs can change their miscibility depending on the temperature or acidity of the system [106, 107]. Examples of ILs that can have their water miscibility modified are 1-butyl-3-methylimidazolium tetrafluoroborate ([Bmim][BF₄]) and protonated betanium bis(trifluoromethane)sulfonimide ([HBet][NTf₂]). It is important to note, however, that all the ILs are

hygroscopic regardless of their hydrophobicity and may make up a significant molar percentage of ILs. The hydrophilicity or hydrophobicity of ILs is mostly determined by the anion although the cation may also have an influence. The hydrophobicity of ILs is basically determined by the ability of the anion to form hydrogen bonds, thus anions such as hexafluorophosphate ($[\text{PF}_6]^-$), tetrafluoroborate ($[\text{BF}_4]^-$) and bis(trifluoromethane)sulfonimide ($[\text{NTf}_2]^-$) usually produce hydrophobic ILs, whilst anions such as chloride (Cl^-) and iodide (I^-) generally produce hydrophilic ILs [117]. The length of alkyl chains also plays an important role in the hydrophilicity or hydrophobicity of ILs. Long alkyl chains in the cations or anions increase the hydrophobicity of an IL due to an intensification of the non-polar regions of the IL structure, product of a stronger Van der Waals force contribution [107, 117, 118]. For instance, in the case of Cyphos 101 ($[\text{P}_{6,6,6,14}][\text{Cl}]$), even pairing a hydrophilic chloride anion, the large alkyl chain cation ($\text{P}_{6,6,6,14}$) confers the final hydrophobicity of the IL.

2.5.1.7 Surface tension

Surface tension also plays an important role in the mass transfer in leaching and extraction processes and affect the efficiencies in emulsion and phase-separation processes. In general, ILs present slightly higher surface tension (>33 dyn/cm) than conventional organic solvents such as toluene (32 dyn/cm) and hexane (18 dyn/cm), and lower than water (73 dyn/cm). Furthermore, it has been reported that the surface tension of ILs decreases as the temperature increases. This is probably due to the alkyl groups of the ILs preferring the orientation towards the surface and are enriched there, whilst the charged parts of the molecule are shifted into the bulk phase [118]. The same study suggested that longer alkyl chains have the greatest impact on the surface tension in imidazolium, ammonium, and phosphonium ILs, due to an increase in the van der Waals force.

2.5.1.8 Conductivity

Electrical conductivity of ILs is an important physicochemical property for the recovery of metals because of the potential for their use in electrochemical processes. ILs have typical conductivity values in the range from 1.0 mS/cm to 10.0 mS/cm and it has been concluded that the interaction between cation and anion is the major factor in determining the conductivity [114]. Studies on the effect of the cation on conductivity, have shown that pyrrolidinium-based ILs present yield the highest conductivities, following the trend: pyrrolidinium $>$ pyridinium $>$ imidazolium $>$ other $>$ ammonium. On the other hand, in studies on the effect of anions on conductivity, it has been reported that the conductivity follows the trend: $[\text{N}(\text{CN})_2] > [\text{OTf}] > [\text{BF}_4] > [\text{NTf}_2] > \text{sulfate} > [\text{PF}_6] > \text{PO}_2$ [114]. In addition, the conductivity of an IL has been found to be inversely related to its viscosity as conductivity depends on ion mobility. The self-diffusion coefficient of ILs also plays a crucial role in the conductivity, which, similar to the viscosity, is a transport property that depends strongly on the movement of ions

[114]. Moreover, it has been reported that the conductivity of ILs tends to decrease as the cationic alkyl chains are lengthened due to the presence of a stronger van der Waals forces, which impact the electron mobility [119]. Other factors such as ion size, ion shape, and density have been found to have negligible or little influence on the conductivity of ILs, confirming that the conductivity of ILs is mainly determined by the ion mobility [114].

2.5.1.9 Toxicity

Although ILs are also known as '*green solvents*' because of their properties previously described (non-volatile, high thermal stability, low combustibility, etc.), concern exists and their '*green*' properties questioned, since several studies suggest that ILs have relatively high toxicity and poor biodegradability, which could have extremely negative impact on humans and the environment [115, 116]. The initial studies of the toxicity of ILs began in the early 2000s, and although the toxicity of ILs can be difficult to measure the data suggest the following trends: the toxicity of ILs is stronger with the increase in the length of the alkyl chain, the presence of oxygen atom in the side chain significantly reduces the toxicity of the ILs, and symmetrical chains result generally in lower toxicity. The effect of anions on the toxicity of ILs has been shown to be secondary compared to the effect of the cations; however, more detailed studies are considered necessary [115, 116, 120]. The elemental IL composition also has revealed that different groups can have different impacts on the toxicity of ILs. Fluorinated anions are normally toxic (example bis(trifluoromethanesulfonyl)imide), whilst common anions (acetate, chloride, methylsulfate) have been found to be nontoxic. Furthermore, it has been predicted that the toxicity of ILs increases slightly with the number of nitrogen atoms in an aromatic cation ring [120]. It is important to point out that most of the studies on the toxicity of ILs is done on human cell, algae, enzyme and aquatic organisms, showing negative impacts on the environment; however, dermal toxicity of all ILs are considerably low and no mutagenicity effects have been observed so far.

2.5.2 Recovery of metals by ionic liquids from WEEE

Due to their environmentally friendly behaviour, including non-volatile and ionic nature, ILs have been widely studied in the extraction and leaching of metals in the recent years. The extraction mechanism of metals by ILs involves anionic or cationic exchange and it depends on the IL selected, the chemical structures of the anionic or cationic metal complexes in aqueous solutions, the chemical interaction of the IL with the target metal, among other factors. Anionic exchange, however, has been commonly identified as the main mechanism. In addition, ionic pairing reaction has been also identified to have an influence in the metal extraction. These two reactions can occur simultaneously, subsequently by starting from the anionic exchange reaction or individually [107, 113, 119, 130]. Janssen et al. reported an in-depth study on the relationship between structure, mechanism and application of metal extraction by ILs [131]. Briefly, it was described that the mechanisms of metal extraction by ILs can be divided in three types: neutral extraction mechanism, ion exchange mechanisms, and the neutral coextraction mechanism. Table 2.8 shows the mechanisms and the prototype equation, which represents every possible means by which a metal can be moved from the aqueous phase to the IL phase while preserving electroneutrality. The electroneutrality is an important and fundamental principle of the IL mechanism and it states that regardless of how the metal enters the IL phase, the net charge of the aqueous and the IL phases cannot change. Table 2.8 presents general mechanisms although there are many variations possible that depends on each system. Several authors have reported the recovery of metals using ILs, and as expected, they conclude that mechanisms are specific to the system [105, 107, 110-112, 131]. In this thesis, copper, gold, indium and REEs are recovered from EoL mobile phones and their mechanisms are developed and explained in each of the following chapters.

Table 2.8: Mechanisms for the transfer of metals from an aqueous phase [131].

Mechanism		Prototype Equation
Neutral Extraction		$M_{(aq)}^+ + L_{(aq)} + X_{(aq)}^- \rightarrow [M \cdot L \cdot X]_{(IL)}$
Ion Exchange	Native Ion Exchange	$M_{(aq)}^+ + L_{(aq)} + C_{(IL)}^+ \rightarrow [M \cdot L]_{(IL)}^+ + C_{(aq)}^+$
	Sacrificial Ion Exchange	$M_{(aq)}^+ + L_{(aq)} + X_{(IL)}^+ \rightarrow [M \cdot L]_{(IL)}^+ + X_{(aq)}^+$
Neutral Coextraction		$M_{(aq)}^+ + L_{(aq)} + X_{(aq)}^- \rightarrow [M \cdot L]_{(IL)}^+ + X_{(IL)}^-$

Each equation represents a prototype of the mechanism of interest. M^+ denotes a monovalent metal, L is a neutral ligand and C^+ and A^- are the component ions of the IL.

2.6 Summary

WEEE is one of the fastest growing municipal solid waste streams worldwide and is forecasted to continue to increase in the coming decades. The generation of WEEE is closely related to the GDP, where high-income countries generate more WEEE per capita than low-income countries. WEEE is a serious problem. Only 17% of global WEEE was formally treated and recycled in 2019 with the rest being discarded into landfill or exported to low-income countries, where WEEE is treated in informal recycling systems. These practices are potentially dangerous due to the likely release of hazardous substances such as heavy metals, flame-retardants, aromatic hydrocarbons, etc., which can have significant impact on human health and the environment.

The consumption of raw materials has increased greatly in the last decades, which has created an imbalance in the supply and demand of natural resources. Without these raw materials, technological developments and advancements will be seriously compromised. To address this problem, the European Commission has developed a list of critical raw materials (CRMs), based on their scarcity and vulnerability. Several of these CRMs are widely used in the production of EEE, and they are fundamental to the development of clean technologies such as electric vehicles, photovoltaic panels, wind turbines, etc. This scenario of scarcity and vulnerability of CRMs is worsened with the very poor levels of WEEE recycling coupled with the huge loss of material value as WEEE ends up in landfills in low-income countries. Although current global metal reserves can meet the short-term demand, the scenario for a long-term demand is seriously threatened with some metals reaching their limit of supply within the next decades.

To protect the environment and human health and reduce the scarcity and vulnerability of natural resources, the recycling of valuable and critical materials from WEEE through the development of sustainable processes is essential. While secondary material production from WEEE requires much less energy and contributes to an important reduction in carbon footprint compared to primary production of metals, the use of the traditional methods of mechanical recovery, pyrometallurgy and hydrometallurgy which offer routes to the recovery metals from WEEE, also present challenges because of the relatively high energy consumption and the generation of waste that must be further processed. Due to the complex nature of WEEE therefore, novel 'tailored' recovery processes are required, and, with ILs, because of their unique properties, showing promise over the last few years, as potential leachants and extractants, it is this potential that is exploited in this work to develop environmentally friendly integrated solutions for recovery of strategic metals from key value components of EoL-mobile phones that can minimise the use of reagents and energy consumption.

3 Detailed Characterisation of Multigenerational Mobile Phones to Determine Potential for Recovery of Value

3.1 Introduction

The aim of the work described in this thesis is to investigate the potential for use of ionic liquids (ILs) to selectively extract key value strategic materials (and specifically metals) for their recovery from waste electrical and electronic equipment (WEEE) using mobile phones as a case study. As a first step to this research, a detailed characterisation of multigenerational mobile phones is carried out to determine the scope for recovery of value from mobile phones in the form of material value (metal and non-metallic fractions) and as energy. This chapter begins with a brief contextual introduction to waste electrical and electronic equipment and specifically mobile phones as an example of a popular consumer electronic device classified as a fast-moving consumer electronic. This is followed by a section which describes the methodology deployed in terms of (i): the collection and classification of used mobile phones referred to as end-of-life mobile phones (EoL-MPs), (ii) the dismantling processes developed to permit access to the component fractions, (iii) the partitioning of key fractions to permit detailed analysis and (iv) the suite of analytical techniques used in the characterisation of the component fractions to provide a comprehensive characterisation. The results of this study are reported in terms of the metallic fraction, the non-metallic fraction, and its potential for recovery.

Waste electrical and electronic equipment (WEEE), also known as e-waste, has been catalogued as one of the fastest growing waste streams in the world with an annual growth rate of 3-5% [2, 4]. According to the United Nations, in 2019 the global WEEE generated reached 53.6 Mt, with an annual growth of almost 2 Mt, and it was forecasted to reach 74.7 Mt by 2030, almost doubling in the last 16 years [132]. This is a serious problem as only 15% of global WEEE is formally treated with the rest discarded to landfill, incinerated, exported to middle- and low-income countries, often illegally, where a WEEE management infrastructure is not yet fully developed.[26, 96, 132]. These practices pose serious risk due to the uncontrolled release of large numbers of hazardous substances such as heavy metals, flame retardants, aromatic hydrocarbons, etc. [6-8, 96], which impact significantly human health and the environment [6-8, 12, 133].

Information and telecommunication technologies (ITT) equipment, such as mobile phones, tablets, laptops, computers, printers, etc., is a major category of WEEE in the EU [18]. Among all ITT equipment, mobile phones have been reported to represent the most valuable of the WEEE's streams

[133]. In addition, the international telecommunication union's (ITU) estimated that more than 9 billion mobile phone subscriptions existed globally by the end of 2020 [37]. This prediction is of concern since the lifespan of a mobile phone has been reduced considerably from an average of 5 years in the 1990's to currently less than 2-3 years [37, 38]. In high-income countries, the lifetime of mobile phones is even shorter. In China, which is the largest producer of mobile phones with over one billion mobile phones produced in 2019 [134], mobile phones are replaced between 1-2 years [135]. The rapid replacement of mobile phones as well as their low recycling rate in the commercial market of approximately 9% [53], leads to large tonnages of EoL-MPs; increased demand for raw materials, energy and water consumption; and where uncontrolled and poor disposal at end-of-life occurs, impacts on health and the environment. In addition, with increasingly limited access to resource some elements key to mobile phone products, due to greater difficulty to extract them from their natural ores and to maintain product supply, it will become necessary to identify alternative sources of these elements.

Mobile phones comprise a complex and heterogeneous combination of materials; the nature of their composition depends largely on the producer, the year of production and category of phone [7, 13]. In general, mobile phones can be divided into 3 categories: *feature phones* (with no operating system, touchscreens and third-party applications), *multimedia phones* (with operating system, touchscreen, but no third-party applications) and *smartphones* (with highly responsive touchscreen, robust operating system and third-party applications) [38]. The major mass fractions of a mobile phone are metals, plastics, ceramic and other trace materials, and its production utilises between 60 and 64 elements [8]. This material composition includes trace amounts of strategically/economically important metals such as rare earth elements, critical raw materials, platinum group metals, and base metals such as copper, aluminium, and iron. Furthermore, several elements, referred to as high-tech minerals that are used extensively in green technologies such as solar panels, wind and marine turbines, low carbon technologies, and play a fundamental role in the energy industry and the development towards a more environmentally friendly and sustainable society, are found in mobile phones. These high-tech minerals, known also as energy metals, are not abundant in the Earth's crust and the majority of them are produced primarily as by-products of base metals [136]. In this context, WEEE offers a resource-rich source of material for potential recovery; EoL-MPs with their fast replacement and low recycling rate, especially are a most valuable WEEE stream [37, 133]. Moreover, use of EoL-MPs as a secondary source offers a route to close the materials loop, is resource efficient, helps to mitigate the threat to natural resources, relieves supply demands, reduces the environmental impacts associated with improper management and contributes to the economy. This contributes to a win-win scenario by achieving both ecological and economic benefits.

WEEE recycling at present is not simple but requires complex and multi-step processes. The “mineralogy” of WEEE such as mobile phones is very different compared to natural ores, as sources of many metals. WEEE is a heterogeneous mix of materials and components, and the legal definition of recycling according to the Waste Framework Directive is *‘any recovery operation by which waste materials are reprocessed into products, materials or substances whether for the original or other purposes’* [71], requires that products are dismantled into their component parts before reprocessing. As a fundamental step towards establishing routes to recycle, detailed characterisation of the components and fractions is critical. To date, manual dismantling and sorting of WEEE is the most utilised technique to separate the different components of mobile phones due to its high complexity and for the maximisation of material recovery [137]. Nevertheless, because current literature related to the qualitative and quantitative characterisation of EoL-MPs is mostly focused on the metal concentration of printed circuit boards (PCBs), there is limited data on composition of the other key components of screens, electronics, and the non-metallic fraction of mobile phones. Thus, the aim of the research described in this chapter presents a detailed assessment of all components of EoL-MPs to provide a comprehensive analysis and provide a significant and valuable information base to aid and inform recovery processes.

3.2 Materials and Methodology

3.2.1 Materials

3.2.1.1 Chemicals and Reagents

All chemicals used in this work were of reagent grade and obtained from either Sigma-Aldrich (USA), VWR (USA) and Fisher Scientific (USA), Alfa Aesar (USA), Fluorochem (UK) and Agar scientific (UK). All the chemicals and reagents were used as received.

3.2.1.2 End-of-Life Mobile Phones (EoL-MPs)

At the start of the research an advert was prepared announcing the Mobile Phone Recycling Project and was displayed in the Department of Civil and Environmental Engineering at Imperial College London inviting staff and students to deposit old/spare mobile phones that were no longer in use (Figure 3.1). A total of 25 mobile phones were collected and from these, 15 mobile phones, representative of three generations of mobile phone from different brands and production years, were selected for detailed compositional analysis, namely: feature phones (F) – F1-F5 (Table 3.1), produced from before 2000 to 2015, multimedia phones (M) – M1-M5 (Table 3.2), produced between 2004 and 2010, and smartphones (S) – S1-S5 (Table 3.3), produced between 2009 and 2013.

Mobile Phone Recycling Project

Do you have any old/spare mobile phones at home?

A new research project is in progress to recover critical metals from mobile phones and we invite you to donate your old phones as feedstock for compositional analysis and recovery trials.

When? → From 22nd January, 2018

Where? → Leave your mobile phones in the Reception at the Skempton building (from 10.00 am to 17.30 pm, Monday to Friday)

The devices will be crushed and pulverised, so no personal information will be released. Please check that you have removed relevant parts (SIM, memory card, etc.).

KEEP CALM AND RECYCLE

If you have any queries please contact us at phoneman@ic.ac.uk

Imperial College London

Figure 3.1: Poster used for the collection of EoL-MPs.

Table 3.1: EoL Feature Phones utilised in this study.

Code	Manufacturer/model	Production year	Weigh [g]	Phone
F1	Motorola Sp	-	121.2	
F2	Nokia 3410	2002	108.1	
F3	Nokia 3510	2002	109.4	
F4	Samsung GT-E1270	2013	82.7	
F5	Nokia 105	2015	70.2	

Table 3.2: EoL Multimedia Phones utilised in this study.

Code	Manufacturer/model	Production year	Weigh [g]	Phone
M1	Motorola V547	2004	120.2	
M2	Nokia RM217	2007	91.4	
M3	LG KU990	2009	112.2	
M4	Samsung GT-S3100	2009	102.5	
M5	Nokia C5	2010	89.6	

Table 3.3: EoL Smartphones utilised in this study.

Code	Manufacturer/model	Production year	Weigh [g]	Phone
S1	IPhone 3GS	2009	135.4	
S2	Samsung GT-I9100	2011	116.2	
S3	Motorola XT910	2011	126.3	
S4	i-Phone 5S	2013	113.1	
S5	Samsung GT-I9500	2013	130.7	

3.2.2 Pre-treatment for Selection of Key Component Fractions for Analysis

The as-received mobile phones were separated into the three generations of phone type: feature phones (F), multimedia phones (M) and smartphones (S), and each set of phones was dismantled by hand and separated into five key components: (i) printed circuit boards (PCBs), (ii) screens, (iii) casings, (iv) electronics (cameras and speakers) and (v) batteries. Prior to detailed physical and chemical analysis, the component fractions, except batteries, which were removed and kept safely stored for a separate study, were shredded into pieces of approximately $1 \times 1 \text{ cm}^2$ using pliers, scissors and a Dremel (Dremel 8220-2/45, USA), and using a cryomill (Retsch CryoMill, Germany), were subjected to cryomilling in liquid nitrogen (freezing the samples at -196°C) for 15 min at 150 rpm in a closed system. The milled samples were sieved to a particle size $\leq 150 \text{ }\mu\text{m}$. This particle size was selected to permit complete metals liberation from the non-metallic and ceramic fractions, being more representative for a total metal analysis [96]. In the shredding and milling processes of WEEE in open systems, loss of precious metals can reach up to 40% in the form of metal fines and dust [94]. To permit a comprehensive metal characterisation and avoid loss of material, the cryomilling process was carried out in a closed vessel. In the shredding and milling processes, the material was weighed before and after each process, and mass losses were found to be $\leq 2 \text{ wt.}\%$. Figure 3.2 Illustrates the sequence of mechanical processes for the metal liberation of each component of EoL-MPs. Each key component fraction from the feature, multimedia and smartphones was weighed separately and the average of the fraction weights is presented later in this chapter (Figure 3.7, in Section 3.3.1) as G1 (average F1-F5), G2 (average M1-M5) and G3 (average S1-S5), where G denotes the generation of the mobile phones.

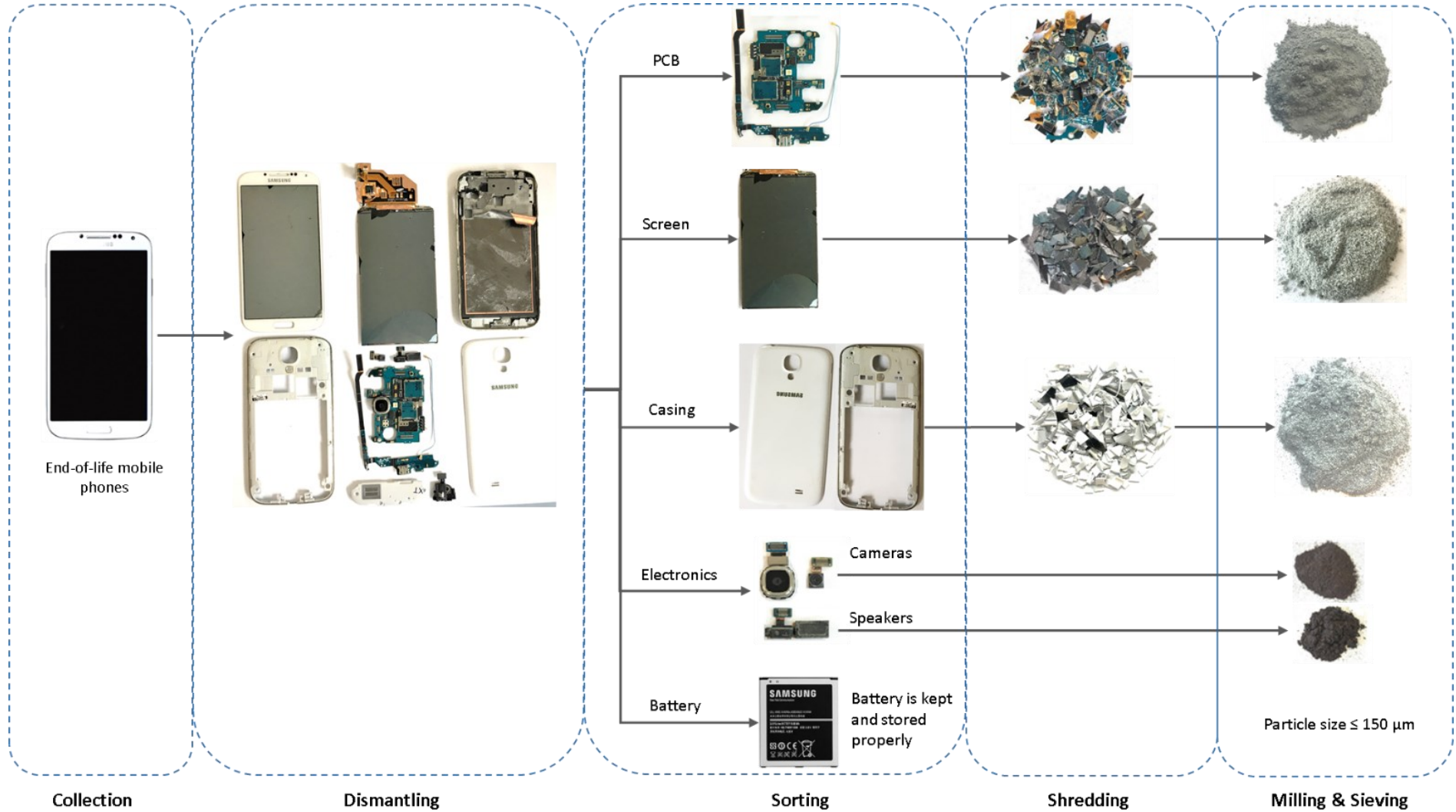


Figure 3.2: Flowsheet of processing methods and products obtained.

3.2.3 Analytical Techniques

To conduct a full characterisation of the five key component fractions of EoL-MPs a suite of analytical techniques is deployed. These include methods (as illustrated in Figure 3.3) to determine (i) the elemental composition using Inductively coupled plasma optical emission spectrometry (ICP-OES), Elemental Analysis, and Ion Chromatography (IC), (ii) the organic fraction using Thermogravimetric Analysis -Differential Scanning Calorimetry (TGA-DSC), and Fourier-transform infrared spectroscopy (FTIR), (iii) the morphology and phase distribution using Scanning Electron Microscopy with Energy Dispersive X-Ray Spectroscopy (SEM-EDS) for morphology, X-ray Diffraction (XRD) for Mineralogical composition (XRD), and a Malvern Particle Size Analyser for Particle size distribution, and (iv) the thermal properties using Bomb Calorimetry and Thermogravimetric Analysis -Differential Scanning Calorimetry (TGA-DSC)). Each of these methods is described in detail in the following sub-sections.

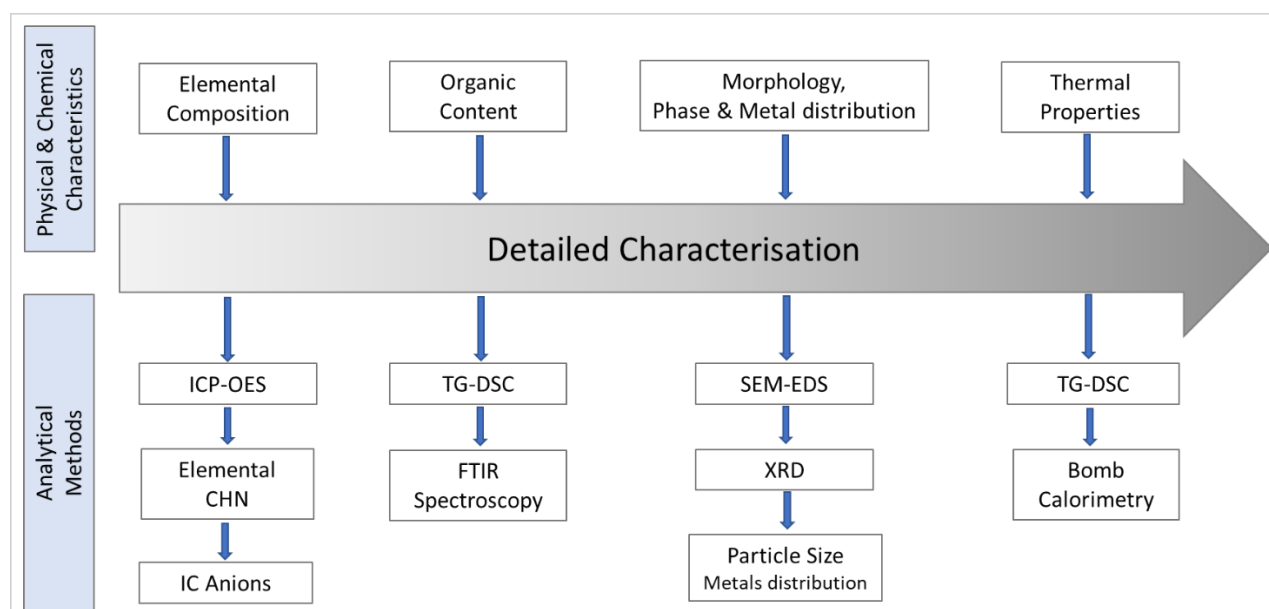


Figure 3.3: Methods used in the characterisation of EoL-MPs.

Elemental analysis of each generation of EoL-MPs was carried out in triplicate for *feature phones (F1-F5), multimedia phones (M1-M5), and smartphones (S1-S5)*, and the results averaged to provide an elemental concentration for each generation of phone recorded as G1, G2 and G3 respectively in Table 3.4 in Section 3.3.

3.2.3.1 Elemental Composition

Inductively coupled plasma optical emission spectrometry Inductively (ICP-OES)

ICP-OES is an analytical technique used to determine the concentration of certain elements contained in a sample based on atomic spectrometry. The ICP-OES principle uses the fact that atoms and ions can absorb energy to move electrons from the ground state to an excited state and those excited atoms release light at specific wavelengths as they transition to a lower energy level. ICP-OES converts a liquid sample into an aerosol by nebulisation with argon before it enters the plasma. The plasma at 10,000 Kelvin excites the atoms or ions that travel through it, enabling electrons to jump from a lower to higher energy level. Once the excited atoms or ions decay to their initial ground state, energy is emitted in the form of photons, which is measurable by the equipment. The amount of light released at each wavelength is proportional to the number of atoms or ions making the transition, thus the concentration of an element can be obtained using the Beer Lambert law, which describes the relationship between light intensity and element concentration by $A = \epsilon cl$, where A is the absorbance, ϵ is the molar absorption coefficient, l is the length of the cell and c is the concentration.

To calibrate an ICP-OES, solutions containing known amounts of each element are measured. From this data, a calibration curve is created, which determines the concentration of a specific element, by comparison, the sample with the calibration. In this study, elements and their concentrations were determined using a Perkin Optical Emission Spectrometer ICP-OES (PerkinElmer Avio™ 500, USA). Multi-element ICP standards ranging between 0.5 ppm and 100 ppm were prepared from different multi-element ICP standards. All calibration curves for metals had a correlation coefficient of $R^2 > 0.999$, with a total of 65 metals and metalloids analysed. Blanks and reagent solutions were prepared to provide a zero baseline and subtracted from the results. Quality control samples were prepared and checked every 10 to 15 samples in each run to guarantee the accuracy and quality of the results. Each sample was analysed in triplicate to ensure reproducibility and precision. Precision defined as relative standard deviation (RSD), was calculated as a percentage using the standard deviation divided by the mean of replicated samples [138, 139]. Precision and accuracy were satisfactorily obtained to be within <15% and 80–120% for all elements, respectively.

Sample preparation methodology for ICP-OES analysis is critical and depends on the sample to be analysed. In this research, two digestion methods were used: Aqua Regia Digestion (ARD) and Lithium Tetraborate Fusion (LTF). Three different spikes (blank, blank+spike, sample+spike) were used. The matrix spikes were deemed acceptable with a recovery of 85-115% and precision being <15%, and quality-assurance checks were made with every 15 samples. The element content in the blanks and reagent solutions were close to or below the detection limit, indicating a null contamination effect in

both digestion methods. Before the determination of elements, samples were roasted in a furnace (Gallenkamp Muffle Furnace, UK) at 600 °C for 1 hour to remove the polymer content which might still conceal the metallic fraction after the milling process, and to ensure a total separation of the polymer and metallic fractions. Before and after each experiment, all the equipment and apparatus used for the digestion methods (graphite crucibles, beakers, volumetric glasses, etc.) were decontaminated by immersing them in a 5% (v/v) nitric acid bath for 24 h, rinsed using reverse osmosis (RO) water and dried in an oven at 60°C for 3 h.

a) Aqua Regia Digestion (ARD)

In this method, an accurately weighed comminuted sample (of 0.1g) was leached with aqua regia (2mL conc. HNO₃ and 6mL conc. HCl). The solid/liquid ratio was set as 1/80 to achieve the total leaching of metals [47]. The leaching process was carried out on a block heater at a temperature of 90°C for 2 h without agitation. The sample was cooled to room temperature and transferred to a volumetric flask and made up to 25 mL with RO water.

b) Lithium Tetraborate Fusion (LTF)

An accurately weighed comminuted sample (0.1g) was poured into a graphite crucible and mixed with lithium tetraborate (0.5 g). The graphite crucibles were then heated to 1000 °C for 30 minutes. After 30 minutes, the molten mixture was poured immediately into a beaker to which was added nitric acid (50 mL, 5M), and stirred at 150 rpm for 2 hours to aid the dissolution [139]. The solution was then quantitatively transferred into a 250 mL volumetric flask and diluted with water.

Solutions obtained from both digestion methods (ARD and LTF) were separately filtered through a 0.45 µm pore diameter cellulose nitrate Millipore filter paper; the samples were then stored in a refrigerator (at 4°C) prior to analysis. A schematic flowchart of the sample preparation is illustrated in Figure 3.4.

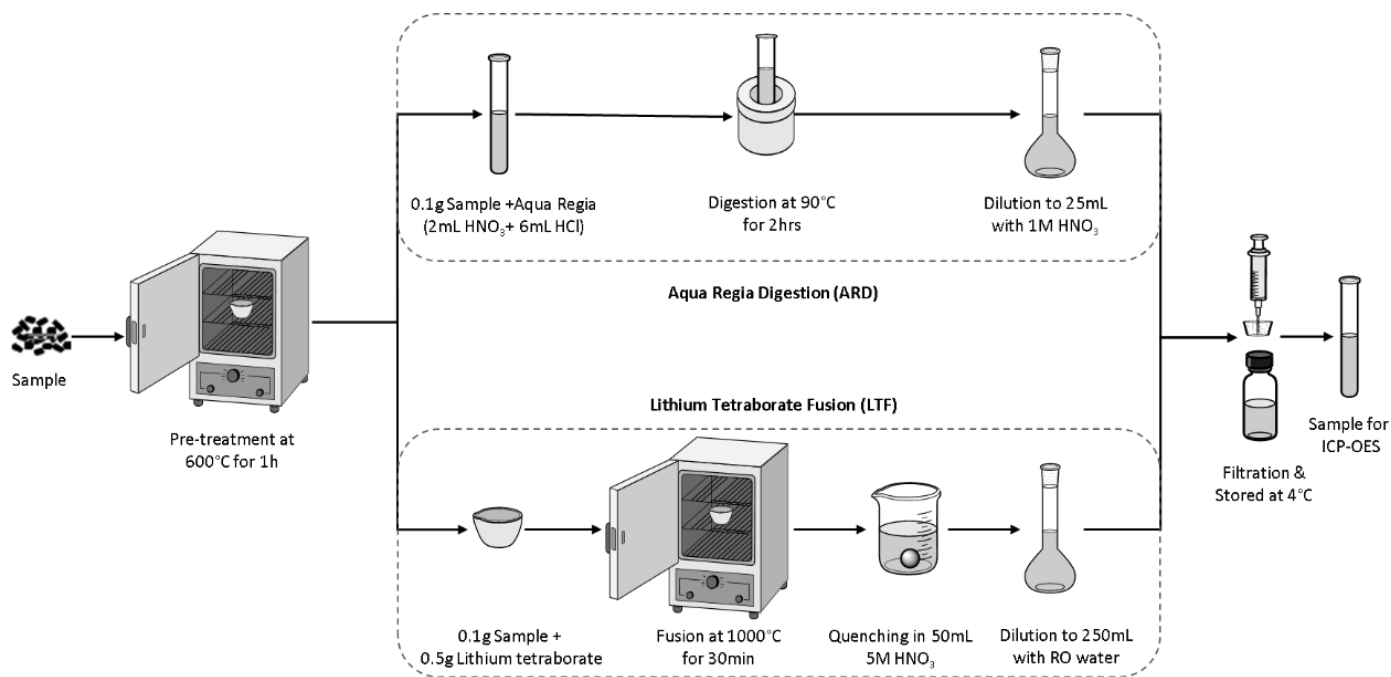


Figure 3.4: Schematic flowchart for sample preparation of ARD and LFT methods.

Elemental Analysis

Carbon, hydrogen, nitrogen, and sulfur content was determined using combustion analysis by MEDAC Ltd. (Surrey, UK). The analysis was carried out in a Flash EA 1112 Series CHNS-O Analyser using approximately 5 mg of each sample. The original analytical method is based on the complete and instantaneous oxidation of the sample by dynamic flash combustion which converts all organic and inorganic substances into combustion products. The resulting combustion gases pass through a reduction furnace and are carried into a chromatographic column by He carrier gas. In the column, the gases are separated and eluted as nitrogen, carbon dioxide, water, and sulfur dioxide, and detected by a thermal conductivity detector (TCD) which gives an output signal proportional to the concentration of the individual components of the mixture. The instrument is calibrated with the analysis of known standard compounds [140]. Each sample was analysed once. The oxygen content was estimated by the difference knowing the percentage C, H, N, and S content.

Ion Chromatography (IC)

Ion Chromatography is the separation and quantitative analysis of anions and cations in an ionic solution using ion exchange resins. The chromatographic process separates the different ions within the sample. The ions in the sample solution are carried through a column packed with an ion exchange resin (stationary phase) by an ionic solution, or eluent (mobile phase). Due to the interaction between the ionic species, coming from a sample, and the polar resin, the ionic species are separated

based on their affinity, species type and size. If cations are to be analysed, the active sites will have a fixed negative charge to attract the anions. Resins for anion analysis will have a positive charge. Individual ions attach and detach from the resin at a rate that depends on the affinity of the specific ion to the active sites. Ions with greater affinity for the stationary phase are retained in the column for a longer time than those with less affinity for the stationary phase. Thus, species in the solution exit or elute from the column at different time bands. At the end of the column, a detector continuously measures the conductivity of the eluent to determine the quantity of the eluting ions as a function of time. The data from the detector are compiled into a plot of ion abundance versus time, known as chromatogram. The position of a peak in the chromatogram is characteristic of a specific ion. Thus, comparing these peaks with different ionic standards solutions (with the ion species under study), the concentration can be determined as a function of the peak size in the obtained chromatogram.

A Dionex ICS-2100 ion chromatograph (Thermo Scientific, USA) was used to analyse the concentration of anions including fluoride, chloride, nitrite, bromide, nitrate and sulphate by ion chromatography (IC). Dionex AS19 2 mm Analytical Column with a Dionex AG19 4u 2 mm Guard Column was used as the ion exchange column. Calibration standards from 1 ppm to 500 ppm were prepared from either individual standards or made in the laboratory using salts of the interested anions. The mobile phase used was potassium hydroxide (KOH), and a gradient of KOH eluent of 10 nM to 45 nM was used, with a flow rate of 0.25 mL/min and an injection loop of 5.0 μ L. The typical backpressure of the pump was around 2,000 psi. A blank solution was analysed prior to any analysis and samples with and without spikes were run as quality control every 10 samples. The samples for the determination of bromide and chloride in the organic fraction from EoL-MPs were obtained by bomb calorimetry, as explained in section 3.2.3.40. Chromeleon 7 Chromatography Data System Software was used to collect and analyse the results.

3.2.3.2 Organic Content

Thermogravimetric Analysis -Differential Scanning Calorimetry (TGA-DSC)

Thermogravimetric analysis (TGA) is a method used for the characterisation of the thermal stability of materials and their fraction of volatiles over time by heating the sample at a constant rate in a selected atmosphere. In TGA, the weight loss of a sample in a particular atmosphere with respect to the temperature is measured over time. These measurements can indicate the phase changes including boiling points or decomposition points, oxidation, or dehydration of a sample. Differential scanning calorimetry (DSC) is technique that measures the difference in the amount of heat required to increase the temperature of a sample when compared with a reference (usually alumina), as a

function of temperature. This information can be used to determine physical (phase) and chemical (endo- or exo-thermic) changes of the sample during the heating process. Thus, TGA-DSC provides relevant information about the thermal behaviour and stability of a material and the different reactions that occur in different atmospheres.

TGA-DSC measurements were carried out using a Rheometric Scientific Simultaneous thermogravimetric-differential scanning calorimeter (STA-1500 Series, Austria). The sample, approximately 10-15 μg (depending on its density), is placed in an alumina crucible, and, is heated at a heating rate of 10°C/min under nitrogen atmosphere from room temperature (~25°C) until 1000 °C (in the case of ionic liquids, the temperature range up to 700 °C). Simultaneous data were recorded for TG and DSC at 5 second intervals.

Proximity analysis was carried out to determine the volatile matter, ash content and fixed carbon in the sample, as illustrated in Figure 3.5. For proximate analysis, a heating rate of 20 °C/min was chosen. The method used was as follows; the temperature was raised at a heating rate of 20 °C/min from the room temperature (25 °C) to 105 °C, where it was held for 5 min to remove the moisture completely. The temperature was then raised from 105 °C to 950 °C with a heating rate of 40 °C/min, held at this temperature isothermally for 20 minutes to remove the volatile matters completely. Finally, the combustion starts by manually switching the nitrogen gas (flow rate at 58 ml/min) to air (flow rate at 57 ml/min), and the final temperature (950 °C) was held for 20 min to allow complete combustion. The ash was calculated as the difference of the initial mass minus the moisture, volatile matter and fixed carbon.

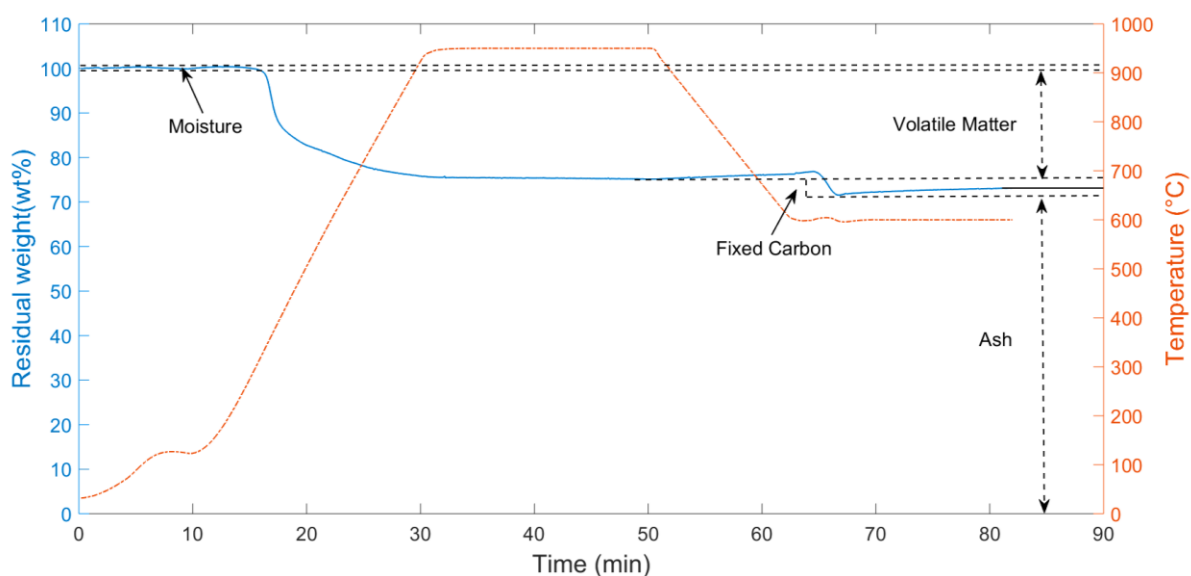


Figure 3.5: Proximity analysis of a feature mobile phone casing.

Fourier-transform infrared spectroscopy (FTIR)

Fourier transform infrared spectrometry (FTIR) is an analytical technique used to identify the presence of organic material in a sample. Samples are subjected to infrared (IR) radiation, inducing excitation in the molecules, causing them to vibrate, stretch and bend. Specific bond vibrations absorb IR radiation of a particular energy, with stretches occurring at higher wavenumbers (lower energy), and bends, at lower wavenumbers (higher energy). This technique measures the absorption of infrared radiation by the sample material versus wavelength, and the infrared absorption bands can be used to identify specific bonds, functional groups and structures. The region of an IR spectrum at the lowest wavelength (between 400 cm^{-1} and 1500 cm^{-1}) is known as the fingerprint region due to the presence of a large number of peaks, which makes it difficult to identify individual peaks, however, together they are characteristic and unique to a given compound. FTIR spectra are commonly used as a fingerprint for comparison with a reference spectrum, helping in the identification of contaminants or sample degradation of the sample shown by changes in the absorption peaks in the spectrum.

FTIR spectra were recorded on a FTIR spectroscopy (Nicolet Magna 560, USA) using a Quest single reflection germanium attenuated total reflection accessory. Transmittance data were collected within the range of 525 cm^{-1} to 4000 cm^{-1} , with a resolution of 4 cm^{-1} and 50 scans. A background spectrum was collected before each sample analysis. The peaks on the transmission FTIR spectra were identified using Thermo Scientific™ OMNIC™ FTIR Software.

3.2.3.3 Morphology, Phase & Metal Distribution

Morphology (SEM-EDS)

The morphology of samples is determined using Scanning Electron Microscopy (SEM) with Energy-Dispersive X-ray Spectroscopy (EDS). SEM is a method used to determine the morphology of samples, showing the contrast between organic and metallic materials, whereas EDS is a semi-quantitative elemental analysis used in specific locations. Essentially, an electron beam strikes the sample's surface, where the electrons within the atoms of this area are excited. Then, the electrons of these atoms return to their ground level state, emitting a characteristic x-ray. The beam swings across the sample causing some of the electrons to be reflected by the specimen and some to be absorbed. Specialized detectors receive these electrons and process the signal into a topographical micrograph of the sample. In the case of EDS, those same x-rays emitted by the electron beam are detected by an EDS x-ray detector, measuring the relative abundance of emitted x-rays versus their energy. When an incident x-ray strikes the detector, it creates a charge pulse that is proportional to the energy of the x-ray. This pulse is converted to a voltage pulse by a charge-sensitive preamplifier.

The signal is then sent to a multichannel analyser where the pulses are sorted by voltage followed by a software analysis to determine the elemental composition. A spectrum of x-ray energy versus voltage is generated, permitting the determination of the element composition of the area of sample under observation.

In this work, SEM-EDS was used to determine the morphology of samples and their elemental composition. SEM coupled with an EDS system makes it possible to show the element distribution, permitting the determination of the efficiency of mechanical release of the metal from the non-metallic fraction. Scanning electron microscope (Hitachi TM4000Plus, Japan) equipped with EDS (Oxford Instruments, UK) and a Back-Scattered Electrons (BSE) detector was utilised. Before sampling, all the samples were placed in an oven at 105 °C for 2 hours to ensure they were completely dry and oil-free to prevent contamination and potential damage to the equipment. The SEM images are presented with the magnification and the parameters used in the equipment recorded.

Mineralogical composition (XRD)

X-Ray diffraction (XRD) relies on the dual wave/particle nature of X-rays to obtain information about the atomic and molecular mineralogical composition of materials. Solids have a crystalline structure, which corresponds to a microscopic arrangement of atoms that is repeated periodically. By using X-rays directed to a sample, some rays are diffracted from the sample and collected by a detector at a particular angle and intensity. The scattering of the radiation produced by the sample creates a regular pattern due to the planes of the internal structure, and a 3-D structure can be generated. Based on the Bragg's law, the angle and intensity of the diffracted radiation (θ) depends upon the lattice spacing (d) of the sample and the wavelength of radiation (λ), based on the relationship $n\lambda = 2d\sin \theta$, where n is an integer.

The detector is moved around the sample to collect diffracted radiation at different angles to produce a plot of 2θ (the angle) vs intensity which is specific to that material. XRD was used to analyse and determine the mineralogical composition of samples. Crystalline phases present in the samples were determined by MiniFlex 600-C (Rigaku, Japan), which has a copper anode with a 1.540593 Å wavelength for $K\alpha$ and operates at a voltage of 40 kV and a current of 15 mA. The diffraction patterns obtained for the samples were compared with the equipment database and with patterns found in the literature.

Particle size distribution

Particle size distribution was measured using either a series of sieve shakers of varying mesh sizes or a particle analyser. For those samples with a size range above 150 μm , the proportion distribution was measured by weights of different fractions after screening the samples through sieves. More precise particle size data was achieved using a laser diffraction particle size analyser MasterSizer 3000 (Malvern, UK). The Mastersizer 3000 uses the technique of laser diffraction to measure the particle size and particle size distribution of materials. It does this by measuring the intensity of light scattered as a laser beam passes through a dispersed particulate sample. This data is then analysed to calculate the size of the particles that created the scattering pattern.

Sieves, with a mesh size of 150 μm to 2000 μm , were used. Sample dispersion for the MasterSizer 3000 was achieved by wet dispersion units using RO water as the distribution media. Pre-spreading of samples in a little RO water was done to ensure a stable state of particle dispersion in the measurement area of the optical bench. Both methods were utilised to classify the particle size and determine its elemental composition, and to determine the degree of metals liberation, confirmed by SEM-EDS.

3.2.3.4 Thermal Properties

Bomb Calorimetry

Bomb calorimetry is used to measure the thermal properties specifically the heat capacity or heat of chemical reaction as well as heat of physical changes of the material during combustion. The measurement is obtained by burning a representative sample in a high-pressure oxygen atmosphere under constant volume conditions within a metal pressure vessel, known as bomb or reaction chamber. The vessel is immersed in a stirred water bath to stabilise the water temperature. After the temperature has been stabilised the reaction, within the vessel, is initiated by discharging a capacitor through thin wires which are connected to the sample which is then ignited. The energy released by this combustion is absorbed by the surrounding water and the resulting change in temperature within the absorbing medium is noted, and the heat released by combustion of the sample is calculated. The calorimeter is designed to be isolated from the surroundings, therefore there is not heat loss.

A Bomb Calorimeter (Parr 6100, USA) was utilised to determine the High Heating Value (HHV), also known as gross calorific value or gross energy. The powder samples were compressed into pellets for use in the bomb calorimeter. The HHV of the samples were determined placing 0.5-1 g of sample in a metallic vessel. In samples with incomplete combustion, the HHV determination was aid with benzoic tablets (1.0 g) to facilitate complete combustion. The tablets were placed in the vessel and the samples were placed on the tablets. Benzoic acid is used due to its constant calorific value (26.454 KJ/g) and it is also utilised for the calibration of the bomb. Triplicate measurements were made for each sample.

A bomb calorimeter was used to determine bromide and chloride species in the plastic components of the EoL-MPs, applying the test method 5050 from the United States Environmental Protection Agency (EPA) for the determination of total chloride in solid waste and liquid fuel [26]. The method involves oxidising the sample in a calorimeter and collecting the gases generated (HCl and HBr) in a 0.25 M NaOH basic solution placed with the sample inside the bomb calorimeter [141]. In this study, 0.10 g of samples was placed in a bomb calorimeter with 10 ml of 0.025 M sodium bicarbonate/sodium carbonate ($\text{NaHCO}_3/\text{NaCO}_3$) solution to capture the acid gases generated by combustion. After the combustion, 10 mL of solution was captured from within the bomb calorimeter, was diluted to 1L, and analysed by ionic chromatography to determine the chloride and bromide contents.

3.3 Results and Discussion

Detailed characterisation of three generations of mobile phones is described in terms of (i) the physical classification of key components of mobile phones, (ii) characterisation of the metallic and non-metallic fractions, and (iii) interpretation of the data in terms of potential for mobile phones as a source of energy and material recovery or recycle.

3.3.1 Key Component Fractions of EoL-Mobile Phones

3.3.1.1 Key Component Distribution in EoL-MPs

End-of-life mobile phones (EoL-MPs) were classified into three groups: feature phones (with no operating system, touchscreens and third-party applications), multimedia phones (with operating system, touchscreen, but no third-party applications) and smartphones (with highly responsive touchscreen, robust operating system and third-party applications) [38]. The dismantling of a typical multimedia phone, as shown in Figure 3.6, revealed that mobile phones comprise at least 14 components, most of which are made up of a large variety of materials such as plastics, metals, ceramics, and other substances. In general, material locked through fastening by screws, clinks, and rivets, etc., can be easily removed, however, there are materials locked by means of welding, alloying, filling, binding, and coating which are difficult or impossible to separate by mechanical means. Furthermore, it was observed that components in mobile phones were not designed for easy and rapid disassembly, so careful manual disassembly was essential for the effective separation of their components. These components can be classified based on their properties and characteristics as *mechanical components* (supporting structure of the mobile phone, frames, keypad, and buttons), *electromechanical components* (LCD screen, speakers, vibration motor, keypad assembly, and other small components), *electronic components* (PCB assemblies and cameras), and *others*, which include batteries and chargers. If all the components are unlocked, between 50 and 100 constituent parts can be found. This number of components varies largely depending on the year of production, producer, and mobile phone generation.

Due to the large number and variety of mobile phone parts, the components were grouped into five key categories for characterisation: *printed circuits boards* (PCBs), *screens*, *casings*, *electronics* (cameras and speakers) and *batteries*. Following manual disassembly and separation each component was weighed and the proportion of mobile phone weight (averaged within a generation type) contributed by each category was determined and presented in Figure 3.7. PCBs in EoL-MPs showed small differences in their weight percentage across the generations, representing between 17% and 20% of the total weight. Screens, however, were the component that unsurprisingly showed the

largest increase in mass fraction through the generations, from 5% and 7% in feature and multimedia phones to 28% in smartphones. The presence of large touchable screen in smartphones has become one of the most important characteristics for consumers' use. Casings in feature phones represented 43% of the total mobile phone weight and 52% in multimedia phones but showed a marked reduction to about 25% in smartphones. Batteries weighed 26 wt.% on average in a feature phone and reduced to 19 wt.% in multimedia phones. The multimedia phone had a smaller and thinner battery, which usually covered half of the device (Figure 3.6). Although batteries in smartphones were thin, the weight percentage of these batteries was higher at 26% of the total weight of a smartphone. The weight of the electronics component showed little variation across the generations representing approximately 1-2% of the total weight, and the other components (plastic keyboard, buttons, etc.) also contributed little to the overall weight but had decreased through the generations, to the smartphone in which there is an increased integration of circuits and components embedded in the phone. In summary, on average (Figure 3.7b), the weight of components in a mobile phone, was dominated by casings (39%), with the other components decreasing in the order: batteries (24 wt.%) > PCBs (18 wt.%) > screens (15 wt.%) > others (3 wt.%) > electronics (1 wt.%).

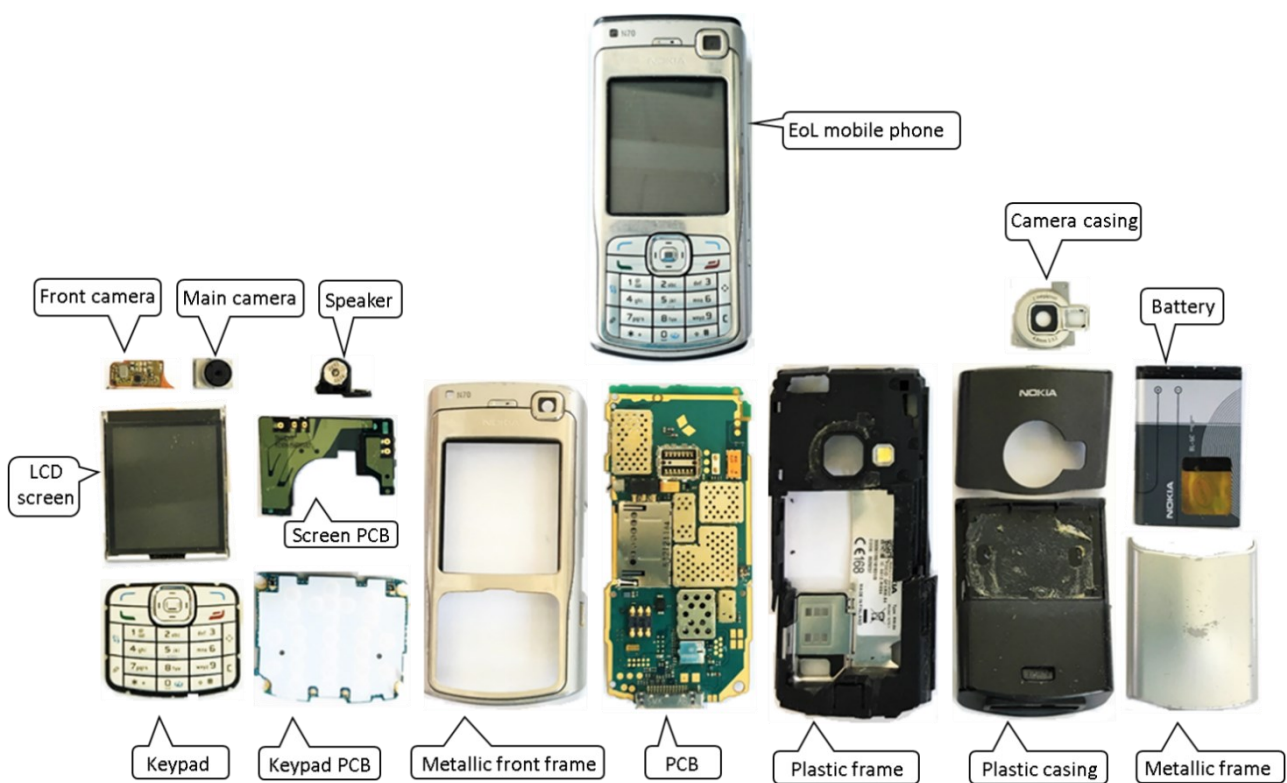


Figure 3.6: Main components of a mobile phone (Nokia N70).

The average metal, non-metal and ceramic content in multigenerational EoL-MPs, derived from this work is shown in Figure 3.8. In general, it was found that an average mobile phone contains approximately 40% plastics, 35% metals and metalloids, and the remaining 25% as ceramics and glass. In terms of metal content, batteries (Li-ion) comprising cathodes, anodes, electrolyte plastic separators and metal cases, as expected, account for the largest fraction, followed by speakers, PCBs and cameras with 47 wt.%, 43 wt.% and 25 wt.%, respectively, and screens with only about 5 wt.%. The high fraction of ceramics and glass in screens come from the LCD displays, where its main material is glass, accounting for nearly 50% of the total weight. The other components in screens are connectors, adhesives, diffusive and reflective sheets, polarizing films and plastic frames [142]. The total metal content was determined as the sum of all the metals analysed and reported in detail for the metallic and non-metallic elements in section 3.3.2

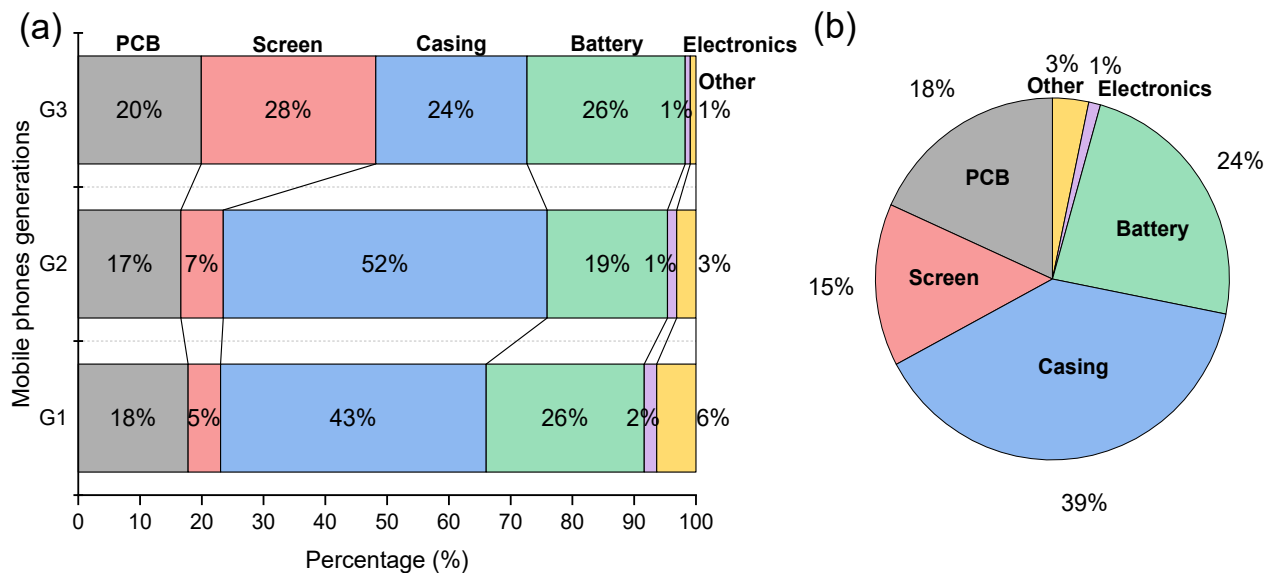


Figure 3.7: Average mass fraction (wt. %) of components of EoL-MPs by (a) by generations and (b) on average.

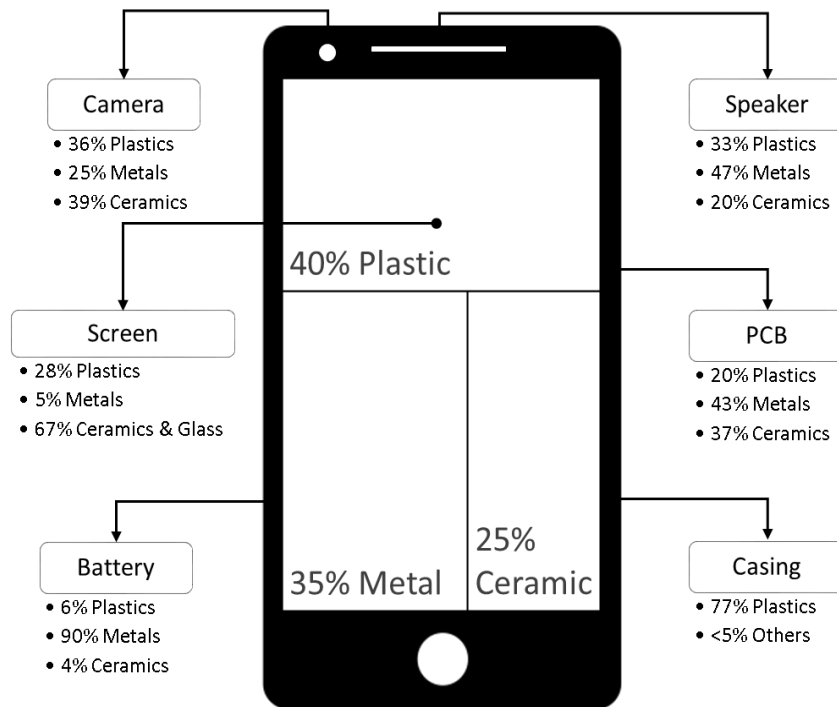


Figure 3.8: Average material composition of mobile phones.

3.3.1.2 Pre-treatment for Analysis

The mobile phone has a complex and heterogeneous material composition and representative analysis requires adequate separation of the metallic and non-metallic fractions to determine the elemental composition and concentration. The degree of liberation is critical as it indicates how much of a target element is liberated from the non-valuable components. Efficient metal liberation is crucial for a detailed characterisation of the metallic and non-metallic fractions, as incomplete metal liberation from e-waste is the key reason for resource loss.

A preliminary comminution step was carried out on PCBs using hammer milling to produce an optimal particle size for metal liberation. Figure 3.9 shows the particles obtained after milling: with the size fraction of $\leq 150 \mu\text{m}$ in powder form, the fraction from $150 \mu\text{m}$ to $710 \mu\text{m}$, appearing acicular, and the fraction above $710 \mu\text{m}$, as flakes. ICP-OES analysis showed that the smallest fraction ($\leq 150 \mu\text{m}$) presented the optimum metal liberation based on the metal content of 42%, 38%, and 35% for $< 150 \mu\text{m}$, $110\text{-}710 \mu\text{m}$, and $> 710 \mu\text{m}$ samples respectively. This preliminary step revealed that hammer milling and ball milling generated a large amount of dust and by weighing the samples before and after the shredding process, a material loss of approximately 15% was observed. To avoid material losses and to permit full metal characterisation of the samples, cryomilling was conducted in a closed system prior to analysis.



Figure 3.9: PCB samples obtained after milling; (a) $\leq 150 \mu\text{m}$, (b) $150\text{-}710 \mu\text{m}$, (c) $710\text{-}2000 \mu\text{m}$.

To ensure that the smallest fraction effectively releases the metallic fraction, liberation assessment was qualitatively achieved using the scanning electron microscope coupled with X-ray microanalysis by energy dispersion system (SEM-EDS) images, as shown in Figure 3.10. The morphology showed that the metallic particles were presented in very random sizes and shapes. It can also be observed that most of metals were unlocked in all the components from the non-metallic fraction. Casings are not shown due to their low metal content. With the aid of EDS analysis, the composition of the different particles was determined. In PCBs (Figure 3.10a), the acicular particles were found to be glass fibres attributed to the high proportion of Si, used to reinforce and insulate PCBs. Copper particles, observed as layered flakes, and particles of Fe, Ti, Ba, and Pb, observed in spherical shapes were well separated from the non-metallic fraction. Carbon was observed at sites away from the metal concentrations, and in some cases linked to Br or Cl elements, likely coming from halogenated flame retardants, indicating an effective metallic and non-metallic separation. In the case of screens (Figure 3.10b), particles showed a high purity composition of silicon and metallic elements such as Al and Mg, suggesting that metal liberation was effectively achieved. Mobile phone screens particles were smaller and generally more homogeneous in sizes and shapes, than the particles of the other mobile phones components. This is likely due to the high glass content in screens, a brittle material, which facilitates a fast and more homogenous comminution. In the case of cameras and speakers, Figure 3.10c and Figure 3.10d, respectively, there was good evidence of liberation of the metallic from the non-metallic fraction. Although in some cases some metallic particles coexisted with other metals, consistent with, alloy fractions, namely Al-Si and Ba-Ti alloys found in cameras. Characteristic of the speakers was the predominance of neodymium and iron derived from magnets. The SEM-EDS data confirm effective liberation of the metal fraction from the non-metallic fraction.

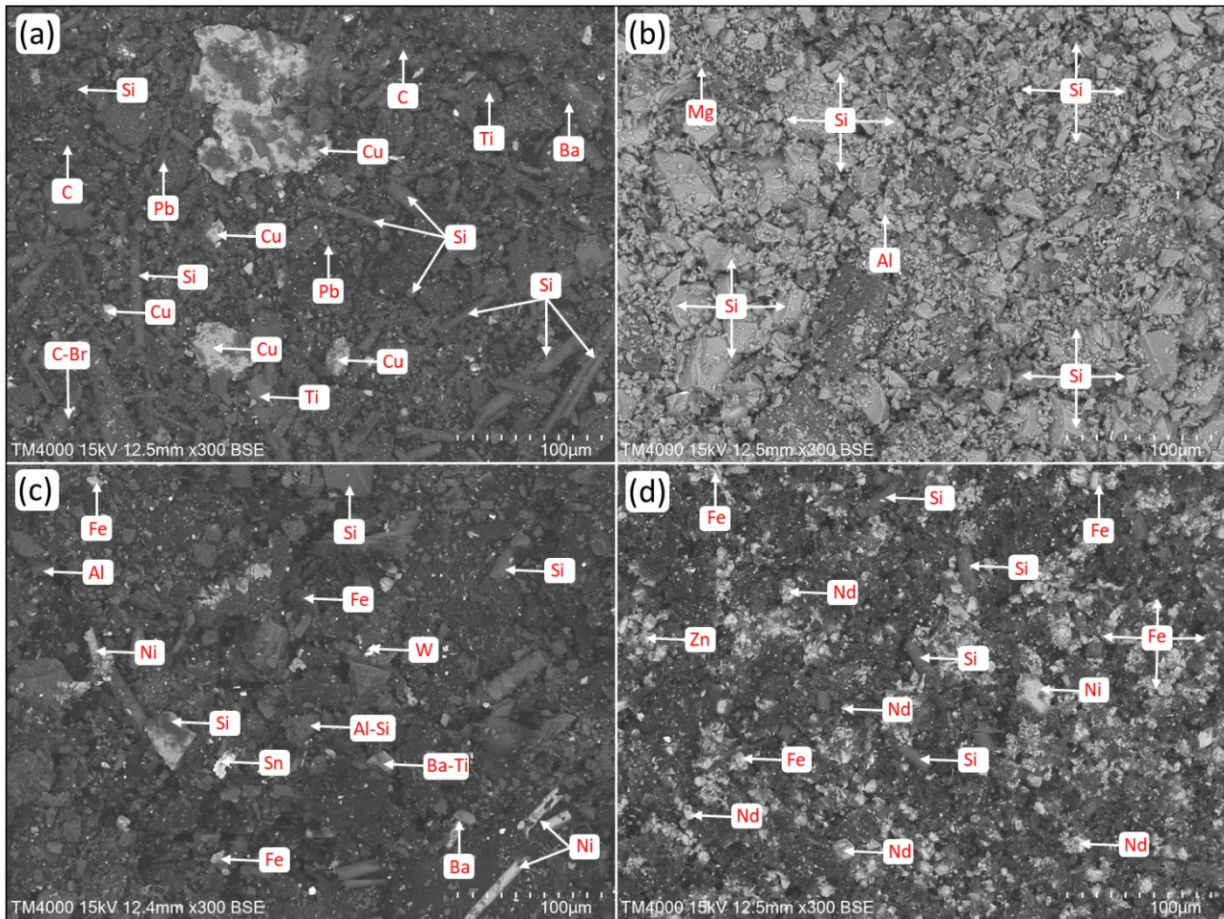


Figure 3.10: BSE-EDS images of comminution fines after cryomilling ($\leq 150 \mu\text{m}$); a) PCBs, b) screens, c) cameras and d) speakers.

3.3.1.3 Discussion

The average weight distribution of PCBs (18%), screens (15%), casings (39%), batteries (24%), electronics (1%) and other (3%) found in this study (Figure 3.7b) is in good agreement with data reported by Tan and Palmieri where PCB accounts for 18%, screen for 8%, plastic for 26% (primarily from casings), and batteries for 21% of the total weight [38]. Elsewhere Palmieri et al. reported similar results with a distribution of 19%, 2%, 26% and 27% by weight for PCBs, screens, frames and batteries, respectively [143]. The only substantial difference was the weight distribution of screens; a difference explained because as the authors utilised feature and multimedia phones in their characterisations, but in this study the characterisation was made using an equivalent amount of feature, multimedia and smartphones, providing a more representative sample. This is corroborated with the data in Figure 3.7a, where excluding the weight attributed to the smartphone fraction, shows the average proportion of weighted screens from feature and multimedia phones alone were 5 wt.% and 7 wt.%,

respectively, consistent with small display screens. The notable increase in screen sizes of smartphones, accounts for more than a quarter of the total weight.

Regarding metal liberation from the non-metallic fraction, extensive studies have focussed on the metal liberation from waste printed circuit boards (WPCBs) as a function of different particles sizes [92, 144-146]. Size reduction that involves crushing, grinding, or shearing is generically referred to as '*shredding*'. Metals in PCBs can be difficult to liberate from non-metals; however, in the fraction of 0.3-1 mm, almost all the metals can achieve complete liberation [144]. Yoo et al. investigated the structural features of PCB scraps before and after mechanical treatments with SEM images. The results indicated that metals could be separated from the non-metallic components if the particle size was below 1.2 mm [92]. Zhao et al. treated WPCBs with a high-speed pulveriser, finding that metals and polymers could be completely separated when the particle size was less than 450 μm [146]. The differences in the optimal particles sizes found by authors differ due to the fact that mechanical comminution is a technology created for reducing the dimensions of ore aggregates, being natural ores fragile or brittle, and the liberation occurs as a side effect [144]. Thus, metal liberation can occur at different particles sizes, depending on the comminution process applied and the material being shredded. The mechanism of the comminution process in WEEE is typically by means of impact, with shear, compression, abrasion or a combination [145]. In this study, it was found that the smaller the particle size, the better metal liberation, with almost complete metal liberation achieved with a particle size of $\leq 150 \mu\text{m}$. Although unliberated composites were observed in SEM-EDS images, they were found to be minimal, suggesting an excellent metal liberation for elemental analysis. It is worth mentioning that the objective in this work is to effectively separate the metallic and non-metallic fraction, without considering the energy utilised. It is acknowledged that the smaller the particle size, the more energy is needed. Thus, for an optimal metal recovery, the energy used for shredding would need to be considered.

3.3.2 Characterisation of the Metallic Fraction

In this section, detailed characterisation of the metal and metalloid content in PCBs, screens, cameras and speakers for multigenerational EoL-MPs is described and a comprehensive analysis is presented in Table 3.4. The data are reported as averages of triplicate measurements for each metal/metalloid in each component fraction. The reported metals and metalloids are classified as base metals (BM), precious metals group (PMG), rare earth elements (REEs, where L and H refer respectively to light and heavy elements), critical raw materials (CRMs), hazardous substances (HS) which refers to those metals classified as hazardous metals according to the RoHS Directive [147] and other metals (OMs). Each component of the mobile phone was analysed separately, but for presentational purposes and ease of interpretation, their concentrations are expressed as average concentrations for each generation of phone: as G1 (feature phones), G2 (multimedia phones), and G3 (smartphones). The characterisation of the metallic fraction showed that 63 metal and metalloid elements are present in EoL-MPs. Figure 3.11 illustrates the average metal and metalloid concentration in EoL-MPs (average elemental concentration per mobile phone unit).

Table 3.4: Metal and metalloid composition of PCBs, screens, cameras and speakers from feature, multimedia and smart phones.

		PCBs			Screens			Cameras			Speakers			Detection limit (mg/L)	
	Element	G1	G2	G3	G1	G2	G3	G1	G2	G3	G1	G2	G3		
<i>BM</i> (wt.% for PCBs and Screens, mg/g for Cameras and speakers)	Cu	21.8	29.5	32.2	3.0	18.1	5.4	120.8	92.6	112.4	126.2	21.8	100.1	8.6x10 ⁻³	
	Al	2.2	2.9	2.3	16.7	16.7	27.1	7.6	9.3	7.0	84.0	7.3	8.5	8.8x10 ⁻³	
	Ba	1.8	2.1	3.0	8.0	2.5	0.5	10.3	12.4	14.9	5.7	0.3	0.5	1.0x10 ⁻³	
	Ni	1.1	1.7	3.2	1.1	1.8	0.7	19.7	16.3	20.1	4.3	21.8	17.4	3.4x10 ⁻³	
	Sn	0.2	1.2	3.1	0.4	0.9	0.3	1.8	3.2	10.2	24.3	7.1	6.3	4.2x10 ⁻³	
	Fe	0.5	0.9	2.5	1.7	2.5	1.1	20.1	25.0	62.6	113.0	186.3	133.4	2.8x10 ⁻³	
	Zn	0.2	0.5	0.8	0.0	0.1	0.0	8.5	0.8	3.1	19.0	7.5	11.5	9.0x10 ⁻⁴	
	B	0.4	0.4	0.3	5.1	5.2	4.8	2.4	2.8	1.4	<DL	<DL	<DL	2.2x10 ⁻²	
	Ti	0.3	0.3	0.5	0.4	0.5	0.1	1.4	1.1	2.0	1.1	0.1	<DL	6.0x10 ⁻⁴	
	Ca	2.3	2.0	1.1	0.5	0.5	0.2	0.7	1.0	1.0	1.2	0.7	0.8	4.1x10 ⁻³	
<i>PMG</i> (ppm)	Ag	1095.1	1246.7	1611.1	35.4	122.9	85.6	<DL	689.4	890.3	1755.3	245.4	114.6	2.1x10 ⁻³	
	Au	502.1	588.2	765.4	64.3	45.9	15.7	1668.2	954.2	1040.4	65.3	83.0	79.2	2.9x10 ⁻³	
	Pd	106.7	109.1	85.8	0.7	2.7	2.2	8.9	15.6	<DL	<DL	<DL	<DL	5.8x10 ⁻³	
	Pt	26.4	29.4	59.2	9.8	14.4	21.3	33.5	23.0	75.6	78.3	93.2	57.6	1.0x10 ⁻²	
	Re	3.4	4.1	6.0	0.5	0.7	<DL	4.2	<DL	20.5	85.6	120.3	90.5	4.0x10 ⁻³	
	Rh	<DL	<DL	<DL	<DL	<DL	<DL	<DL	<DL	<DL	<DL	51.7	30.5	52.7	1.0x10 ⁻²
	Ru	<DL	<DL	<DL	<DL	<DL	<DL	<DL	<DL	<DL	<DL	<DL	<DL	<DL	2.0x10 ⁻³
<i>LREE</i> (ppm)	Sc	3.8	4.9	5.1	<DL	0.2	<DL	1.7	5.4	10.1	24.1	38.2	34.3	1.0x10 ⁻⁴	
	La	439.5	61.0	4.7	0.4	0.3	0.5	1.7	998.4	75.1	145.5	240.5	214.3	9.0x10 ⁻⁴	
	Ce	9.9	2.5	<DL	0.7	0.1	<DL	<DL	<DL	<DL	<DL	<DL	<DL	7.6x10 ⁻³	
	Pr	130.0	114.9	64.8	<DL	3.0	3.6	25.8	592.1	3468.4	12175.8	12435.8	8820.7	4.9x10 ⁻³	
	Nd	1657.5	1627.9	982.6	3.0	28.3	12.3	141.3	7731.5	31498.3	73264.7	97525.5	85449.4	8.0x10 ⁻³	
	Sm	20.8	18.4	12.1	<DL	<DL	<DL	7.2	158.1	561.5	1230.4	1884.1	1800.4	2.7x10 ⁻³	
	Eu	2.3	2.1	0.7	0.4	0.3	<DL	1.7	5.4	10.1	136.2	232.6	198.8	4.0x10 ⁻⁴	

<i>HREE</i> (ppm)	Y	28.7	17.1	20.1	0.7	2.0	1.3	4.7	258.5	5.7	7.9	3.6	3.6	4.0x10 ⁻⁴
	Gd	9.5	56.3	45.9	4.1	6.5	2.6	135.3	31.6	17.6	232.7	54.6	181.3	2.3x10 ⁻³
	Tb	10.0	50.3	3.7	0.6	0.6	0.4	<DL	8.0	224.5	193.3	1577.6	48.6	4.0x10 ⁻³
	Dy	46.4	91.1	125.7	0.2	9.0	1.8	24.4	572.4	1826.0	3159.8	8251.5	5642.0	1.2x10 ⁻³
	Ho	13.5	4.2	<DL	<DL	<DL	<DL	<DL	<DL	<DL	94.1	55.9	38.4	1.3x10 ⁻³
	Er	7857.8	7977.6	11731.1	954.3	1185.3	206.3	3499.2	2654.4	4599.6	136.2	232.6	198.8	3.3x10 ⁻³
	Tm	<DL	<DL	<DL	<DL	<DL	<DL	<DL	<DL	11.5	28.2	44.1	28.6	7.0x10 ⁻⁴
	Yb	0.6	0.5	1.4	0.1	0.1	0.1	0.3	2.1	8.9	22.3	36.4	29.4	2.0x10 ⁻⁴
	Lu	0.4	0.1	1.0	<DL	0.1	<DL	0.5	8.9	3.8	0.3	2.4	5.5	2.0x10 ⁻⁴
<i>CRM</i> (ppm)	In	<DL	<DL	<DL	190.0	262.5	64.9	<DL	<DL	<DL	<DL	<DL	<DL	2.5x10 ⁻²
	Ga	74.4	149.0	248.8	5.0	6.9	5.1	25.9	242.3	1317.1	4196.3	4684.3	3468.6	5.3x10 ⁻³
	Ge*	100.3	164.4	222.7	8.8	11.8	10.2	40.6	<DL	<DL	50.5	<DL	<DL	2.3x10 ⁻²
	Co	136.4	92.7	51.4	2.2	3.3	0.8	58.3	165.9	1091.5	<DL	<DL	<DL	1.0x10 ⁻³
	Hf	8.1	11.8	15.0	0.7	1.6	0.7	35.6	13.1	5.2	<DL	<DL	<DL	2.0x10 ⁻³
	Be	<DL	<DL	<DL	<DL	<DL	<DL	<DL	37.0	<DL	1.0	4.0	2.2	1.0x10 ⁻⁴
	Sb*	103.8	78.4	<DL	16.6	16.2	42.4	86.4	<DL	<DL	<DL	85.7	1595.1	1.2x10 ⁻²
	Mg	1421.2	1535.7	3967.0	1309.6	2193.4	3250.1	1352.5	1961.0	8741.5	838.3	365.1	465.2	1.1x10 ⁻³
	Nb	98.8	60.3	64.3	10.0	4.8	11.1	44.2	108.8	22.6	96.7	109.8	80.7	1.1x10 ⁻²
	W	110.0	141.9	702.1	5.9	32.0	7.2	160.1	6247.6	1926.2	215.5	140.0	1707.2	1.1x10 ⁻²
	Bi	<DL	<DL	<DL	<DL	<DL	<DL	<DL	351.0	<DL	<DL	<DL	<DL	8.9x10 ⁻³
	Ta	94.5	125.6	143.3	4.0	8.9	2.5	49.5	95.0	72.7	87.8	94.0	92.4	1.5x10 ⁻²
	V	7.1	11.5	18.4	0.4	2.8	11.2	25.3	ULD	1.1	4.7	11.4	3.7	1.9x10 ⁻³
<i>HS</i> (ppm)	Cd	0.8	4.4	4.9	1.0	0.1	<DL	<DL	<DL	<DL	<DL	<DL	<DL	8.0x10 ⁻⁴
	Pb	7304.2	999.3	469.1	35.0	77.1	2.0	108.5	3066.2	295.5	629.0	1163.5	2834.4	7.7x10 ⁻³
	Hg	<DL	<DL	<DL	<DL	<DL	<DL	<DL	<DL	<DL	<DL	<DL	<DL	2.5x10 ⁻³
<i>OM</i> (ppm)	As*	63.6	114.2	172.4	400.6	205.8	<DL	66.9	97.5	13.2	20.8	18.9	20.6	1.2x10 ⁻²
	Cr	133.0	104.6	1017.3	83.2	124.7	53.9	2817.1	790.3	250.1	113.3	228.7	101.0	1.3x10 ⁻³
	U	678.5	1223.1	3575.5	242.3	351.8	140.3	2845.1	3854.0	10436.8	22882.7	45894.9	29113.7	5.1x10 ⁻³

K	150.2	150.5	193.5	174.8	175.0	1883.2	297.9	1220.1	1012.0	84.1	23.0	148.0	1.8x10 ⁻³
Na	951.5	848.7	846.8	2974.7	1298.1	12839.3	2090.5	5073.6	4224.2	649.3	533.4	554.4	3.5x10 ⁻³
Li	31.2	30.3	24.3	0.8	1.1	0.9	7.0	371.1	<DL	9.0	11.6	5.8	1.0x10 ⁻⁴
Sr	743.3	1002.8	628.1	<DL	<DL	<DL	474.0	529.2	<DL	205.0	128.5	134.2	2.0x10 ⁻⁴
Mo	53.0	28.2	73.8	41.0	24.5	69.3	155.4	607.2	343.8	69.9	118.2	106.9	1.1x10 ⁻³
Zr	497.3	749.1	448.5	14.3	33.2	28.5	42.7	371.2	33.5	150.2	141.5	36.6	8.0x10 ⁻⁴
Te*	208.4	247.6	259.8	12.1	15.3	22.2	47.7	58.6	95.4	234.0	238.4	162.7	1.2x10 ⁻²
Mn	1106.9	269.0	533.5	16.1	24.8	9.3	333.7	189.2	100.1	130.5	330.1	215.8	2.0x10 ⁻⁴
Tl	<DL	<DL	<DL	<DL	<DL	<DL	74.1	741.2	215.7	16.0	18.6	164.2	1.7x10 ⁻²
Ir	<DL	<DL	<DL	<DL	<DL	<DL	<DL	<DL	<DL	1077.1	<DL	<DL	1.4x10 ⁻¹
Rb	<DL	<DL	<DL	<DL	<DL	<DL	<DL	<DL	<DL	<DL	<DL	<DL	2.8x10 ⁻²
Se	<DL	<DL	<DL	<DL	<DL	<DL	<DL	93.3	<DL	<DL	<DL	<DL	2.9x10 ⁻²
Total* (wt.%)	33.5	43.6	51.9	4.8	5.9	4.8	21.6	21.5	31.8	52.2	44.5	43.6	
Average (wt.%)		43.0			5.2			25.0			47.0		

G1, G2, and G3 stand for feature, multimedia and smartphones, respectively, also known as generation 1, 2, and 3.

<DL: Below detection limit.

*: Metalloid.

+: The total metallic fraction is the addition of all the metals analysed.

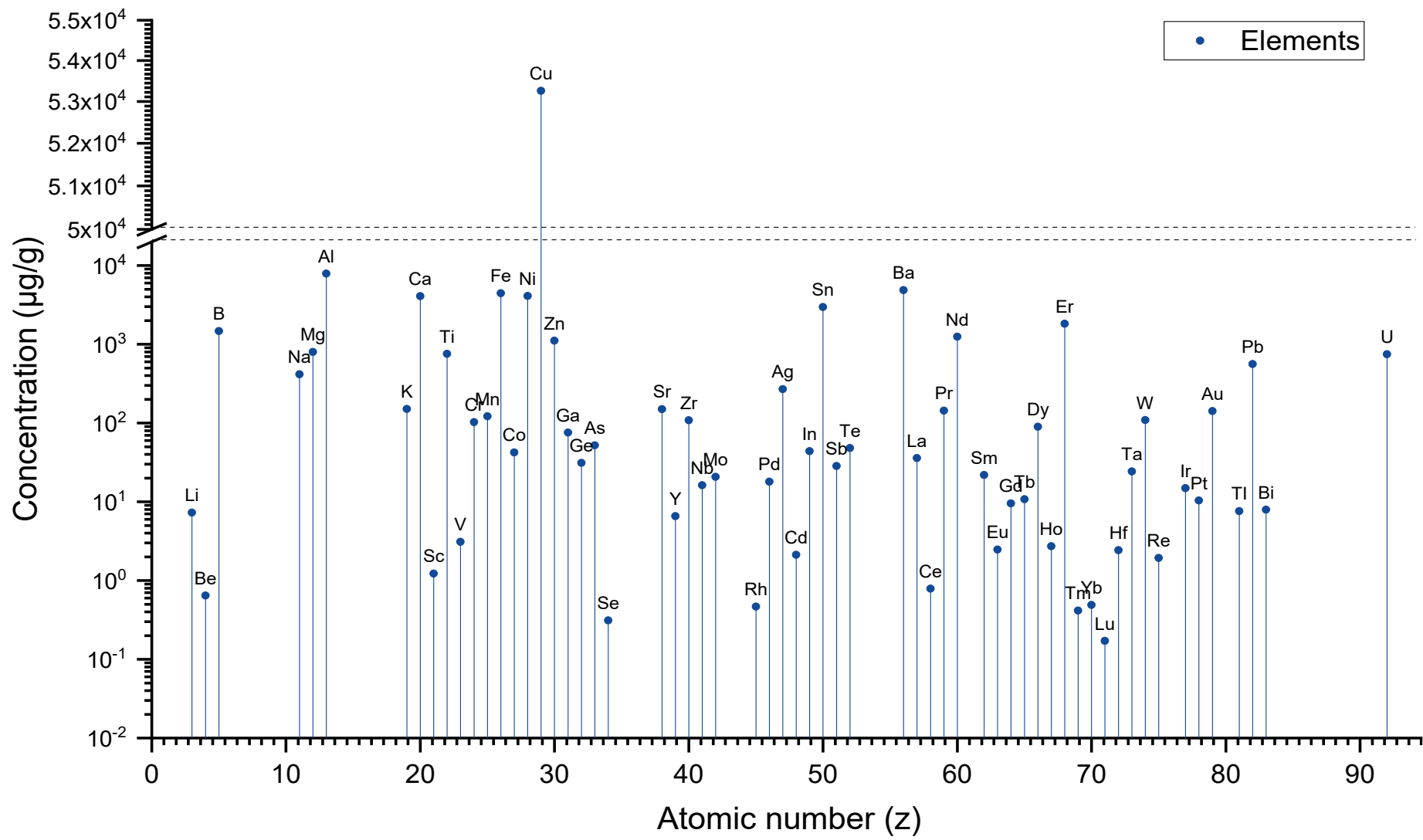


Figure 3.11: Average metal and metalloid concentrations per EoL mobile phone unit.

3.3.2.1 Printed Circuit Boards (PCBs)

Results in Table 3.4 show the main metal present in mobile phone PCBs to be copper with an average of 27.8 wt.%, which represents almost 65% of the total metallic content by weight. This high level of copper in PCBs is due to a typical mobile phone PCB (FR-4 type) composed of a multilayer of epoxy resin, fiberglass, and copper layers, which give the PCB its conductive properties [12, 96]. The cross-section of a PCB detected using BSE-EDS (Figure 3.12a) and its reconstruction (Figure 3.12b) confirm the high levels of copper found, which are used as conductive layers in PCBs. Silicon and aluminium are also observed, residing in the long acicular shape which represents the fiberglass, which is used as a reinforcement material in PCBs. Pb-Sn alloy was observed on the PCB surface, consistent with its use as solder. The darker layers in Figure 3.12a are mainly composed of carbon and oxygen, confirming the polymeric layers of epoxy resins. These observations suggest that copper, lead, and tin are the key metals present within the PCBs and the other metals found (Table 3.4) are mainly present in the electronic components mounted on the PCBs.

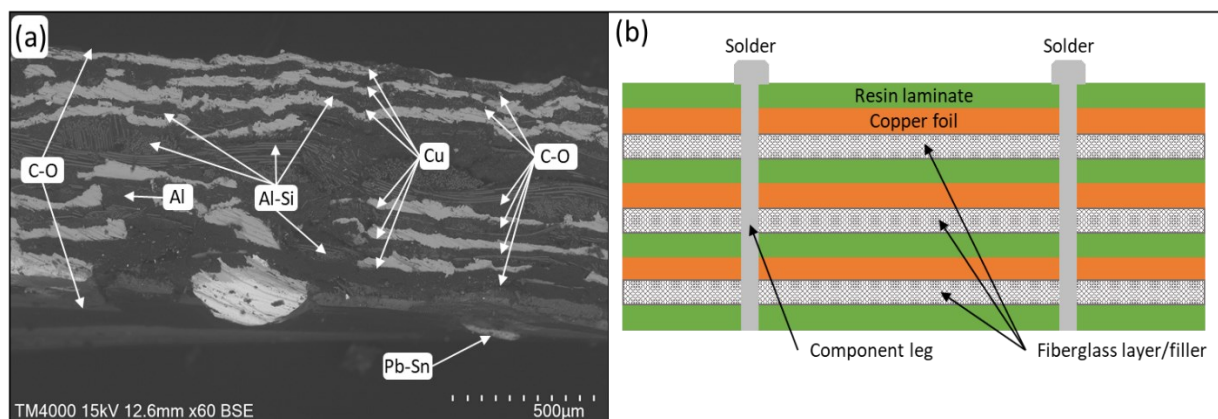


Figure 3.12: BSE-EDS image of (a) PCB cross-section, (b) PCB reconstruction of layers.

In general, an increase in the amount of copper is observed through the generations of mobile phone, with an average of 21.8 wt.%, 29.5 wt.% and 32.2 wt.% for feature phone, multimedia phones and smartphones, respectively; a factor likely to be due to the increase in the size and level of technology sophistication in mobile phones, that require larger and more conductive PCBs. This is consistent with the observed increase in the weight of PCBs through the generations, recorded in Figure 3.7, where PCBs weighed on average 17.3 g in feature phones and 24.2 g in smartphones, representing an increase of approximately 48%. Other base metals such as Al, Ba, Ni, Sn, Fe, are also present in PCBs, increasing with the generation of mobile phone. Aluminium and nickel are mostly used in welding and in the cover case of the screen which provides strong internal support in the mobile phone [148]. The concentration of nickel was considerably increased through the generations of mobile phones, with a rise of approximately 300% from feature phones to smartphones, whereas

the amount of aluminium was almost the same in all devices studied. The increase in use of nickel may arise due to its properties of lightweight, hardness and ductility. On average, base metals constitute approximately 39 wt.% of a PCB and share nearly 90% of the total metallic content by weight. Titanium is also one of the top ten most abundant elements in mobile phones PCBs, likely because of its use in chips [8].

Among the precious metals group, Ag, Au, Pd and Pt were found in high concentration in PCBs, with increasing concentrations through the generations. The average content of Au was 0.62 mg/g, varying between 0.50 mg/g and 0.76 mg/g. The amount of Ag was nearly twice that of Au, with an average content of 1.32 mg/g. These results and trends are in good agreement with those reported in the literature [22, 23, 38]. Au and Ag are used as connectors between electronics and PCBs due, for example, to their excellent conductive properties, thermal stability, and fine ductility [12, 22].

Rare Earth Elements (REEs) were also found in PCBs, accounting for 2.6% of the total PCB weight. Two REEs were found in significantly high concentration; neodymium from the LREEs and erbium from the HREEs, with average concentrations of 1.42 mg/g and 9.18 mg/g, respectively. These findings may be attributed to the use of REEs in microphones and vibrators because of their magnetic properties.

Analytical data are reported for the first time for uranium and those metals defined as critical raw materials (CRM) present in mobile phones. The concentration of uranium (U-238) has increased through the generations, from 0.68 mg/g to 3.58 mg/g for feature phones and smartphones, respectively. U-238 is weakly radioactive with a half-life of 4.5×10^9 years; however, uranium is a harmful element to human health due to its chemical toxicity, which can pose a threat if the product at end-of-life is not managed properly. PCBs contain various CRMs such as Ga, Ge, Hf, Be, Sb, Mg, Nb, W, Ta, and V with significant high concentrations. The concentration of those metals and metalloids increases through the generations of EoL-MPs. For instance, the concentration of Mn increases from 1421.2 ppm in feature phones to 1535.7 ppm and 3967.0 ppm for multimedia and smartphones, respectively. Cobalt and niobium are the only two CRMs that show a decrease in their concentration through the generations.

In summary the metal and metalloid content in EoL-MP PCBs, is observed to change significantly through the generations with an average of 33.5 wt.%, 43.6 wt.% and 51.9 wt.% for feature phones, multimedia phones and smartphones, respectively. The concentrations of the metals suggest PCBs represent a resource-rich stream of precious metals, 'high-tech' metals, CRMs and base metals such as copper. A detailed investigation of methods to recover some of these metals follows in the remaining chapters of the thesis.

3.3.2.2 Screens

Table 3.4 records the average metal and metalloid composition of screens in feature phones, multimedia phones and smartphones, with no significant difference through the three generations, averaging at 5.2 wt.%. Liquid crystal displays (LCD) are widely used in mobile phone screens [149, 150], and typically comprise thin conductive electrodes placed between two glass plates, accounting for nearly 50% of the total mass of the screen. The other components include connectors, adhesives, diffusive and reflective sheets, polarizing films and plastic frame [150, 151]. Figure 3.13 presents images of the components following dismantling of an EoL-MP screen, and a cross-sectional image of the screen analysed by BSE-EDS, and a reconstruction of a screen. These show that glass is the main component of screen, which explains the low metal content present. The large ceramic fraction, which was found to be approximately 65 wt.%, comprises the aluminosilicate glass fraction (a combination of alumina (Al_2O_3) and silicon dioxide (SiO_2)), and traces of potassium ions to increase the strength of the screen. The polymer content (28 wt.%) exists in the sheets, films, adhesives, and plastic frames of the screens. The conductive electrodes in the LCD screens are made of indium tin oxide (ITO), which is a mixture of In(III) and Sn(IV) oxides, with a typical distribution of 90% In_2O_3 and 10% SnO_2 by weight [149, 150, 152], so not surprisingly indium, a CRM, is detected with an average concentration of 0.17 mg/g in screens. Aluminium was the metal found with the highest concentration in screens, most likely because of its use as a frame to support the LCD screens due to its light weight, corrosion resistance, strength, lack of permeability and non-magnetic properties. Magnesium was also found in high concentration, increasing through the generations from 1309.6 mg/g to 2193.4 mg/g and 3250.1 mg/g for feature phone, multimedia phone and smartphone screens, respectively. In terms of PGMs, the amount of gold in screens has decreased through the generations of phones while palladium and platinum have increased.

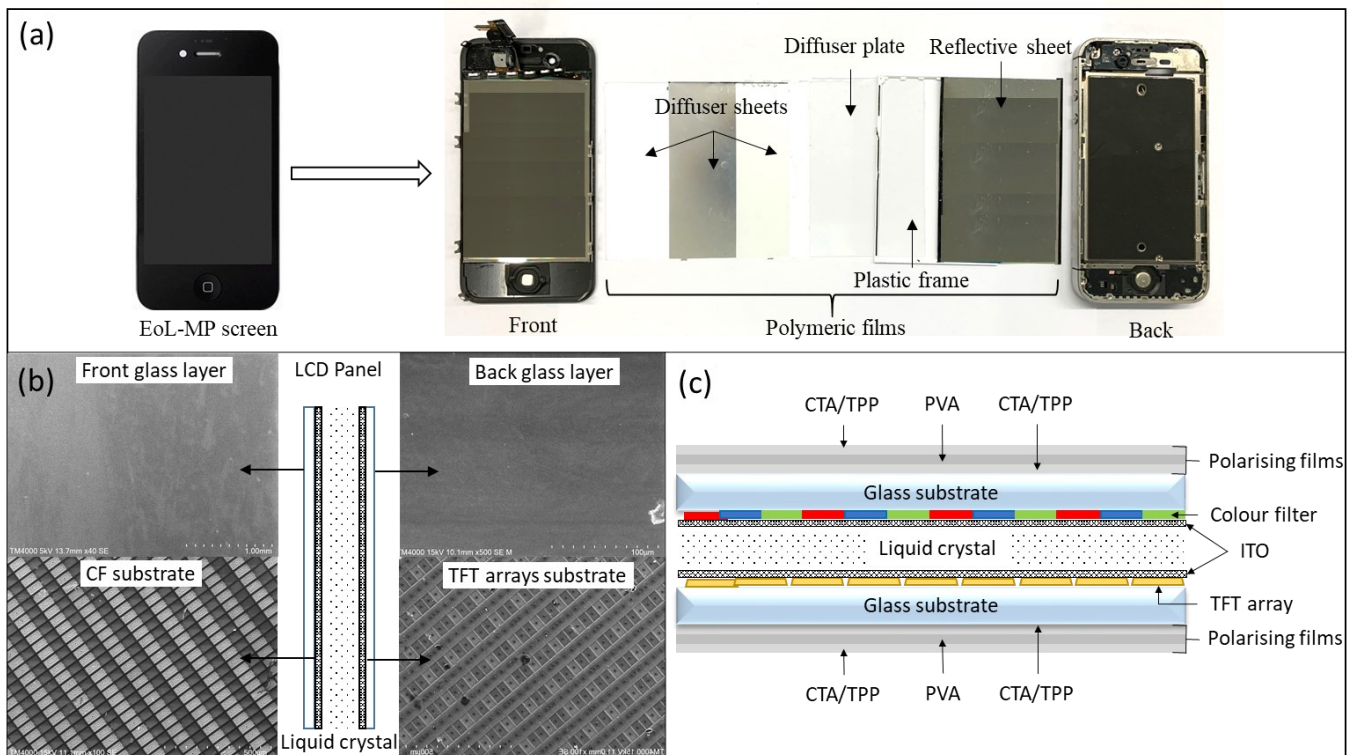


Figure 3.13: Mobile phone screen a) polymeric set, b) BSE-EDS images of a cross-section screen, and c) reconstruction of a cross-section of an LCD screen.

In terms of hazardous substances, it was found in screens that there is a considerable reduction in the amount of Cd and Pb through the mobile phone generations, consistent with the intentions of the RoHS Directive in 2002 requiring the banning of specified hazardous materials from electrical and electronic equipment put on the market after 2006 [75]. In the case of Cd, 1.0 $\mu\text{g/g}$ was found in screens of feature phones, decreasing to 0.1 $\mu\text{g/g}$ in the multimedia phones and being undetectable in smartphones. The amount of lead in the multimedia phones (77.1 $\mu\text{g/g}$) was nearly twice that in feature phones (35.0 $\mu\text{g/g}$) but decreased to 2.0 $\mu\text{g/g}$ in smartphones. The higher Pb content in multimedia phones is likely due to the increase in the screens size and their technological development, possibly requiring more solder for connecting electronics. This is consistent with other metals such as Ag and Au, used as connectors showing higher concentrations in these screens (Table 3.4). Another interesting finding is that the concentration of As in screens, on average (202.2 $\mu\text{g/g}$), was nearly twice the concentration found in PCBs (116.8 $\mu\text{g/g}$), despite the fact that metals account for just 5.2 wt.% in screens, much lower than in PCBs (43 wt.%). The high concentration of As found in mobile phone screens is likely due to the utilisation of As to improve the optical clarity in the glass of LCD displays [151]. This also explains why screens have the highest concentration of As of all the components in mobile phones.

In summary whilst there was little difference in metal and metalloid concentration found in the screens between generations, the screen offers a valuable source of indium, a critical metal under threat, for recovery which forms the basis of the research presented in Chapter 6 of this thesis.

3.3.2.3 *Electronics: Cameras*

The data for the metal and metalloid content in cameras for the three generations of phone are recorded in Table 3.4. Both front and back cameras were removed from the EoL-MPs for analysis. On average, the metal content in cameras was found to be 25% by weight. It is known that cameras in mobile phones have been improved year-on-year, to offer high-resolution photos and videos; especially in smartphones. This technological improvement is linked to the higher metal content found in smartphones cameras, with 31.8 wt.%, compared with approximately 21.5 wt.% found in cameras from feature and multimedia phones; equating to an increase of nearly 50% of metals utilised in smartphones cameras. Notably the presence of the highest concentration of gold across all components was found in cameras with an average of 1220.9 ppm. Silver was not detected in feature cameras; however, it was found in multimedia phones (689.4 ppm) and smartphones (890.3 ppm). In addition, platinum also increased its concentration from 33.5 ppm in feature phones to 75.6 ppm in smartphones. This increase in the PGMs is likely due to their use as connectors. Figure 3.14 shows the components of a main camera, as comprising frames (plastic and metallic), a lens and circuits. The metal content particularly the high copper and gold content in the cameras is most likely associated with the circuit connector and the sensor integrated circuit framework linked to the PCB.

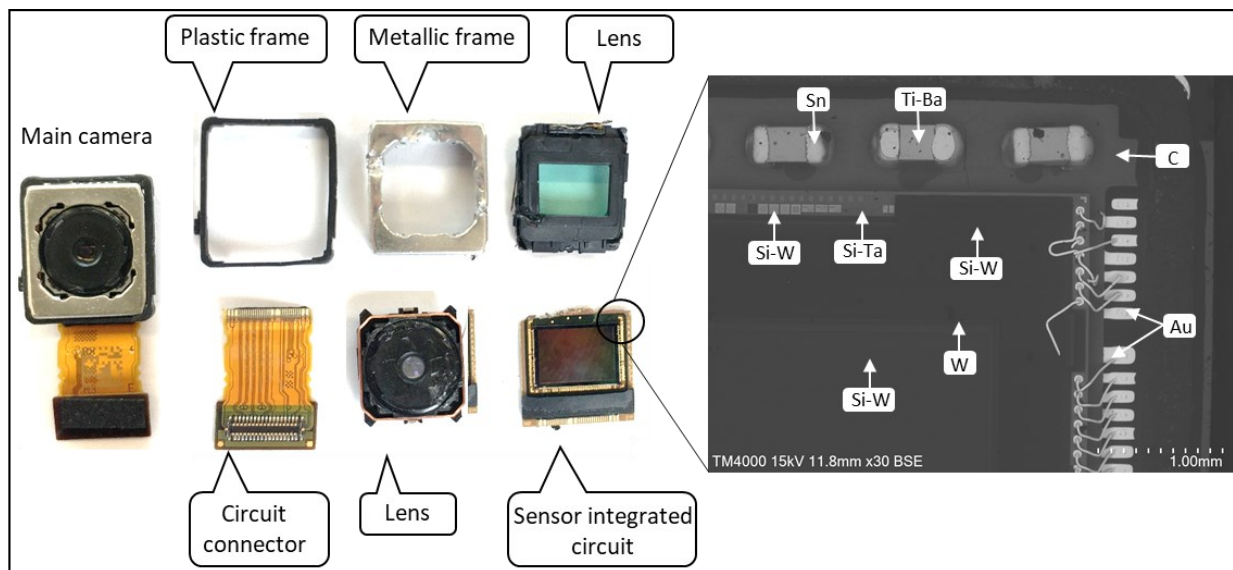


Figure 3.14: Camera components and DSE-EDS image of a sensor integrated circuit found in cameras.

3.3.2.4 Electronics: Speakers

Analysis of the speakers (Table 3.4) showed that on average, the metal content is approximately 50 wt.% and has reduced through the generations, from 52.2 wt.% in feature mobile phones to 43.6 wt.% in smartphones. The metal with the highest concentration in speakers is iron which is used because of its magnetic properties in NdFeB magnets. The REEs, neodymium, praseodymium and dysprosium, are also found in high concentrations in speakers, again because of their magnetic properties [27]. Other metals and metalloids present in speakers are in relatively low concentration, which make speakers likely as an excellent alternative source of REEs. These issues will also stimulate the desire for recycling REEs from EoL-MPs and e-waste in general. Figure 3.15 shows an image of the components of speakers, including frames, magnets and coils. The metals are mainly found in the magnet and coil, with the coil being made of copper, whereas the surface of the magnet is composed of iron and zinc. These findings explain the high concentration of copper and iron found in speakers. REEs metals are embedded in the magnet, and the PMs are found in the connectors linking the speaker to the PCB.

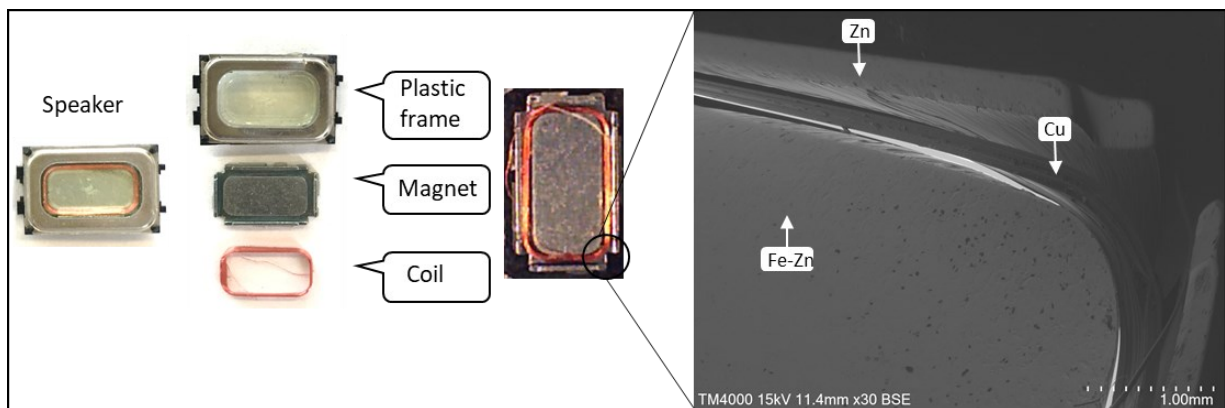


Figure 3.15: Speaker components and DSE-EDS image of a speaker.

3.3.2.5 Discussion

Table 3.5 records the concentration of a selection of metals determined in mobile phone PCBs by different authors compared with the values reported in this study. Copper is the most abundant metal in PCBs with approximately 30.0-57.5 mg/g, and found in this research to be 21.8-32.2 mg/g. The difference in the copper content is likely due to the pre-treatment and experimental methods utilised. For instance, Fontana et al. reported a concentration of 57.47 mg Cu/g PCB, following two leaching processes, the first leach was to separate the electronics from the PCBs, followed by ball milling of the bare PCB and a second aqua regia leach step [46]. Park and Kim [153] reported 47.9 wt.% of copper in PCBs, but the PCBs were obtained from a local e-waste recycling company (Torecom Inc., South Korea), where mechanical pre-treatments were previously carried out. The metal concentrations are listed with a record of the year of the publication to serve as an indicator of the change in metal concentration in EoL-MPs through the years. The results show there is no significant correlation between the metal concentrations in different generations of EoL-MPs and the timeline (assumed to closely represent the production year quoted); it shows, however, an increase in the copper content, a similar trend to that found in this study. The authors also reported that gold and silver in PCBs of mobile phones are in the range of 0.06-0.28 wt.% and 0.06-0.41 wt.%, respectively. In this study, gold was found to be in the range of 0.05-0.07 wt.% and silver 0.11-0.16 wt.%. Again, the differences in the amount of gold and silver in mobile phone PCBs are likely due to the pre-treatment steps followed. The authors concluded that PCBs are an excellent resource for secondary metals, mainly for copper, gold, and silver, where concentrations are observed as much higher than in their natural ores. Other studies have focussed on desktop computers PCBs, finding on average 20 wt.% of copper. Although PCBs from different EEEs such as laptops, desktop computers, television, radio, etc. contain nearly the same metals and metalloids, their concentration is lower than the mobile phone PCBs [154, 155]. It is noteworthy to mention that aqua regia has been widely used in the characterisation of PCBs, mainly because of its great property to dissolve gold.

Despite the low metal content in mobile phone screens accounting for just 5.2 wt.%. (Table 3.2), the amount of indium in screens was high, with an average concentration of 0.17 mg/g. This amount of In found in EoL-MP screens is higher than the average amount of indium reported elsewhere in LCD panels (0.102 mg/g) [150]. Indium has no primary ore but is produced as a by-product during the processing of zinc and lead, typically with a concentration between 0.01-0.02 mg/g [152]. Several authors have focused on the extraction and recovery of indium from LCD panels due to its high content [142, 149, 152, 156]. In addition, it has been reported that when the polymer films attached to the LCD screens are removed, the amount of available indium can be as high as 1400 mg/kg [150]. Ueberschaar et al. reported the concentration of indium in various LCD devices (mobile phones,

notebooks, PC monitors, LCD TVs, and tablets) ranging between 3 and 660 ppm, being by far the greatest indium content per LCD panel found in mobile phones [142]; and observed the indium concentration to be considerably lower in smartphones than other earlier generation mobile phones, attributing this to different LCD technologies applied. In this study, smartphones also showed the lowest indium concentration (64.9 mg/g) compared to feature (190.0 mg/g) and multimedia (262.5 mg/g) phones. These differences in indium content can also be attributed to the technology of the LCDs since all the feature phones analysed had monochrome displays, whereas multimedia and smartphone displays were coloured, with the smartphone screen being much sharper and more colourful. Furthermore, in smartphones, REEs are used to impart colour due to their better brightness and conductivity properties [27].

Mobile phones contain concentrations of hazardous and toxic substances such as antimony, beryllium, copper, nickel, zinc, heavy metals (arsenic, cadmium, chromium, mercury thallium and lead), flame retardants (mostly bromides and chlorides compounds), among others. Most of these hazardous and toxic substances are bio-accumulative toxins, and have been associated with cancer, and a range of neurological, reproductive, and developmental disorders. In addition, when EoL-MPs are discarded to landfills, these toxic substances can be released contaminating soil, seeping into groundwater, and polluting the atmosphere with toxic fume and gases, causing serious damage to the environment and potentially becoming incorporated into the food chain and impacting the human health [41, 148, 157].

Table 3.5: Concentration of metals in PCBs reported by various researchers in comparison to results from this study.

Element (wt.%)	W. Hall J. and P. Williams [48]	A. Kasper et al. [47]		F. Xiu et al. [158]	Q. Tan et al. [38]	D. Fontana et al. [46]	H. Park and Y. Kim [153]	S. Jeon et al. [159]	This Study
	2007	Brand A	Brand B	2015	2017	2019	2019	2020	2021
Al	1.83	0.31	0.99	-	-	0.17	-	1.60	2.47
Ba/ppm	0.11	-	-	-	-	-	-	-	2,300
Cd	<0.56	-	-	-	-	-	-	-	0.0034
Cu	32.31	39.56	38.33	40.80	41.8	57.47	47.90	30.00	27.93
Fe	0.54	1.42	6.53	0.28	0.66	25.23	0.5	4.70	1.3
Mn	0.65	-	-	-	-	0.24	-	-	0.63
Ni	0.69	3.42	1.67	0.39	1.93	5.10	0.80	2.10	2.03
Pb	0.25	1.17	1.26	1.36	0.19	0.85	-	1.30	5.11
Sn	-	2.09	3.11	1.60	4.57	3.49	2.00	-	1.51
Zn	0.96	3.43	0.97	0.41	-	4.9	-	0.90	0.52
Ag	0.41	0.06	0.06	0.11	0.20	0.15	0.13	-	1.32
Au	0.28	0.06	0.10	0.0065	0.12	0.12	0.1	0.10	0.62
Pd	<0.56	-	-	0.005	0	-	0.01	-	0.11
Particle size (mm)	<0.6	<1	<1	<4	-	<1	-	0.085-0.224	≤0.150
Characterisation process	Metals present in char produced by pyrolysis at 800 °C and acid digested. Analysed by ICP-MS.	Manual disassembly, hammer mill grinding and knife milling. Digestion: aqua regia, 2 h at 60 °C without agitation. Analysed by ICP-AES.	Cutting mill Digestion: HNO ₃ -HCl-HClO ₄ -HF mixture Analysed by ICP-OES.	Manual dismantling, PCBs crushed. Digestion: unmentioned. Analysed by XRF and ICP-AES	Ball milling. Digestion: Aqua regia at 25 °C. Analysed by AAS.	Digestion: unmentioned. Analysed by ICP-AES.	Cutting mill. Pre-treated in an ashing furnace to burn the plastics. Digestion: aqua regia, 2h, 90 °C. Analysed by ICP-AES	Cutting. Pre-treated in a furnace to burn the plastic. Cryomilling, aqua regia digestion. Analysed by ICP-AES	

Hazardous and toxic metals present in mobile phones are reported in Table 3.2 with only the three metals, cadmium, lead, and mercury listed under the category of hazardous metals (HM) as referenced in the RoHS Directive [ref]. More than these, however, although listed elsewhere in Table 3.2, fall under the category of hazardous metals deemed toxic to human health and the environment. A detailed analysis of these metals (As, Ba, Be, Cd, Cr, Pb, Sb, Sn, V and Zn) is shown graphically (Figure 3.16) as concentrations in the different components across the three generations of mobile phone. Within the components of mobile phones, PCBs are the most hazardous component, followed by screens. It is interesting to note that since the Directive 2002/95/EC came into force in 2003, mobile phones entering the market after that year, mainly smartphones, have not reduced the content of hazardous substances, indeed the opposite is true; the concentration of many hazardous elements has risen. Narendra et al. studied and reported the trends and impact on human health and ecotoxicity of 19 elements present in EoL-MPs manufactured between 2001 and 2015. They grouped the EoL-MPs into basic phones and smartphones, and it was found that smartphones contained a significant increase in the content of toxic materials from 2006 to 2015, whereas no significant changes were found in basic phones. Among the 19 elements studied, nickel, lead and beryllium were reported to contribute the greatest risk as carcinogens in mobile phones, whilst copper dominated the ecotoxicity risks in EoL-MPs [148]. These findings are confirmed in this study, with smartphones being potentially the most hazardous handset among the generations. Although their concentrations are still below the maximum concentration values tolerated by the RoHS, it will likely not be long before their presence will be under threat.

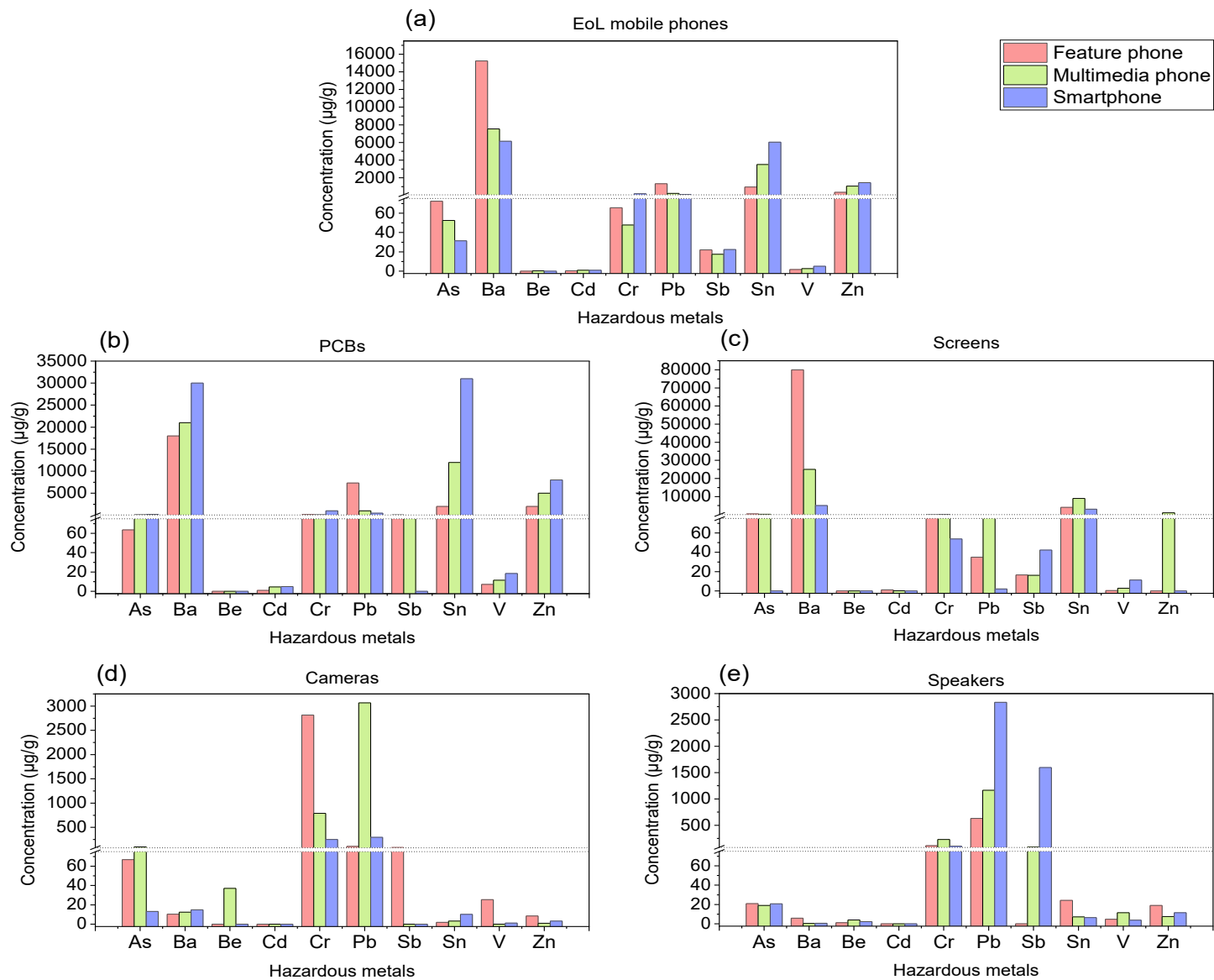


Figure 3.16: Hazardous metals (selected as those most commonly cited as toxic in WEEE) in EoL multigenerational mobile phones and in their components: PCBs, screens, cameras, and speakers.

3.3.3 Characterisation of the Non-Metallic Fraction

The non-metallic fraction in EoL-MPs comprises mainly plastics and ceramics with the primary focus here on plastics. Characterisation of the non-metallic fraction was completed using FTIR analysis to confirm the functional groups of the plastic components, elemental analysis to confirm the carbon to hydrogen ratio as an indicator of aromaticity of the organic fraction, and thermogravimetric analysis to further confirm the polymer type by measuring the thermal properties.

3.3.3.1 Fourier Transform Infrared Analysis of Polymer Fractions

To determine the different polymers in the plastics, FTIR analysis was used to characterise the functional groups present in each of the main plastic-based components of mobile phones (casings, screens, and PCBs) through the three generations. Cameras and speakers were not considered because plastic is not part of their composition.

Casings: In all casing samples the FTIR spectra (Figure 3.17) show two small peaks at around 3030 cm^{-1} and 3059 cm^{-1} representing the presence of aromatic C-H bonds in the range of $3100\text{-}3000\text{ cm}^{-1}$. Within the range of $3000\text{-}2840\text{ cm}^{-1}$, there are four peaks (2850 cm^{-1} , 2871 cm^{-1} , 2918 and 2966 cm^{-1}) which indicate the presence of aliphatic C-H bonds. The peaks at 1768 cm^{-1} and the multiple peaks in the range of $1300\text{-}1000\text{ cm}^{-1}$ are associated with C=O and C-O bonds of an ester group, present and characteristic of polycarbonate (PC). All the casings show peaks at 1601 cm^{-1} that are attributed to aliphatic C=C double bond in the butadiene units of acrylonitrile butadiene styrene (ABS), present in the polymer because of its flame retardant properties. The peak at 1500 cm^{-1} is associated with aromatic C=C stretches within the styrene unit of ABS. The fingerprint regions below 1500 cm^{-1} of all three casing samples are similar. The peaks around 552 cm^{-1} are likely to be associated with C-Cl (range $850\text{-}550\text{ cm}^{-1}$) or C-Br (range $690\text{-}515\text{ cm}^{-1}$), attributed to the presence of halogenated flame retardants. These findings indicate that casings most likely comprise PC, ABS, and PC/ABS polymer blends, confirmed by the composition data on the printed plastic code found in some of the casings, as shown in Figure 3.18.

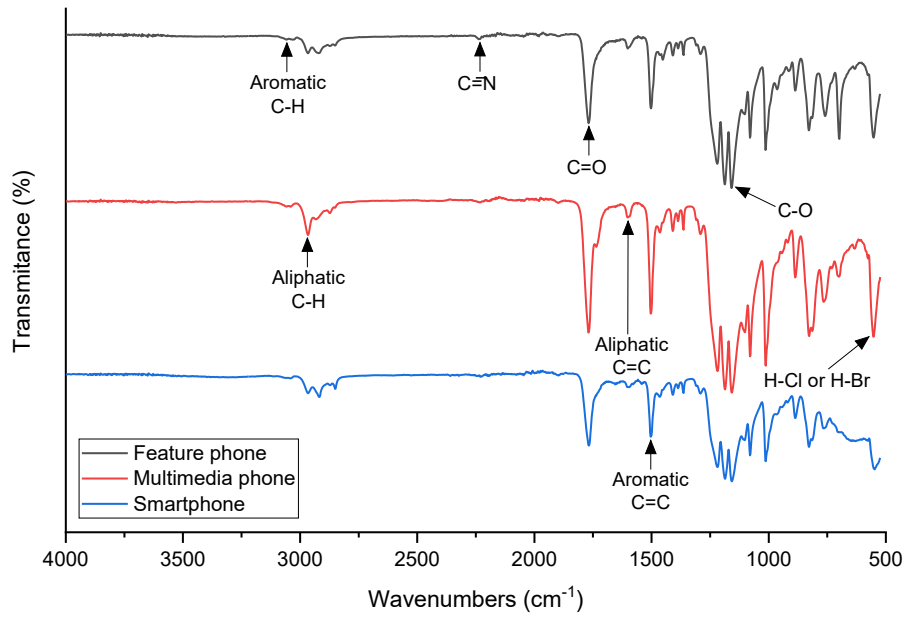


Figure 3.17: FTIR Spectrum of a milled sample of casings of feature phone, multimedia phone and smartphone.

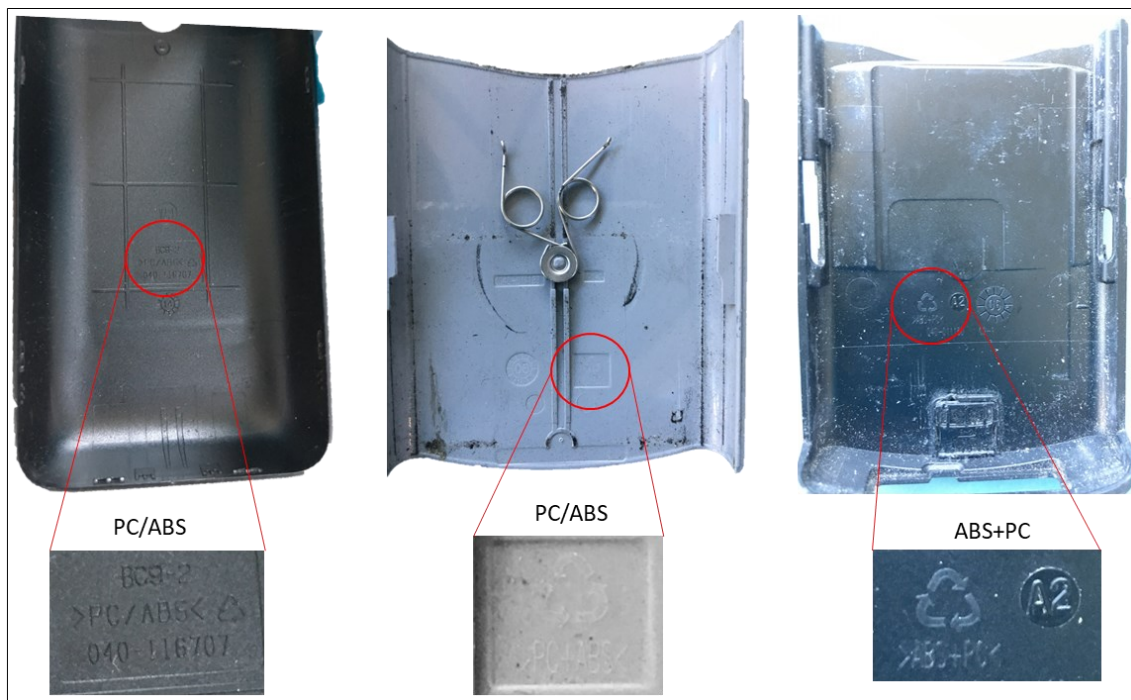


Figure 3.18: Printed plastic code in EoL-MPs casings.

PCBs: Figure 3.19 shows the FTIR spectra of PCBs from the three generations of mobile phones. Aliphatic C-H bonds between 3000-2840 cm^{-1} are present in all the phones with similar intensity (peaks at 2960 cm^{-1} , 2920 cm^{-1} , and 2870 cm^{-1}). The peak at around 1730 cm^{-1} corresponds to the carbonyl group C=O stretch, which together with the broad peak at 1014 cm^{-1} related to the C-O bond, is indicative of the presence of an ester group. The two peaks at 1600 cm^{-1} and 1500 cm^{-1} are associated with aliphatic C=C bonds and aromatic C=C bonds respectively. The fingerprint regions below 1500 cm^{-1} of the PCBs for each generation of mobile phone show similar patterns. The absorption band of the hydroxyl group (-OH) in the region of 3200-3600 cm^{-1} is evident in the PCB of the multimedia phone, but only slightly visible in the other two types of mobile phone. The hydroxyl group and aromatic C=C bonds together indicate the presence of bisphenol-A (BPA) epoxy resins in the PCBs, while the ester group and the aromatic C=C bonds indicate the presence of unsaturated polyester resin (UPR). It is likely that PCBs from the three generations of mobile phones comprise a mixture of BPA epoxy resins and UPR.

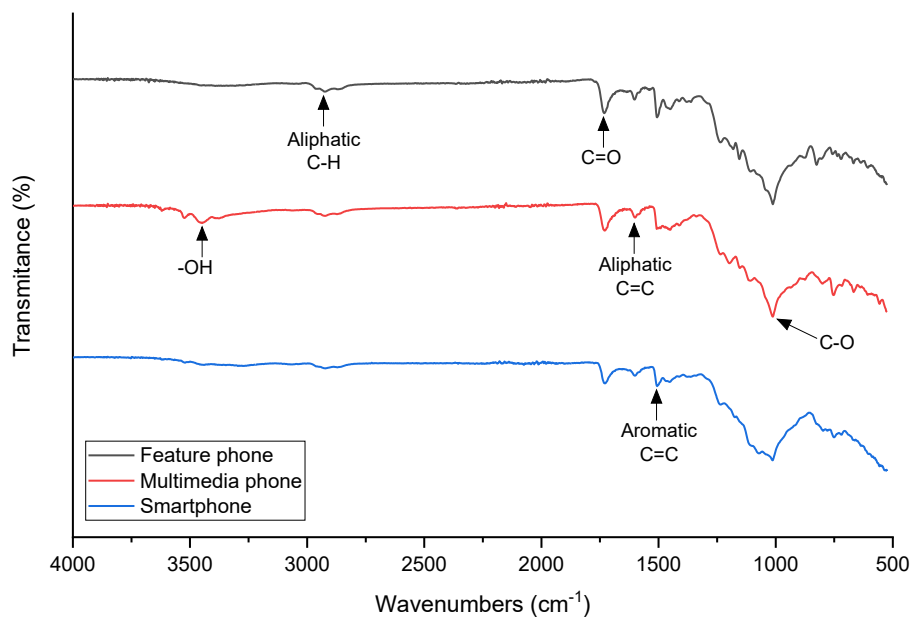


Figure 3.19: FTIR Spectrum of a milled sample of PCBs of feature phone, multimedia phone and smartphone.

Screens: The FTIR spectra of the screen samples (Figure 3.20) show peaks between 3000-2840 cm^{-1} which indicate the presence of aliphatic C-H bonds in all samples and appear more intense in the smartphone. The peak at 1730 cm^{-1} is related to C=O and together with the broad peak at 1014 cm^{-1} , which is associated with the C-O bond, are representative of an ester group. The peak at 1500 cm^{-1} is associated with the aromatic C=C bonds. The fingerprint regions below 1500 cm^{-1} are similar for all three samples of screen across the generations of phone.

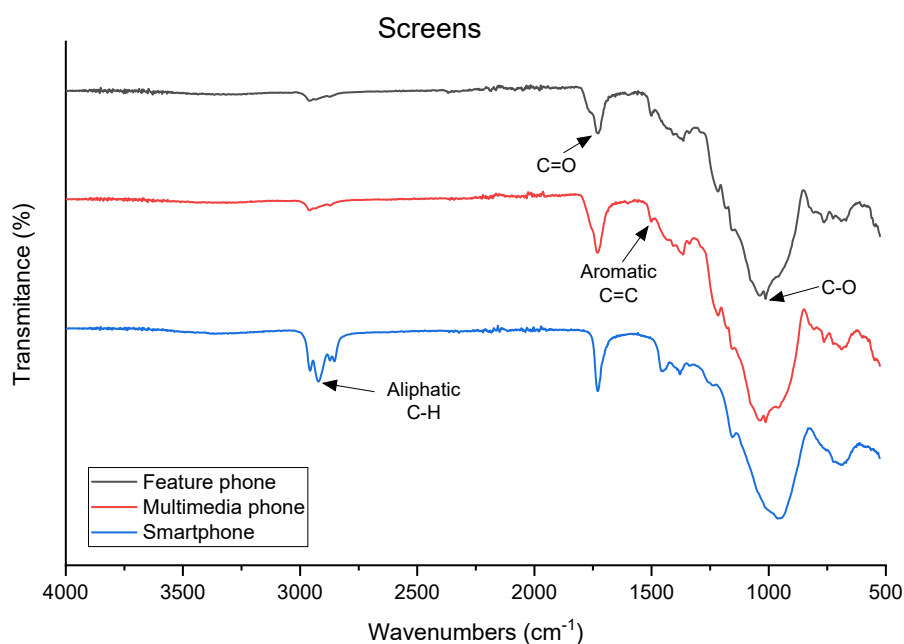


Figure 3.20: FTIR Spectrum of a milled sample of Screens of feature phone, multimedia phone and smartphone.

Screens of mobile phones comprise liquid crystal displays (LCDs), which contain thin conductive electrodes, glass plates, connectors, adhesives, and polymeric films (Figure 3.13) with the latter comprising a complex matrix of diffuser sheets, diffuser plates, plastic frames, and reflective sheets. Each of the three generations of mobile phone screens has similar polymeric composition (Figure 3.21). FTIR characterisation was used to better understand the polymeric composition of this matrix, and the spectra for each component are presented in Figure 3.22, and interpretation of the peaks was based on matching with a database of polymer reference patterns and matches were found to be greater than 90% in all cases (Table 3.6). It was found that *diffuser sheets* were composed of poly(ethylene terephthalate) (PET) and poly(methyl methacrylate) (PMMA), *diffuser plates* were made of polycarbonate (PC), *plastic frames* were composed of PC and PET, and *reflective sheets* were made of PET. Characteristic peaks for these polymers are presented in Table 3.7. It is noted that the FTIR

patterns of screen presented in Figure 3.20, which correspond to the FTIR pattern of the whole screen (without separation of the polarising films) shows aromatic C=C bonds, which are found in TPP and PET, and ester bonds that are present in CTA and PET, confirming the polymeric composition previously found. In addition, in all the samples and especially in smartphones there are peaks in a range of 2900-3100 cm^{-1} , associated with aliphatic C-H bonds, and characteristic of PET. These PET peaks are found with higher intensities in smartphones, probably due to the use of screen protectors, which are made principally of PET.

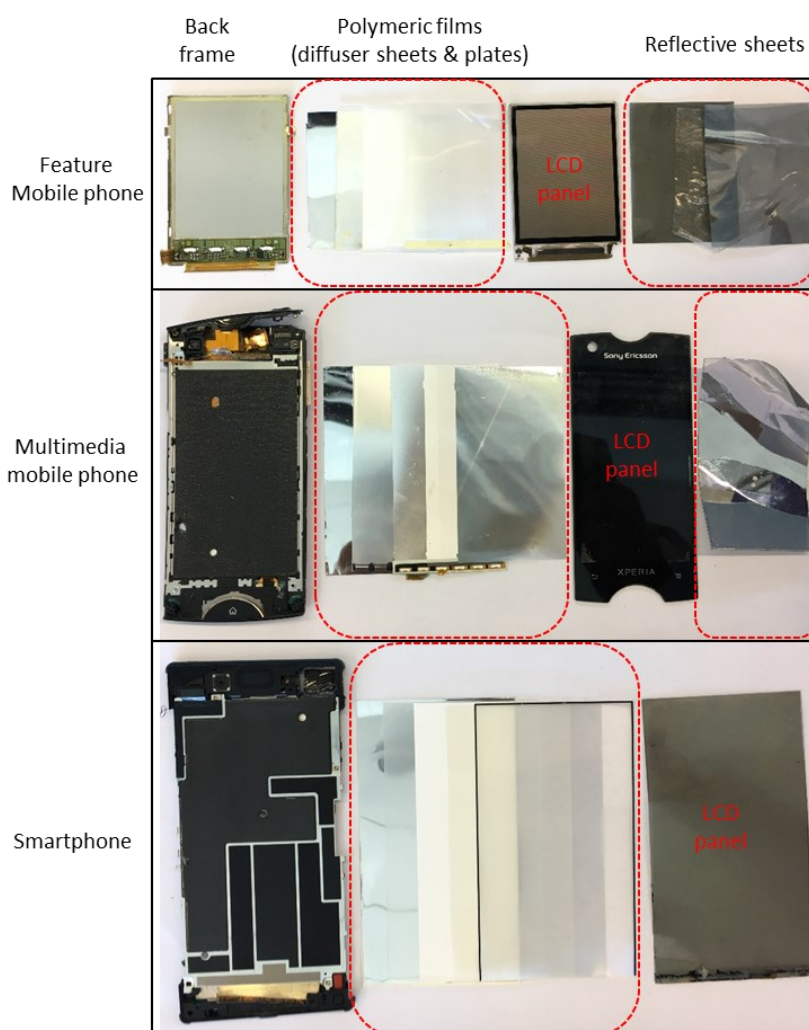


Figure 3.21: Main components of LCD screens from EoL-MPs.

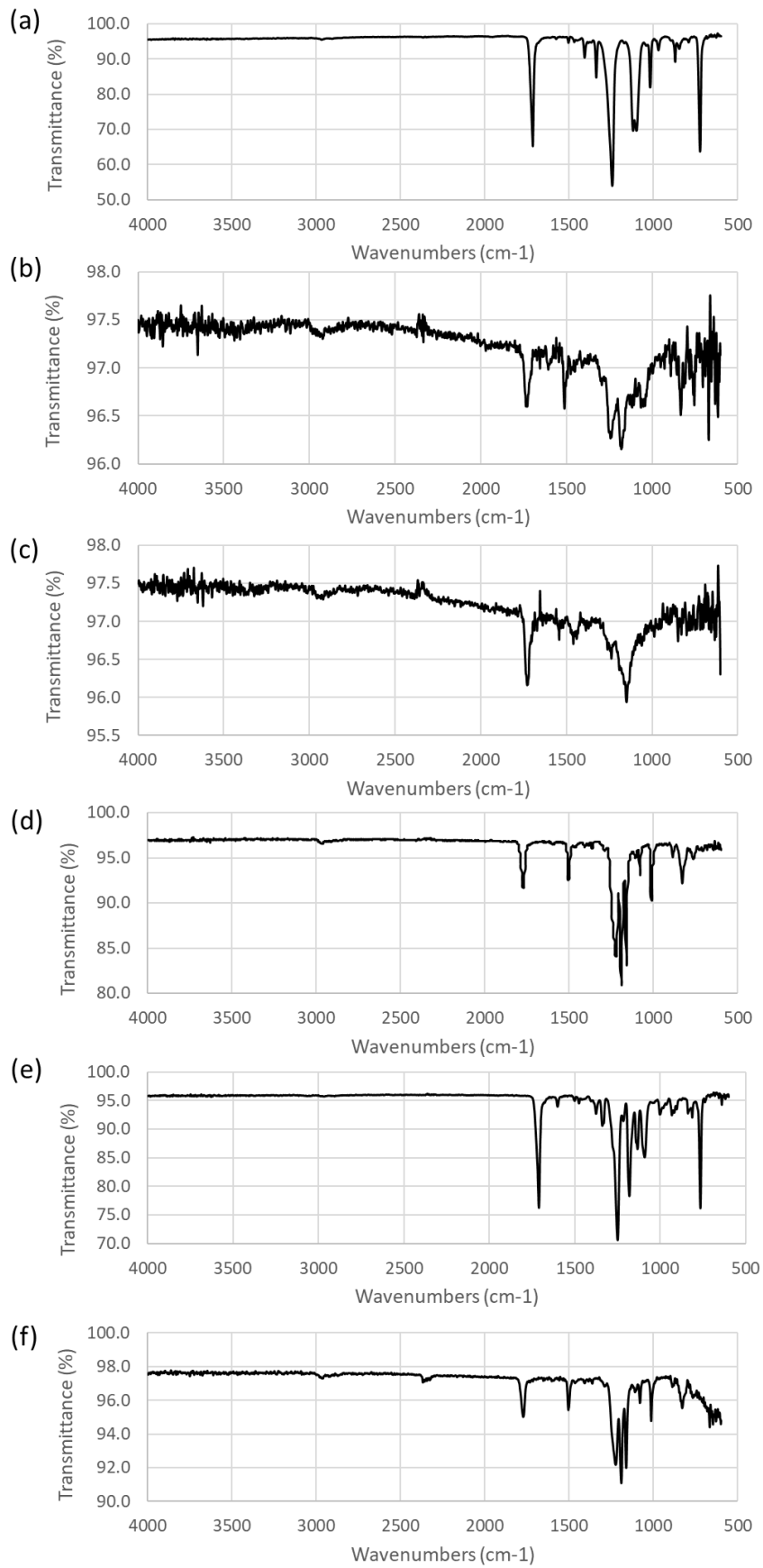
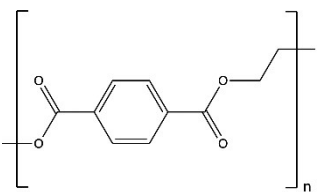
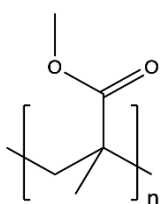
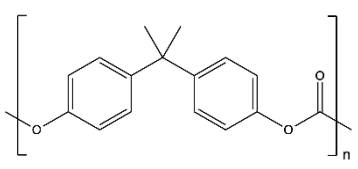


Figure 3.22: FTIR Spectrum of (a) diffuser sheet 1, (b) diffuser sheet 2, (c) diffuser sheet 3, (d) diffuser plate, (e) reflective sheet, and (f) plastic frame

Table 3.6: Characterisation of the polymeric films in LCD mobile phone screens.

Component of LCD panel	Material	Match (%)	Weight composition (%)	Thickness (mm)
Diffuser sheet 1	PET	>95	1.0 ± 0.01	0.060 ± 0.001
Diffuser sheet 2	PMMA	>90	1.0 ± 0.01	0.060 ± 0.001
Diffuser sheet 3	PMMA	>90	0.6 ± 0.01	0.045 ± 0.001
Diffuser plate	PC	>95	6.5 ± 0.50	0.430 ± 0.030
Plastic frame	PC-PET	>90	1.1 ± 0.25	0.055 ± 0.001
Reflective sheet	PET	>90	1.2 ± 0.50	0.085 ± 0.002

Table 3.7: FTIR characterisation of the polymers in the polymeric set of LCD screens.

Compound	Structure	FTIR characterisation		
		Functional group	Absorptions (cm ⁻¹)	Intensity
Poly(ethylene terephthalate) (PET)		Alkane: -C-H	1350-1480	variable
		Alkene: C=C	1620-1680	variable
		Alkene: -C-H	675-1000	strong
		Ester: C=O	1735-1750	strong
		Ester: C-O	1000-1300	two bands or more
Poly(methyl methacrylate) (PMMA)		Alkane: -C-H	1350-1480	variable
		Ester: C=O	1735-1750	strong
		Ester: C-O	1000-1300	two bands or more
Polycarbonate (PC)		Alkane: -C-H	1350-1480	variable
		Alkene: C=C	1620-1680	variable
		Alkene: -C-H	675-1000	strong
		Ester: C=O	1735-1750	strong
		Ester: C-O	1000-1300	two bands or more

3.3.3.2 Elemental Analysis of Polymer Fractions

For a complete compositional analysis of polymers in mobile phones, CHN and S elemental analysis was carried out and the results are presented in Table 3.8. Also included are the carbon to hydrogen(C:H) ratios for each component determined as a measure of aromaticity. The C:H ratios range from 0.68 to 1.15. FTIR data (Figure 3.17) suggest the casings in the EoL-MPs used in this work are made of PC, ABS and PC/ABS blends. Assuming that the casings are made of pure PC and ABS, C:H ratios of above 1.0 suggest that the casings are mainly composed of PC with the addition of ABS to modify its mechanical properties since the C:H ratio of PC and ABS are 1.14 and 0.88, respectively. PC and ABS are the commonly used polymers for casings due to their high stability to different environmental conditions, heat resistance, flame retardancy, dimensional stability as well as excellent mechanical properties such as rigidity and mechanical strength [143, 160].

FTIR results for PCBs (Figure 3.19) identified the presence of the unsaturated polyester resin (UPR), which would lower the C:H ratio (to below 1.0). The FTIR is in good agreement with results from Table 3.8, confirming that PCBs are mostly made of UPR since UPR has one less aromatic ring per structural unit than BPA epoxy resin. In the case of mobile phone screens, the smartphone screens showed the lowest C:H ratio (0.68) of the generations, which might suggest a change in the materials used for its manufacturing, containing a lower fraction of aromatic compounds.

Table 3.8: Elemental analysis of casings, screens and PCBs of multigenerational EoL-MPs.

Element (wt.%)	Casings			Screens			PCBs		
	G1	G2	G3	G1	G2	G3	G1	G2	G3
C	71.76	65.43	56.11	21.80	31.66	12.44	17.94	18.76	17.87
H	5.19	5.17	4.30	1.68	2.64	1.51	1.58	1.66	1.61
N	0.32	0.30	0.40	<0.10	<0.10	<0.10	0.47	0.36	0.56
S	<DL	<DL	<DL	<0.10	1.75	<0.10	1.84	1.65	<0.10
O and others*	22.73	29.10	39.19	54.72	63.95	86.05	78.16	77.58	79.95
C:H	1.15	1.05	1.08	1.08	0.99	0.68	0.94	0.94	0.92

G1, G2, and G3 stand for feature, multimedia and smartphones, respectively, also known as generation 1, 2, and 3.

<DL: Below detection limit.

*: Determined by difference.

Flame retardants (FRs) are used to delay the ignition of flames and prevent the spread of fire, and residual heavy metals are the main concern of hazardous substances. Brominated flame retardants (BFRs) have been extensively used in EEEs to increase the flame resistance since they are considered the most effective flame-retarding agents [161]. FTIR spectra of the casings (Figure 3.17) show peaks at wavelengths consistent with the presence of halogenated flame retardants (C-Cl and

C-Br bonds) in casings. To determine the total bromine and chlorine content in mobile phones, ion chromatography was used based on a method derived from the US EPA Method 5050. It was found that, on average, the content of Cl was 2300 ppm, whereas for Br was 690 ppm. These concentrations are per mobile phone unit, representing only 0.0023% for Cl and 0.00069% for Br of the total mobile phone weight. The maximum concentration values of FRs permitted by the RoHS are 0.1 wt.%, so the detected levels of Cl and Br are well below the maximum permitted under these regulations. Although BFRs have been or planned to be phased out in new products, their presence in historical WEEE will continue threaten human health and the environment if these products at end-of-life are not properly managed.

3.3.3.3 Thermal Analysis of Polymer Fractions

Combined TG/DSC analysis was used to further characterise the polymer fractions in casings, PCBs, and screens by heating the samples in an inert atmosphere (N₂). The results are presented as plots in Figure 3.23 for the three polymeric components from each generation of mobile phone recorded for comparison. Details of polymeric decomposition and final residue are listed in Table 3.9

Table 3.9: Temperatures of polymer degradation zones and residue material from TGA-DSC ((10 °C/min, N₂ atmosphere).

Generation of Mobile phone	Zone 1 (°C)	Zone 2 (°C)	Zone 3 (°C)	Zone 4 (°C)	T _{onset} * (°C)	Residue (%)
Casings						
Feature phone	280-345	335-415	415-500	500-615	280	23
Multimedia phone	295-420	420-600	-	-	280	29
Smartphone	290-385	385-500	500-600	-	285	32
PCBs						
Feature phone	310-380	380-500	-	-	300	78
Multimedia phone	235-340	340-510	510-700	-	225	72
Smartphone	230-330	330-500	500-575	575-875	230	84
Screens						
Feature phone	330-415	415-600	-	-	300	67
Multimedia phone	205-340	340-415	415-635	-	200	65
Smartphone	300-355	355-405	405-500	-	300	84

The zones of degradation were calculated based on the weight loss rate calculated as the derivate of the residual weight with respect to the temperature (wt.%/ °C).

*: Temperature onset was calculated as the intersection point of the extrapolated baseline and the inflectional tangent at the beginning of the melting or crystallization peak.

Casings: A first-stage reaction (Figure 3.23a), occurs between 280-345 °C, followed by a one-step decomposition in the range of 415-500 °C to leave a residue of 23 wt.%, 29 wt.%, and 32 wt.%, for feature phone, multimedia, and smartphones, respectively. The onset of the phase change at 280 °C is consistent with the melting of PC.

PCBs: The PCBs from each generation of mobile phone show multiple phase changes (Figure 3.23b), accompanied by weight loss with maximum decomposition in the range 300-500 °C, and a total loss following incomplete decomposition at 1000 °C of between 15 and 25 wt.%. A PCB typically comprises a substrate of epoxy resin and glass fibre coated with thin layers of copper films, used as mechanical support for electric components (resistors, capacitors, transistors, integrated circuits, etc.), which principally contain metals and ceramics [47, 96, 162], as seen in Figure 3.12. This explains the high residue content of PCBs (>70 wt.%) seen in Figure 3.23b and reported earlier in Table 3.1.

Screens: The screens of all mobile phones show a main decomposition occurring in the temperature range of 330-400 °C; the temperature range that corresponds to thermal degradation of CTA [163]. This result and the characteristic ester peaks in the FTIR (b) confirm CTA to be the main polymer found in screens of mobile phones. The second decomposition step above 400 °C in the screens from multimedia phones and smartphones are consistent with the presence of PET especially in the smartphones. The high residue in screens, heated to above 400°C, is likely due to the presence of glass, which accounts for more than 70% of the total weight of screens. The high content of glass in screens was also observed in Figure 3.13.

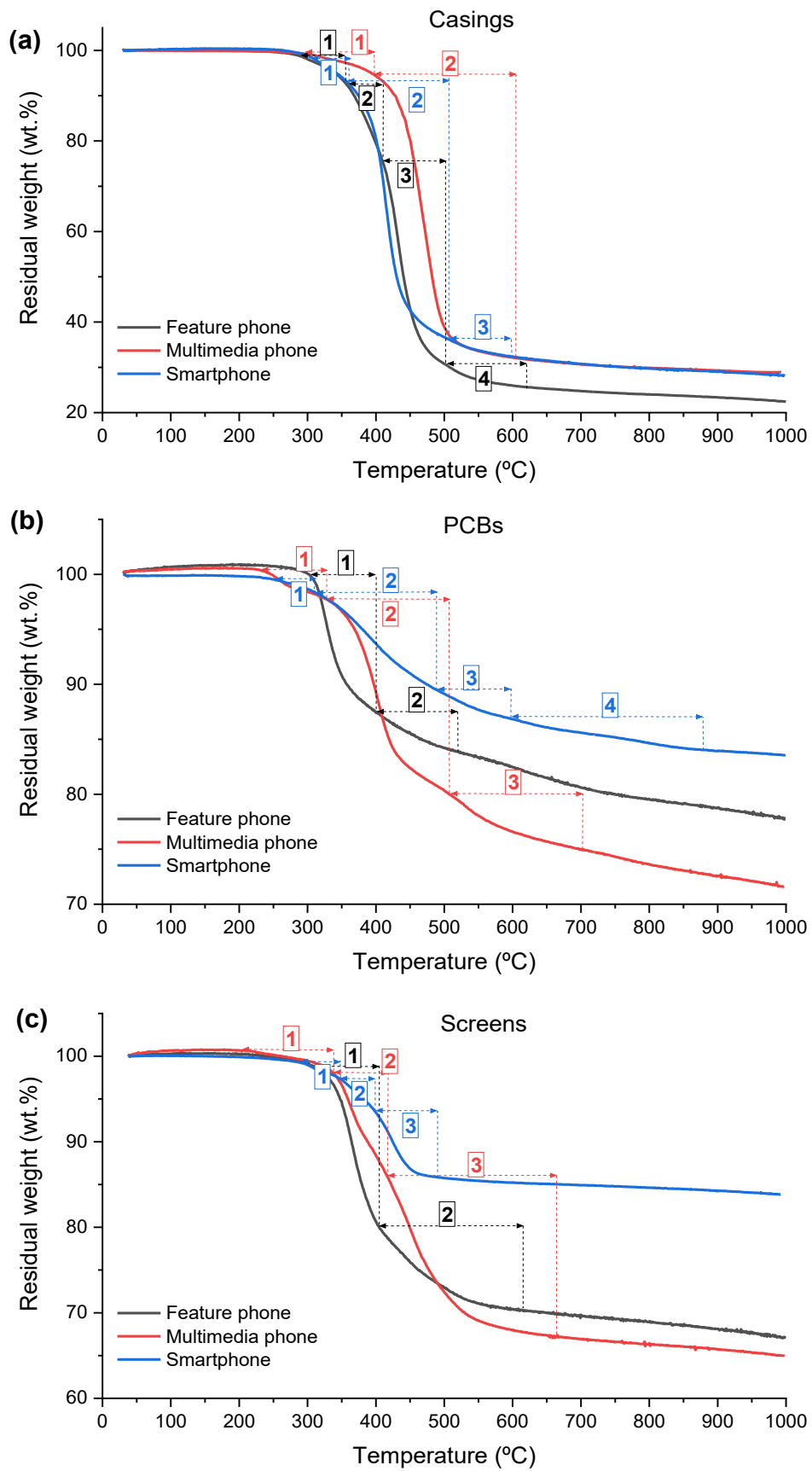


Figure 3.23: TGA of milled sample of (a) casings (b) PCBs and (c) screens of feature phone, multimedia phone and smartphone (10 °C/min, N₂ atmosphere).

3.3.3.4 Intrinsic Energy Value in Polymer Fractions

A combination of thermogravimetric analysis and bomb calorimetry was used to determine the proximate analysis and intrinsic energy value of the key components of the mobile phones containing the non-metallic fraction. Table 3.10 presents the results from the proximate analysis with the weight percentage of the moisture content, volatile content, black carbon content, and ash residue ash and the higher heating value (HHV) of casings, screens, and PCBs of the multigenerational EoL-MPs. From the proximate analysis, negligible moisture is found in all the samples (0-0.57 wt.%), and of the three components, the casings contain the highest volatile content (77.9 wt.% on average), with the volatile content of screens and PCBs being much lower at 27.9 wt.% and 23.8 wt.% respectively. Likewise, the casings have the most fixed carbon content (11.6 wt.%) compared screens (3.7 wt.%) and PCBs (4.6 wt.%). PCBs have the most inorganic ash residue after combustion with oxygen, at 71.2 wt.%, followed by screens at 68.0 wt.%, and casings with the least amount of ash (10.2 wt.%). The ash residue is consistent with the high metallic and ceramic content in PCBs and high content of glass and ceramics in screens. It is noted that the weight of ash from the feature phone and smartphone PCBs, although not observed in the multimedia phone, increased by 1.6 wt.% and 1.0 wt.% respectively, as the ash was held under oxidation condition, suggesting oxidation of some metals present in PCBs.

Table 3.10: Proximate analysis and HHV from multigenerational mobile phones.

Unit (wt.%)	Feature phone	Multimedia phone	Smartphone
	Casings		
Moisture	0.00	0.57	0.50
Volatile matter	78.60	83.28	71.75
Fixed carbon	9.385	12.99	11.96
Ash residue	11.56	3.15	15.78
HHV (MJ/Kg)	34.29	24.76	28.28
	Screens		
Moisture	0.41	0.53	0.31
Volatile matter	32.54	35.92	15.23
Fixed carbon	4.22	6.34	0.51
Ash residue	62.83	57.22	83.96
HHV (MJ/Kg)	12.43	10.48	6.59
	PCBs		
Moisture	0.42	0.54	0.45
Volatile matter	24.86	29.93	16.48
Fixed carbon	5.32	5.66	2.83
Ash residue	69.38	63.88	80.23
Oxidised ash	1.60	n/a	1.03
HHV (MJ/Kg)	7.88	7.73	8.96

Determination of the HHV values for each component show casings to have the highest calculated calorific value, with an average HHV of 29.11 MJ/kg, which is comparable to bioethanol (26.8 MJ/kg), coke (29.8 MJ/kg) and tyres (30.4 MJ/kg) [164]. Mobile phone screens and PCBs have much lower HHVs, with an average of 9.83 MJ/kg and 8.19 MJ/kg, respectively. The average HHV for a mobile phone is calculated as the sum of the weight fraction of each component multiplied by its HHV value ($HHV_{MP} = \sum [\text{weight fraction} \times HHV_{\text{each component}}]$), giving an estimated HHV for a feature phone as 16.8 MJ/kg, a multimedia phone as 14.59 MJ/kg and a smartphone as 10.32 MJ/kg. The decrease in the HHV value through the generations is likely due to the increase in the metallic content through the generations, as reported in Table 3.4.

3.3.3.5 *Discussion*

The non-metallic fraction of EoL-MPs was studied in casings, screens, and PCBs. Due to the low representation of cameras and speakers in mobile phones and the fact that plastics in those electronics are mainly attached and not an intrinsic part of their composition, electronics were not analysed further for non-metallic fraction.

FTIR, elemental analysis and TGA-DSC results confirm the casings to be composed of PC, ABS, and PC/ABS blends. Li et al. analysed samples of raw PC, ABS and PC/ABS blend under FTIR, identifying the same functional groups as found in this study, and a peak at 2237 cm^{-1} for $\text{C}\equiv\text{N}$ bond [165]. Palmieri et al. [143] and Fontana et al. [46] also found that PC/ABS blends, PC, and ABS were the most abundant polymers in casings, in that order respectively. Kasper et al. conducted TGA on a mixture of mobile phone casings in a nitrogen atmosphere with a heating rate of $20 \text{ }^\circ\text{C}/\text{min}$ [166]. They found that casings, which mainly consisted of PC/ABS blends, started to degrade at $280 \text{ }^\circ\text{C}$, which agrees with the onset temperature (T_{onset}) of decomposition found for the casings tested in this study ($280\text{-}285 \text{ }^\circ\text{C}$), and the maximum weight loss reported at $478 \text{ }^\circ\text{C}$, is also consistent and within the range of the derivative thermogravimetric (DTG) maximum found in this work for the casings. Caballero et al. [18] reported a C/H ratio of 1.0 for the plastic-rich mobile phone, which is close to the average found for the casings in this study (1.09). The findings from the literature conclude that PC, ABS, and PC/ABS blends were the main polymers in EoL-MPs casings, which is in good agreement with the results reported in this characterisation study.

In the case of PCBs, it was found that bisphenol-A (BPA) epoxy resins and unsaturated polyester resins (UPR) were the main polymers. Normally, FR-4 PCBs are used in mobile phones, which are composed of a multilayer of epoxy resin, fiberglass, and copper layers, and give the PCB its conductive

properties [12, 96]. Kasper et al. obtained FTIR spectra of baseboard PCB samples and found mainly BPA epoxy resins, whereas the polymers used to embed electronic components in PCBs consists of unsaturated polyester resins [47]. Hence, it is likely that PCBs from the three generations of mobile phones were made up of a mixture of BPA epoxy resins and UPR.

In the case of screens, it has been reported that in the LCD screen the polarising films are mainly made up of cellulose triacetate (CTA), triphenyl phosphate (TPP), polyvinyl alcohol (PVA) and polyethylene terephthalate (PET) [163, 167], while liquid crystal composition is usually complex, comprising more than 20 compounds with elements such as C, H, O and halogens, and organic compounds such as biphenyl, azomethine, phenylcyclohexane, pyrimidine and difluorophenylene, depending on their applications and fabrication patents [168]. In this work, it was not possible to analyse the liquid crystal due to the small size of the mobile phone screens, and due to the mix of polymers, it is considered unlikely that they could have been detected using the analytical (FTIR, TGA & CHN) methods applied in this study. the FTIR, TGA and CHN analysis.

In terms of intrinsic energy, the low HVV value for screens (9.83 MJ/kg) and PCBs (8.19 MJ/kg) make them unsuitable for energy recovery; but the casings showed the highest HVV (29.11 MJ/kg), which is comparable to bioethanol (26.8 MJ/kg), coke (29.8 MJ/kg) and tyres (30.4 MJ/kg) [164], making the casing fraction most suitable as a feedstock for energy recovery. Elsewhere Caballero et al. reported that mixed plastics of casings from mobile phones had an HHV of 26.4 MJ/kg [18] consistent with HHV levels reported here.

3.3.4 Potential Key Value Components for Recycle and Recovery

The results presented in this chapter, confirm a high metal and plastic content in EoL MPs and suggest these offer a resource rich stream. To evaluate the potential for material and energy recovery and recycle a high-level analysis is now reported.

3.3.4.1 Recovery from the metallic fraction

The average concentration and weight-related distribution of 63 metals and metalloids in a mobile phone unit is represented using the Sankey diagram (Figure 3.24), which illustrates the complexity and diversity of the metal composition of EoL-MPs, distributed across key component fractions, with an average total metal content of 93,809 $\mu\text{g/g}$. To construct this diagram, each of the key components of the mobile phone was considered in terms of its representative weight percentage (average mass) derived from the data in Figure 3.7, multiplied by the metal content determined and listed in Table 3.4, resulting in the final metal concentration on average per component per mobile phone. The total amount of metal in PCBs, for example, was found to be 430,370 $\mu\text{g/g}$, and, based on the calculated average weight percentage of PCB in mobile phones quoted in Figure 3.8, the final amount obtained is 77,504 $\mu\text{g/g}$, as shown in Figure 3.24. PCBs account for the largest concentration of metal, with approximately 83% of the total metal fraction, followed by screens, speakers, and cameras at 8%, 5% and 4%, respectively. It is noted that although speakers and cameras account for only 2% of the total weight of a mobile phone (1% each), the metallic content found in them is nearly the same as in screens, which represent 15% of the total mobile phone weight. This is because of the low metal content in screens, and the high content of glass, plastics, and ceramics. Extrapolation of the data in Figure 3.24 on the content of metal per mobile phone ($\mu\text{g metal/g mobile phone}$), permits an estimate that 1 tonne of EoL-MPs can contain up to 53 Kg of copper, 141 g of gold, 270 g of silver, 10 g pf platinum, 18 g of palladium and 3.3 kg of REEs, among other precious and critical metals. In waste PCBs (WPCBs), these amounts are much higher. One tonne of WPCBs can contain up to 278 Kg of Cu, 1.3 Kg of Ag, 678 g of Au, 98 g of palladium, 38 g of platinum, and 11.1 Kg of REEs (mainly erbium, neodymium, and dysprosium).

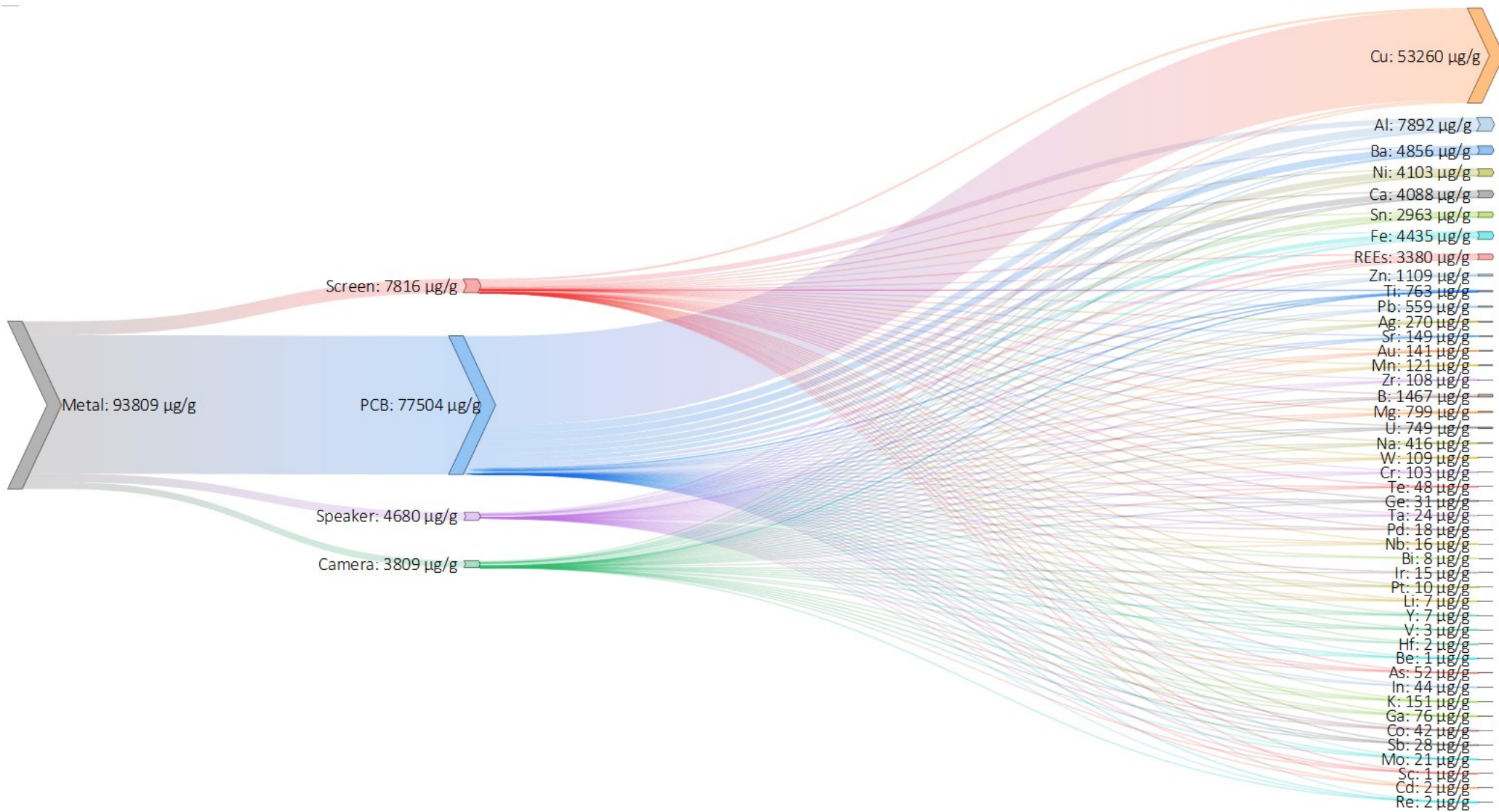


Figure 3.24: Average concentration and distribution of metals and metalloids in EoL-MPs.

The metallic fraction of EoL-MPs showed the presence of 63 metals and metalloids in different components of mobile phones. To permit comparison of the metals concentration in EoL-MPs and the primary ores of the metals used in EEE, Table 3.11 was compiled with data derived from the literature, expressed in terms of economic value and risk supply, their concentration in primary ores, energy use in metal extraction, estimation of the peak production, recycling rates and prices. Peak production values quoted were estimated by Sverdrup et al. using the Hubbert's model, which was first developed to estimate the oil peak production in the 1950's, being successfully applied to other materials such as coal, gas, and uranium [64]. Comparison of the metal concentrations of EEE metals found in primary ores and the corresponding values, derived in this work for EoL-MPS and WPCBs, show that the concentration of base metals is higher in the respective natural ores. The exception, however, is copper, where the concentration is between 5 and 28 times higher in EoL-MPs and WPCBs, respectively than in primary ores, and precious metals are found in much higher concentrations in the EoL products and waste components than in their natural ores. For the PMG metals, silver is between 5 to 26 times higher in EoL-MPs and between 26 to 131 times higher in WPCBs; gold has a concentration in EoL-MPs of more than 100 times its natural ore, and in WPCBs is more than 600 times higher; and platinum and palladium also show considerably higher concentrations in EoL-MPs and WPCBs from 5 to 32 times higher than their natural ores. REEs are present in relative high concentration with neodymium leading the list, with a concentration of 1,243.6 g/t in EoL-MPs and 1,422.7 g/t in WPCBs. Even though REEs are present in WPCBs, Table 3.4 showed that cameras and speakers were the components with the highest concentration of REEs, especially Pr, Nd, Sm, and Dy. So dismantling and selective separation of the different components of EoL-MPs will be a crucial step for optimum recovery of targeted metals.

The peak production year shows that several of the most important metals for society may run into scarcity within the next decades. Without these metals and oil, peak year of production is estimated to occur in the year 2028, which can bring serious limitations to the development of society, and it could face one of its most severe challenges ever [169]. Gold, platinum, and palladium have already reached their peak production and reserves for production, without any new reserve, could run out as soon as in 20 years, without taking account the increased demand for these precious metals. Furthermore, many of these metals coexist in metallic mineral ore bodies and they are extracted in combination with other metals, or as subsidiary processes. In some cases, the concentration of a desirable metal in the crust can be economically unviable for production in primary ore. Indium is a clear example of this, in which it is obtained almost exclusively as a by-product of zinc mining and processing [79, 149, 152].

From an environmental perspective, it has been demonstrated that recycling or secondary production can greatly reduce the consumption of energy, water, carbon dioxide, fumes, chemicals, waste generated, among others [21, 24, 41, 157, 162, 170]. Table 3.11 also includes values for energy use in metal production from primary (ore) and secondary (scrap) production, in which there is a clear reduction in energy consumption, especially for the PMGs. The real environment impacts, however, are difficult to determine due to limited data. In addition, since several elements are extracted in combination with others, environmental impacts of a single element can be difficult. In some cases of major elements such as iron and aluminium, the environmental impacts are well quantified. For instance, for each tonne of aluminium produced, there is an associated waste generation of 150-250 tonnes, known as red mud [79]. This large amount of waste is generated where the amount of the Al in the ore is approximately 20-24% (high-grade ore), which is considerable higher compared to other elements. In the case of elements with lower concentration, the waste generated is much larger.

Table 3.11: Main metals used in EEE, concentration in primary ores, estimates of peak production, recycling rates, and prices.

Metal	Conc. primary ores (% w/w or g/t)	Conc. EoL-MPs (%w/w or g/t)*	Conc. WPCBs (%w/w or g/t)*	Energy use in metal extraction (MJ/Kg) ⁱⁱⁱ		Global production USGS ¹ (ton)	Reserves USGS ¹ (ton)	Peak production year ⁱⁱ	Reserves to production ² (years)	Recycling rate (%)	Price ³ (US\$/Kg)
				Scrap	Ore						
Base Metals											
Iron	30-60 ⁱ %	0.5 %	1.3%	6	20-100	2,500,000,000	170,000,000,000	2055	68	60 ⁱⁱ	0.2
Aluminium	20-24 ⁱ %	0.8 %	2.5 %	10	238-925	64,000,000	50,000,000,000-75,000,000,000	2020-2040	781-1172	75 ⁱⁱ	2.0
Chromium	0.1-0.5 ⁱ %	0.01 %	0.04 %	6	22-51	44,000,000	570,000,000	2050	13	22 ⁱⁱ	7.2
Copper	0.5-3 ⁱ %	5.3 %	27.8 %	14	31-2,040	20,000,000	870,000,000	2034	44	60 ⁱⁱ	8.0
Manganese	35-55 ⁱ %	0.01 %	0.06 %	-	-	19,000,000	810,000,000	2050	43	45 ⁱⁱ	2.2
Zinc	0.2-0.7 ⁱ %	0.1 %	0.5 %	11	32-63	13,000,000	1,900,000,000	2030	146	20 ⁱⁱ	2.7
Lead	3-15 ⁱ %	0.05 %	0.3 %	9	32-45	11,760,000	2,000,000,000	2020	170	65 ⁱⁱ	2.0
Titanium	35 ⁱⁱ %	0.08 %	0.4 %	-	-	6,000,000	940,000,000	2038	157	40 ⁱⁱ	4.8
Nickel	1-5 ⁱ %	0.4 %	2.0 %	20	130-370	2,700,000	89,000,000	2025	33	60 ⁱⁱ	18.2
Zirconium	8 ⁱⁱ %	0.01 %	0.06%	230	1,320-1,500	1,400,000	62,000,000	2025	44	10 ⁱⁱ	22.5
Magnesium	40 ⁱⁱ %	0.08 %	0.2 %	10	165-230	1,100,000	Large to virtually unlimited ⁴	No data	-	40 ⁱⁱ	2.4
Tin	0.6-8 ⁱ %	0.3 %	1.5 %	15	480-2,180	310,000	4,700,000	2036	15	20 ⁱⁱ	47.3
Molybdenum	0.6-8 ⁱⁱ %	0.002 %	0.005 %	-	-	300,000	17,000,000	2045	57	40 ⁱⁱ	26.0 ⁵
Antimony	0.5-5 ⁱⁱ %	0.003 %	0.006 %	-	-	160,000	1,500,000	2018	9	15-20 ⁱ	5.5
Cobalt	0.5-5 ⁱⁱ %	0.004 %	0.01 %	20-140	140-2,100	140,000	7,000,000	2026	50	40 ⁱⁱ	41.4
Tungsten	0.1-3 ⁱⁱ %	0.01 %	0.04 %	-	-	85,000	3,200,000	2029	38	40	13.5
Lithium	0.1-1.5 ⁱⁱ %	0.0007 %	0.003 %	-	-	77,000	17,000,000 ⁶	2030	221	10 ⁱⁱ	69.8
Niobium	0.5-5 ⁱ %	0.002 %	0.007 %	-	-	74,000	>13,000,000	2025	176	60 ⁱⁱ	12.9

Cadmium	No data ⁷	0.0001 %	0.0003 %	-	-	26,000	4,750,000-9,500,000 ⁸	1998	183-365	80 ⁱⁱ	2.7
Indium	0.1-0.2 ⁱ % 20-50 ⁱⁱ g/t	0.004 %	0.01 %	-	-	760	- ⁹	2022	-	<1 ⁱ	180.0

Metal	Conc. primary ores (% w/w or g/t)	Conc. EoL-MPs (%w/w or g/t)*	Conc. WPCBs (%w/w or g/t)*	Energy use in metal extraction (MJ/Kg) ⁱⁱⁱ		Global production USGS ¹ (ton)	Reserves USGS ¹ (ton)	Peak production year ⁱⁱ	Reserves to production ² (years)	Recycling rate (%)	Price ³ (US\$/Kg)
				Scrap	Ore						

Precious Metals

Rare Earth Oxides	0.3-5 ⁱⁱ %	-	-	-	-	210,000	120,000,000 ¹¹	2060	571	<1 ⁱ	212.8 ¹²
Praseodymium	0.1-4.5 ⁱ %	103.3 g/t	143.8 g/t	1,000-5,000	5,500-1,200	6,100,000 ⁱ	No data	No data	-	<1 ⁱ	95.0
Lanthanum	0.5-20 ⁱ %	36.0 g/t	168.4 g/t	-	-	32,000 ⁱ	No data	No data	-	<1 ⁱ	4.1
Neodymium	0.1-15 ⁱ %	1,243.6 g/t	1,422.7 g/t	-	-	19,000	No data	No data	-	<1 ⁱ	96.5
Yttrium	0.05-2.5 ⁱ %	5.1 g/t	22.0 g/t	-	-	8,900 ⁱⁱ	540,000 ⁱⁱⁱ	2035	61	<1 ⁱ	31.5
Dysprosium	0.1-8.6 ⁱ %	81.3 g/t	87.8 g/t	-	-	100 ⁱ	No data	No data	-	<1 ⁱ	390.7

Metal	Conc. primary ores (% w/w or g/t)	Conc. EoL-MPs (%w/w or g/t)*	Conc. WPCBs (%w/w or g/t)*	Energy use in metal extraction (MJ/Kg) ⁱⁱⁱ		Global production USGS ¹ (ton)	Reserves USGS ¹ (ton)	Peak production year ⁱⁱ	Reserves to production ² (years)	Recycling rate (%)	Price ³ (US\$/Kg)
				Scrap	Ore						
Precious Metals											
Silver	10-50 ⁱⁱ g/t	269.9 g/t	1317.6g/t	80-180	480-4,280	27,000	560,000	2034	21	80 ⁱⁱ	909,7
Gold	1-3 ⁱⁱ g/t	141.4 g/t	678.3 g/t	140- 230	13,300- 52,300	3,300	50,000	2016	15	95 ⁱⁱ	65891,8
Platinum	3-5 ⁱⁱ g/t	10.4 g/t	38.3 g/t	-	-	180	69,000 ¹⁰	2020	-	70 ⁱⁱ	38,444.1
Palladium	3-5 ⁱⁱ g/t	18.0 g/t	98.0 g/t	-	-	210	69,000 ¹⁰	2020	-	60 ⁱⁱ	83,581.7

References and notes:

i; [13], ii; [64], iii; [170].

*: Concentration values in this study.

1: Global production and reserves of metals were obtained from U.S. Geological Survey (USGS), 2021.

2: Reserves to production was obtained by the division of the reserves by the global production.

3: Metal prices were obtained in January 2021 from MineralPrices.

4: Magnesium metal is derived from seawater, natural brines, dolomite, serpentine, and other minerals. The reserves for this metal are sufficient to supply current and future requirements. Magnesium is also globally widespread.

5: Metal prices were obtained in January 2021 from Metalary.

6: Owing to continuing exploration, identified lithium resources have increased substantially worldwide and total about 80 million tonnes.

7: Quantitative estimates of reserves are not available. Cadmium is generally recovered from zinc ores and concentrates.

8: Cadmium is generally recovered as a by-product from zinc concentrates. Zinc-to-cadmium ratios in typical zinc ores range from 200:1 to 400:1, and the reserves of Cadmium was estimated based on these ratios.

9: Indium's abundance in the continental crust is estimated to be approximately 0.05 ppm, so it is economically unviable its production from primary ore. Indium is most often recovered from the zinc-sulfide ore mineral sphalerite. The indium content of zinc deposits from which it is recovered ranges from less than 1-100 ppm.

10: Production and reserves are based on Platinum Group Metals (PGMs; Palladium, platinum, iridium, osmium, rhodium, and ruthenium).

11: Rare Earth Oxides (REOs) are relatively abundant in the Earth's crust, but discovered minable concentrations are less common than for most other ores.

12: REOs' prices were calculated as the average of the all the REOs' prices. Heavy RREs are more scarce and therefore more expensive, with an average of 345.5 US\$/Kg, whilst light REEs have an average price of 27.2 US\$/Kg. Prices obtained in January 2021 from MineralPrices.

3.3.4.2 Recovery from the non-metallic fraction

Incineration has been widely used in the recycling of plastics from WEEE, from which energy can be recovered and used for electricity [45, 143, 166, 167, 171, 172]. Figure 3.25 shows the calculated intrinsic energy from 1 tonne of EoL-MPs, as 14,405 MJ/ton. The figures were calculated multiplying the HHV of PCBs, screens and casings from Table 3.10 with their respective polymeric content showed in Figure 3.7. In result from the intrinsic energy, casings accounts for 80% of the total value, followed by PCBs and screens with both 10%. The relevance of casings to the total intrinsic energy value is that they account for nearly 40% of the total weight of a mobile phone and has the highest HHV (29.11 MJ/kg).

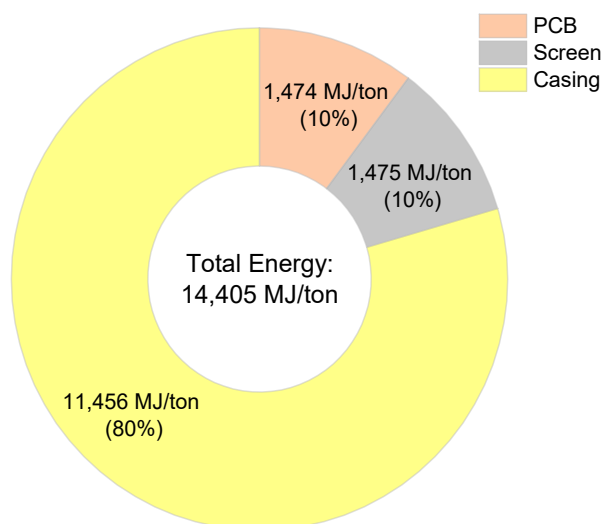


Figure 3.25: Polymeric composition and potential energy recovery per ton of EoL-MPs.

Pyrolysis offers an excellent route to energy and material recovery from the non-metallic organic fraction, and because of its size and operation it is particularly suitable for handling small volume feedstocks of organic materials typical of those found in mobile phone casings. With the presence of flame retardants, especially in casings and PCBs, however, the potential reuse of the pyrolysis products may be limited. In this context, work published by Lateef & Grimes [173] reported the development of a method using ionic liquids to selectively extract brominated flame retardants from composite electronics industry polymer to achieve 100% pure polymer fraction for recycle. This may offer a pre-treatment step, particularly for historical WEEE, before pyrolysis for energy and material recovery.

3.4 Summary

A comprehensive characterisation of multigenerational EoL mobile phones, in which 71 elements, from the metallic and non-metallic fractions, is reported for the first time, and the suite of elements found and expressed in terms of concentration is summarised in the periodic table illustrated in Figure 3.26. These elements were quantified in five main streams: PCBs, screens, casings, cameras, and speakers. EoL-MPs weigh on average 109 g, with the major mass fractions being plastics (40%), followed by metals (35%), and ceramic and other trace materials (25%).

EoL-MPs contain a vast range of precious metals, high-tech minerals and critical raw materials with a clear increase in metals present through the generations of mobile phones. Copper was the metal found with the highest concentration in all the components of EoL-MPs, accounting for approximately 58% of the total metal content in a mobile phone. High-tech elements, REEs, PMG, among other elements were found to be at least twice or up to 600 times more concentrated than in their natural ores, with an upward trend through the mobile phone generations. It is estimated that 1 tonne of EoL contains up to 53 Kg of copper, 130 g of gold, 264 g of silver, 10 g of platinum, 18 g of palladium and 3.3 kg of REEs, among other valuable metals. Quantification of the hazardous elements in EoL-MPs shows that they present a severe risk due to the high content of toxic metals and substances, making smartphones the most 'harmful' of the three generations of mobile phone. Although the concentration of these hazardous substances is found to be below the maximum concentration values tolerated by the RoHS Directive, a proper WEEE management system is crucial to prevent release of these elements to the environment and their likely impact on humans.

The polymeric composition in EoL-MPs shows the main polymers are a blend of polycarbonate and acrylonitrile butadiene styrene (PC/ABS) in casings, cellulose triacetate (CTA), polycarbonate (PC), poly(methyl methacrylate) (PMMA), and polyethylene terephthalate (PET) in screens, and bisphenol-A (BPA) epoxy resins and unsaturated polyester resins (UPE) in PCBs. Among these polymers, casings have the highest HVV (29.11 MJ/kg). The potential intrinsic energy value in 1 tonne of EoL-MPs was estimated to be 431.2 MJ/tonne, where casings accounted for 80% of this value, followed by PCB (10%) and screens (10%). There is a potential for recovery of energy and materials from the polymeric fraction by pyrolysis.

This detailed characterisation of EoL-MP composition reported here shows this e-waste stream to be a resource-rich source of energy and critical metals. The challenges of unlocking this value to recover these secondary resources, (through urban mining) cannot be underestimated but in the chapters that follow the potential for development of methods for selective recovery of the key metals of copper, gold, indium, and rare earth elements is described.

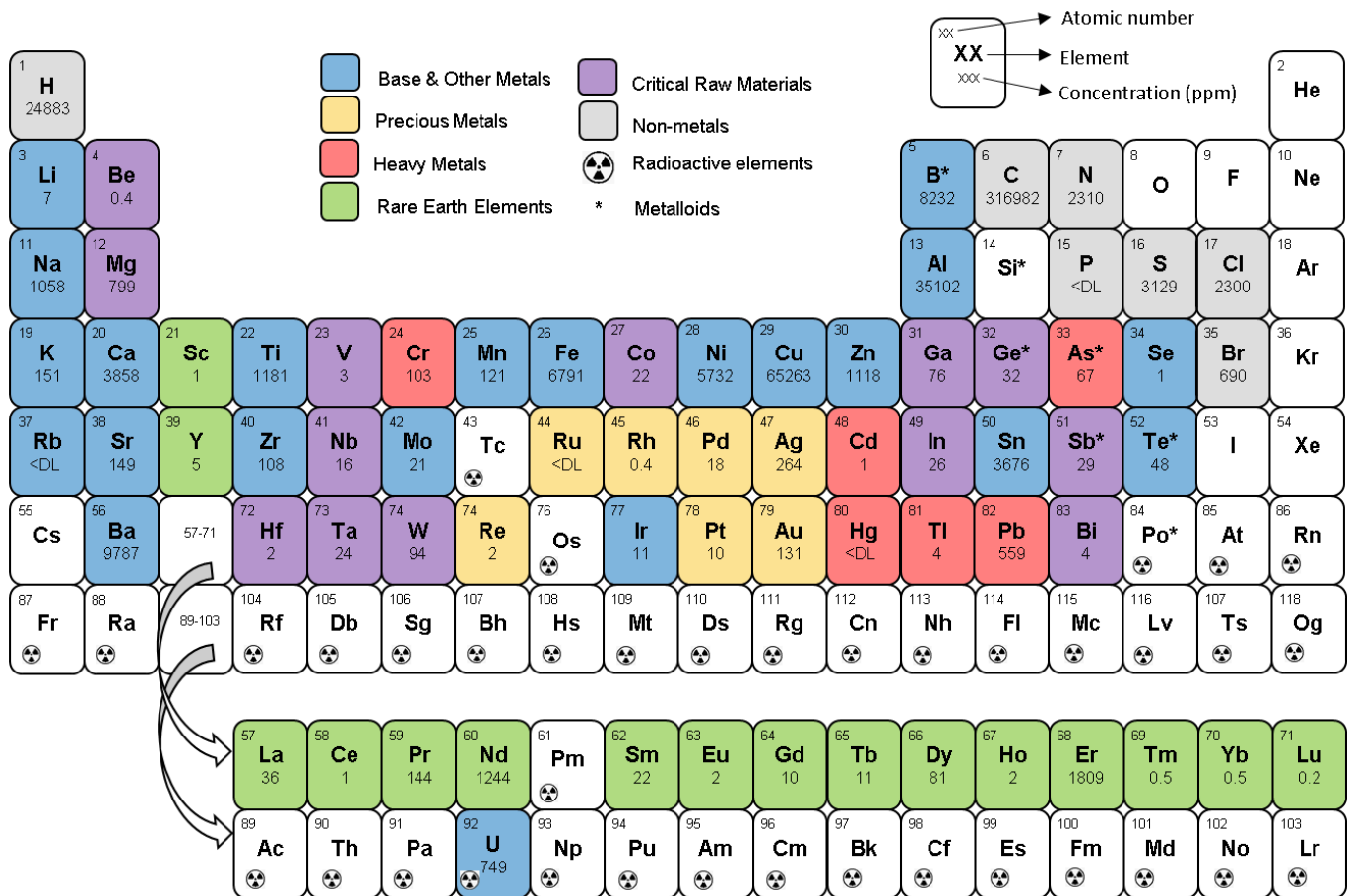


Figure 3.26: Periodic Table to show concentrations of metals, metalloids and non-metallic elements present in EoL multigenerational mobile phones.

4 Copper Recovery from End-of-Life Mobile Phone Printed Circuit Boards Using Ionic Liquids and Electrolysis

4.1 Introduction

Global E-waste Monitor 2020 reported that an estimated 53.6 Mt of waste electrical and electronic equipment (WEEE) was generated globally in 2019, a figure representing a 21% jump in the previous 5 years and with e-waste likely to reach 74Mt by 2030 equating to a growth rate of 2Mt per annum. In 2021, the current estimate stands at 57.4Mt [5]. Although WEEE represents about 3-5% of the total waste, its growth is 2-3 times faster than other solid waste and represents more than 70% of the hazardous in landfill [174-176]. Printed circuit boards (PCBs), which are essential components of WEEE, account for approximately 3% of its total weight and has also shown a dramatic increase in rate of 17-25% per year [105, 175]. Despite the small size of PCBs, they have a high pollution potential, being one of the most hazardous components of WEEE due to the presence of several heavy metals such as cadmium, arsenic, chromium, lead, and organics, dioxins, furans, for example among other hazardous substances. With improper management of WEEE at end-of-life, these substances can be released and pollute the air, water, and soil, presenting a serious impact on human health and the environment [12, 47].

PCB is a complex composite material containing valuable components such as metals and engineering plastics as well as hazardous materials that include heavy metals and halogenated flame retardants [96, 97, 176, 177]. A typical PCB contains approximately 40% metallic, 30% plastic and 30% ceramic and other materials [12]. This composition can vary depending on the device, its year of production and manufacturer. In the characterisation of EoL mobile phones reported in Chapter 3, it was shown that copper is the most abundant metal in multigenerational mobile phone PCBs, with an average of 28% by weight, which accounts for nearly 70% of the total metal composition in PCBs; and there is a clear increase in copper content through the generations. Other authors have also reported copper as the most abundant metal in different PCBs, within a range of 20-35% by weight [12, 91, 97, 105, 176, 177]. In 1 tonne of waste PCBs (WPCBs), there is approximately 280 kg of copper; a level which is between 10 and 26 times higher than its ore [104, 177]. The International Copper Study Group (ICSG) had estimated a copper deficit of 320,000 tonnes in 2019 and 600,000 tonnes in 2020 [178]. In addition, it was reported that more than 70% of WPCBs are not treated and are incinerated or landfilled [12]. Recent publications assessing global copper demands and environmental implications

of supply to meet that demand [179-181] confirm the greater need to recycle copper from the copper-rich source of WPCBs to mitigate these challenges.

The high economic value and the environment issues associated with poor management of WPCBs has led to several studies reporting on the recycling of WPCBs, using a number of methods which fall broadly under three types: (i) *mechanical separation* including crushing, grinding, magnetic separation, electrostatic separation, gravity separation and density-based separation [12, 92, 95, 96], (ii) *pyrometallurgical processes* including smelting, calcination, roasting and pyrolysis [18, 97-99], (iii) *hydrometallurgical processes* [12, 96, 100], extending to biohydrometallurgical methods [96, 101], and the use of supercritical fluids [102]. Nevertheless, many of these processes have constraints associated with their use. Mechanical separation methods can present high material losses, mainly of precious metals, dust, which can contain halogenated flame retardants and dioxins, and dangerous metal fines such as lead, chromium, cadmium [96, 103, 104]. Pyrometallurgical methods are energy intensive with high operational costs and may liberate toxic gases to the atmosphere [12, 104]. Although hydrometallurgical processes use milder operating conditions, require lower capital cost, energy and have less environmental impact than pyrometallurgical methods, the processes can consume a substantial amount of toxic, corrosive and flammable reagents, generating a large volume of wastewater that has to be further treated [12, 91, 104]. Biohydrometallurgical leaching is more environment-friendly, requires low cost of investment and has high selectivity of metals, however, toxic influence of ingredients on the growth of micro-organisms, long reaction times and the high sensibility of the microorganisms for pH and temperature are the major drawbacks [12, 96, 101, 104]. Supercritical fluids are an energy-intensive processes due to the high pressure and temperatures required [12, 102-104]. To overcome the limitations associated with these conventional technologies, several researchers have reported the use of greener technologies for the recovery of copper from WPCBs using ionic liquids (ILs) as leaching agents [104, 109, 154, 176, 182]. The remarkable properties of ionic liquids which include wide liquid range (from room temperature to above 300 °C), negligible vapour pressure, excellent thermal, chemical and electrochemical stability, low viscosity, and high recyclability, make them attractive alternatives to conventional volatile organic compounds (VOCs) [104, 105]. Several authors report the success of ILs in metal leaching, including copper, for recovery from WPCBs [104, 105, 112, 176, 177]. The potential of ILs, however, look promising and form the basis for investigation in the current research. Although researchers have reported the use of ILs for copper recovery [105, 112, 176, 177], there has been little focus on the importance of their role as part of a complete copper recovery process centred on sustainability which forms the basis of the research investigation reported here.

4.2 Methodology

4.2.1 Materials

4.2.1.1 Chemicals and Reagents

All chemicals used were of reagent grade and obtained from either Sigma-Aldrich (USA), VWR (USA) and Fisher Scientific (USA), Alfa Aesar (USA), Fluorochem (UK) and Agar scientific (UK). Unless stated otherwise all chemicals and reagents were used as received.

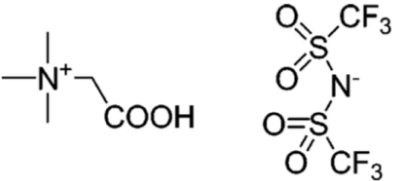
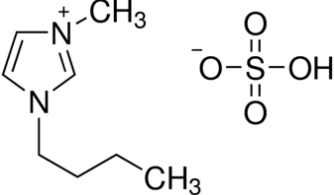
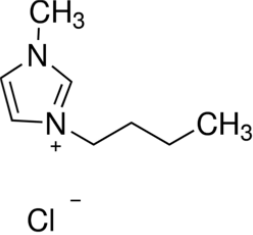
4.2.1.2 Ionic Liquids (ILs)

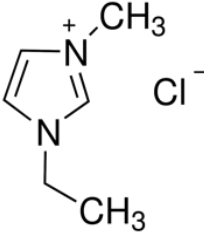
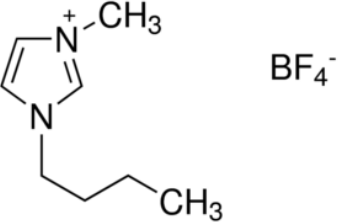
Based on the literature review, five ionic liquids were selected for use in this work. Four of the ILs, namely, *1-butyl-3-methylimidazolium hydrogen sulfate* ($[Bmim]HSO_4$), *1-butyl-3-methylimidazolium chloride* ($[Bmim]Cl$), *1-ethyl-3-methylimidazolium chloride* ($[Emim]Cl$), and *1-butyl-3-methylimidazolium tetrafluoroborate* ($[Bmim][BF_4]$), were purchased and used as received. The fifth IL, *betaine bis(trifluoromethylsulfonyl)imide* ($[Hbet][Tf_2N]$) was synthesised using an equimolar metathesis reaction [107]. In this reaction, 26.7g (0.174 mol) of $[Hbet]Cl$ and 50.0g (0.174 mol) of $Li[Tf_2N]$ were mixed together and dissolved in 50 mL of reverse osmosis (RO) water, stirred at 600 rpm at room temperature for 1h. Two layers were obtained, with the ionic liquid in the lower layer and an aqueous phase in the upper layer. The IL was separated and washed with cold RO water several times until no trace of chloride was detected in the water effluent using the silver nitrate test. The IL was allowed to stand in a fridge for 2h until frozen, and then dried in a vacuum dryer for two days. $[Hbet][Tf_2N]$ appears as a white solid which was ground before use. All ILs were kept in a nitrogen atmosphere bag. Their properties and characterisation (obtained in this work) are summarised in Table 4.1. Four ILs, $[Bmim]HSO_4$, $[Bmim]Cl$, $[Emim]Cl$, and $[Hbet][Tf_2N]$, were selected for testing their potential to leach and extract copper from the printed circuit boards present in the end-of-Life mobile phones (EoL-MPs); the fifth IL, $[Bmim][BF_4]$ was used in the pre-treatment study to remove solder from the WPCBs.

4.2.1.3 Metals and WPCB samples

To determine the solubility of copper in the different ILs, samples of copper metal in different forms - powder, granules, wire, and foil were tested. Other major metals present in WPCBs such as Fe and Zn were also tested for their solubility (as powders) in the ILs to determine the IL that could selectively separate out the target metal, copper. Using the chosen IL, solubility testing was then performed on the as-received WPCBs, either as strips or powder form. These WPCB fractions were obtained using the methods described in Chapter 3. To provide a more representative sample for testing, the WPCB powders from different mobile phone generations were mixed, ground together, and the metal and metalloid concentrations were determined by ICP-OES, using the aqua regia digestion method for characterisation described in Chapter 3. In addition to the 15 EoL-MPs used for characterisation studies in Chapter 3, a further 10 mobile phones selected from the three generations of mobile phone were used in this study to provide a larger source of representative material for the experimental trials.

Table 4.1: Properties, characterisation and structure of the ionic liquids used in this study.

Ionic liquid	Properties & characterisation	Structure
[Hbet][Tf ₂ N]	<p>Appearance: White powder in dry form; colourless, viscous liquid in fluid form Upper Critical Solvent Temperature (UCST) 55 °C M_w: 398.33 g/mol Density: 1.727 g/cm³ (20°C), 1.541 g/cm³ (60 °C) Flash point: 60°C FTIR: 3292 (OH), 2998 (CH), 1768 and 1758 (C=O), 1721 (COO), 1495 (CH₂), 1477 (OH), 1423 (COOH), 1348 and 1138 (νSO₂), 1178 (CN), 1049 (νSNS), 928 (OH), 793 (νCS), 741 (δCF₃), 669 (δSNS), 607 (δSO₂) TGA-DSC: Onset decomposition temperature: 350 °C. Residue: <1 wt.% at 700 °C</p>	
[Bmim]HSO ₄	<p>Appearance: Light-yellow liquid M_w: 236.29g/mol Density: 1.277 g/cm³ (25 °C) Flash point: 284 °C FTIR: 3200-2500 (OH), 3105/ 2961 (CH), 1573/1466 (C=C, aromatic), 1229/1166 (CN), 1070-1033 (S=O), 841/655 (C=C), 759 (C-H) TGA-DSC: Onset decomposition temperature: 340 °C. Residue: 5 wt.% at 700 °C</p>	
[Bmim]Cl	<p>Appearance: White to light-yellow crystalline powder M_w: 174.67 g/mol Density: 1.086 g/cm³ (20 °C) Flash point: 192 °C FTIR: 2973 and 2870 (C-H), 3330–3450 (quaternary amine salt formation with chlorine), 1635 (C=C), 1600 (C=N), 840 (C-N) TGA-DSC: Onset decomposition temperature: 270 °C. Residue: <1 wt.% at 700 °C</p>	

[Emim]Cl	<p>Appearance: Pale yellow crystalline powder</p> <p>M_w: 146.62g/mol</p> <p>Density: 1.11 g/cm³ (20 °C) 1.435</p> <p>Flash point: 186 °C</p> <p>FTIR: 3051/2979/2866 (C-H, alkane), 1573-1459 (C=C, aromatic), 1360-1080 (C-N, Amine), 892-665 (C=C, alkene)</p> <p>TGA-DSC: Onset decomposition temperature: 270 °C. Residue: <1 wt.% at 700 °C</p>	
[Bmim]BF ₄	<p>Appearance: Colourless, viscous liquid</p> <p>M_w: 226.03 g/mol</p> <p>Density: 1.21 g/cm³ (20 °C)</p> <p>Flash point: 288 °C</p> <p>FTIR: 2941 (CH, aliphatic asymmetric), 2877 (CH, symmetric), 1193 and 1112 (CH₃), 1655 (CC), 1465 (CN), 748-623 (C-N) , 3124–3200 (quaternary amine salt formation with tetrafluoroborate).</p> <p>TGA-DSC: Onset decomposition temperature: 370 °C. Residue: <1 wt.% at 700 °C.</p>	

Molecular weight (M_w), densities and flash point values were obtained from Sigma Aldrich, Chemical Book and PubChem in 2020. FTIR vibrations were obtained as part of this work and compared with references. TGA-DSC information reported were obtained in this study.

4.2.2 Analytical Techniques for Characterisation

The analytical techniques used for characterisation of materials in this study are described in Chapter 3. Figure 4.1 summarises the analytical methods applied, and the measures used to determine the effectiveness of the steps towards extraction and recovery of copper from WPCBs, reported in this chapter, under the four key process stages of *Leaching*, *Pre-treatment*, *Electrowinning*, and *IL Recyclability*.

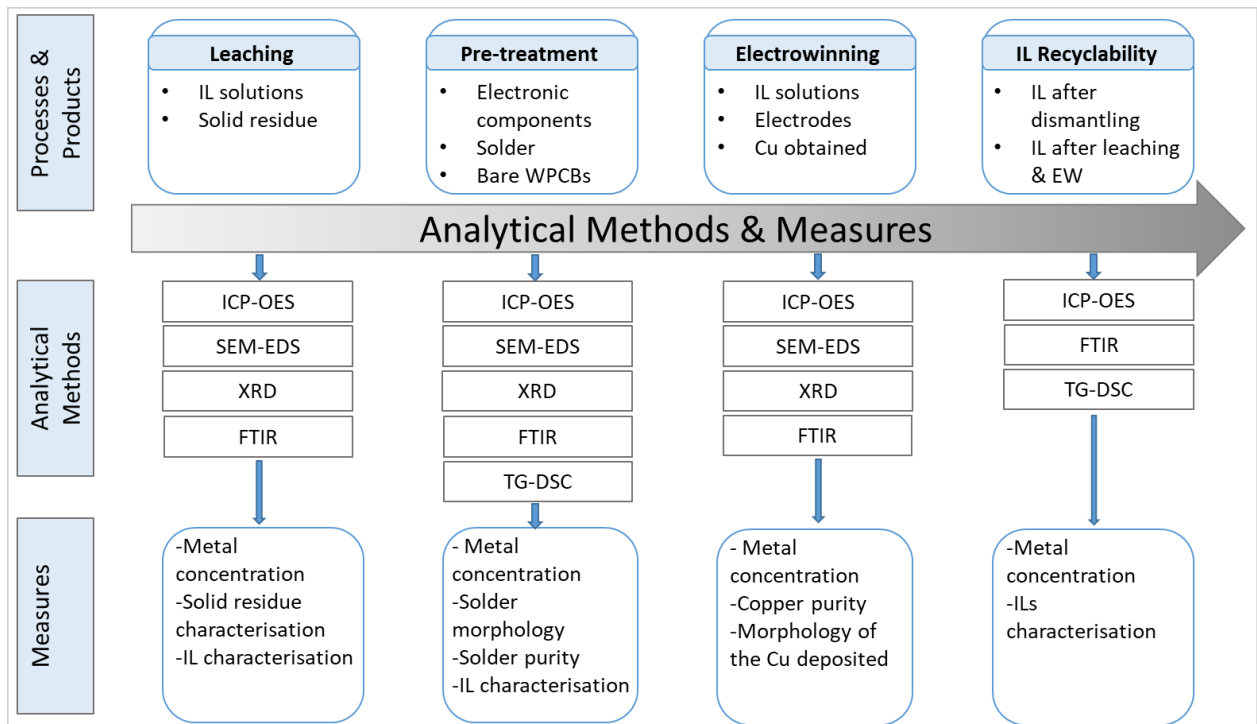


Figure 4.1: Analytical methods Applied and Measures Used to Determine the Effectiveness of the Extraction and Recovery Methods Proposed.

4.2.3 Experimental Procedures

To investigate the potential for recovery of copper from WPCBs derived from multigenerational mobile phones, a four-step approach is followed: (i) solubility testing to determine the selective solubility properties of ionic liquids for copper, and other non-target metals, as a step towards establishing the optimised conditions for IL-leaching of copper from as-received WPCBs, (ii) pre-treatment of as-received WPCBs to remove solder and electronic components to permit the selective IL extraction of copper into solution, (iii) electrowinning of copper from the leached solution to achieve full copper recovery, and (iv) the potential for recovery of the ionic liquids for recycle and reuse. An overview of the experimental procedure followed is set out in Figure 4.2.

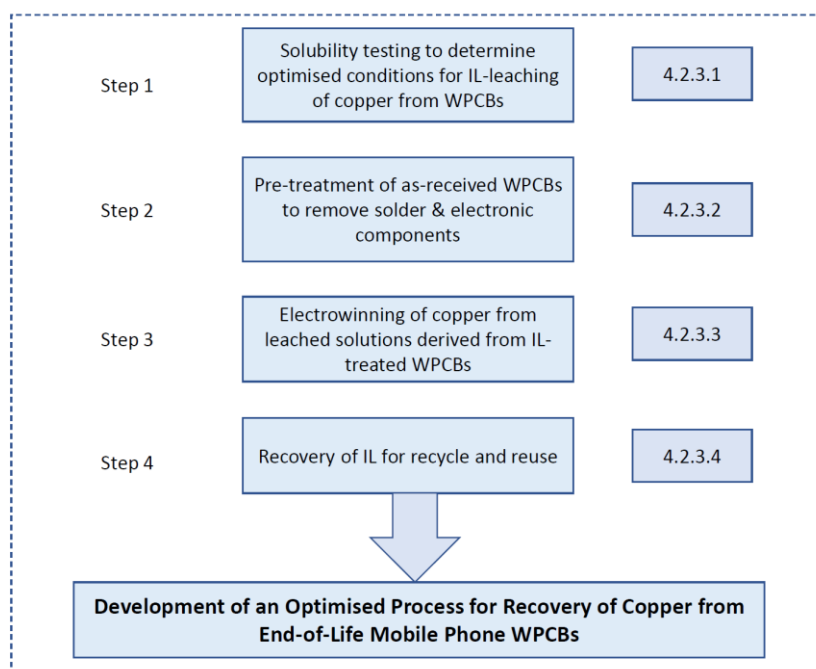


Figure 4.2: Overview of Experimental Procedure.

4.2.3.1 Solubility Testing to Determine the Optimised Conditions for Leaching of Copper from WPCBs Using Ionic Liquids

Solubility tests were carried out to investigate the potential for ILs to leach copper and determine the extent of solubility of copper and other metals present in WPCBs in each of the four ILs ([Bmim]HSO₄, [Emim]Cl, [Bmim]Cl and [Hbet]NTf₂). A stepwise approach to the investigation involved as a first step tests on (i) a mono-metal system using copper, presented in its different forms of powder, granules, wire, and foil, (ii) a mixed metal system that included the dominant metals present in WPCBs alongside copper, and (iii) a WPCB as-received sample derived from EoL-MPs. Using the detailed characterisation data reported in Chapter 3 for WPCBs, simulated solutions were prepared for testing. Solubilities were determined in g/L and due to the high viscosity of the ILs, which makes it difficult to measure volume transfer of an IL from one piece of equipment to another, ILs were weighed to obtain a volume of 1 mL, based on their densities listed in Table 4.1. All tests were performed in triplicate.

4.2.3.1.1 *Mono-metal system*

The mono-metal system using copper, presented in its different forms of powder, granules, wire, and foil was carried out to determine the most suitable IL for copper leaching. Prior to the leaching process, the solubility of copper in ILs was tested by adding a small amount (10 mg) of copper, the solute, to the IL (1 mL). The tests were carried out using test tubes, each containing the solute and the IL, placed in a water bath on a temperature-controlled heating plate to permit measurements of the extent of solubility over a temperature from room temperature to 80°C. Additional amounts of copper (10 mg) were added if the initial 10 mg had fully dissolved. After each experiment, the undissolved copper remaining in the test tubes was filtered using Fluoropore Membrane Filter with 1.0 µm pore size and washed with methanol three times. The residual copper was dried in an oven for 3 h and weighed. The solubility of a copper was calculated using the relationship $[S = (m_i - m_f)/V]$, where m_i is the total metal mass added (mg), m_f is the mass of residual metal after the experiment (mg) and V is the volume of the IL (mL). The effects of temperature (50°C, 60°C, 70°C, and 80°C), time (0.5h, 1h, 1.5h, 2h, and 3h), and dosage of oxidant (H₂O₂) (10 vol.%, 20 vol.%, 30 vol.%, 40 vol.%, and 50 vol.%) on the solubility of copper leaching using copper powder were investigated. The above procedure was followed for each form of copper, as powder, granules, wire, and foil to determine the effect of the particle size and shape of the copper form in the leaching efficiency.

4.2.3.1.2 *Mixed-metal system*

Mixed-metal solutions were studied to investigate the behaviour of copper in the presence of the major metals present in a real WPCB samples. From the characterisation data presented in Chapter 3,

the two key metals selected for study were Fe and Zn. Each metal was separately tested with the selected IL and then with a metal mixed system was prepared for testing. To better simulate the real WPCB, metallic powders were used. All the mixed-metal solutions were prepared using equal amounts of metal powder to produce a Cu:Fe:Zn system, which were tested in each of the four ILs to determine the selectivity of the chosen IL for the target (Cu) or non-target metals (Fe and Zn). The concentration of metals was determined by ICP-OES, and the extraction/leaching efficiency (E) was calculated using the relationship:

$$\%E = \frac{C_i \cdot V_i}{M_i} \cdot 100 \quad \text{Eq. 4.1}$$

where C_i , and V_i are the concentration (mg/L) and volume (L) of the target metal i in the solution, and M_i is the initial amount (mg) of metal i added.

4.2.3.1.3 WPCB as-received sample system

The mixed metal system study confirmed the optimal conditions for the selective leaching of the target metal (copper) from non-target metals (Fe and Zn) from simulated solutions to be achieved using the IL, [Bmim]HSO₄. This IL was selected as the best leaching agent to use for testing the leaching of copper from real WPCB samples and to determine the optimum conditions for extraction. In these studies, the effects of IL concentration (10-100%v/v [Bmim]HSO₄), temperature (from room temperature up to 80 °C), reaction time (from 15 minutes to 3 hours), solid-liquid ratio (from a solid/liquid: 1/1 to 1:20), oxidant agent (hydrogen peroxide, from 10 vol.%, to 50 vol.%), were tested for the leaching of copper from milled WPCBs and separately from WPCB strips. The testing was extended to the use of a more representative sample of WPCB powder which was derived from a mix of mobile phone samples were mixed (described in section 4.2.1.3). The leaching efficiency was calculated using *Eq. 4.1*; but in this case the M_i (mg) was determined using the aqua regia digestion method, as detailed in Chapter 3. In the study of the leaching kinetics, data was obtained from the temperature (20 °C- to 80 °C) and time (15 min. to 180 min.) effect on the metal leaching, used for the determination of optimal leaching conditions.

4.2.3.2 Pre-treatment of As-received WPCBS Using Ionic Liquids

The WPCBs comprise multilayers of epoxy resin and fibreglass coated with layers of thin copper film which gives the PCB its conductive properties, and this substrate structure is used to mechanically support various electronic components (ECs) such as resistors, relays, capacitors, transistors, integrated circuits/chips, etc. To access the copper in the substrate layer requires the ECs and the solder (typically Sn-Pb alloy) which binds them to the resin substrate, to be removed through a pre-treatment step. Based on a method reported in the literature [182] using water-soluble ionic liquids to remove the solder from WPCBs, the ionic liquid 1-butyl-3-methylimidazolium tetrafluoroborate ([Bmim]BF₄) was selected as the medium for trialling the pre-treatment step in the current research, because of its physical properties, low cost, and potential for recyclability. The conditions for trialling included using [Bmim]BF₄ as the heating medium over a temperature range 200 °C to 250 °C, with variable mechanical stirring speeds of up to 150rpm, for variable times from 5 minutes up to 15 minutes, to achieve complete removal of the solder and EC components from the WPCB substrates. Prior to trialling, the WPCB samples were shredded, or cut into strips of approximately 1x1cm², and placed in a small container for solder removal under the conditions described above. WPCBs were cut due to IL constraints, however, WPCBs can be treated without being shredded.

4.2.3.3 Electrowinning of Copper from Leached Solutions Derived from IL-treated WPCBs

The recovery of copper from leach solutions derived from IL-treated WPCBs has been trialled using (i) cementation, and (ii) electrolysis.

4.2.3.3.1 *Cementation*

To recover copper from the IL-leach solutions (in the presence of other metals such as Fe and Zn) a preliminary investigation into the use of the cementation was trialled, based on the standard electrode potentials of copper and the non-target metals of Fe and Zn (Table 4.2).

To a copper sulphate solution, used as the source of copper iron powder was added in stoichiometric proportions. A mixture of 5 mL of 0.1M CuSO₄ with iron powder (Cu:Fe ratios of 1:1, 1:1.5, 1:2, and 1:3) was placed in a test tube and the mixture stirred at 600 rpm for periods of 10 min, 30 min, 60 min and 120 min. After each reaction, the test tubes were centrifuged at a speed of 3000 rpm for 10 min. Cementation to recover copper from an IL-leach system was then tested using the selected optimal conditions, of a Cu:Fe ratio of 1:1.5, 2 h and 500 rpm of agitation. Every test was carried out in triplicate.

Table 4.2: Standard reduction potentials of metals used in this study (25 °C, 101 kPa, 1 M).

Reaction	E° (V)
$\text{Au}_{(\text{aq})}^{3+} + 3\bar{\text{e}} \rightarrow \text{Au}_{(\text{s})}$	1.42
$\text{Pt}_{(\text{aq})}^{2+} + 2\bar{\text{e}} \rightarrow \text{Pt}_{(\text{s})}$	1.20
$\text{Ag}_{(\text{aq})}^{1+} + \bar{\text{e}} \rightarrow \text{Ag}_{(\text{s})}$	0.88
$\text{Fe}_{(\text{aq})}^{3+} + \bar{\text{e}} \rightarrow \text{Fe}_{(\text{aq})}^{2+}$	0.77
$\text{Cu}_{(\text{aq})}^{2+} + 2\bar{\text{e}} \rightarrow \text{Cu}_{(\text{s})}$	0.34
$\text{Cu}_{(\text{aq})}^{2+} + \bar{\text{e}} \rightarrow \text{Cu}_{(\text{aq})}^{1+}$	0.16
$\text{In}_{(\text{aq})}^{3+} + 3\bar{\text{e}} \rightarrow \text{In}_{(\text{s})}$	-0.34
$\text{Fe}_{(\text{aq})}^{2+} + 2\bar{\text{e}} \rightarrow \text{Fe}_{(\text{s})}$	-0.44
$\text{Zn}_{(\text{aq})}^{2+} + 2\bar{\text{e}} \rightarrow \text{Zn}_{(\text{s})}$	-0.76
$\text{Al}_{(\text{aq})}^{3+} + 3\bar{\text{e}} \rightarrow \text{Al}_{(\text{s})}$	-1.66

4.2.3.3.2 Electrolysis

Electrowinning (EW) is a process that has been widely used in the recovery of metals, such as gold, silver, copper, etc. [183, 184], enabling the electrodeposition of metals from dilute solutions, effective metal separation, recovery of the target metal in a directly reusable without further processing and a reduction in problems associated with the effluent disposal, among others [185]. EW critical factors in the design of an electrowinning process are control of pH, cathode surface area and current density.

In this study, a flat-plate electrolytic cell was designed as shown in Figure 4.3. The electrolytic cell comprised a 5mL beaker (to serve as the reservoir chamber), into which were placed a platinum mesh anode and a cathode. The cathode was made of different materials (carbon, copper, nickel, lead, and steel), being a copper mesh the most effective and suitable as cathode. The electrodes were cut as rectangles of 10 mm width and 20 mm length, with a separation of 10 mm. The current was generated using a power supply (RS PRO Digital Bench Power Supply 150W, UK). The electrowinning experiments were carried out in triplicate and maintaining constant currents.

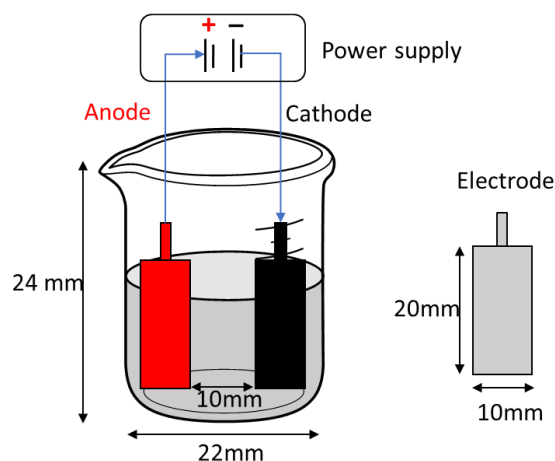


Figure 4.3: Scheme of the flat-plate electro-winning cell developed and used in this work.

For each electrolysis run, the electrolyte, (the IL-leach solution), was placed in the chamber and the electrodes immersed in the solution. The effects of current density (10 mA, 50 mA, 100 mA, and 500 mA) and electrolysis time (15, 30, 45, 60, 90, 120, 180, 240, and 300 minutes) on the target metal recovery were examined. After each run, the electrolyte was sampled and analysed by ICP-OES for metal composition. The cathode deposit was collected and dissolved in concentrated nitric acid and diluted before analysis by ICP-OES to determine the purity of the recovered metal. Samples of the recovered metal powders were further characterised by SEM-EDS and XRD. The metal recovery rate (M_R), purity (P_{Cu}) and current efficiency (η_{Cu}) were calculated, and the specific energy consumption (kWh/kg) determined for the recovery of copper from WPCBs by:

$$E = \frac{zFE_{cell}}{3600\eta M} \quad \text{Eq. 4.2}$$

where z is the number of electrons (2, in the case of copper), F is the Faraday constant (96485 C/mol), E_{cell} is the cell voltage observed during the experiment (V), η is the current efficiency and M is the molar mass of copper (63.546 g/mol).

4.2.3.4 Recovery of the ILs For Recycle and Reuse

Regeneration of the ionic liquid, [Bmim]HSO₄, following leaching and electro-winning was investigated to determine its potential for reuse in further leaching cycles to extract copper from WPCBs and subsequent recovery by electrolysis. Following an optimised leaching and recovery

process by EW, the residual IL-bearing solution was frozen at -10 °C for 1 h, followed by water separation using a freeze vacuum. Once the water was evaporated, the frozen IL changed from solid to liquid, and was used in a further leaching cycle under optimised conditions, followed by electrodeposition. Tests on the recycle of the IL were also carried out on solutions that had not undergone a pre-treatment step (described in Section 4.2.3.2) to determine the extent to which impurities could affect the next leaching cycle; and these tests involved the use of a solvent impregnated resin - XAD-7 resin impregnated with di-(2-ethylhexyl) phosphoric acid (DEHPA). The impregnated resins were added after each cycle (leaching and EW), shaken for 1 h, and then separated using a filter to remove the resins. The IL solution was frozen at -10 °C for 1 h and put in a freeze vacuum for water evaporation, before reuse. The results showed that the use of impregnated resins did not have any considerable effect on the leaching and EW efficiencies. Therefore, the method without the impregnated resins was selected. This procedure was utilised in five consecutive cycles, and triplicates were done in each test.

4.2.3.5 Summary

The four-step approach to investigate the potential for recovery of copper from waste WPCBs derived from multigenerational mobile phones, and to optimise the selective recovery of the target metal, copper, is elaborated further in Figure 4.4 in terms of the processes followed and the component fractions involved.

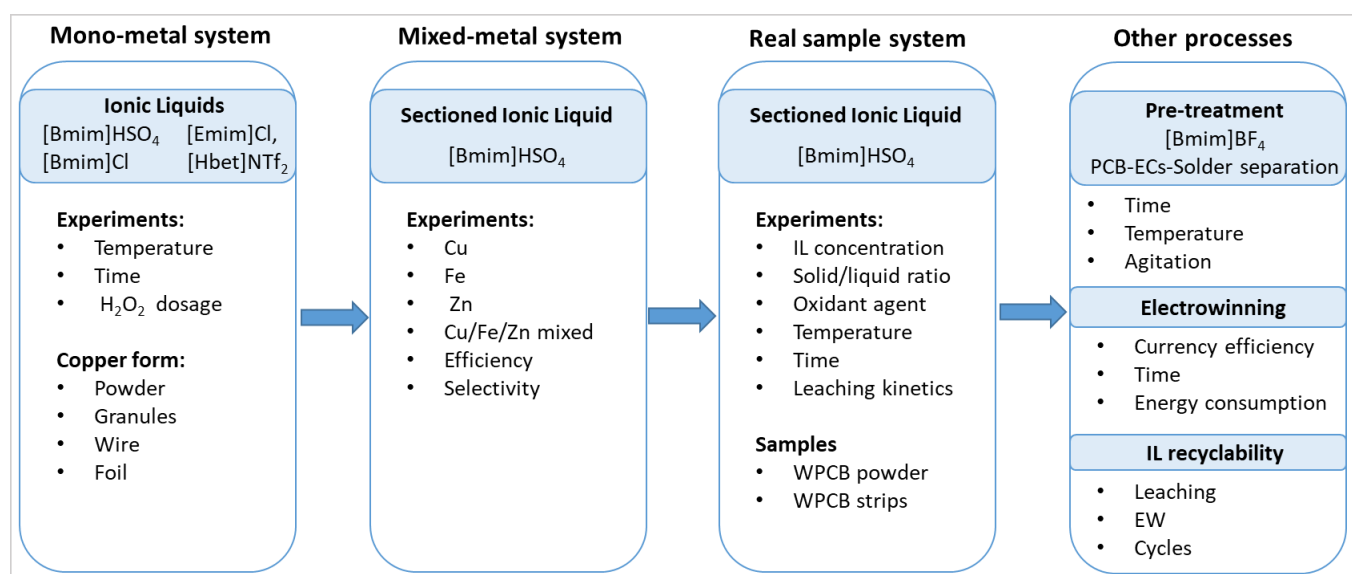


Figure 4.4: Overview of the experimental procedure in the copper recovery process.

4.3 Results and Discussion

4.3.1 Solubility Testing to Determine Optimised Conditions for IL- Leaching of Copper from WPCBs

4.3.1.1 Selection of an ionic liquid for copper leaching from WPCBs in a mono-metal system

The ionic liquids 1-butyl-3-methylimidazolium hydrogen sulfate ([Bmim]HSO₄), 1-butyl-3-methylimidazolium chloride ([Bmim]Cl), 1-ethyl-3-methylimidazolium chloride ([Emim]Cl), betaine bis(trifluoromethanesulfonyl) [Hbet]NTf₂ were selected as potential copper leaching agents based on a literature review. The effects of temperature, time, and oxygen peroxide (H₂O₂) dosage as an oxidant reagent on copper solubility were studied and the results are shown in Figure 4.5. The solubility of copper in all the ionic liquids (ILs) showed a substantial increase with the rise in temperature from 50 °C to 80 °C (Figure 4.5a) In the case of [Bmim]HSO₄, the solubility of copper rose significantly from 1.44 g/L at 50 °C to 3.68 g/L at 80 °C. In the cases of [Emim]Cl, [Bmim]Cl and [Hbet]NTf₂, copper solubility increased gradually reaching a maximum leaching at 80 °C, with 1.94 g/L, 0.70 g/L and 1.39 g/L, respectively. The effect of time is presented in Figure 4.5b, in which it can be seen that in all four ILs, copper leaching increased rapidly until 1.5 h and then plateaued, showing no significant increase when the leaching time was extended beyond 2 h, where Cu leaching in [Bmim]HSO₄ was 4.8 g/L, approximately double that for [Hbet]NTf₂ (2.3 g/L) and [Emim]Cl (2.8 g/L), and six times higher than for [Bmim]Cl (0.8 g/L) after 2 h. The effect of temperature revealed a similar pattern with leaching of copper into the IL in the order: [Bmim]HSO₄ > [Emim]Cl > [Hbet]NTf₂ > [Bmim]Cl. The leaching of copper improved with increased hydrogen peroxide (H₂O₂) dosage (Figure 4.5c), because hydrogen peroxide is a strong oxidant, that assists the acid in the solution and accelerates the oxidation of copper in WPCBs to Cu²⁺ ions in solution [105, 176, 177, 186]. The selection of H₂O₂ as oxidant is due to its decomposition products are oxygen and water, making it more suitable for industrial applications compared to others oxidant such as hypochlorite or permanganate. The oxidised copper (Cu²⁺), produced by addition of the oxidant, hydrogen peroxide, can readily react with the acidic IL [Bmim]HSO₄ to form copper sulphate; and with of the ILs, [Bmim]Cl and [Emim]Cl, to form [CuCl₄]²⁻. In the case of [Hbet]NTf₂ a dual behaviour can be observed. [Hbet]NTf₂ has shown great ability in dissolving metal oxides [107]. Copper oxide (CuO), as a product of the oxidation reaction between the oxidant and copper, can be dissolved by [Hbet]NTf₂, which explains the pronounced increase in copper leaching seen in Figure 4.5c. Additionally, the reaction between [Hbet]NTf₂ and CuO can be facilitated by the addition of water [107]. The decrease in the solubility after addition of 30 vol.% of H₂O₂ could be due to two factors; firstly, as the H₂O₂ dosage increases, copper peroxide can be formed [105] and

secondly, an overdose of H_2O_2 may cause the oxidation of the ionic liquid [Hbet]NTf₂, thereby reducing its efficiency [176].

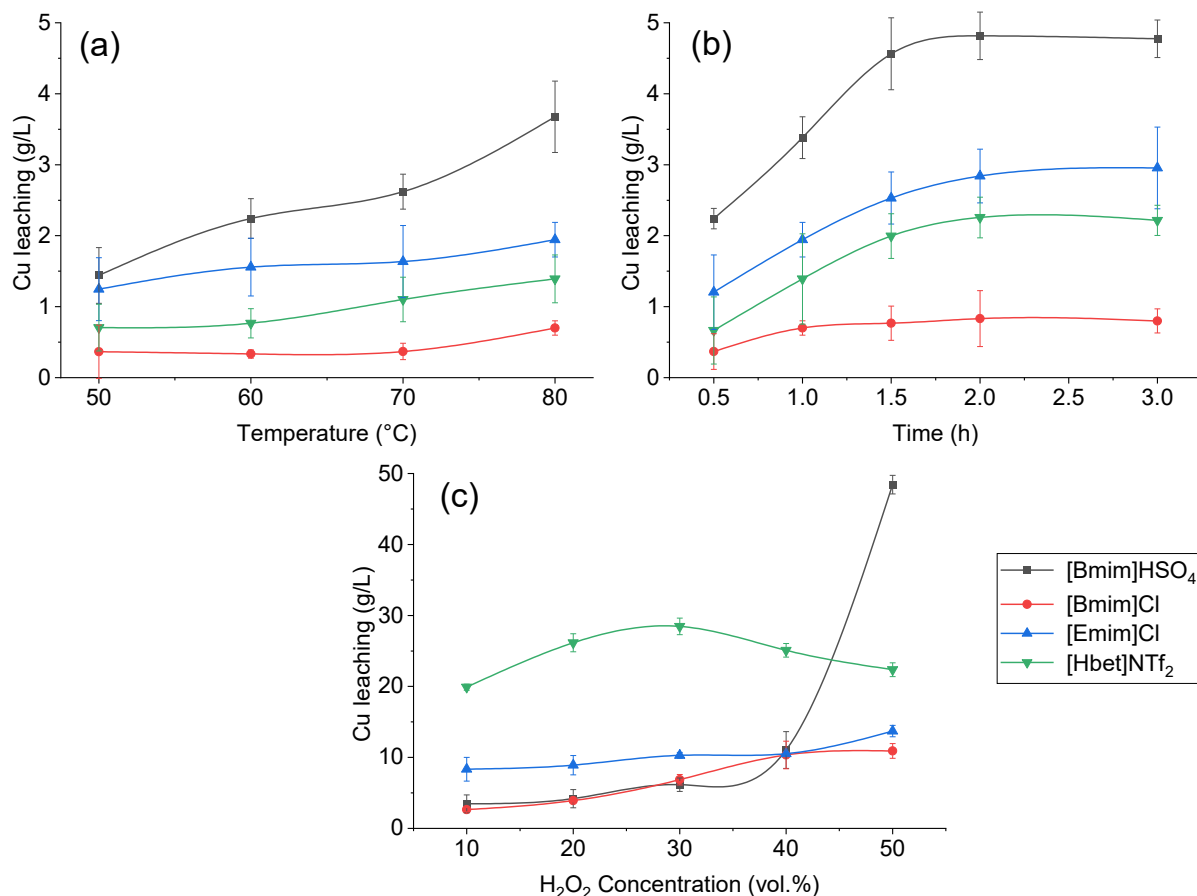


Figure 4.5: Study of different conditions on copper solubility (using powdered copper); (a) effect of temperature, (b) effect of reaction time and (c) effect of the oxidant (H_2O_2) dosage.

Using the optimum conditions identified for temperature, time, and hydrogen peroxide dosage, on the leaching of copper powder, other forms of copper presented as granules, wire and foil were studied to determine the effect of different particle size and shape on the leaching of copper. The comparative results are shown in Figure 4.6. It can be seen from Figure 4.6a that the leaching of wire and foil in the four ILs are all less than 0.3 g/L, which is much lower than that for copper granules, which is not surprising as the copper granules have a much larger surface area, to facilitate the interaction with the ILs. [Bmim]HSO₄ presented a similar trend to that observed in Figure 4.5, showing the highest copper leaching among the ILs. The effect of the different forms of copper was studied further by adding H_2O_2 to aid the copper dissolution. The experiments were carried out under the

optimal conditions (80 °C and 2 h). The highest levels of copper leached with 48.4 g/L, 68.0 g/L and 63.3 g/L for granules, wire, and foil, respectively were achieved with the IL, [Bmim]HSO₄. For [Emim]Cl, the maximum leaching was 13.39 g/L with copper granules and approximately 18.4 g/L for [Bmim]Cl with copper wire. In the case of [Hbet]NTf₂, the solubilised copper wire and copper foil were close to 28 g/L, slightly higher than for copper granules. It can be concluded that whilst the form of copper can significantly impact the leaching process when only ILs are present in the solution, there is little impact on copper solubility in presence of H₂O₂. Based on these results, [Bmim]HSO₄ was selected as the IL that presented the best performance and used as extractant medium for the copper from WPCBs. Furthermore, [Bmim]HSO₄ has several advantages over the other ILs such as solubility in water, environmental friendliness, low cost, and easy availability.

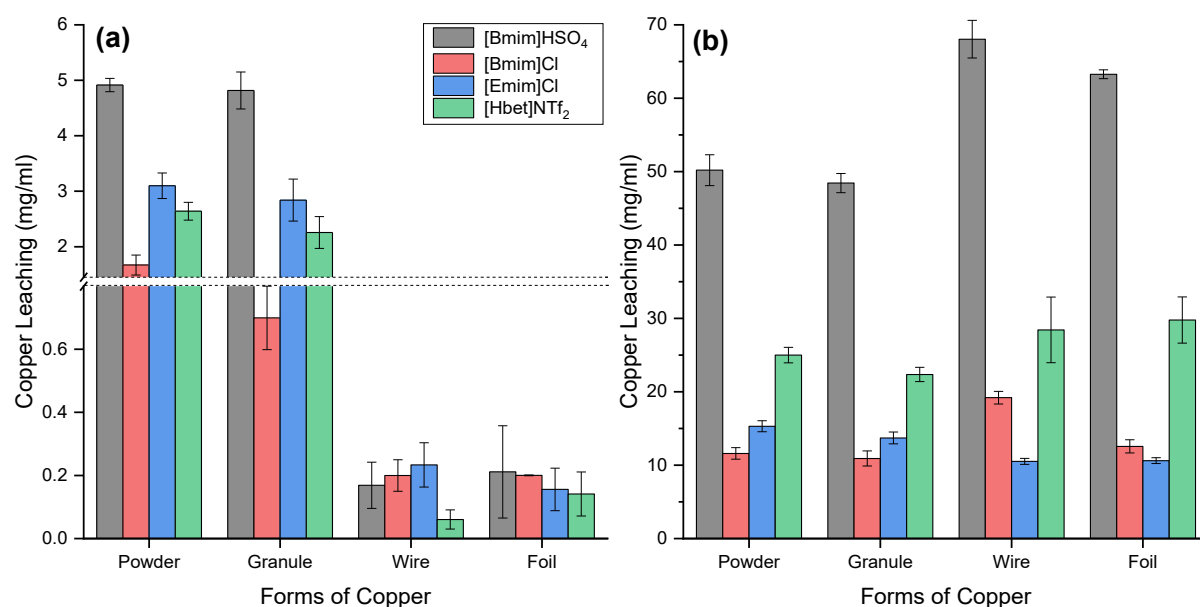


Figure 4.6: Effect of the copper form on leaching; (a) without H₂O₂, (b) optimal condition of H₂O₂ of each IL (50 vol.% for [Bmim]HSO₄, [Emim]Cl and [Bmim]Cl, 30 vol.% for [Hbet]NTf₂). Copper leaching were at 80 °C, 2 h and 500 rpm.

4.3.1.2 Investigation of the Impact of the presence of non-target metals on the solubility of the target metal, copper in a mixed-metal system

Characterisation of WPCBs, reported in Chapter 3, showed copper to be the main metal present with a content between 27% and 32% by weight. Nevertheless, high concentrations of other metals such as iron and zinc are also found, and their presence could impact the copper leaching process. To investigate the IL selectivity for copper, the target metal, in the presence of other metals that co-exist in WPCBs, copper, iron and zinc powder were tested separately in each ionic liquid (Figure 4.7a) and then as a simulated mixture in a 1:1:1 Cu:Fe:Zn ratio (Figure 4.7b) in [Bmim]HSO₄. Figure 4.7a shows that, of the three metals, copper has the greatest dissolution in [Bmim]HSO₄ (76.8 mg/g), followed by zinc (50.6 mg/g) and iron (37.8 mg/g). Nevertheless, in the mixture of these three metals, the solubility of copper decreased to 2.4 mg/g, representing only 3% of its selectivity. The amounts of iron and zinc dissolved in the IL from the mixed metal system, and individually were similar, with a selectivity of 37% for Fe and 60% for Zn. This indicates that when equivalent amounts of metals co-exist, zinc and iron are leached more favourably than copper, significantly reducing the copper leaching efficiency.

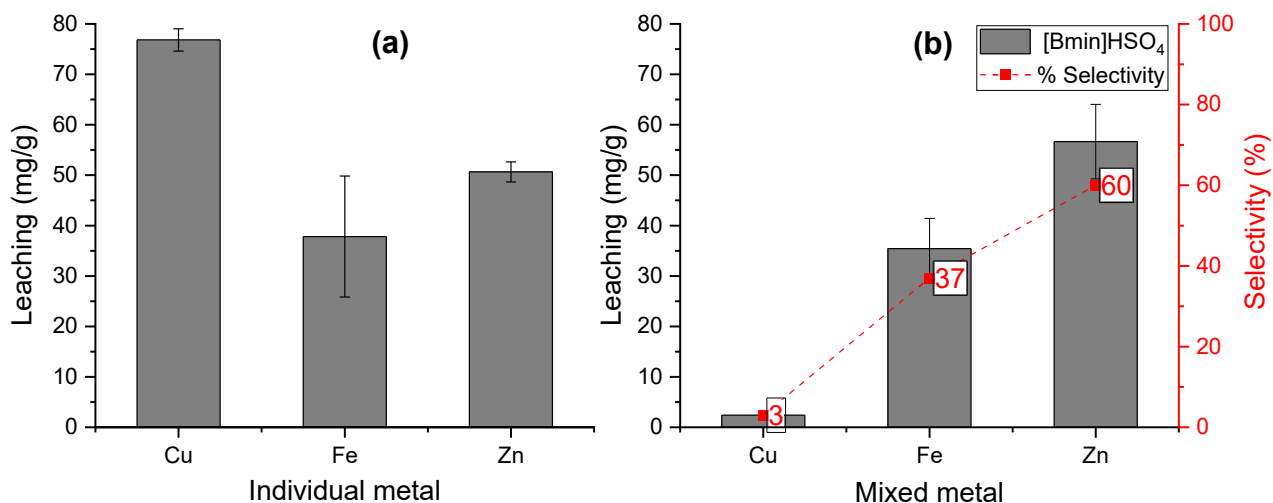


Figure 4.7: Leaching of Cu, Fe and Zn: (a) from single metal solutions, and (b) from a simulated Cu:Fe:Zn 1:1:1 mixed metal solution. Optimal conditions (80 °C, 2 h, 50%v/v H₂O₂, 500rpm).

4.3.1.3 Determination of the optimal conditions for copper leaching from as-received WPCB samples

Among the four ILs studied for the mono-metal system, [Bmim]HSO₄ was shown to be the most effective ionic liquid for copper leaching. This IL was further tested to investigate the impact of the presentation of copper in its different forms, and separately, using simulated mixed metal solutions with zinc and iron to investigate the impact of the presence of other metals found in significantly high levels alongside copper in WPCBs. The inhibiting effect of the non-target metal impurities on the selective leaching of the target metal, copper using the chosen IL, required further investigations into the effects of (i) the IL concentration, (ii) the solid to liquid ratio, (iii) the oxidant dosage, and (iv) time and temperature to optimise the conditions of leaching copper from as-received WPCB samples. The results of these investigations are now described.

4.3.1.3.1 Effect of the [Bmim]HSO₄ concentration

The influence of [Bmim]HSO₄ concentration on copper leaching is presented in Figure 4.8 and confirms that the presence of water is beneficial to the copper leaching. In the zone of 10%-30% (v/v) of IL, the copper leaching increased from 23.1 mg/L to 30.0 mg/L with a maximum achieved at 30% (v/v), after which the concentration decreased to 6.5 mg/L at 100 % (v/v) of [Bmim]HSO₄. This increase in the Cu leaching with the addition of water is due to water helping the sulphate anion present in the ionic liquid to dissociate, acting as an acid. In addition, water can break the hydrogen bonds within the IL, which lowers the IL viscosity, allowing a greater mixing and increasing the dissolution kinetics [105, 177]. As the concentration of IL is higher than 30 % (v/v), the viscosity of the solution is increased, slowing the diffusion and consequently, decreasing the Cu leaching. Thus, 30 % v/v [Bmim]HSO₄ in H₂O is the concentration selected for further copper leaching.

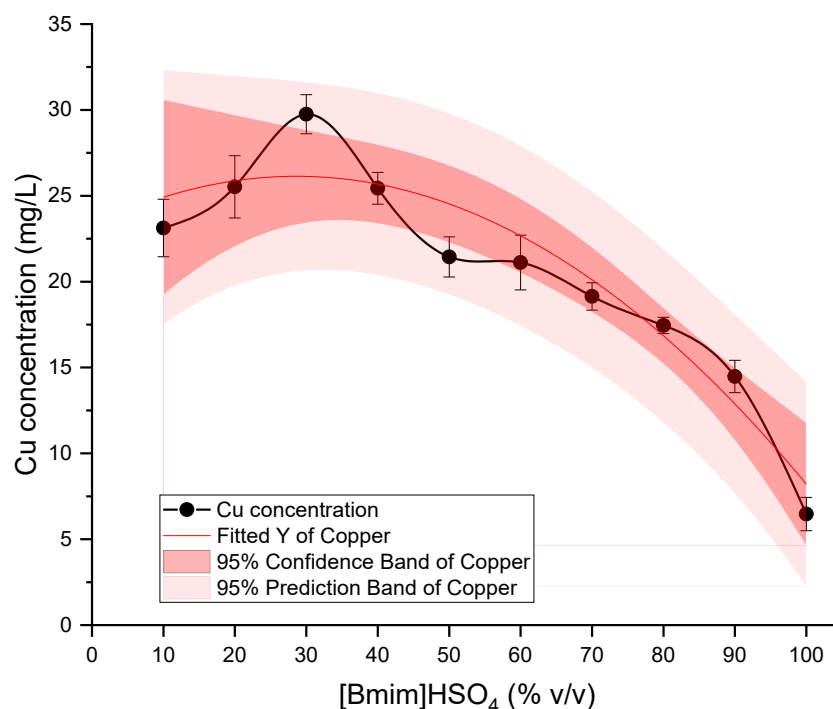


Figure 4.8: Effect of the [Bmim]HSO₄ concentration on copper leaching.

4.3.1.3.2 Effect of the Solid to Liquid Ratio

The effect of the solid-liquid (s/l) ratio (g WPCBs/L [Bmim]HSO₄) on copper and the other significant metals present in WPCBs is shown in Figure 4.9. It can be seen from Figure 4.9a that copper leaching increased significantly (from 60% at s/l of 1.5) with a decrease in the solid-liquid ratio reaching 100% at 1:15 s/l ratio and maintaining this level at solid-liquid ratios lower than 1:15. A decrease in the solid-liquid ratio for the leaching process means an increase in the solution volume allowing greater interaction between the WPCB particles and the IL, increasing the mass transfer efficiency and hence the leaching efficiency [105, 176, 177]. When the solid-liquid ratio is too low, in this case lower than 1:15, although the mass transfer efficiency increases, the leaching of copper (interpreted as yield) remains almost unchanged since the reaction occurs with the same amount of WPCBS powder albeit with a larger solution volume. This also explains the continuous decrease in the copper concentration in the final solution after reaction with the increase of the solid-liquid ratio, which can be considered as a dilution of the solution (Figure 4.9b).

Concentration of other metals in solution (metals considered as impurities) also varied depending on the solid-liquid ratio. Barium showed negligible variation on its leaching efficiency and concentration across the whole range, which showed no interaction with [Bmim]HSO₄. Aluminium showed a slight increase in the leaching efficiency, reaching a plateau of 11% at a solid-liquid ratio of 1:30. Iron, nickel and lead showed a similar trend with a steady leaching rate around 25-30% from a

solid-liquid ratio of 1:5 up to a ratio of 1:15, with maximum leaching peaking at a solid-liquid ratio of between 1:20 (for Fe and Pb) and at 1:30 for Ni. Zinc was the only metal that decreased its leaching efficiency substantially with the decrease in the solid-liquid ratio, from 62% to 0% after a solid-liquid ratio of 1:30. This does not mean that Zn was not leaching out, this is likely due to equipment measures limits since the concentration of Zn was 237 mg/L at a S/L ratio of 1:5, consequently, as the solid-liquid ratio decreases, the volume solution increases drastically, diluting the Zn concentration until it is under the detection limit of the equipment. It is interesting to note that with a large solid-liquid ratio (1:5), the leaching of copper, zinc and iron were 60%, 62% and 45%, respectively. This result confirms the selectivity of [Bmim]HSO₄ towards Zn and Fe over Cu, as confirmed in Figure 4.7b. This is significant since the concentrations of Fe and Zn are 62 and 483 times lower respectively than the concentration of Cu in WPCBs, and even with such differences, the IL still leaches high amounts of Zn and Fe from the mixture. Copper can be leached completely from WPCBs with a solid-liquid ratio of 1:15 and above, thus the selected solid-liquid ratio for the leaching process is 1:15. This solid-liquid ratio minimises the use of reagents, the volume of reaction, the energy used, and the unwanted impurities. The main impurities at this solid-liquid ratio are Ni, Fe and Pb; however, their concentrations are two orders of magnitude less, representing minor impurities in the leaching process.

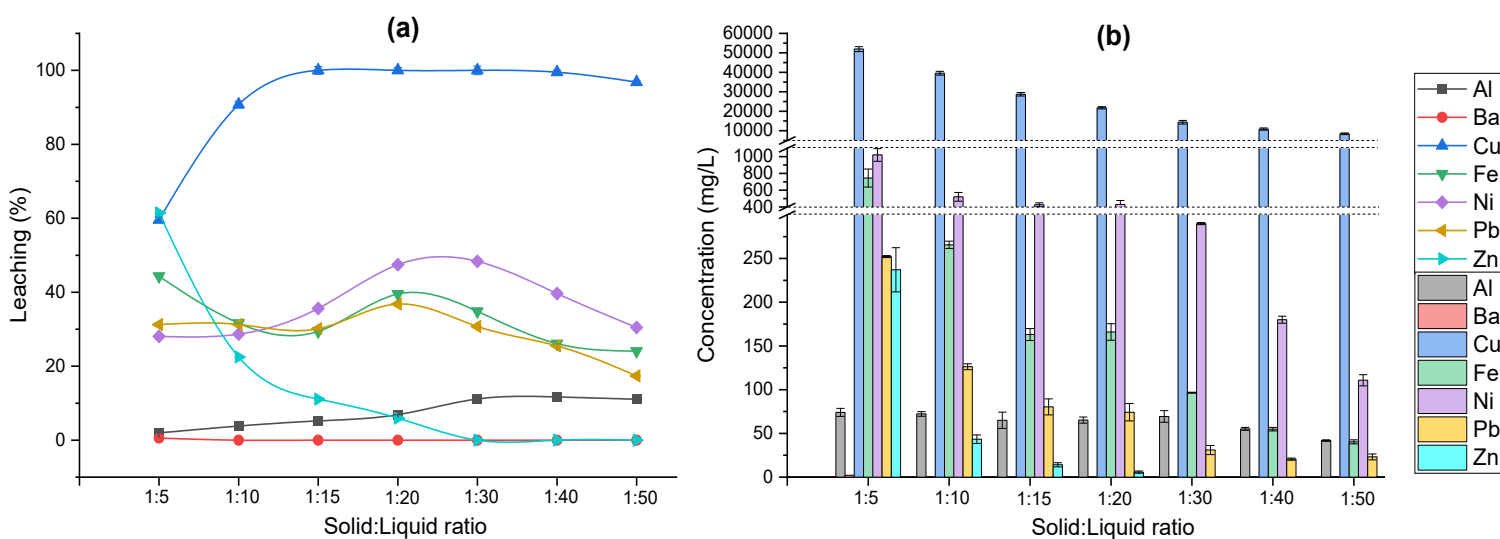


Figure 4.9: Effect of the solid/liquid ratio on WPCBs leaching; (a) leaching efficiency, and (b) metal concentration.

4.3.1.3.3 Effect of Hydrogen Peroxide Dosage

The effect of hydrogen peroxide dosage on the leaching and concentrations of copper and other major metals present in WPCBs is shown in Figure 4.10. The results indicate that copper leaching efficiency is dramatically improved by the addition of H₂O₂. As it can be seen in Figure 4.10b, copper concentration increased from 161 mg/L to 19,697 mg/L with only 5 % (v/v) H₂O₂, leaching 90% of

copper from WPCBs. At a dosage rate of 10 %(v/v) H₂O₂ and above, the leaching of copper is complete, reaching a concentration of 21,647 mg/L. This increase is due to the oxygen produced from the decomposition of hydrogen peroxide reacting with metallic copper to form copper(II) oxide which can further react with the IL to form copper(II) compounds [105, 111, 177].

Aside from Al and Ba, which showed negligible leaching, the other metals present in WPCBs, showed an increase in concentration and consequently their leaching efficiency in the presence of hydrogen peroxide. The hydrogen sulphate anions in the [Bmim]HSO₄ dissociates in the presence of water, and the solubility of metals from the second group of the periodic table (Ba, Ca, etc.) are low, likely due to their precipitation as sulphate salts. Nickel and lead showed an increase in their leaching rate, reaching a plateau from 5 %(v/v) onwards, with Zn and Fe showing generally high leaching but with variable behaviour across the dosages range studied. Although the leaching of nickel was nearly 30%, it is the main unwanted element in the leaching process, with an average concentration of 290 mg/L. Nevertheless, this concentration is much lower when compared to copper (22,700 mg/L), accounting for only 1.2% of the total metals leached. According to previous studies reported in the literature, the use of hydrogen peroxide with ILs has been found to reduce leaching of metals as the dosage rate increases; an observation that is related to a possible oxidation of the IL thus reducing its leaching capacity [105, 176]. In this case, the increase in the dosage of hydrogen peroxide in the IL-water solution did not seem to decrease its leaching efficiency, showing a good stability of the IL. Hence, the optimal hydrogen peroxide dosage for copper leaching is 10 %(v/v), which leaches completely the copper from WPCBs as well as minimises the use of the oxidant agent and the potential oxidation/decomposition of the IL.

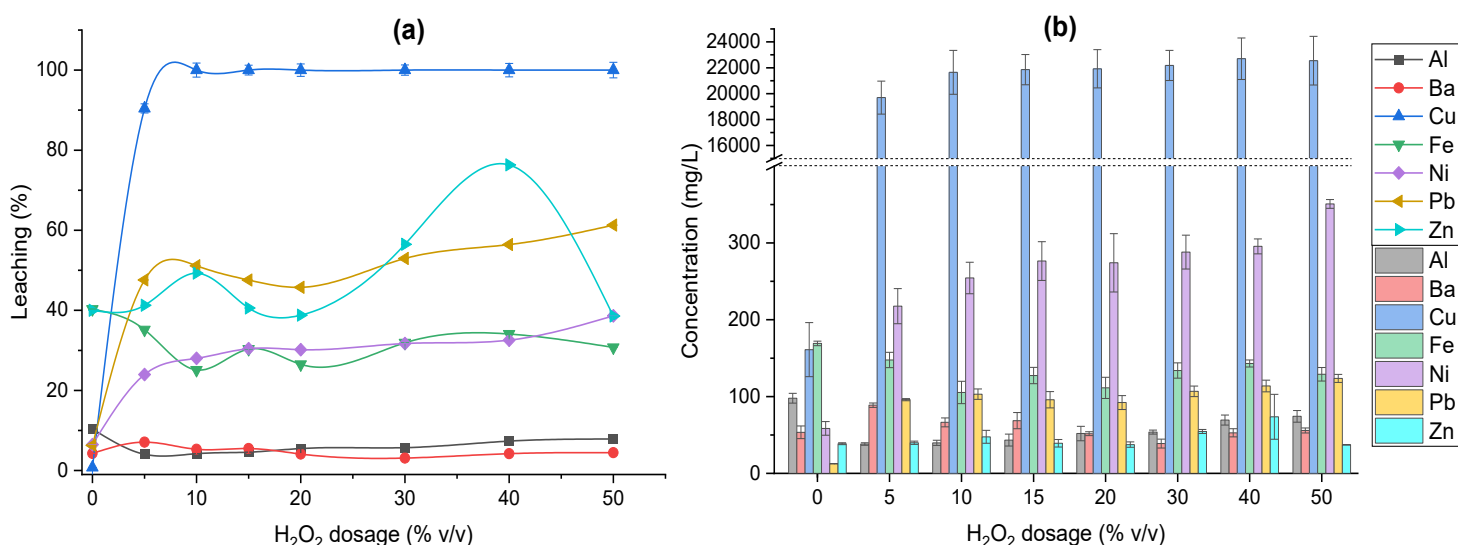


Figure 4.10: Effect of the H₂O₂ dosage on leaching from WPCBs; (a) leaching efficiency, and (b) metal concentration.

4.3.1.3.4 Effect of Time and Temperature

Figure 4.11 shows the effects of leaching time and temperature on the leaching of copper from WPCBs using [Bmim]HSO₄. Increasing the temperature from 20 °C to 80 °C, with time showed that the copper leaching rate increased gradually within the first 60 min, and stabilised as time continued, reaching copper leaching efficiencies of 55%, 66% and 92% at 20 °C, 40 °C and 80 °C, respectively. At 60 °C, the copper leaching efficiency increased steadily over the 2 h, with a greater level of copper leaching (up to 85%) in the first hour, followed by a steadier copper efficiency rate, reaching a 90% of Cu leaching in 2 h. The increase in copper leaching with temperature arises because the kinetic energy of the reactant particles increases, leading to a higher frequency of collisions between the particles, and thus overcoming the activation energy. These observations are consistent with the temperature acting as a catalyst and speeding up the reaction [111, 177].

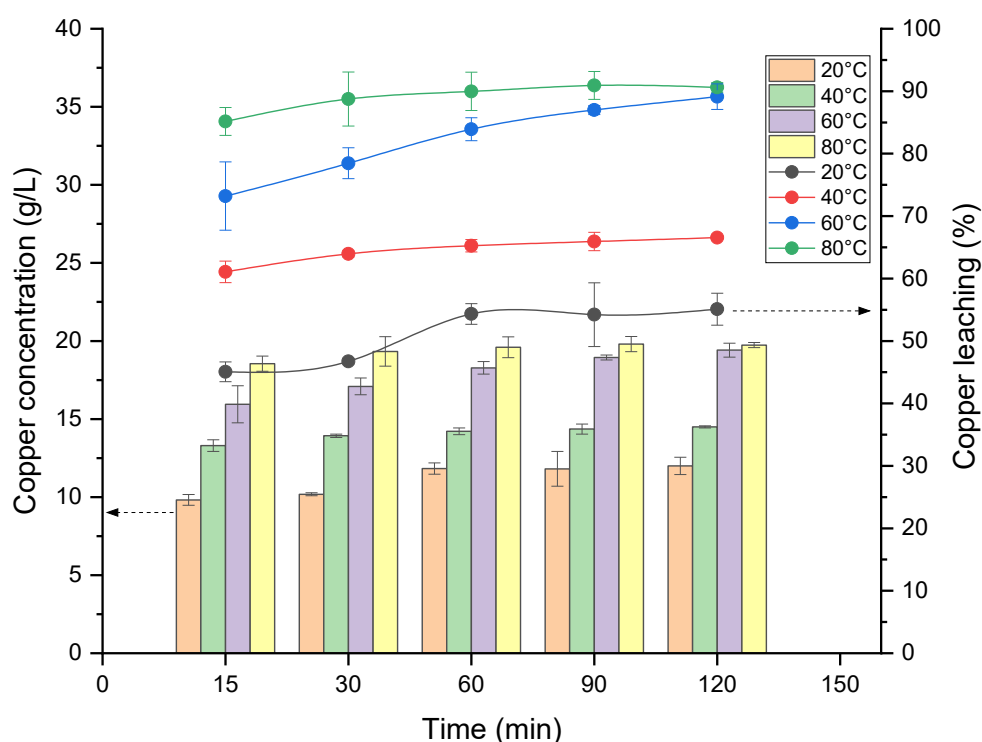


Figure 4.11: Effect of time and temperature on copper leaching from WPCBs.

Figure 4.12 shows the effect of time and temperature on the major metals present in WPCBs leaching. In general, as the temperature increased, the leaching of major metals in WPCBs also increased. Al and Ba showed a slight increase with the rise of temperature, demonstrating once again the poor affinity for [Bmim]HSO₄. Although Fe exhibited a leaching of approximately 20%, its leaching

rate did not increase despite the increase in the reaction temperature. Lead presented a similar behaviour, achieving approximately 50-55% of leaching independent of temperature after 2 h. Nickel showed a relatively low leaching efficiency of 9%, 12% and 19% by 2 h at 20 °C, 40 °C and 60 °C, respectively; however, it presented a marked increase in its leaching at 80 °C after 2 h, reaching 57%. Zinc is the only metal that showed variable behaviour, leaching 50%, 27%, 32%, and 70% at 20 °C, 40 °C, 60 °C and 80 °C after 2 h, respectively. This behaviour could be due to the competition of other metals present in WPCBs. With respect to the concentration, Figure 4.13 illustrates that Pb and Zn were the main impurities at lower temperatures, whilst Ni was of greater concern at higher temperatures. Although [Bmim]HSO₄ can leach several metals with high leaching rates, their concentration is considerably lower than that of copper, with at least two orders of magnitude less. These results suggest that copper leaching at 60 °C for 2 h maximises the copper leaching and minimises the energy consumption and impurities in the leached solution, being selected as the optimal temperature and time for leaching.

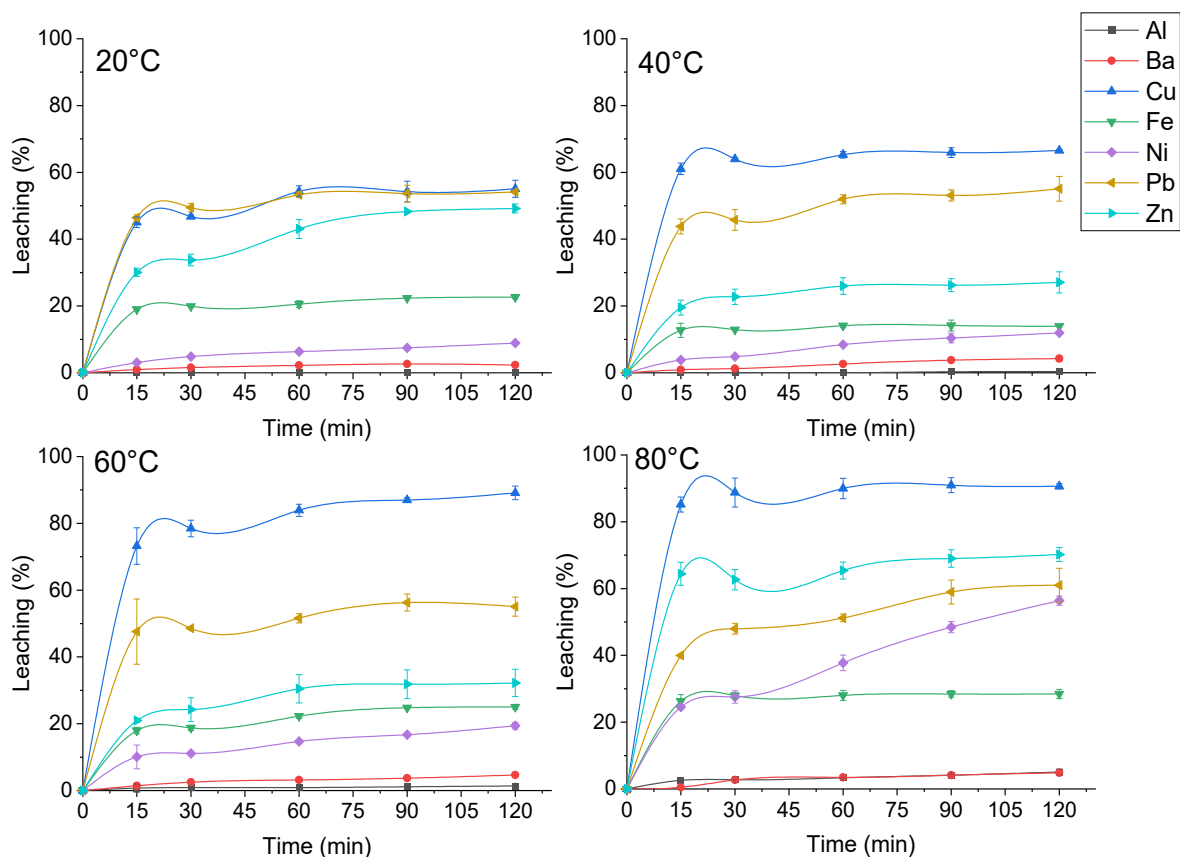


Figure 4.12: Effect of time and temperature on the leaching of major metals present in WPCBs.

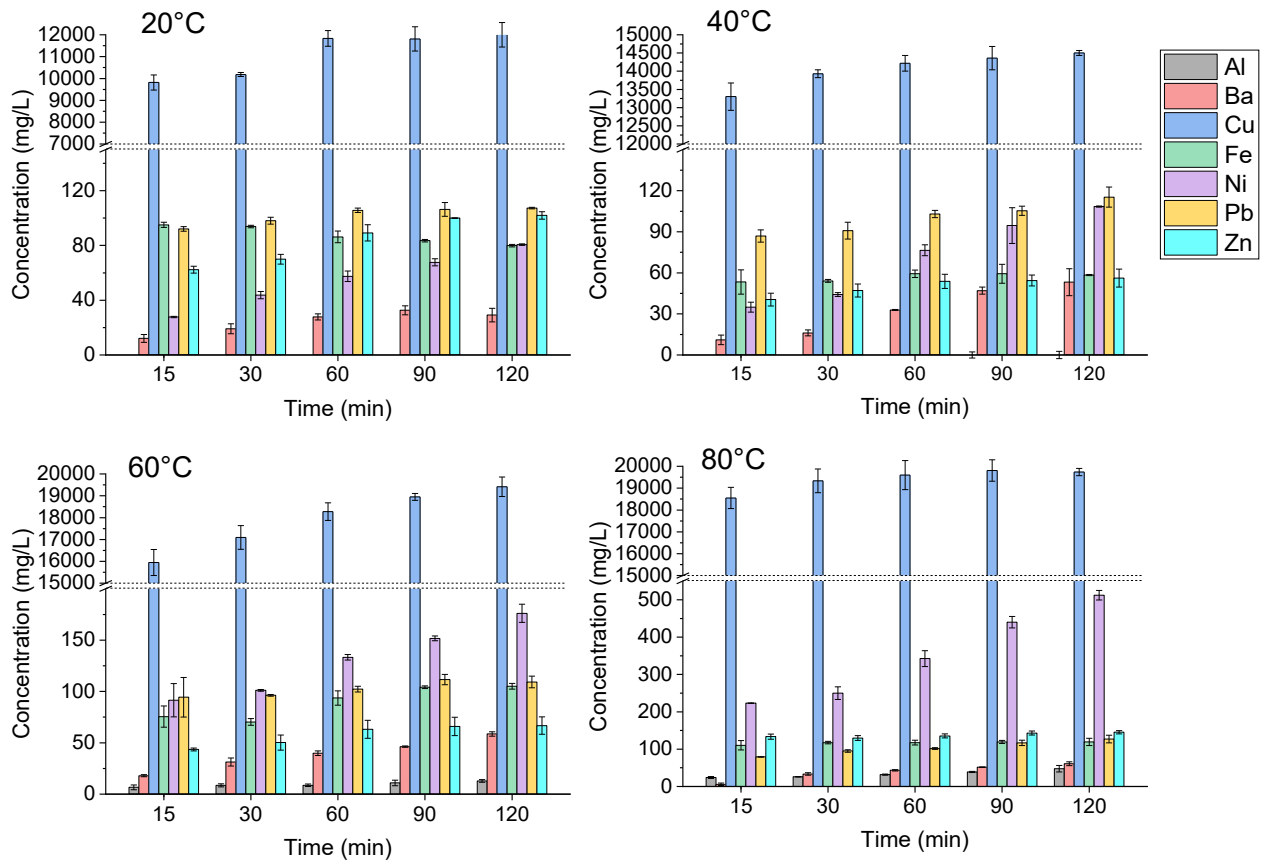


Figure 4.13: Effect of time and temperature on the concentration of major metals present in WPCBs.

4.3.1.3.5 Selection of Optimal Leaching Conditions

Results from investigation of the effect of the [Bmim]HSO₄ concentration, solid to liquid ratio, hydrogen peroxide dosage, temperature and time suggest that leaching of the target metal, copper, can be successfully achieved by careful control of these parameters. The combined optimal conditions for Cu leaching from WPCBs are 30 %v/v [Bmim]HSO₄, 10 %v/v H₂O₂, and 60 %v/v H₂O at 60 °C, 1:15 solid to liquid ratio for 2 h. Under these conditions, the average metal concentrations, their leaching efficiency, and their proportion in the leaching solution of the major metals present in WPCBs achieved are presented in Figure 4.14. It can be observed that the reaction under optimal conditions can leach copper completely from WPCBs, with minor contaminants accounting for approximately 5% of the leached solution (Figure 4.14b), and the major impurities of nickel and zinc with concentrations of 18.5 mg/L and 18.7 mg/L for Ni and Zn, respectively.

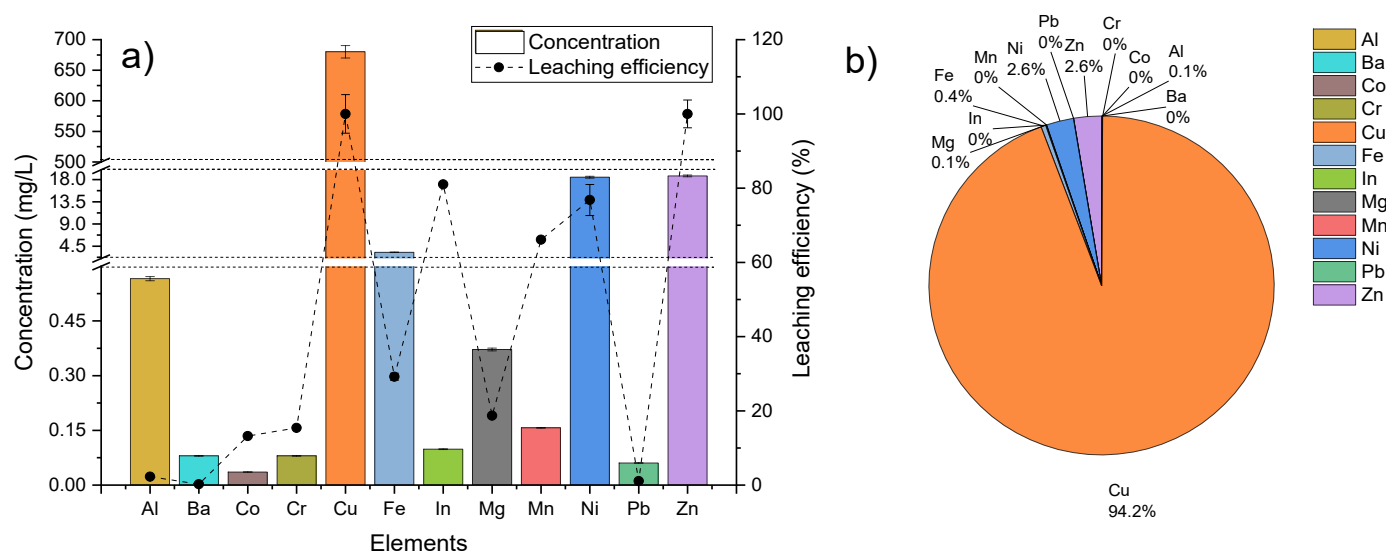


Figure 4.14: Metal leaching from WPCBs using optimal conditions; (a) metal concentration and leaching efficiencies, and (b) metal proportion in solution

Figure 4.15 shows SEM-EDS images of the WPCBs powders before and after the leaching reaction under optimal conditions. As it can be seen from Figure 4.15a and b, WPCBs contain a large variety of metals in different forms and shapes, with copper as the most abundant (shown in red colour). Figure 4.15c and d show that the residual WPCB powder from the leaching reaction, after being centrifuged and dried. The SEM-EDS images confirm that copper has been effectively leached out from the WPCBs, confirming the efficiency of the leaching condition for extracting copper into the IL for further recovery.

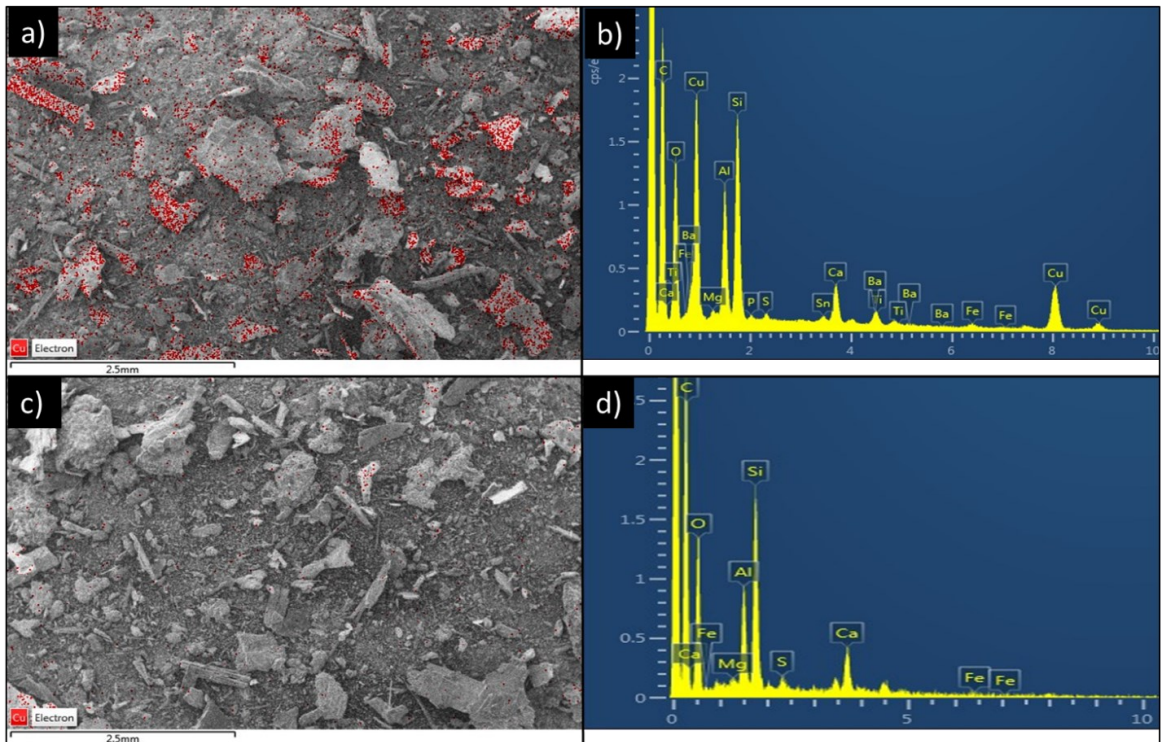


Figure 4.15: SEM-EDS images of WPCBs powders (a) and (b) before reaction, (c) and (d) after reaction.

X-ray diffraction of the WPCBs powder before and after leaching under optimal condition is presented in Figure 4.16. It can be observed that in the WPCBs powder the dominant metal is Cu, with Al, Pb, Sn and Zn also evident to a lesser degree, which is consistent with the composition analysis by ICP-OES. After leaching under optimal conditions, the leached residue (depicted in red) showed a total reduction in the intensity of the Cu peaks, confirming that copper was effectively leached from WPCBs by the [Bmim]HSO₄ solution under optimal conditions.

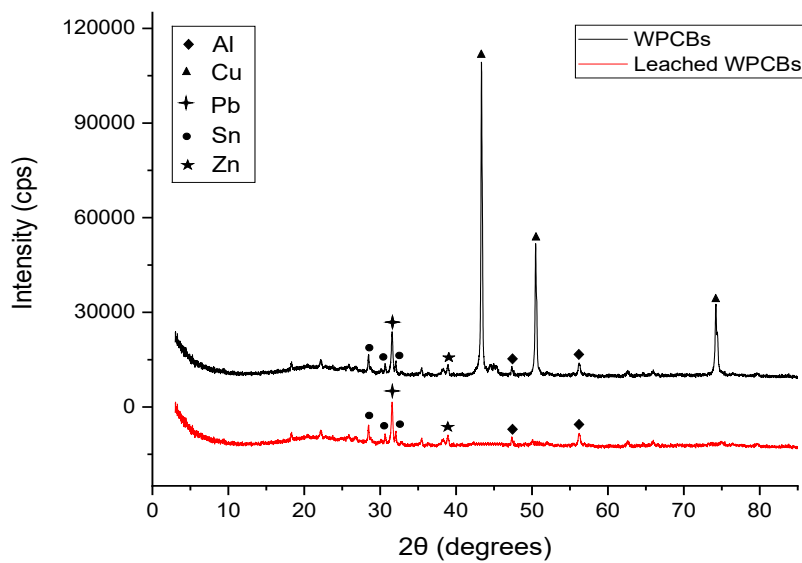


Figure 4.16: XRD patterns of WPCBs powders before reaction and after reaction.

4.3.1.4 Leaching kinetics in [Bmim]HSO₄

To obtain a greater insight into the leaching process and to determine its mechanism, which explain the most effective path of causing the reaction to occur, the leaching kinetics were made targeting Cu as well as the major metals present in WPCBs; Al, Ba, Fe, Ni, Pb, and Zn. Copper leaching in the presence of several other metals is a complex and heterogeneous reaction. In this heterogeneous system, if the metal particles are considered as spherical particles, the copper leaching process can be described by the shrinking core model (SCM). SCM was chosen because it approximates real particles more closely than does the other conversion models in a wide variety of situations [187]. SCM model describes the dissolution or reaction of solid particles, which are consumed by a reagent, in this case the IL/H₂O₂/H₂O solution. The amount of material being consumed in these solid particles is “shrinking”. The solid reacted is considered a non-porous material with spherical and cylindrical shapes, which are surrounded by a fluid which enables mass transfer between the solid and the bulk of the fluid [91, 176, 187].

An attempt has been made to study the kinetics of dissolution of copper and the major metals leaching present in WPCBs using the SCM model. All standard equations of the shrinking core models were tested for reaction kinetics. The step with the greatest resistance is considered the rate-controlling step. According to this model, the following steps are considered to occur in succession during the dissolution [91, 187]:

1. Transport of the reactant through the solution to the surface of the solid.
2. Reaction on the surface between the reactant and the solid.
3. Formation of the products on the surface layer of the reaction zone and their transport from the interface into the bulk of solution.

In this study, both spherical and cylindrical shapes were considered due to the metal liberation (Figure 4.15) exposed both geometries, representing better a real system. The kinetic equations to describe the process are [91]:

- 1 Film diffusion control dense constant size small particles – all geometries

$$X = K_c t \quad \text{Eq. 4.1}$$

- 2 Film diffusion control dense shrinking spheres

$$1 - (1 - X)^{2/3} = K_c t \quad \text{Eq. 4.2}$$

- 3 Chemical reaction control dense constant size cylindrical particles model

$$1 - (1 - X)^{1/2} = K_c t \quad \text{Eq. 4.3}$$

- 4 Chemical reaction control dense constant size or shrinking spheres

$$1 - (1 - X)^{1/3} = K_c t \quad \text{Eq. 4.4}$$

- 5 Ash diffusion control dense constant size-spherical particles

$$1 - 3(1 - X)^{2/3} + 2(1 - X) = K_c t \quad \text{Eq. 4.5}$$

where, K_c is the reaction rate constant (min^{-1}), t = time (min), and X = metal leaching rate (% leaching).

Figure 4.17 shows the model fitting for copper leaching using the shrinking core equations. The coefficient of determination R^2 value was adopted to compare the goodness of fit. Comparing the R^2 values, it was found that data fitted best with the ash diffusion control dense constant size-spherical particles, with the highest value of R^2 in the range of 0.4652 and 0.7559. This result pointed out that the kinetics may be controlled by diffusion; however, leaching kinetics are difficult to determine especially for a heterogeneous reaction such as WPCB with ILs, and both physical and chemical factors should be considered. Figure 4.17 also shows relatively close R^2 values for the chemical reaction control (Figure 4.17c and d), being slightly higher values with the dense constant size or shrinking spheres model. Figure 4.11 showed a sharp increase in the metal leaching within the first 15 minutes, followed by a steady rise to 2 h. This sharp increase in the metal concentration is due to the chemical reaction between the metals, the IL and the oxidant, in which the concentration of hydrogen ions and the oxidant decrease, and as the reaction progresses, the reaction slows down towards completion after 2 h. Thus, both the chemical and the diffusion factors are relevant in the copper leaching kinetics. In addition, WPCBs contain several metals, which may impact significantly in the copper leaching process. For instance, if the content of iron is high, leached iron (Fe^{3+}) in the solution could accelerate the copper leaching [12].

In the case of other major metals present in WPCBs, the ash diffusion control dense constant size-spherical particles were also the step with the greatest resistance, controlling the leaching process (Figures of all the models for Fe, Ni, Pb and Zn are presented in Appendix). Aluminium and barium were not evaluated due to their low leaching rates. Although the ash diffusion presented the highest R^2 values for Fe, Ni, Pb, and Zn, the models also showed similar R^2 values to the chemical reaction control processes, suggesting that chemical reaction also could play a role in their kinetics. In the leaching kinetics with inorganic acids (HCl , H_2SO_4 , HNO_3), the surface chemical reaction usually is the controlling step of the process [187]. In this case, the anionic part (HSO_4^-) of the $[\text{Bmim}]\text{HSO}_4$ is also part of sulphuric acid, which may favour the chemical reaction as the control stage. The conclusion

that can be drawn from these results is that diffusion plays a more important role than surface reaction; however, both are relevant in the metal leaching process from WPCBs.

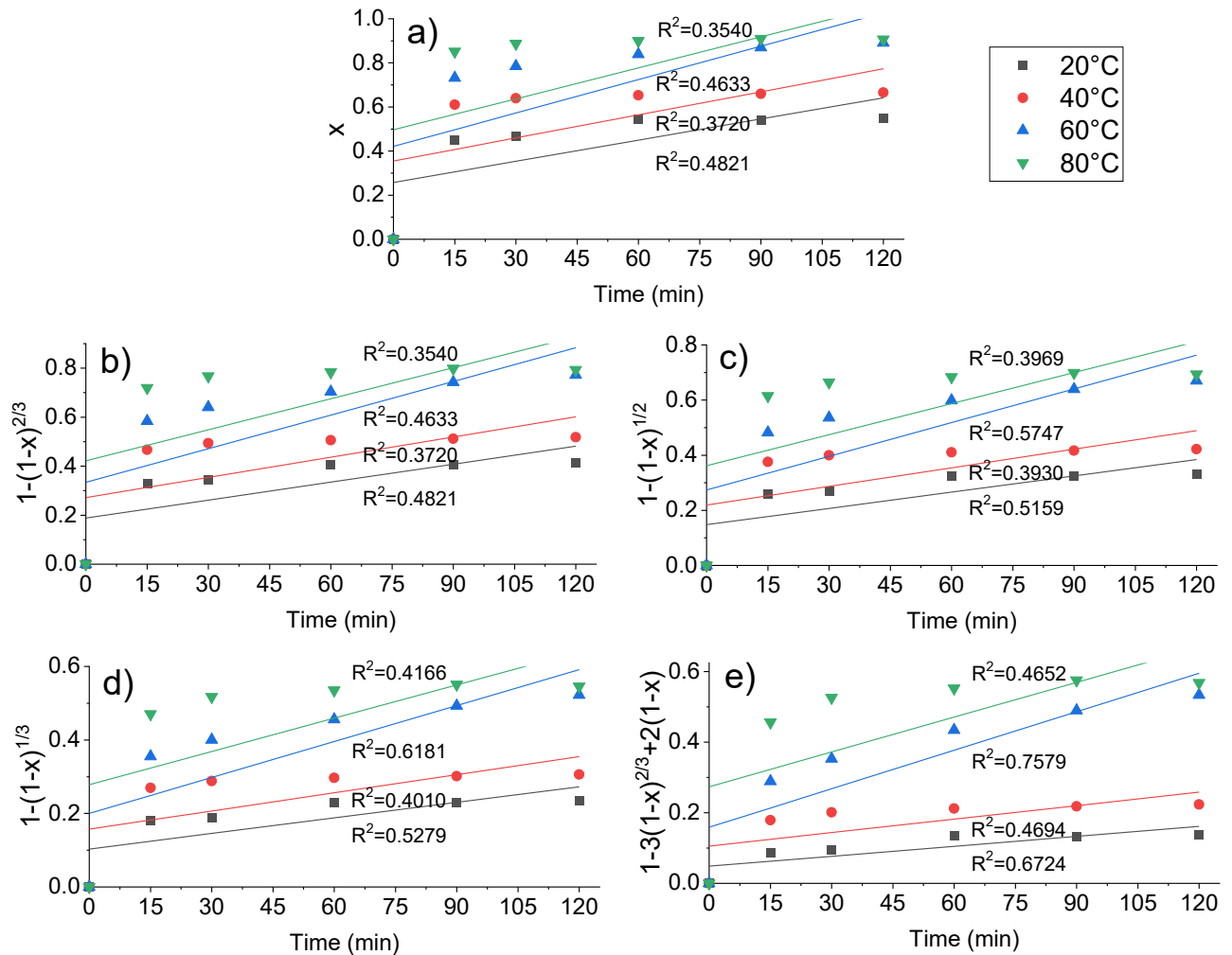


Figure 4.17: Model fitting for leaching kinetics of Cu from WPCBs by [Bmim]HSO₄; a) Film diffusion control dense constant size small particles – all geometries, b) Film diffusion control dense shrinking spheres, c) Chemical reaction control dense constant size cylindrical particles, d) Chemical reaction control dense constant size and e) Ash diffusion control dense constant size-spherical particles.

Although the metal leaching kinetics are complex and both chemical reaction and physical diffusion are relevant in the process, it was found that the ash diffusion control dense constant size-spherical particles presented the highest resistance in the SCM. The slope of the linear fit in the representation of the model (Figure 4.17e for copper) is the apparent rate constant k_d , which is listed in Table 4.3. The relationship between the leaching rate (K_d) and the temperature can be described by the Arrhenius equation [91, 105, 111, 177]:

$$K = Ae^{-E_a/RT}$$

Eq. 4.6

where k is the rate constant (min^{-1}), A is the frequency factor (min^{-1}), E_a is the activation energy of reaction (J/mol), R refers to the universal gas constant (8.3145 J/mol·K), and T is the temperature (K).

Table 4.3: Linear fitting parameters of ash diffusion control dense constant size-spherical particles model.

	K_c (min^{-1})				E_a (KJ/mol)
	20 °C	40 °C	60 °C	80 °C	
Cu	5.32×10^{-4}	2.63×10^{-4}	2.28×10^{-3}	7.82×10^{-4}	25.61
Fe	4.11×10^{-5}	1.20×10^{-4}	1.75×10^{-4}	1.71×10^{-4}	20.56
Ni	2.22×10^{-5}	4.33×10^{-5}	1.06×10^{-4}	1.20×10^{-3}	54.27
Pb	8.36×10^{-4}	9.13×10^{-4}	9.3×10^{-4}	1.30×10^{-3}	5.66
Zn	1.97×10^{-4}	3.18×10^{-4}	8.61×10^{-4}	1.54×10^{-3}	30.70

The Arrhenius plot shown in Figure 4.18 was obtained by using the apparent rate constant k_d from Table 4.3 and data from Figure 4.11, Figure 4.12 and Figure 4.13, which shows the effect of temperature on metal leaching. The linear regression with an R^2 of 0.9507 shows that the copper leaching process fitted well with the controlling model. Using the Arrhenius equation, the activation energy for copper leaching from WPCBs was calculated to be 25.61 KJ/mol in the temperature range of 20 °C and 80 °C. The magnitude of E_a suggests that the process was controlled by diffusion since high activation energies ($\geq 30\text{-}40$ kJ/mol) generally indicate that the chemical reaction is the rate limiting step, whilst lower activation energies are associated with transport-controlled reactions [111, 177]. Iron and zinc have an activation energy of 20.46 KJ/mol and 30.70 KJ/mol, respectively, also suggesting that diffusion controlled the leaching process. Lead showed an activation energy of 5.66 KJ/mol, the lowest of all the metals analysed. Lower activation energy generally leads to higher speed rate. This low activation energy could explain the steady Pb leaching of 50-55% observed in Figure 4.12, in which the Pb leaching was not significantly dependent on temperature. Whilst the activation energies of Cu, Fe, Pb, and Zn correlate well with their respective dissolution kinetics, Ni however, presented the highest activation energy with 54.27 KJ/mol, suggesting that the chemical reaction control is the rate limiting step for its leaching.

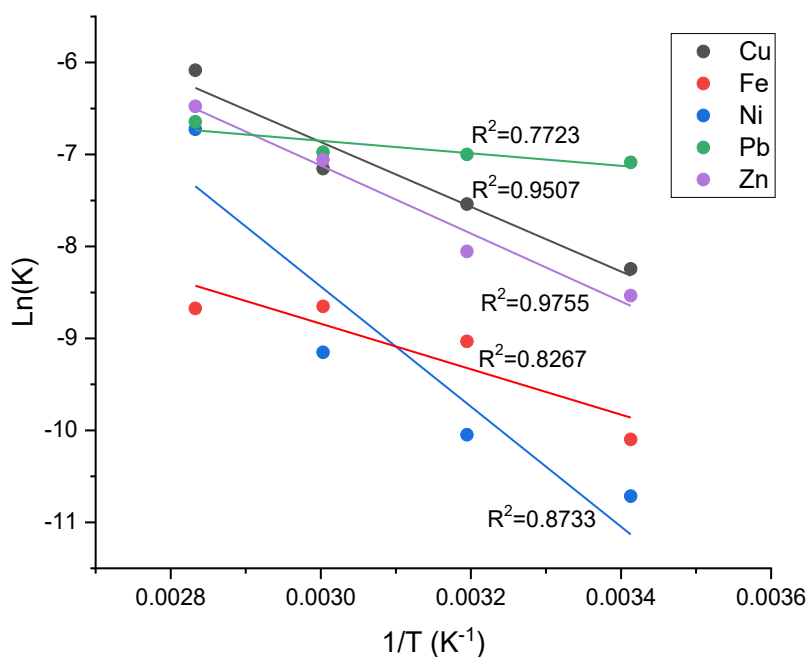


Figure 4.18: Arrhenius plot for metal leaching from WPCBs.

4.3.1.5 Discussion

The major impurities found in leaching of copper from WPCBs are iron, nickel and zinc, representing less than 5% of the total metals leached. Preliminary solubility testing to determine selective extraction for the target metal copper, shows that whilst [Bmim]HSO₄ preferentially leaches Fe and Zn in presence of Cu, control of the conditions can overcome this challenge and lead to the extraction of copper. Kilicarslan et al. investigated the copper and zinc leaching from brass ash using [Bmim]HSO₄, obtaining a leaching efficiency of 99% for Zn and 25% for copper. They found that addition of 50 vol% H₂O₂, led to more than 82% of copper being leached [186]. Due to the high amount of copper in WPCBs, the leaching process under optimal condition leached all the Cu, accounting for nearly 95% of the total metal leached. Chen et al. reported a comparative study on copper leaching from WPCBs using five ILs ([BSO₃HPy]OTf, [BSO₃Hmim]OTf, [BSO₄HPy]HSO₄, [BSO₄Hmim]HSO₄ and [mim]HSO₄). They demonstrated that copper can be successfully leached out, leaching nearly 100% with all the ILs under optimal conditions. Furthermore, they found that ILs with the hydrogen sulphate anion group (HSO₄⁻) were more efficient than ILs with the trifluoromethane sulfonate anion group (-OTf, CF₃SO₃⁻) [176]. This result is in good agreement with the results found in this work, where the IL with the sulphate anion group proved to be the most effective for Cu leaching. Zang et al. studied the copper leaching efficiency of five sulphuric ILs ([Bmim]HSO₄, [PS-mim]HSO₄, [CM-mim]HSO₄, [di-Ac-IM]HSO₄, and [C₆(di-Ac-IM)]HSO₄) from WPCB powders, reporting [CM-mim]HSO₄ as the most

effective leaching agent under optimal conditions (8.5 mL of a 90 %v/v IL solution and 1.5 mL 30% hydrogen peroxide at a solid-to-liquid ratio of 1/20 at 80 °C for 2 h), leaching out 98.3% Cu [105]. The same work also reported that the IL can be recovered by rotary evaporation, although it was not reused in subsequent cycles. Huang reported a copper leaching of 99.9% with [Bmim]HSO₄, when 1 g WPCB powder was leached under the optimum conditions with 25 mL 80 %v/v ionic liquid, 10 mL 30% hydrogen peroxide, solid/liquid ratio of 1/25, 70 °C and 2 h [177]. Whilst the optimal conditions reported are close to those used in the current work, a major difference lies in the IL concentration used, where IL concentrations were nearly three times higher (80-90 %v/v) than the optimal IL concentration used in this work (30 %v/v), leading to a considerable reduction in IL required. Furthermore, these studies focussed mainly on leaching of copper without taking account of other metals present in WPCBs, and as potential impurities their likely impact the overall recovery process.

In terms of kinetics, Huang et al. reported that, when copper is leached from WPCBs by a solution of 25 mL 80 %v/v [Bmim]HSO₄ and 10 mL 30% hydrogen peroxide, the reaction rate is controlled by diffusion through a product [177]. He et al. reported that when copper is leached from WPCBs using [Emim]Cl and [Bmim][BF₆] with hydrogen peroxide as an oxidant, the reaction was also controlled by the solid membrane diffusion [111]. In the current research it is shown that the ash diffusion control dense constant size-spherical particles presented the highest resistance in the SCM, although the R² values of the chemical reaction and physical diffusion were, albeit smaller, were not that different, suggesting that both the chemical reaction and the physical diffusion are of significance in the process. The authors mentioned that using higher concentration of ILs could have helped to overcome the chemical reaction as the slowest process. The concentrations used in the current work, of 30 %v/v of IL and 10 %v/v H₂O₂ for the leaching process, could make the chemical reaction more relevant. Huang et al. reported that the activation energy of leaching copper from WPCBs in the range of 40 °C and 70 °C with a Brønsted acidic ionic liquid was 25.36 KJ/mol [177], which it is similar to the activation energy calculated in the current work of 25.61 KJ/mol in the temperature range of 20 °C and 80 °C. Although kinetics from copper leaching from WPCBs can be complex and difficult to determine due to the presence of several metals, where other parameters such as particle size, metallic and non-metallic separation, ceramic composition, among other can also influence, the kinetic study suggests that the reaction rate is controlled by diffusion through a product or that it has a higher predominance.

4.3.2 Pre-treatment of As-received WPCBs to Remove Solder and Electronic Components

4.3.2.1 Separation and removal of solder, electronic components, and copper enrichment from WPCB

Copper is the major metal present in WPCBs with approximately 28 wt.% in EoL-MP PCBs, representing nearly 65% of the total metallic content by weight. This is due to a typical PCB comprising a multilayer of epoxy resin and fiberglass, coated with layers of thin copper film, which give the PCB its conductive properties. PCBs are used to mechanically support and electrically connect electronic components (ECs) including resistors, relays, capacitors, transistors, and integrated circuits/chips. Hence, copper is mostly found in the bare PCB substrate, whilst precious metals, CRMs and other metals are found in the ECs mounted on the substrate [12, 91, 96, 188]. These ECs are mounted on PCB assemblies using various types of connections such as socket pedestal device (press-fit), through-hole device (solder wave type), surface mounted device (solder by reflux), screw joint device, and rivet joint device. The removal of these components can be achieved through a number of different methods which may be simple mechanical methods or physicochemical methods such as the removal of solder or pins, using liquid medium heating [96].

Most of the ECs attached to PCBs are by means of welding/soldering and can be dismantled by melting the solder. Welding/soldering is a process where two or more metals are chemically and mechanically joined at a low melting point [188]. Sn-Pb solder alloys is commonly used for electrical soldering, with 63Sn-37Pb alloy being the most common Pb-based solder in PCBs. Researchers have studied methods of removing solder, being infrared heating (using a heating tube), liquid medium heating, solder bath heating, and chemical reagent the most commonly methods used. These methods, however, present difficulties such as the disposal of the used hot fluid and selection of adequate chemical reagents, and they are often inefficient and highly polluting [182, 189, 190]. The method of hot bathing PCBs in a heated liquid assisted by mechanical vibration, is currently considered as a promising technology for opening solder connections and liberation of ECs [182]. The use of the ionic liquid ([Bmim]BF₄) as the heating medium was therefore tested in the current work.

The key prerequisite for separating the ECs from PCBs is the opening of the solder. Based on the physical state of Sn-Pb alloy, the melting temperature predominantly ranges from 183 °C (eutectic alloy) to 232 °C (lead-free solder). Nevertheless, it is important to note that temperatures over 250 °C can be unfavourable due to the release of flame retardants (chlorinated/brominated dibenzo-p-dioxins and furans) from PCBs [182]. Therefore, temperatures ranging from 200 °C to 250 °C could

effectively separate ECs and solder from WPCBs. Preliminary studies using $[Bmim]BF_4$ as the heating medium from 200 °C to 250 °C with different mechanical stirring speeds and timing were carried out to determine the optimal parameters. Figure 4.19 provides an illustration of the dismantling and solder recovery process from WPCBs using $[Bmim]BF_4$. Temperature plays a crucial role, and it was found that the higher the temperature reduced the viscosity of the molten solder, and with the decreased flow resistance removal of the solder from WPCBs was faster [190]. The slightly higher temperature end of 240-250 °C, however, damage the WPCBs, releasing toxic substances. So, a temperature of 210 °C was selected, being the minimum temperature that effectively removed the ECs from WPCBs minimising the release of toxic substances. Experiments were carried out without mechanical stirring and, although the ECs were successfully separated from WPCBs, the solder remained attached. With the addition of mechanical stirring the molten solder was easily peeled from the WPCBs and along with the ECs were taken into the IL. The optimal conditions for the dismantling of the ECs and removal of solder from WPCBs (Figure 4.19) were a temperature of 210 °C, mechanical stirring speed of 150 rpm and reaction time of 15 min. This pre-treatment can effectively separate all the ECs and solder from WPCBs, even exposes the copper surface on the PCB pins.

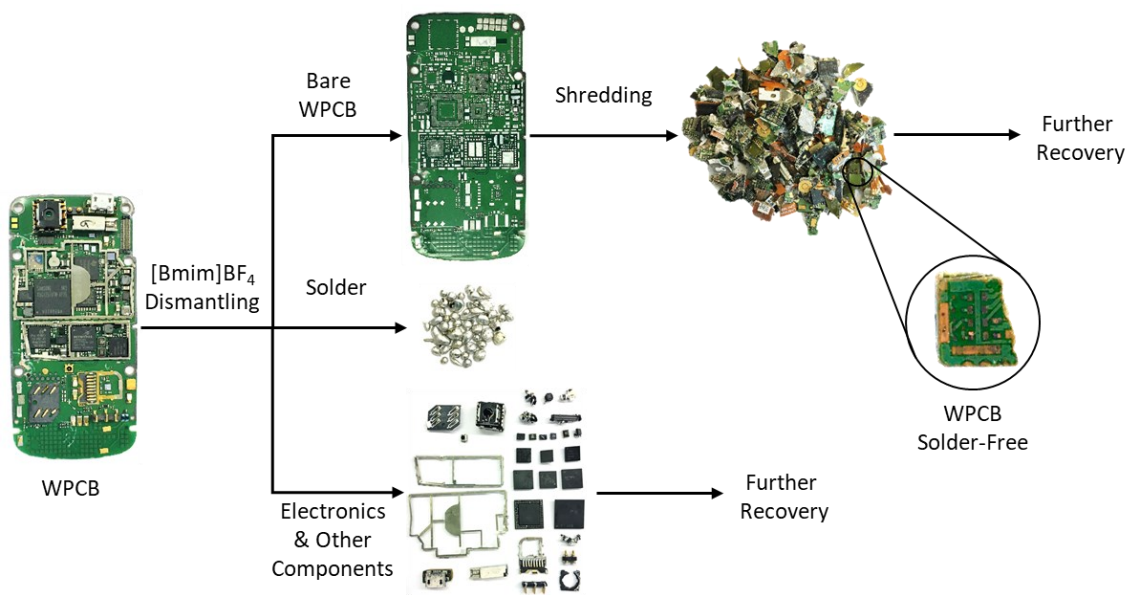


Figure 4.19: Process for dismantling ECs from the WPCBs using $[Bmim]BF_4$.

An SEM-EDS image of the solder separated from WPCBs, is shown in Figure 4.20, as smooth spheres, and the EDS in Figure 4.20b, c and d, shows that the solder is mainly composed of lead and tin without any contaminant/undesirable metal. The clean removal of the solder using [Bmim]BF₄ with the chemical properties of the solder remaining intact, suggests the IL acts as an excellent heating medium for solder separation.

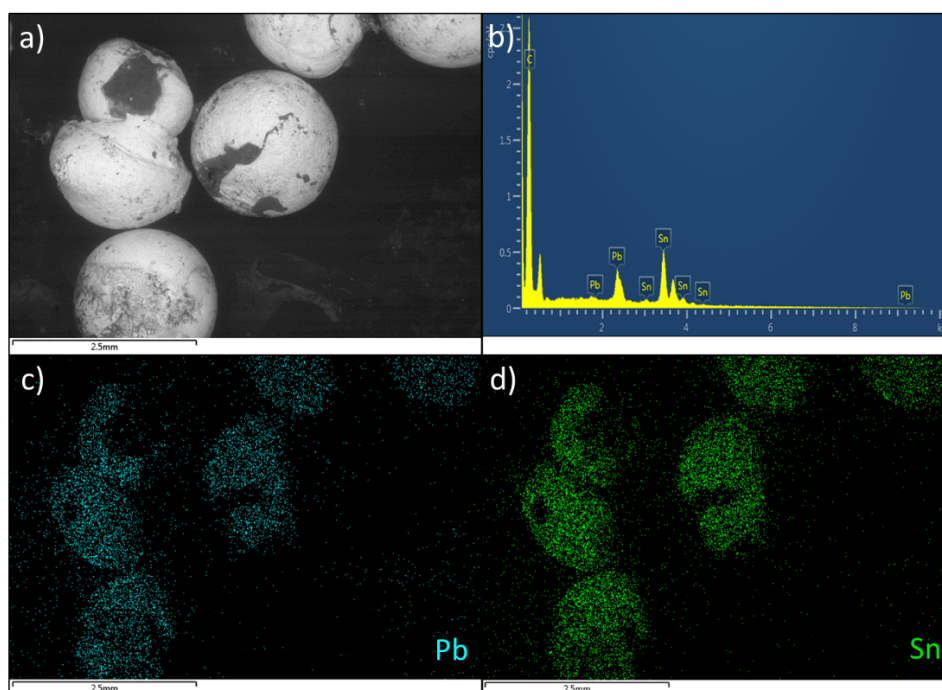


Figure 4.20: SEM-EDS images of recovered solder from WPCBs using [BMIM]BF₄.

The bare WPCBs, stripped of any ECs and solder, represents approximately 70% by weight of an average WPCB. Table 4.4 shows the metal composition of the as-received WPCB before and after the separation of ECs and solder. As a result of the solder separation, the concentration of lead and tin decrease from 3.6 mg/g and 1.5 mg/g, respectively to be undetectable, confirming the successful separation of solder from WPCBs. Copper concentration in the bare WPCBs after the separation nearly doubled from 435.7 mg/g to 838.2 mg/g, representing approximately 84% of the total weight of the bare WPCBs. As expected, most of the other metals, such as B, Ba, Cr, Fe, Ni, present in as-received WPCBs decreased and were not detected in the bare WPCBs, because most of these metals are found in the ECs mounted on PCBs. The significant increase in silver from 5.8mg/g in as-received WPCBs to 32.7mg/g in bare WPCBs, is likely due to the use of Ag in contacts, which can be seen plated on some parts of the PCBs.

Table 4.4: Metal concentration of As-received WPCBs and bare WPCBs.

Elements	As-received WPCBs (mg/g)	Bare WPCBs (mg/g)	Elements	As-received WPCBs (mg/g)	Bare WPCBs (mg/g)
Ag	5.8	32.7	In	<DL	0.3
Al	14.0	18.7	K	1.4	0.3
B	3.4	1.9	Li	<DL	4.2
Ba	24.0	0.5	Mg	0.5	0.5
Bi	<DL	<DL	Mn	<DL	<DL
Ca	28.9	13.7	Na	4.0	1.5
Cd	<DL	0.1	Ni	12.9	<DL
Co	<DL	<DL	Pb	3.8	<DL
Cr	0.4	0.0	Sr	0.5	0.1
Cu	435.7	838.2	Sn	1.5	<DL
Fe	6.6	0.2	Tl	<DL	<DL
Ga	<DL	<DL	Zn	0.9	1.1

<DL: Below detection limit.

Figure 4.21 shows the XRD patterns of as-received WPCBs and bare WPCBs, which confirmed that Cu is the main element presented by the diffraction angles (2θ) of 43.5° , 50.6° and 74.2° , with the strongest peak at 43.5° . The intensity of the Cu peaks is much higher in the bare WPCBs pattern, showing an increase in its content. [Bmim]BF₄ proved to be a clean, efficient and non-polluting pre-treatment for the separation of solder and ECs from WPCBs, favouring the enrichment of copper for subsequent recovery process. Whilst ECs did not appear to be damaged in the pre-treatment step, and therefore could potentially be reused, it is possible that the temperatures used in the heating process involved might impact their future performance. Nevertheless, the ECs could be further treated to recover the precious metals. The recovered solder was shown to be chemically unchanged by the process and without any impurities, making it suitable for direct reuse.

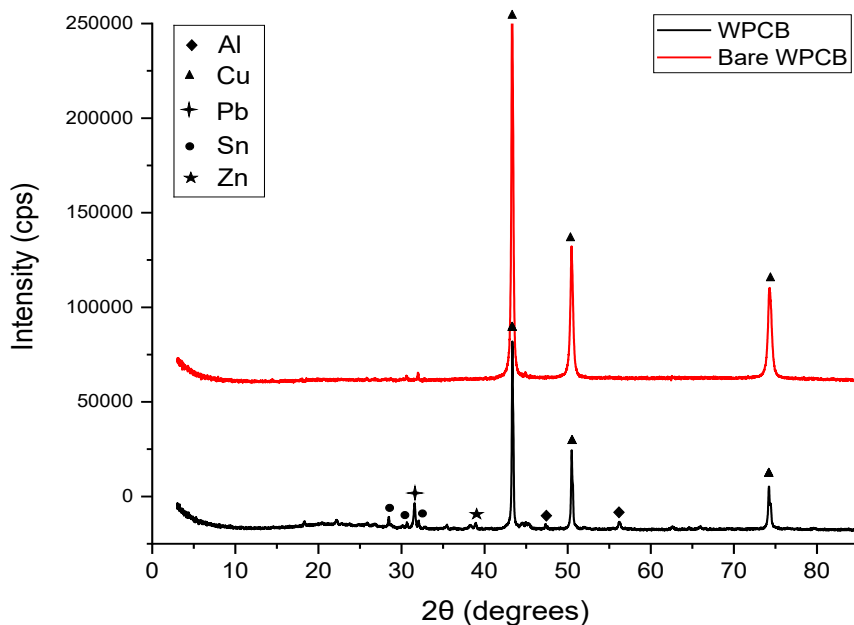


Figure 4.21: XRD patterns of WPCBs powders before reaction and after solder and ECs removing by $[Bmim]BF_4$.

4.3.2.2 Discussion

Since copper is mostly found in the bare PCB, dismantling of the electrical components and solder separation is a critical step to provide direct access to the available copper. The use of $[Bmim]BF_4$ trialled under the optimal conditions at 210 °C, 150 rpm and 15 minutes has been successfully used as a heating medium in this pre-treatment step for separation of lead (present as solder) from WPCBs. Elsewhere, Zhang at al. reported separation of solder and ECs from strips of PCBs using $[Bmim]BF_4$ as the heating medium at 200 °C, 150 rpm, with only 3 minutes of contact time [105], showing that contact time can be significantly reduced when strips are used. In the current research, due to the amount of the IL available, the IL was effective in separating the ECs from the WPCBs, but not achieve complete separation of the solder. Hence, the WPCBs were cut in strips of approximately $1 \times 1 \text{ cm}^2$, and applying the pre-treatment again, the solder was completely separated from the WPCB strips. Experiments, where the WPCBs were cut first (with the ECs), showed that the time required to separate the ECs and the solder completely was significantly lower (<5 min.). This can be explained in terms of the greater surface area contact and increased collisions helping agitation and mixing of the solution.

4.3.3 Electrowinning of Copper from Leached Solutions Derived from IL-Treated WPCBs

Following the leaching process, different methods were utilised to strip the copper from the solution under its optimal conditions (30 %v/v [Bmim]HSO₄, 10 %v/v H₂O₂, and 60 %v/v H₂O at 60 °C for 2 hours with 1:15 solid to liquid ratio). This is the last step of the recovery process, where copper, the target metal, is recovered by mean as pure metal or compound. In this process, three methods of stripping were studied: precipitation, cementation, and electrowinning. These methods were selected because of they are more environmentally friendly, simple operation, low cost, and energy consumption as well as their use in the industry of metals. Preliminary studies suggested that electrowinning is the most promising recovery process, and it was further studied.

4.3.3.1 Precipitation

Precipitation of copper was carried out using sodium hydroxide and aqueous ammonia. Studies were carried out using copper sulphate solutions. Stoichiometric amount of sodium hydroxide and ammonia were added to the solutions, precipitating a light blue copper hydroxide. Preliminary experiments were carried out mixing the copper sulphate solutions with raw IL ([Bmim]HSO₄) and, although copper hydroxide was obtained, precipitation was not further studied with leached copper from WPCBs due to the presence of sodium, in the case of sodium hydroxide, and ammonium cation from ammonia, which introduces ions to the solution, making the recyclability of the IL more difficult. Furthermore, copper hydroxide needs further treatment to convert it to pure copper, increasing the steps of the recovery copper process from WPCBs.

4.3.3.2 Cementation

A preliminary investigation into the use of cementation for the recovery of copper was carried out using iron as the cementing metal, based on its reduction potential. Figure 4.22 shows the effect of the Cu:Fe ratio with time in the cementation of copper from sulphate solutions. Copper recovery increased with the time, reaching an equilibrium after 2 h. With higher levels of iron, the more copper was stripped, reaching 91.3%, 95.1%, 98.7% and 99.8% of copper for Cu:Fe ratios of 1:1, 1:1.5, 1:2, and 1:3, respectively. Although 100% of copper recovery was expected from a 1:1 Cu:Fe ratio, only 91.3% was obtained, which suggested that to recover copper from solution, a Cu:Fe ratio between 1:1.5 and 1:2 for 2 h should be applied.

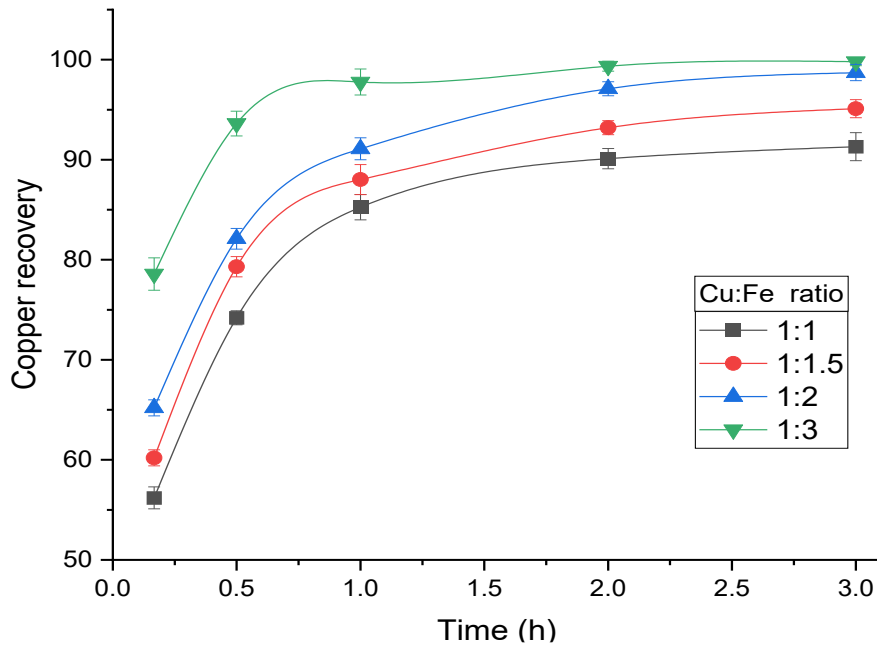


Figure 4.22: Effect of the Cu:Fe ratio and time in the cementation of copper from copper sulphate solutions.

Cementation was trialled for the recovery of copper from an IL-leaching under optimal conditions, using a Cu:Fe ratio of 1:1.5, 2 h and 500 rpm of agitation. Figure 4.23 shows the metal concentration and percentage of metals after cementation. It was found that 67.6% of copper was recovered after cementation, leaving one-third of the total leached copper in solution (220 mg/L). In addition, and as expected, the concentration of iron in solution increased more than 100 times from 4.5 mg/L (Figure 4.14) to 480.3 mg/L (Figure 4.23a). The final solution after cementation still had a high amount of Cu (30.5%) which would require an additional recovery step. A factor that could contribute to the incomplete Cu recovery using cementation could be the higher density and viscosity of the IL compared to the copper sulphuric solution test solution, which might have made mixing more difficult. The final Cu recovered showed a purity of 75.6%, with the remainder contaminated with iron. In addition, the solution after cementation had copper, iron, and other unwanted metals, requiring further purification methods to recover the copper and recycling of the IL. Due to these issues, cementation was discarded as a method deemed unsuitable for copper stripping.

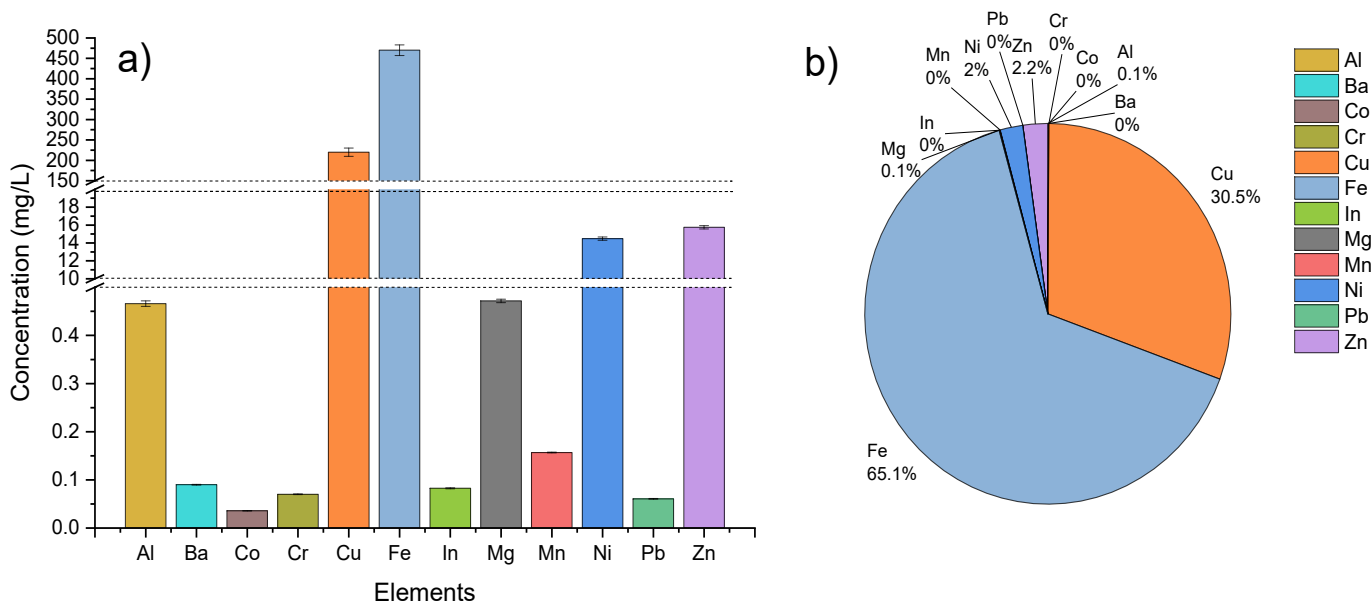


Figure 4.23: Cementation of Cu by Fe from leached WPCBs; (a) concentration and (b) metal percentage in solution.

4.3.3.3 Electrowinning (EW)

Electrowinning (EW) is a well-established technique for the industrial production of high purity copper, with nearly 20% of its annual production coming from EW. EW is a clean single-step method, which consume relatively low energy, produces no secondary waste, and can be directly applied to solutions without requiring additional chemicals [184, 191]. An important factor in EW is the selection of the correct electrodes. The electrodes are chosen based on the galvanic series, where the active metal acts as anode and the passive or inert metal acts as cathode. In this work a review of suitable electrodes was carried out and Table 4.5 provides a summary of the advantages and disadvantages of different electrodes reported as used in the EW of leached solutions under optimal conditions, where copper mesh and titanium mesh electrodes were chosen as the cathode and anode, respectively.

Table 4.5: Advantages and disadvantages of different electrodes in the copper EW.

Cathodes	Advantages	Disadvantages
Glassy carbon (sheet)	Reusable Easy Cu removing	Slow Cu deposition
Copper (sheet)	-	No reusable Slow Cu deposition
Copper (mesh)	Fast Cu deposition	No reusable
Stainless steel (sheet)	-	No reusable Slow Cu deposition
Stainless steel (mesh)	-	No reusable Difficulties in Cu removing
Anodes	Advantages	Disadvantages
Glassy carbon (sheet)	Excellent conductivity	Disintegration after 3 cycles
Copper (sheet)	Good conductivity	Disintegration after 3 cycles
Copper (mesh)	Good conductivity	Disintegration after 2 cycles
Stainless steel (sheet)	Good conductivity	Disintegration after 2 cycles
Stainless steel (mesh)	Good conductivity	Disintegration after 2 cycles
Nickel (sheet)	Good conductivity	Disintegration after 4 cycles
Lead (sheet)	Good conductivity	Disintegration after 3 cycles
Platinum(mesh)	Excellent conductivity No corrosion	Costly

The leached solution (30 %v/v [Bmim]HSO₄, 10 %v/v H₂O₂, and 60 %v/v H₂O at 60 °C for 2 hours with 1:15 solid to liquid ratio) was centrifuged for 10 minutes at 3500 rpm for a complete separation of the supernatant from the WPCB residue. The supernatant then was transferred to an electrolytic cell, designed in the laboratory for EW (Figure 4.3). The effect of the current densities on copper concentration, recovery and current efficiency are presented in Figure 4.24. It can be observed that the higher the current density, the faster was the electrodeposition of copper on the cathode; thus, copper recovery reaches 100% within 30 minutes at 500 mA, 90 minutes at 100 mA, and 180 minutes with 50 mA, whereas at 10 mA, 70% of Cu is recovered within 5 h, requiring more time for a complete deposition. This increase in recovery with increasing current density is consistent with acceleration of the electrodeposition process and improved mass transfer in the solution [183]. The current efficiency shows a similar trend for all the current densities applied; an initial increase in the current efficiency until reaching 100% (except for 500mA, which reached 85%) followed by a decrease. During recovery by electrowinning, the concentration of copper in the electrolyte is constantly decreasing, leading to a decrease in current efficiency with time as the electrowinning process continues. In the beginning, a higher copper concentration reduces the mass transfer limitation, resulting in higher current efficiency [191]. At a current density of 10 mA, there is a current efficiency higher than 100%, reaching

approximately 120% between 2 and 3 h. This could be due to the release of hydrogen, although it is associated with a reduction in the cathode efficiency, it can occasionally auto-catalyse the reaction by increasing agitation and favouring mass transfer.

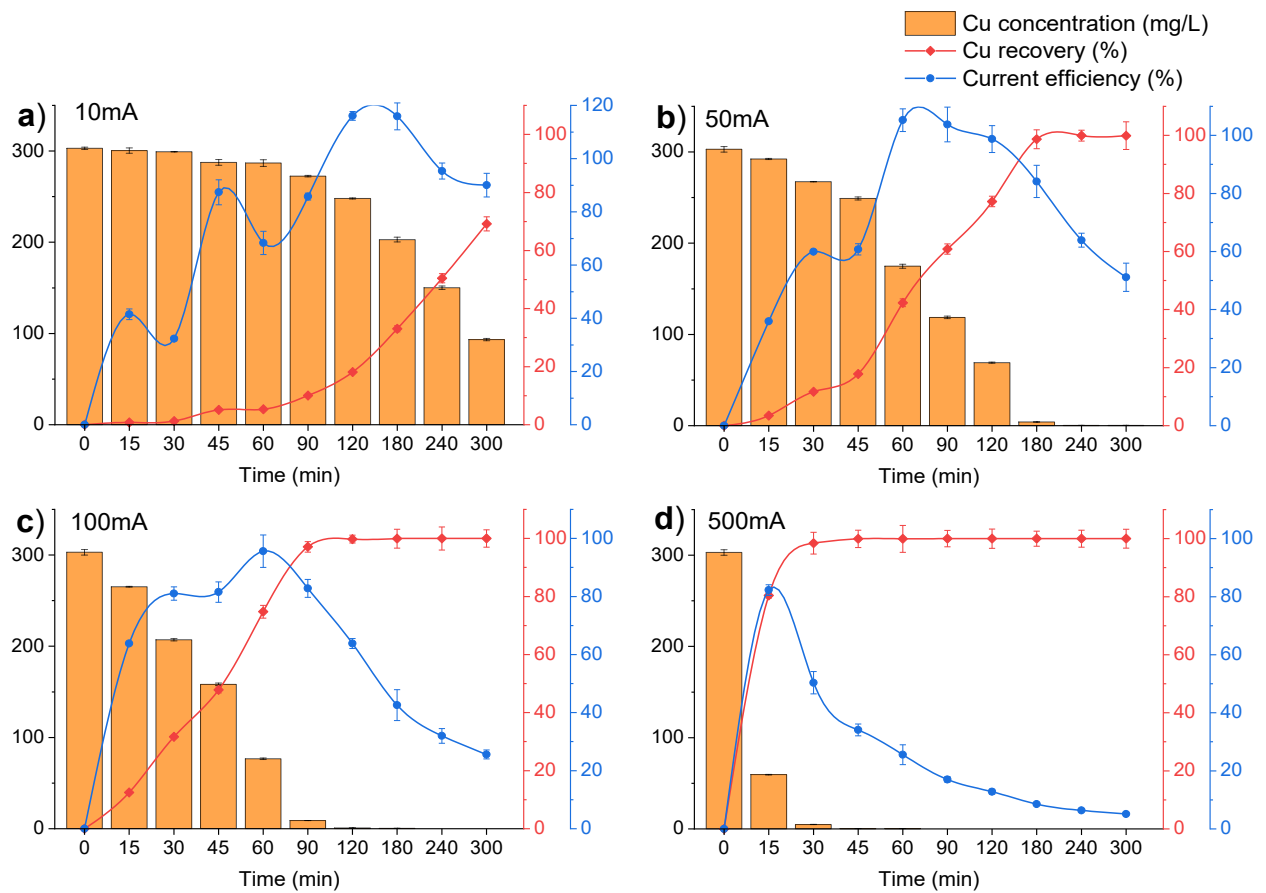


Figure 4.24: Effect of electrolysis time on copper concentration, copper recovery and current efficiency from WPCBs using different currents; (a) 10mA, (b) 50mA, (c) 100mA and (d) 500mA.

Figure 4.25 shows SEM images of the copper deposits on the cathodes following EW at different current densities. In general, the morphology of copper particles appeared to be mainly dendritic, with a decrease in grain size with the increase in the current density. Generally, electrocrystallisation has two principal stages, nucleation and growth, and the size and shape of the deposited metal particles are affected by both the rate of nucleation and nuclei growth [192]. If the rate of nucleation is much faster than the growth of nuclei, more crystal nuclei can be formed, leading to finer powders [192, 193]. Thus, as the electrolysis time increases, it is expected that the growth of nuclei is faster than the rate of nucleation, obtaining larger particles [184]. As the current density is increased more discharged ions would be produced on the cathode per unit time, allowing the formation of more nuclei and as a consequent, smaller particles of copper powders are obtained.

Copper purity was determined by dissolving 12 mg of the deposited copper obtained by EW in 2 mL of concentrated nitric acid for 3 hours. This solution was diluted and the concentration of 30 metals were determined by ICP-OES. The copper purity was over 99% at all the current densities; 99.12%, 99.22%, 99.35%, and 99.15% for 10 mA, 50 mA, 100 mA and 500 mA, respectively. The increase in the current density did not impact the copper purity, although with a higher current density, the hydrogen evolution is intensified, making the structure of the metal powders in the cathode loose, and enabling impurities to easily adhere to the metal powder surface, causing a decrease in copper purity [183, 184]. Nevertheless, due to the leached solution was mostly copper (>95%), small percentages (<1%) of impurities were found in the final copper product.

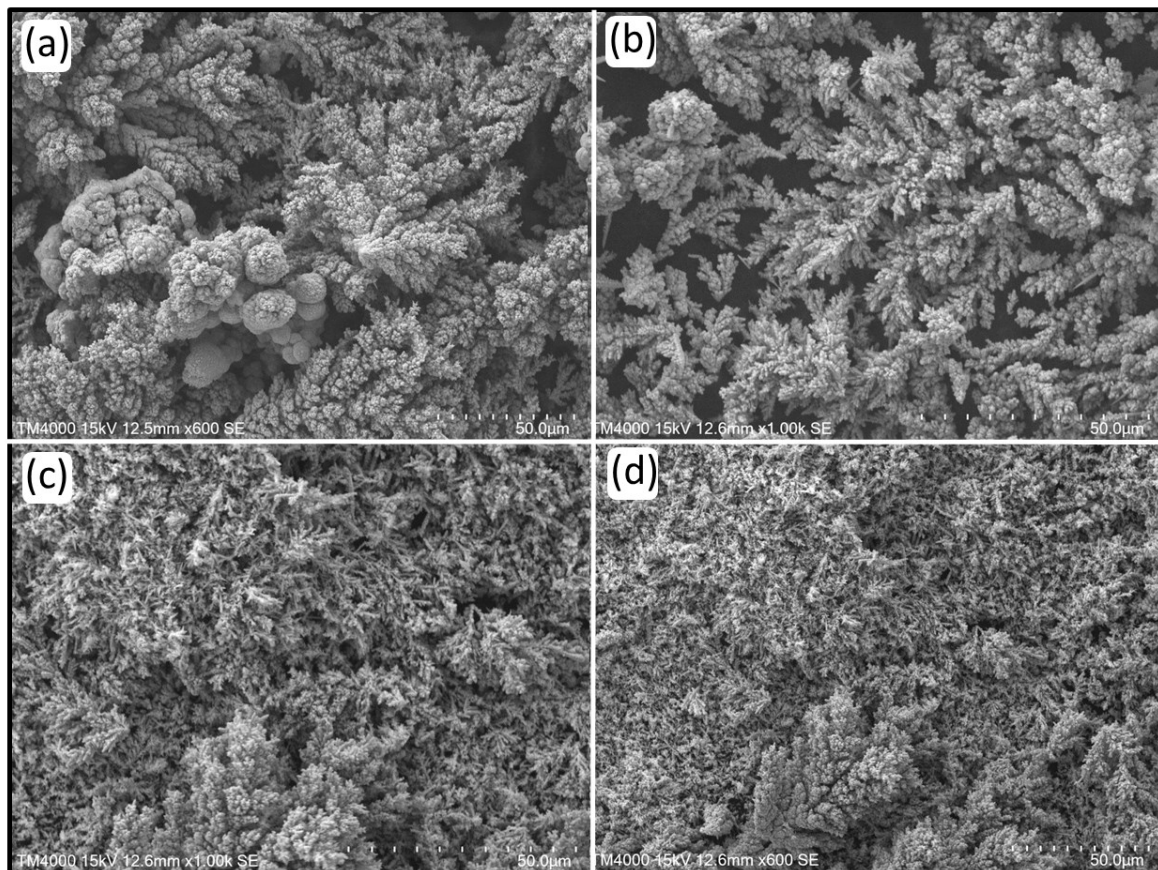


Figure 4.25: SEM images obtained at different current densities; a) 10 mA, b) 50 mA, c) 100 mA and d) 500 mA.

Table 4.6 records the current efficiency, observed cell voltage and the calculated specific energy consumption of all the solutions with different current densities. The current efficiency shown is the average of the efficiencies over the period of electrolysis. These timescales represent the

electrolysis period for recovery efficiency to be reached. In all experiments, the cell voltage stabilised quickly, on average in less than 15 min; however, there was a slight increase in the voltage at the end of each electrodeposition. The results show that the energy consumption increased with the increase in current density from 3.2 kWh/kg at 10 mA to 4.1 kWh/kg, 4.5 kWh/kg and 8.3 kWh/kg at 50 mA, 100 mA and 500 mA, respectively. This is due to a high current density during EW, the ohmic resistance losses also increase in the solution, consuming more energy in the deposition process. Small operational current densities tend to correlate with low power consumption [191]. The most energy efficient current (81.4%) seemed to be at 10 mA; however, the Cu recovery reached only 70% after 5 hours, requiring more time for complete electrodeposition. Furthermore, as the Cu in solution is lower, more energy will be required for the EW process. This will certainly decrease the current efficiency and increase the energy consumption. The energy consumption at 50 mA and 100 mA were similar, with nearly the same current efficiency; however, the EW at 50 mA requires 3 hours for complete Cu electrodeposition whilst at 100 mA it takes only 2 hours. A current of 500 mA electrodeposits all the copper in 45 minutes, with a high energy consumption and low current efficiency. According to these results, it can be concluded that the best deposit in terms of purity, morphology, time, current efficiency, and energy consumption is obtained at a current density of 100 mA for 2 h, recovering 100% of copper with a purity of 99.35%.

Table 4.6: Energy consumption parameters from EW of copper from WPBC.

Current (mA)	Time (min)	Recovery (%)	Current efficiency (%)	Cell voltage (V)	Energy consumption (kWh/kg Cu)
10	300	70	81.4	3.1	3.2
50	180	100	78.8	3.8	4.1
100	120	100	78.1	4.2	4.5
500	45	100	55.6	5.5	8.3

4.3.3.4 Discussion

Copper stripping from leaching solutions was carried out by cementation and electrowinning (EW). The method of cementation was discarded as the process involved addition of substances to the IL solution, which then needs further treatment to recycle the IL. In addition, with cementation not all the copper was recovered, requiring either addition of more cementing metal or additional copper recovery stages. Electrowinning was therefore selected as the stripping method. EW was optimised, with a current density of 100 mA for 2 h, where 100% of copper is recovered with a purity of 99.35%, current efficiency of 78.1% and an energy consumption of 4.5 kWh/kg Cu. The copper concentration in the WPCBs solutions in this study was on average 681.2 mg/L. The energy consumption for copper

deposition is one of the most important parameters for consideration of an industrial scale operation. In industrial electrowinning, the typical operating conditions are cell voltage of ca. 2V, copper ion concentration of ca. 50 g/L, current density of 20-45 mA/cm², temperature of 40-60 °C, current efficiency of 89-94% and specific energy consumption of 1.8-2.5 kWh/ kg Cu [191]. Gorgievski et al. reported a specific energy consumption of 7 kWh/kg Cu from acid mine drainage solution containing 1.3 g/L Cu, with approximately 92% copper recovered, >60% average current efficiency in a 5 V cell voltage [194]. Peng et al. studied the EW of diluted solutions (150 ppm Cu), recovering 90% of copper with an energy consumption of 11.1 kWh/kg Cu [195]. Both authors reported higher energy consumption than that used in this study, which achieved 100% recovery of copper with low impurities. In the work reported by Gorgievski et al. [37] and Peng et al. [38] copper was dissolved in inorganic acids, mostly sulphuric acid, whereas in the current research, the copper was dissolved in a solution of [Bmim]HSO₄, which can be recycled with no further purification/treatments, making the proposed process with IL attractively viable.

A novel approach to recovery copper from WPCBs has been slurry electrolysis. Slurry electrolysis is a process that combines the leaching, solution purification, electrowinning, and electrodeposition in one single procedure within one apparatus, and it could directly obtain products from finely ground ores or concentrates in one step [111, 183]. He et al. studied the copper recovery from WPCBs by slurry electrolysis, finding that under optimal conditions, copper recovery of 92.7% was obtained with a current efficiency of 79.9% in the ionic liquid solution of CuSO₄-NaCl-H₂SO₄-[Bmim][PF₆] [111]. Li et al. studied the copper and gold recovery from CPU sockets by one-step slurry electrolysis. They reported that under optimum conditions (4 mol/L HCl, 75 g/L pulp density, 80 mA/cm² and 4 h), one third of copper can be electrodeposited at the cathode (with a purity of 98.2%), whilst the other two-thirds remained in the electrolyte, needing further steps for its recovery [183]. Zhang et al. also studied the copper recovery from WPCBs using slurry electrolysis, using a simulated solution with 30 g/L copper sulphate pentahydrate (CuSO₄·5H₂O), 60 g/L sodium chloride (NaCl) and 170 g/L vitriol oil (H₂SO₄) and 10% of N-butyl sulfonate pyridinium hydrosulfate ([BSO₃HPy]HSO₄), with a copper recovery rate (90,9%), current efficiency (70.6%) and purity (81.7%), with an electric current of 0.5 A for 3 h [154]. Although slurry electrolysis was trialled as part of the current research using the same electrochemical cell set-up developed for this work (Figure 4.3) and applying the same optimal leaching and EW conditions, the trial was aborted as the addition of hydrogen peroxide to the solution, caused rapid foaming of the electrolyte within the first 15-20 minutes, trebling volume of liquid, causing the contents to overspill. Further trials using this slurry electrolysis method were aborted, as a new EW cell would have to be redesigned.

4.3.4 Recovery of the Ionic liquids for Recycle and Reuse

From an environmental and economic perspective, in the context of conserving resources the recyclability of reagents is crucial. In this study two ionic liquids have been successfully used in (i) the pre-treatment step to remove a Pb-Sn solder from as-received WPCB and (ii) the selective leaching of the target metal from WPCBs. The recyclability of each IL was investigated and the performance over three or more cycles judged.

4.3.4.1 Recovery of [Bmim]BF₄ for recycle and reuse

After the successfully separating solder, ECs and bare WPCBs, all the reagents were collected and used in a following cycle. The recovered IL was successfully heated, cooled, and used in 3 cycles under the optimal conditions without loss of performance. Figure 4.26 shows the FTIR and TGA of [Bmim]BF₄ after three cycles of use. The FTIR spectra (Figure 4.26a) indicates that the IL did not change after 3 cycles of heating and cooling, suggesting excellent recyclability. TGA (Figure 4.26.b) also did not show major differences through the cycles, indicating very good thermal stability, and a consistent small percentage mass loss in the temperature range 100-250 °C traces over three cycles of use.

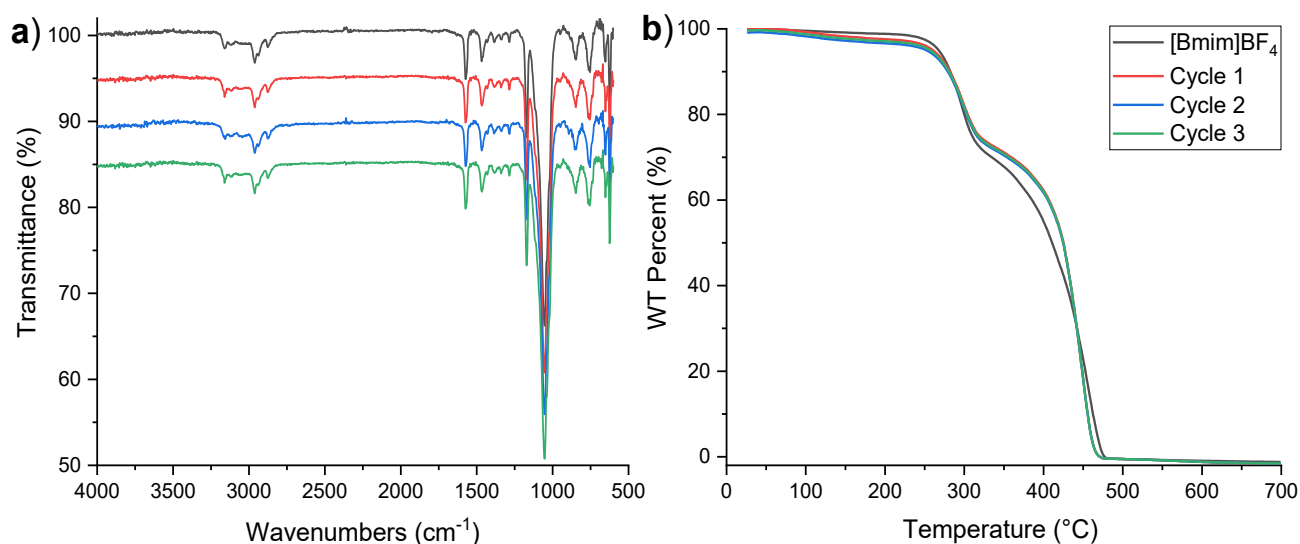


Figure 4.26: FTIR and TGA of [BMIM]BF₄ used in 3 cycles of ECs and solder separation from WPCBs.

The use of [Bmim]BF₄ trialled under the optimal conditions at 210 °C, 150 rpm and 15 min has been successfully used as a heating medium for separation of lead (in the form of solder) from WPCBs without any loss of the IL properties after 3 cycles of reuse. The yellow colour of the IL was observed to change to brown and dark brown on recycle, suggesting that some compounds might have been dissolved in the IL. Zhu reported the complete separation of ECs from WPCBs using [Emim]BF₄ as the heating medium at 240 °C, 150 rpm for 12 min; however, an initial delamination of the WPCBs was observed, implying that the IL was dissolving bromine and chlorine from the epoxy resins of WPCBs [190]. In the current research no delamination was observed, although some WPCBs changed colour from green to pale suggesting some decomposition of resins in the WPCBs was taking place. FTIR and TGA of the IL, [Bmim]BF₄, showed no major changes, suggesting that although the IL can be contaminated, its heating medium property was not affected.

Zeng et al. separated nearly 90% of the ECs from WPCBs also using [Bmim]BF₄ as the heating medium and compared this method with two dismantling approaches that can be used in industrial scale, namely manual dismantling (driven by pneumatic screwdrivers) and mechanical dismantling (in semi-automatic mode) [182]. In their economic assessment of different dismantling processes, which includes the alternative of an IL-heating medium dismantling process of the type described in the current research, it was found that as the amount of WPCBs for treatment increased to over 3 kt, the IL heating medium turned out to be the least expensive process, although the challenge remained in terms of the cost of the IL [182]. The successful reuse of [Bmim]BF₄, reported in the current work, for 3 cycles, without reduced performance, would overcome the challenge of costs of IL and lead to a viable process. Thus, using [Bmim]BF₄ as pre-treatment for separating EC and solder from WPCBs can be environmentally friendly and economically viable on a large industrial scale.

4.3.4.2 Recovery of [Bmim]HSO₄ for recycle and reuse

To develop a process that is environmentally friendly and cost-efficient for Cu leaching from WPCBs, the stability of the IL [Bmim]HSO₄ under the conditions of use, and the ability to reuse the IL are important factors. It should be chemically stable throughout and retain high leaching efficiency. To evaluate the recyclability of [Bmim]HSO₄, five cycles with leaching combined with the electrowinning process were carried out. After the leaching reaction (30 %v/v [Bmim]HSO₄, 10 %v/v H₂O₂, and 60 %v/v H₂O at 60 °C for 2 hours with 1:15 solid to liquid ratio), the copper was stripped by EW in 2 h with a current density of 100 mA. Figure 4.27 presents the leaching, electrowinning, and overall efficiencies over five cycles of copper recovery under optimised conditions. The leaching of copper remains largely unaffected over five leaching and electrowinning cycles, suggesting that

[Bmim]HSO₄ can be successfully recycled and reused without any loss in efficiency. In fact, the overall efficiency of copper recovery remains >99% in each cycle Table 4.7.

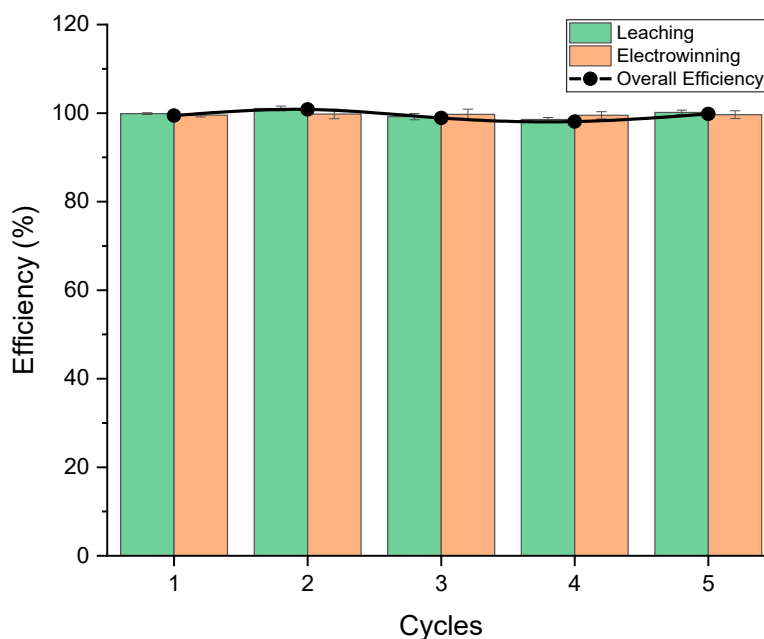


Figure 4.27: Leaching, electrowinning, and overall efficiency over five cycles by [Bmim]HSO₄.

In the leaching solution, several minor metals were also leached and presented in the solution. Although it was previously found that copper accounts for nearly 95% of all the leached metals, there is still a 5% of undesirable impurities present, which can be accumulated in each cycle of the process. Table 4.7 shows the leaching concentration and efficiency of copper and the major metals present in WPCBs over five cycles of leaching and EW. As previously found, nickel and zinc are the main contaminants in the leaching process with an initial concentration of 18.5 mg/L and 18.7 mg/L for Ni and Zn, respectively. As the number of cycles increases the concentration of Ni and Zn, following leaching and electrowinning, decreases. The concentrations of other major metals present at four significant figures less than that of copper, are deemed inconsequential. Although the concentration of these metals increases slightly during the leaching process, their leaching efficiency remains relatively unchanged and even decrease over the cycles. Thus, any increase in their concentration is likely due to their accumulation through the cycles.

Table 4.7: Leaching of Cu and major metals present in WPCBs over five cycles of leaching and EW.

Element	1 st Cycle		2 nd Cycle		3 rd Cycle		4 th Cycle		5 th Cycle	
	mg/L	%	mg/L	%	mg/L	%	mg/L	%	mg/L	%
Al	0.5	2.2	1.0	2.1	1.2	0.8	1.3	0.3	1.5	0.4
Ba	0.1	0.2	0.2	0.23	0.3	0.2	0.4	0.2	0.4	0.1
Co	0.0	13.2	0.1	12.3	0.1	2.3	0.1	3.4	0.1	2.1
Cr	0.1	15.1	0.1	2.3	0.1	3.3	0.2	10.2	0.2	1.5
Cu	680.2	100.0	689.8	100.0	676.1	100.0	679.2	100.0	683.5	100.0
Fe	3.2	29.2	5.2	14.3	5.7	1.5	7.1	4.6	8.2	3.5
Mg	0.4	53.2	0.7	39.4	0.9	25.4	0.9	1.4	0.9	1.6
Mn	0.2	29.1	0.2	1.2	0.2	1.1	0.2	0.8	0.2	0.5
Ni	18.5	76.1	16.5	0.0	14.5	0.0	13.7	0.0	12.2	0.0
Pb	0.1	1.1	0.1	0.6	0.2	0.5	0.1	0.0	0.1	0.0
Zn	18.7	73.2	17.8	0.0	12.6	0.0	8.5	0.0	6.3	0.0

During the leaching and EW processes, although [Bmim]HSO₄ showed no loss in performance and efficiency of copper recovery, the IL changed its colour slightly through the cycles from light yellow to dark yellow. This change in colour may suggest some degradation of the IL. Figure 4.28 shows the FTIR of [Bmim]HSO₄ before and after each cycle of leaching and EW. The FTIR of the recycled IL was compared to the virgin [Bmim]HSO₄ (black line), indicating no major changes in the fingerprint regions below 1500 cm⁻¹. Nevertheless, the IL showed an indication of degradation with the appearance of two peaks in the range of 1710 to 1650 cm⁻¹, consistent with two C=O stretch bands. The formation of these bands can be linked to the degradation of the IL due to the presence of H₂O₂ present in the leaching process and consequently of the EW process [176]. M. Muñoz et al. found that in imidazolium based ionic liquids, the presence of H₂O₂ can degrade the IL, generating acid carbon-bearing compounds such as acetic, oxalic, and formic [196]. In addition, ILs containing methanesulfonate and methylsulfate anions were found to oxidise faster than those with chloride or acetate anions. Thus, the emergence of C=O stretch in recycled IL of Figure 4.28 depicted by the features in spectra within the hatched box, can be associated with the degradation of the 1-butyl-3-methylimidazolium group present in [Bmim]HSO₄, suggesting its oxidation through the cycles.

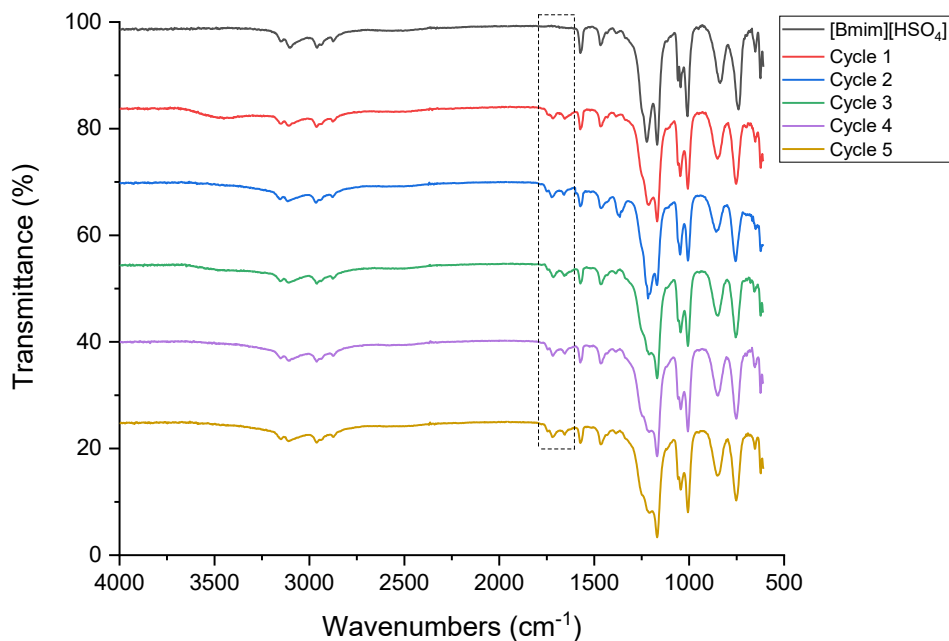


Figure 4.28: FTIR spectra of virgin of [Bmim]HSO₄ and recovered [Bmim]HSO₄ after 5 cycles – the hatched box indicates the emergence of feature linked to C=O stretch frequencies.

The TG and DTG curves of the virgin [Bmim]HSO₄ and the recovered [Bmim]HSO₄ over 5 cycles are presented in Figure 4.29. The conclusions that can be drawn from these traces include: (i) The virgin [Bmim]HSO₄ displays a single-step weight loss of 90%, with decomposition of the IL starting at approximately 380 °C. The recovered [Bmim]HSO₄, however, after each cycle shows a two-stage weight loss at 100-250 °C and 250-400 °C, with the major weight loss occurring in the second step at the higher temperature range. These decomposition zones are consistent with the volatilisation of compounds arising from the decomposition of the imidazolium group in the IL due to the leaching and EW processes. The DTG and energy (heat) flow traces (Figure 4.29b and c) respectively show the detailed phase changes and confirm the volatilisation of two compounds in the virgin and recycled IL. The first decomposition could be due to the volatilization of the butyl group present in the 1-butyl-3-methylimidazolium cation of the IL. The recycled IL did not present many differences after the first cycle, suggesting that the degradation of the IL occurs in the first leaching and EW cycle.

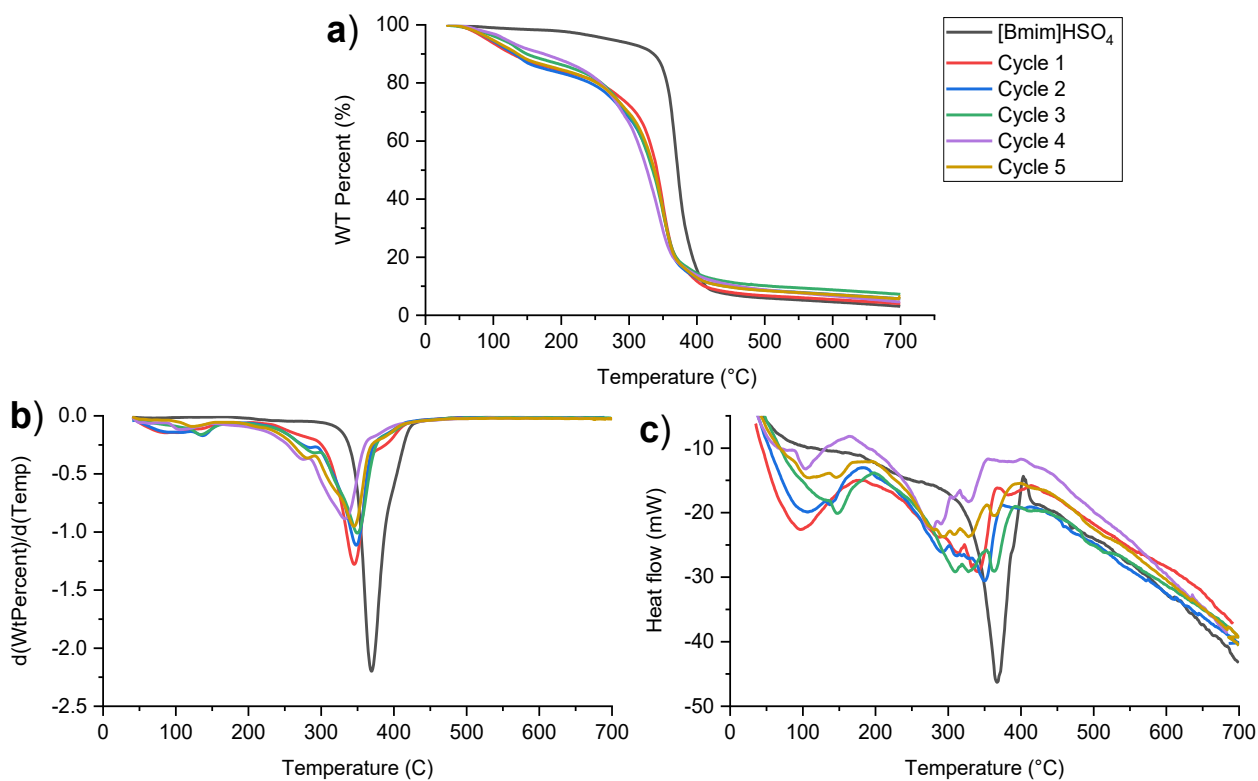


Figure 4.29: Thermogravimetric results of virgin [Bmim]HSO₄ and recovered [Bmim]HSO₄ after 5 cycles; a) TGA, b) DTG and c) heat flow.

The leaching of Cu from WPCBs remains largely unaffected over five leaching and EW cycles, confirming that [Bmim]HSO₄ can be successfully recycled and reused several times without losing its leaching efficiency. In addition, the recycling of that [Bmim]HSO₄ does not need any extra reagent or pre-treatment, making the copper recovery more environmentally friendly and cost-effective. The integrity of the IL remains for five cycles but will likely reach a limit and require addition or replacement beyond five cycles.

4.3.5 Proposed copper recycling process from WPCBs

The potential for recovery of copper from WPCBs derived from multigenerational mobile phones is proposed as a four-step approach involving the use of two task-specific ionic liquids, under optimised conditions, using one to remove solder and electronic components from as-received WPCBs, and the second to selectively leach the target metal, copper from the bare WPCB substrate, before using the process of electrowinning to recover copper in high levels of purity from the IL-leach medium. The fourth step involves the recovery of both ILs for recycle and reuse in their respective processes to minimise resource use and consequently reduce cost of materials. The four steps of *pre-treatment, leaching, electrowinning* and *IL recovery* proposed to recover copper from EoL-MP WPCBs are illustrated in the a flowsheet shown in Figure 4.30 and in a schematic in Figure 4.31. The process achieves a copper recovery efficiency is >95%, obtaining copper with a purity >99%. The optimised laboratory scale process developed shows excellent results for the recovery of high-level purity copper from EoL-MP WPCBs which can be extended to treat other sources of WPCBs and, with efficiencies around material resources, and simplicity of processes involved could be developed for application on a larger scale.

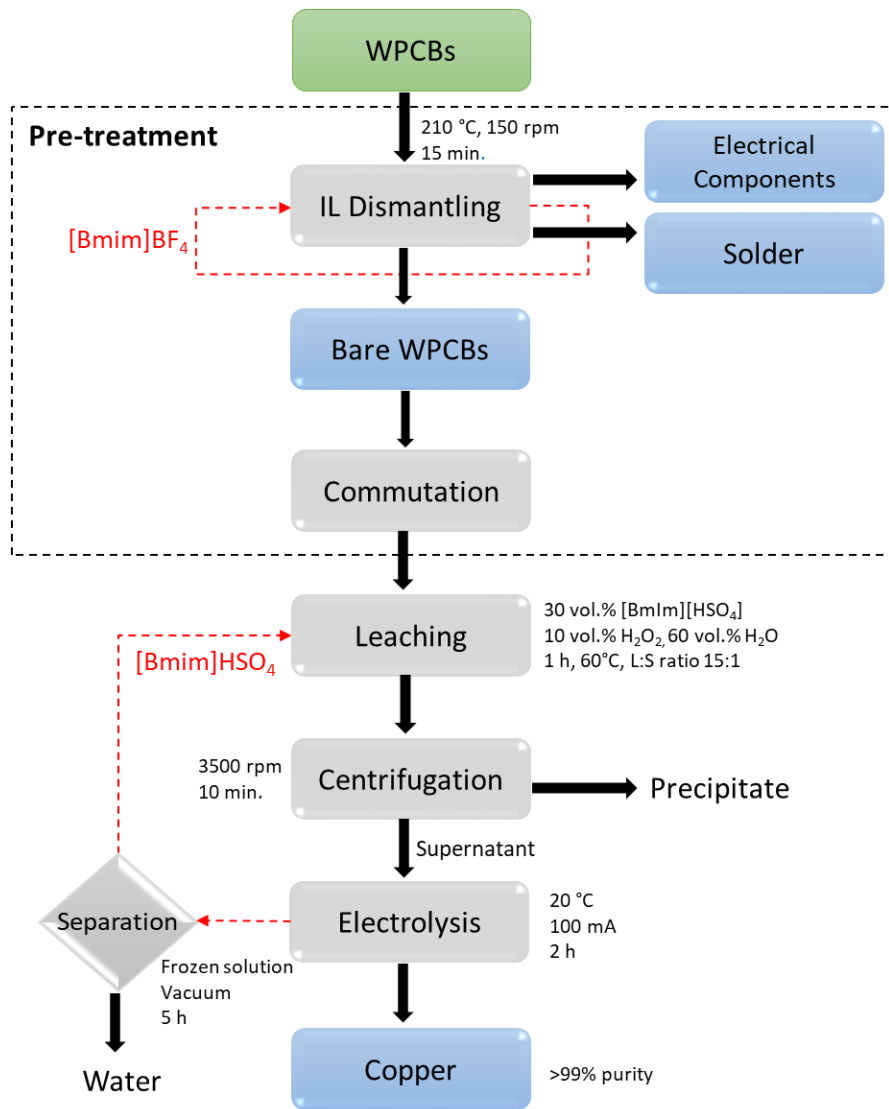


Figure 4.30: Flowsheet of copper recovery process from WPCBs.

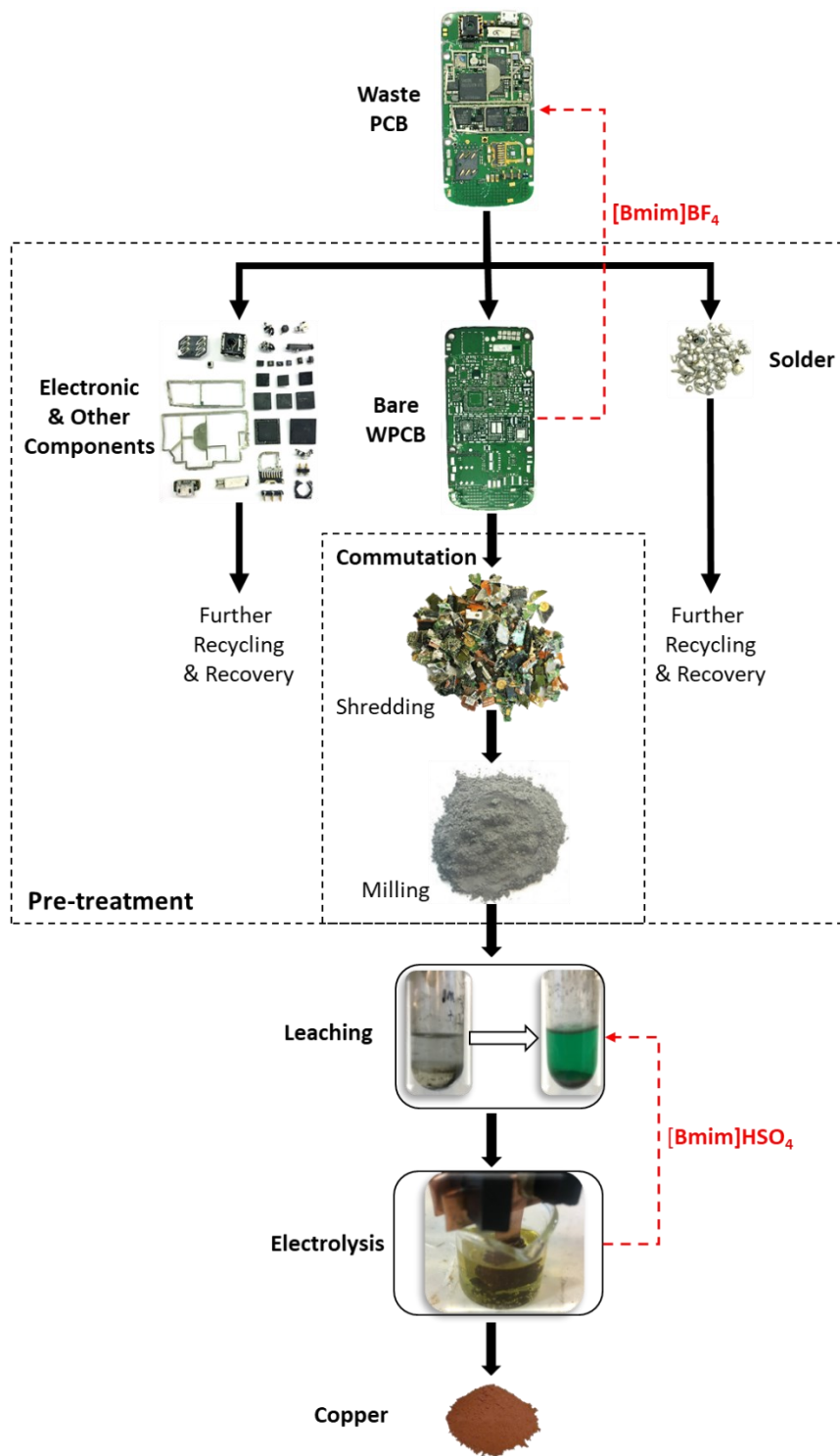


Figure 4.31: Schematic diagram of the experimental process for the recovery of copper from WPCBs.

4.4 Summary

Pre-treatment, leaching and electro-winning processes were studied and optimised to recover copper from WPCBs. Different ionic liquids were tested for their selective leaching of copper, namely: [Bmim]HSO₄, ([Bmim]Cl, ([Emim]Cl, and [Hbet]NTf₂, and the task-specific IL, [Bmim]HSO₄ was shown to be the most promising with the highest copper leaching efficiency. Temperature, time, solid to liquid ratio, oxidant and water dosages were studied and optimised. The optimal leaching conditions were 30 %v/v [Bmim]HSO₄, 10 %v/v H₂O₂, and 60 %v/v H₂O at 60 °C for 2 hours with 1:15 solid to liquid ratio and 150 rpm. Aqueous solutions of [Bmim]HSO₄ leached almost 100% of copper, with minor contaminants such as Ni, Zn and Fe, accounting for roughly 5% of the leaching solution. The kinetics analysis showed that diffusion plays a more important role than surface reaction, however, both are relevant in the metal leaching process from WPCBs.

To provide greater access to copper in the substrate, and so enrich the copper content for recovery, a pre-treatment step was studied. Pre-treatment of the WPCBs was achieved using the task-specific IL, [Bmim]BF₄. The optimal parameters for the dismantling of the ECs and removal of solder from WPCBs are shown to be a temperature of 210 °C, mechanical stirring speed of 150 rpm for 15 min. This pre-treatment step resulted in the doubling of copper content in the bare WPCBs compared to the original WPCBs. The ECs did not show any superficial damage, so have potential for reuse in new and/or refurbished PCBs. Alternatively, ECs can be further processed for metal recovery, as they are a rich source of precious metals. The solder recovered was shown to be chemically unchanged by the separation process and without any impurities, has potential to be reused. [Bmim]BF₄ was successfully used for up to three cycles without impact on its properties as an effective stripping medium.

Copper recovery by cementation and separately by electrowinning (EW) was investigated, and electrowinning was found to be the most effective and cleanest method to achieve excellent recovery of high-purity copper from the IL-leach medium. Thus, copper stripping was achieved by direct electrowinning from the [Bmim]HSO₄-leach solution, as electrolyte. Under controlled deposition conditions of 100 mA during 2 h, 100% of copper can be recovered with an average current efficient of 78.1% and an energy consumption of 4.5 kWh/kg Cu. The copper deposits were found to be of 99.35% purity. The leaching of copper from WPCBs remains largely unaffected over five leaching and electrowinning cycles confirming that [Bmim]HSO₄ can be successfully recycled and reused several times (despite some minor degradation of the imidazolium group in the [Bmim]HSO₄ by H₂O₂ during the leaching) without losing its leaching efficiency. In addition, the recycling of [Bmim]HSO₄ does not

need any extra reagent or pre-treatment, making the copper recovery more environmentally friendly and cost-effective.

In summary the results of the detailed investigation of the four key stages have led to the proposal of a process for the complete recovery of copper from EoL-MP WPCBs, which, following pre-treatment to remove solder and electronic components, makes use of an ionic liquid as a leaching medium for selective extraction of copper which is then used as an electrolyte medium, from which pure copper can be recovered. The process combining a dual two-step leaching and electrowinning system that is clean and environmentally friendly, minimising reagent use, minimising spent wastes, and maximising resource conservation through recovery of copper metal and return of secondary streams (electronic components and solder) for reuse in new or refurbished components or products. Furthermore, the proposed process can be applied not only to EoL-MP WPCBs, but to other WPCBs derived from all types of waste electrical and electronic equipment.

5 Development of a Process for Gold Recovery from Gold-rich E-Waste Components Using Ionic Liquids

5.1 Introduction

Printed circuit boards (PCBs) are essential components in electrical and electronic equipment (EEE). PCBs have a very complex structure with a heterogeneous composition, which contains a variety of more than 70 elements, as shown in Chapter 3. PCBs are rich in recyclable high-value materials, especially precious metals in concentrations higher than in their natural ores [22, 183]. Among these precious metals, gold is regarded as the most value metal in PCBs and EEE [159, 197]. Due to its excellent electrical conductivity, inertness, corrosion resistance, malleability, etc., gold is widely used in EEE in plating contacts, connectors, terminals, and pins as well as in electronic components such as chips, RAM, IC, CPU, etc. The content of gold in PCBs is between 200-500 times higher concentrated than in its natural ores (1-3 g/ton) and, although the weight percentage of gold in a PCB is less than 1%, its monetary value is more than 70% of all metals present in PCBs [22, 64, 159, 183, 197].

According to the US Geological Survey (USGS), the natural reserves of gold are 53,000 tonnes, with an average world production of 3,212 tonnes/year in the last five years (2016-2020) [198]. Based on these production levels, and without access to any new reserves, and the increasing demand for EEE, gold could run into scarce supply in the next two decades. Furthermore, it was estimated that the peak production of gold was in 2016, suggesting scarcity, lower concentrations of gold in natural ores, and an increase in mining cost production post 2016 [64]. Annually, approximately 267.3 tonnes of gold are being consumed for manufacturing mobile phones, laptops and other EEEs. Nevertheless, only 15% of this gold is recovered from these EEEs and the rest lies in storage yards or landfills [22]. The increase in the demand for gold for EEE and the limited availability have led to a steep rise in the market price of gold, making gold recycling an excellent source to meet this demand. Despite regulations controlling the handling, treatment and disposal of e-waste at end-of-life, e-waste is still poorly managed and ends up either in landfill or shipped for illegal dumping to developing countries, where gold is informally recycled; activities that give rise to serious impact on human health and the environment [45, 148, 197, 199]. Therefore, recycling gold from WEEE should be required to secure the metallic resources and to prevent environmental pollution.

Currently, recovery of valuable metals from waste PCBs (WPCBs) can be divided into two major methods: (i) upgrading the metal content by mechanical pre-treatment (commutation, magnetic separation, eddy current separation, corona electrostatic separation, etc.), and (ii) extraction and

refining to recover metals by pyro/hydro-metallurgical processes [92, 103, 200]. Mechanical pre-treatment methods are highly effective for metal liberation from the non-metallic fraction and offer excellent means of separating ferrous and non-ferrous metals; however, they usually lead to loss of precious metals [12]. Jiang et al. reported that shredding can lead up to 40% loss of precious metals as well as the process generating dangerous metal fines and dust containing brominated flame-retardants and dioxins[94] . Pyrometallurgy is the traditional approach for metal recovery from e-waste, has the advantage of requiring no pre-treatment and more than 70% of the recycled WPCBs are treated in smelters [12]. Nevertheless, pyrometallurgical is an energy intensive high-cost process that generates large amount of slag, and can result in the loss of precious metals in the process [12, 93].

In the last decades, hydrometallurgical processes have been given considerable attention for recovery of precious metals due to milder conditions involved, good selectivity for target metals, lower cost processing, and more environmentally friendly approach [12, 199]. Cyanide has been the dominant leaching agent for gold for more than a century due to the selectivity and stability properties of the dicyanoaurate complex. Nevertheless, cyanide is a highly poisonous/toxic reagent. Aqua regia (AR) and thiosulfate have mostly been used in the recent decades as gold leachants [200]. AR (1:3 molar mixture of nitric and hydrochloric acid) has been used due to its rapid and complete dissolution [201]. Lee et al. compared four leaching solutions; sulphuric acid, ammonia, aqua regia and thiourea for gold recovery from scrap integrated circuits (ICs), and found AR to be the best leaching reagent with a 100% gold leached [202]. Cyganowski et al. reported a gold removal of 86% from central processing units (CPUs) and pin contact elements (PINs) using aqua regia, an anion exchange resin and elution with a 5% thiourea-0.1 M HCl solution [203]. Park and Fray reported an effective gold recovery process from WPCBs using aqua regia for leaching precious metals, followed by a liquid-liquid extraction with toluene, recovering 97% of the gold [49]. More recently Jeon et al have reported a >99% gold extraction by ammonium thiosulfate from mobile phone PCBs and with a subsequent recovery of dissolved metals from pregnant leach solution via cementation, approximately 80% of the gold was recovered [159]. Ha et al found high gold leaching efficiencies from two types of mobile phone waste streams of 98% from keyboards and 90% from PCBs of mobile phones using thiosulfate [204]. Although high recovery efficiencies can be achieved, the methods are not without their drawbacks - these leaching reagents are costly, highly corrosive, do not achieve selectivity, have an excessive consumption of reagents, and generate toxic waste which needs further treatment [200, 203]. An alternative for gold extraction is the use of ionic liquids (ILs), also known as green solvents, with excellent solvent properties - non-flammable, negligible vapour pressure, excellent thermal, chemical and electrochemical stability, low viscosity, and high recyclability [104, 105]. Among the ILs,

imidazolium-based and phosphonium-based ILs, authors have reported their use in the metal recovery due to their cost-effectiveness and high recovery efficiencies [205, 206]. Most recently Masilela and Ndlovu have reported high and selective gold extraction over 90% using [Bmim][Tf₂N], [Bmim][PF₆], and Cyphos 101 from chloride leach liquors from WPCBs, with Cyphos 101 being reported as the most effective extracting IL [207].

Following gold leaching by hydrometallurgical processes, the steps to recover gold from leach solution include processes such as solvent extraction, sorption and electrochemical deposition, and a number of papers report the use of sorption as a more appropriate method for metal recovery from dilute solutions containing metals such as gold [203, 205, 206]. An alternative method that has attracted attention for recovery from dilute solutions is the use of solvent impregnated resins (SIRs). In the SIRs, a liquid complexing agent is dispersed homogeneously in a solid polymeric medium (resins). SIRs have excellent advantages in recovering metals from dilute solutions since they combine the benefits of solvent extraction and ion exchange, making the process highly selective, usually with fast mass-transfer rate, operational simplicity and a lack of solvent emulsification [208]. In addition, ion exchange reaction are reversible reactions, which offers the potential for reuse of the SIRs, favouring the economic and environmental aspects of the process [203, 208]. The SIRs limit the release of extractant by confinement of the extractant in a porous support resin allowing higher extraction efficiencies [205, 209]. Although gold recovery can be achieved using ILs, most studies reporting on gold extraction have been investigated using synthetic solutions and investigation on the recovery of gold direct from an e-waste source is much needed. The work described in this chapter, therefore, is focussed on the development of a process to achieve gold recovery from as-received e-waste (derived from EoL Mobile Phone WPCBs and EoL Computer PCB components) that combines the use of ILs in two hydrometallurgical processes of liquid-liquid extraction and sorption extraction.

5.2 Methodology

5.2.1 Materials

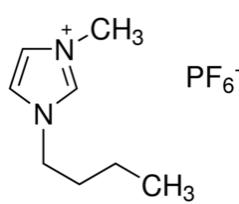
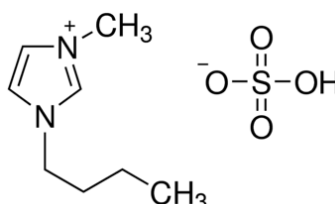
5.2.1.1 Chemicals and Reagents

All chemicals were of reagent grade and obtained from either Sigma-Aldrich (USA), VWR (USA) and Fisher Scientific (USA), Alfa Aesar (USA), Fluorochem (UK) and Agar scientific (UK). Unless stated otherwise all chemicals and reagents were used as received.

5.2.1.2 Ionic Liquids (ILs)

Based on the literature review, three potential ionic liquids were selected for trialling the extraction of gold, namely; *1-butyl-3-methylimidazolium hexafluorophosphate* ($[Bmim][PF_6]$), *1-butyl-3-methylimidazolium hydrogen sulphate* ($[Bmim][HSO_4]$), and *trihexyl(tetradecyl)phosphonium chloride* known as *Cyphos 101* ($[P_{6,6,6,14}][Cl]$). All ILs were purchased and used as received. Their properties and characterisation details (obtained in this work) are summarised in Table 5.1.

Table 5.1: Properties, characterisation and structure of the ionic liquids used in this study.

Ionic liquid	Properties & characterisation	Structure
$[Bmim][PF_6]$	<p>Appearance: Light yellow, viscous liquid</p> <p>MW: 284.18g/mol</p> <p>Density: 1.38 g/cm³ (20°C)</p> <p>Flash point: 350 °C</p> <p>FTIR: 3158 and 3119 (C-H, stretching from imidazole ring), 2964-2938 (CH, CH₂ and CH₃), 1574 and 1467 (imidazole ring) 1170 (CH, imidazole ring)</p> <p>TGA-DSC: Onset decomposition temperature: 400 °C. Residue: 1 wt.% at 700 °C</p>	
$[Bmim][HSO_4]$	<p>Appearance: Light-yellow liquid</p> <p>MW: 236.29g/mol</p> <p>Density: 1.277 g/cm³ (25°C)</p> <p>Flash point: 284 °C</p> <p>FTIR: 3200-2500 (OH), 3105/ 2961 (CH), 1573/1466 (C=C, aromatic), 1229/1166 (CN), 1070-1033 (S=O), 841/655 (C=C), 759 (C-H)</p> <p>TGA-DSC: Onset decomposition temperature: 340°C. Residue: 5 wt.% at 700 °C</p>	

Cyphos 101
[P_{6,6,6,14}][Cl]

Appearance: colourless, viscous liquid

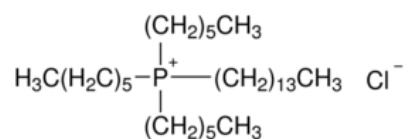
MW: 519.3 g/mol

Density: 0.895 g/cm³ (20°C)

Flash point: 118 °C

FTIR: 2954 (νCH₃), 2920 and 2952 (νCH₂), 1465 and 1377 (δCH₃), 1458/1111/1003 (νP-C), 1415 (δCH₂), 988(δC-H), 812 (νC-C), 719 (δP-C))

TGA-DSC: Onset decomposition temperature: 370 °C. Residue:<1 wt.% at 700 °C



Molecular weight (MW), densities and flash point values were obtained from Sigma Aldrich , Chemical Book and PubChem. FTIR vibrations were obtained experimentally and compare with references FTIR patterns in this study symbol; i) ν: stretching, ii) δ: bending, iii) ρ: rocking, iv) ω: wagging and v) τ: twisting. TGA-DCS information were obtained experimentally.

5.2.1.3 Metal samples

Samples of gold foil were used to determine the solubility of gold in the different ILs, and the gold salt of chloroauric acid (HAuCl₄) was used for the extraction studies described in Section 5.2.1.5. Copper samples used for IL solubility testing were as copper powder.

5.2.1.4 Amberlite™ XAD-7 Resin

Amberlite™ XAD-7 was supplied by Sigma-Aldrich (Saint-Louis, U.S.A.). Amberlite™ XAD-7 is an acrylic ester polymer of intermediate polarity and relatively hydrophilic character; its structure is shown in Figure 5.1 and physicochemical properties are presented in Table 5.2. Resins are generally conditioned with NaCl and Na₂CO₃ to prevent bacterial growth and may contain some mineral ions and residual monomers [205]. Prior to use, the Amberlite™ XAD-7 resins were placed in contact with acetone for 24 h followed by vacuum filtration and rinsing with RO water to remove residual monomers. For removal of mineral ions, the resins were then put in contact with 0.1 M HNO₃ for 24 h, vacuum filtered and rinsed with RO water until the eluate pH was the same as the RO water (using a pH paper indicator). Finally, the resins were put in contact with acetone for 12 h and dried using a vacuum roto-vapour at 80 °C.

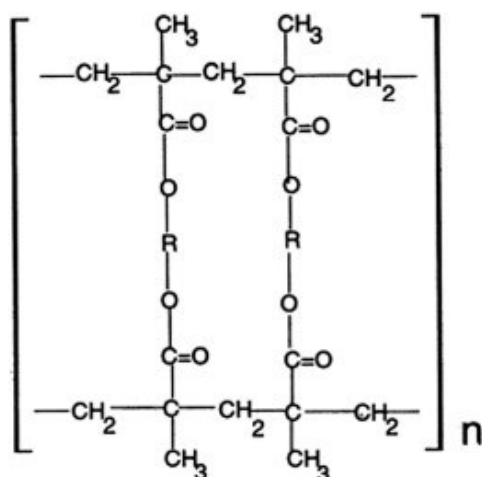


Figure 5.1: Chemical structure of Amberlite™ XAD-7 resin [210].

Table 5.2: Physical properties of Amberlite™ XAD-7 [210].

Physical property	Value
Superficial area (m ² /g)	450
Particle size (mesh)	20/60 (250/850 μm)
Resin porosity	0.55
Pore size (Å)	85-90
Pore volume (cm ³ /g)	0.97-1.14
Dry/wet density (g/cm ³)	1.24/1.05
Dipole moment	1.8
Vapour pressure (at 20 °C)	17 mm Hg
Auto ignition temperature (°C)	427

5.2.1.5 Model Test Solution

A stock synthetic solution, referred to in this work as the Model Test solution, containing gold in hydrochloric acid was prepared by dissolving chloroauric acid (HAuCl₄) (0.5g) in 290 mL of 0.1 M HCl solution, producing a stock solution of 1000 ppm Au. This stock solution was diluted to the desirable gold concentrations with hydrochloric acid for use in the liquid-liquid extraction and sorption/desorption studies to determine optimal process conditions for the recovery of gold.

5.2.1.6 E-Waste Printed Circuit Boards and Components

For the extraction and recovery of gold trials reported in this work two sources of gold-rich fractions from e-waste PCBs were investigated:(a) EoL Mobile Phone WPCBs and (b) EoL Computer PCB Components.

EoL-Mobile Phone WPCBs: The as-received WPCBs prepared as a powder for testing were from: (i) as-received samples EoL-MP WPCBs and (ii) stripped WPCB samples following copper extraction and recovery methods described in Chapter 4 of this thesis. A total of twenty-five EoL-MPs PCBs were used in this study for a more sensitive analysis and to provide a larger source of representative material for the experimental trials.

EoL Computer PCBs: As-received integrated circuits (ICs) and central processing units (CPUs) derived from EoL computers were trialled for gold recovery due to their high gold content for comparison and to provide insight on optimising experimental methods. ICs and CPUs were manually removed from EoL computer PCBs and were cut into pieces of 1x1 cm² prior to cryomilling. The shredding process used was the same as that used for shredding WPCBs described in Section 3.2.2, Chapter 3). The final product was a powder of ≤150 μm.

5.2.2 Analytical Techniques for Characterisation

The analytical techniques used for characterisation of materials in this study are described in Chapter 3. Figure 5.2 summarises the analytical methods applied, and the measures used to determine the effectiveness of the proposed process steps: *Leaching*, *Liquid-liquid Extraction*, *Sorption Extraction*, *Elution/Desorption*, *Reduction* and *Recovery of ILs and Resins* in extraction and recovery of gold from simulated solutions and from real samples e-waste components.

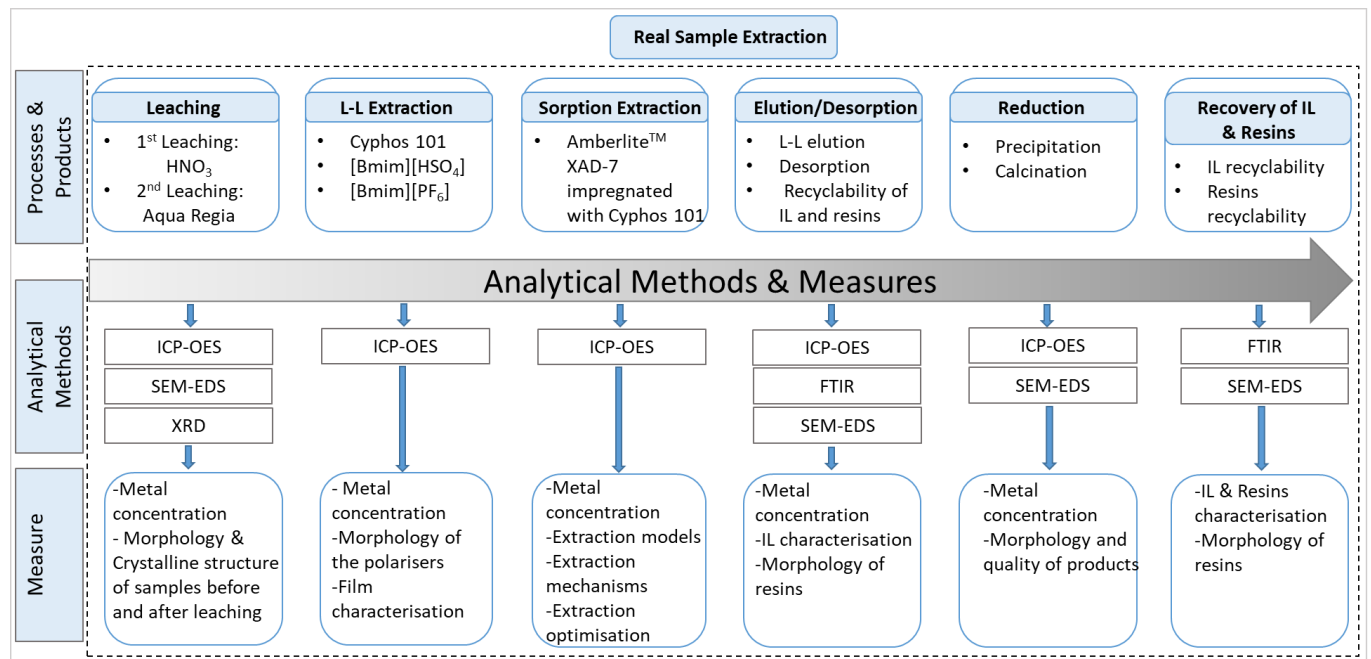


Figure 5.2 Analytical methods Applied and Measures Used to Determine the Effectiveness of the Extraction and Recovery Methods Proposed.

5.2.3 Experimental Procedure

To investigate the potential for recovery of gold from waste PCBs derived from multigenerational mobile phones and from components of computer PCBs, a four-step approach is followed: (i) solubility testing of ILs to identify selectivity for the target metal, gold, (ii) determination of the optimised conditions for gold extraction and recovery using a gold salt as a model test system to simulate a gold-rich source, (iii) pre-treatment of the as-received WPCBs and PCB components for gold recovery trials, and (iv) application of the optimised conditions for gold extraction and recovery of pre-treated real samples derived from the two e-waste streams of EoL-MP WPCBs and EoL Computer PCBs. An overview of the experimental procedure followed is set out in Figure 5.3.

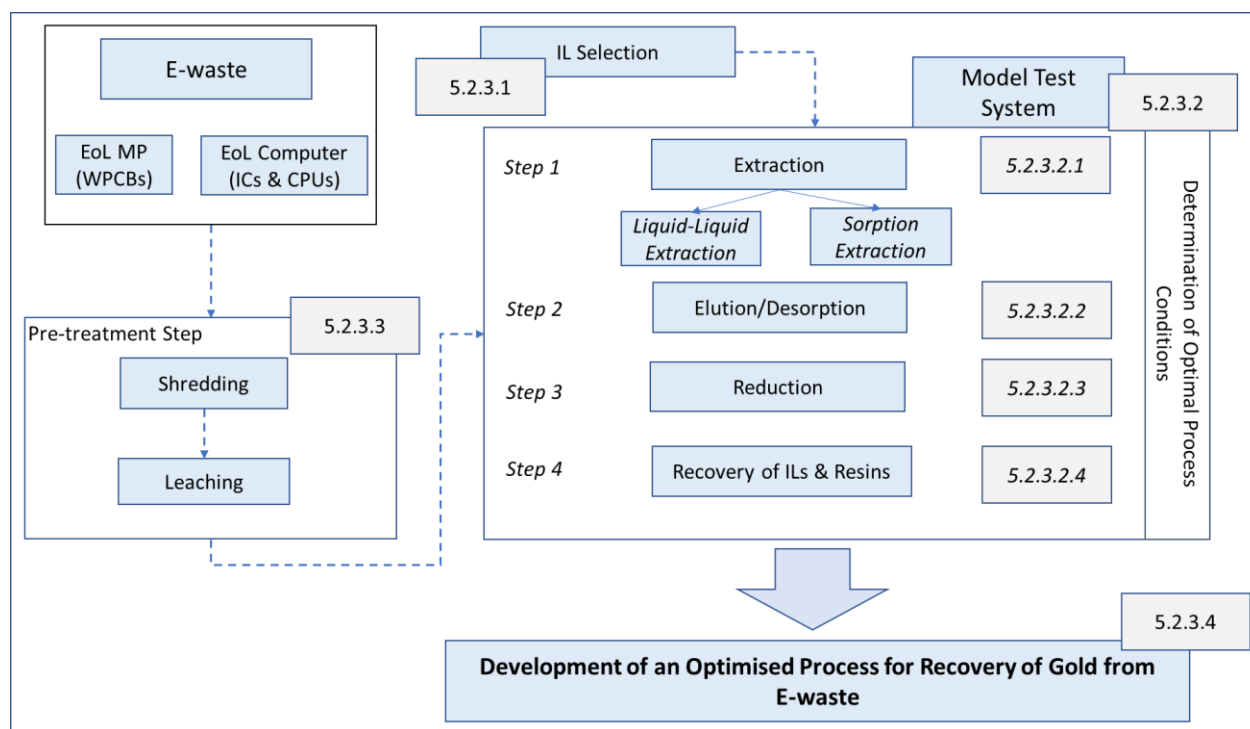


Figure 5.3: Overview of Experimental Procedure.

5.2.3.1 Solubility Testing of ILs for Gold Extraction

Solubility testing of the three potential ionic liquids (*[Bmim][PF₆]*), (*[Bmim][HSO₄]*), and *Cyphos 101* (*[P_{6,6,6,14}][Cl]*) were tested for their selectivity for gold (as foil) and separately for copper (as powder). The solubility of each metal in the ILs was tested under adding 0.1 g of target metal in 2 mL of IL at room temperature, 510 rpm for 1 h. To test the selectivity of the ILs for gold in the presence of a copper a mix of the two metals, the same amount of gold and copper (0.1 g each) was added with 4 mL of IL at room temperature, 510 rpm for 1 h.

5.2.3.2 Determination of Optimised Conditions for Gold Extraction and Recovery using A Model Test System

To determine the optimised conditions for recovery of gold from gold-rich samples, a Model Test solution was prepared as described in Section 5.2.1.4 and diluted to desirable gold concentrations with hydrochloric acid for use as a first step in each of the extraction processes using ionic liquids as either a *liquid-liquid extraction* or a *sorption extraction* system. Each of these extraction processes was followed by an *elution* and a *reduction* step. The potential for recovery of the ionic liquids and resins for recycle and reuse to minimise reagent use was also investigated as part of the determination of optimised conditions for gold extraction and recovery – an important and necessary aspect when using ionic liquid systems to mitigate the cost of ILs. Each of process steps investigated using simulated gold solutions is now described under the headings: *Extraction*, *Elution*, and *Reduction*.

5.2.3.2.1 Extraction

Two extraction methods were investigated for comparison using the Model Test System – *liquid-liquid extraction* and *sorption extraction*. The two methods were trialled to determine the effectiveness and impact of each on the recovery process.

Liquid-Liquid Extraction: Extraction experiments were conducted by mixing a prepared 510 ppm gold solution from the stock solution with the selected IL, *Cyphos 101*, in a liquid-to-liquid ratio of 1:1 (3 mL for organic and aqueous phases). The investigated parameters for liquid-liquid extraction are listed in Table 5.3. In each experiment, only one parameter at a time was changed while keeping the others constant. The solution was agitated using magnetic stirrers on a temperature-controlled heating plate. Once the extraction reaction was complete, the solutions were then centrifuged at 3500 rpm for 10 min to achieve complete phase separation. Following separation of the two phases 1 mL

of the aqueous phase was transferred to an ICP test tube and diluted with 4 mL of 1M HCl for ICP-OES analysis. Each experiment was conducted in triplicate. The extraction efficiency was calculated as:

$$Extraction (\%) = \frac{(C_i - C_f)_{(aq)} \cdot V_{org}}{(C_i \cdot V_{aq})_{(aq)}} \cdot 100 \quad Eq. 5.1$$

where C_i and C_f represent the initial and final metal concentration in the aqueous phase (mg/L), respectively, and V_{aq} and V_{org} are the volume (L) of the aqueous and organic phases, respectively. Due to the organic nature of Cyphos 101, the metal concentration in Cyphos 101 was calculated as the difference between the initial concentration and the final concentration in the aqueous phase, as shown in *Eq. 5.1*. This relationship was used to determine the metal concentration in all the extraction experiments.

In this study different diluents for Cyphos 101 in the L-L extraction, were tested, which included pentane, hexane, heptane, cyclohexane, and toluene. Their selection was based on their low polarity, where low polarity diluents can favour the formation of hydrogen bonds and other secondary bonding between the extractant molecules and contribute to the strength and selectivity of an extractant [211]. Diluents with high dielectric constant such as n-butyl alcohol, cyclohexanone, etc., however, can present strong interactions between diluents and phosphonium/ammonium extractants, which lead to low extraction rates [156]. Table 5.3 sets out the experimental conditions tested to (i) determine the optimal parameters for liquid-liquid extraction of gold in terms and the influence of variable process conditions, (ii) understand the mechanism of the extraction, and (iii) interpret the thermodynamics of the extraction process.

Table 5.3: Experimental parameters for determination of optimal gold liquid/liquid extraction conditions, mechanism, and thermodynamics Cyphos 101.

Liquid/liquid Extraction				
Temperature (°C)	HCl concentration (M)	IL concentration (M)	Time (min)	Diluent
20, 30, 40, 50, 60, 70, 80	1	0.005	15	Toluene
20	0.1, 0.5, 1, 2, 3	0.01	15	Toluene
20	1	0.001, 0.005, 0.01, 0.05, 0.1	15	Toluene
20	1	0.01	1, 2, 3, 4, 5, 7.5, 10, 15, 20, 30	Toluene
20	1	0.01	15	Pentane, hexane, heptane, cyclohexane, toluene

Extraction mechanism				
Temperature (°C)	[Cl ⁻] (M)	[IL] (M)	Time (min)	Diluent
20	0.1, 0.2, 0.5, 0.7, 1.0	0.001	15	Toluene
20	1	0.001, 0.002, 0.003, 0.004, 0.005, 0.007, 0.01, 0.05, 0.1	15	Toluene
Extraction thermodynamics				
Temperature (°C)	[Cl ⁻] (M)	[IL] (M)	Time (min)	Diluent
20, 30, 40, 50, 60, 70, 80	1	0.01	15	Toluene

Sorption Extraction: The process involved the use of resin impregnation. There are different processes for physical impregnation of resins such as the dry method, the wet method, the dynamic method, and the impregnation in the presence of a modifying agent [206]. Researchers have found that the dry method increases the stability of the extractant on the resin [205, 206, 209]. Thus, the selected IL (Cyphos 101) was immobilised on the resin by the dry impregnation method where Amberilite™ XAD-7 resin (5 g) was mixed with (Cyphos 101) (0.5 M), diluted in acetone (25 mL), and contained in a stoppered glass bottle. The bottle was placed in a reciprocating shaker and the mixture was agitated for 24h at 150rpm. Varying amounts of Cyphos 101 diluted in acetone (0.5 M) were added to the resin under these conditions and allowed to equilibrate over a period of 24 h under 150 rpm of agitation. The acetone was then slowly removed by evaporation in a roto-vapour. Three samples of SIRs were prepared with IL loadings of 100, 300 and 500 mg IL/g resins. It has been reported that an excessive loading of ILs in resins, with amounts over 600 mg of ILs, could result in a partial leakage of the IL and iridescence (typical of hydro-carbon release) can also be observed [212]. To avoid this, IL loadings were maintained at ≤500 mg IL/g resin for the sorption experiments.

The loading levels were determined by mixing impregnated resin (0.2g) with methanol (3ml) for 24h to remove the IL by dissolution. This washing procedure was carried out three times to ensure a total extractant dissolution. The resin was separated and dried at 50 °C for 24 h. The amount of IL extractant immobilised on the resin was calculated as:

$$q_{IL} = \frac{M_{resin/IL} - M_{resin}}{M_{resin/IL}} \quad \text{Eq. 5.2}$$

where $M_{resin/IL}$ and M_{resin} represent the mass of the impregnated resin and washed resin (mg). The amounts of extractant immobilised on the resin obtained were close to the theoretical values calculated, resulting in 95, 289, and 508 mg IL/g resin.

Sorption studies were carried out using the Model Test solution with concentrations of gold (from 5 mg/L to 300 mg/L) in different HCl acid concentrations (0.1 M-5 M). The sorption experiments were performed by mixing the impregnated resins with the gold solutions for 24 h to ensure that equilibrium was achieved with a fixed sorbent dosage (solid to liquid ratio, g sorbent/ L solution). Table 5.4 lists the parameters studied for gold sorption; temperature, HCl concentration, time, and initial gold concentration. In each experiment, only one parameter was changed at a time while keeping the others constant. The selection of a 24 h period for sorption was based on previous studies reported for recovery of Pd, Au and Cd using Amberlite™ XAD-7 resin [206, 209, 212], however, preliminary kinetic experiments carried out as part of the current research showed that the equilibrium was reached within 3 h.

For each experiment, a gold solution (of known concentration in the range 5 to 300 mg/L) was poured into a 25 mL capped bottle with a respective amount IL-impregnated resin, sorbent dosage listed in Table 5.4, and agitated in a reciprocating shaker at 150 rpm and at room temperature (20 ± 2 °C). To study the effect of temperature on the sorption, the capped bottles (containing the mixture) were placed in a water bath on a temperature-controlled heating plate, and the solution was agitated using magnetic stirrers at 50 rpm (in place of the reciprocating shaker). The lower agitation was selected to avoid deterioration of the resins which can occur at higher mechanical agitation levels. Once the sorption period ended, the samples were filtered and the solution was analysed by ICP-OES (1 mL of the aqueous phase was transferred to an ICP test tube and diluted with 4 mL of 1 M HNO₃ or 1 M HCl, depending on the experiment). Each experiment was repeated in triplicate. Resins, without Cyphos 101, were also studied to provide a control. The amount of gold adsorbed was calculated by [205]:

$$q = \frac{V \cdot (C_0 - C_{eq})}{m} \quad \text{Eq. 5.3}$$

where V is the solution volume (L), C_0 and C_{eq} are the initial and equilibrium concentrations (mg/L), respectively, and m is the mass of resin used (mg).

Table 5.4: Experimental parameters of sorption; Amberlite™ XAD-7 impregnated with Cyphos 101.

Sorption				
Temperature (°C)	HCl concentration (M)	Time (h)	C _{0, Au} (mg/L)	Sorbent Dosage (mg/mL)
20, 30, 40, 50, 60, 70, 80	1	2	300	0.5
20	0.1, 0.5, 1, 2, 3, 4, 5	24	300	3
20	1	0.5, 1, 1.5, 2, 3, 3.5, 4, 4.5, 5, 6, 7, 8, 20, 22, 24, 30, 44	200	0.5
20	1	24	5, 10, 25, 50, 75, 100, 150, 200, 300	0.5

All experiments were carried out for the three loading resins (100, 300, and 500 mg IL/g resin) and raw Amberlite™ XAD-7. Models and kinetics were determined based on the sorption results.

5.2.3.2.2 Elution and Desorption

Elution of gold in the **L-L extraction** was tested under conditions set out in Table 5.5, by placing the loaded organic phase (3 mL) after extraction in a stoppered glass bottle, in contact with a thiourea solution (3 mL) at different concentrations of hydrochloric acid and of thiourea. The bottle was placed in a reciprocating shaker at 150 rpm for 15 minutes. After the reaction, the metal concentration in the aqueous phase was determined by ICP-OES. The elution efficiency was calculated by:

$$Elution (\%) = \frac{(C_f - C_i)_{(aq)} \cdot V_{aq}}{[M]_{(org)}} \cdot 100 \quad Eq. 5.4$$

where C_i and C_f represent the initial and final metal concentration in the aqueous phase (mg/L), respectively, V_{aq} is the volume (L) of the aqueous phase, and $[M]_{(org)}$ represents the amount of metal (mg) in the organic phase, calculated for the L-L extraction. For the evaluation of L-L extraction and elution cycles, the same procedure was repeated five times.

In the case of loaded resins, from the **Sorption** Extraction studies, the desorption of gold was achieved by mixing the loaded resin (20 mg) with thiourea (10 mL), at different concentrations of hydrochloric acid (0.1-3M) and of thiourea (0.1-3M); the mixture was agitated at 150 rpm for 3 h (Table 5.5). It has been reported that gold desorption from resins with thiourea can reach equilibrium in two hours [213], but to ensure complete equilibrium was achieved, a duration of 3 h was chosen. The solutions were then filtered and the concentration in the eluent was determined by ICP-OES. The desorption efficiency was calculated as the amount of desorbed metal as a fraction of the amount of metal in the impregnated resins, using Eq. 5.4. For the evaluation of sorption and desorption cycles,

the same procedure was repeated five times. After each desorption step, the resin was washed three times with 0.01M HCl to eliminate residual thiourea that may be retained in the resin.

Table 5.5: Experimental parameters for Elution & Desorption.

Elution & Desorption			
Temperature (°C)	HCl concentration (M)	Thiourea concentration (M)	Time* (min)
20	0.1, 0.5, 1, 1.5, 2, 3	1	15/180
20	1	0.1, 0.5, 1, 1.5, 2, 3	15/180
20	1	1	1, 5, 10, 15, 20, 30, 45, 60, 90, 120, 180

*: For elution after L-L extraction, 15 minutes was used, whilst in the case of desorption, 3 h were utilised. In the case of elution, all experiments were carried out with an Organic:Aqueous (O:A) ratio of 1:1. In the case of desorption, all experiments were carried out with a sorbent dosage of 2 (mg/mL).

5.2.3.2.3 Reduction

The recovery of gold from eluted solutions (using the conditions of 0.5M thiourea in 0.5M HCl) was carried out by a reduction-precipitation step using sodium borohydride (NaBH_4), a strong and efficient reducing agent resulting in precipitation of metallic gold. NaBH_4 solution with a concentration of 0.5 M was freshly prepared using ice cold RO water. A double beaker was utilised as an ice-bath, where the external beaker was filled with a mixture of ice and RO water to maintain a low reaction temperature. Ice-cold water is necessary because NaBH_4 reacts violently and quickly with water at room temperature, and, if added to water without cooling, it will start to react quickly with the water before reduction of gold can take place. Thus, ice-cold water can sufficiently slow the reaction to allow the reduction of gold ions. In the absence of any reducible species in solution, sodium borohydride decomposes into sodium metaborate and hydrogen gas. Controlled precipitation was achieved with dropwise of a solution of 0.1 M NaBH_4 in 0.1 M NaOH. Total gold reduction was obtained within 20 minutes at room temperature and 150 rpm.

5.2.3.2.4 Recovery of ILs and Resins for Recycle and Reuse

To study the recyclability of the organic phase (0.1 M Cyphos 101 in toluene) in the **L-L extraction**, and the recyclability of impregnated resins (300 mg IL/g resins) in the **sorption extraction**, the whole extraction process was carried out for five continuous cycles of L-L extraction or sorption extractions followed by elution/desorption processes using the same organic phase and resins. A synthetic gold solution of 300 ppm Au in 1 M HCl was utilised as the aqueous phase. In the case of L-L

extraction, 5 mL of organic phase was put in contact with 5 mL of aqueous solution at 20 °C, 150 rpm for 15 min. After extraction, the loaded organic phase was separated from the aqueous phase and then put in contact with 5 mL of 0.5 M thiourea in 0.5 M HCl at 20 °C, 150 rpm for 1 h. After elution, the organic phase was washed 3 times with RO water and was utilised in the next cycle. In the case of sorption/desorption extraction, the sorption was done by contacting 10 mg of impregnated resins with 5 mL of aqueous solution (SD=2 mg/mL) at 20 °C, 150 rpm for 4 h. After 4 hours of sorption, the resins were filtered and put in contact with 5 ml of 0.5 M thiourea in 0.5 M HCl (SD=2 mg/mL) at 20 °C, 150 rpm for 2 h. After desorption, the resins were washed 3 times with 0.01 M HCl solution, dried at 40 °C for 5 h and then utilised in the next cycle.

FTIR was used for characterisation of the organic phase in each cycle. SEM-EDS was used to characterise the resins before and after the five cycles, and ICP-OES was used in both extraction methods to determine the metal concentration following each cycle.

5.2.3.3 Pre-treatment of As-Received WPCBs and PCB Components for Gold Recovery

The leaching of gold was carried out using a two-step leaching of the as-received fractions with nitric acid leaching followed by aqua regia (AR) leaching. The use of a two-step leaching is due to the high copper content in WPCBs, which makes the extraction of gold difficult, requiring a first leaching for the extraction of copper. Previous leaching studies of WPCBs with traditional acids carried out as part of this research showed that nitric acid was more efficient than sulphuric and hydrochloric acids for copper leaching. Based on these findings and reports in the literature, the first leaching was carried out with nitric acid using the reported optimal Cu leaching conditions of 3M HNO₃, 30 °C, 50 g/L pulp density, and 500 rpm for 3h rather than the reported 2h to ensure complete copper leaching [214]. Once the first leaching was complete, the solution was filtered under vacuum and the filtrate was rinsed 5 times with RO water. The solid residue was then dried at 50 °C for 24 h before being used in the second leaching step (gold leaching), which the dried powder was mixed with aqua regia (AR, 1:3 solution of concentrate HNO₃ and HCl) with a solid to liquid ratio of 1:20. The solid to liquid ratio of 1:20 was selected since it had been widely reported to be the optimal ratio [49]. The leaching was carried out at room temperature (20 ± 2 °C) and pressure since the reaction is exothermic and releases adequate heat for optimum leaching temperature (~80 °C), stirred at 150 rpm for 3 h under a fume hood. After AR leaching, the solution was centrifuged at 3500 rpm for 15 minutes and the supernatant was separated from the sediment passing it through a paper filter paper of 0.45 µm. The metal concentration after each leaching was analysed by ICP-OES. The leaching efficiency was determined by:

$$\text{Leaching (\%)} = \frac{[M_i]_{\text{solution}}}{[M_i]_{X,\text{digestion}}} \cdot 100 \quad \text{Eq. 5.5}$$

where $[M_i]_{\text{solution}}$ is the amount of metal 'i' in solution (mg), and $[M_i]_{X,\text{digestion}}$ represents the total amount of 'i' metal (mg) in the 'X' sample (WPBCs, ICs, CPUs).

The total metal concentrations of WPBCs, ICs and CPUs were previously determined by AR digestion, using the methodology described in section 3.2.3.1, Chapter 3. Each experiment was done at least in triplicate. Characterisation of the initial sample and leached residue, after each leaching process was made using scanning electron microscope (SEM), energy dispersive X-ray spectroscopy (EDS) and X-Ray diffraction (XRD) analyses.

5.2.3.4 Application of the Optimised Conditions for Gold Extraction and Recovery from E-Waste Components

Following these trials for gold recovery using a Model Test system, and after pre-treatment of EoL Mobile Phone WPBCs and the EoL Computer PCBs to obtain a gold-rich stream the optimised process conditions were tested on real samples to determine the potential for the complete recovery of gold from these e-waste streams.

The process of **L-L extraction** followed by **elution**, and **Sorption extraction** followed by **desorption** were both tested for comparison. The conditions for trialling are set out below.

Liquid-liquid extraction was carried out using the leach solution derived from the two-stage leaching process reported in the pre-treatment step (Section 5.2.3.3). The organic phase used was 0.1 M Cyphos 101 in toluene, and the extraction was carried out with an O:A ratio of 1:1, at room temperature (20 ± 2 °C), 150 rpm, and 15 minutes (Table 5.3). The loaded organic phases were eluted using 0.5 M thiourea in 0.5 M HCl with an O:A ratio of 1:1, room temperature (20 ± 2 °C), 150 rpm for 1 h (Table 5.5).

Sorption extraction was carried out using the leach solution derived from the two-stage leaching process reported in the pre-treatment step (Section 5.2.3.3). The sorption was carried out using Amberlite™ XAD-7 impregnated with 300 mg Cyphos™ 101/g resins, with a sorbent dosage (SD) of 25 g/L, room temperature (20 ± 2 °C), 150 rpm, and 3 h (Table 5.4). Loaded SIRs were desorbed/eluted by 0.5 M thiourea in 0.5 M HCl with SD=25 g/L, room temperature (20 ± 2 °C), 150 rpm for 2 h (Table 5.5).

The optimised conditions for **Reduction** to recover gold following both extraction methods used on the real samples was carried out by reduction/precipitation using sodium borohydride (NaBH_4) present as a 0.1 M NaBH_4 in 0.1 M NaOH solution. The **recovery of ILs and resins** for reuse and recycle were trialled on the real samples using the optimised conditions.

5.2.3.5 Summary

The four-step approach to investigate the development of an optimised process for recovery of gold from gold-rich sources in e-Waste PCBs derived from EoL WPCBs and EoL Computer ICs and CPUs using ionic liquids is elaborated further in Figure 5.4 in terms of the process steps, the conditions tested, and the component fractions involved.

Leaching	L-L Extraction	Sorption Extraction	Elution & Reduction	Gold Recovery
Acids HNO_3 & Aqua Regia	Ionic Liquid Cyphos 101 + Toluene	Amberlite™ XAD-7 Resin XAD-7 + Cyphos 101	Reagents Thiourea, NaBH_4	Samples WPCBs, ICs, CPUs
Copper Leaching <ul style="list-style-type: none"> Nitric acid leaching 	Experiments: <ul style="list-style-type: none"> Diluent influence Time Temperature IL concentration Acid concentration 	Experiments: <ul style="list-style-type: none"> IL loadings in resins Acid concentration Sorption isotherms Time Temperature Thermodynamics 	Elution & Desorption <ul style="list-style-type: none"> HCl concentration Thiourea concentration Time 	Experiments: <ul style="list-style-type: none"> Copper leaching Gold leaching
Gold Leaching <ul style="list-style-type: none"> Aqua regia leaching 	Extraction mechanism <ul style="list-style-type: none"> Effect of [IL] Effect of $[\text{Cl}^-]$ Thermodynamics 	Kinetics and models <ul style="list-style-type: none"> Adsorption isotherm models Sorption kinetics Sorption models 	Reduction <ul style="list-style-type: none"> Gold precipitation by NaBH_4 solution 	<ul style="list-style-type: none"> Gold L-L extraction Gold elution
ILs Selection <ul style="list-style-type: none"> $[\text{Bmim}][\text{HSO}_4]$ $[\text{Bmim}][\text{PF}_6]$ Cyphos 101 			Materials reusability <ul style="list-style-type: none"> L-L extraction & elution for 5 cycles Sorption & desorption for 5 cycles 	<ul style="list-style-type: none"> Gold sorption Gold desorption
				<ul style="list-style-type: none"> Gold precipitation Reagents & materials reusability

Figure 5.4: Overview of the experimental procedure applied in the development of an optimised process for gold recovery

5.3 Results and Discussion

5.3.1 Selection of IL for Gold Extraction

Gold in e-waste is present as solid metal, so as a first step to gold recovery using ionic liquids, a preliminary investigation involved the testing of three ILs, ($[Bmim][PF_6]$), ($[Bmim][HSO_4]$), and *Cyphos 101* ($[P_{6,6,6,14}][Cl]$), to evaluate their potential as leaching reagents and determine their selectivity, or not, for gold. Since copper is the most abundant metal in e-waste, it was also necessary to investigate the behaviour of copper in the three ILs. The leaching efficiency of gold foil and copper powder were studied separately with the three ILs, and the results are presented in Figure 5.5. The leaching efficiency of all three ILs for gold is similar but *Cyphos 101* shows the highest at 7.4%, followed by $[Bmim][HSO_4]$ and $[Bmim][PF_6]$ with 6.4% and 5.3%, respectively. The highest leaching efficiency obtained by *Cyphos 101* could be due to the presence of Cl^- as anion in *Cyphos 101*, which has better affinity towards gold than the anions HSO_4^- and PF_6^- present in the other ILs. In the case of copper, $[Bmim][HSO_4]$ shows a markedly higher leaching efficiency of approximately 25%, followed by *Cyphos 101* and $[Bmim][PF_6]$ with 5.3% and 4.2%, respectively. The difference in performance can be attributed to the greater affinity of the Cu^{2+} cation towards the HSO_4^- anions present in the IL; a factor explained in Chapter 4. Although gold can be leached with the three ILs, their leaching efficiencies are low and in presence of more metals, the effectiveness of the leaching is expected to be negligible.

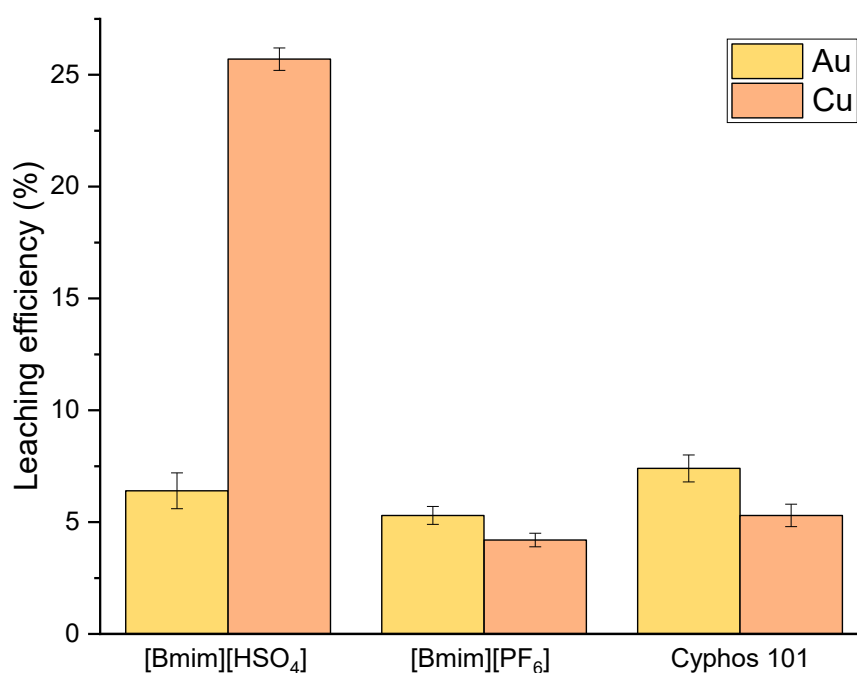


Figure 5.5: Leaching efficiency of IL from gold and copper.

Gold can also be recovered from acidic solutions, where ILs can act as extractant agents. Due to the hydrophilic nature of [Bmim][HSO₄], and its higher affinity for copper over gold which could make the separation process more difficult or require the need of further separation processes, it was not selected, in this work, as a suitable extractant for gold recovery. On the other hand, because of the hydrophobicity of [Bmim][PF₆] and Cyphos 101, two phases are observed, making them ideal for liquid-liquid extraction. Figure 5.6 shows a gold extraction efficiency of [Bmim][PF₆] and Cyphos 101 from a 510 ppm model gold solution as function of time and temperature. In both ILs, almost complete extraction of gold was achieved, reaching 99.5% and 97.5% extraction efficiency for Cyphos 101 and [Bmim][PF₆], respectively. Furthermore, the gold extraction was rapid, reaching the equilibrium within 15 minutes of reaction (Figure 5.6a). Temperature (Figure 5.6b) did not appear to impact the extent of gold extraction, showing only an increase of 0.5% extraction efficiency from 25 °C to 80 °C. In general, both ILs presented high extraction efficiencies, with Cyphos 101 being marginally better. The extraction mechanism for each of these ILs is different. The phosphonium group in Cyphos 101 extracts AuCl₄⁻ through largely anion exchange whilst in the case of [Bmim][PF₆], the imidazolium group extracts gold through a complexing reaction [207].

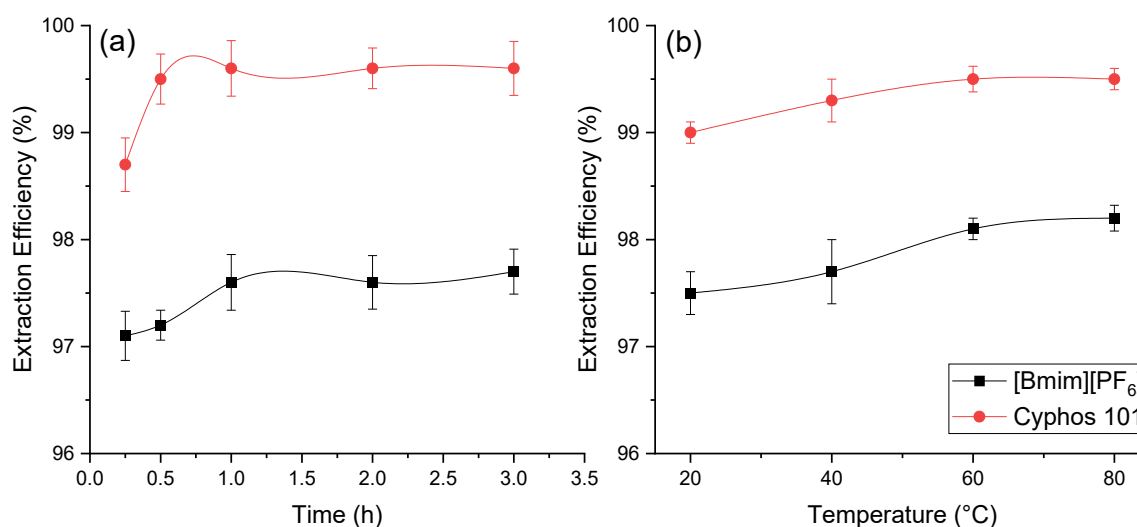


Figure 5.6: Extraction efficiency of gold from HCl solution; (a) effect of the time and (b) effect of the temperature.

Cyphos 101 has been used in the recovery of other metals such as cadmium [212], palladium [206], indium and tin [156, 215], among others [112, 206]. [Bmim][PF₆] has also been used in the recovery of other metals such as copper [111], silver [207], nickel [216], etc. Thus, although Cyphos

101 and [Bmim][PF₆] can be effectively used for gold extraction in a liquid-liquid process, the lack of selectivity becomes a major disadvantage, especially in processing WEEE, in which more than 60 metals can be found, as reported in Chapter 3. Since WEEE contains only trace amounts of gold any solutions containing gold will be very dilute, thus making the challenge of extracting gold from diluted media even greater. In metal extraction from diluted solution, ion exchange is a promising and often economically viable method to concentrate and recover a target metal [203], and so ion exchange was used in this work for separation and enrichment of gold, using the well-documented aqua regia medium in the pre-treatment method for real samples (discussed in Section 5.3.3). The use of these highly acidic conditions, therefore, rendered the IL, [Bmim][PF₆], unsuitable as an extractant in this medium since it has been reported that [Bmim][PF₆] in highly acid conditions shows weak chemical stability, because the [PF₆]⁻ ion decomposes through hydrolysis of the anion, deteriorating the IL and leading to lower efficiency of extraction. Furthermore, this hydrolysis can produce and liberate highly toxic gases such as hydrogen fluoride [207]. As part of the solubility testing, it was observed that the behaviour of the two ILs, [Bmim][PF₆] and Cyphos 101 in a range of organic solvents was different, with the former having limited or no solubility in simple organic solvents such as toluene, pentane, hexane, etc., making the selection of diluent more difficult. Therefore, Cyphos 101 was selected for as a complexing agent in liquid-liquid extraction and solvent impregnated resins (SIRs) trials for the recovery of gold in hydrochloric solutions.

5.3.2 Optimised Conditions for Gold Extraction and Recovery Using a Model Test System

To determine the optimal conditions for gold extraction and recovery from gold-rich samples, a Model Test system was used in which a gold solution in hydrochloric acid was prepared to simulate a gold solution leached from pre-treated real samples. The extraction processes using ionic liquids as either a liquid-liquid extraction or a sorption extraction system (trials for comparison), followed by an elution and reduction step were developed, and the potential for recovery of the ionic liquids and resins for recycle and reuse to minimise reagent use was investigated. The results of the optimised process steps using simulated gold solutions are now described under the headings: *Liquid-Liquid Extraction, Sorption Extraction; Elution and Desorption including Recycle of ILs and Reuse of Resins; and Reduction.*

5.3.2.1 Liquid-Liquid Extraction

5.3.2.1.1 Influence of the diluent

The influence of five diluents; pentane, hexane, heptane, cyclohexane, and toluene on the extraction of gold by diluted Cyphos 101, was studied and the results are presented in Figure 5.7. The use of different diluents did not show any major change in extraction efficiency with extractions in a range of 94-96% for pentane, hexane, heptane, and cyclohexane; with toluene showing complete extraction of gold. Among these diluents, toluene is more economic and easily available. Furthermore, toluene has the highest boiling point (110 °C), resulting beneficial if working with higher temperatures is needed, so toluene was selected as the preferred diluent.

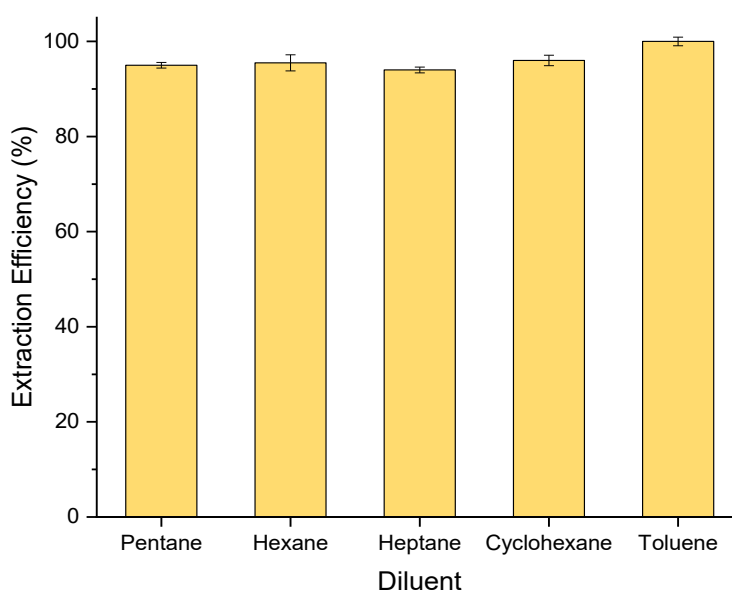


Figure 5.7: Effect of diluents on gold extraction.

5.3.2.1.2 Effect of time, temperature, Cyphos 101 concentration, and HCl concentration on the gold extraction

The effect of time, temperature, Cyphos 101 concentration, and hydrochloric acid concentration on gold extraction was studied and the results are presented in Figure 5.8. The time required to achieve equilibrium was approximately one minute (Figure 5.8a), with more than 99% gold extracted, suggesting that the extraction kinetics are reasonably fast. No adverse effects were observed with prolonged agitation time, so to ensure equilibrium was attained a time of 15 minutes was selected. There was no change in extraction efficiency with temperature with 100% gold extraction (Figure 5.8b), achieved across the range (20-80 °C). The influence of Cyphos 101 concentration, from 0.001 M to 0.1 M on gold extraction is presented in Figure 5.8c. The results show an extraction of 67% at 0.001M Cyphos 101, followed by a sharp increase in the gold extraction. At 0.005 M Cyphos 101, the gold extraction was 93%, followed by 100% extraction with higher Cyphos 101 concentrations (of $\geq 0.01\text{M}$). The influence of the hydrochloric acid concentration is shown in Figure 5.8d. It was observed that the HCl concentration did not affect the extraction of gold, with only a minor decrease in the extraction of only 1-3% with low HCl concentration (0.1 M-0.5 M). This is beneficial for the gold extraction as no changes in pH are required for complete extraction. An observation that is promising, as aqua regia, which is highly acidic, is used to leach gold from WPCBs, ICs and CPUs, as described in section 3.2.3.1, Chapter 3. The results of the study of the effect of variations in time, temperature, Cyphos 101 and HCl concentrations confirm that gold extraction is only slightly affected and high gold extraction efficiencies are achieved under a variety of conditions.

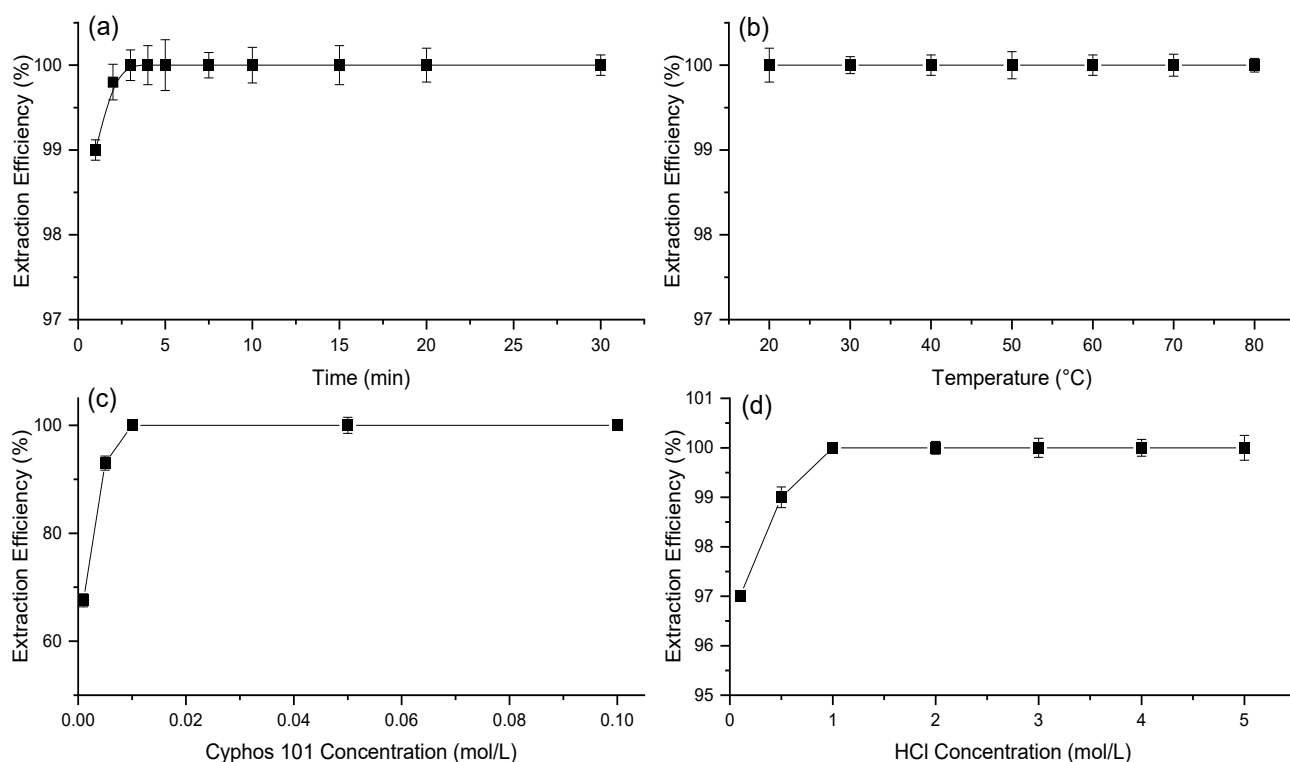
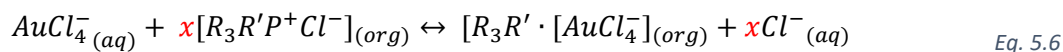


Figure 5.8: Effect of different condition on gold extraction: (a) time, (b) temperature, (c) Cyphos 101 concentration, and (d) hydrochloric acid concentration.

5.3.2.1.3 Extraction mechanism

To determine the mechanism of gold extraction using Cyphos 101 diluted in toluene, further studies were carried out, varying the IL and HCl concentrations. The gold solution used in these studies was 1 g/L in 0.5M HCl, which is approximately 5 mmol/L Au. In an excess of chloride ions, gold is present in the form as tetrachloroaurate ion ($AuCl_4^-$) [209, 213, 217], therefore the extraction mechanism from acidic chloride solution by the ILs in equilibrium can be expressed by the following reaction:



where x represents the number of extractant molecules utilised in the extraction, and $R_3R'P^+$ represents the tetradecyl-(trihexyl)-phosphonium group in Cyphos 101.

The equilibrium constant of the above reaction is given by:

$$K_{eq} = \frac{[R_3R' \cdot [AuCl_4^-]_{(org)}}{[AuCl_4^-]_{(aq)} \cdot x[R_3R'X^+Cl^-]_{(org)}} \quad Eq. 5.7$$

The distribution ratio D of gold in the organic and aqueous phases (Au_{org}/Au_{aq}) during the extraction process can be expressed as:

$$D = \frac{[Au]_{(org)}}{[Au]_{(aq)}} = \frac{[R_3R' \cdot [AuCl_4^-]_{(org)}}{[Au^{3+}]_{(aq)}} \quad Eq. 5.8$$

Replacing Eq. 5.8 in Eq. 5.7, the equilibrium constant can be expressed as:

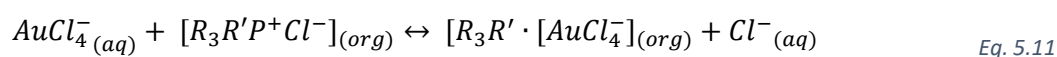
$$K_{eq} = \frac{D}{x[R_3R'P^+Cl^-]_{(org)}} \quad Eq. 5.9$$

Applying the logarithm and rearranging the terms in Eq. 5.9, the logarithm of the distribution ratio can be expressed as:

$$\text{Log}(D) = \log(K_{eq}) + x \log([R_3R'P^+Cl^-]_{(org)}) \quad Eq. 5.10$$

Thus Eq. 5.10 can be used to determine the effect of Cyphos 101 molecules in the gold extraction. Varying the IL concentration, whilst keeping the other factors constant, its contribution in the extraction can be deduced.

Figure 5.8 showed almost 100% gold extraction was achieved irrespective of the changes in time, temperature, Cyphos 101 and HCl concentrations; likely due to an excess of Cyphos 101 being present in the working range used. Figure 5.8c showed that at 0.001 M Cyphos 101, 67% of gold extraction was achieved with an aqueous phase containing 300 ppm Au. Therefore, to study the effect of the IL and to ensure a wider working window, lower concentrations of Cyphos 101 and a higher concentration of gold solution were utilised. Figure 5.9 shows the effect of changes in Cyphos 101 concentration on the gold extraction, which was found to increase with increase in IL concentration (Figure 5.9a), from 20.7% to 93.6% with 0.001 M and 0.005 M Cyphos 101, respectively. The gold solution used was approximately 5 mmol/L, and the gold extraction by the IL showed a linear trend, reaching approximately 100% at 5 mmol/L of Cyphos 101, suggesting a stoichiometric ratio of 1:1. This was confirmed by the $\log[IL]$ versus $\log D$ graph (Figure 5.9b), where the slope of the straight line (0.9817), obtained by linear fit ($R^2=0.9807$), suggests that the ion exchange mechanism engages one molecule of Cyphos 101 per gold chloroanionic ion present in the extractable complex:



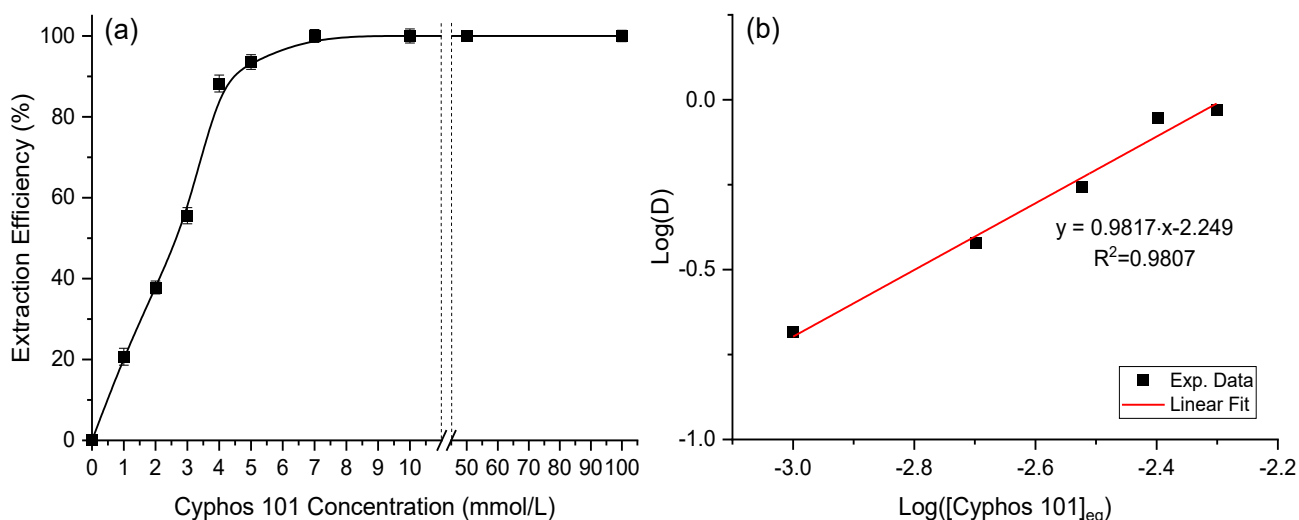


Figure 5.9: Effect of Cyphos 101 concentration on gold extraction vs; (a) extraction efficiency, and (b) $\log(D)$.

To confirm that the HCl concentration does not affect the gold chloroanionic extraction mechanism, further experiments were carried out. Figure 5.8d showed that varying the HCl concentration did not affect the extraction, however, since the IL concentration was in excess, the effect of the HCl concentration on gold extraction could be hidden. Thus, using a lower IL and a higher gold solution concentration, any effects can be observed. Figure 5.10a shows the gold extraction at different HCl concentrations. The effect of the HCl concentrations did not show any major change in the gold extraction, confirming the results from Figure 5.8d. In addition, further experiments were carried out where NaCl was added to evaluate the effect of the chloride ions alone on the gold extraction, as presented in Figure 5.10b. Varying the Cl^- ion concentration from 0 to 1 M Cl^- showed a minor increase in the extraction from 52% to 57%. To further study the relation between Cl^- ion concentration and the extraction, Figure 5.10c shows a plot of $\log[\text{Cl}^-]$ versus $\log D$. The linear fit presented a slope of 0.240, indicating a weak relationship between these two parameters. Therefore, it can be concluded that the concentration of HCl and Cl^- in the aqueous phase do not affect the gold extraction, and only minor increases can be seen with an increase in the concentration of HCl and Cl^- .

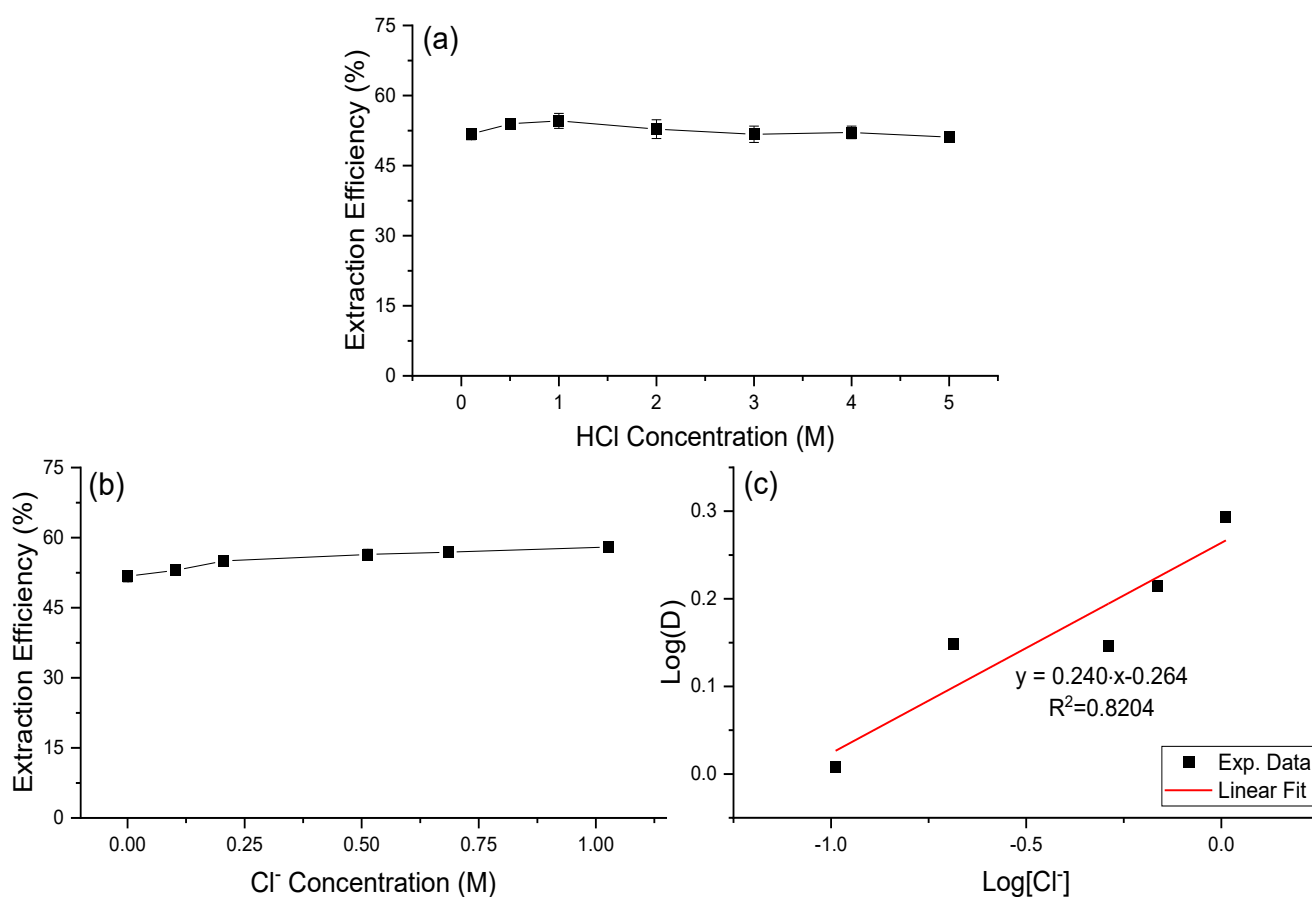


Figure 5.10: Effect of the gold extraction by; (a) HCl concentration, (b) chloride concentration, and (c) $\log [Cl^-]$ vs $\log (D)$.

5.3.2.1.4 Thermodynamics parameters of gold extraction

The results in Figure 5.8b show that gold extraction was completed independent of the temperature, however, the IL concentration was in excess. Consequently, to study the thermodynamics of the gold extraction, 0.003 M Cyphos 101 and a solution of 1000 ppm Au were used. Figure 5.11a shows the effect of the temperature on gold extraction, where an increase in temperature of 60 °C (from 20-80 °C) has only a minor effect (up 2%) on the gold extraction, consistent with the results reported in Figure 5.8b. The low dependence of the gold extraction on the temperature, even in the presence of a deficit of IL to extract all the gold, shows the high affinity of Cyphos 101 for gold ions, which is beneficial for extraction purposes.

The thermodynamics parameters were calculated using the Gibbs free energy from the Gibbs-Helmholtz and Van't Hoff equations [209, 218]:

$$\log(D) = \frac{-\Delta H}{2.303 \cdot RT} + C \quad \text{Eq. 5.12}$$

$$\Delta G = -2.303 \cdot RT \cdot \log(D) \quad \text{Eq. 5.13}$$

$$\Delta G = \Delta H - T\Delta S \quad \text{Eq. 5.14}$$

where ΔS is the change in entropy (J/mol), ΔH is the change in enthalpy (J/mol), ΔS is the entropy change (J/mol·K), T is the absolute temperature (K), R is the universal gas constant (8.314 J/mol·K), and D is the distribution coefficient (Au_{org}/Au_{aq}).

Using the slope and intercept values of Figure 5.11b and equations 5.12-5.14, the calculated values for ΔH , ΔG , and ΔS are 963.3 J/mol·K, -123.7 J/mol, and 3.4 J/mol·K, respectively. The positive values of the enthalpy and entropy, respectively, suggest that the gold extraction is endothermic, and entropy driven in nature. On the other hand, the negative value of the Gibbs free energy indicates that the extraction is a spontaneous process.

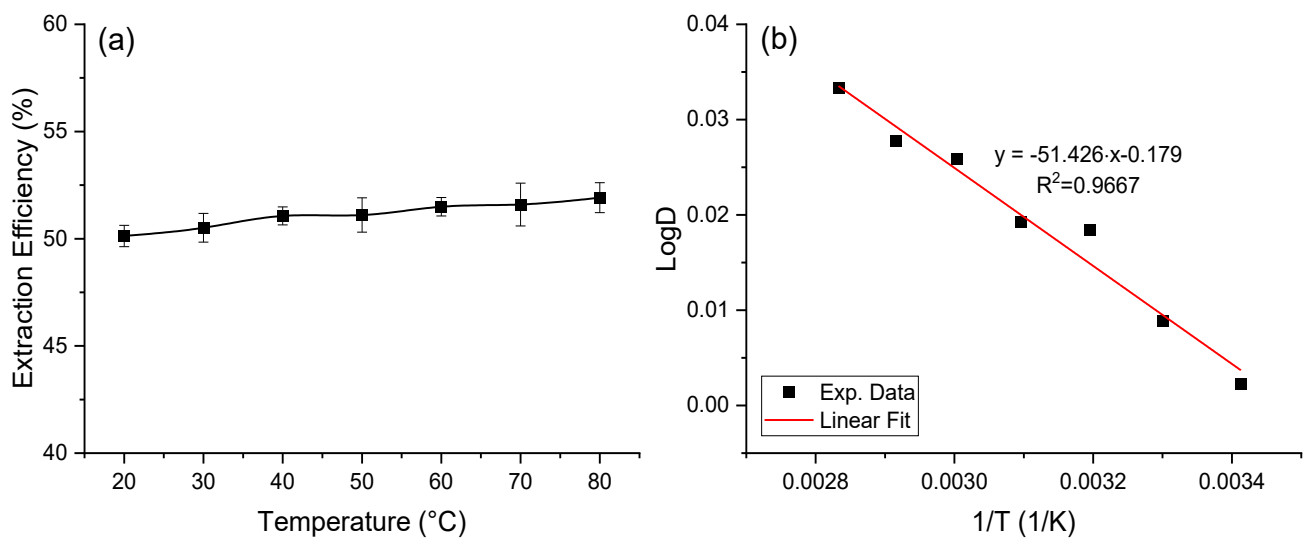


Figure 5.11: Effect of the temperature on gold extraction: (a) extraction efficiency, and (b) $1/T$ vs $\log(D)$.

Based on these gold liquid-liquid extraction studies, the optimal extraction parameters are confirmed as 0.1 M Cyphos 101, room temperature, 150 rpm and 15 minutes. The concentration of Cyphos 101 can be modified depending on the gold concentration of the feedstock; and the HCl and Cl⁻ concentrations do not present a major change in the gold extraction, over a large range, suggesting no extra reagents are needed to pH changes.

5.3.2.1.5 Discussion

The first studies on gold extraction were carried out to evaluate the leaching and extraction efficiencies of three ILs; [Bmim][HSO₄], [Bmim][PF₆], and Cyphos 101. Among these ILs, Cyphos 101 is observed as the most efficient IL for gold extraction, and furthermore the most suitable for gold extraction under acidic (AR) conditions. Masilela et al. reported high gold extraction efficiencies (>92%) using Cyphos 101, [Bmim][PF₂N], and [Bmim][PF₆] from chloride leach solutions (PCB powder in aqua regia). They also found that Cyphos 101 proved to be the most effective extractant for all metals from chloride solution at O:A=1:1, extracting 95% , 97% and 99% for Ag, Au, and Cu, respectively [207]. Although Cyphos 101 has also been reported to be efficient in the extraction of several metals such as cadmium [212], palladium [206], indium and tin [156, 215], among other [112, 206], by tailoring the leaching systems and using different leaching agents, these metals can be successfully separated and extracted. In this work, a first nitric acid leaching was carried out, removing ≥99% of the copper.

Due to the high viscosity of Cyphos 101, different organics were studied as diluent, with toluene being the most suitable. Campos et al. reported that Cyphos 101 diluted in hexane and toluene showed similar gold extraction efficiencies from HCl solutions [213]. In the current research, the five diluents tested showed similar gold extractions, with the difference in extraction being only 3-6% (Figure 5.7). Since none of the diluents showed significant difference in the extraction, toluene was selected because it has the highest boiling point of the organic solvents studied, it is readily available and has a lower price. Dhiman and Gupta studied the extraction of indium in Cyphos 104 with different diluents, reporting toluene as the best diluent [156]. The study of the effect of time showed that the equilibrium is reached within five minutes, extracting ≥97% of gold even after one minute. The fast extraction kinetics of Cyphos 101 observed for gold (in this work) and for other metals (reported elsewhere) has been reported by other authors, reporting that the equilibrium of extraction can be reached within five minutes in all the cases [156, 207, 215]. The fast kinetics is a sign of a high affinity between the Cyphos 101 and gold. In addition, it was found that temperature and hydrochloric acid concentration had a minimal effect on gold extraction. In the same work by Campos et al., it was found that gold extraction efficiency did not significantly change with varying HCl concentration in the range

of 0.1-5.0 M. They calculated the speciation of gold in the concentration range using the MEDUSA software, finding that gold is only present in the form of tetrachloroaurate ion (AuCl_4^-) consistent with reports that in an excess of chloride ions, gold is found as AuCl_4^- [209, 213, 217]. This indicates that, due to an excess of chloride ions, the presence of additional Cl^- , through HCl, does not affect the speciation of gold and consequently, is unlikely to alter the extraction mechanism, maintaining the extraction efficiency. Regarding the extraction mechanism, it was found it involves one molecule of Cyphos 101 per gold chloroanionic ion present in the extractable complex. This 1:1 stoichiometric ratio suggests that the extraction mechanism corresponds to an anion exchange, rather than a complexing reaction. The 1:1 stoichiometric ratio between Cyphos 101 and Au(III) in gold extraction has also been reported, confirming the mechanism is likely to be an anion exchange [213].

5.3.2.2 Sorption Extraction

5.3.2.2.1 Gold sorption from hydrochloric solutions using solvent impregnated resins (SIRs):

Solvent impregnated resins (SIRs) are ideal for separation and recovery of metals from dilute solutions. In SIRs, a liquid complexing agent is dispersed homogeneously in a solid polymeric medium (the resin). SIRs have excellent advantages in recovering metals from dilute solutions since they combine the benefits of solvent extraction and ion exchange [208]. In addition, ion exchange reactions are reversible, which offers the potential for reuse of the SIRs, favouring the environmental and economic perspectives of the process [203, 208]. In this study, based on previous studies carried out in this research and reports in the literature, Amberlite™ XAD-7 was selected as the support resin and Cyphos 101 as the complexing agent. The impregnation of Cyphos 101 on Amberlite XAD-7 was described in Section 5.2.3.2.1.

To verify the incorporation and distribution of the IL in the resin, SEM-EDS analysis was used to examine the cross-section of raw and impregnated resins (Figure 5.12). The cross-section of the individual resin was obtained by freezing the resins in liquid nitrogen for 1 minute, before cutting the resin with a knife. The cartography of elements for raw Amberlite™ XAD-7 (Figure 5.12a and c) showed C and O elements, which are characteristic elements of polymers. In the Amberlite XAD-7 impregnated with Cyphos 101 at 300 mg IL/g resin (Figure 5.12b and d), C, O, P and Cl elements are also detected, where C and O are characteristic of the Amberlite™ XAD-7 resin, and P and Cl elements are tracers of Cyphos 101 (red dots represent P and green dots represent Cl), confirming good IL impregnation. No gradient of P and Cl was observed between the inner and outer zones (Figure 5.12b) and a homogeneous cartography of P and Cl was also observed, suggesting a homogeneous distribution of Cyphos 101 in the resin.

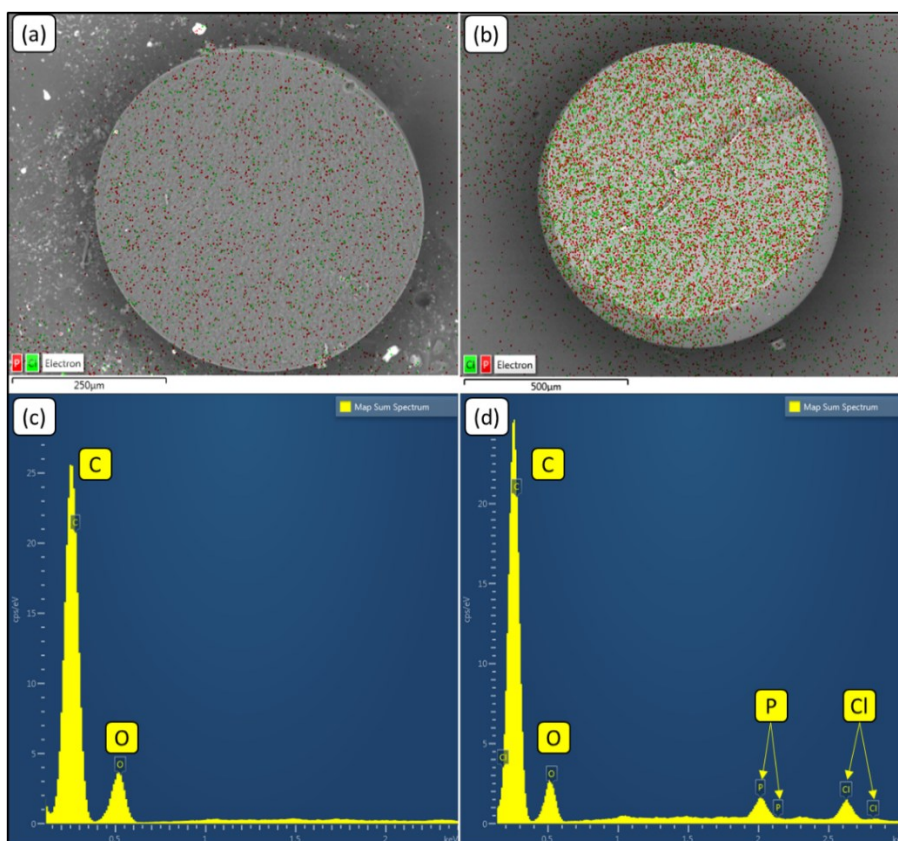


Figure 5.12: SEM–EDS analysis (element cartography) of raw Amberlite™ XAD-7 resin (a) and (c), and Cyphos 101 impregnated resin (b) and (d). Red and green dots denote P and Cl, respectively.

The effect of IL loadings (from zero (0) denoting non-impregnated), to 100, 300, and 500 mg IL/g resin) and the concentration of HCl (0.1-5.0 M) on gold sorption efficiency is presented in Figure 5.13. In general, the HCl did not have a significant effect on the adsorption of gold in the range of 0.1-5.0 M. The sorption efficiencies reached nearly 94%, 97%, and 99% for resins with IL loadings of 100 mg/g, 300 mg/g, and 500 mg/g respectively. In the case of raw resin (Amberlite™ XAD-7), the sorption efficiency reached 77%, with a reduction of 5% at low HCl concentrations (0.1-0.5 M). The SIR 100 mg IL/g also showed a slight decrease of only 2% in sorption efficiency at low HCl concentration.

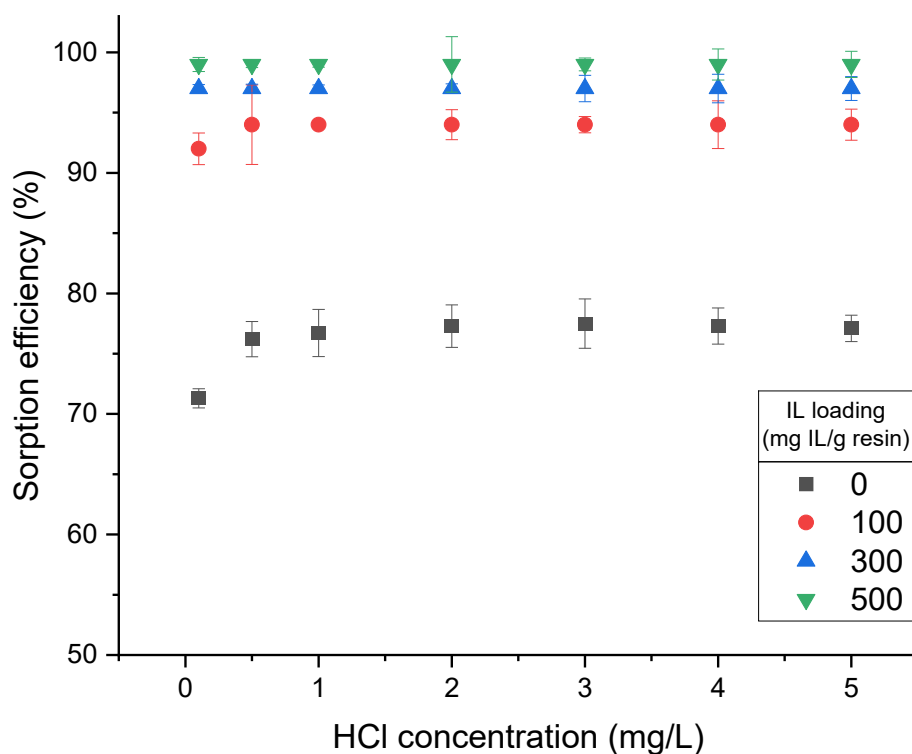


Figure 5.13: Influence of HCl concentration and IL loading on Au(III) sorption efficiency using Amberlite™ XAD-7 (SD: 3 g/L, 150 rpm, 20 °C, 24 h, $C_0 = 300$ mg Au/L)

The influence of the IL content on the sorption isotherms was studied in 1M HCl solutions at different gold concentrations (5-300 ppm), and the results are shown in Figure 5.14. The profile of the isotherms shows a steep initial slope, reaching a saturation plateau. Raw Amberlite™ XAD-7 showed a maximum gold sorption of 20.2 mg Au/g, whilst impregnated Amberlite™ XAD-7 showed a clear trend: the higher the IL, the greater the saturation. The maximum gold sorption for 100 mg IL/g, 300 mg IL/g and 500 mg IL/g were 40.4 mg Au/g, 136.2 mg Au/g and 175.2 mg Au/g, respectively. These increases in the gold loading capacity represent a rise of 2, 6.7, and 8.7 times the loading capacity of the raw resin, for the 100 mg IL/g, 300 mg IL/g and 500 mg IL/g, respectively. The initial steep slope in the impregnated resins indicates a higher affinity of the SIRs for gold compared to the raw resins (with a lower initial slope) [209]. The steepness of the gradient confirms the sorbents to be very efficient for gold recovery even at low concentrations from acidic solutions, which is beneficial for the gold extraction process.

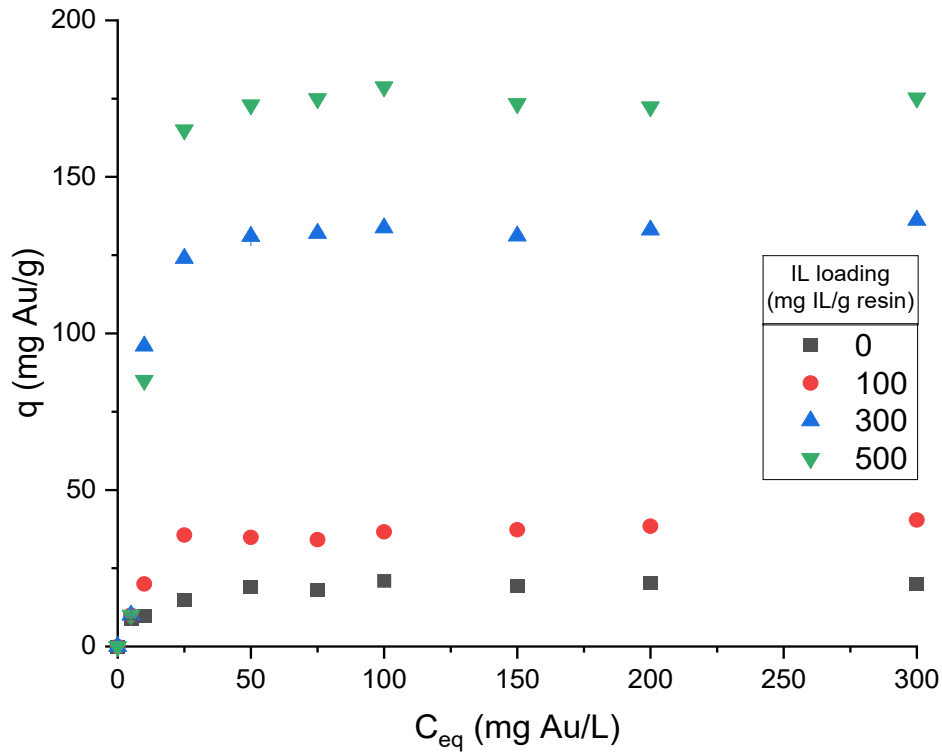


Figure 5.14: Influence of IL loading on Au(III) sorption isotherms using Amberlite XAD-7 (SD: 2 g/L, 150 rpm, 20 °C, 24 h).

5.3.2.2.2 Models of Gold Sorption

The experimental data for gold sorption were fitted to two well-known sorption isotherm models, Langmuir model and Freundlich model, by a linear regression method. The Freundlich isotherm model and its linear form can be mathematically expressed by [219]:

$$q_e = K_f \cdot C_e^{1/n} \quad \text{Eq. 5.15}$$

$$\log(q_e) = \log(K_f) + \frac{1}{n} \log(C_e) \quad \text{Eq. 5.16}$$

where K_f is the Freundlich equilibrium adsorption capacity and n is the Freundlich equation constant representing the deviation from linearity of adsorption.

The Langmuir isotherm model and its linear form are represented by [219]:

$$\frac{C_e}{q_e} = \frac{C_e}{q_m} + \frac{1}{K_l \cdot q_m} \quad \text{Eq. 5.17}$$

$$\frac{1}{q_e} = \left(\frac{1}{q_m}\right) + \left(\frac{1}{K_l \cdot q_m}\right)\left(\frac{1}{C_e}\right) \quad \text{Eq. 5.18}$$

where K_l represents the energy constant relevant to the heat adsorption (L/mg) and q_m represents the maximum adsorption capacity (mg/g).

The separation factor (R_l) is a dimensionless constant which is a useful characteristic of the Langmuir model, and it is given by the following equation [218]:

$$R_l = \frac{1}{(1 + bC_0)} \quad \text{Eq. 5.19}$$

where b is the Langmuir biosorption constant (L/mg), which is related to the free energy of biosorption and C_0 is the initial concentration. R_l indicates whether the isotherm is either unfavourable ($R_l > 1$), linear ($R_l = 1$), favourable ($0 < R_l < 1$), or irreversible ($R_l = 0$).

The calculated Langmuir and Freundlich isotherms parameters are listed Table 5.6. Figure 5.15 shows the experimental data fitted with both Langmuir and Freundlich isotherm models at different gold concentrations. The regression correlation coefficients (R^2) of the Freundlich model (0.454-0.852) (Table 5.6) is lower than the values obtained by the Langmuir model (0.901-0.957), suggesting that the Langmuir model is a better fit to the experimental data (linear fit graphics of the models are shown in Figure A.5 and Figure A.6 in Appendix). This is confirmed in Figure 5.15. The maximum adsorption capacities calculated by the Langmuir model (q_m) are close to the experimental data, which provides a better prediction of the gold adsorption. Due to the better fit of the Langmuir model, it can be assumed that there is a monomolecular layer of AuCl_4^- on the surface of the resins with no stacking of adsorbed molecules. Furthermore, the separation factor (R_l) values between 0 and 1 indicate that the adsorption process is favourable. From the Freundlich model it can be observed that the Freundlich equation constant (n) is lower with the increase in the amount of IL impregnated, which translates to a higher $(1/n)$ values at higher IL impregnations. In this model, the higher the $1/n$, the more favourable is the adsorption. Thus, both models suggest that the adsorption process is favourable.

Table 5.6: Freundlich and Langmuir parameters for Au adsorption at different initial gold concentrations.

IL loading (mg IL/g resin)	Freundlich			Langmuir			
	K_f	n	R^2	q_m (mg/g)	K_m (L/mg)	R_L	R^2
0	6.58	4.46	0.852	20.41	0.13	0.013	0.923
100	9.44	3.49	0.712	45.45	0.06	0.014	0.955
300	15.89	2.24	0.454	138.89	0.23	0.139	0.957
500	14.06	1.89	0.534	185.15	0.08	0.075	0.901

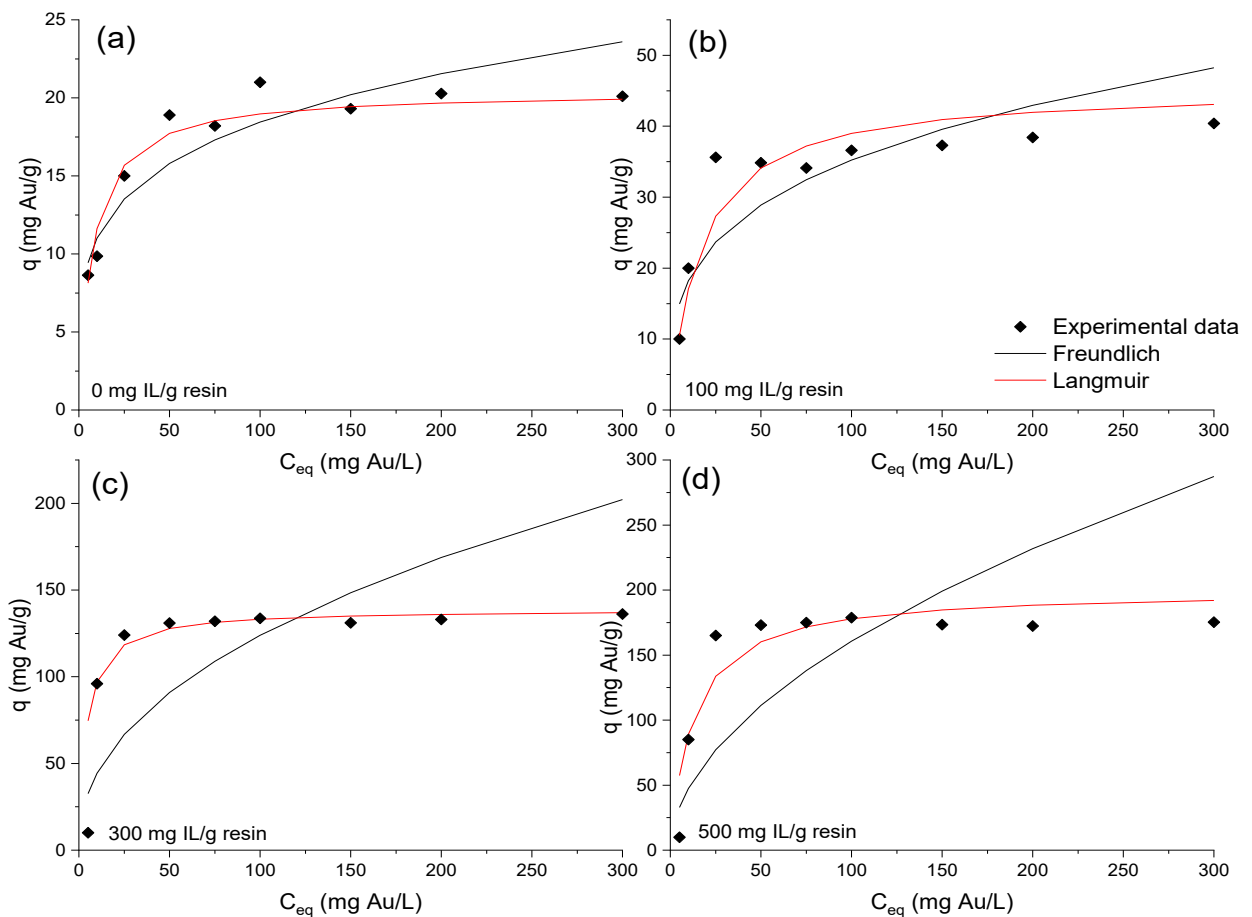


Figure 5.15: Experimental adsorption isotherms fitted with Freundlich and Langmuir isotherms at different gold concentrations.

5.3.2.2.3 Kinetics of Gold Sorption

The influence of time on the sorption of gold with the different Cyphos 101 loadings is presented in Figure 5.16. An increase in sorbent dosage increases the sorption, as previously discussed, and decreases the time required for reaching the equilibrium. In all the cases, the equilibrium was reached within 3 h, with 1 h being sufficient for equilibrium to be attained for the 300 mg IL/g and 500 mg IL/L impregnated resins.

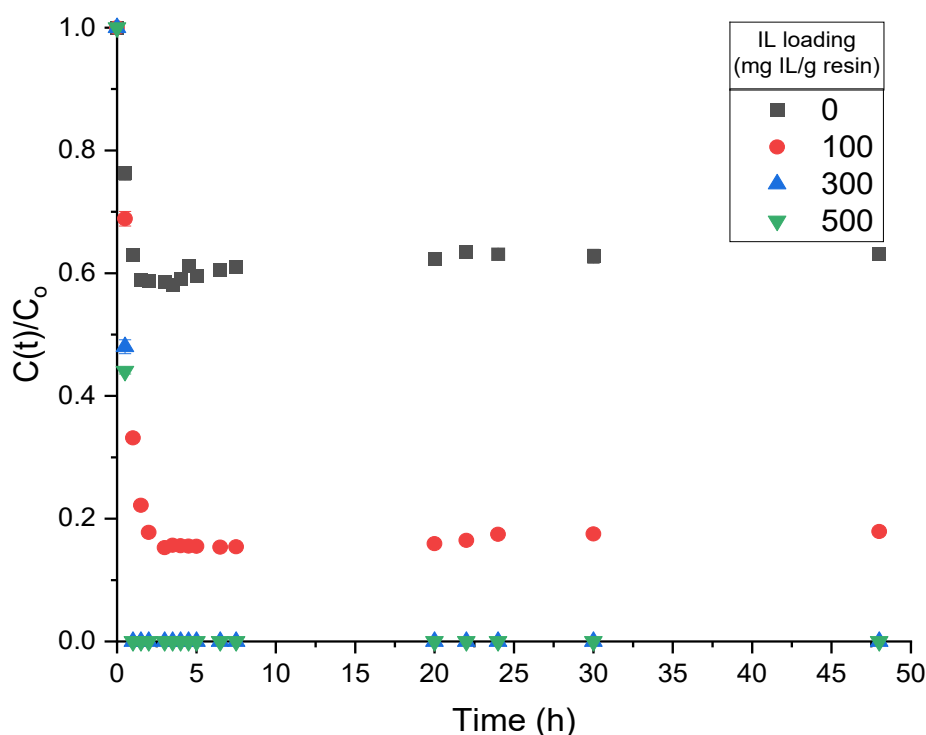


Figure 5.16: Influence of IL loading on Au(III) sorption kinetics.

The sorption kinetics can be controlled by various mechanisms including a diffusion mechanism (bulk diffusion, film diffusion, intraparticle diffusion, and sorption and desorption within the particle and solid's surface) and chemical reaction [205, 209, 213]. Identification of the controlling step is important to allow the selection of optimal experimental conditions and optimise the use and design of sorbent [209]. To determine the limiting step of the sorption, four models were studied; the Lagergren equation (pseudo first order equation), the pseudo second order equation described by Ho and the intraparticle diffusion models defined by Weber–Morris and Boyd et al. model. Two diffusion models were selected due to reports in the literature that diffusion is often the limiting step in similar systems [205, 206, 209]. In general, within the diffusion mechanism, the intraparticle diffusion and the film diffusion are generally the rate-limiting steps of the process of sorption [218].

The non-linear and linear form of the pseudo-first-order equation [219]:

$$q(t) = q_e(1 - e^{-k_1 t}) \quad \text{Eq. 5.20}$$

$$\log(q_e - q(t)) = \log(q_e) - \frac{k_1}{2.303} t \quad \text{Eq. 5.21}$$

The non-linear and linear form of the pseudo second order equation [219]:

$$q(t) = \frac{k_2 q_e^2 t}{1 + q_e k_2 t} \quad \text{Eq. 5.22}$$

$$\frac{t}{q(t)} = \frac{1}{k_2 q_e^2} + \frac{t}{q_e} \quad \text{Eq. 5.23}$$

The Weber–Morris intraparticle diffusion equation [218]:

$$q(t) = k_3 t^{1/2} + C \quad \text{Eq. 5.24}$$

The Boyd particle diffusion equation [218]:

$$B(t) = -0.4977 - \log \left(1 - \frac{q(t)}{q_e} \right) \quad \text{Eq. 5.25}$$

where $q(t)$ is the amount of adsorbate on the surface of the adsorbent at the time t (mg/g), k_1 is the equilibrium constant of the pseudo-first order sorption (min^{-1}), k_2 is the pseudo-second order rate constant (g/mg/h), k_3 is the intraparticle diffusion rate constant (g/mg/h) and C is the slope which represents the thickness of the boundary layer.

The rate constants, q_e , regression coefficient (R^2), and model parameters obtained by fitting the data are presented in Table 5.7. The model fittings are illustrated in Figure 5.17. Linear fit graphics of the models are shown in Figure A.7 and Figure A.8 in Appendix B. Among the models applied and comparing the R^2 values obtained, there is a clear indication that the gold adsorption process likely follows a pseudo-second order kinetics ($R^2 > 0.995$), as observed in Figure 5.17b. In addition, the calculated $q_{e, \text{model}}$ are also consistent with the experimental $q_{e, \text{experimental}}$, validating the pseudo-second order mechanism. The calculated pseudo-second-order rate constant K_2 decreased with the increase in Cyphos 101 impregnated in the resin, which is likely due to lower competition for the adsorption of active sites at higher Cyphos 101 concentration, thus decreasing the absorption rate. This pseudo-second order kinetic model also suggest that the adsorption may be dominantly controlled by

chemical processes. In the Weber-Morris model (Figure 5.17c), when the plot of $q(t)$ versus $t^{1/2}$ passes through the origin, the intraparticle diffusion mechanism is considered as the rate-limiting step. On the other hand, in the Boyd model (Figure 5.17d), when the linear plot of $B(t)$ versus t passes through the origin, the particle diffusion is the rate-limiting step. If none of these models go through the origin, the film diffusion is suggested to be the rate-limiting step of the process [218]. The intraparticle diffusion model is commonly divided into three phases: (1) external surface adsorption, (2) intraparticle diffusion phase and (3) equilibrium phase where low adsorbate concentration in solution results in the slowing down of the intraparticle diffusion [220]. As observed in Figure 5.17c, the curve determined by the Weber-Morris model presents two linear regions for all the resins. This phenomenon indicates that the external diffusion occurred quickly, and the first step was not observed in the data, thus the first linear region represents the intramolecular diffusion stage, whilst the second linear region represents the equilibrium stage. The rate constant of the region 1 ($k_{3, \text{region1}}$) is larger than the rate constant of the region 2 ($k_{3, \text{region2}}$), indicating that the diffusion of the adsorbate through the macro pores is faster than the diffusion of the adsorbate in the equilibrium phase.

As shown in Table 5.7, none of the regions had C values equal to zero, indicating that these linear regressions do not pass through the origin. This suggests that the intraparticle diffusion is not the rate-limiting step of the process. Similarly, none of the Boyd plots passed through the origin (Table 5.7), suggesting that the particle diffusion is not the rate-limiting step. These results indicate that the film diffusion could be considered the rate limiting step, but trials carried out at varying agitation speeds (100-400 rpm) showed no observed major change in the sorption kinetics. This suggests that the film diffusion is unlikely to be the limiting mechanism. It appears, therefore, that the kinetics of gold adsorption in Amberlite™ XAD-7 is likely governed by chemical process. This conclusion is in good agreement with that in ion-exchange resins [219].

Table 5.7: Parameters of the kinetics models for Au(III) sorption on Amberlite™ XAD-7/Cyphos 101 resins.

Amberlite™ XAD-7/Cyphos 101				
	0 mg/g	100 mg/g	300 mg/g	500 mg/g
$q_{e,experimental}$	20.2	40.4	136.2	175.2
Pseudo first order model				
$q_{e,model}$	2.951	4.612	20.101	26.782
K_1	0.093	0.085	0.098	0.096
R^2	0.712	0.639	0.742	0.739
Pseudo second order model				
$q_{e,model}$	21.013	41.924	136.212	175.212
K_2	0.177	0.122	0.025	0.019
R^2	0.999	0.999	0.998	0.997
Weber–Morris model				
$K_{3,region\ 1}$	12.028	33.712	154.971	200.572
R^2	0.779	0.827	0.862	0.745
C	4.115	-5.877	-72.365	-91.959
$K_{3,region\ 2}$	0.476	0.242	0.394	0.444
R^2	0.776	0.674	0.179	0.367
C	20.308	39.442	132.97	172.301
$t_{1/2}$	30	45	45	45
Boyd model				
Slope	0.006	0.051	0.101	0.119
Intercept	1.662	1.683	2.193	2.602
R^2	0.054	0.302	0.444	0.404

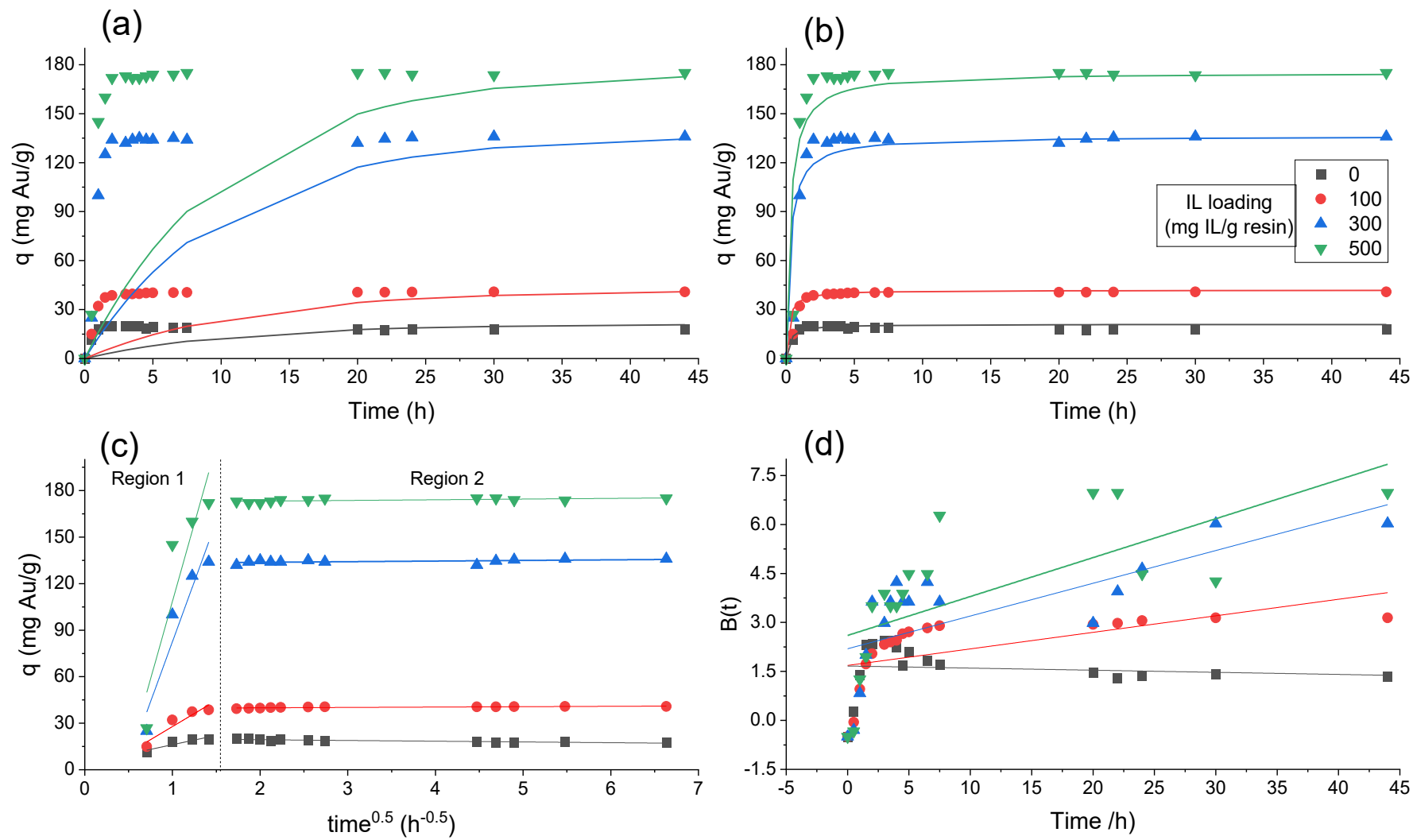


Figure 5.17: Sorption models for Au(III) onto Amberlite™ XAD-7/Cyphos 101 resins; (a) Pseudo-first order model, (b) Pseudo-second order model, (c) Weber–Morris model, and (d) Boyd model.

5.3.2.2.4 Effect of Temperature and Thermodynamic Parameters on Gold Sorption

The effect of the temperature on the sorption efficiency of gold is presented in Figure 5.18; the sorption increases with increase in temperature in all the cases. Loaded resins with 500 mg IL/g show the highest efficiencies rising from 20% at 20 °C to 37% at 80 °C. It is noted that raw Amberlite™ XAD-7 resin, and resins with loadings of 100 mg IL/g and 300 mg IL/g, show slight increases in sorption with temperature. The raw Amberlite™ XAD-7 resin shows a sorption increase of only 3% when the temperature increases from 20 °C to 80 °C, whilst in the case of the 100 mg IL/g and 300 mg IL/g resins, a rise of approximately 4% was observed in both cases. The marked increase in the gold sorption by the 500 mg IL/g resin with temperature could be due to more rapid movement gold ions, greater number of collision and increased chances of ion exchange with the IL. Furthermore, the rise of the temperature could also slightly expand the pores of the resin, facilitating the movement of the ions through it.

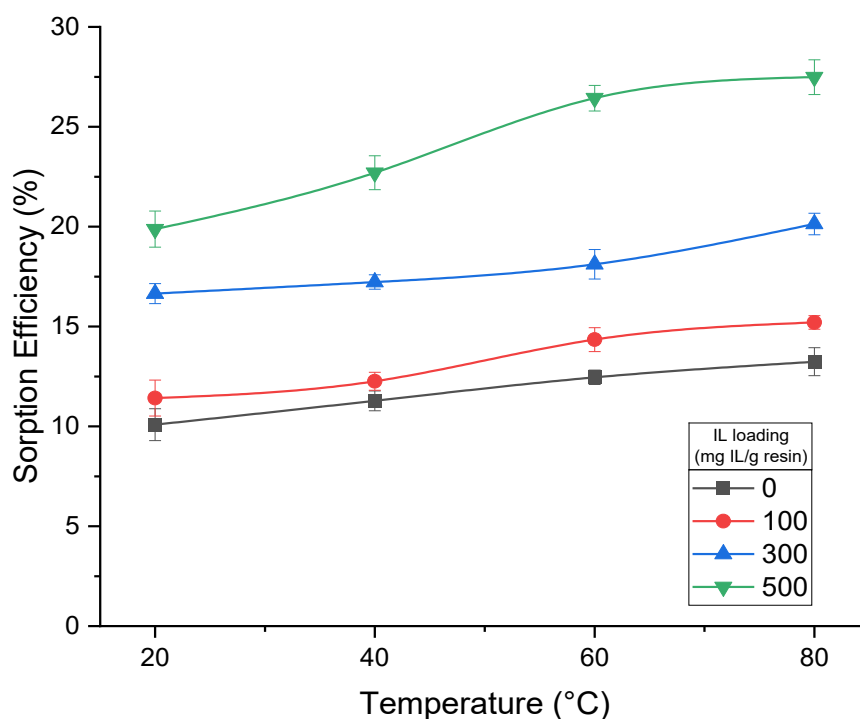


Figure 5.18: Effect of the temperature on the sorption efficiencies.

The thermodynamics parameters were calculated using Eqs 5.12-5.14, presented in section 5.3.2.1.4. Figure 5.19 shows the effect of the temperature over the logarithm of the distribution coefficient (linear plot of Eq. 5.14) with linear fits of the experimental data. The linear fits have relatively high R^2 values (>0.92 in all the cases), indicating a good linear regression. Using the slope and intercept values of Figure 5.19 and Eqs 5.12-5.14, the calculated values for ΔH , ΔS and ΔG were obtained, and presented in Table 5.8. In all cases, the enthalpy was positive consistent with the

endothermic nature of the sorption process as indicated by the increase of sorption capacity with temperature (Figure 5.18). The positive values obtained in the entropy indicate that the sorption of gold is correlated with an increase of randomness of adsorbate at the solid/liquid interface, which can occur due to desorption of water molecules from adsorbent surface [218]. The negative values of the Gibbs free energy indicate that the gold extraction is a spontaneous process.

Table 5.8: Thermodynamics parameters of gold extraction by SIRs.

	0 mg/g	100 mg/g	300 mg/g	500 mg/g
ΔH (KJ/mol·K)	4.38	3.56	2.76	7.91
ΔG (KJ/mol)	-5.41	-5.14	-4.69	-2.93
ΔS (J/ mol·K)	30.41	27.05	23.17	33.75

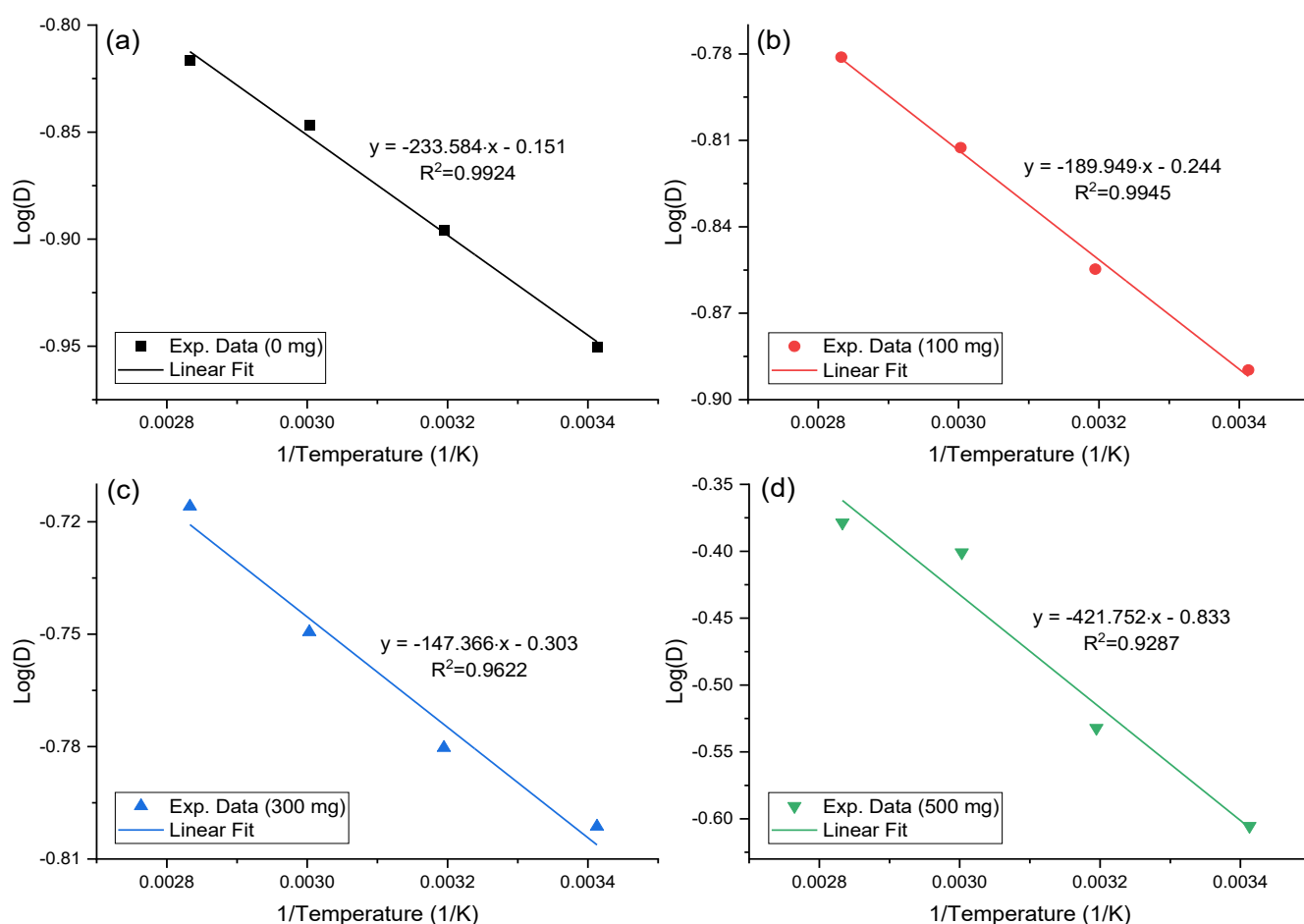


Figure 5.19: Effect of the temperature on the equilibrium thermodynamics for different Cyphos 101 loadings; (a) raw Amberlite™ XAD-7, (b) 100 mg IL/g resin, (c) 300 mg IL/g resin, (d) 500 mg IL/g resin.

5.3.2.2.5 Discussion

It was found that the concentration of HCl did not have a significant effect on the gold sorption within the range of 0.1-5.0 M HCl. A decrease of only 2-5% on gold sorption efficiencies at low HCl concentrations (0.1-0.5 M) for the raw Amberlite™ XAD-7 and 100 mg IL/g resins was observed. These results are consistent with those reported by Lira et al. [205], where the concentration of HCl was observed not to affect the Au(III) sorption using Amberlite™ XAD-7/Cyphos 101 resins, and raw Amberlite™ XAD-7 showed a decrease in sorption efficiencies at low HCl concentrations. Similar limited effect of the HCl concentrations has been observed in the sorption of metals such as Cd (II), Pd(II), and Pt(IV) using similar resins [212, 213]. This result indicates that gold sorption can be achieved efficiently over a wide range of hydrochloric acid concentration, with no requirements for additional reagents to control pH. This is of particular benefit given the pre-treatment step used for e-waste which involves leaching using highly acidic AR, so the gold liquor after leaching could be directly used without the need for dilution or additional reagents.

Sorption isotherms showed that raw Amberlite™ XAD-7 has a maximum Au (III) sorption of 20.2 mg Au/g. The sorption mechanism of Au(III) on the acrylic ester resins such as Amberlite™ XAD-7 has been well documented [205, 206, 209, 213, 221]. The mechanism under very acidic conditions is due to the resins being chemically modified by partial hydrolysis of the acrylic ester group ($\text{O}=\cdots\text{H}^+\text{Cl}^-$), and Au(III) is extracted as an anionic chloro-complex ($\text{O}=\cdots\text{H}^+\text{AuCl}_4^-$). Hydrophobic interactions of the resin matrix with tetrachloroauric acid have also been proposed to explain the high sorption of Au(III) in mild acid conditions [206, 209]. Navarro et al. described the Au sorption on Amberlite™ XAD-7 by a two-step process; the extraction of HCl by the resin through the interaction with the oxygen of the polyacrylic matrix, followed by metal binding through the ion exchange between chloride anion and metal chloro-anion [209]. Laatikainen and Paatero reported that Au(III) sorption on Amberlite™ XAD-7 can also involve hydrophobic interactions between AuCl_4^- and the resin by analogy with FeCl_4^- sorption on Amberlite™ XAD-7 since both metals have a similar tetrahedral structure for their chloro-complex and do not contain water ligands [221]. The impregnation of Cyphos 101 substantially improves the sorption loading, as observed in Figure 5.13 and Figure 5.14. The maximum gold sorption for 100 mg IL/g, 300 mg IL/g and 500 mg IL/g were 40.4 mg Au/g, 136.2 mg Au/g and 175.2 mg Au/g, respectively. In the liquid-liquid extraction it was found that gold is extracted by an anion exchange mechanism between gold chloroanionic species and chloride anions bound to the IL. Campos et al. studied the liquid-liquid extraction of Au(III) in HCl solutions with Cyphos 101 in toluene and hexane solvents. They reported that gold extraction increased with the IL concentration, also finding a 1:1 stoichiometric ratio between Au(III) and the IL [213]. This mechanism of gold extraction has been reported elsewhere [205, 206, 209], confirming that the increase in the sorption efficiency and

capacity of the impregnated resins is due to a combination of extraction processes, including sorption on the polymer matrix (anionic chloro-complex and hydrophobic interactions) and ionic extraction IL (anion exchange by Cyphos 101). It is noteworthy that the 100 mg IL/g resin did not show a sorption increase as pronounced as the 300 mg IL/g and 500 mg IL/g did. Navarro et al. observed that at low Cyphos 101 loading (57 mg/g), the sorption efficiency of Au(III) in HCl solutions were similar to the obtained with raw resin. They suggested that is likely that part of the IL interacts with the resin, decreasing its ability to gold binding [209]. Thus, a degree of interaction between the IL and the resin could have decreased the Au(III) efficiency and capacity of the 100 mg IL/g resins. The experimental data of the isotherms were fitted with two well-known models: the Freundlich model and the Langmuir model. The Langmuir model fitted better the experimental data, suggesting that there was a monomolecular layer of gold (AuCl_4^-) on the surface of the resins with no stacking of adsorbed molecules. This may be the result of Cyphos 101 impregnation on the internal porous surface of Amberlite XAD-7 resins. As gold ions interact with Cyphos 101 in a 1:1 stoichiometric ratio, the anion exchange occurs on the surface of the resin, where Cyphos 101 is impregnated, forming a monomolecular layer of gold. This process reduces the stacking of more adsorbed gold ions on the already occupied space.

The study of sorption kinetics showed that the equilibrium was reached within 2-3 h for raw Amberlite™ XAD-7 and impregnated resins, regardless of the Cyphos 101 loadings impregnated. This result disagrees with the sorption kinetics in similar systems. Navarro et al. reported that Au(III) sorption in Amberlite™ XAD-7/Cyphos 101 resins can be reached within 8 h of contact time for 95% of total sorption, and up to 24 h for complete sorption, also regardless of the IL loadings [209]. Lira studied the effect of different Amberlite™ resins (XAD-2, XAD-4, XAD-7, XAD-8, XAD-16, XAD-1180, XAD-2000, and XAD-2010) impregnated with Cyphos 101 (200 mg IL/g resin) on the Au(III) sorption from HCl solutions. They found that Amberlite™ resins can reach equilibrium within the first 10–12 h of contact time, with some requiring as much as a week. Based on those results, they classified the resins in three groups: (a) the fastest and the most efficient (XAD-1180, XAD-8, XAD-7 and XAD-2), (b) XAD-2010, and (c) the slowest (XAD-4, XAD-2000 and XAD-16) [205]. Thus, although Amberlite™ XAD-7 was found to be fast and efficient for gold sorption, it reached equilibrium in approximately 10 h and only in the XAD-2 resins, the equilibrium was reached within 6 h. In another study, Au(III) sorption from HCl solutions using Cyphos 101 impregnated in biopolymer capsules (alginate and gelatin) the equilibrium was reached within 24 h of contact for the smallest particles, whilst 48 h was required to achieve the equilibrium for the largest particles [213]. For the extraction of Pd(II) with Amberlite™ XAD-7/Cyphos 101 resins, it was reported that lower IL loadings can reduce considerably the contact time to reach sorption equilibrium, from approximately 24 h at 401 mg IL/g resins to less than 3 h at

106 mg IL/g resins [206]. It is noted that the kinetics of the 300 mg IL/g and 500 mg IL/g resins were not faster than the raw Amberlite™ XAD-7 and 100 mg IL/g, due to a deficit of gold in the solution. The raw Amberlite™ XAD-7 adsorbed approximately 60% of the gold from the solution, whilst the 100 mg IL/g resins adsorbed nearly 85%, consequently, with higher Cyphos 101 loadings, gold could have been adsorbed before reaching equilibrium due to a deficit of gold in the solution. Thus, although those resins extracted all the gold in nearly 1 h, the expected time for equilibrium to be reached similar the raw and 100 mg IL/g resins, is approximately 3 h. In this work, the distribution of Cyphos 101 in the Amberlite™ XAD-7 resin shown in the SEM-EDS image, was found to be distributed homogeneously (Figure 5.12), which is beneficial for an efficient sorption, and can reduce the equilibrium time required. Another factor that can increase the kinetics is the type and rate of agitation. Although this effect was not studied in detail, preliminary tests on gold sorption, without shaking, showed the process to be slower, by at least 2 times. Due to the high gold sorption efficiencies of the SIRs system, however, once the threshold of a minimum agitation is exceeded, it will not have such a marked effect. Experiments carried out at agitation speeds of 100 to 400 rpm, showed no major change in the sorption kinetics, consistent with the findings reported for the recovery of Pd(II) from HCl solutions with Amberlite™ XAD-7 impregnated with Cyphos IL-101, where increasing the agitation speed hardly affects Pd(II) sorption kinetics [206].

To determine the limiting step of the gold sorption, four models were used to describe the kinetic of experimental data, where the pseudo second order model was considered as the best-fit model in describing the gold sorption from HCl solutions. Thus, the sorption kinetics of Au(III) in impregnated Amberlite™ XAD-7 was concluded to be governed by chemical process. It has been reported that, in most cases, binding in sorbents is controlled by diffusion mechanisms, generally by intraparticle diffusion, rather than chemical processes [205, 209, 212]. Nevertheless, other sorption kinetics have been shown the process to be controlled by a reaction mechanism in relation with the parallel ionic reactions [212]. In a similar study, the sorption kinetics of Au(III) in immobilised Cyphos 101 in biopolymer capsules found that physical (resistance to mass transfer) and chemical reaction rate processes can govern the kinetics depending on the working conditions. They reported that the intraparticle diffusion governed the kinetics at high metal concentration and for poorly favourable conditions (i.e., low sorbent dosage), whereas at low metal concentration (or excess of sorbent) the kinetics were governed by the reaction rate [213]. In this study, as it was previously mentioned, gold sorption was complete with resin loadings of 300 mg IL/g and 500 mg IL/g due to a deficit of gold in the solution, i.e., an excess of sorbent, which could explain the kinetics governed by chemical reaction. Furthermore, experiments varying the agitation speed (100-400 rpm) showed no significant changes in the sorption, confirming that the intraparticle diffusion was not the controlling step. Kinetic sorption

controlled by chemical processes is known particularly to be involved in ion exchange resins [219], supporting the findings of this work.

5.3.2.3 Elution and Desorption of Gold including Recycle of ILs and Reuse of Resins

Recovery of the target material, gold, following the two hydrometallurgical steps requires the use of an elution step to follow liquid-liquid extraction, and a desorption step to follow sorption extraction. The results of both these processes are discussed; and consideration is also given to the potential for recycle of the IL and for reuse of the resins through subsequent cycles for gold recovery without loss of efficiency and effectiveness, and to ensure any process developed is sustainable in environmental and economic terms.

5.3.2.3.1 Gold Elution in Liquid-Liquid extraction and The Potential for Recycling of the IL

Investigation of the effects of hydrochloric acid concentration, thiourea concentration and contact time on the elution of gold in the Liquid-Liquid extraction was carried and the results are presented in Figure 5.20. It can be seen from that neither HCl nor thiourea concentration has a noticeable effect on the gold elution, stripping practically the same amount of gold across the range tested. In the case of the HCl concentration (Figure 5.20a), it was found that the elution reached 91% at 0.1M HCl and 94% at 3M HCl. Varying the concentration of thiourea (Figure 5.20b) did not affect the gold elution, with almost complete elution (97-100%) in the studied range (0.1-3.0 M). The effect of time in the elution (Figure 5.20c) showed a relatively fast reaction, eluting 41% in the first minute and reaching the equilibrium within one hour (with 97% of gold eluted). Thus, to minimise the use of reagents and to ensure a complete gold desorption, 0.5 M thiourea in 0.5 M HCl for 1 h were selected as the elution parameters.

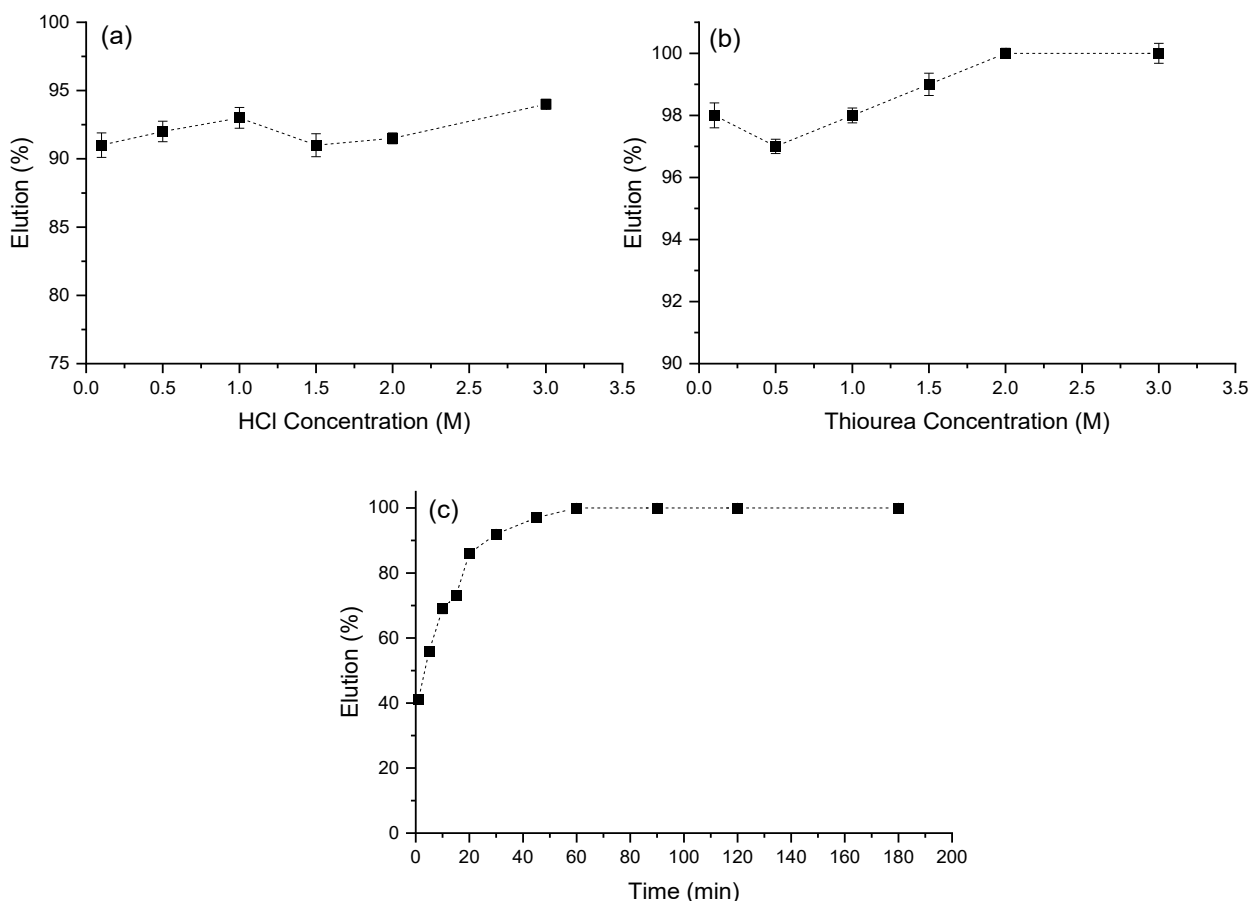


Figure 5.20: Gold elution from 0.1 M Cyphos 101 in toluene; (a) Effect of the HCl concentration (1M thiourea), (b) effect of the thiourea concentration (1M HCl), and (c) Effect of the contact time.

An important aspect of the process development in terms of sustainability in the metal recovery process is the ability to mitigate costs of reagents through the recycle of the IL. The recyclability of Cyphos 101 was therefore tested through five cycles of the whole process. Figure 5.21 shows the effects of recycle through the liquid-liquid extraction, elution steps over five cycles of gold recovery under the optimised conditions (0.1 M Cyphos 101 in toluene for extraction and 0.5 M thiourea in 0.5 M HCl for elution, both process at 20°C and 150 rpm), with excellent results confirming that the extraction and stripping of gold remains largely unaffected over five cycles, suggesting that Cyphos 101 can be successfully reused without any loss in efficiency. In addition, the overall efficiency of gold recovery remains $\geq 98\%$ in each cycle.

To check that the IL (organic phase, 0.1 M Cyphos 101 in toluene) was not affected physically or chemically through the recycle process, FTIR was used to record any changes in the structure of the organic extractant over the five cycles, as shown in Figure 5.22. The FTIRs after extraction and elution over 5 cycles did not show any noticeable difference, suggesting that the organic phase can be reused

at least five times without changes to its structure and loss in extraction efficiency. After each elution, the organic phase was rinsed three times with a 0.01 M HCl solution to mitigate the potential loss of Cl⁻ from the Cyphos 101. This rinsing process with hydrochloric acid was used because preliminary experiments, not involving a rinsing step, had indicated a slight decrease in the extraction of gold in subsequent cycles, which was likely due to the elimination of chloride ions present in the IL.

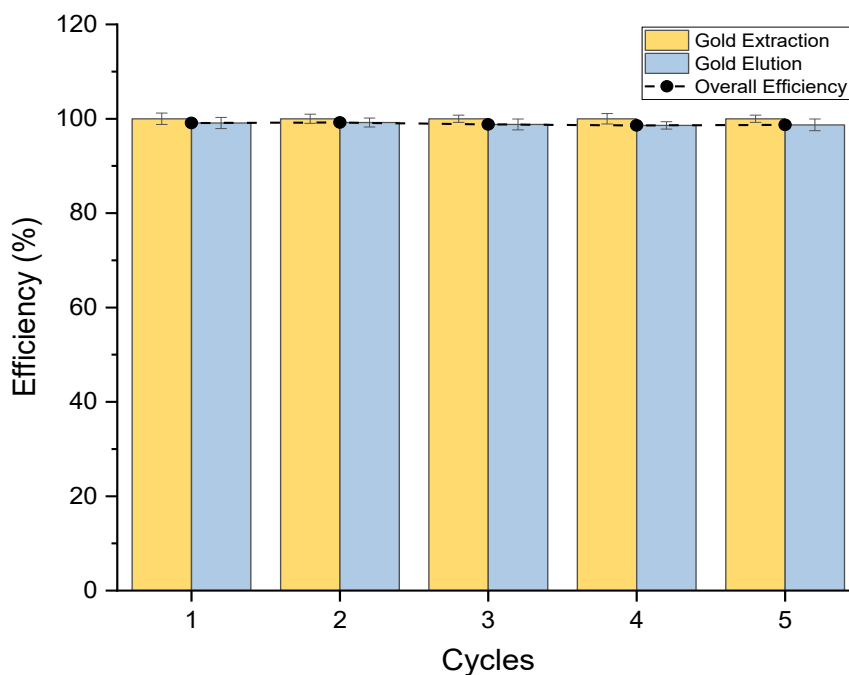


Figure 5.21: Gold extraction, elution desorption, and organic phase (0.1 M Cyphos in toluene) reusability over five cycles.

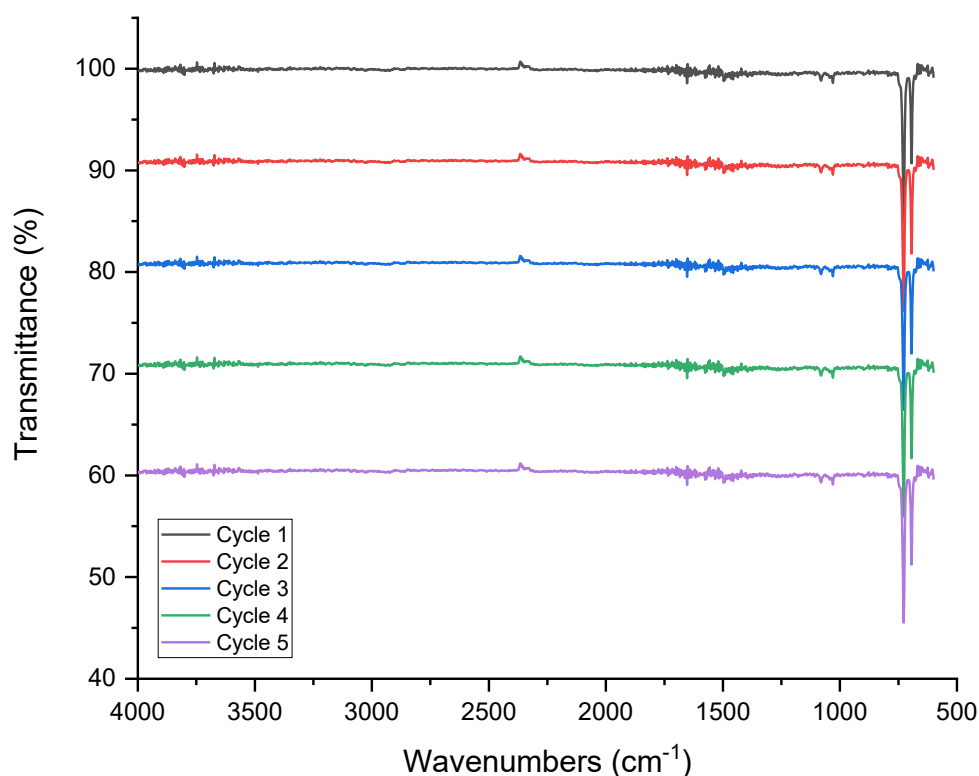


Figure 5.22: FTIR spectra of the organic extractant (0.1 M Cyphos 101 in toluene) over five cycles.

5.3.2.3.2 Gold Desorption and The Potential for Reuse of the Impregnated Resins

Investigation of the effects of hydrochloric acid concentration, thiourea concentration, and the contact time of gold on the desorption from loaded XAD-7 resins (300 mg IL/g) was carried out and the results are shown in Figure 5.23. Like gold elution from the liquid-liquid extraction, it was found that neither HCl nor thiourea concentration has a noticeable effect on the gold desorption. With different HCl concentrations, the desorption increased from 78% at 0.1 M HCl to 81% at 1.0 M HCl and 83% at 3.0 M HCl; at other concentrations tested the percentage change was marginal. The variation in the concentration of thiourea (Figure 5.23b) was also observed to have little impact on the desorption of gold, reaching nearly complete desorption across the range tested (0.1-3.0 M). The effect of the contact time (Figure 5.23c) showed that complete desorption can be reached within 2 hours, twice the time required for elution following the liquid-liquid extraction. This is likely due to the gold ions being attached to the interior of the resins, making it more difficult for ionic interchange. The optimal desorption parameters that minimise the use of reagents and ensure a complete gold desorption are 0.5 M thiourea in 0.5 M HCl for 2 h.

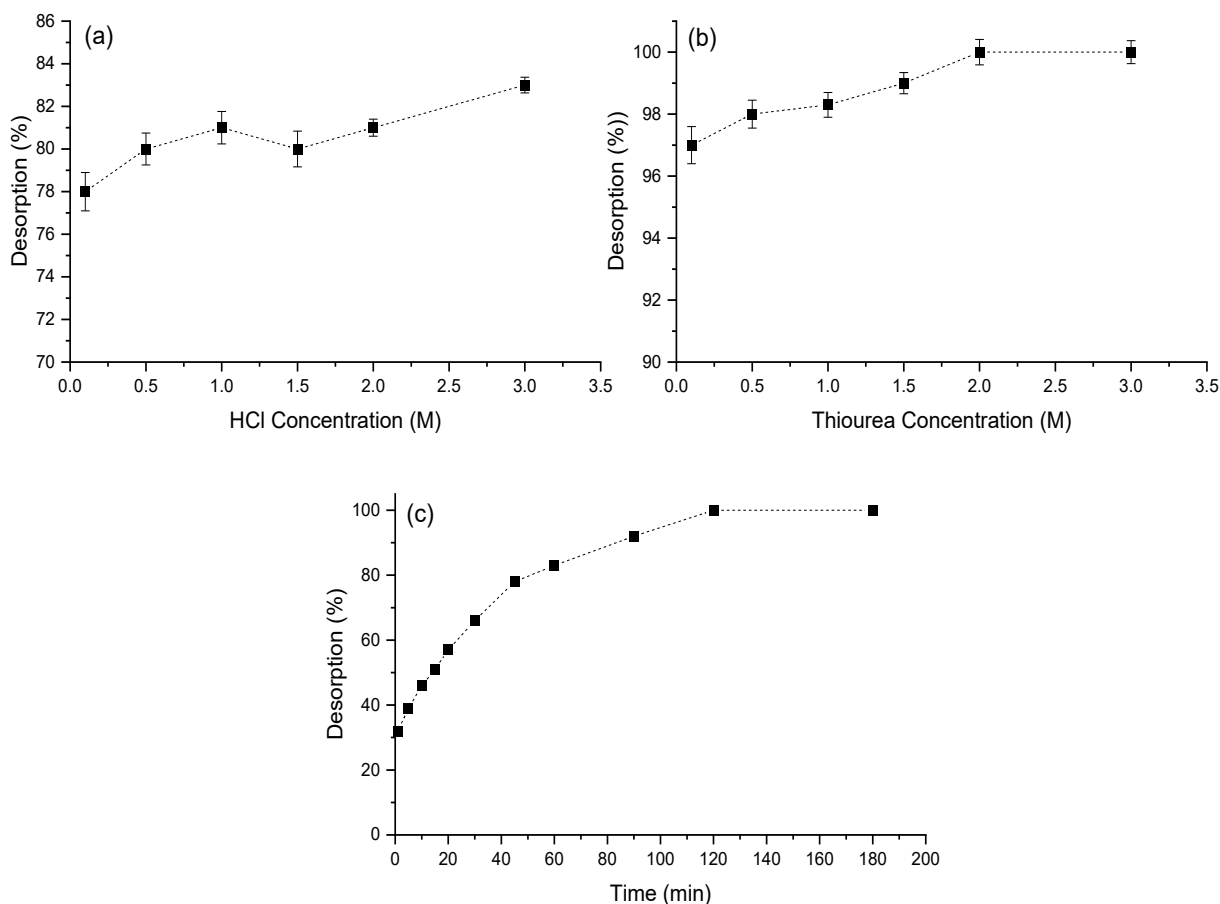


Figure 5.23: Gold desorption from XAD-7 impregnated with Cyphos 101 (300 mg IL/g); (a) Effect of the HCl concentration (1M thiourea), (b) effect of the thiourea concentration (1M HCl), and (c) Effect of the contact time.

Again, to ensure any process development is sustainable and the use of reagents minimised, the loaded resins should be chemically stable throughout the process, retain high efficiencies after gold sorption and desorption, and be able to be reused through several cycles. To evaluate the reusability of the sorbent, five successive cycles of sorption and desorption were carried out, and the results are shown in Figure 5.24. The sorption and desorption of gold remained largely unaffected over five consecutive cycles, suggesting that the loaded resin can be successfully reused without any major loss in efficiency. In addition, although the overall efficiency slightly decreases over subsequent cycles, the overall efficiency of gold recovery remains $\geq 95\%$ in each cycle. After each desorption a rinsing step was carried out using a 0.01 M HCl solution to mitigate the potential loss of Cl^- of the impregnated Cyphos 101 due to the sorption/desorption. In the preliminary experiments only one rinse step after desorption was used but this led to a decrease in the subsequent sorption/desorption

efficiencies. Increasing the number of rinses to three however ensured high sorption and desorption efficiencies were maintained through the cycles.

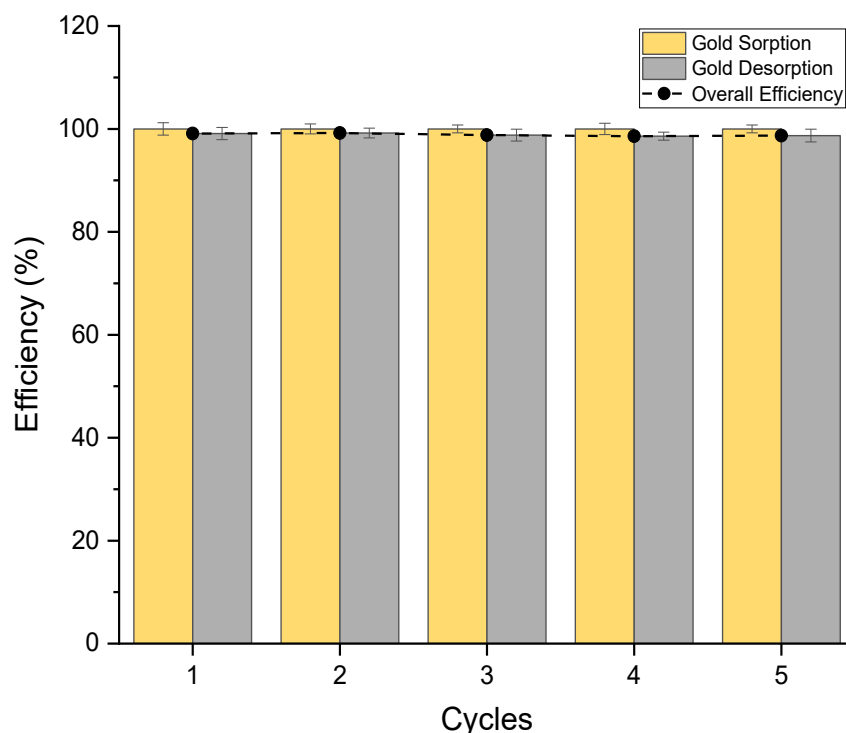


Figure 5.24: Gold sorption, desorption, and resin recyclability over five cycles.

The impregnated resins can be used in at least five consecutive cycles of sorption and desorption (Figure 5.24) without major losses in the efficiencies. To investigate any change in the integrity of the resins (such as cracks, rift, breakage, etc.) following the sorption and desorption cycles, BSE images of the impregnated Amberlite™ XAD-7 before and after five cycles were recorded and analysed (Figure 5.25). The images confirm no changes in the resin shape, suggesting no damage or degradation has taken place after five cycles of sorption and desorption. The only noticeable difference is the presence of shine marks in the reused resins (Figure 5.25c and d), which may be the result of dust and contamination in their handling. In Figure 5.25d, a small fracturing of the resin is observed, which could be due to osmotic shock generated by repeated sorption and desorption in acidic conditions. In general, the differences were negligible, suggesting no major damage was generated after five sorption and desorption cycles, however, a further study is needed to confirm the physical robustness of the resins with extended sorption and desorption cycles for a large-scale process.

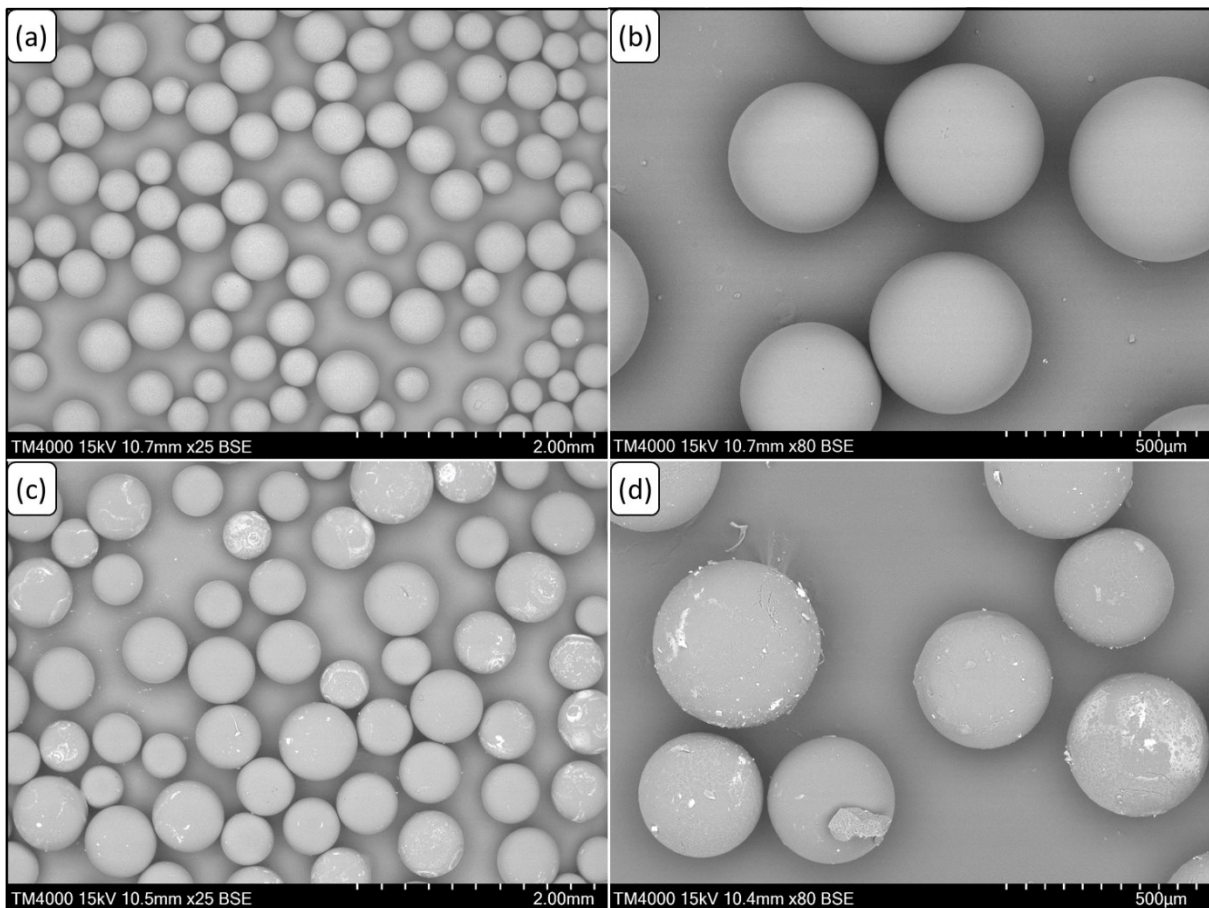


Figure 5.25: BSE images of impregnated Amberlite XAD-7: (a) and (b) before cycles, (c) and (d) after 5 cycles of sorption/desorption.

5.3.2.3.3 Discussion

Thiourea was selected for the elution in both extraction methods because it has been widely reported to be an excellent eluent for gold from acidic solutions [203, 205, 206, 209, 213]. Campos et al. reported the gold desorption from biopolymer capsules impregnated with Cyphos 101 in three solutions: 1M thiourea (in 1M HCl solution), 1M KI (in 1M HCl solution), and 6M HNO₃ solutions. They found that gold can be effectively desorbed from loaded resins using thiourea (1 M) with over 95% of desorption within 2 hours, whilst KI and HNO₃ presented a desorption of nearly 60% and 15%, respectively [213]. Cyganowski et al. also reported a complete gold desorption from shell type anion exchange resins using a 5% thiourea in 0.1 M HCl solution [203]. Navarro et al. studied the desorption of gold in Amberlite™ XAD-7/Cyphos 101 resins with nitric acid (5 M) and thiourea (1 M in 0.5 M HCl solution), observing a complete metal removal with thiourea over 5 cycles (in simulated solutions), whereas nitric acid led to a decrease in the efficiency of the resin over the cycles [206]. They pointed out that careful washing must be included as a step to prevent a later release of binding metal with

thiourea during the following sorption step, which can reduce the availability of the metal for binding to the IL, decreasing the sorption efficiency [206, 209].

The reusability of the organic phase in the L-L extraction and reusability of the impregnated resins in the sorption extraction are key factors that contribute to the development of a process that is environmentally sound and economically viable; one that conserves resources minimises process reagent costs. In this study both the organic phase and impregnated resins are shown to be reusable in five cycles of extraction/elution, with no loss in extraction/elution efficiencies. This is good agreement with similar systems reported in literature [156, 206, 209, 213, 215, 219]. In indium liquid-liquid extraction, Cyphos 101 diluted in toluene, a system similar to that the used in this study, has been shown that it can be reused up to up to 13 times without decreasing the extraction or elution efficiencies [156]. In the case of impregnated Amberlite™ XAD-7, it has also been shown that resin impregnated with Cyphos 101 can be reused for at least five times with slight decrease in the Pd(II) sorption; where the slight decrease was associated with the incomplete washing of the resins [206]. Several authors pointed out the importance of multiple rinsing/washing steps before subsequent cycles. In this study, three washings after metal elution were performed using a 0.01 M HCl solution to ensure replacement of any chloride ion that could be lost through the process and to remove any residual metal.

5.3.2.4 Reduction

The recovery of gold from the eluted solution (0.5 M thiourea in 0.5M HCl) was carried out by reduction/precipitation using sodium borohydride (NaBH_4). Sodium borohydride was chosen as the reducing agent for precipitation of gold from acidic thiourea, because the reaction is very fast, and is more selective for the precipitation of gold than other reducing agents [222]. Previous studies of the gold reduction were carried out using a 500 ppm Au solution in 0.5 M HCl. The solution was put in contact with 0.1 M Cyphos 101 in toluene with a O:A ratio of 1:1 for 15 minutes, followed by elution with 0.5 M thiourea in 0.5 M HCl with an O:A=1:1 for 1 h. The eluent solution was separated, and the precipitation was achieved with dropwise addition of a 0.1 M NaBH_4 in 0.1 M NaOH solution. Total gold reduction was obtained within 20 minutes at room temperature and 150 rpm.

5.3.3 Pre-treatment of As-Received E-Waste Components

As-received fractions of e-waste derived from EoL Mobile Phones and EoL Computers, as waste PCBs, CPUs, and IC components were required to undergo pre-treatment prior to application of the optimised process developed for gold recovery to real waste samples. The results of the development of a two-stage leaching process used to maximise copper removal and deliver a gold-enriched source for recovery are now described.

5.3.3.1 Two-stage Leaching Pre-treatment Step with Nitric Acid and Aqua Regia

Waste PCBs (WPCBs), CPUs and ICs can contain high amounts of gold, as previously reported in Chapter 3. Nevertheless, base metals represent most of the metal composition of these components, with copper being the most abundant. Previous results showed that copper represents $\geq 70\%$ of all the metals presents in WPCBs, CPUs, and ECs, whereas gold represents only $\leq 1\%$. To develop a process for gold recovery requires a pre-treatment step which involves a two-stage leaching to achieve enrichment of gold. The first stage involves the leaching of copper in the presence of nitric acid under optimal Cu leaching conditions of 3M HNO_3 , 30 °C, 50 g/L pulp density, and 500 rpm for 3 h [214]. Figure 5.26 shows the nitric acid leaching for ICs, CPUs, and PCBs. The WPCBs were leached using nitric acid (Figure 5.26e and f) and separately using [Bmim]HSO₄ (Figure 5.26g and f) under the optimal conditions (30 %v/v [Bmim]HSO₄, 10 %v/v H₂O₂, and 60 %v/v H₂O at 60 °C, 1:15 solid to liquid ratio for 2 h), reported in Chapter 4. It can be observed that nitric acid effectively leaches $>99\%$ of copper in all the cases, representing between 82% and 89% of the total metals leached. Gold was not leached by the nitric acid leaching, indicating that the first leaching stage was successful in selectively targeting copper for removal along with other base metals such as Al, B, Ba, Co, Ga, Mg, Ni, Pb and Zn which helped to achieve the gold enrichment. The main drawback of the nitric acid leaching is that Pd, a precious metal, was partially leached with approximately 50% from ICs and WPCBs, and completely removed from CPUs. In the case of the [Bmim]HSO₄ leaching, copper was completely removed, representing 94% of the total metals leached. Gold and other precious metals were not leached using this IL. The first leaching stage was successful in removing copper and other base metals, leaving gold intact in the solid residue. After nitric acid leaching, the residue was rinsed with RO water and dried for the next leaching stage. It is worth noting that the leach solution had a high copper concentration, where electrowinning can be applied for its recovery using methods described in Chapter 4, where it was demonstrated that copper can be almost completely leached and recovered by [Bmim]HSO₄ leaching, followed electrowinning. This IL was also used for the potential recovery of copper and gold in the same process.

In the second leaching stage, aqua regia (AR) was selected as the leachant as it dissolves most of the precious metals, with gold being completely dissolved. AR leaching was carried out at room temperature (20 ± 2 °C), 20 g/L pulp density, and 150 rpm for 3 h. Figure 5.27 shows the results of AR leaching for ICs (Figure 5.27a and b), CPUs (Figure 5.27c and d), WPCBs (Figure 5.27e and f), each following a nitric acid leach, and for WPCBs following a [Bmim]HSO₄ leaching (Figure 5.27g and h). The gold concentration after AR leaching in ICs was 289.3 mg/L, representing 52.1% of the total metals leached. In CPUs, the gold concentration reached 38.9 mg/L, representing 13.4% of the total metals leached. In WPCBs, both after nitric acid and separately [Bmim]HSO₄ leaching, showed similar gold concentrations of 30.5 mg/L, representing nearly 30% of the total metals present in solution. In all cases, the main impurities were Al, Fe, and remnant Cu. In WPCBs derived from EoL-MPs, Pd represented 17.4% of the total metals leached, with a concentration of 6.1 mg/L. Although complete gold leaching was achieved by AR, other metals present in the solution might interfere in the gold extraction. To overcome this potential problem, another leaching process after the nitric acid and before AR may be required. This leaching process could be carried out by nitric acid, hydrochloric acid, or sulphuric acid. Table 5.9 summarises the concentration and leaching efficiencies of metals obtained in the two-leaching process.

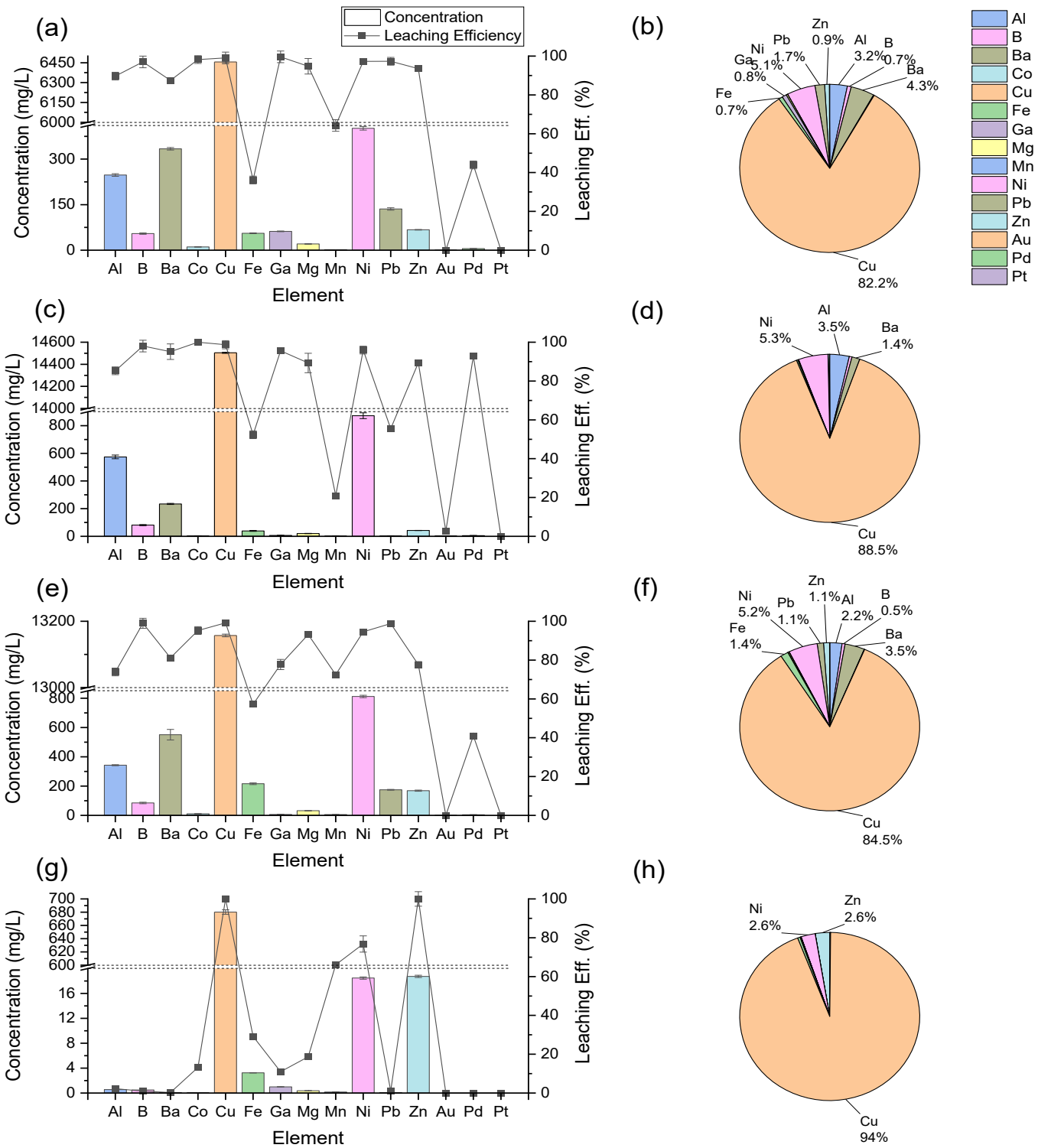


Figure 5.26: First leaching stage with nitric acid: (a) and (b) for ECs, (c) and (d) for CPUs, (e) and (f) for WPCBs, (g) and (h) for WPCBs with [Bmim]HSO₄.

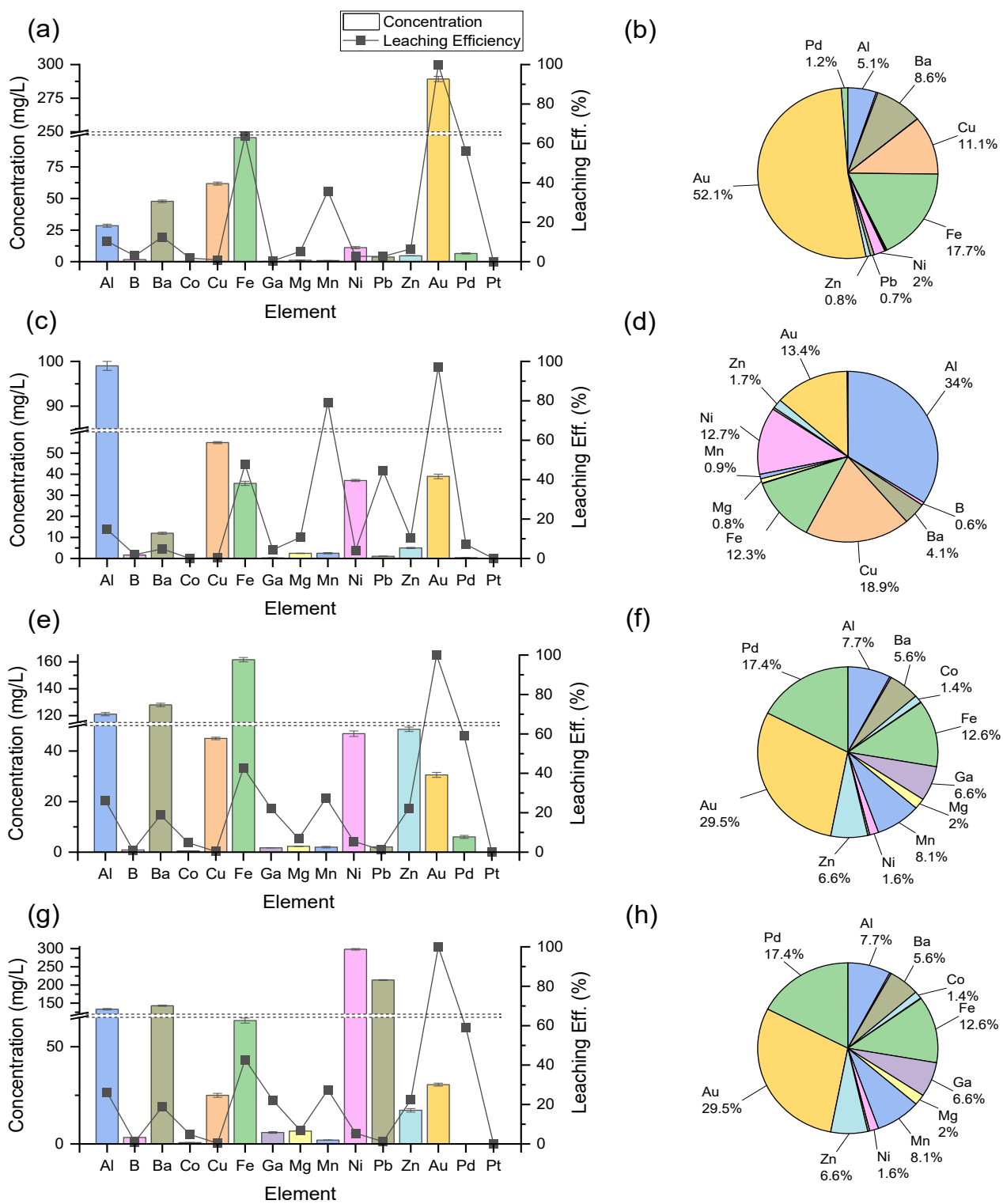


Figure 5.27: Second leaching stage with aqua regia: (a) and (b) for ECs, (c) and (d) for CPUs, (e) and (f) for WPCBs, (g) and (h) WPCBs with [Bmim]HSO₄.

Figure 5.28 shows the leaching liquors obtained from waste ICs, CPUs, and WPCBs after the first leaching stage with nitric and the IL, followed by the second leach with aqua regia. The blue colour after the first leaching is characteristic of copper nitrite, whilst the greenish colour obtained in [Bmim]HSO₄ is likely due to the copper sulphate formed in the presence of the sulphate group of the IL. The more intense blue colour in CPUs and PCBs compared to ICs is due to the higher copper concentration, with 14.5 g/L and 13.2 g/L for CPUs and PCBs, respectively, compared to 6.5 g/L in the IC fraction (Table 5.9). The golden yellow colour of the leach liquor following the second leaching stage is characteristic of the AR reaction.

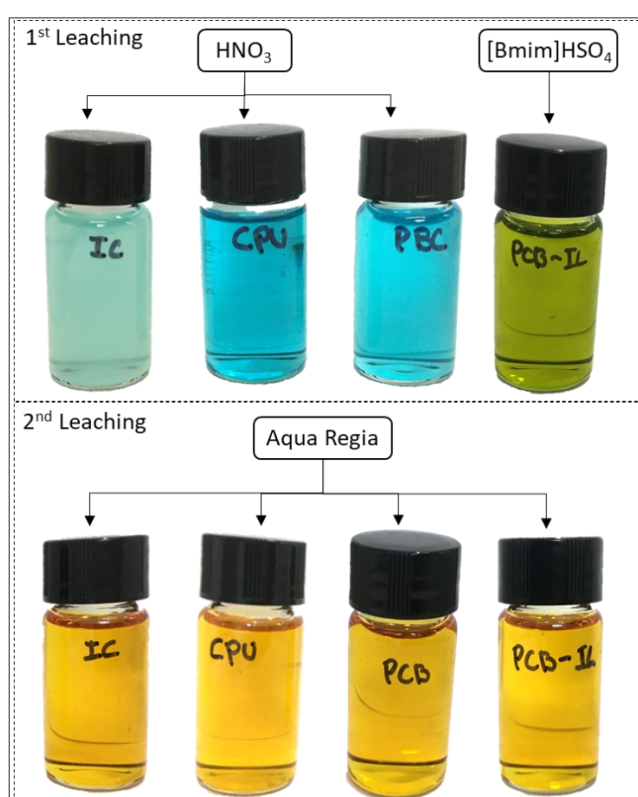


Figure 5.28: Images of the first and second leaching liquors.

Table 5.9: Metal concentration and leaching efficiencies of the two-leaching process.

First Leaching								
Element	Concentration (mg/L)				Leaching Efficiency (%)			
	ICs	CPUs	PBCs	PBCs-IL	ICs	CPUs	PBCs	PBCs-IL
Al	247.5	574.2	342.7	0.6	89.7	85.3	73.9	2.3
B	54.6	81.2	84.9	0.5	97.0	98.0	99.0	1.0
Ba	334.1	234.2	551.0	0.1	87.5	95.1	81.2	0.2
Co	10.7	1.6	10.7	0.0	98.2	100.0	95.2	13.2
Cu	6455.5	14504.1	13157.1	680.2	99.1	99.6	99.7	100.0
Fe	55.7	39.2	216.0	3.3	36.2	52.4	57.2	29.2
Ga	62.1	6.5	6.0	1.0	99.6	95.6	77.7	11.0
Mg	20.5	20.3	31.8	0.4	94.8	89.3	93.2	18.7
Mn	1.6	0.7	5.2	0.2	64.3	21.0	72.5	66.1
Ni	401.5	872.0	811.9	18.5	97.3	95.9	94.5	76.8
Pb	135.7	1.3	174.8	0.1	97.4	55.5	98.8	1.1
Zn	67.2	42.3	168.7	18.7	93.5	89.4	77.6	100.0
Au	0.0	1.1	0.0	0.0	0.0	2.7	0.1	0.0
Pd	5.1	5.2	4.2	0.0	43.9	92.8	41.0	0.0
Pt	0.0	0.0	0.0	0.0	0.0	0.0	0.0	0.0
Second Leaching								
Element	Concentration (mg/L)				Leaching Efficiency (%)			
	ICs	CPUs	PBCs	PBCs-IL	ICs	CPUs	PBCs	PBCs-IL
Al	28.5	99.0	121.1	133.4	10.3	14.7	26.1	32.0
B	1.7	1.6	0.9	3.3	3.0	2.0	1.0	4.3
Ba	47.8	12.0	128.0	142.9	12.5	4.9	18.9	21.2
Co	0.2	0.0	0.5	0.7	1.8	0.0	4.8	4.9
Cu	61.8	55.0	45.0	25.0	1.0	0.4	0.3	0.2
Fe	98.2	35.7	161.6	63.5	63.8	47.7	42.8	21.2
Ga	0.3	0.3	1.7	5.9	0.4	4.4	22.3	65.2
Mg	1.1	2.4	2.3	6.6	5.2	10.7	6.8	18.2
Mn	0.9	2.5	2.0	2.0	35.7	79.0	27.5	27.0
Ni	11.1	37.0	46.9	298.2	2.7	4.1	5.5	34.2
Pb	3.7	1.1	2.1	213.6	2.7	44.5	1.2	98.0
Zn	4.7	5.0	48.6	17.3	6.5	10.6	22.4	9.3
Au	289.3	39.0	30.6	30.5	99.9	97.3	99.9	99.9
Pd	6.5	0.4	6.0	0.0	56.1	7.2	59.0	0.0
Pt	0.0	0.0	0.0	0.0	0.0	0.0	0.0	0.0

The standard deviation of each result was ≤5%.

5.3.3.2 Discussion

Copper from WEEE can be dissolved by mineral acids (HCl, HNO₃, H₂SO₄); however, nitric acid typically has the highest leaching efficiency for copper. Dhanunjaya et al. studied the copper leaching from EoL-MP PCBs using sulphuric and nitric acids. They found that nitric acid was more effective, leaching 99.9% of Cu with 3 M HNO₃ at 30 °C with a 50 g/L pulp density, 2 h residence time, and 500 rpm stirring [214]. With the focus of the research described in this chapter on the recovery of gold, and the similarity of the material (WPCBs from EoL MPs), these leaching conditions were adopted with a residence time of 3 h used instead of 2 h, as the shorter time was not enough to leach all the copper (90% of Cu leached in 2 h). Thus, in the first leaching stage from e-waste, copper was leached with an efficiency $\geq 99\%$ in nitric acid (3 M HNO₃, 30 °C, 50 g/L pulp density, 500 rpm, 3 h), with no gold dissolved. Due to the trace amount of gold and other precious metals in e-waste, copper, despite the fact that 99% is leached in the first stage, is still found as a major contaminant present in the solution after L-L extraction and sorption extraction (discussed later in Section 5.3.4 and evidenced in Figures (Figure 5.29b and Figure 5.31b), although this did not affect subsequent gold extraction from real samples. Dutta et al. compared copper leaching using HCl, HNO₃, H₂SO₄, also finding that nitric acid leached copper more efficiently than hydrochloric and sulphuric acids, due to the stronger oxidising properties of nitric acid. They reported that copper 91.6% can be leached from WPCBs under optimal conditions (3 M HNO₃, 75 °C, 75 g/L pulp density, 2 h), and a two stages leaching (with nitric acid) under similar conditions resulted in 99.99% of copper leached [91]. Behnamfard also leached copper from WPCBs in a two-stages leach, using sulphuric acid (2 M H₂SO₄, 20 °C, 96 g/L pulp density, 3 h) and H₂O₂ (35%), with H₂SO₄:H₂O₂ =5:1. In the first stage, 85.8% of Cu was leached, with complete leaching achieved following a second sulphuric acid leach under same conditions [222]. Although copper can also be completely leached by sulphuric acid in a two-stages process, additional oxidising agents such as hydrogen peroxide are required, which increase the consumption of reagents in the process. Thus, the selection of nitric acid was deemed adequate.

In the second leaching stage, gold was dissolved using aqua regia (AR) at 20 °C, 20 g/L pulp density, and 150 rpm for 3 h, leaching gold completely (99.9%). Although other leachants for gold are possible such as cyanide, ammonia, thiourea, thiosulphate, halide, they have been categorised as extremely toxic for the human health and the environment, present relatively low efficiencies and can be very expensive [19, 203]. Although AR is also an extremely toxic leachant and can cause serious pollution, it shows high leaching efficiency, fast kinetics, is a well-established method, and inexpensive, and still shown to be a most efficient leachant for gold [19]. Although AR leaching conditions like those used in this work are reported in the literature to have involved higher temperatures (60-90 °C) [19, 23, 202], in the current research, no heating was required since the

reaction is exothermic and releases adequate heat for optimum gold leaching ($\sim 80\text{ }^{\circ}\text{C}$). Others authors have also leached gold and other metals with AR at room temperature [49, 207]. In all the cases, $\geq 95\%$ of gold was leached. The two-stages leaching process was effective for the enrichment of gold, with copper being removed in the first leaching ($\geq 99\%$), leaving gold in the solid residue for the second leaching with AR.

5.3.4 Application of the Optimised Conditions for Gold Extraction and Recovery from Pre-treated E-Waste Components

The optimal conditions developed for gold extraction and recovery from gold-rich samples using a Model Test system have been applied to pre-treated real samples of e-waste and the results are now described. The results of the extraction processes using ionic liquids as either a **liquid-liquid extraction** or a **sorption extraction** system (trialled for comparison) followed by an elution/desorption and reduction step are discussed here. The potential for recovery of the ionic liquids and resins for recycle and reuse to minimise reagent use described elsewhere in this chapter are discussed in terms of the real sample investigation.

5.3.4.1 Liquid-liquid Extraction Applied to Pre-treated E-Waste Components

Liquid-liquid extraction was carried out using the leach solution from Section 5.2.3.3 (ICs and WPCBs after the two-step leaching process) as the aqueous phase (metal concentration presented in Table 5.9), and the organic phase of 0.1 M Cyphos 101 in toluene. The extraction was carried out with an O:A=1:1, room temperature (20 ± 2 °C), 150 rpm, and 15 minutes. The results of the liquid-liquid extraction are presented in Figure 5.29, with the gold extraction (Figure 5.29a) complete, at $\geq 99.5\%$. The concentration in the organic phase after L-L extraction is 344.2 mg/L. In addition to gold, iron is also completely extracted, with a concentration of 80.7 mg/L in the organic phase. Following Au and Fe, Ga and Pb are extracted at 76.8% and 45.9%, respectively. Other metals present are partially extracted with values of approximately 11-21%. Nevertheless, although several metals are partially extracted, their concentration varies between 0.06 and 12.51 mg/L. Among the extracted metals (Figure 5.29c), gold represents 74.8 %, followed by iron (17.5%), silver (2.7%), and others (5.0%). In the aqueous phase (Figure 5.29b), silver, copper, barium, and aluminium (i.e., the metals not extracted) are present in the highest concentrations with 57.4 mg/L, 41.9 mg/L, 35.0 mg/L, and 20.3 mg/L for Ag, Cu, Ba, and Al, respectively. The aqueous phase after extraction is rich in silver, a valuable precious metal, which can be further treated to recover Ag, which will increase the economic benefits of the recycling process. In addition, although palladium is partially extracted in the organic phase (19.7%), nearly 80 % of the Pd is left in the aqueous phase, with a concentration of 5.6 mg/L, which could be also recovered. The metal distribution (Figure 5.29d) shows that the liquid-liquid extraction has potential to also separate the precious metals, separating gold from silver, palladium, and platinum, which are left in the aqueous phase. This separation is completely efficient, as a loss of approximately 20% of Ag, Pd, and Pt is extracted by the organic phase. Nevertheless, the aqueous

phase after extraction is a solution rich in Ag, Pd and Pt, representing a potential secondary source of these metals. The liquid-liquid extraction applied to real e-waste samples is shown to be effective and a fast process for the extraction of gold, with minimal gold losses in the process ($\leq 0.5\%$).

5.3.4.1.1 *Discussion*

Gold extraction from real leach solution (aqueous phase) was carried out using 0.1 M Cyphos 101 in toluene at 20 °C, 150 rpm, with an O:A=1:1 for 15 minutes. The gold extraction from the leach solution (344.2 mg Au/L) was complete ($\geq 99.5\%$), with the gold transferred entirely to the organic phase. Using the volume extraction (5 mL:5 mL), it can be calculated that the organic phase contains 0.5 mmol of Cyphos 101, whilst the aqueous phase contains 8.7×10^{-3} mmol of Au. The mmol of Cyphos 101 in the L-L extraction was approximately 57 times higher than the mmol of Au in the aqueous phase and based on the extraction mechanism of 1:1 stoichiometric ratio between Cyphos 101 and gold, there was a large excess of Cyphos 101. This can explain the complete gold extraction and the extraction of other metals. This also suggests that with lower concentration of Cyphos 101, gold can still be completely extracted, requiring less extract reagent, which in turn lowers the cost of the process. Among all the metals extracted, apart from gold, iron was the main and practically the only pollutant present, which could potentially decrease the gold extraction efficiency in a continuous process. It has been reported that in concentrated chloride solution such as AR leach liquor, iron is mostly found as tetrachloroferrate anion (FeCl_4^-), having a tetrahedral structure which does not contain water ligands [221]. This hydrophobicity and absence of dipole moment, facilitates the mobility of iron towards the organic phase. In addition, as the tetrachloroferrate anion (FeCl_4^-) has a similar symmetry than tetrachloroaurate anion (AuCl_4^-), its extraction mechanism could be potentially very similar. Nevertheless, the stability of FeCl_4^- has been found to be far less than that of the AuCl_4^- and in different chloride concentrations, it can be found as $\text{FeCl}_2(\text{H}_2\text{O})_4$ (1-3 M), $\text{FeCl}_3(\text{H}_2\text{O})_2$ (5.6 M), having a mix of Fe(III) complexes in the other ranges of HCl concentrations [221]. Therefore, as the gold extraction is not affected by the HCl concentration, an alternative could be the addition of a basic salt of solution to modify the iron complex, and consequently, decreasing its extraction. Indeed, it was reported that in a gold adsorption in presence of iron, the iron uptake was negligibly small when the HCl concentration was low (1 M) [221].

Alternatively, as the organic phase is not fully loaded, counter-current with several stages can be used. McCabe-Thiele diagrams for gold extraction can be constructed by varying the O:A ratio from 1/ 5 to 5/1 by keeping the total volume of phases constant. Nevertheless, this alternative has a great potential for gold extraction and the increase of its concentration in the organic phase, which can favour an increase in the gold concentration for the elution stage. Masilela and Ndlovu reported an extraction of 97% of gold by undiluted Cyphos 101 from chloride AR leach liquors of WPCBs [207]. Nevertheless, as only one leaching stage was used, copper and silver (the metals studied) were also leached, making the separation process more difficult. Furthermore, the viscosity of Cyphos 101 can be challenging to handling since it sticks on the walls of the container where the extraction occurs, it is hard to remove completely between containers for further processes. Furthermore, as Cyphos 101 is less dense than water, it is found in the upper layer, making it difficult to access to the lower aqueous phase layer. Due to these and other complications, diluted Cyphos 101 was preferred.

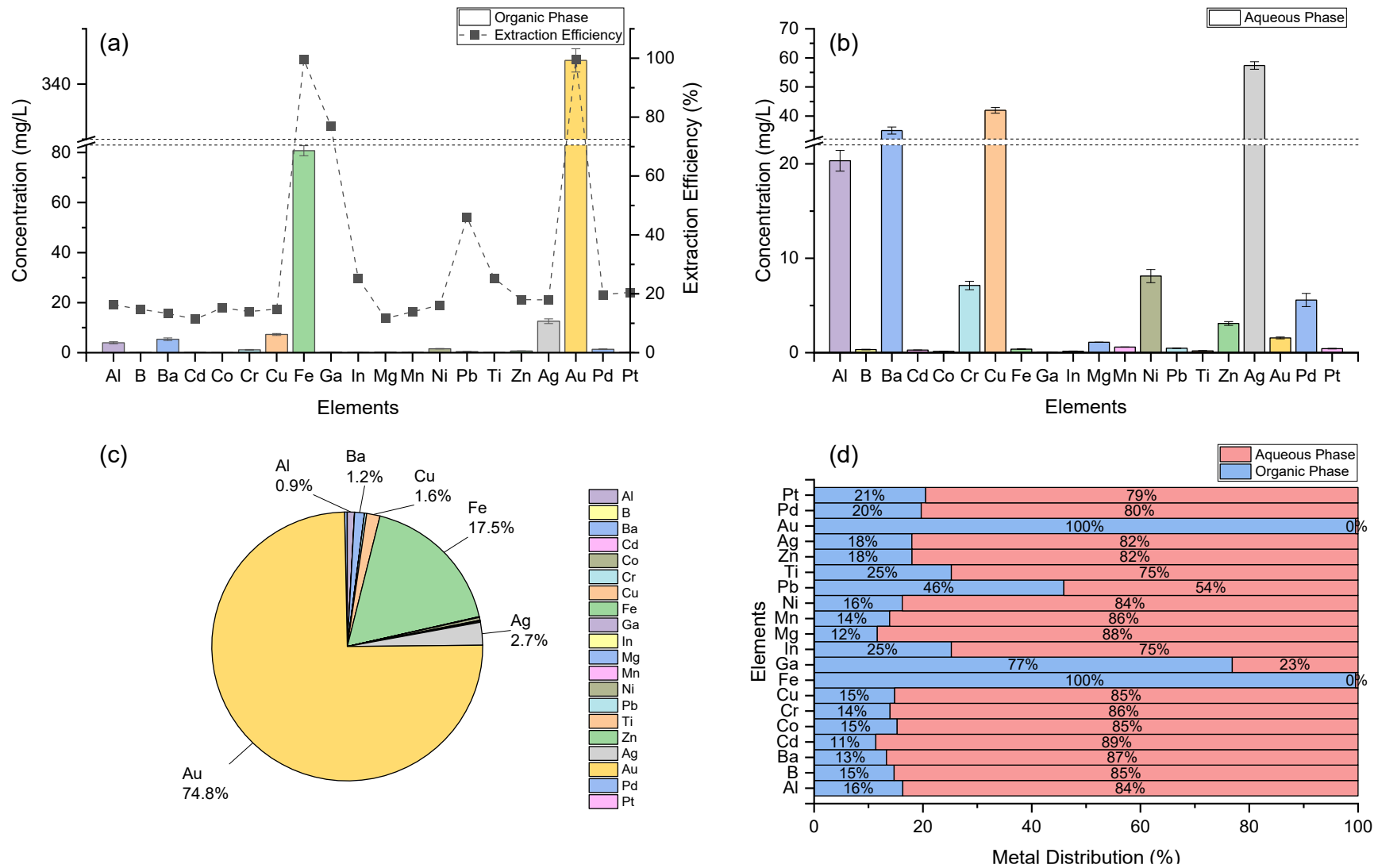


Figure 5.29: Gold extraction from ICs leaching liquor by 0.1 M Cyphos 101: (a) metals in the organic phase, (b) metals in the aqueous phase, (c) metal distribution of the extracted metals, (d) metal distribution in the organic and aqueous phases after extraction. Conditions: O:A=1:1, 150 rpm, 20 °C, 30 min.

5.3.4.2 Elution following Liquid-Liquid Extraction for Gold Recovery from Pre-treated E-Waste Components

The loaded organic phases were then eluted using 0.5 M thiourea in 0.5 M HCl with an O:A=1:1, room temperature (20 ± 2 °C), 150 rpm for 1 h. Elution results are shown in Figure 5.30. In Figure 5.30a, it can be seen that gold is effectively eluted (99.2%), with a concentration of 341.4 mg/L in the eluent, representing the 90.5% of the total metals present in the eluent (Figure 5.30b). Indium and titanium are also completely eluted, however, their concentrations are < 0.4 mg/L, representing a minor contamination. Although iron is partially eluted (41.3%), its concentration is 33.4 mg/L, representing 8.8% of the total metals eluted. The other metals present in the loaded organic phase are found in low concentrations in the eluent (< 0.8 mg/L), representing only 0.7% of total metals in the eluent, which are considered as minor contaminants. The elution process is observed to be very effective in the recovery of gold with only iron as an undesirable contaminant; and, the eluent, requiring no further processing for the reduction of gold, can be reused in subsequent elutions from loaded organic phases. The only potential problem is the possible accumulation of iron in the eluent; this would need to be carefully monitored as high levels of iron could impact formation of thiourea-gold complexes and subsequently decrease the gold extraction.

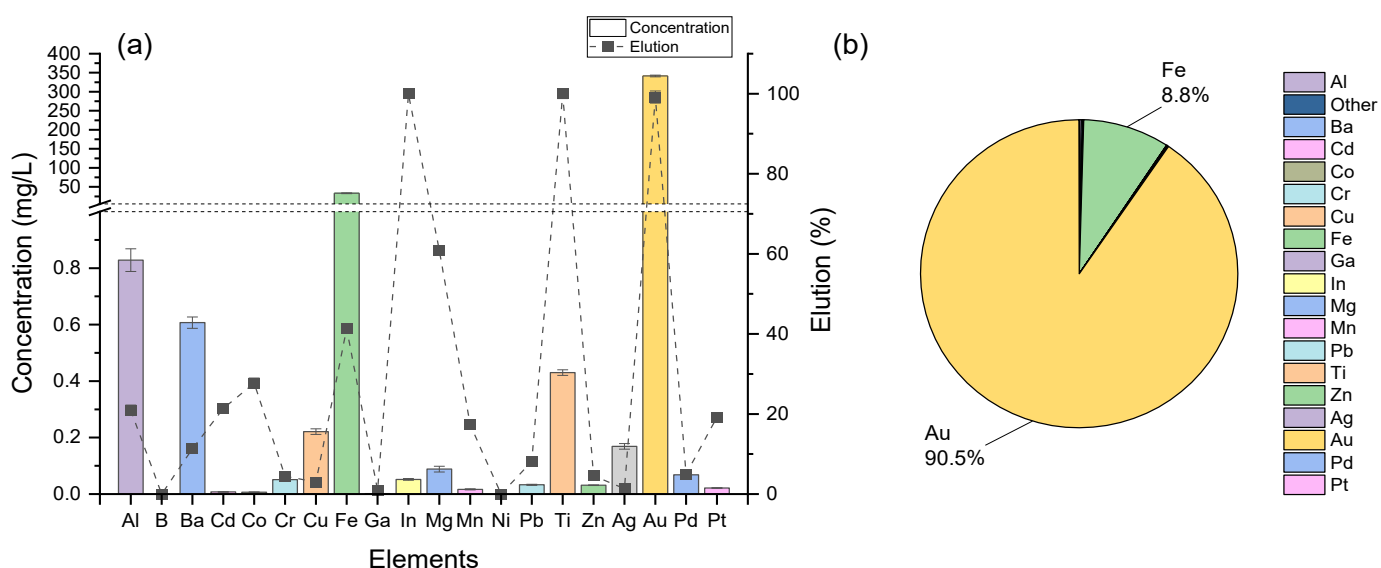


Figure 5.30: Elution of loaded organic phase (0.1 M Cyphos in toluene) with thiourea: (a) concentration and elution efficiency, and (b) metal distribution in the elution solution. Conditions: 0.5 M thiourea in 0.5 M HCl, O:A=1:1, 150 rpm, 20 °C, 2 h.

5.3.4.3 Sorption Extraction Applied to Pre-treated E-waste Components

Sorption extraction was carried out using the leach solution from Section 5.2.3.3 (ICs and WPCBs after two leaching steps process) as the aqueous phase (metal concentration presented in Table 5.9). The sorption was carried out using Amberlite™ XAD-7 impregnated with 300 mg Cyphos 101/g resins, with a sorbent dosage (SD) of 25 g/L, room temperature (20 ± 2 °C), 150 rpm, and 3 h. The sorption results are presented in Figure 5.31. The gold extraction by sorption is complete (99.3%), being adsorbed at 13.7 mg Au/g SIRs (Figure 5.31a), representing 79.4% of the total metals adsorbed (Figure 5.31c). Iron, the main contaminant is also completely adsorbed (99.2% at 3.2 mg Fe/g SIRs), representing 18.6% of the total metal adsorbed. The other metals adsorbed represent only 2%, suggesting that iron is the main and essentially the only undesirable metal present in the gold sorption. In the aqueous phase after the sorption process (Figure 5.31b), silver, copper, barium, aluminium, nickel, and palladium are found in relatively high concentrations. There is a particular interest in Ag and Pd, with concentrations of 67.7 mg/L and 6.4 mg/L, respectively. These metals can be potentially recovered from the aqueous phase after sorption, increasing the value of the gold recovery process. The metal distribution (Figure 5.31d) confirms that gold is successfully extracted at level of more than >99%, while small percentages of silver and palladium are extracted with 3% and 8%, respectively. Other metals extracted can be considered as minor impurities, since their sorption is at levels, at least 340 times lower than gold. The gold sorption process is successful since gold can be completely extracted and only minor impurities are observed, except for iron, which may need a further separation.

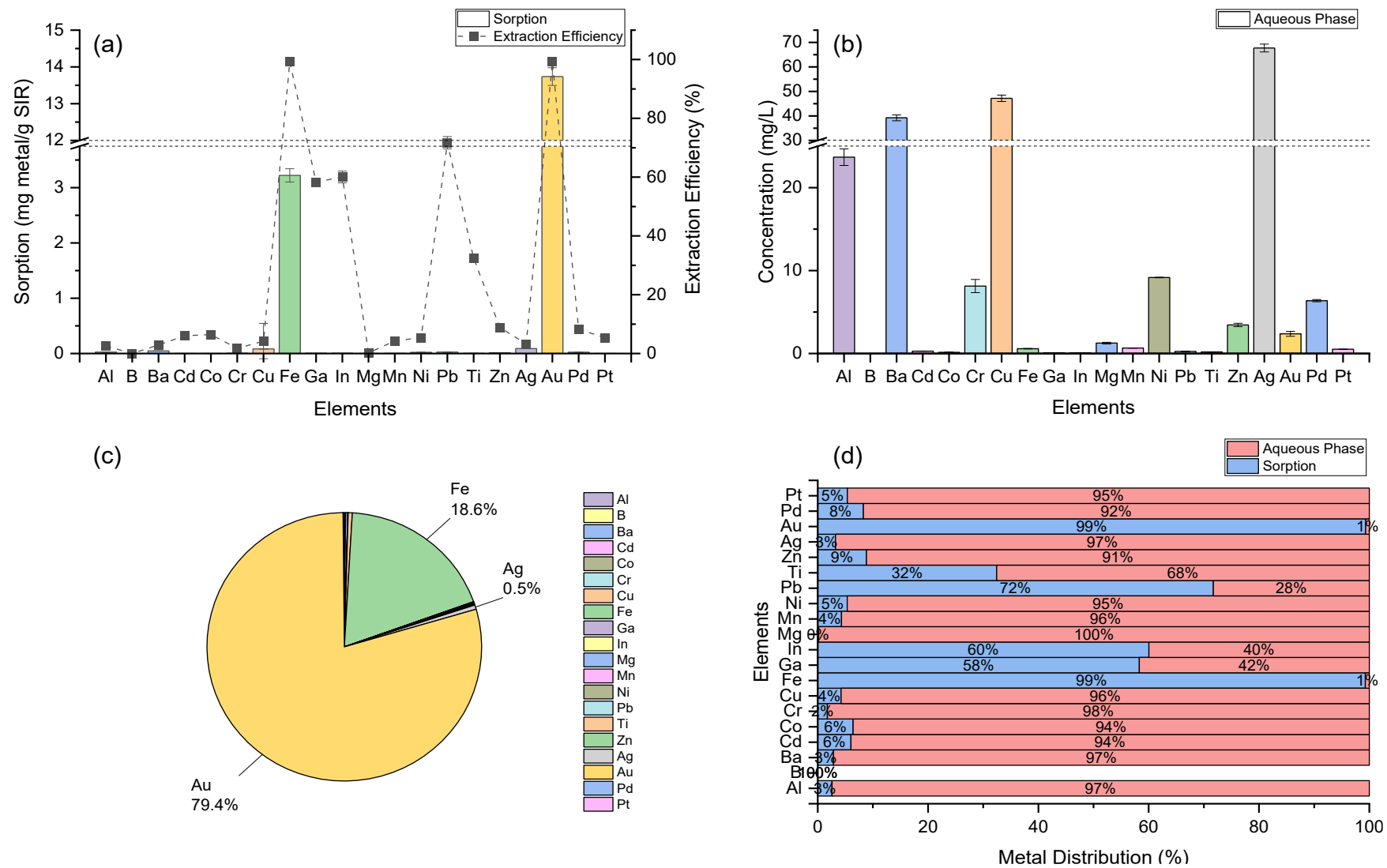


Figure 5.31: Gold sorption from ICs leaching liquor by SIRs (Amberlite™ XAD7-300mg Cyphos 101): (a) metal sorption, (b) metals in the aqueous phase, (c) metal distribution of the extracted metals, (d) metal distribution in the organic and aqueous phases after extraction. Conditions: SD:25 g/L, 150 rpm, 20°C, 4h.

5.3.4.4 Desorption following Sorption Extraction for Gold Recovery from Pre-treated E-waste Components

The loaded SIRs from were desorbed/eluted under the conditions: 0.5 M thiourea in 0.5 M HCl with SD=25 g/L, at room temperature ($20 \pm 2 \text{ }^\circ\text{C}$), 150 rpm for 2 h. The desorption results are presented in Figure 5.32. Gold is effectively desorbed (97.3%), giving a concentration of 334.1 mg/L in the eluent Figure 5.32a, representing 84.0% of the total metals present in the eluent (Figure 5.32b). Iron is 75% eluted with a concentration of 60.8 mg/L, representing the 15.3% of the total metals eluted. Other metals such as Al, Cr, In, Mg, Mn, and Ti are also completely eluted; their concentrations of <0.8 mg/L, represent only 0.7% of the total desorbed metals present in the eluent, which are considered as minor contaminants. The desorption process is very effective in the recovery of gold with just iron as the undesirable contaminant. Like the elution stage of the liquid-liquid extraction process, a problem that might arise is the possible accumulation of iron in the eluent; this would need to be carefully monitored as high levels of iron could impact formation of thiourea-gold complexes and subsequently decrease the gold extraction. Figure 5.33 shows photographic images of SIRs during the sorption and desorption stages. It can be observed that the white colour of the resins turned to golden yellow after sorption and turned to light yellow/white colour after desorption. Apart from this colour change there was no noticeable that the resins confirming that no damage or degradation of the SIRs has occurred.

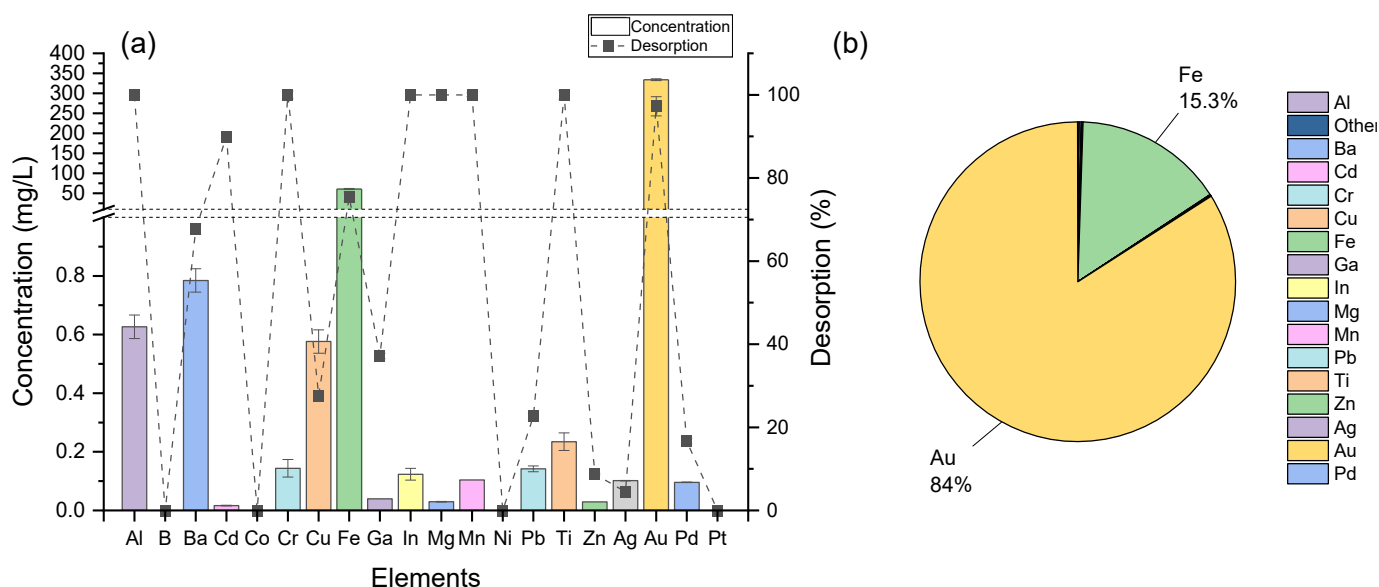


Figure 5.32: Desorption of loaded SIRs (Amberlite™XAD7-300mg Cyphos 101) with thiourea: (a) concentration and elution efficiency, and (b) metal distribution in the elution solution. Conditions: 0.5 M thiourea in 0.5 M HCl, SD=25 g/L, 150 rpm, 20 °C, 3 h.

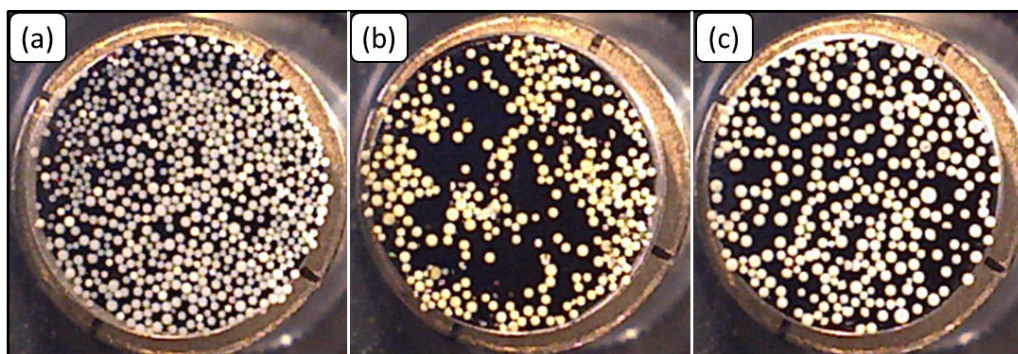


Figure 5.33: Photographic images of SIRs: (a) before sorption, (b) after sorption, and (c) after desorption.

5.3.4.5 Reduction Step for Gold Recovery from E-waste Components

Using the reduction step developed in the trials on the Model Test System the same procedure was applied using the real e-waste-derived sample (ICs), using both extraction methods studied in this work (liquid-liquid extraction and sorption-desorption under the optimal conditions determined). The extraction/sorption and elution/desorption efficiencies in both processes were >97%. Due to the low amount of gold and the scale of the experiments, both elution solutions were mixed (as they both were similar in gold concentration in the same elution solution of 0.5 M thiourea in 0.5 M HCl), and the gold reduction was carried out with dropwise addition of a solution of 0.1 M NaBH₄ in 0.1 M NaOH, stirring at 150 rpm for 20 minutes. Controlled addition was carried out until the final solution turned from pink (due to the first drop) to dark wine-colour (after several drops) – the point at which reduction of Au³⁺ to Au⁰ was complete. Figure 5.34 shows SEM-EDS images of the gold nanoparticles precipitated from the gold extraction using real sample (ICs). Gold nanoparticles appear as irregular shapes with a large size dispersion, estimated between 1 μm and 150 μm (Figure 5.34a and b). EDS analysis confirms that gold is the only metal present (Figure 5.34c and d). The purity of the precipitated gold was further confirmed with ICP-OES by dissolving the gold nanoparticles in aqua regia, obtaining a gold purity >99 %.

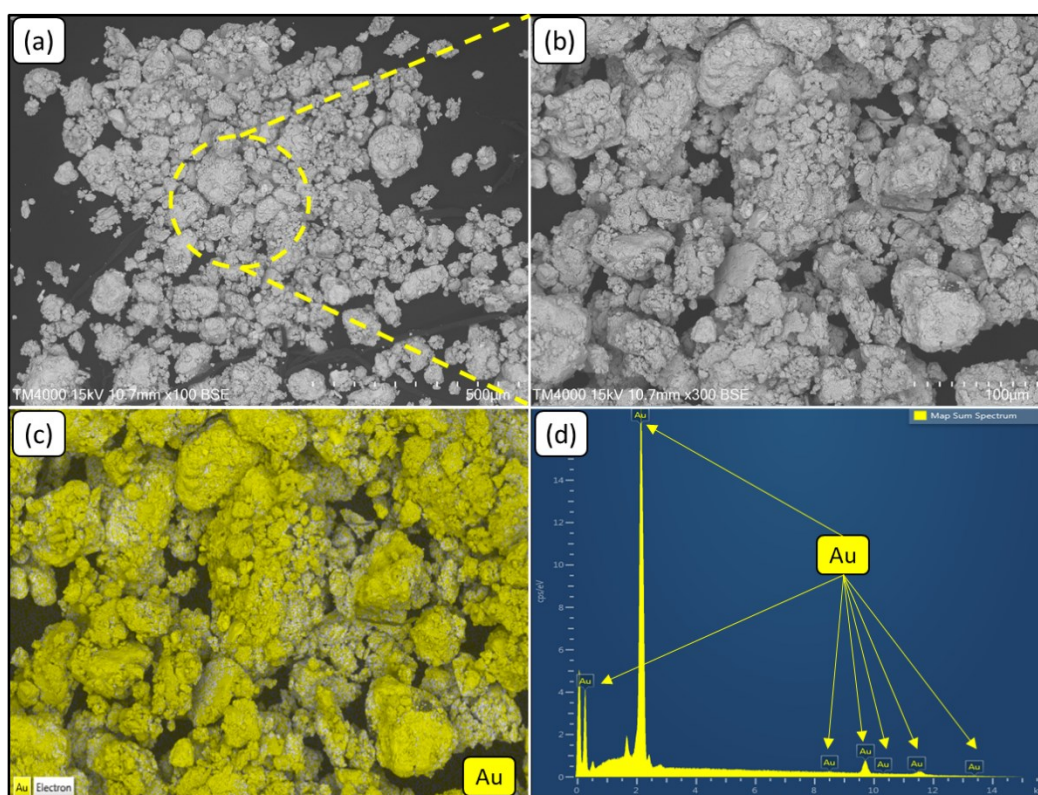


Figure 5.34: SEM-EDS images of the precipitated gold nanoparticles by NaBH₄: (a) SEM image (500 μm), (b) SEM image (100 μm), (c) EDS (100 μm), and (d) EDS map sum spectrum.

The process used in this work for gold reduction with the controlled addition of sodium borohydride is a method that has the advantage of being a simple, quick, and low-cost process, and consistent with reports in the literature confirms the high selectivity of sodium borohydride for gold reduction. Alguacil tested different potential precipitation reagents (ascorbic acid, hydrazine sulphate, and sodium borohydride), finding that only sodium borohydride solution in alkaline medium could effectively precipitate gold from the gold-thiourea solutions, precipitating 90% of gold in less than five minutes and achieving complete gold precipitation in 20 minutes [223]. They obtained a very fine gold powder of varying particles sizes. Behnamfard et al. reported complete precipitation of gold from NaClO-HCl-H₂O₂ leach solutions following addition of sodium borohydride directly to the leach solution at room temperature, requiring only 15 minutes for complete precipitation. Elsewhere, Jingyue and Bernd reported that in the formation of gold nanoparticles by NaBH₄ precipitation, the gold and NaBH₄ concentrations, and the temperature are significant parameters that contribute to the uniformity of the precipitate [224]. They found that with high concentration of both gold and NaBH₄ at room temperature, the reduction rate is very fast, generating irregularly shaped gold nanoparticle (nanorods, triangles, and irregular shapes). Diluting the gold and NaBH₄ solution and keeping the temperature low (0 °C), regular and spherical gold nanoparticles are obtained. The gold nanoparticles precipitated in the current research, however, despite maintaining sodium borohydride at a low temperature through use of an ice-bath, precipitated as irregular shapes with a large size dispersion (1-150 µm). The important outcome of the current research is on the effectiveness of the gold reduction and precipitation rather than the regularity of the precipitate formed. Where regular sizes and shapes are required, this can be achieved by tailoring the sodium borohydride solution and controlling the temperature.

5.3.5 Proposed Hydrometallurgical Process for Gold Extraction and Recovery from E-Waste Components

The potential for recovery of gold from e-waste components derived from EoL Mobile Phones and EoL Computers, where gold present in these streams, in trace amounts, is found in the WPCB, IC and CPU components is proposed as a four-step approach using task-specific ionic liquids under optimised conditions. An initial pre-treatment of the as-received waste is carried out to produce a gold-enriched feedstock from which gold can be extracted and recovered using one of two alternative hydrometallurgical processes. The pre-treatment involves the manual separation of the electronic components (WPCBs, ICs, CPUs) containing gold, albeit in trace amounts, followed by shredding to decrease the particle size to benefit the chemical processes involved. A two-stage leaching follows involving first, a nitric acid leach to remove copper, and second, an aqua regia leach to obtain an enriched gold solution.

Based on an IL selection study the IL, Cyphos 101 was chosen and used in the two extraction processes developed for recovery of gold. The first process, presented in Figure 5.35, a liquid-liquid extraction using 0.1 M Cyphos 101 in toluene is followed by elution with 0.5 M thiourea. The second process, Figure 5.36, a sorption extraction is carried out using Amberlite™ XAD-7 impregnated with Cyphos 101, followed by desorption by a 0.5 M thiourea solution. The difference between the two processes lies in the extraction/elution stages, with each followed by a reduction step (using sodium borohydride) leading to the precipitation of gold, as gold nanoparticles with a purity $\geq 99\%$.

Using the Model Test system with synthetic gold solutions, the overall gold recovery efficiencies for both processes was $\geq 97\%$, even after 5 cycles. Application of the processes to treat real samples, led to overall recovery efficiencies of $\geq 95\%$, with a recovery of 97% achieved using liquid-liquid extraction, slightly higher than the 95% recovery using sorption extraction. The two hydrometallurgical processes differed in that liquid-liquid extraction was faster (with the elution time half that required for complete desorption) and achieved a higher level of gold recovery whilst sorption extraction used less chemicals to recover the same amount of gold.

All the experiments were carried out on a laboratory scale with excellent results and have potential to be applied on a larger scale, although for the handling of larger volume of e-waste, further studies may be required. In addition to the gold recovery, there are by-products in the processes which can be used as part of other recovery processes. In particular, the leach solution after the first leaching is rich in copper, which it would be relatively easy to recover by means of electrowinning. This formed part of the process developed described in Chapter 4; a process combining a dual two-step leaching

and electrowinning system applied to the recovery of copper from WPCBs derived from EoL Mobile Phones with an overall efficiency of $\geq 95\%$. The copper recovery process reported in Chapter 4 was repeated using WPCBs and the solid residue was utilised for gold recovery using the processes developed and reported in this chapter to demonstrate the success of the combined processes in recovery of both metals. Furthermore, the aqueous phase after liquid-liquid and sorption extractions was found to be rich in precious metal group (PMG) metals, particularly rich in silver and palladium. These precious metals are very valuable, and their recovery should be further studied.

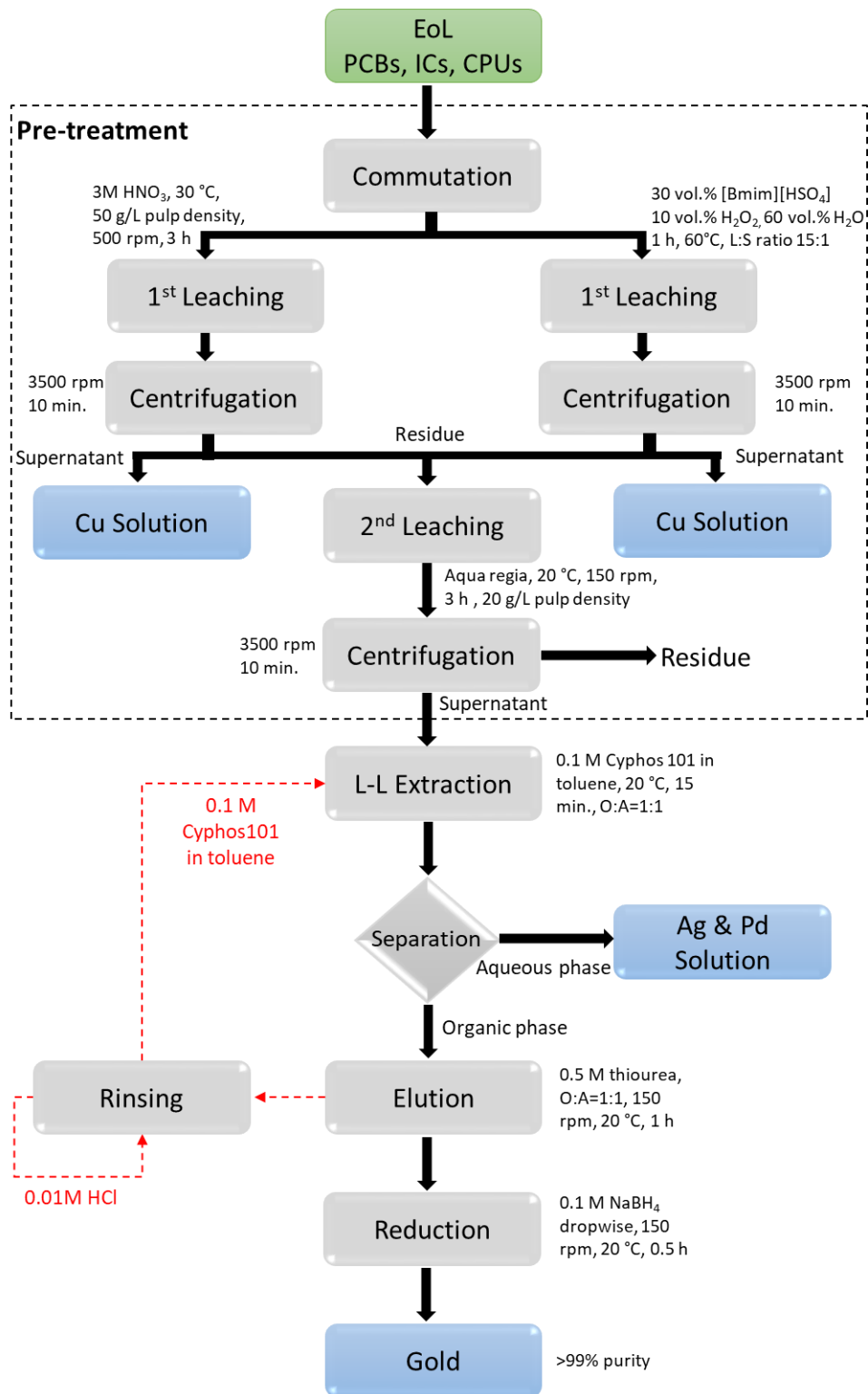


Figure 5.35: Gold recovery process from WEEE (WPCBs, ICs, CPUs) by liquid-liquid extraction.

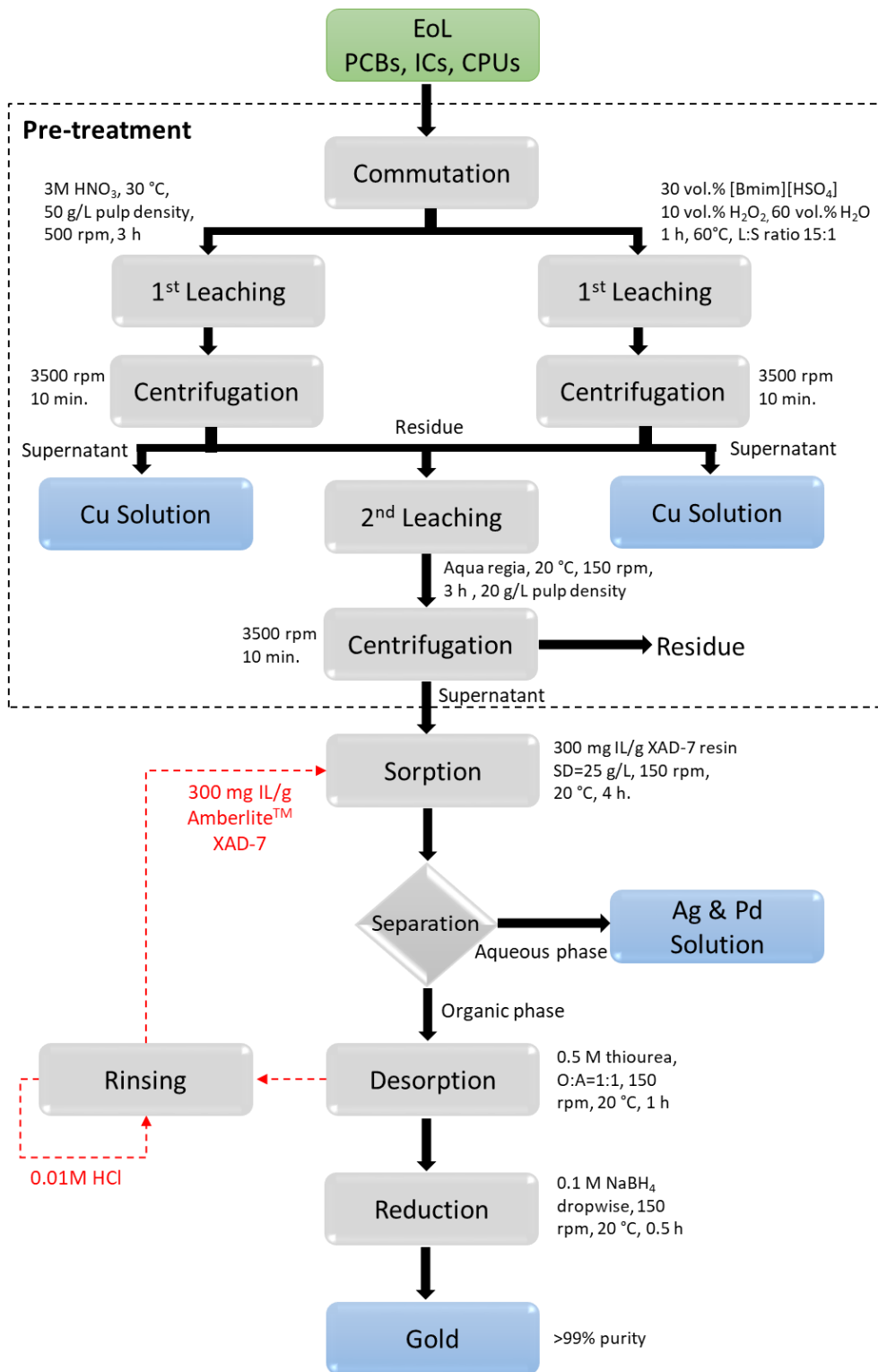


Figure 5.36: Gold recovery process from WEEE (WPCBs, ICs, CPUs) by sorption extraction.

5.4 Summary

In this chapter, two hydrometallurgical processes are developed for the recovery of gold from e-waste components derived from EoL Mobile Phones and EoL Computers. The gold present in these streams is found in WPCB, IC and CPU components. The proposed hydrometallurgical processes developed in this work for gold extraction and recovery were trialled using a Model Test System (a simulated gold solution) to determine the effectiveness of each process step before application on real as-received e-waste components.

Recovery of gold from e-waste (PCBs, ICs, and CPUs) is successfully achieved using the two alternative hydrometallurgical processes. Due to the low traces of gold and high content of copper present in e-waste, a pre-treatment step involving two-stage leaching is developed. The first leaching, nitric leaching (3 M HNO₃, 30 °C, 50 g/L pulp density, 500 rpm, 3 h), removed ≥99% of the copper with no gold dissolved. The second leaching, followed the nitric leaching, was carried out by aqua regia (20 °C, 20 g/L pulp density, and 150 rpm for 3 h), achieving complete gold leaching (99.9%). As a by-product, the leach liquor from the nitric leaching can be used for recovery of copper.

Liquid-liquid extraction was carried out by Cyphos 101 as extractant. Different organic solvents were investigated as potential diluents and toluene found to be the most effective. Factors, such as HCl concentration, temperature, and contact time did not influence the gold extraction. The extraction mechanism of gold in chlorinated medium showed a one-to-one gold to Cyphos 101 molecule complex, suggesting an anion exchange mechanism. The evaluated thermodynamic parameters indicated the gold extraction is spontaneous and endothermic. Sorption extraction was carried out by immobilisation of Cyphos 101 in the porous network of Amberlite™ XAD-7. SEM-EDS analysis showed that the IL was homogeneously distributed in the resin. It was found that the IL loading increases the gold sorption capacity, with maximum gold capacities of 20.2 mg Au/g, 40.4 mg Au/g, 136.2 mg Au/g and 175.2 mg Au/g observed for raw Amberlite™ XAD-7, 100 mg IL/g, 300 mg IL/g and 500 mg IL/g, respectively. The increase in the gold sorption capacity is due to a combination of extraction processes including sorption on the polymer matrix of the resin and anion exchange by the impregnated Cyphos 101. Further studies showed that the gold adsorption process is hardly affected by the HCl concentration and agitation, reaching equilibrium within 3h in all the cases studied. Sorption kinetics were governed by the chemical reaction rate, whereas thermodynamic studies showed that the gold adsorption process was spontaneous and endothermic.

In both processes, elution and desorption was operated using thiourea (0.5 M, in 0.5 M HCl solution), with gold being completely removed. After gold elution, the organic phase and resins have

been shown to be successfully reused for at least five cycles. The reusability of the organic phase and resins is optimised with extensive washing (0.01 M HCl) after each elution/desorption to remove any trace of thiourea, which might affect the next extraction cycle, and to replace any chloride ions lost in the Cyphos 101 through the process. Gold precipitation was achieved by dropwise addition of a sodium borohydride solution (0.1 M NaBH₄ in 0.1 M NaOH) at 150 rpm for 20 minutes in the thiourea gold-rich solutions. Another by-product in the processes, it is the liquor left after gold extraction, which is rich in silver and palladium and can be used for their recovery.

Under the optimised conditions of liquid-liquid extraction (0.1 M Cyphos 101 in toluene, 20 °C, 150 rpm and 15 minutes), and sorption extraction (loaded resins at 20 °C, 150 rpm and 3 h), gold can be extracted almost completely (≥98%) from the e-waste leach solution (obtained using the two-stage leaching process). The proposed hydrometallurgical processes developed in this work can achieve overall efficiencies as high as >95% for gold recovery; and offer a promising approach to the recovery of gold from any e-waste stream rich in gold.

6 Recovery of Indium from EoL Mobile Phone Liquid Crystal Display Screens Using Ionic Liquids

6.1 Introduction

Indium has emerged as an important strategic metal in the last decades, which is extensively utilised in the electronic and energy related industries due to its excellent chemical, physical, and mechanical performance [142, 156]. Indium has been catalogued as a critical material by the European Commission (EC), the U.S. Department of Energy (DOE), United Nations Environment Programme (UNEP), US National Academy of Sciences (NAS) and American Physical Society and Materials Research Society, and it is one of the most frequently cited metals in terms of material criticality due to its economic importance, scarcity, lack of substitutes, and limited future availability [78, 225, 226]. In 2015, 820 tonnes of indium was produced, reaching 900 tonnes in 2020 [198]. The worldwide production of indium is mainly used in the indium tin oxide (ITO) industry, representing approximately 70-80% of its consumption [152, 227]. ITO is a mixture of In(III) and Sn(IV) oxides with a typical distribution of 90% In_2O_3 and 10% SnO_2 , used in the production of liquid crystal displays (LCD), which are widely utilised in screens of mobile phones, televisions, laptops, etc. [142, 152, 228]. End-of-life (EoL) LCDs account for up to 90% of the indium-bearing components in WEEE [142]. Indium concentration in LCDs varies from 100 to 400 ppm, whereas in its commercial production it is found with a concentration of only 1-100 ppm [156, 198, 229]. Due to indium's low concentration in the Earth's crust (250 ppb) it is primarily produced as a by-product of zinc refining, with production dominated by China and South Korea [152, 198]. In the most recent study published in 2015 reporting on the availability of indium in the present, medium and long term, Lokanc et al make the point that the current and likely future demand of indium is driven by LCD and photovoltaic panels, with an annual growth of 15%, whilst the expansion of zinc production (from which indium is derived) is estimated to have an annual growth of only 1-3% [230]. These differences in demand and production will create shortages of indium in the medium and long term as well as rising of the indium price. Ciacci and co-authors conducted a material flow analysis focussed on European indium recycling potentials which examined secondary sources in European urban mines and in-use stocks, identifying them as potential sources of 500 tonnes of indium [231]. They emphasised the unique properties of indium that make it most suitable for applications linked to rising demand for sustainable energy, thin film PV applications, and larger LCD screens and the need for recycling of these end-of-life products is becoming an imperative. In 2011, Graedel et al cited that according to UNEP, barely 1% of indium-bearing end-of-life (EoL) waste was being recycled [232]. The challenges of supply of indium (as a by-

product of zinc production and the monopoly of China for production) and increasing demand for indium (with applications in PVs, flat screen TVs, laptops, tablets, and mobile phones, etc.), investigation into the recovery of indium from secondary sources such as LCDs described in this work is necessary and timely to balance this dilemma. Furthermore, LCD recycling will be also important due to environmental and human health aspects as LCDs are categorised as one of the most hazardous materials according to the Directive 2002/95/EC, due to the content of hazardous substances such as toxic metals (In, Cd, Pb, As, among other), flame-retardants, among others [147].

Indium recovery from EoL-LCDs can be achieved using pyrometallurgical [152, 167, 233], hydrometallurgical [156, 234-236], and bioleaching [237, 238] processes. Particular attention has been given to the use of hydrometallurgical processes due to their suitability for metal recovery from low concentration solutions, use of mild operation conditions, reported high efficiencies, lower energy consumption and lower capital investment, which can lead to excellent materials and energy balances due to the potential reuse of reagents [211]. Hydrometallurgical processes consist of a series of operations including: leaching, concentration, separation, and reduction of the desirable metal [211]. Among the different hydrometallurgical processes, solvent extraction (SX) has been shown to be a simple and eco-friendly method for metal recovery and purification from dilute solutions [156, 235]. Several extractants have been reported for the extraction of indium from aqueous and waste solutions including: bis(2-ethylhexyl) phosphate (D2EHPA) [90, 239], bis(2,4,4-trimethylpentyl)phosphinic acid (Cyanex 272) [240], tributyl phosphate (TBP)[241], 2-ethylhexyl phosphonic acid mono-2-ethylhexyl ether (PC88A) [242], sec-nonylphenoxy acetic acid (CA100) mixture with N,N-di(1-methyl-heptyl) acetamide (N503) [243], 2-ethyl-hexyl phosphonic acid mono-2-ethylhexyl ester (IONQUEST 801) [244], and di(1-methylheptyl)methyl phosphate (P350) [244-246]. A major problem with these acidic solvents is that their H⁺ ions released in the aqueous phase have an adverse effect on the metal ion extraction [156, 211, 247], furthermore, most of these organic extractants are toxic, flammable, volatile and expensive.

A novel, more sustainable and safer SX process involves the replacement of conventional molecular solvents by ionic liquids [235]. Ionic liquids (ILs) reported elsewhere in the current research are solvents that possess excellent properties such as non-flammability, negligible vapour pressure, excellent thermal, chemical and electrochemical stability, and high recyclability, among other [104, 105]. Among the ILs, phosphonium ionic liquids (PILs) generally exhibit better selectivity and extraction efficiency than conventional extractants [247], and among PILs, tetradecyl-(triethyl) phosphonium chloride (Cyphos IL 101) [205, 215, 235], tetradecyl-(tri-hexyl)phosphonium bis-(2,4,4-trimethylpentyl) phosphinate (Cyphos IL 104) [156, 236, 247] and tricaprilmethylammonium chloride (Aliquat 336) [215, 235, 248] have been widely utilised. Deferm et al. reported that undiluted Cyphos

101 and Aliquat 336 had a high affinity for indium(III), achieving extraction of >95% over a large range of HCl concentration (0.5M to 12 M) from simulated solutions [215]. In the process, indium was recovered as $\text{In}(\text{OH})_3$ by precipitation stripping with NaOH; this stripping step had the advantage that no IL was lost to the aqueous phase and the ILs could be regenerated for reuse. Dhiman and Gupta reported the recovery of indium, tin and zinc separately with purities >98.9% from discarded LCD screen using Cyphos 104 diluted in toluene [156]. The LCD panels were manually cut and ground in a ball mill to obtain a powder (75 μm); the powder was thermally treated at 80 °C for 24 h, followed by leaching with a mixture of 90% 3M HCl and 10% H_2O_2 (30%) at 75 °C for 2 h. Although it was developed as a complete process of indium recovery, no other materials were recovered from the LCD panels.

An LCD panel is a complex multi-layered structure, consisting of organic materials such as polarisers, liquid crystal, and inorganic materials such as sodium or boron-silicate glass substrate with ITO film. The glass substrates contribute to about 70-85 wt.% the weight of the panel and are usually about 1 mm in thickness. The outer sides of the glass substrate are attached in contact with the polarizers and the inner sides are coated with functional films and a transparent conductive electrode, including indium tin oxide [142, 151, 228]. With multiple components embedded in the structure it is likely, therefore, that indium is not the only material that can be recovered from EoL-LCD panels. Silveira et al. identified acetone as the most appropriate solvent for removal of the polarising films as it is inexpensive and relatively less toxic than other common organic solvents, however, the process takes 20 h [150]. Traditional separation of polarisers from LCD panels in acetone takes long hours, ≥ 15 h [150, 249]. Recently, Cui et al. reported that a two-step immersion of the waste LCDs in a bath of hot water (80-100 °C) followed by a bath of acetone, enabled the polarisers to be effectively separated within 1 h, allowing the liquid crystal to be potentially recovered [237]. Zhang et al. enriched liquid crystals from waste LCDs from 0.3 wt% to 53 wt.% by pyrolysis with inert gas, which also enriched the indium content [250]. Examples such as these suggest that pre-treatments of LCD panels are not only beneficial to material recovery, but they also enrich the amount of indium which further benefits any recovery processes.

Although several studies have reported the determination of optimal indium leaching from LCDs [89, 251, 252], indium extraction [156, 205, 236, 239, 246-248], and some pre-treatment methods [142, 150, 237, 249], a full recycling of LCD panels has not yet been developed. In this chapter, a whole material and indium recovery process, from LCD panels derived from EoL-MPs, is proposed.

6.2 Methodology

6.2.1 Materials

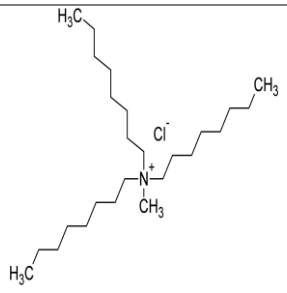
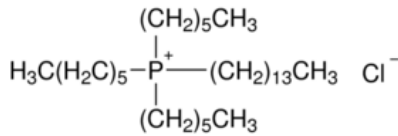
6.2.1.1 Chemicals and Reagents

All chemicals were of reagent grade and obtained from either Sigma-Aldrich (USA), VWR (USA) and Fisher Scientific (USA), Alfa Aesar (USA), Fluorochem (UK) and Agar scientific (UK). Unless otherwise stated, all the chemicals and reagents were used as received.

6.2.1.2 Ionic Liquids (ILs)

Based on the literature review, two potential ionic liquids were selected for trialling the extraction of indium, namely: tricaprylmethylammonium chloride known as Aliquat 336 ($[\text{CH}_3(\text{CH}_2)_7]_3\text{NCH}_3\text{Cl}$) and trihexyl(tetradecyl)phosphonium chloride known as Cyphos 101 ($[\text{P}_{6,6,6,14}][\text{Cl}]$). All ILs were purchased and used as received. Table 6.1 shows their properties and characteristics.

Table 6.1: Properties, characterisation and structure of the ionic liquids used in this study.

Ionic liquid	Properties & characterisation	Structure
Aliquat 336 $[\text{CH}_3(\text{CH}_2)_7]_3\text{NCH}_3\text{Cl}$	<p>Appearance: pale orange, viscous liquid</p> <p>M_w: 404.164 g/mol</p> <p>Density: 0.884 g/cm³ (20°C)</p> <p>Flash point: 132 °C</p> <p>FTIR: 747–1080 (C–H, sp²), 2883 (CH, symmetric), 2976 (CH, asymmetric), 1514 (CH₂)</p> <p>TGA-DSC: Onset decomposition temperature: 347 °C. Residue: 2 wt.% at 700 °C</p>	
Cyphos 101 $[\text{P}_{6,6,6,14}][\text{Cl}]$	<p>Appearance: colourless, viscous liquid</p> <p>M_w: 519.3 g/mol</p> <p>Density: 0.895 g/cm³ (20°C)</p> <p>Flash point: 118 °C</p> <p>FTIR: 2954 (νCH₃), 2920 and 2952 (νCH₂), 1465 and 1377 (δCH₃), 1458/1111/1003 (νP–C), 1415 (δCH₂), 988 (δC–H), 812 (νC–C), 719 (δP–C))</p> <p>TGA-DSC: Onset decomposition temperature: 370 °C. Residue: <1 wt.% at 700 °C</p>	

Molecular weight (MW), densities and flash point values were obtained from Sigma Aldrich, chemicalbook and PubChem. FTIR vibrations were obtained experimentally and compared with reference FTIR patterns in this study symbol; i) ν: stretching, ii) δ: bending, iii) ρ: rocking, iv) ω: wagging and v) τ: twisting. TGA-DSC information were obtained experimentally.

6.2.1.3 Metals and LCDs samples

Solutions of indium oxide powder were prepared in varying concentrations of indium in different acids (HCl, H₂SO₄, and HNO₃) solutions. A stock synthetic solution of 500 ppm In in 1M HCl, referred to in this work as a Model Test solution, was used for the indium extraction in chloride medium.

LCD panels were manually separated from as-received EoL-MPs using methods described in Chapter 3. The mobile phones used in this study were manufactured within the last 12 years and were received in good condition. A total of 25 EoL-MPs were used for a more sensitive analysis and to provide a larger source of representative material for the experimental trials. To ensure a representative sample for testing, the milled LCD screens from the 25 mobile phones were mixed. LCD panels were used as received, and for experimental purposes were cut into strips or used in powdered form.

6.2.2 Analytical Techniques for Characterisation

The analytical techniques used for characterisation of materials in this study are described in Chapter 3. Figure 6.1 summarises the analytical methods applied, and the measures used to determine the effectiveness of the steps towards extraction and recovery of indium from LCD panel from EoL-MPs. The six key process steps trialled and reported here include: *Leaching, Polymer Films Removal, Extraction, Stripping, Reduction, and IL Recyclability*.

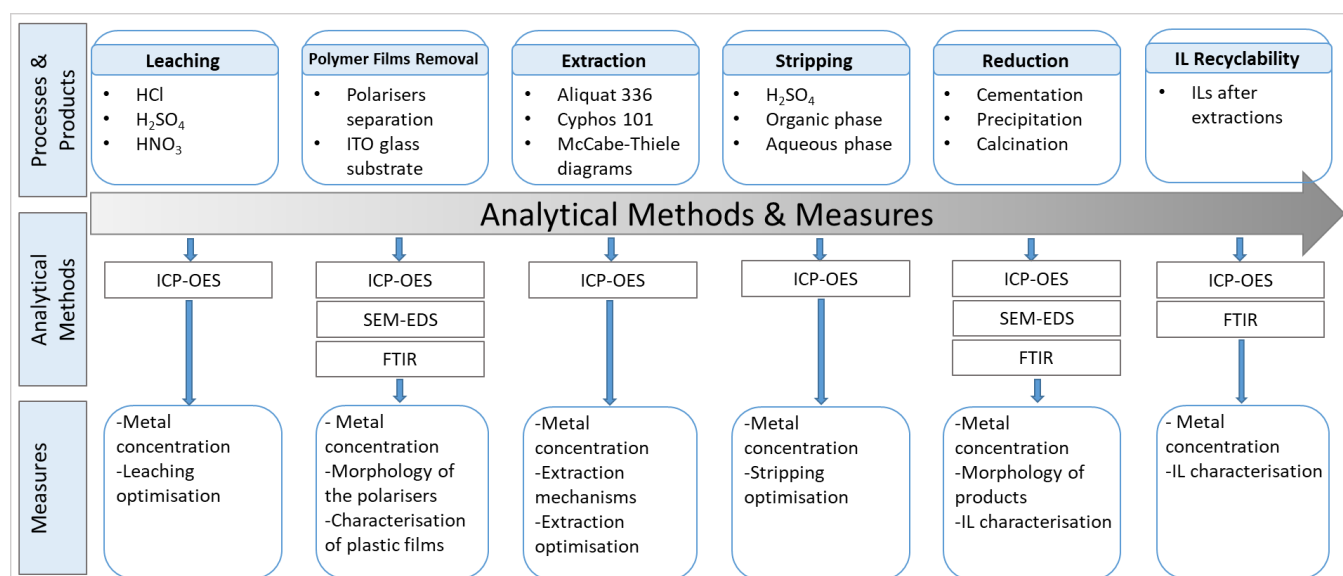


Figure 6.1: Analytical methods applied and measures used to determine the effectiveness of the extraction and recovery methods proposed.

6.2.3 Experimental Procedures

To investigate the potential for recovery of indium from EoL LCD panels derived from multigenerational mobile phones, a three-step approach is followed: (i) determination of the optimised conditions for indium extraction and recovery, including conditions for recovery of ILs for recycle and reuse using a Model Test System, (ii) pre-treatment of the as-received LCD panels to remove the polymeric films attached to the panels for material recovery and enrichment of the target metal, indium, and (iii) application of the optimised conditions for indium extraction and recovery to pre-treated waste LCD panels. An overview of the experimental procedure followed is set out in Figure 6.2.

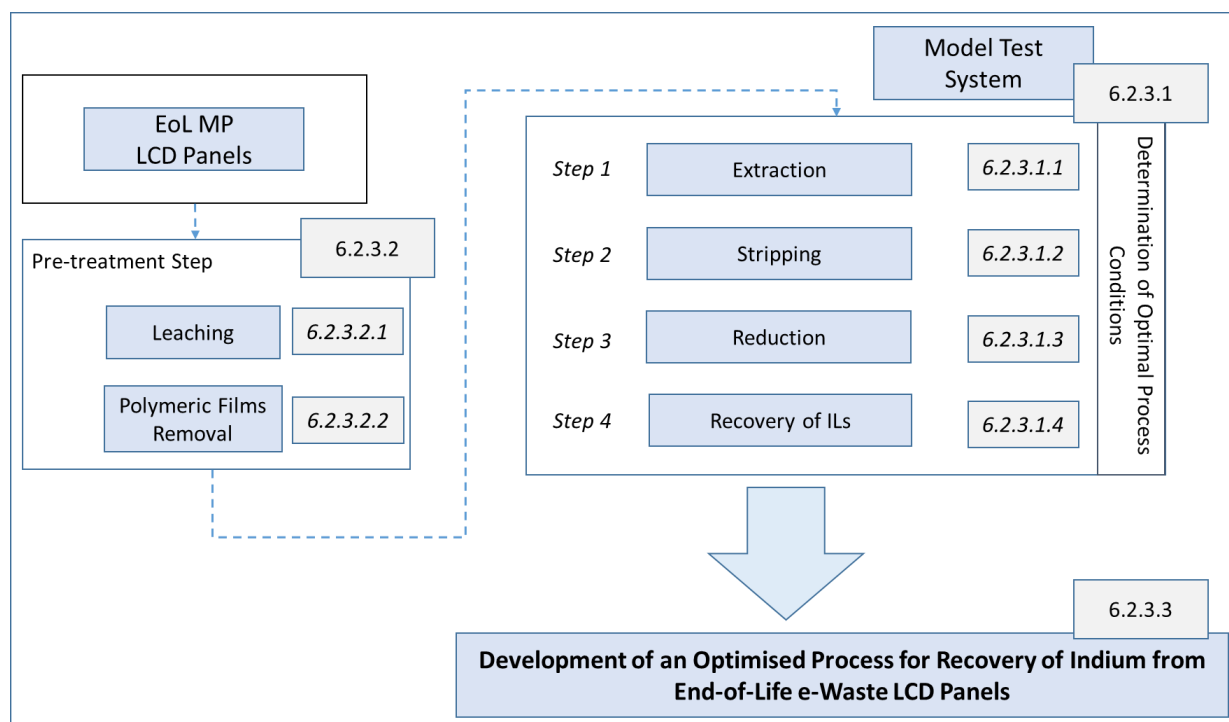


Figure 6.2: Overview of Experimental Procedure.

6.2.3.1 Determination of Optimised Conditions for Indium Extraction and Recovery using A Model Test System

To determine the optimised conditions for recovery of indium from EoL MP-derived LCD screens trials were initially conducted on a Model Test System containing indium alone, prepared as described in Section 6.2.1.3. The process steps trialled include liquid-liquid extraction using the two ionic liquids, followed by stripping of indium from the organic phase to permit (i) reduction to recover indium metal, and (ii) recovery of the ionic liquids for recycle and reuse to minimise reagent and mitigate the cost of ILs. Each of process steps investigated using simulated indium solutions is now described under the headings: *Extraction*, *Stripping*, and *Reduction*.

6.2.3.1.1 Extraction

As a first step towards determination of the optimal extraction conditions, the extraction mechanism, and the thermodynamics of the extraction, variable process conditions listed in Table 6.2 were tested for their influence on the extraction using each of the ILs, Aliquat 336 and Cyphos 101. These included the effects of acid type, acid concentration, diluent, time, temperature, IL concentration, chloride ion concentration, hydrogen ion concentration, etc. In each experiment, only one parameter at a time was changed while keeping the others constant. After separation of phases, the metal content was measured by taking 1 mL of sample diluted in 4 mL of 1M HNO₃ using ICP-OES. Due to the nature of the ILs, which cannot be dissolved by inorganic acids, the metal concentration in the ILs was calculated as the difference between the initial concentration and the final concentration in the aqueous phase as:

$$\%_0E = \frac{(C_i - C_f)_{(aq)} \cdot V_{IL}}{(C_i \cdot V_i)_{(aq)}} \cdot 100 \quad \text{Eq. 6.1}$$

where C_i and C_f represent the initial and final metal concentration in the aqueous phase, respectively, and V_i and V_{IL} are the initial and the IL volume, respectively.

Table 6.2: Experimental parameters for determination of optimal extraction conditions, mechanism, and thermodynamics for Aliquat 336 and Cyphos 101.

Extraction				
Temperature (°C)	Acid conc. (M)	IL conc. (M)	Time (min)	Diluent
20, 30, 40, 50, 60, 70, 80	2	0.005	15	Toluene
20	0.01, 0.5, 1, 2, 3, 4, 5*	0.01	15	Toluene
20	2	0.001, 0.003, 0.007, 0.01, 0.03, 0.07, 0.1	15	Toluene
20	2	0.01	1, 2, 3, 4, 5, 7.5, 10, 15, 20, 30	Toluene
20	2	0.01	15	Pentane, hexane, heptane, cyclo- hexane, toluene
Extraction Mechanism				
Temperature (°C)	[Cl ⁻] (M)	[H ⁺] (M)	[IL] (M)	Time (min) - Acid conc. (M)-diluent
20	0.1, 0.5, 1, 2, 3	2	0.01	15- 2 - Toluene
20	2	0.05, 0.1, 0.5, 1, 2, 3, 4, 5	0.01	15- 2 - Toluene
20	2	2	0.001, 0.003, 0.007, 0.01, 0.03, 0.07, 0.1	15- 2 - Toluene
Extraction Thermodynamics				
Temperature (°C)	[Cl ⁻] (M)	[H ⁺] (M)	[IL] (M)	Time (min) - Acid conc. (M)-diluent
20, 30, 40, 50, 60, 70, 80	2	2	0.01	15- 2 - Toluene

All experiments were carried out with an organic to aqueous ratio of 1:1.

*: In the study of acid concentration, HCl, H₂SO₄, and HNO₃ were studied separately. The results showed that HCl presented the highest indium extraction rate, being selected as the leaching acid. All other experiments were carried out using hydrochloric acid.

6.2.3.1.2 Stripping

To determine the optimal conditions for the stripping step, a feed solution containing In (100 ppm) in 3M HCl was prepared as this acid concentration was observed to have the highest leaching capability to leach indium (Section 6.2.3.2.1). Once the ILs were loaded with indium, trials were carried out to test the stripping of the loaded IL phase with H₂SO₄ under different conditions (Table 6.3) where only one parameter at a time was changed while keeping the others constant. Sulphuric acid was selected as the stripping medium based on its performance in leaching indium as well as due to its

lower corrosivity. All stripping experiments were performed using equal volumes of IL and sulphuric acid at room temperature (20 ± 2 °C); with the effects of variation in the ratios studied only under conditions of 0.1 M H_2SO_4 for the 15 min trial. After stripping, the phases were separated by centrifugation at 3000 rpm for 10 min. After separation of the phases, the metal content was measured by taking 1 mL of sample diluted in 4 mL of 1M HNO_3 using ICP-OES. The stripping efficiency was calculated using the extraction eq. 6.1.

Table 6.3: Experimental parameters for determination of optimal stripping conditions

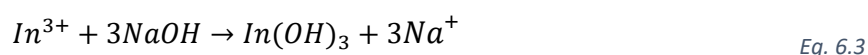
Acid conc. (H_2SO_4) (M)	Time (min)	$V(H_2SO_4):V(IL)$
0.1, 0.5, 1, 3, 5	15	1:1
0.1	5, 10, 15, 30, 45, 60, 90	1:1
0.1	15	1:1, 1.25:1, 1.5:1, 2:1, 2.5:1, 3:1

6.2.3.1.3 Reduction

Two methods were trialled to recover indium from the stripped solution of 0.1M H_2SO_4 to simulate the stripping reagent (with In (100ppm) in 0.1M H_2SO_4) namely, cementation with zinc to recover indium as powder, and precipitation using NaOH to recover indium oxide. Cementation tests were initially carried out and the effects of time (up to 5h) and stoichiometric ratio of Zn with respect to In (1.00 to 3.00) were investigated. The pH of the solution was maintained at 2 using a NaOH solution. After each stripping, the strip liquor from extraction and leaching of LCD panels was reused for further cementation analysis keeping the pH at 2 with NaOH solution. The In-Zn cementation reaction is:



Precipitation using sodium hydroxide was also trialled with a pH of 12, reported as the most effective, being maintained. A white powder of indium hydroxide was filtered, washed with RO water, and dried in an oven at 50 °C for 3h. The hydroxide was dehydrated by calcination at 500 °C for 3 h, to yield indium oxide. The precipitation and calcination reactions are:



6.2.3.1.4 Recovery of the IL

To study the recyclability of ILs the extraction process was carried out for five continuous cycles of extraction using a simulated solution of indium (100 ppm In solution in 2M HCl) under optimised conditions of O:A ratio of 1:1, 20 °C, and 15 min for indium extraction with 0.1 M IL (Aliquat 336 or Cyphos 101) in toluene, followed by stripping with 0.1 M H₂SO₄ under optimised conditions (V(H₂SO₄):V(IL)=1.5:1, 20 °C, and 15 min). After the stripping, the ILs were recovered for use in the next extraction cycle. Each experiment was carried out in triplicate. The recovered IL was characterised using FTIR following the extraction and stripping steps and ICP-OES was used to determine the metal concentration following each cycle. To further establish the integrity of the ILs following recycle, each IL alone was recycled (without the solvent) for 3 cycles using a leaching LCD panel's solution.

6.2.3.2 Pre-treatment of As-received LCDs

To establish the need, if any, for pre-treatment of as-received LCDs panels, a preliminary investigation was carried out to determine (i) the concentration of indium, and the presence of other metals in the as-received LCD panels, (ii) the location of the indium in the screen composition and the ability to leach indium without pre-treatment, (iii) the impact of feedstock as powdered LCD or strips of LCD to reduce the need for milling on leaching, (iv) a method to remove the polymeric film to provide access to an indium-rich source, and improve leaching capability; and (v) the effectiveness of leaching of indium following this pre-treatment step. This investigation made use of two key methods: *leaching* and the *removal of polymeric films* which are now described.

6.2.3.2.1 Leaching

Preliminary investigations involved the leaching of milled LCD powder to determine the concentration of indium and other metals and establish if a pre-treatment step is necessary. Leaching trials were carried out on the as-received LCD panels without polymer removal (*untreated LCDs*) to determine the optimum leaching conditions, and subsequently on treated LCD panels in both powder and strip form, following polymer removal, referred to in Section 6.3.2 as *pre-treated powder LCD panels* and *pre-treated strip LCD panels* respectively.

To determine the optimal leaching conditions milled LCD powder from as-received EoL MPs was subjected to acid leaching (HCl, H₂SO₄, and HNO₃) under the different experimental conditions, in terms of temperature, acid concentration, time, and solid:liquid ratio, listed in Table 6.4. In each experiment, only one parameter at a time was changed while keeping the others constant. For each

test, LCD powder (0.1 g) was added to an acid solution in a beaker containing a magnetic stirrer (500 rpm) to assist mixing and the beaker was placed on a heating plate for temperature control. After each test, the solution was centrifuged at a speed of 3000 rpm for 10 min. and the solution analysed for indium and other metals. A 1 mL sample of solution was diluted with 4 mL of 1M HNO₃ for analysis by ICP-OES. All measurements were recorded in triplicate. The leaching efficiency was obtained by:

$$\%L = \frac{C_{f,j} \cdot V}{m_j} \cdot 100 \quad \text{Eq. 6.5}$$

where $C_{f,j}$ represents the final concentration of element j (mg/L), V is total leaching volume (L), and m_j represents the total mass of element j (mg) in 0.1g of LCD powder. The total mass of the elements present in the LCD powder was determined using aqua regia digestion, as described in Section 3.2.3.1, Chapter 4. For consistency and accuracy, for each different LCD panel investigated, a metal analysis using an aqua regia digestion was made and the metal content in the as-received sample determined.

Table 6.4: Experimental parameters for determination of optimal leaching conditions.

Temperature (°C)	Acid concentration (M)	Time (h)	Solid/liquid ratio (g/mL)
20, 30, 40, 50, 60, 70, 80	1	2	1:20
20	0.1, 0.5, 1, 2, 3, 4, 5	2	1:20
20	1	0.5, 1, 2, 3, 4, 5	1:100
20	1	2	1:10, 1:20, 1:30, 1:50, 1:100

All experiments were carried out with an organic to aqueous ratio of 1:1.

HCl, H₂SO₄, and HNO₃ was studied first for indium leaching varying the temperature, resulting HCl and HNO₃ promising leaching reagent. Because of that, HCl and HNO₃ were further studied for indium leaching.

6.2.3.2.2 Removal of Polymeric Films

EoL-MP screens were first manually dismantled and separated into three component fractions: frames, polymeric films (composed by reflective films, diffuser sheets, and frame as showed in Figure 3.13, in Chapter 3), and LCD panels. To optimise the recovery of indium from the screens a pre-treatment step was required to provide access to the indium-rich source and improve leaching capability involving the removal of the polymeric films adhered to the glass substrate in the LCD panels.

As a first step to this pre-treatment, two methods were investigated to remove the polymeric films from the LCD panels. The first method involved soaking the disassembled LCD panels in acetone at room temperature (20 ± 2 °C) for 24 hours until the polarizers could be easily removed. The second

method involved a two-stage soaking of the disassembled LCD panels: the first in hot water at 80-90°C for 1h, after which the cellulose triacetate (CTA) and polyvinyl alcohol (PVA) films of the polarizers were peeled off manually with tweezers; followed by a second soaking of the panels in acetone at room temperature (20 ± 2 °C) for another hour to reduce the viscosity of the pressure-sensitive adhesive (PSA), allowing the final CTA films to be peeled off from the glass substrates. Different solid to liquid ratios (g of LCD panel/mL of solvent) were studied. The vessels used for the hot bath and the acetone bath were glass beakers and aluminium foil perforated with tiny holes was used to seal the vessels and reduce evaporation of the solvents. Both vessels were set up to operate with magnetic stirring at 500 rpm.

6.2.3.3 Development of an Optimised Process for Recovery of Indium from End-of-Life E-Waste LCD Panels

The conditions optimised for recovery of indium from a Model Test System were used to treat waste LCD leach liquor derived from pre-treatment of EoL Mobile Phone LCDs. The waste LCD leach liquor (5 mL) was mixed with an equal volume of organic (Aliquat 336 and Cyphos 101 in toluene) and aqueous phase using a mechanical shaker for 15 min to ensure equilibrium at room temperature (20 ± 2 °C). The McCabe-Thiele diagrams for the indium extraction from these leach liquor solutions using 0.1M Aliquat and 0.1M Cyphos 101 in toluene were constructed by varying the aqueous to organic ratio (A/O) from 1/ 5 to 5/1 keeping the total volume of phases constant to 10 mL. All measurements were made in triplicate and the results averaged.

6.2.3.4 Summary

The three-step approach to investigate development of an optimised process for recovery of indium from indium-rich sources in LCDs from EoL Mobile Phones using ionic liquids is elaborated further in Figure 6.3 in terms of process steps, the conditions tested, and the component fractions involved.

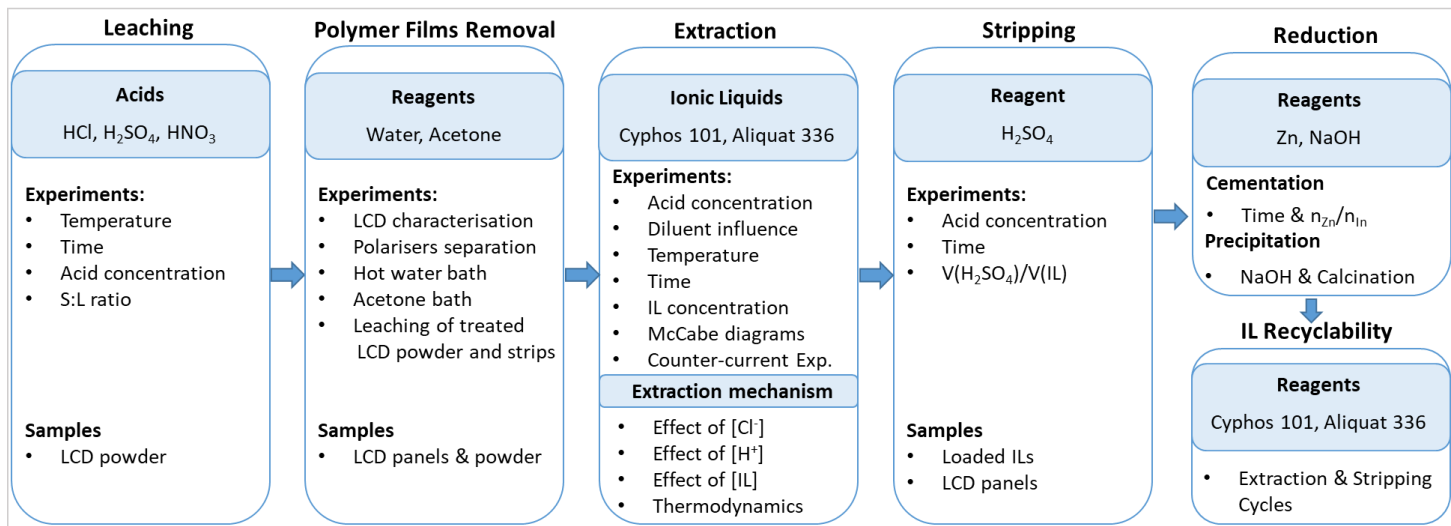


Figure 6.3: Overview of the experimental procedure applied in the development of an optimised process for indium recovery.

6.3 Results and Discussion

6.3.1 Optimised Conditions for Indium Extraction and Recovery Using a Model Test System

To determine the optimal conditions for recovery of indium from EoL MP-derived LCD screens a Model Test System was used in which an indium solution in hydrochloric acid was prepared to simulate an indium solution leached from pre-treated LCD samples. The extraction process using ionic liquids as solvent extraction media followed by a stripping and reduction step was developed, and the potential for recovery of the ionic liquids for recycle and reuse to minimise reagent use was investigated. The results of the optimised process steps are now described under the headings: *extraction of indium using the ionic liquids, stripping, reduction, and recovery of ILs.*

6.3.1.1 Extraction of Indium Using the Ionic Liquids: Aliquat 336 and Cyphos 101

6.3.1.1.1 Influence of different acids and their concentration on indium extraction

The effect of sulphuric acid, hydrochloric acid, and nitric acid on the extraction of indium from the Model Test solution of indium solution (100 ppm) was carried out using Cyphos 101 and Aliquat 336 diluted in toluene (0.01 M for both ILs) with varying acid concentration from 0.01M to 5M, is shown in Figure 6.4. In the case of Cyphos 101 (Figure 6.4a), HCl showed the highest extraction rates across the concentration range studied from 7.5% at 0.01M to 96% at 5M, showing an initial sharp increase in indium extraction in the range of 0.01M-2M of HCl, plateauing out at higher HCl concentrations. Sulphuric acid showed a low indium extraction, from 7% at 0.01M to 24% at 5M H₂SO₄. With nitric acid, indium extraction peaked at low acid concentration (11% at 0.5M) and remained below 10% extraction for higher concentrations of acid. Thus, indium extraction using Cyphos 101 at low acidity follows the order HCl>HNO₃>H₂SO₄, whilst at higher acidity the indium extraction follows HCl>H₂SO₄>HNO₃.

In the case of Aliquat 336 (Figure 6.4b), hydrochloric acid also displayed the highest indium extraction, followed by sulphuric and nitric acids. HCl showed a continuous increase in indium extraction, reaching 74% at 5M. H₂SO₄ and HNO₃ showed a slow and steady increase in indium extraction, reaching only 21% and 5% of In extraction, respectively. Although both of these acids performed better at concentrations below 0.5M, HCl performed better at concentrations ≥ 0.5 M. Thus, indium extraction by Aliquat336 at low acidity follows the order H₂SO₄>HNO₃>HCl and HCl>H₂SO₄>HNO₃ at higher acidity. The performance of both ILs was similar with HCl proving to be the most

promising acid for indium extraction and therefore it was used as the chosen acid medium in further trials.

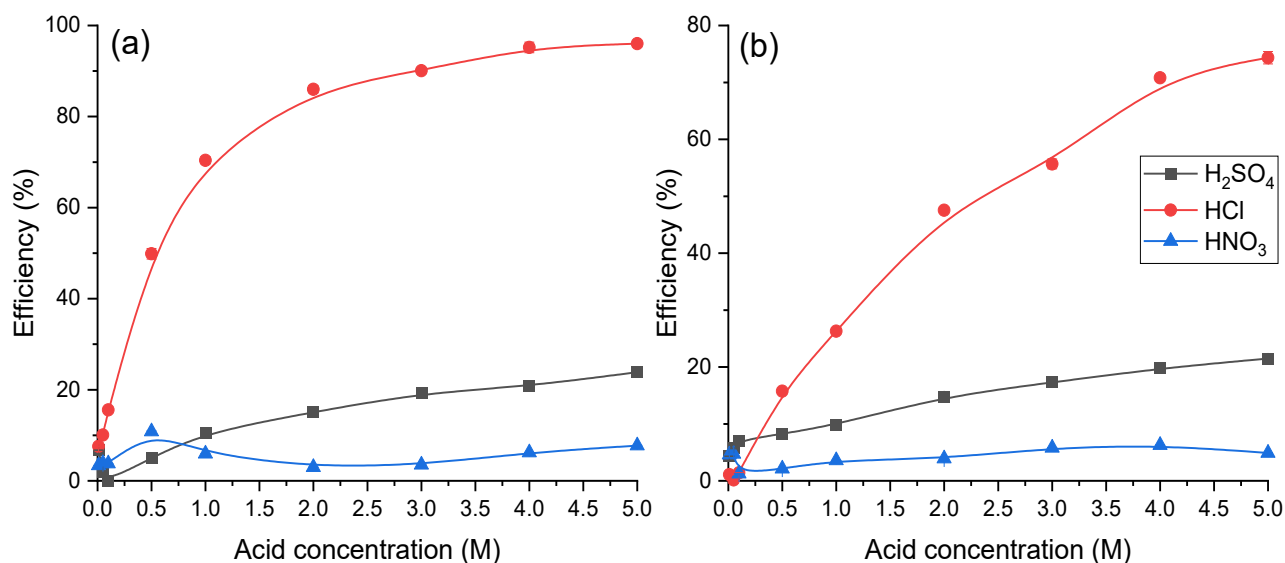


Figure 6.4: Effect of different acids in the indium extraction with; (a) Cyphos 101 and (b) Aliquat 336.

6.3.1.1.2 Influence of the diluent

The influence of five diluents; pentane, hexane, heptane, cyclohexane, and toluene on the extraction of indium using Cyphos 101 and Aliquat 336 was studied, and the results are presented in Figure 6.5. The diluents were selected based on the fact that low polarity diluents can favour the formation of hydrogen bonds and other secondary bonding between the extractant molecules, which interactions can contribute to the strength and selectivity of an extractant [211]. Furthermore, diluents with high dielectric constant such as n-butyl alcohol, cyclohexanone, etc. can present strong interactions between diluents and phosphonium/ammonium extractants, leading to low extraction rates [156]. In the case of Cyphos 101, there was no noticeable difference in indium extraction between the diluents, with extractions in the range of 84-86%, dipping just below to 80% for cyclohexane. In the case of Aliquat 336, poor extraction levels were achieved with all diluents except toluene which showed an extraction of 48%. Based on the results, toluene was selected as the diluent for further studies.

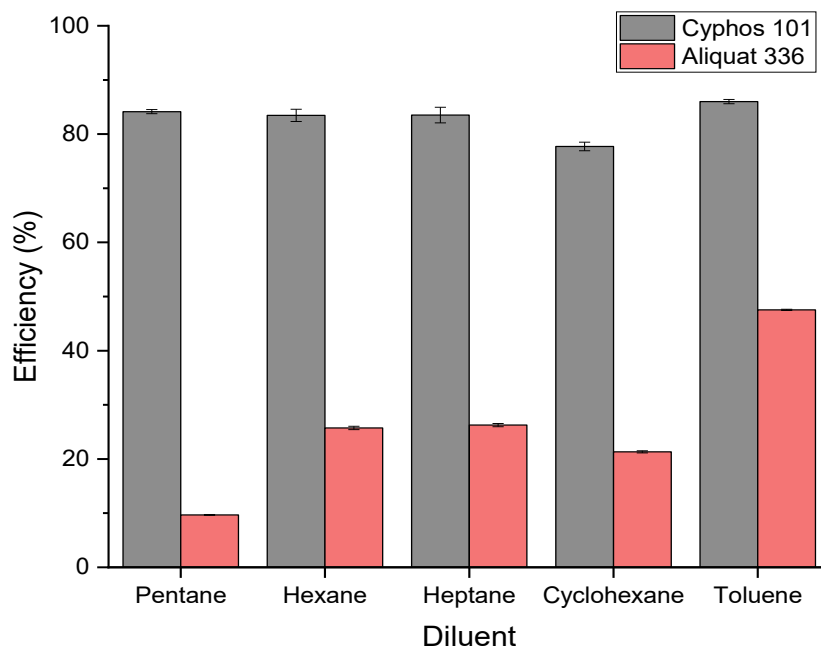


Figure 6.5: Effect of different diluents in the indium extraction.

6.3.1.1.3 Effect of the time, temperature, and IL concentration

The effect of time, temperature, and IL concentration on indium extraction was studied and the results are presented in Figure 6.6. The time required to achieve equilibrium, trialed in the time range from 1 min. to 30 minutes (Figure 6.6a), was rapid (and achieved in 3 mins) for both ILs, with indium extractions of 75% and 85% for Aliquat 336 and Cyphos 101, respectively. To ensure equilibrium was attained, a time of 5 minutes was selected for further experiments. The effect of the temperature on indium extraction is shown in Figure 6.6b. The general trend is that the higher temperature, the higher the indium extraction. In the case of Cyphos 101, the extraction increases from 61% at room temperature (20 °C) to 71% from 60 °C up to 80 °C. In the case of Aliquat 336, a constant upward trend in the extraction was observed from 34% at 20 °C to reach 58% at 80 °C. The increase in indium extraction is likely due to a decrease in the viscosity of the ILs with increasing temperature; as viscosity is inversely proportional to the temperature, which favours the mass transfer [156]. This result suggests that 60 °C and 80 °C are the optimal temperatures for indium extraction with Cyphos 101 and Aliquat 336, respectively. It was noted that in the case of Cyphos 101, the indium extraction increased by only 10% from 20 °C to 80 °C, so to reduce the energy consumption in the process room temperature was selected. The influence of the IL concentration, from a range of 0.001M to 0.1M, on indium extraction was investigated and the results are presented in Figure 6.6c. The results show a sharp increase in the indium extraction at low IL concentrations (0.001M-0.01M) for both ILs, with limited change in extraction when concentrations were used. The indium extraction using Cyphos 101 increased from 20% at 0.001M to 99% at 0.1M, reaching a plateau at 0.07M (>97%

extraction). In the case of Aliquat 336, the indium extraction increased from 18% at 0.001M to 82% at 0.1M and no plateau was observed. Under the different conditions investigated (Figure 6.6), the IL, Cyphos 101 performed better than Aliquat 336, showing a greater affinity for In(III). This can be explained in terms of the lower water uptake of Cyphos 101 (13.7%) compared to Aliquat 336 (21.3%), which allows more molecules in Cyphos 101 to interact with indium. In ILs with a common anion, the hydrophobicity depends on the total number of carbon atoms in the alkyl chain attached to the corresponding central atom, thus the larger alkyl chains attached to the phosphonium cation core contributes to the higher hydrophobicity (and lower miscibility with water) of Cyphos 101 compared to Aliquat 336. Moreover, the charge delocalization at the ammonium cations of Aliquat 336 makes the central part of these cations more highly charged, and consequently more polar, than the corresponding phosphonium cations which favours the interaction with water [215].

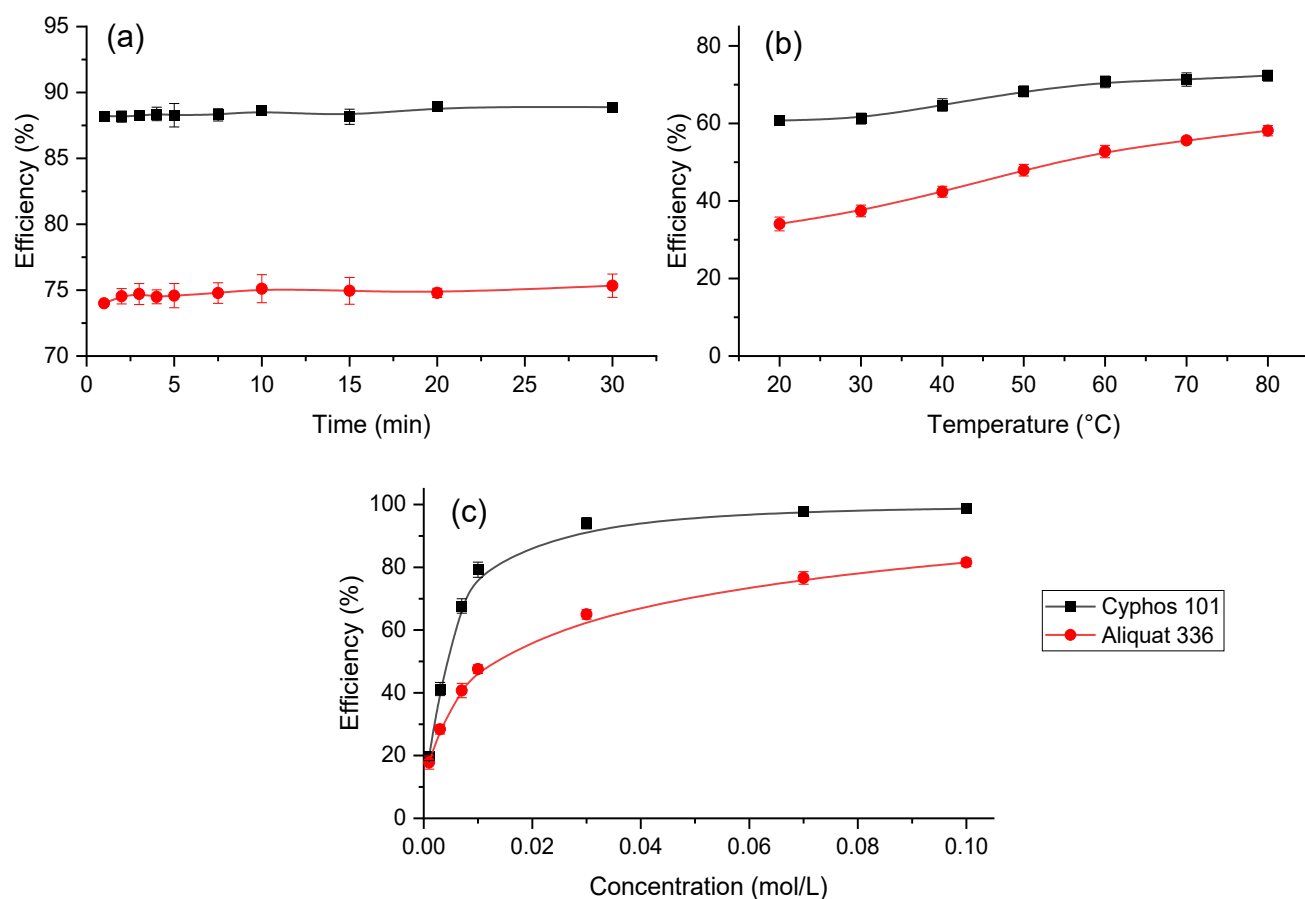
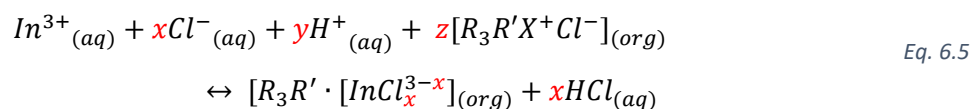


Figure 6.6: Effect of the indium extraction in (a) time, (b) temperature, and (c) IL concentration.

6.3.1.2 Extraction mechanism of indium

To determine the mechanism of indium extraction, detailed studies were carried out using HCl as the acid medium, selected as the best medium for indium leaching, as reported in Section 6.3.2.1.1. The In(III) extraction from acidic chloride solution by the ILs in equilibrium can be expressed by the following reaction:



where x and y represent the number of hydrogen and chloride ions in the complex formation, respectively; and z is the number of extractant molecules utilised in the extraction. Subscripts (aq) and (org) indicate the aqueous and organic phases, respectively. $\text{R}_3\text{R}'\text{X}^+$ represents the tetradecyl(trihexyl)phosphonium group in Cyphos 101, and $\text{R}_3\text{R}'\text{X}^+$ represents the trioctylmethylammonium in Aliquat 336.

The equilibrium constant of the above reaction is given by:

$$K_{eq} = \frac{[\text{R}_3\text{R}' \cdot \text{InCl}_x^{3-x}]_{(org)}}{[\text{In}^{3+}]_{(aq)} \cdot [x\text{Cl}^{-}]_{(aq)} \cdot [y\text{H}^{+}]_{(aq)} \cdot z[\text{R}_3\text{R}'\text{X}^+\text{Cl}^{-}]_{(org)}} \quad \text{Eq. 6.6}$$

The distribution ratio D of indium in the organic and aqueous phases ($\text{In}_{org}/\text{In}_{aq}$) during the extraction process can be expressed as:

$$D = \frac{[\text{In}]_{(org)}}{[\text{In}]_{(aq)}} = \frac{[\text{R}_3\text{R}' \cdot \text{InCl}_x^{3-x}]_{(org)}}{[\text{In}^{3+}]_{(aq)}} \quad \text{Eq. 6.7}$$

Replacing Eq. 6.8 in Eq. 6.7, the equilibrium constant can be expressed as:

$$K_{eq} = \frac{D}{[x\text{Cl}^{-}]_{(aq)} \cdot [y\text{H}^{+}]_{(aq)} \cdot z[\text{R}_3\text{R}'\text{X}^+\text{Cl}^{-}]_{(org)}} \quad \text{Eq. 6.8}$$

Applying the logarithm and rearranging the terms in Eq. 6.9, the logarithm of the distribution ratio can be expressed as:

$$\text{Log}(D) = \log(K_{eq}) + x\log([\text{Cl}^{-}]_{(aq)}) + y\log([\text{H}^{+}]_{(aq)}) + z\log([\text{R}_3\text{R}'\text{X}^+\text{Cl}^{-}]_{(org)}) \quad \text{Eq. 6.9}$$

Thus Eq. 6.10 can be used to determine the effect of chloride ions, hydrogen ions and IL molecules in the indium extraction. Varying one parameter, whilst keeping the others constant, the contribution of each factor on the indium extraction can be deduced.

6.3.1.2.1 Effect of the chloride ion concentration

To investigate the effect of chloride ion concentration on the indium extraction, the concentration of chloride ions was adjusted in the feed solution with the addition of NaCl, while keeping the hydrogen ion concentration constant with a 100ppm In solution in 1M HCl. Each IL was diluted in toluene. The chloride ion concentration was varied from 0.1 M to 3.0 M. Figure 6.7 presents the plot of logD versus log[Cl⁻], which gives a straight line by linear fit with high R² values (>0.98 for both ILs), suggesting a good agreement between the variables. For both ILs, the increase in the chloride concentration was reflected as a rise in indium extraction. In the case of Cyphos 101, the indium extraction increased from 23% to 53% at 0.1M and 3M Cl⁻, respectively, whilst with Aliquat 336, the In extraction showed a more marked increase from 15% to 49% at 0.1M and 3M Cl⁻, respectively. Aliquat 336 and Cyphos 101 are basic extractants (anion exchangers), and their extraction driving force is the presence of chloride anions [215]; unsurprisingly therefore with the increase in the Cl⁻ concentration an increase in the IL extraction is observed. The slopes for the linear fittings were calculated as 2.787 for Cyphos 101 (Figure 6.7a) and 2.668 for Aliquat 336 (Figure 6.7 b). These numbers suggest that in the formation of the extracting species for indium, 3 chloride ions are likely incorporated in for Cyphos 101 and Aliquat 336.

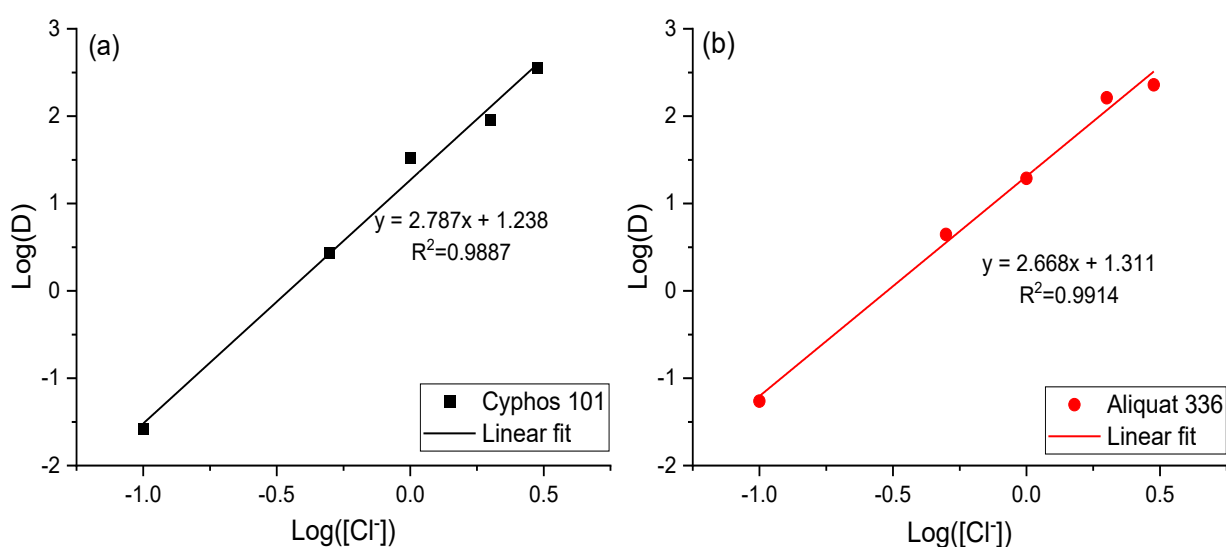


Figure 6.7: Effect of the Cl⁻ concentration on indium extraction.

6.3.1.2.2 Effect of the hydrogen ion concentration

The effect of hydrogen ion concentration on the distribution of indium extraction was investigated by adding a calculated amount of H_2SO_4 , to maintain the concentration of HCl at 1M. Sulphuric acid was selected over nitric acid due to the presence of two molar hydrogen ions per mole of acid. Figure 6.8 shows a $\log D$ versus $\log[\text{H}^+]$ graph with the linear fit of the experimental result (R^2 values >0.97 for both ILs), suggesting that one mole of hydrogen-ion participates in the indium extraction with Cyphos 101 and Aliquat 336.

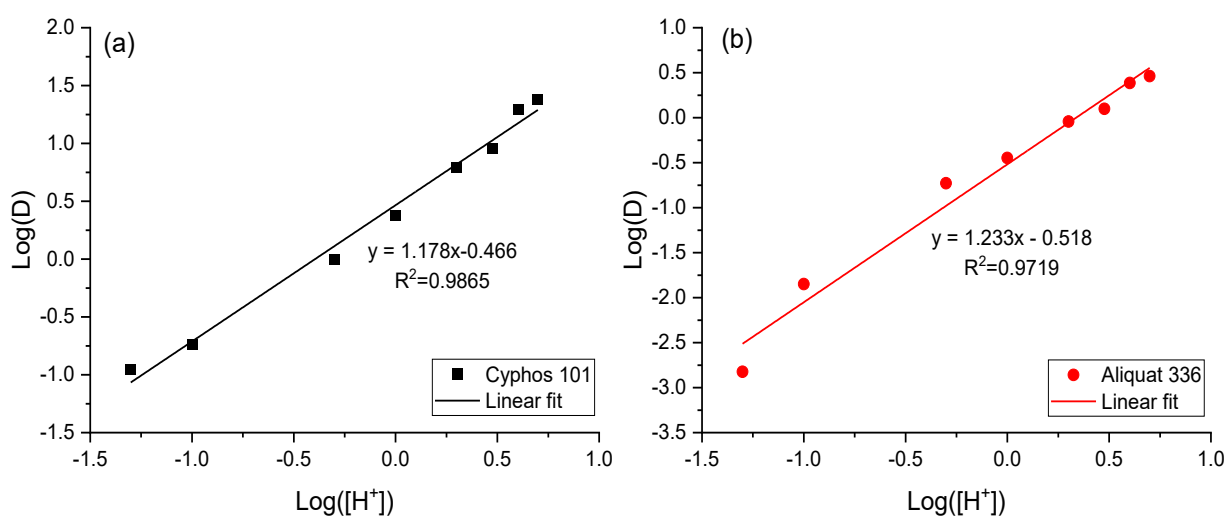


Figure 6.8: Effect of the H^+ concentration on indium extraction.

6.3.1.2.3 Effect of the ionic liquid concentration

The influence of the IL concentration on the extraction of indium from a solution of 100 ppm In in 1M HCl was carried out by varying the IL concentration in a range of 0.001M-0.1M. The ILs were diluted in toluene. Figure 6.9 shows a log-log plot of D and the IL equilibrium concentration with linear fits to the experimental data which had high R^2 values (>0.99 for both ILs), indicating a good linear regression. The slope of the linear fit of 0.78 for Cyphos 101, implies the involvement of one mole of extractant per one mole of the metal ion, suggesting the formation of 1:1 complex between indium ions and Cyphos 101, and in the same way, for Aliquat 336, the slope of 1.314, suggests the formation of 1:1 complex between indium ions and the IL.

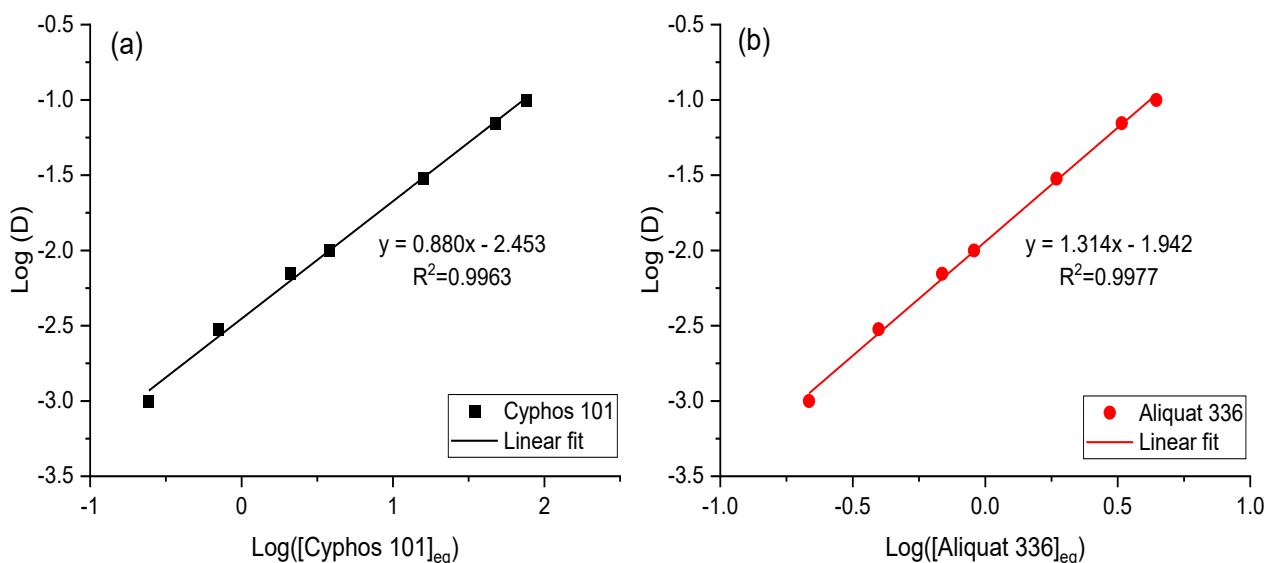
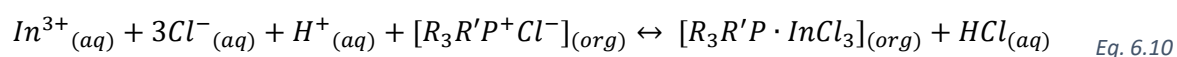


Figure 6.9: Effect of the IL equilibrium on indium extraction.

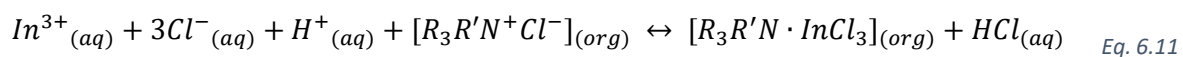
6.3.1.2.4 Proposed indium extraction mechanism

Based on the studies investigating the effect of ionic liquid concentration, chloride ion concentration, and hydrogen ion concentration on the indium extraction by Cyphos 101 and Aliquat 336, diluted in toluene, the following extraction mechanisms are proposed. The proposed mechanisms are supported by the slope values obtained in the respective plots from Figure 6.7 (Cl^- ion concentration), Figure 6.8 (H^+ ion concentration), and Figure 6.9 (IL concentration).

Extraction of indium by Cyphos 101:



Extraction of indium by Aliquat 336:



where $\text{R}_3\text{R}'\text{P}^+$ = Tetradecyl(trihexyl)phosphonium (for Cyphos 101), and $\text{R}_3\text{R}'\text{N}^+$ = Trioctylmethylammonium (for Aliquat 336).

6.3.1.2.5 Thermodynamics parameters of indium extraction

The results presented in Figure 6.6b, show temperature to have a considerable effect on the extraction of indium, with a more pronounced rise in the indium extraction with Aliquat 336 than Cyphos 101. In Figure 6.10 the effect of temperature on the thermodynamics of indium extraction is expressed showing the values of $\log(D)$ of In vs $1000/\text{temperature}$ in the range of 20 °C to 80 °C. Extractions were carried out using 100 ppm In in 1M HCl and 0.005M IL with A/O=1/1. Based on earlier tests using a higher concentration (0.01M IL) any effect was masked so a lower IL concentration of 0.005M was used to permit a wider range of extraction available for variation with increase in temperature. The thermodynamics parameters ΔH , ΔG and ΔS were determined by using the following equations [156]:

$$\log(D) = \frac{-\Delta H}{2.303 \cdot RT} + C \quad \text{Eq. 6.12}$$

$$\Delta G = -2.303 \cdot RT \cdot \log(D) \quad \text{Eq. 6.13}$$

$$\Delta G = \Delta H - T\Delta S \quad \text{Eq. 6.14}$$

where D refers to distribution ratio, C refers to constant of integration and R is gas constant with a value of 8.314 J/mol·K.

Using the slope and intercept values derived from Figure 6.10 and equations 6.13-6.15, the values for ΔH , ΔS and ΔG are calculated and presented in Table 6.5. The positive values of the enthalpy and entropy suggest that the indium extraction is endothermic, and entropy driven in nature, respectively. On the other hand, the negative value of the Gibbs free energy indicates that the indium extraction is a spontaneous process. The enthalpy of Cyphos 101 (10.9 KJ/mol·K) was lower than the Aliquat 336 (13.0 KJ/mol·K), indicating that Cyphos 101 requires less energy for the extraction, which can favour the process. The Gibbs free energy was considerably lower in Cyphos 101, suggesting a more spontaneous process which is likely the reason of the higher extraction rate observed with Cyphos 101.

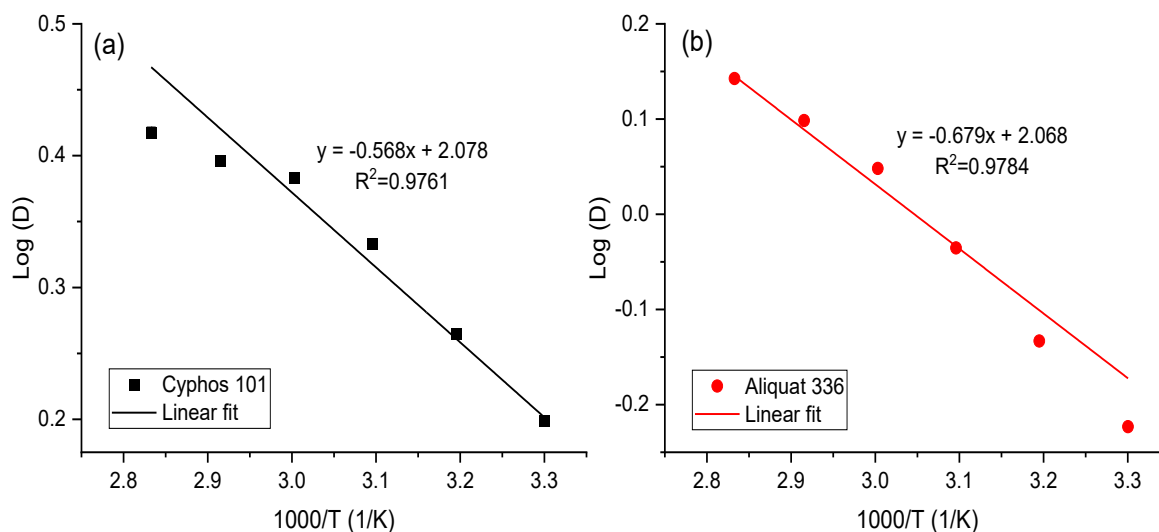


Figure 6.10: Effect of the temperature on the thermodynamics parameters of indium extraction.

Table 6.5: Thermodynamics parameters of indium extraction.

ΔH (kJ/mol·K)	ΔG (kJ/mol)	ΔS (kJ/ mol·K)
Cyphos 101		
10.9	-2110.6	6.6
Aliquat 336		
13.0	-704.9	2.2

6.3.1.2.6 Discussion

Previous authors have reported that indium extraction with different extractant can be achieved within 5 minutes [156, 235, 239, 246-248], and even within 30 seconds [239]. In this work however a contact time of between 5 and 15 minutes was chosen to ensure complete extraction. The fast extraction of indium is due to a very strong affinity for the extractant. Deferm et al. found that undiluted Aliquat 336 and Cyphos 101 can achieve indium extraction equilibrium after 10 minutes [215]. In the current research equilibrium was reached within 8 minutes using undiluted Aliquat 336 and Cyphos 101, but the viscosity of the ILs then presented a major problem for separation and handling in the further stages of the recovery process.

Regarding the mechanism for indium extraction, it was found that in the case of Cyphos 101, that the extraction involved one mole of the Cyphos 101, 3 moles of Cl^- , and one mole of H^+ per mole

of In^{3+} , whereas in Aliquat 336, the extraction per mole of In^{3+} extracted involved 1-2 moles of Aliquat 336, 3 moles of Cl^- , and 1-2 moles of H^+ . Deferm et al. reported that In^{3+} in chloride medium can be present in different forms, where some species are dominant over others at different HCl concentrations [235]. They found that at low HCl molarities ($< 1\text{ M HCl}$), the dominant species is $[\text{In}(\text{H}_2\text{O})_4\text{Cl}_2]^+$, changing to a neutral $[\text{In}(\text{H}_2\text{O})_4\text{Cl}_3]$ complex at HCl concentrations between 1 and 6 M HCl, whereas at higher HCl molarities (6-10 M HCl), the predominant species is $[\text{In}(\text{H}_2\text{O})_2\text{Cl}_4]^-$, and at very high HCl concentrations (10-12 M HCl), $[\text{In}(\text{H}_2\text{O})\text{Cl}_5]^{2-}$ is the dominant form of dissolved indium [235]. The current work was carried out using 2 M HCl, where the neutral $\text{In}(\text{H}_2\text{O})_4\text{Cl}_3$ should be the dominant species in the aqueous phase solution. This is in good agreement with the mechanism proposed, where 3 moles of Cl^- were involved in both mechanisms, which is consistent with the predominant neutral $\text{In}(\text{H}_2\text{O})_4\text{Cl}_3$ species at that HCl concentration. Deferm and co-authors also studied indium extraction using Cyphos 101 and Aliquat 336 in a chloride medium, reporting that each indium ion is extracted by one molecule of each IL [235], confirming the results found in the current study. The focus of their work, however, was only on understanding the mechanism of IL extraction and not the whole extraction mechanism, as determined here in this work. Nayak and Niharbala studied the extraction of indium from aqueous chloride medium using Cyphos 104, finding that the mechanism involved the formation of a 1:1 complex between In^{3+} and Cyphos 104, including four Cl^- and one H^+ [236]. Dhiman and Gupta, who also studied the mechanism of indium extraction by Cyphos 104 in HCl solution, however, reported the formation of a 1:2 complex between In^{3+} and Cyphos 104, involving three chloride ions [156]. The differences in complex formation and chloride ion representation observed in these two studies using Cyphos 104 as the extractant for indium, despite the fact that both studies were carried out at similar temperatures (25-27 °C) and used similar chloride medium (1-3 M HCl), suggesting the dominance of neutral $[\text{In}(\text{H}_2\text{O})_4\text{Cl}_3]$ species, can only be explained in terms of the interpretation of the slope value of the linear fit used for the determination of the indium-Cyphos 104 complex. In the 1:1 complex formation, the slope was 0.9357, whilst in the 1:2 complex the slope obtained was 1.68. The 1.68 slope suggested the formation of 1:2 complex, however, it was not that clear. In this study, the linear fit slope of the indium-ILs complex result from Figure 6.9 was 0.880 and 1.314 for Cyphos 101 and Aliquat 336, respectively. These slopes have values closer to one than two, consistent with the 1:1 indium-IL complex proposed.

6.3.1.3 *Stripping*

The stripping of indium from the organic phase and the regeneration of the organic phase for recycle and reuse are crucial steps for a sustainable separation process. Based on the acid leaching behaviour for extraction of indium observed in this work and reported later in this chapter in Figure 6.17 and Figure 6.18 (under Section 6.3.2), the variation of the acid concentration affects the indium extraction from the IL. Whilst it was found that HCl and H₂SO₄ could each be used as potential extractant reagents (in the stripping process) because of their high leaching efficiencies, due to ease of handling and the less corrosive properties of H₂SO₄, this acid was chosen. The effect of varying the acid concentration on the extraction of indium from the IL phase, was therefore examined and the results are presented in Figure 6.11. It was revealed that indium can be stripped at low H₂SO₄ concentration (0.1-0.5M) in both ILs. In the case of Aliquat 336, indium can also be completely stripped at 1M of H₂SO₄. At higher acid concentrations, the stripping of indium was considerably reduced, especially for Cyphos 101 with stripping efficiencies of 7.5% and 0.5% at 3 M and 5 M of H₂SO₄, respectively. The stripping of Aliquat 336 at higher H₂SO₄ concentration was not as pronounced as with Cyphos 101, stripping 70% and 18% at 3M and 5 M of H₂SO₄, respectively. The decrease in indium stripping at higher H₂SO₄ concentration could be due to the addition of ions into the solution, which increases the ionic strength, promoting complex formation between Cl⁻ and In³⁺ present in the solution. Thus, the re-extraction of indium into the ILs is faster than the stripping. For environmental reasons and for ease of reagent use, therefore, a 0.1 M of H₂SO₄ was selected as the stripping agent at room temperature (20 °C).

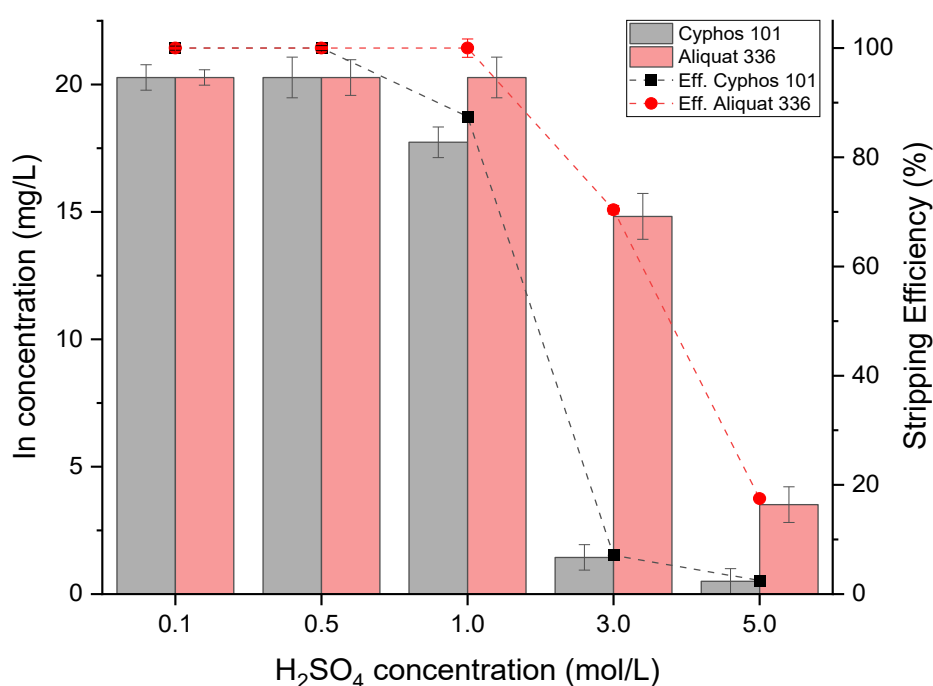


Figure 6.11: Indium stripping at different H₂SO₄ acid concentration

To determine the optimal conditions required for indium stripping, a simulated indium solution with a concentration equivalent to that obtained in the extraction step (33 g/L) in 0.1M H₂SO₄ was investigated as a function of time and the results are shown in Figure 6.12a. The stripping process reaches equilibrium within 30 minutes at 150 rpm, however analysis showed that not all indium was stripped from the simulated solution. Thus, further stripping tests were carried out to determine the impact of increasing the volume of the stripping solution (adjusting the stripping agent to IL ratio), as observed in Figure 6.12b. The stripping agent to organic ratio (V(H₂SO₄)/V(IL)) of 1:1 stripped approximately 75% of In, and an increase of 25% of the stripping volume can strip up to 95% of the indium. An V(H₂SO₄)/V(IL) of 1.5/1 can effectively strip indium from both organic phases, without the need for larger volumes of 0.1M H₂SO₄ solution. Therefore, the conditions of the stripping solution (0.1M H₂SO₄) selected were a V(H₂SO₄)/V(IL) ratio of 1.5:1, 150 rpm, and 30 minutes.

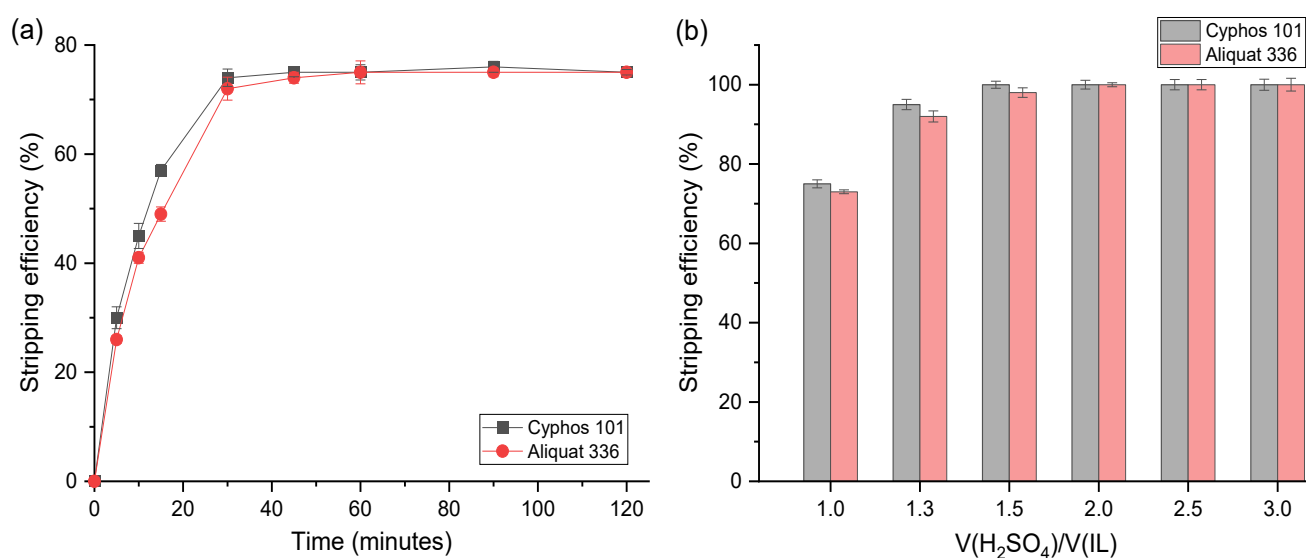


Figure 6.12: Indium stripping from simulated solution; (a) effect of time, and (b) effect of stripping solution volume.

6.3.1.4 Reduction

The recovery of indium from stripped solution (0.1M H₂SO₄) was trialed using two methods: cementation with zinc to recover indium powder, and precipitation, using NaOH to recover indium oxide following calcination at 500 °C for three hours. The trials were carried out using in a 100 ppm In solution in 0.1M H₂SO₄ (as the stripping agent) to determine the optimal conditions for reduction.

6.3.1.4.1 Cementation

To separate indium from the stripping agent, the indium cations need to be reduced. Cementation relies on the addition of metals with lower reduction potentials compared to indium, causing the indium ions to be reduced. Whilst there are several candidate metals that could be used for cementation, zinc, which has been widely used in the recovery processes of indium on a commercial scale, was selected for this study. The effect of time and amount of zinc on the cementation of indium from simulated solutions was studied, and the results presented in Figure 6.13. The amount of zinc or excess of Zn was calculated as the stoichiometric moles excess Zn/In based on Eq. 6.2. The effect of time (Figure 6.13a), where an excess of 1.5 of Zn was used, shows that the cementation is a relatively slow process, compared to the process times involved in the leaching, extraction, and stripping steps. The cementation reached an equilibrium within 4 hours. The stoichiometric moles excess Zn/In (Figure 6.13b) showed that in 4 hours, the stoichiometric reaction reached 85% of conversion, cementing 92% and 96% of indium at moles excess of 1.25 and 1.5, respectively. From an excess of 1.75 onwards of Zn, 100% of In was cemented. Thus, a time of 4 hours and ratio of 1.5 n_{Zn}/n_{In} were selected as the optimum conditions for the recovery of indium.

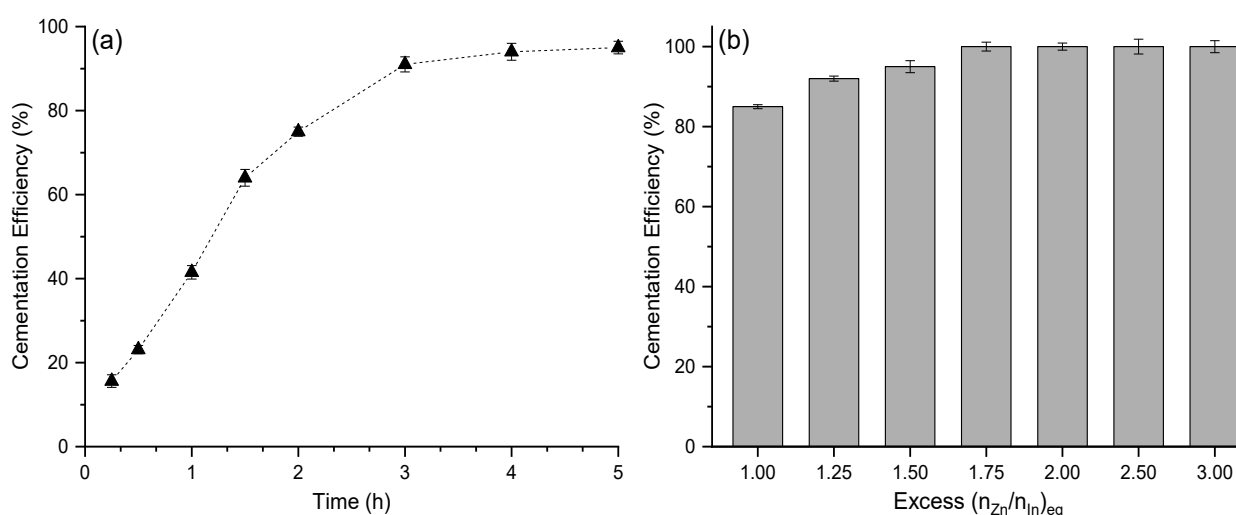


Figure 6.13: Indium recovery from 0.1M H₂SO₄ by cementation; (a) effect of time, and (b) effect of stoichiometric excess Zn moles/In moles.

Previous cementation studies done in this research, however, carried out on real stripped solutions showed that 4 h and 1.5 n_{Zn}/n_{In} conditions were found not to be sufficient to recover all the indium. This is likely due to tests being carried out on simulated solutions with indium present as the only metal. Furthermore, it was found that agitation plays a crucial role. In the simulated solutions, a vortex shaker was used, whereas with real samples, agitation was carried out using magnetic stirrers, which create lower agitation conditions. Due to this, a molar excess n_{Zn}/n_{In} of 2 was used. With this higher ratio, the cementation of indium from stripped solution was complete, recovering 98.5% indium. Indium recovered by cementation has benefits such as simple operation, low energy consumption, and low cost.

6.3.1.4.2 Precipitation

The second method for indium recovery from the stripping solution was the use of precipitation by NaOH. The effect of the pH in the precipitation of indium by NaOH has been widely studied, reporting the highest precipitation rates at pH 12 [156, 239]. Thus, the pH of the solution was maintained at 12 by adding NaOH. A white precipitate ($In(OH)_3$) was obtained, which was filtered, washed with RO water, and dried at 50 °C in an oven for 3 h. Thermogravimetric analysis of indium hydroxide in the temperature range of room temperature to 1000 °C, showed that the hydroxide is completely dehydrated at 400 °C [239]. On this basis to ensure the formation of indium oxide, the filtered product was calcined at 500 °C for 3 h. Figure 6.14 shows SEM-EDS images of the indium oxide obtained from precipitation of indium by NaOH, followed by a calcination. In the SEM image (Figure 6.14a), it can be observed that indium oxide is present in its characteristic rhombohedral shape. EDS image (Figure 6.14b) confirms that the yellow powder obtained is composed mainly of indium and oxygen.

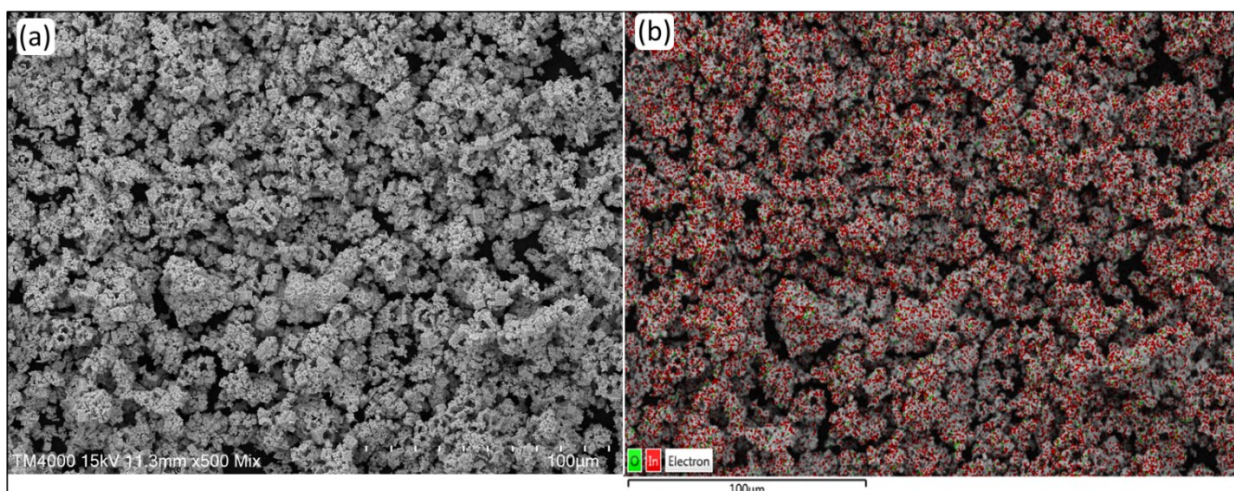


Figure 6.14: Indium oxide obtained by precipitation of In by NaOH; (a) SEM, and (b) EDS images.

6.3.1.4.3 Discussion

The recovery of indium was achieved by two methods; cementation, and precipitation followed by calcination. The final product obtained were indium from cementation and In_2O_3 from precipitation followed by calcination. From data contained in Table 6.8 (presented at the end of Section 6.3.2) compiled from the literature as part of this study, the two methods of cementation and precipitation are the most used for indium recovery due to simplicity of the processes and high efficiency rates achieved. Although indium is recovered, any industrial process developed would need to consider, as an additional step, treatment of the wastewater generated; in the case of cementation, the stripping solution is saturated with zinc, whereas in the precipitation, it is saturated with sodium. Hence, new alternatives should be explored. Alternatively, electrodeposition of indium can be used. Song et al. reported a two-step electrodeposition, using platinum and carbon rod as electrodes, from leach liquor from LCD monitors (previously treated by manual dismantling, pyrolysis and ball milling). The first electrodeposition was copper, followed by indium electrodeposition [253]. Grimes et al. described an In, Sn and Pb separation process involving a novel three-stage electrodeposition, using a novel cylindrical mesh electrode electrolysis cell, from nitric acid media from dilute indium-tin-lead solutions. Under optimised conditions, 97%, 94% and 98% recovery can be achieved for Sn, Pb and In, respectively [254]. Electrodeposition offers an excellent alternative for the recovery of indium in this work, as the stripping solution contains predominantly indium with minimal impurities, and so recovery of a pure metal is possible. Preliminary trials using electrowinning of the type described in Chapter 4 of this work were made to recover indium but due to time constraints and limited supply of LCD panels to achieve a sufficiently rich indium source no further experiments were carried out. A recommendation for further work in this area, however, is made at the end of this thesis.

6.3.1.5 Recovery of ILs

To ensure an optimised process is designed that conserves the use of reagents and mitigate costs, the potential to recover and recycle the ILs, through the indium recovery process developed, was investigated. The ILs should be chemically stable throughout and retain high efficiencies after indium extraction and stripping. To evaluate the recyclability of Cyphos 101 and Aliquat 336, five cycles through the whole process were performed. The results in Figure 6.15 show the extraction, stripping and the overall efficiencies over five cycles of indium recovery under optimised conditions (0.1M ILs for extraction and 0.1M H₂SO₄ for stripping, both processes at 20°C and 300 rpm). The extraction and stripping of indium remained largely unaffected over five cycles, suggesting that Cyphos 101 and Aliquat 336 can be successfully reused without any loss in efficiency. In addition, the total efficiency of indium recovery remains >95% in each cycle.

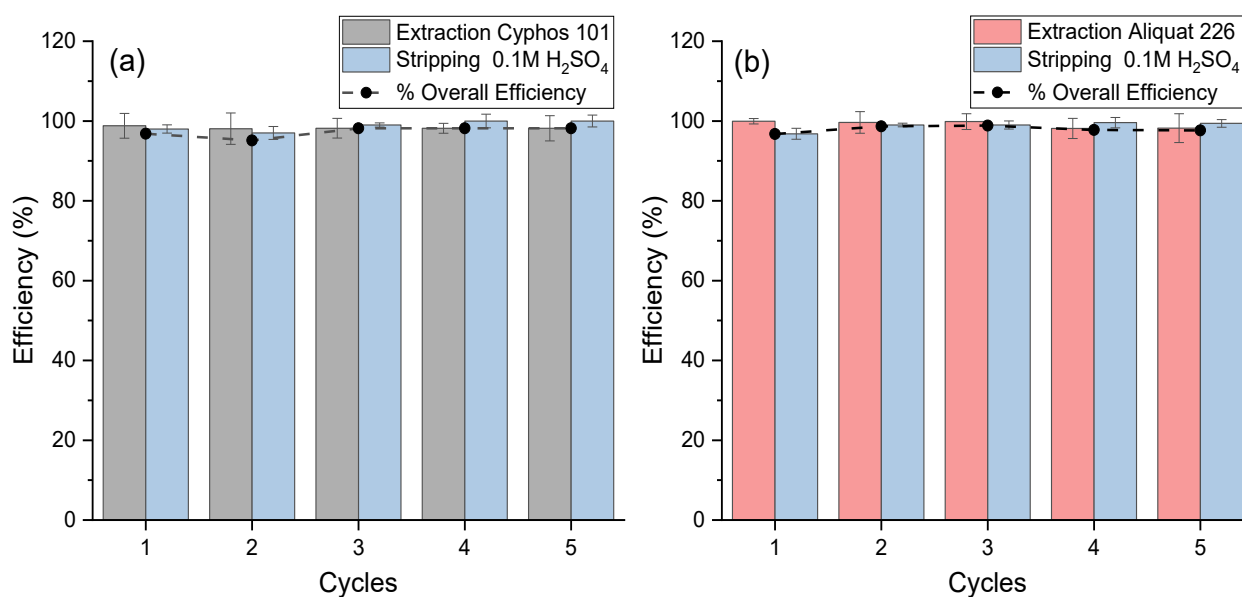


Figure 6.15: Efficiencies of extraction and stripping over 5 cycles: (a) Cyphos 101, and (b) Aliquat 336.

To check the integrity of the ILs was not affected through the recycle and reuse process, FTIR was used to record any changes in the structure of the ILs, following each cycle. Figure 6.16a shows the FTIR spectra of toluene, 0.1M Cyphos 101 and 0.1M Aliquat 336, both diluted in toluene. The FTIR spectra showed that Cyphos 101 and Aliquat 336 modified the toluene spectra, where several peaks were observed, however, the fingerprint of toluene at 500-1500 cm⁻¹ is preserved. Both ILs solutions presented 3 different zones. Zones 1 and 3 are associated with noisy spectra due to the fast volatilization of toluene. Changes in the analysis were carried such as performing the sample

measurement as soon as possible after the background measurement, decreasing the numbers of scans, however, results were very similar. The FTIRs after extraction and stripping over 5 cycles did not show any noticeable difference between the reference (virgin 0.1M IL in toluene) and the used ILs solutions. Due to the low IL concentration, the FTIR patterns were mostly characteristic of the toluene pattern, and the characteristic wavenumbers of Cyphos 101 and Aliquat 336 were not easily observed, thus the result was not clear whether the ILs had suffered any degradation or not. Therefore, to study the effect of the indium extraction and stripping on the ILs, experiments with pure Cyphos 101 and Aliquat 336 were carried out. The ILs were used in 3 cycles and the FTIR patterns after extraction and stripping are shown in Figure 6.16b and c.

In Cyphos 101 (Figure 6.16b) three different zones can be seen. The first zone, with a wide peak at 3407 cm^{-1} , which corresponds to -OH stretching, suggesting the existence of water, which has probably remained after the washing of the IL after each cycle. In the second zone, there is a peak in the range of $1550\text{-}1700\text{ cm}^{-1}$, which can be associated with a C=O stretch. The most significant change observed in the third zone ($500\text{-}1100\text{ cm}^{-1}$), which is the fingerprint zone, was not associated with the presence of new peaks, but simply a change in intensity of the peaks. It was inferred therefore that degradation of the IL through the cycles was unlikely. In the case of Aliquat 336 (Figure 6.16c), two different zones can be observed. The first zone, with a wide peak at peak at 3407 cm^{-1} is due to the existence of water, similar peak was found in Cyphos 101. The most significant change is in the second zone ($800\text{-}1260\text{ cm}^{-1}$), where peaks at 1185 cm^{-1} , 1046 cm^{-1} and 862 cm^{-1} can be associated with the symmetrical vibration of SO_4^{2-} group, suggesting that sulphate ions, coming from the stripping ($0.1\text{M H}_2\text{SO}_4$), are transferred into the organic phase of the IL. In both cases, it is difficult to determine specific substances and complexes in the range of $800\text{-}1500\text{ cm}^{-1}$, known as the fingerprint region, which usually contains a large number of peaks, making it difficult to identify individual peaks. Furthermore, the complex composition of the leached solution also makes the identification difficult. Nevertheless, the FTIR spectra of the pure ILs did not show any major difference after 3 cycles of reuse, and extraction efficiencies did not diminish either after 5 cycles, suggesting no or minor degradation of the ILs occurred through the indium recovery process.

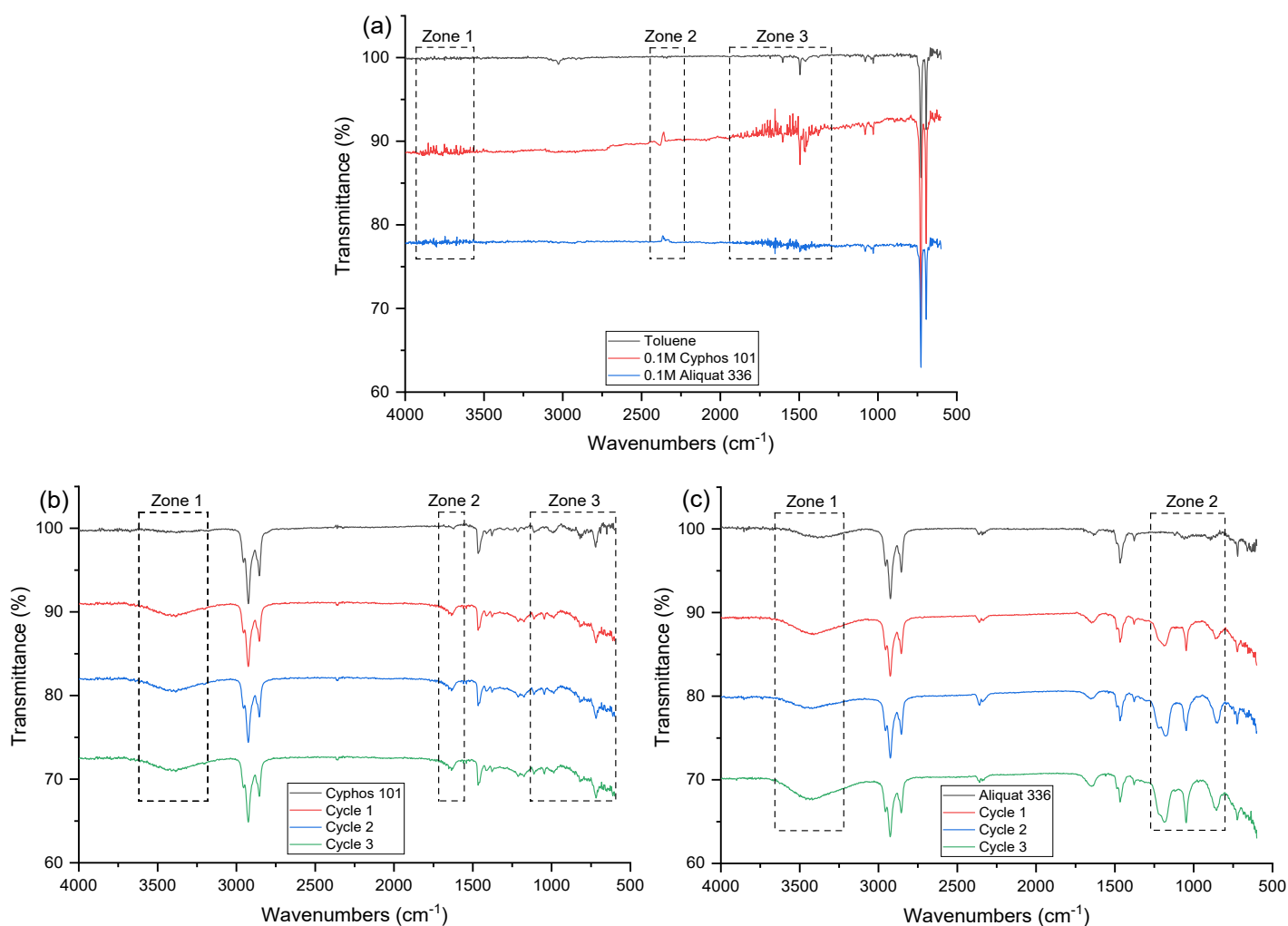


Figure 6.16: FTIR spectra of (a) toluene and 0.1M IL, virgin ILs and after 3 cycles for (b) Aliquat 336, and (c) Cyphos 101.

6.3.1.5.1 Discussion

The regeneration of the extractants was checked by contacting the 0.1M ILs in toluene with a 100 ppm In solution (3 M HCl). The loaded ILs were stripped with a 0.1 M H₂SO₄ solution. The stripped ILs were washed with RO water and the process was repeated five times with no variation on the extraction and stripping. Cyphos 104 has been reported to be reused up to twelve cycles without loss in extraction [156]. The experiments were carried out with a 100 ppm In solution (3 M HCl) for IL loading and stripping with 3 M HNO₃ [156]. Undiluted Aliquat 336 and Cyphos 101 showed no losses in indium extraction over two cycles of extraction and stripping [215]. The same study also reported that the solubility of the Cyphos 101 and Aliquat 336 in the aqueous phase is very limited, which minimises the loss of the ILs to the aqueous phase. The avoidance of IL loss to the aqueous phase is important in creating a sustainable and environmentally friendly process. In this study, the whole

process was carried out twice with leach treated LCD panels liquor (representative of real samples), confirming the recyclability of the ILs.

6.3.2 Pre-treatment of waste LCD screens

To establish the need, if any, for pre-treatment of as-received LCDs panels, a preliminary investigation involved a series of leaching studies to determine the concentration of indium and other impurities, the steps to be taken to access the indium embedded in the LCD panels, and the optimal conditions for extracting the target metal. The results of these studies along with the necessary pre-treatment steps developed to extract indium from as-received LCD panels derived from EoL-MPs are now described.

6.3.2.1 Leaching

The leaching efficiencies of H_2SO_4 , HCl , and HNO_3 on indium from LCD screens was studied and the results are presented in Figure 6.17 . It is seen that indium leaching increases considerably with an increase in temperature, reaching 71%, 90% and 100% of leaching at 80°C for HNO_3 , H_2SO_4 and HCl , respectively. Nitric acid and sulphuric acids reached a plateau at approximately 60 °C, whereas hydrochloric acid reached a plateau at nearly 70 °C. From these results, hydrochloric and sulphuric acids are shown to be the most effective acids for indium leaching from LCD panels. Indium leaching with HCl over 60 °C, however can lead to volatilization of HCl , reduction in acid concentration and liberation of toxic fumes [234]. Furthermore, HCl is highly corrosive which makes it difficult to handle. Sulphuric acid, on the other hand, remains relatively stable as temperature increases due to its higher boiling point, is more environmentally friendly and cost effective than HCl . Therefore, although hydrochloric acid shows a better performance in leaching indium, H_2SO_4 promises to be an excellent leaching agent.

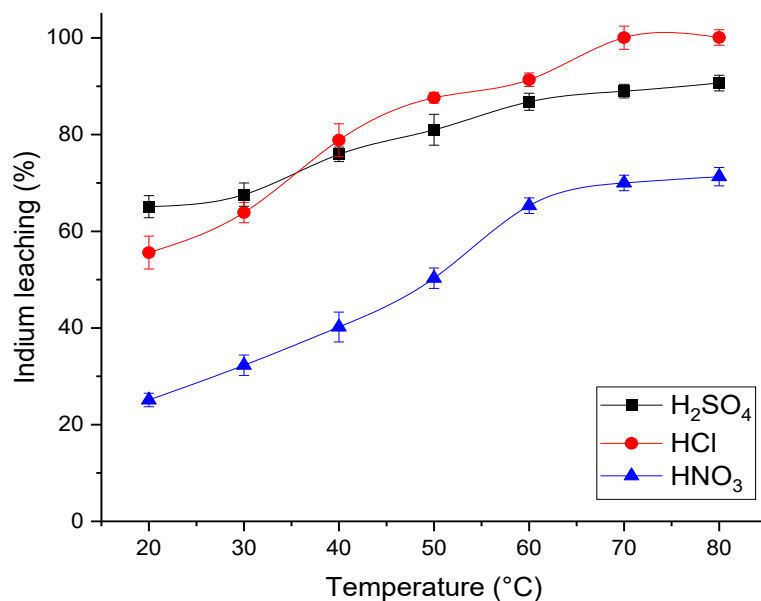


Figure 6.17: Effect of the temperature in the indium leaching from LCD screens with different acids.

6.3.2.1.1 Determination of the optimal indium leaching conditions from Waste LCD Screens

To determine the optimal indium leaching conditions from LCD panels, the effects of time, acid concentration (using HCl and H₂SO₄), and, solid to liquid ratio were investigated and the results are presented in Figure 6.18. From Figure 6.18a, it is observed that as the leaching time increases, the indium leaching efficiency also increases. After 0.5 hours, the indium leached is 56% and 44% for HCl and H₂SO₄, respectively. In both acids, the leaching yield curve flattened out and complete leaching is achieved after 2 h for HCl and 3 h in the case of H₂SO₄. The effect of the acid concentration (Figure 6.18b) shows a direct, almost linear, relationship with the indium leached. At low concentrations (0.1M-<1M), H₂SO₄ shows a slightly higher leaching efficiency but as acid concentrations are increased, HCl favours indium leaching. Indium leaching was complete at a concentration of 4M for HCl and 5M for H₂SO₄. The solid-to-liquid (s/l) ratio (Figure 6.18c) shows that as the volume of acid increases, the amount of indium leached also increases. In the case of HCl, a 1:10 s/l ratio leaches 66% of indium, whilst a 1:20 s/l ratio achieves 94%, and 100% leaching after a 1:30 s/l ratio. In the case of H₂SO₄, the indium leaching is 77% at 1:10 s/l ratio, reaching a plateau of approximately 90% of indium leached after a s/l ratio of 1:20. The temperature effect on indium leaching is shown in Figure 6.17, reaching a plateau at 70 °C and 60 °C for HCl and H₂SO₄, respectively. In terms of optimal indium leaching conditions, each acid has different optimal conditions and slightly different one to another, however, from an economic and environmental perspective and preventing an excessive use of reagents, the optimal conditions of 60 °C, 2 h, 3 M with a s/l ratio of 1:20 are proposed for both acids.

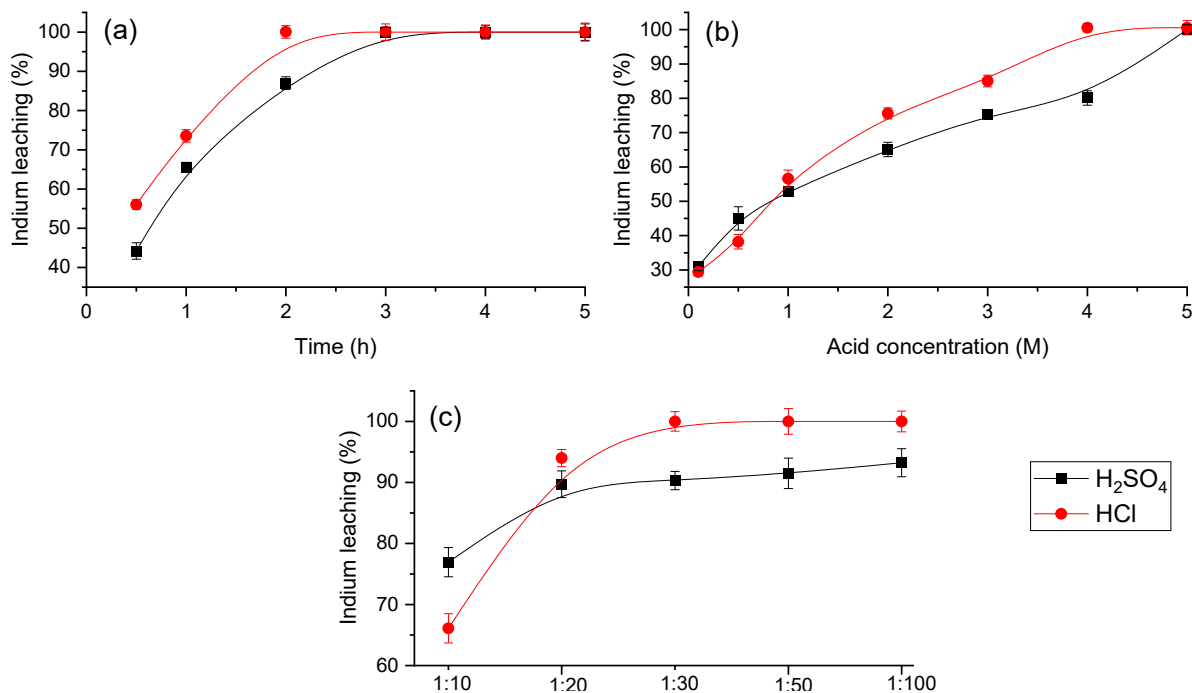


Figure 6.18: Effect of (a) time, (b) acid concentration, and (c) solid/liquid ratio on the indium leaching.

6.3.2.1.2 Leaching of Indium under Optimal Conditions

Based on the results reported in Section 6.3.2.1.1, powdered LCD panels were leached separately with hydrochloric acid (Figure 6.19a and b) and sulphuric acid (Figure 6.19c and d). Complete leaching of indium is achieved with both acids, with an average concentration of 0.73 mg/L, representing the 1.2% and 1.5% of the total leached species in HCl and H₂SO₄, respectively. The major metal present in the leached solution is copper with a concentration of 31 mg/L, followed by iron, aluminium, and nickel. These four elements (Al, Fe, Cu and Ni) together represent more than 90% of the total metal leached by both acids; other metals present include Mg, Zn and Pb. Although indium can be effectively leached by the two acids, the presence of other metals in significantly higher concentrations than indium will likely impact the recovery of indium from any process developed. The glass fraction in LCD screens accounts for nearly 67 wt.%, (as reported in Chapter 3), which further contributes to a decrease the efficiency of the process, with an increase in reagent use, and energy to leach indium. These results confirm that a pre-treatment step is needed for the enrichment of indium, and the results of this part of the study are described in the next section.

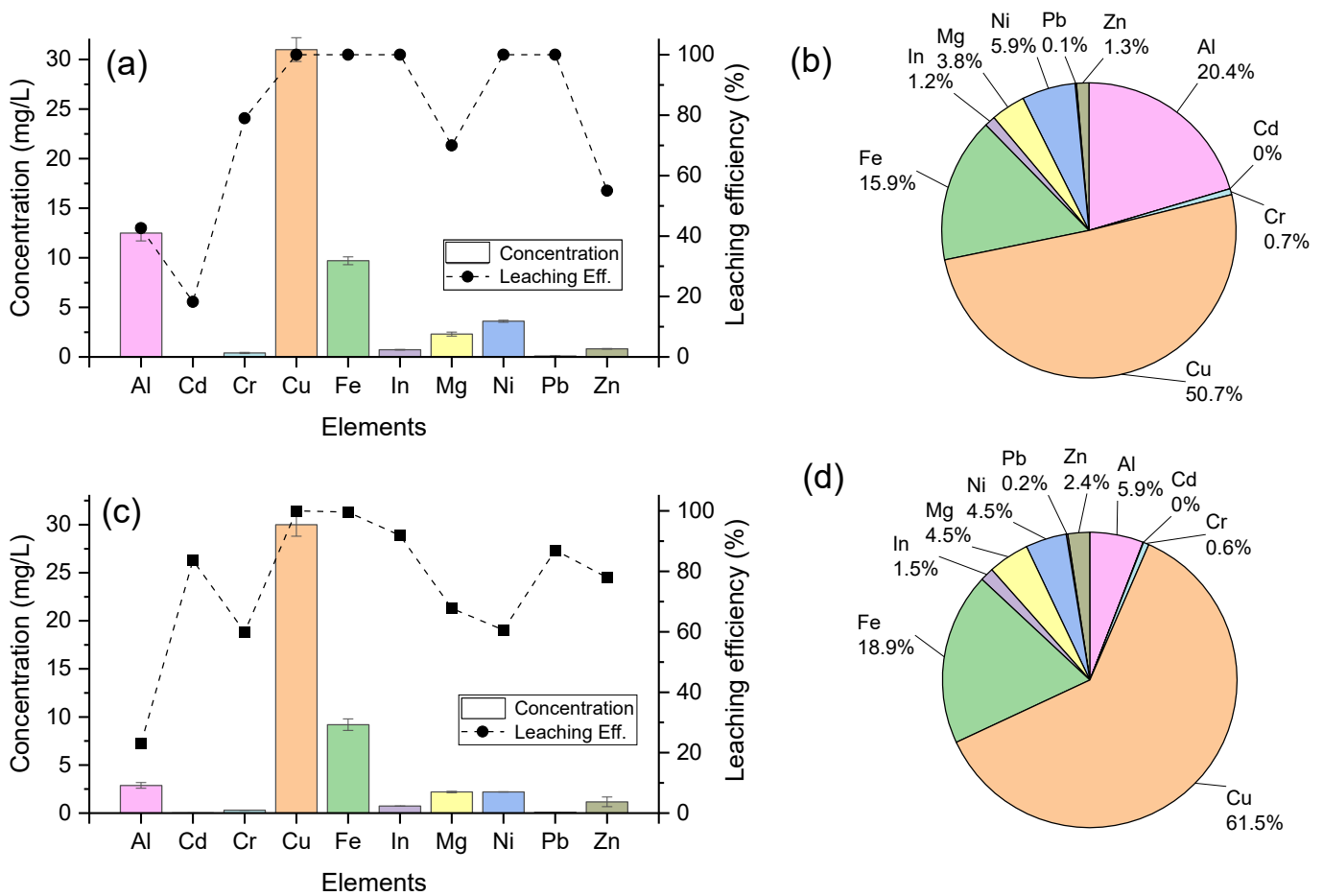


Figure 6.19: Metal leaching of LCD screens under optimal conditions (a) and (b) HCl, (c) and (d) H₂SO₄.

In summary, the use of the two acids (HCl and of H₂SO₄) as leaching agents are each shown to be promising in terms of efficiency for indium, with neither showing a greater selectivity for indium, in the presence of other metals, over the other. Considering the results here and in the results reported in Section 6.3.1.1 (explained in the extraction section), where it was found that hydrochloric acid was the most efficient acid for indium extraction by the ILs, HCl was selected as the leaching agent for testing on as-received LCD panels.

6.3.2.1.3 Characterisation of LCD panels

A pre-treatment was developed to enrich the indium concentration reduce the concentration of undesirable metals, remove the organic materials such as liquid crystal and polarizers from the LCD panels, and remove the glass, which could be recycled.

In Chapter 3, section 3.3.2.2, a detailed characterisation of the EoL-MPs screens and LCD panels was presented. A typical LCD screen is made of thin conductive electrodes placed between two glasses plates, accounting for nearly 50% of the total mass of the screen. The other components include connectors, adhesives, diffusive and reflective sheets, polarising films, and plastic frames [150, 151]. As indium is found within the LCD panels (Figure 3.13, Chapter 3), the LCDs were separated from the connectors, adhesives, polarising films, and frames, as a previous separation.

An LCD panel is a complex multi-layered structure, consisting of ceramic materials such as glass substrate, organic materials such as polarisers, colour filters and liquid crystal, and inorganic materials such as metals (In, Sn, Cu, etc.). Among these materials, glass substrates account for approximately 80 wt.%, followed by the organic materials with nearly 18 wt.%. Figure 6.20 shows an EoL-MP screen and its cross-section of an EoL LCD panel. The LCD panel comprises two glass substrate layers, where polarisers are in contact externally, and liquid crystal is located in between these two glass plates. The polymeric film and the polarisers were analysed as part of the detailed characterisation reported in Chapter 3 and found to be cellulose triacetate (CTA), polyvinyl alcohol (PVA) and triphenyl phosphate (TPP). Adjacent to each polarising film is a glass substrate with an inner colour filter attached to the internal surface of the glass plate, and between the glass substrate layers, is liquid crystal. The chemical composition of liquid crystal used in LCD panels is usually complex and varied depending of the producer, applications and fabrication patents, being usually a mixture of about 10–25 compounds with long structured chemical compounds such as the combination of fluorenyl, cyclohexyl biphenyl, cyano biphenyl and terphenyl groups [151, 228]. Although most toxicities of liquid crystal are still unknown, some of them have been categorized as biologically toxic [228]. In fact, according to the Directive 2002/95/EC, LCD panels are classified as high risk elements because of the hazardous substances in their composition such as toxic metals (In, Cd, Pb, As, Cr, Hg, Cu, etc.) and flame retardants (polybrominated diphenyl ethers, polybrominated biphenyls, etc.) [147]. The first layers on the inner glass substrate include the colour filter and the thin-film transistor (TFT) arrays substrate. The colour filter substrate is used to generate colours, namely red, green, and blue, whilst the TFT arrays substrate is used to control the voltage signal of pixel electrode. The inner sides of the glass substrates are coated with functional films and a transparent conductive electrode, including indium tin oxide (ITO). ITO is a mixture of In(III) and Sn(IV) oxides with a typical distribution

of 90% In_2O_3 and 10% SnO_2 by weight and its thickness varies depending on the manufacturer and the application [149, 150, 152]. Figure 6.20c also shows the SEM-EDS images of the inner sides of the glass substrate, with a predominance of In and Sn, from the ITO inner layers, found on both sides, and other metals such as Al, Cr, Mg, Mo, Sr, Ti, etc., and non-metal elements such as Cl and S.

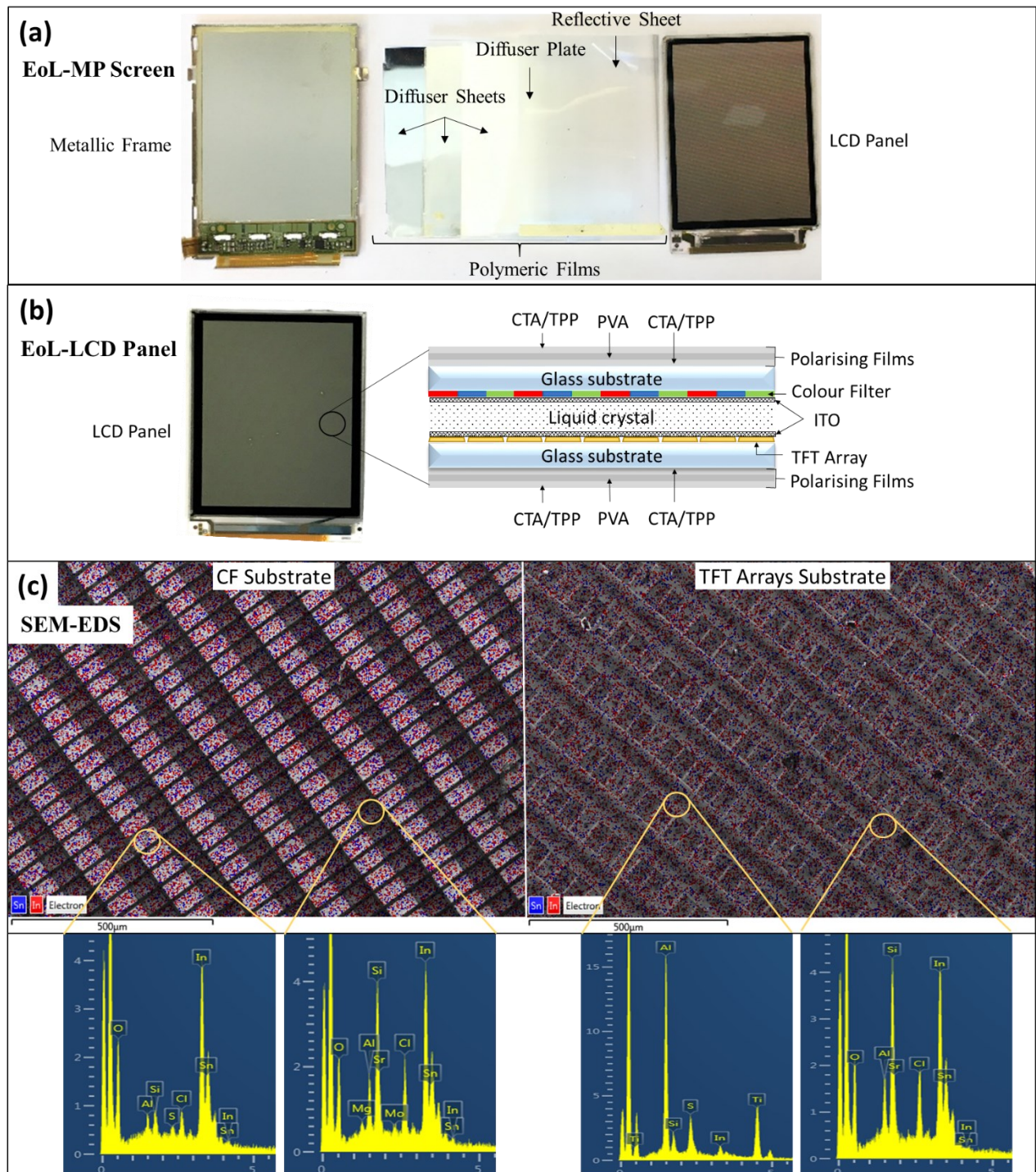


Figure 6.20: Structure of (a) an EoL-MP Screen, (b) EoL-LCD Panel and a cross-section, and (c) SEM-EDS images of the inner glass substrate.

6.3.2.2 Polymer Films Removal

The polarising films are located on the outside of the LCD panels, consisting of a PVA film sandwiched between two CTA/TPP films, as showed in Figure 6.20b. These films are usually secured by a pressure sensitive adhesive (PSA) via hot pressing [237]. This means that manual or mechanical separation of the films can be difficult. At first, manual separation was carried out using knives and pliers but proved ineffective. As the polarising films are organic materials, different organic solvents were used to try to remove the films. Preliminary tests using toluene, hexane, and acetone showed that acetone performed best, with partial removal of the polarising films after 3 h, and was chosen as the preferred solvent. Acetone has the benefits of being less toxic than other common organic solvents, has a low boiling point (56 °C), which favours separation and reuse, and is relatively inexpensive. Its biggest disadvantage is that it is highly volatile and flammable, and due to this, it was used under controlled conditions at room temperature (20 °C) in a closed system to avoid solvent losses through evaporation.

Initial studies were carried out to determine the optimal solid-to-liquid (s/l) ratio of LCDs and acetone. LCD panels were cut into pieces of approximately 2x2 cm², and the samples were immersed in acetone in 1:5, 1:10, 1:30, 1:50, and 1:100 s/l ratios. It was found that the separation of the polarising films from the LCD panels was not greatly influenced by the different s/l ratios employed, although for the s/l ratio of 1:5, stirring was difficult, consuming more time for the separation, so s/l ratio of 1:10 was selected creating a less viscous medium to aid stirring but at the same time keeping the consumption of solvent to a minimum. The effects of acetone on the polarisers are summarised in Table 6.6; the polarisers started to show signs of softening after 3 h and complete separation was achieved after 24 h. Acetone is able to penetrate through the CTA film to reduce the viscosity of PSA, enabling the polarizers to be separated from the glass substrates [150]. In this process, the solvent loss was approximately 8.5 vol.%.

Table 6.6: Effects of acetone on polarisers through time.

Time (hours)	Condition(s) of polarisers
1	No observable changes
3	First sign of softening on the edges
7	Partial separation on the edges from the glass substrates Extremely low physical strength Broke instantly when handled with a pair of tweezers Cannot be recovered as a whole
20	Nearly complete separation, polarisers still adhered in the centre Broke instantly when handled with a pair of tweezers
24	Complete separation from the glass substrates without manual work

Although the polarisers can be effectively removed with acetone after 24 h, stirring the solvent for 24 h increases the energy consumption of the process. This long soak time is required because the PVA film cannot be dissolved in acetone [255], and since PVA is located between the CTA/TPP layers, it is difficult for acetone to penetrate to the PSA. To avoid this, a two stage immersion was used with a hot water bath, followed by an acetone bath [237]. Hot water (80-100 °C) can penetrate the CTA/TPP film and can dissolve the PVA film. The layer of CTA/TPP can then be separated by loosening the PSA with acetone. The use of hot water does not affect the liquid crystal [237]. Hot water at approximately 80-90 °C was first applied with an s/l of 1:20, as the s/l ratio has no impact on the loosening of PVA, however, it must cover completely the LCD panel. The CTA and PVA layers are peeled off manually with tweezers. An acetone bath with an s/l of 1:10, was used to loosen the PSA so the second layer of CTA film was peeled off from the glass substrates. The hot water process lasted 30 minutes, whilst the acetone process lasted 1 hour, giving a total treatment time to separate the polarisers of only 1.5 hours. It is worth noting that the polarisers must be peeled off immediately otherwise the procedure would need to be repeated. Photographs and SEM images of polarising films after separation by hot water and acetone from an EoL-MP LCD panel are shown in Figure 6.21. CTA and PVA films were separated as whole pieces of film without any major scratch to the surface. The SEM images confirm that CTA films did not show any scratch or irregular form because of the separation process, whereas the SEM image of the PVA film showed an irregular form on one of the surfaces of the film; likely due to the glue that joins PVA to the last CTA layer. The photographs and SEM images confirmed that the CTA and PVA films can be separated without any deterioration, allowing them to be reused or recycled.

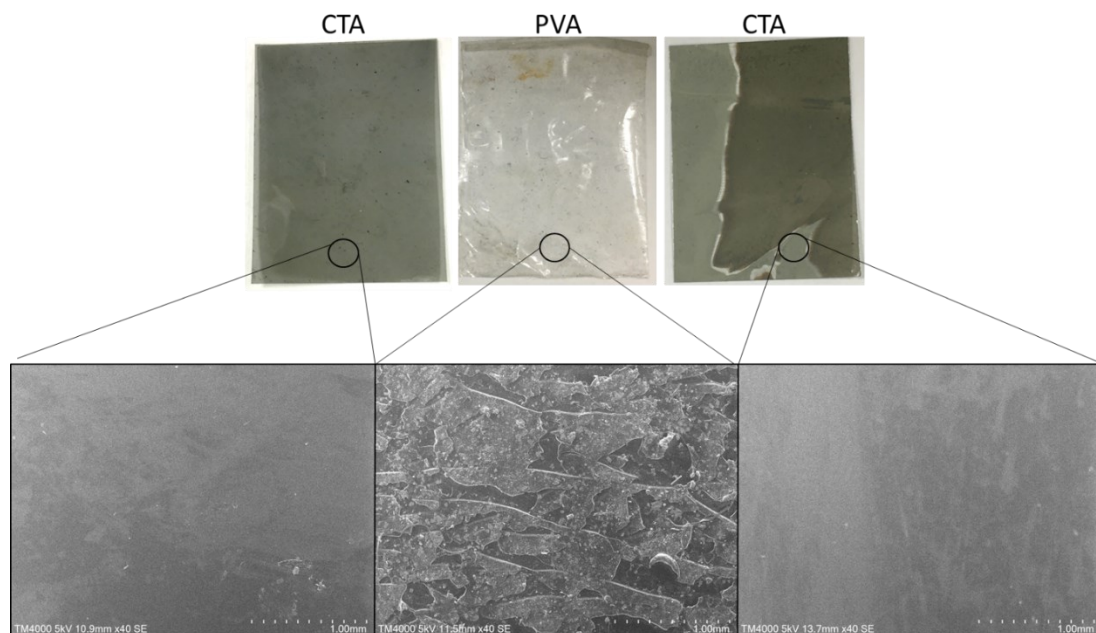


Figure 6.21: Photographs and SE images of the polarisers obtained by hot water and acetone.

6.3.2.2.1 Indium Leaching after Polymer Removal

After the separation of the polymeric films (diffuser sheets, diffuser plate, plastic frame, and reflective sheet) from the EoL-MP screens, the pre-treatment step allowed the separation of the polariser layers (CTA and PVA films) from the LCD panels, which consist of two layers of glass substrate, containing a colour filter, ITO and FTT arrays (Figure 6.20). The treated LCD panels were leached under optimal conditions (60 °C, 2 h, 3 M HCl, and s/l ratio of 1:20) and the results show an increased in indium concentration from 0.7 g/L (shown in Figure 6.19) to 33.2 g/L (in Figure 6.22), representing 51% of the total metal present in the leach solution. The main undesirable metals are aluminium and iron with concentrations of 10.2 mg/L and 14.7 g/L, respectively. These two metals (Al and Fe) represent 38% of the total metal content of the leach liquor (Figure 6.22b), almost identical to their concentrations in the un-treated LCD (12.5 g/L for Al and 9.7 g/L, respectively). Other metals such as Cd, Cr, Cu, Mg, Ni, Pb, and Zn are found with concentration <1.5 g/L. This result demonstrates the significance and value of pre-treatment as a step towards the enrichment of indium, and the separation of polariser films that can be recovered and reused.

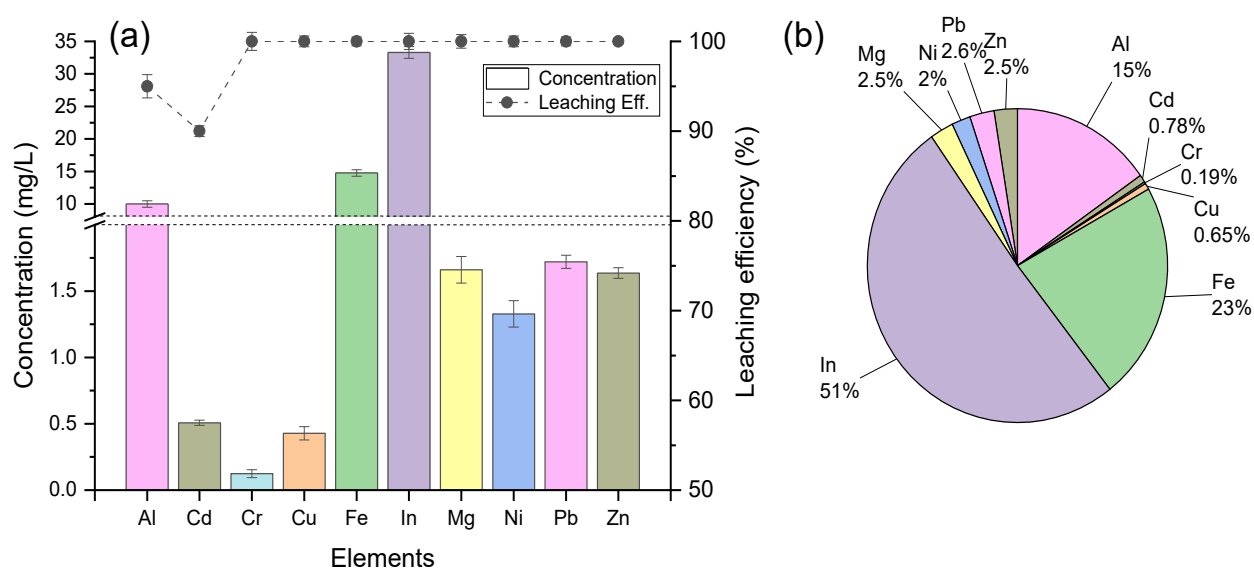


Figure 6.22: Metal leaching of pre-treated LCD panels under optimal conditions; (a) metal concentration and leaching efficiency, and (b) metal distribution after leaching.

To reduce the consumption of energy in the process, (and in the interests of developing an experimental method and conserving material use) pre-treated LCD panel strips of approximately 0.5x0.5 cm² were leached under optimal conditions. Table 6.7 presents a comparison of metal concentrations and their leaching efficiencies when three different feedstock materials were leached, namely: *untreated powder LCD panels*, *pre-treated powder LCD panels*, and *pre-treated strip LCD*

panels. It was found that indium leaching from *strip pre-treated LCD panels* was nearly complete, decreasing a little the concentration of the other metals, which is beneficial for the reduction of undesirable metals. By way of illustration to confirm that indium was leached from the *pre-treated strip LCD panels*, SEM-EDS images from before and after leaching, along with images of the three leaching processes are shown in Figure 6.23. The images show that the leach solution for the *pre-treated strip LCD panels*, is more transparent in colour compared to the leach solutions for both *untreated powder LCD panels*, and *pre-treated powder LCD panels*, which are yellow and dark yellow respectively (Figure 6.23b). The intensity of the colour is likely indicative of a greater leaching of metals which suggests that in the leaching of *pre-treated strip LCD panels*, less metal or undesirable metal was leached. SEM-EDS images, in which red represents In and blue Sn (by EDS), show that indium is present on the colour filter glass substrate (Figure 6.23c) but effectively extracted, as shown in Figure 6.23d. In the case of the *untreated powder LCD panels* (Figure 6.23a) and *pre-treated powder LCD panels* (Figure 6.23d) indium was also completely leached, providing visual confirmation of the results reported in Table 6.7. Since the leaching from treated *pre-treated strip LCD panels* was nearly the same as the leaching of *pre-treated powder LCD panels*, the use of strips is preferred due to the elimination of a milling process, reducing the energy consumption and material losses that occur in the milling process.

Table 6.7: Metal leaching from LCD panels (untreated and treated) under optimal leaching conditions.

Element	Untreated Powder LCD panels		Pre-treated Powder LCD panels		Pre-treated Strip LCD panels	
	Conc. (g/L)	Leaching Eff. (%)	Conc. (g/L)	Leaching Eff. (%)	Conc. (g/L)	Leaching Eff. (%)
Al	12.5	42.6	10.1	95.2	9.5	95.9
Cd	0.004	18.3	0.501	90.6	0.434	88.1
Cr	0.4	79.1	0.1	100.0	0.1	100.0
Cu	31.2	100.0	0.4	100.0	0.4	100.0
Fe	9.7	100.0	14.7	100.0	13.4	91.1
In	0.7	100.0	33.2	100.0	32.5	97.8
Mg	2.3	70.5	1.7	100.0	1.4	82.4
Ni	3.6	100.0	1.3	100.0	1.1	84.6
Pb	0.1	100.0	1.7	100.0	1.5	88.2
Zn	0.8	55.6	1.7	100.0	1.6	94.1

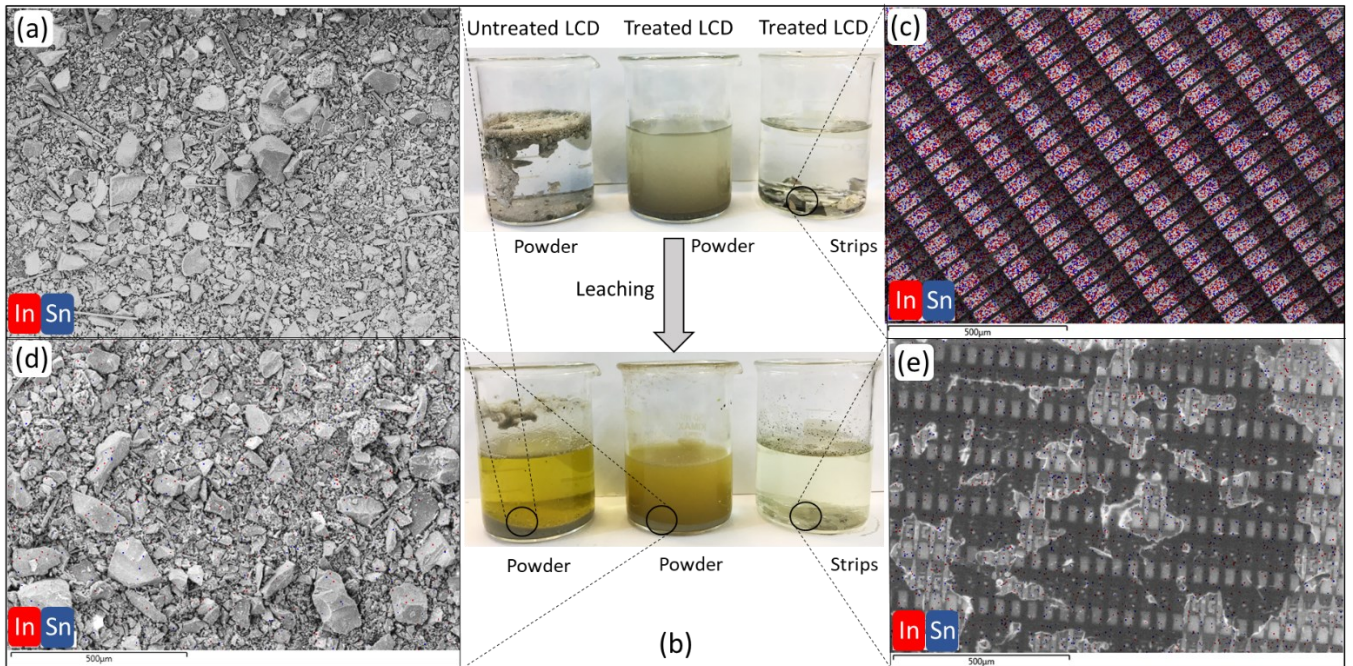


Figure 6.23: LCD leaching and SEM-EDS images before and after reaction.

6.3.2.3 Proposed pre-treatment for Waste LCD Screens

The need for a pre-treatment step is confirmed and Figure 6.24 provides a flowchart of the proposed pre-treatment steps with an indication of valuable materials that can be separated and recovered from EoL-MP LCD screens as part of this process. The pre-treatment process separated all the polymeric films from the EoL-MP screens, increasing the concentration of indium. Furthermore, when acetone is used to separate the final CTA film from the LCD panels, liquid crystal is dissolved, which can be recovered by evaporation, and the acetone can be reused in subsequent cycles. While development of this part of the process was not carried out in this research due to the small number of LCD panels from EoL-MP screens, however, with the difference in the boiling points of acetone (56 °C) and liquid crystal (145°C and 178°C), the recovery of liquid crystal can be justifiably proposed as part of the process. The final product following pre-treatment is a glass substrate rich in ITO, which can be leached directly for further indium recovery process. In addition, after leaching of indium the residual glass can also be recycled.

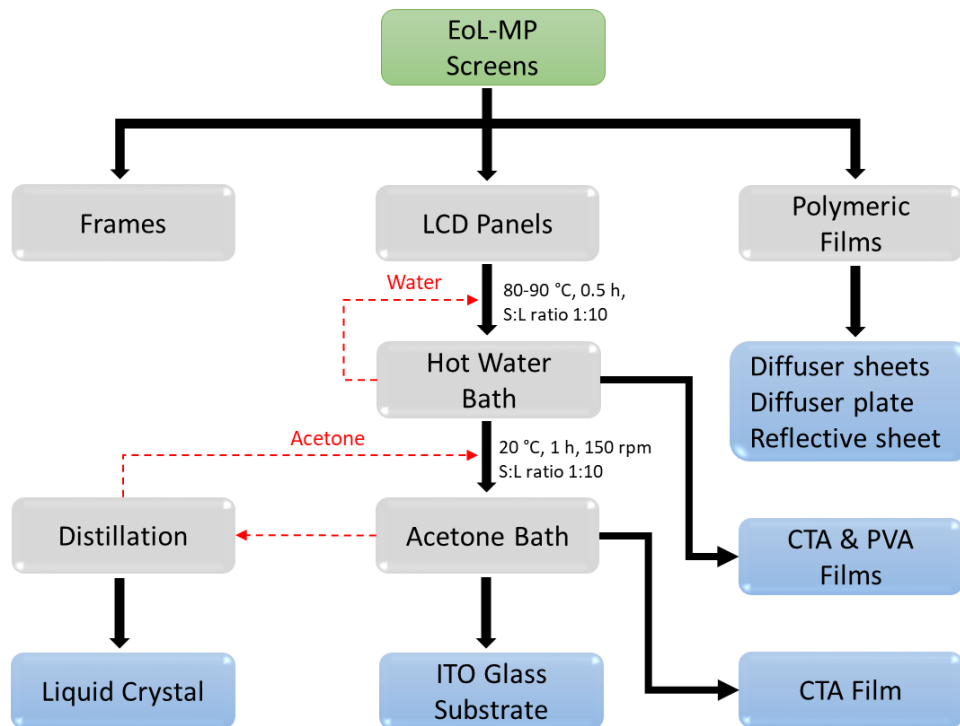


Figure 6.24: Pre-treatment of EoL-MP screens and recovery of valuable materials.

6.3.2.4 Discussion

Following the detailed investigation in this work to establish the optimised conditions for pre-treatment, extraction and recovery for application to as-received waste LCD screens described in the next section (Section 6.3.3), and to put this in the context of current literature, a compilation of the relevant studies reported has been prepared and is presented in Table 6.8 and Table 6.9. Table 6.8 covers the studies reporting on *Leaching* and Table 6.9 covers those reporting on *Extraction*. Since the processes of stripping and reduction for complete recovery are not usually studied on their own, all relevant information on these steps is included in both tables.

As a general observation, most of the reported data cover part of a hydrometallurgical process, focusing on the determination of the optimal parameters, and most of the studies use a simple simulated/synthetic solution for optimisation, usually followed with applications to real LCD samples. It is noted that most of the LCD panels trialled come from TVs and laptops, where indium concentrations are lower than that present in EoL-MPs, where levels are typically higher in mobile phone screens [142].

Table 6.8: Comparative Analysis of recycling approaches for LCD panels focused on Indium leaching.

EoL Material Type	Methodology	Products	Indium Yield	Year of publication	Reference
Leaching					
EoL-MP screens	<p>EoL-MPs screens: Manual dismantling, frames, polymeric films, and LCD panels separated.</p> <p>LCD panels: Pre-treatment with a bath of hot water (80-90 °C, 0.5 h, S:L=1:10), followed by a bath of acetone (20 °C, 1 h, S:L=1:10, 150 rpm). Polarising films separated from ITO glass substrate.</p> <p>The ITO glass substrate was leached as strips (0.5x0.5 cm²) and powder (≥ 150 μm).</p> <p>Leaching: 3 M HCl, s/l ratio of 1:20 (g/L), 60 °C, 2 h,</p>	<p>Frames, polymeric films (diffuser & reflective sheets), polarising films (CTA &PVA)</p> <p>Indium solution</p>	100% leaching	2022	This work
Waste ITO targets	<p>Waste ITO targets obtained from an e-waste recycling plan (38-42 μm).</p> <p>Leaching: 4 M (NH₄)HSO₄, S:L=1:50, 125 °C, oxygen partial pressure 0.3 MPa, 1.75 h.</p> <p>Reduction: Precipitation with ammonia (NH₃: H₂O), 60 °C, 2 h., followed by calcination at 600 °C, 1 h.</p>	In ₂ O ₃	100% leaching	2021	[227]
TV LCD panels	<p>Polarises were removed previously. Crushing LCD (53 μm),</p> <p>Leaching: 10% AR leaching, 90 °C, S:L=1:20 (g/L), 15 min., and sonication.</p>	Indium solution	~100% leaching	2020	[252]
LCD monitors	<p>Manual separation. Mechanical stripping process, followed by pyrolysis to remove liquid crystal. The pyrolysed scraps were pulverized via ball-milling.</p> <p>Leaching: 1 M H₂SO₄ at 70 °C, 1 h.</p>	Cu, In	99.3% leaching Electrodeposition for Cu (95.3%) an In (85.6%)	2020	[253]
TV LCD	<p>Manual dismantling, polarised were removed by a heat gun. Crushing by disc mill, followed by agate mortar (-74+44 μm)</p> <p>Leaching: 1 M citrate, 0.2 M N₂H₄, pH = 5, using sodium hydroxide (NaOH), S:L=20 (g/L), 16.6 h.</p> <p>yielded a remarkably high In recovery of 98.9% after 16.6 h.</p>	Indium solution	99.9% leaching	2019	[256]

LCD panels	Cutting 4x4 cm ² and shredding (0.3-2.8mm) Leaching: 5 M mineral acid (HCl, H ₂ SO ₄ , and HNO ₃), pulp density of 500 g/L, 75 °C, 500 rpm, 2 h.	Indium solution	~100% leaching with small LCD particles sizes	2018	[226]
Laptop LCD	Manual dismantling. Manual shredding 1x1 cm ² and ball milling (37 μm) Bioleaching: <i>Acidithiobacillus thiooxidans</i> , pH=2.6, pulp density of 1.6% (w/v), initial sulphur content 8.6 (g/l).	Indium solution	~100% leaching	2018	[238]
Computer monitor	Manual dismantling. Polariser were peeled off by contact with alcohol. Glass substrate was separate using a knife. Acetone was used to remove the liquid crystal. Cut in 4x4 cm ² for experiments. Non-crushing Leaching Leaching: 0.8 M HCl, ultrasonic waves 300 W, 1h.	Indium solution	96% leaching	2017	[257]
TV LCD	Components mechanically separated, shredding. Leaching: 5 M HCl, pulp density of 500 g/L, 75 °C, 400 rpm, 2 h.	Indium solution	~100% leaching	2016	[258]
TV LCD panels	Manual cutting, big plastic and glass fragments were removed, blade grinding (1.25 mm and 10 mm). Leaching: 2 M H ₂ SO ₄ 3-step cross-current, pulp density of 0.1 Kg/L, 80 °C, 17 min.	Indium solution	~100% leaching in 1 step and 50-55% In leaching after 6 steps	2015	[149]
LCD monitors	Manual dismantling. Removal of polariser with liquid nitrogen. Leaching: 6 N HCl, H ₂ SO ₄ , and HNO ₃ , 25 °C, L:S=3:1 (mL/g), 6h.	Indium solution	>90% leaching	2015	[259]

Table 6.9: Comparative Analysis of recycling approaches for LCD panels focused on Indium extraction.

EoL Material Type	Methodology	Products	Indium Yield	Year of publication	Reference
	Extraction				
ITO glass substrate	<p>Manual dismantling and pre-treatment (Table 6.8). ITO glass substrate strips (2x2 cm²) and powder (≥ 150 μm). Leaching: 3 M HCl, s/l ratio of 1:20 (g/L), 60 °C, 2 h. Extraction: 0.1 M Cyphos 101 & Aliquat 336 in diluted in toluene, room temperature, counter-current and A:O ratio of A:O=7/2 for Cyphos 101 and A:O=2/1 for Aliquat 336. Stripping: 0.1M H₂SO₄, V(H₂SO₄)/V(IL) ratio of 1.5:1, 150 rpm, for 30 minutes. Reduction: Cementation by adding zinc at 20 °C, 4 h and 250 rpm (adding 2 times the amount of zinc required stoichiometrically), and as the oxide via precipitation by adding NaOH at pH 12, followed by a calcination at 500 °C for 3 h.</p>	<p>In (by cementation)</p> <p>In₂O₃ (by precipitation)</p>	<p>In model test system ≥95%. Purity 100%.</p> <p>In real samples using EoL-MP screens >90%. Purity of ≥99%.</p>	2022	This work
TV LCD	<p>Manual dismantling, cutting and ball milling. Powder was treated at 80 °C, 24 h (75 μm) Leaching: 90 %v/v 3 M HCl and 10 %v/v 30% H₂O₂, 75 °C 400 rpm, 2h. Extraction: 0.1 M Cyphos IL 104 in toluene Stripping: In, Zn and Sn from organic phase were stripped quantitatively into 0.001 M HNO₃, 4 M HNO₃ and conc. HCl stripping solutions, respectively at O/A = 3/2 in two stages. Reduction: Precipitation using NaOH at pH 9 for Zn and 12 for In. Sn was precipitated by adding dropwise a Na₂S solution at 80 °C. Calcination at 400 °C, 2h for Zn(OH)₂, and 500 °C, 3 h for In(OH)₃.</p>	ZnO, SnS, In ₂ O ₃	Recovery of 98.9% In, 100% Zn and 99.6% Sn with a purity of 100%, 99.9%, and 100%, respectively.	2020	[156]
LCD monitors	Manual dismantling, polarisers were removed. Shredding by high-speed crushing shear (<0.75 μm).	In ₂ (C ₂ O ₄) ₃	99.8% leaching (hot reaction)	2019	[260]

	<p>Leaching & extraction: 50% (v/v) ionic liquid ([Hbet][Tf₂N])/ascorbic acid, S:L= 20 (g/L), 90 °C, 24 h.</p> <p>Stripping: oxalic acid.</p>		98.6% extraction (cold solution)		
Mobile phone LCDs	<p>Manual dismantling, polymers removing, ball milling (150 μm).</p> <p>Leaching: 1 M H₂SO₄, 90 °C, 1 h, S/L ratio of 1:20, stirring at 500 rpm.</p> <p>Extraction: 30% (v/v) of D2EHPA diluted in kerosene, A:O ratio of 40:1, pH 0.5, 20 min.</p> <p>Stripping: 4 M HCl, A:O of 10:1, 10 min.</p>	Indium solution	96.7% extraction 61.1 % stripping	2018	[90]
Spent GZO/IGZO targets from thin film solar industry	<p>Gallium zinc oxides (GZO), indium gallium zinc oxides (IGZO).</p> <p>Leaching: 3 M HNO₃, L:S ratio of 50 ml/g, 80 °C, 2h.</p> <p>Extraction: 0.02 M D2EHPA, pH 1, A:O = 2, 5 min for indium. 0.015 M D2EHPA, pH 3, A:O=3, 3 min for gallium.</p> <p>Stripping: 1 M HCl, O/A = 1, 5 min for indium. 2 M HCl, O/A = 3, 3 min for gallium.</p> <p>Reduction: Precipitation using NaOH at pH 8, 9 and 12, for Ga, Zn and In, respectively.</p> <p>Calcination at 300 °C, 400 °C and 500 °C for Zn(OH)₂, In(OH)₃ and Ga(OH)₃ respectively.</p>	ZnO, Ga ₂ O ₃ , In ₂ O ₃	Metal recovery: 99.9% (Zn, Ga & In) Metal oxide purities: 99.5%	2017	[239]
Synthetic solution	<p>Extraction: Undiluted Cyphos IL 101 and Aliquat 336, A:O=1:1, 500 rpm for 10 min at 60 °C</p> <p>Stripping & Reduction: Precipitation with NaOH solution</p>	In(OH) ₃	100% extraction 100% stripping	2017	[235]
ITO Etching solution	<p>Solution: indium from hydrochloride-based etching solution of ITO.</p> <p>Extraction: 0.3M D2EHPA at room temperature, O/A ratio of 1:1, pH=1.0–1.5.</p> <p>Stripping: O/A ratio of 1:2 or less, 2 M HCl.</p>	Indium solution	92% leaching	2016	[261]
ITO powder(< 44 μm)	<p>Leaching: 1M H₂SO₄ and 1 M HCl, S:L=1:1 (g/L), 545 rpm, 6 h.</p> <p>Extraction: 1 M D2EHPA in kerosene for indium, 1 M TBP or 0.2 M D2EHPA + 0.8 M TBP diluted in kerosene for Sn.</p> <p>Stripping: 1.5 M HCl, O:A+1:1.</p>	Indium solution	100% leaching 97% extraction 96% stripping	2011	[241]

The optimal leaching conditions found in this study (3M for each acid HCl and H₂SO₄, 60 °C, S:L ratio of 1:20 for 2 h), achieving an efficiency of 100%, are consistent with those reported in the literature (Table 6.8), although, in this work HNO₃ showed a leaching efficiency of 74% under the same conditions. Virolainen et al. reported that ITO can be completely dissolved by 1M HCl and 1M H₂SO₄ after 6 hours at room temperature, however, HNO₃ took significantly longer [241]. In the literature, it is well established that ITO leaching rates are, in general, slow, with nitric acid being the slowest. This could be the result of the strong oxidizing conditions of nitric acid, which could be responsible for indium precipitation [259]. Similar to the findings in the work, acid concentration and temperature were found to have a major effect on both the efficiency and leaching rate. Analysis of the data in Table 6.8 shows the ranking of acids used for indium leaching to follow the order: HCl > H₂SO₄ > AR > HNO₃. Fontana et al. compared indium leaching from LCD panels with 6 N solutions of HCl, H₂SO₄, and HNO₃ at room temperature, reporting HCl as the best acid for indium leaching (>90%) [259]. Other studies have also shown excellent indium leaching efficiencies in presence of HCl [156, 226, 241, 257]. This observation fits well with the findings in this work that showed in the extraction studies developed using Aliquat 336 and Cyphos 101 the best indium extraction was achieved in hydrochloric acid medium, so HCl was selected as the leaching reagent to be applied to LCD panels. Despite the higher cost of HCl with respect to H₂SO₄ and the high concentrations of the acid required which may present challenges in industrial applications, the use of HCl in both parts of the leaching and extraction process permits recycle of HCl within the total process creating a closed-loop cycle.

Although indium was completely leached under optimal conditions (in untreated LCD panels), several other metals were also present with much higher concentration such as Cu, Fe, Al, Ni, Mg, Zn, etc., where indium only represented 1.2% of the total metal content. This problem was solved by development of a two-stage pre-treatment with a hot water bath, followed by an acetone bath. This pre-treatment permits the separation of the polarisers from the LCD panels, leaving an LCD fraction rich in indium, representing 51% of the total metal content. In general, pre-treatments reported in the literature have been carried out with the focus on metal enrichment, and not on the potential for recycle of materials. Rocchetti et al. for example successfully enriched indium in a series of cross-current leaching from EoL LCD panels [149]. In the process, prior to indium leaching, the LCD panels went through two shredding processes; a knife mill, followed by a blade grinding. In between these processes, large plastic and glass fragments were manually removed, representing 10% of the total feed material. Those plastics fragments were considered as a waste product, although they could have been recovered. The findings from the current research however have shown that the shredding of glass substrate with polymers attached can prolong the process time and increase total costs and energy consumption. Fontana et al. reported the study of chemical and thermal treatments for the

separation of the polarisers from discarded LCD monitors [259]. The chemical treatments consisted of soaking of the LCDs in different organic solvents (acetone, ethyl acetate and limonene), using ultrasound (35 KHz), and 3 ml/g LCDs. Polarisers were removed after 3-8 h, however, the films were heavily damaged, with grooves and showing some porosity. The thermal treatment applied liquid nitrogen ($T=-196\text{ }^{\circ}\text{C}$) for 10-20 minutes. Although this method did not show significant damage to the polarisers, it requires 25 L/kg of waste LCDs and work with 'dangerous' temperatures, increasing the process operational cost and risks. Neither study mentioned the potential for liquid crystal to be recovered. In the current research, however, polarisers showed no damaged after pre-treatment, except for the PVA film showing some grooves, and furthermore, an attempt was made to recover liquid crystal. Following the bath treatment with acetone, several polarisers were separated using the recycled acetone, which was separated by vacuum distillation, to conserve reagent use. The amount of liquid crystal, however, was not sufficient for further analysis, likely due to small size of the mobile phone LCD panels. An alternative liquid crystal recovery from LCD monitors was reported by Zhang et al. using pyrolysis, in which liquid crystals can be well separated at $600\text{ }^{\circ}\text{C}$, 40 min and 2 L/min N_2 flow from the crushed powder, where oil and gas produced in the process can be reused as energy and fuel [250]. This process also enriched the indium concentration, favouring its recovery.

Another critical factor in the indium leaching is the particle size of the shredded LCDs. It is well-known that the size of the material is inversely proportional to its leaching capability, however, particles smaller than a size threshold will increase the energy consumption and time, increasing the operational cost of the process. Swain et al. recommended that waste LCD should be crushed to pieces of 1 mm or smaller for optimal indium liberation [226]. Most studies reported in Table 6.8 used LCD panels crushed to 1mm or less. Zhang et al. showed that indium can be leached without shredding [257]. They manually dismantled computer LCDs, peeled off the polarisers by contacting them with pure alcohol, followed by the separation of the glass substrate using a knife (due to the size of the panel, pieces of $4\times 4\text{ cm}^2$ were cut for experiments). They found that since ITO was located on the surface of the glass substrate, there was no need for crushing as it would not affect the leaching due to the exposure of the ITO layers. In the current research, treated LCD panels were cut in pieces of $0.5\times 0.5\text{ cm}^2$, process that was easily carried out manually due to the brittle nature of glass, and leached by HCl on optimal conditions. The results showed that indium was completely leached, dispensing with the shredding process. Although LCDs screens from mobile phones are small and more difficult to separate the substrate glass layers, leaching was still achieved.

6.3.3 Application of the Optimised Conditions for Recovery of Indium from Waste LCD Screens

The optimal conditions developed for indium extraction and recovery from indium-rich samples using a Model Test System have been applied to pre-treated real samples of LCD panels and the results are now described. The results of the extraction process trialled using separately the two ILs, Cyphos 101 and Aliquat 336, followed by stripping and reduction steps are discussed here. The potential for recovery of ionic liquids for recycle and reuse to minimise reagent use described elsewhere in this chapter are discussed in terms of the real sample investigation.

6.3.3.1 Extraction of Indium from Leach Liquor from Pre-treated Waste LCD Screens

Leach liquor derived from the treatment of LCD panels (*pre-treated strip LCD panels*) under the conditions (60 °C, 2 h, 3 M HCl, and s/l ratio of 1:20) was separated from the residue using centrifugation at 3000 rpm for 10 minutes and the solution was kept for further analysis. The leach liquor was contacted with 0.1M Cyphos 101 and separately in 0.1M Aliquat 336 (each in toluene as diluent) at room temperature (20 °C), for 15 minutes (to achieve equilibrium) and with an aqueous to organic ratio of 1:1. The extraction results are shown in Figure 6.25 for Cyphos 101 and in Figure 6.26 for Aliquat 336 and Table 6.10 summarises the metal concentration in the organic and aqueous phases, and the extraction efficiencies of the ILs. Using both ILs the almost complete extraction of indium was achieved with 98% and 96% extracted with Cyphos 101 and Aliquat 336, respectively. The main contaminants in the leach LCD liquor (Al and Fe) were also completely extracted with both ILs, which could be beneficial in two ways. Firstly, as the metals with the highest concentration are extracted in the leach liquor, further stripping methods can be used to selectively recover these metals. Secondly, the metals remaining in the leach liquor have relatively low concentration of impurities, allowing the liquor to be reused for further leaching processes, thereby reducing the use of new hydrochloric acid. The distribution of metals following extraction in both ILs (Figure 6.25c and Figure 6.26 c) shows that indium represented nearly 52%, followed by iron and aluminium with 24% and 16%, respectively. The metal distribution in the organic and aqueous phases (Figure 6.25d and Figure 6.26 d) suggests that metals such as Ba, Mg, Mn, Ni and Sr do not have affinity for the ILs showing almost zero extraction; it is noted strontium, at a concentration of 4.7 g/L in the aqueous phase, is relatively higher than other metals (of <1.5 mg/L). Whilst Ti did not show affinity for Cyphos 101, nearly 50% was extracted by Aliquat 336. The metals Ga and Cr were partially extracted with both ILs, which shows the selectivity of the ILs towards different metals. Although not considered further as part of this research this information about the selectivity of the ILs for certain metals can be used to develop further separation processes, as appropriate. In general, both Cyphos 101 and Aliquat 336

presented very similar extraction efficiencies, with indium being successfully extracted from leached pre-treated LCD liquor.

Table 6.10: Metal concentration in the organic and aqueous phases, and extraction efficiencies of ILs.

Elements	Cyphos 101			Aliquat 336		
	Organic phase (mg/L)	Aqueous phase (mg/L)	Extraction Eff. (%)	Organic phase (mg/L)	Aqueous phase (mg/L)	Extraction Eff. (%)
Al	9.95	0.05	99.5	9.93	0.08	99.3
Ba	<DL	0.13	<DL	<DL	0.13	<DL
Cd	0.51	<DL	100.0	0.51	<DL	100.0
Cr	0.08	0.05	39.6	0.05	0.07	42.3
Cu	0.43	<DL	100.0	0.43	<DL	100.0
Fe ³⁺	14.76	<DL	100.0	14.76	<DL	100.0
Fe ²⁺	0.151	14.14	1.0	0.17	14.21	1.1
Ga	0.127	0.26	66.8	0.27	0.12	69.2
In	32.68	0.61	98.1	32.07	1.22	96.3
Mg	<DL	1.66	<DL	<DL	1.66	<DL
Mn	<DL	1.33	<DL	<DL	1.33	<DL
Ni	<DL	0.31	<DL	<DL	0.31	<DL
Pb	1.72	<DL	100.0	1.72	<DL	100.0
Sr	0.15	4.57	3.2	0.05	4.67	1.1
Ti	<DL	0.06	<DL	0.04	0.04	<DL
Zn	1.64	0.03	100.0	1.64	<DL	100.0

Standard deviation ≤5% in all the cases.

<DL: Under detection limit.

Fe³⁺: Original iron concentration without any addition of ascorbic acid.

Fe²⁺: Iron concentration after a 3-fold molar excess of ascorbic acid in the leach liquor.

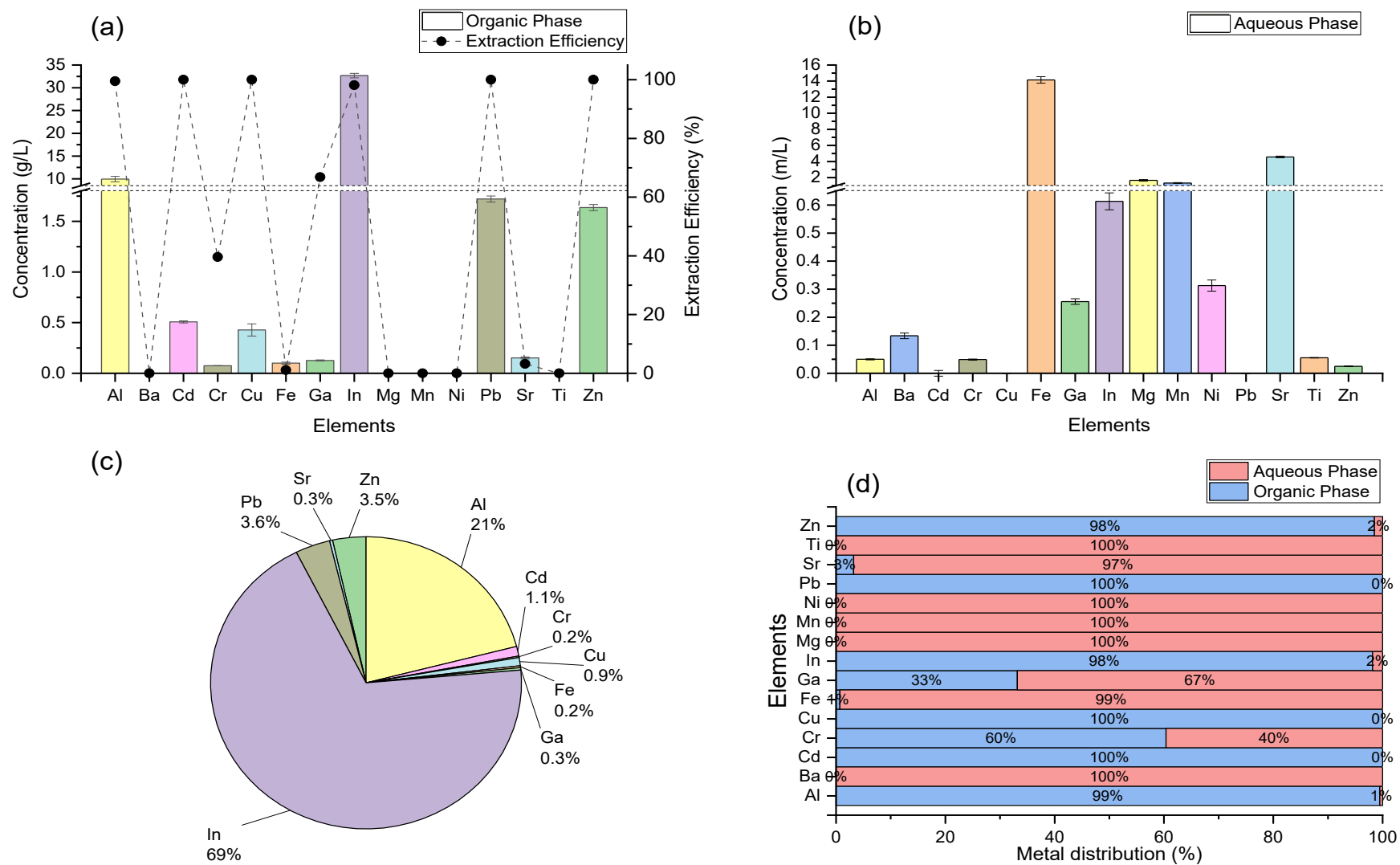


Figure 6.25: Indium extraction from leach liquor derived from pre-treated strip LCD panels by 0.1M Cyphos 101; (a) metals in the organic phase and extraction efficiencies, (b) metals in the aqueous phase, (c) metal distribution of the extracted metals, and (d) metal distribution in the organic and aqueous phases after extraction.

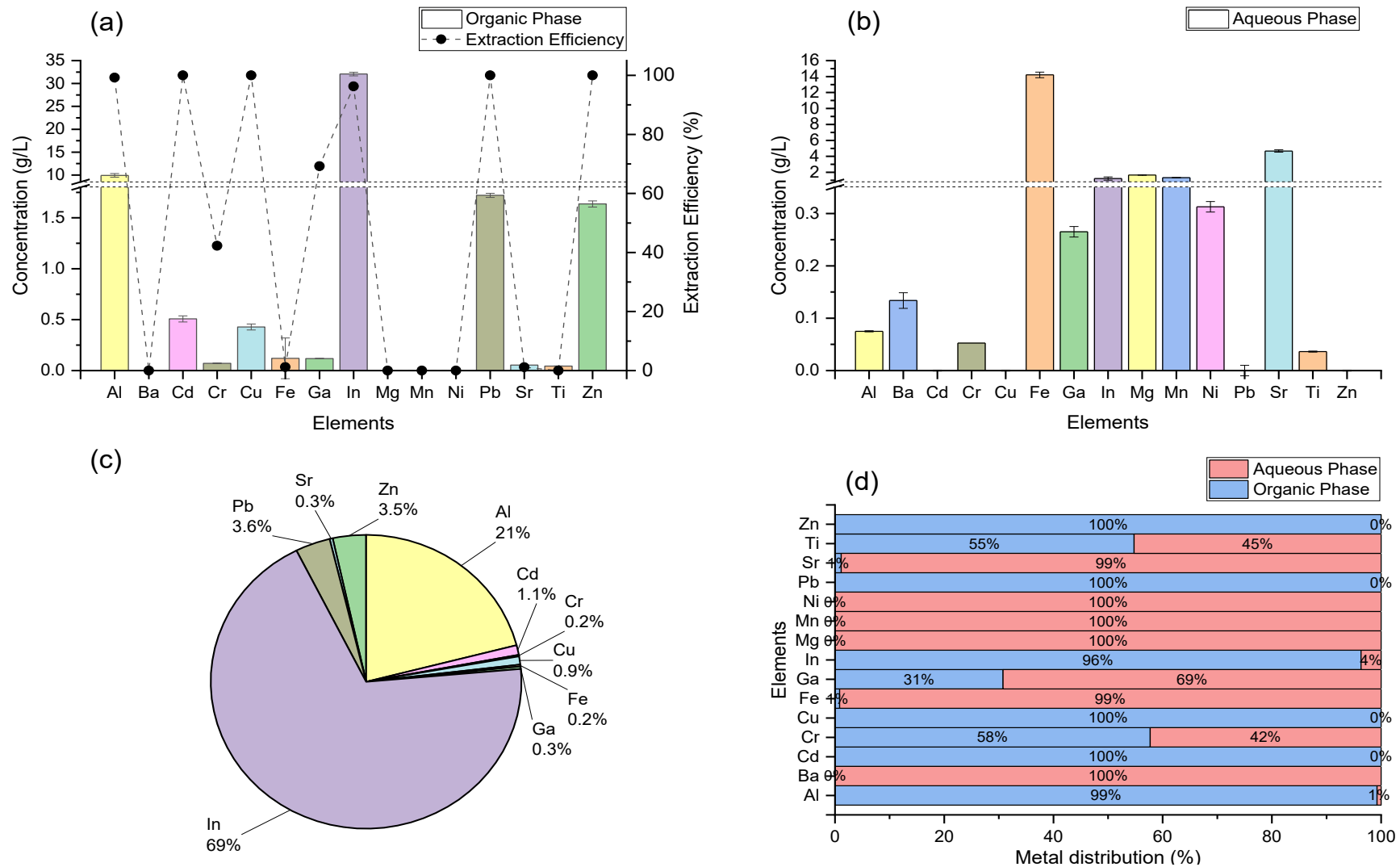


Figure 6.26: Indium extraction from leach liquor derived from pre-treated strip LCD panels by 0.1M Aliquat 336; (a) metals in the organic phase and extraction efficiencies, (b) metals in the aqueous phase, (c) metal distribution of the extracted metals, and (d) metal distribution in the organic and aqueous phases after extraction.

6.3.3.2 Extraction of Indium Using Counter-current Extraction with Ionic Liquids

To increase the concentration of indium counter-current extraction was studied with different volumes of organic and aqueous phases. Extraction isotherms were drawn to calculate the number of extraction stages required for indium by varying the aqueous: organic ratio (A:O), from 1/5 to 5/1, while keeping total volume of phases constant at 12 mL. The feed solution was derived from the leaching of *pre-treated strip LCD panels* at 3M HCl, 60 °C for 2 h, whilst the organic phase was 0.1M of each IL in toluene. McCabe-Thiele diagrams for the indium extraction are presented for Cyphos 101 in Figure 6.27a, and for Aliquat 336 in Figure 6.28a.

The McCabe-Thiele diagrams show that Cyphos 101 has a greater extraction capacity for indium than Aliquat 336. This result agrees with the findings reported earlier in this chapter (Figure 6.6) that show Cyphos 101 to consistently out-perform Aliquat 336 and achieve higher indium extraction. This behaviour is also confirmed by the steeper slope obtained for Cyphos 101 (Figure 6.27a), where at A:O=1:1, Cyphos 101 extracted 100% of indium in one step, whilst Aliquat 336 extracted approximately 90% (Figure 6.28a), requiring 2 stages for complete indium extraction.

To validate the McCabe-Thiele diagrams, a two stage counter-current experiment was carried out in toluene at A:O=7/2 for 0.1M Cyphos 101 (Figure 6.27b) and at A:O=2/1 for 0.1M Aliquat 336 (Figure 6.28b). These ratios were chosen so that the two ILs could be compared. It was expected that with an increase in the A:O ratio more indium will be available for the validation of the McCabe-Thiele diagram. Simply increasing the ratio to A:O=2:1 for Cyphos 101, two stages are theoretically required for complete indium extraction using (shown as the green lines in Figure 6.27a), yet with only one stage, more than 95% of the indium can be extracted. At this ratio of A:O=2:1, however, it was not clear if 1 or 2 stages is required for Cyphos 101, so the McCabe-Thiele diagram cannot be validated. For comparative purposes and for validation, therefore, with the selected ratios two stages of counter-current extraction could be obtained theoretically from the McCabe-Thiele diagrams, and it is easier to corroborate this by measuring the indium concentration at each stage, leading to validation of the diagrams. The results from these experiments indicate that 100% of indium is extracted with 2 stages of counter-current by Cyphos 101, whilst Aliquat 336 extracted 96%, as predicted in the McCabe-Thiele diagrams. The final indium concentration in the loaded Cyphos 101 was 115.3 mg/L, and 63.2 mg/L in the loaded Aliquat 336. Other metals present in the LCD leach liquor were also concentrated in the 2-stage process, namely, aluminium, lead, and zinc as the main contaminants. Of these three metals, aluminium is the main concern since its concentration increased to 33.4 mg/L and 19.1 mg/L in Cyphos 101 and Aliquat 336, respectively. This problem is addressed in the discussion on the stripping of indium from solution (Section 6.3.3.3). It is worth noting that the leach liquor used to draw

these McCabe-Thiele diagrams, ascorbic acid was added, which reduces iron from Fe^{3+} to Fe^{2+} , and Fe^{2+} is not extracted by the ILs. Figure A.9 and Figure A.10 contained in Appendix show the extraction without the addition of ascorbic acid, and iron is completely extracted, with concentration of 48.5 mg/L and 25.6 mg/L for Cyphos 101 and Aliquat 336, respectively.

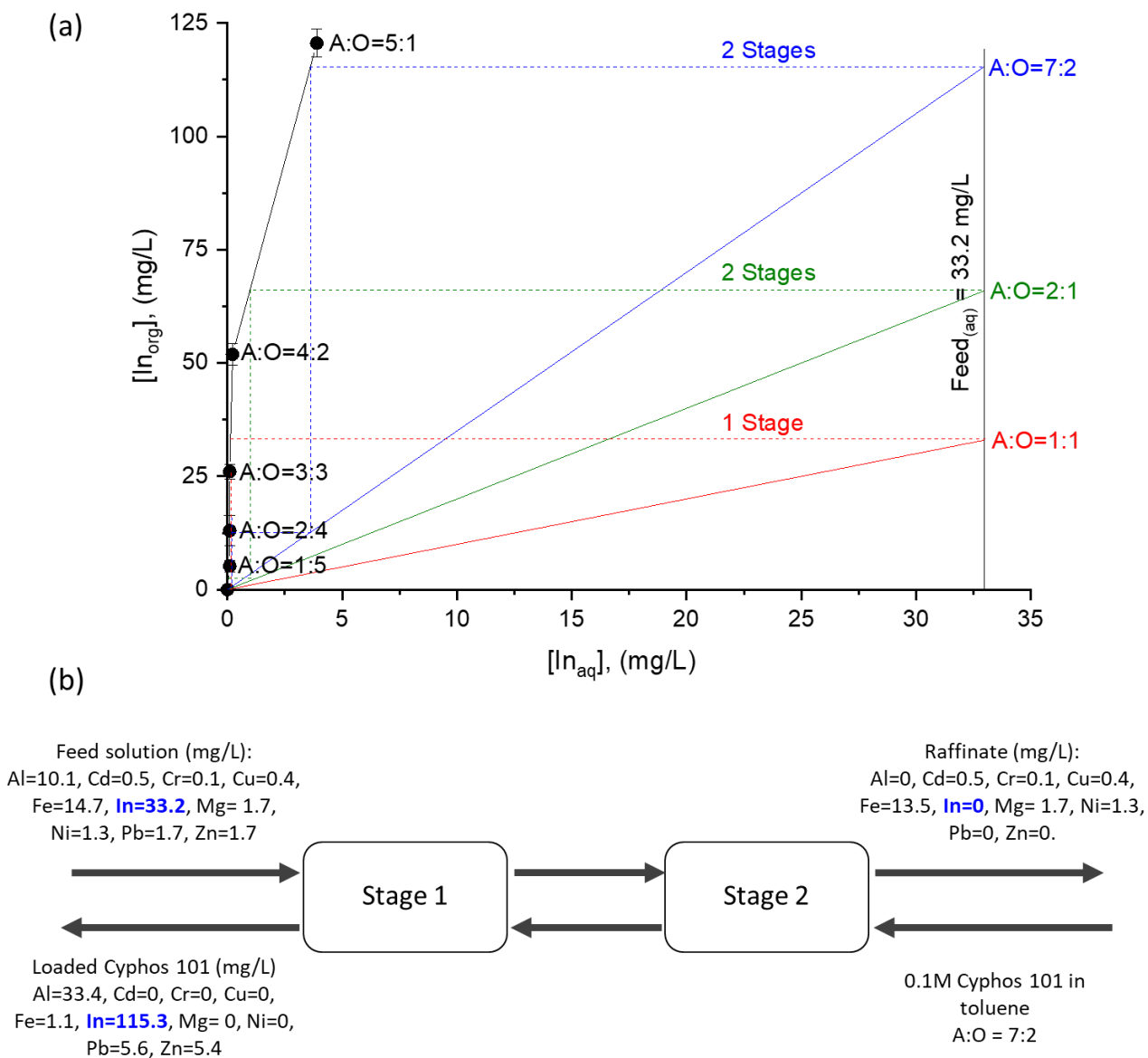


Figure 6.27: Indium extraction by Cyphos 101; (a) McCabe-Thiele plot for In, and (b) Counter-current on the extraction of In from pre-treated strip LCD panels leached in hydrochloric medium.

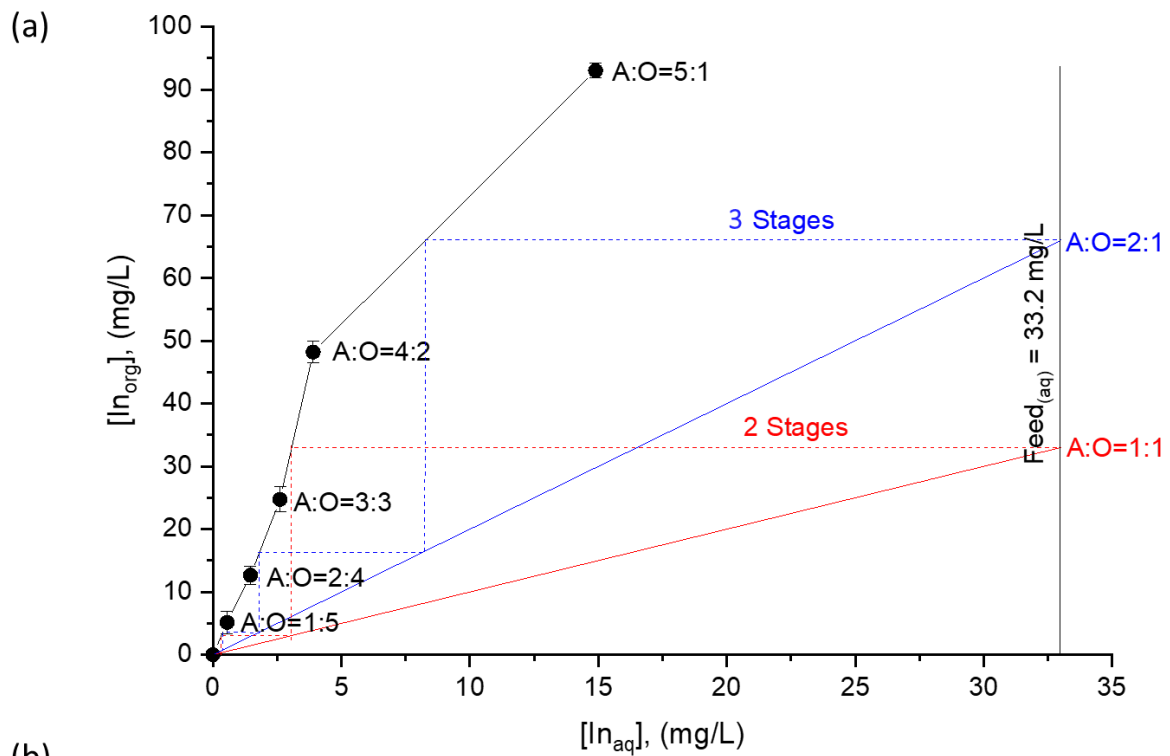


Figure 6.28: Indium extraction by Aliquat 336; (a) McCabe-Thiele plot for In, and (b) Counter-current on the extraction of In from pre-treated strip LCD panels leached in hydrochloric medium.

6.3.3.3 Stripping of Indium from the Loaded Organic Phase

Although indium can be stripped at low H_2SO_4 concentration, several other metals present in the ILs can also be stripped and their presence could also be influenced by changes in acid concentration. To investigate the influence on metal stripping loaded organic phases (obtained from the extraction of leached liquor of *pre-treated strip LCD panels*), were stripped with different H_2SO_4 concentrations under optimal conditions. As observed in Table 6.7 of the metal leaching from *pre-treated strip LCD panels*, the main contaminant metals in the leach liquor are aluminium and iron, with concentrations of approximately 10 mg/L and 15 mg/L for Al and Fe, respectively. It is also observed (in Section 6.3.3.2) that these two metals can be effectively extracted with both ILs (Table 6.10). In the stripping studies trialled with different H_2SO_4 concentrations after extraction of ILs in toluene of real sample, shown in Figure 6.29, it is observed that Al does not strip out from the organic phase, so a complete separation is achieved. It is worth to note that, although 0.1M H_2SO_4 was selected as the stripping solution in the test model solution (Section 6.3.1.3), the effect of the concentration of H_2SO_4 in the stripping step (Figure 6.29) was further analysed with real sample (at room temperature with an A:O ratio of 1.5:1), due to the presence of other metals that can affect the effectiveness of the indium recovery process. In the case of Fe, it was completely stripped at low H_2SO_4 concentrations (0.1M-1M), with the extent of stripping decreasing as the H_2SO_4 concentrations increase. The stripping of iron is a problem since the stripped solution contained approximately 20 mg/L of In and 10 mg/L of Fe, with other minor contaminants (<1 mg/L), suggesting further steps for separation and recovery of indium will be needed. In the literature, it was reported that the use of ascorbic acid can reduce iron from Fe^{3+} to Fe^{2+} , which in the lower oxidation states is not extracted by the ILs [156]. With a 3-fold molar excess of ascorbic acid added to the leach liquor, as observed in the reduced iron in solution (Table 6.10) was not extracted by the organic phase. Thus, complete separation of In, Fe and Al was successfully achieved.

The results of the stripping efficiency and the concentration of the main metals present in the organic phase, after extraction from leach liquor from *pre-treated strip LCD panels* are presented in Figure 6.29. In the same way the indium stripping varied with acid concentration (Figure 6.11), the stripping of other metals varied as a function of H_2SO_4 concentration. Copper was stripped across the full range of H_2SO_4 concentrations studied, however, since its concentration is low (0.428 mg/L), it was considered as a minor impurity of the process. Using a 0.1M H_2SO_4 stripping solution, the results in Table 6.11 show the final metal concentration in the stripping solution with indium completely stripped, with a concentration of approximately 21.7 mg/L from both ILs, representing a 97.1% and 91.4% of total metals stripped for Cyphos 101 and Aliquat 336, respectively. Aluminium and iron, the main undesirable metals, were selectively separated, with iron in the leach liquor and aluminium still

in the organic phase, which can be stripped by other acids. The high indium concentration in both stripped solutions provide a source rich in indium which can be further processed for recovery.

Table 6.11: Final metal composition and concentration of the stripping solution by 0.1M H₂SO₄.

Elements	Cyphos 101			Aliquat 336		
	Concentration (mg/L)	Extraction Eff. (%)	Metal distribution (%)	Concentration (mg/L)	Extraction Eff. (%)	Metal distribution (%)
Al	<DL	<DL	-	0.09	2.21	0.41
Cd	0.12	35.22	0.52	0.06	18.50	0.32
Cr	<DL	1.21	0.00	0.01	2.11	0.01
Cu	0.29	100.00	1.32	0.29	100.00	1.20
Fe	0.11	1.24	0.50	0.12	1.10	0.41
Ga	0.05	29.41	0.21	0.05	29.31	0.20
In	21.82	100.00	97.10	21.61	100.00	91.41
Mn	<DL	<DL	-	<DL	<DL	-
Ni	<DL	<DL	-	<DL	<DL	-
Pb	<DL	<DL	-	0.95	83.31	4.00
Zn	0.08	7.20	0.40	0.48	43.12	2.01

Standard deviation ≤5% in all the cases.

<DL: Under detection limit.

6.3.3.3.1 Discussion

It is shown that a 0.1 M H₂SO₄ solution at room temperature with an A:O ratio of 1.5:1 can completely strip indium but as acid concentration increases the effectiveness of the acid stripping diminishes. The driving force for the extraction with Aliquat 336 and Cyphos 101 is the presence of chloride anions, whilst the stripping of metals is efficient if the distribution ratio (metal in the organic phase/metal in the aqueous phase) is low. Theoretically, a low distribution ratio can be achieved by the addition of water, which decreases the chloride concentration. Nevertheless, although indium can be partially stripped with water, it is not efficient [215]. Thus, slightly acid solutions are advisable for stripping. Nayak and Devi studied several stripping agents such as hydrochloric acid, sulphuric acid, nitric acid and ammonia solution at different concentrations for indium extraction from Cyphos 104, finding that 0.1 M HCl was the best stripping agent [236]. Whilst authors have reported the use of different acids and different concentrations for stripping indium, interrogation of the comparative data contained in Table 6.8 and Table 6.9, compiled from the literature, suggest, HCl and H₂SO₄ as the ones most used.

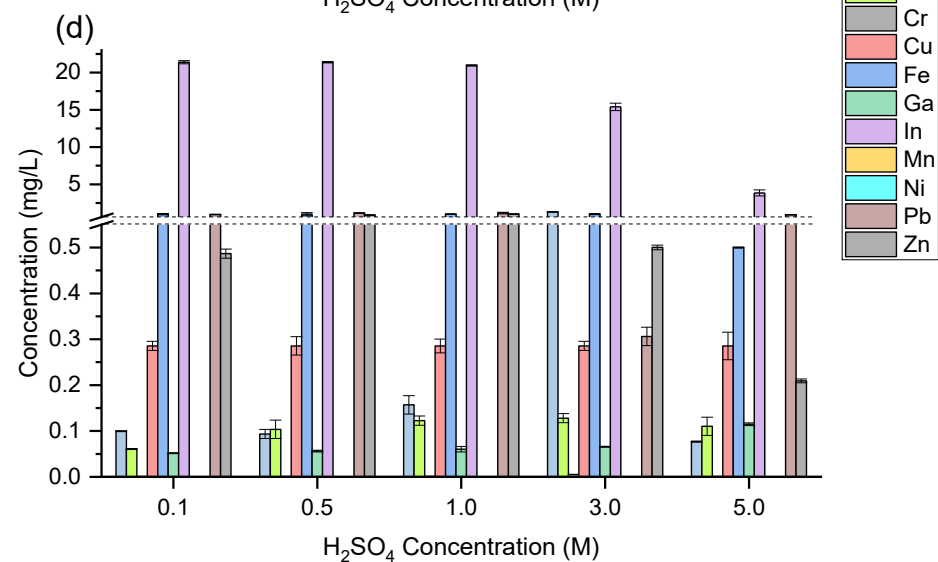
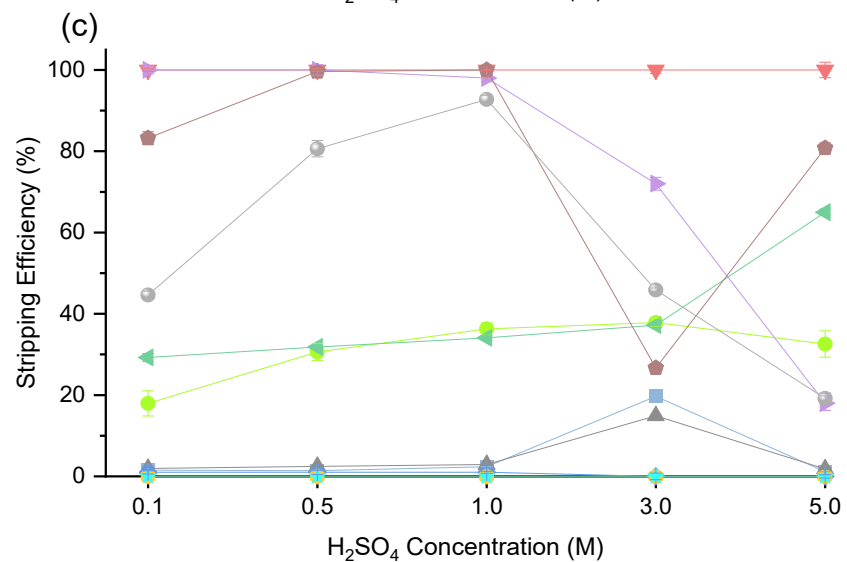
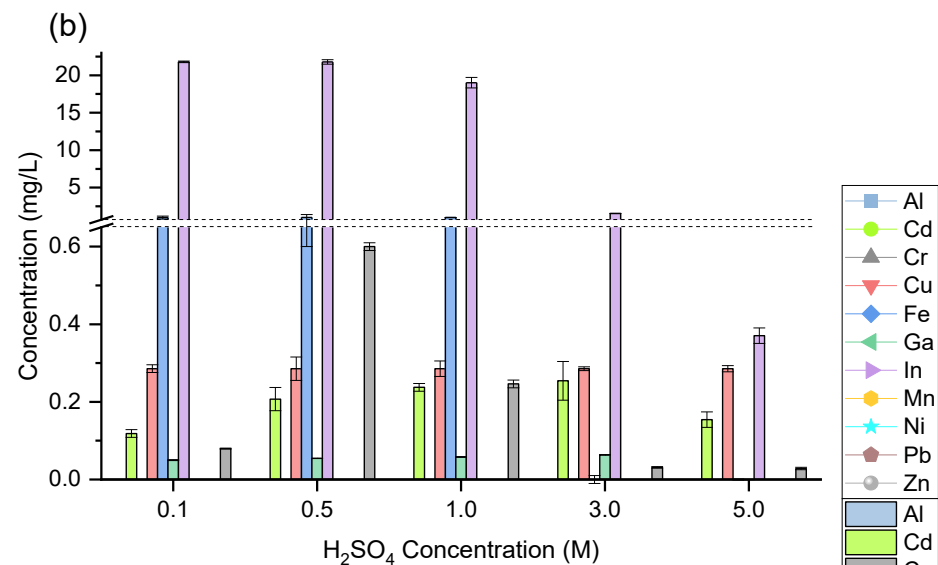
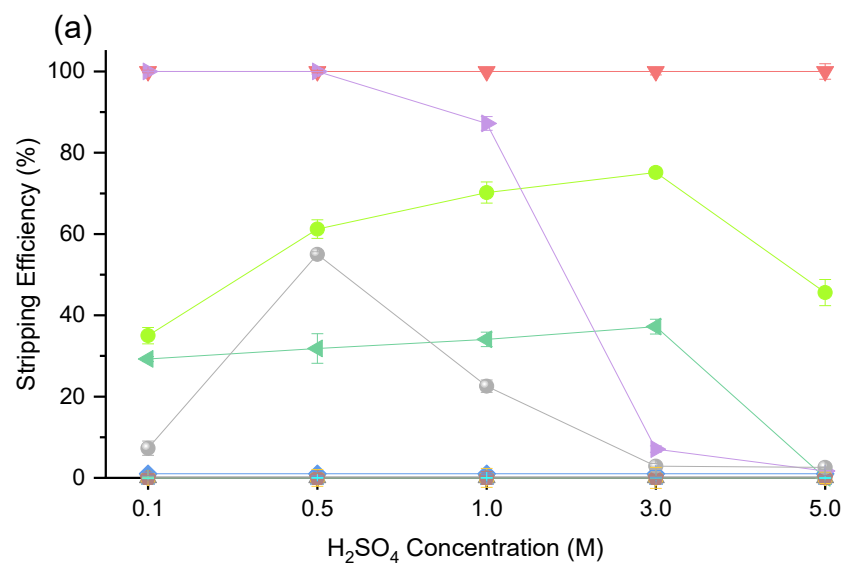


Figure 6.29: Metal stripping from loaded 0.1M ILs with different H₂SO₄ concentrations; (a) and (b) Cyphos 101, (c) and (d) Aliquat 336.

6.3.4 Proposed Hydrometallurgical Process for Indium recovery from LCD Panels (as ITO Glass Substrate Fractions)

The potential for recovery of indium from waste LCD panels derived from EoL Mobile Phones has been investigated and a hydrometallurgical process using the ionic liquids Cyphos 101 and Aliquat 336, is developed. It is shown that pre-treatment of the as-received LCD panels is necessary to concentrate the indium, produce an indium rich source from which the target metal can be recovered in a three-step process of extraction, stripping, and reduction. Important factors in the development of an optimised process for recovery of indium include minimisation of reagent use and reduced energy consumption. In this context the efficiency of leaching was carefully controlled, with the recycle of leach liquors and recovery of ILs for recycle and reuse in the extraction and stripping process being trialled. Using a Model Test System containing indium, a detailed investigation of each step was carried out to maximise material recovery and optimise process parameters, including acid concentration, temperature, IL concentration, solid liquid ratios, reaction time, etc., the process conditions of extraction, separation and recovery were optimised.

A pre-treatment step to remove polymeric films from as-received EoL Mobile Phone screens was developed to provide access to the indium-rich source embedded in the ITO glass substrate. A two-step process involving immersion of *LCD panels* in a hot water bath followed by an acetone bath successfully removed the polarising films leaving a glass substrate rich in ITO from which indium can be recovered and the residual glass can be recycled.

The four-step process of leaching, extraction, stripping, and reduction developed to recover indium metal or indium oxide from the ITO glass substrate using ionic liquids is illustrated in Figure 6.30. The process developed using *strip pre-treated LCD panels* from as-received EoL-MPs can be applied to other waste LCD panels. The overall indium recovery efficiency was >90%, obtaining metallic indium (via cementation) and indium oxide (via a precipitation-calcination step) in pure form for reuse in commercial products. As part of the trials the recycle and reuse of reagents was studied, and the efficiency and effectiveness in recovery of target indium was maintained over multiple cycles. The whole process shown here in Figure 6.30 was repeated for a second cycle to confirm the recyclability of the ILs, and the process efficiency, and a total efficiency >90% was successfully achieved. All the experiments were carried out in a laboratory scale with excellent results, which can now be applied on a larger scale.

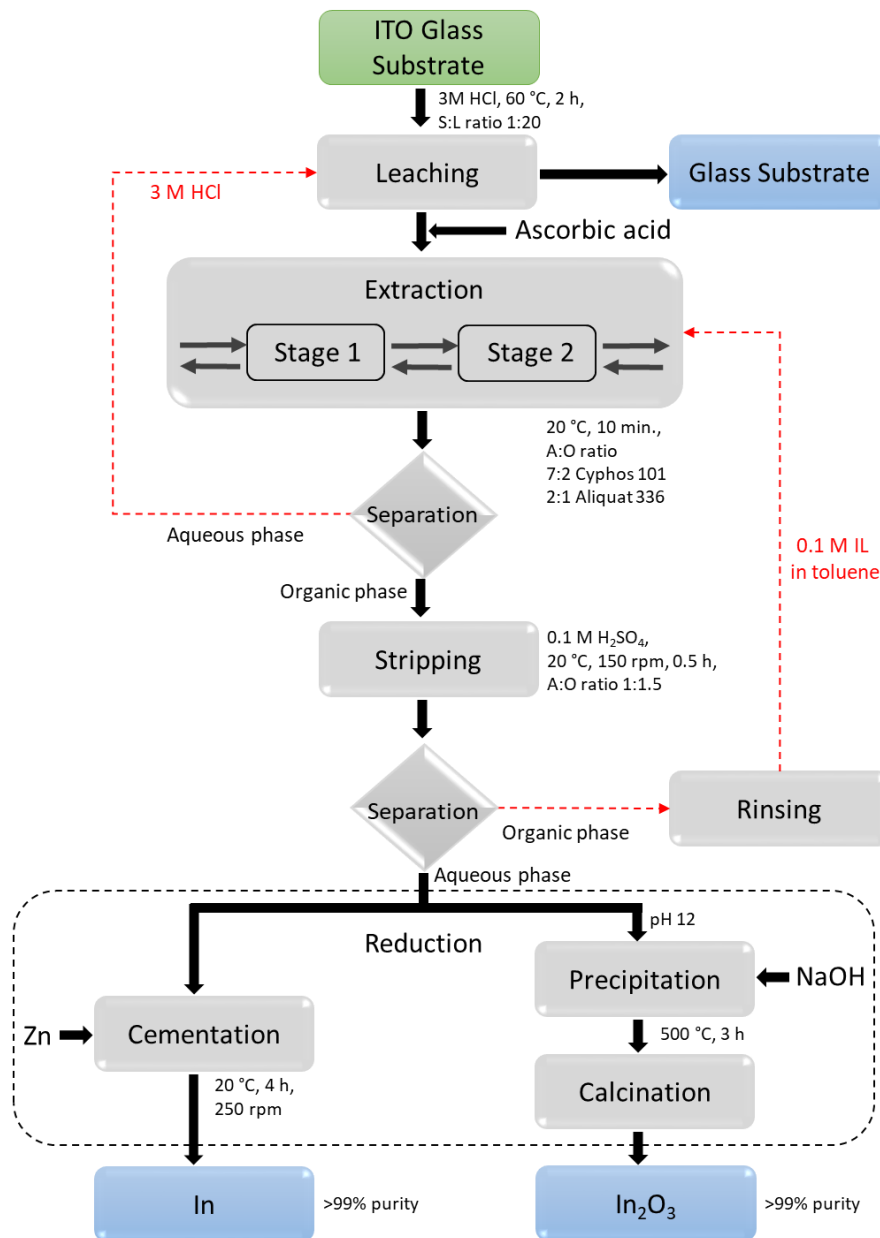


Figure 6.30: Process Developed for Indium Recovery from ITO Glass Substrate.

The complete recovery process developed in this work to produce indium and indium oxide from as-received EoL MP LCD screens is illustrated in Figure 6.31. The total indium recovery efficiency is >90%, and the separated components of frames, polymers films, polarisers, liquid crystal, and glass substrate have also been separated for recovery and for reuse. In the process studies have shown that the ILs can be recovered and recycled as part of the process and, because of the relatively high concentrations of iron and aluminium in the leach liquor, there is potential for them also to be recovered.

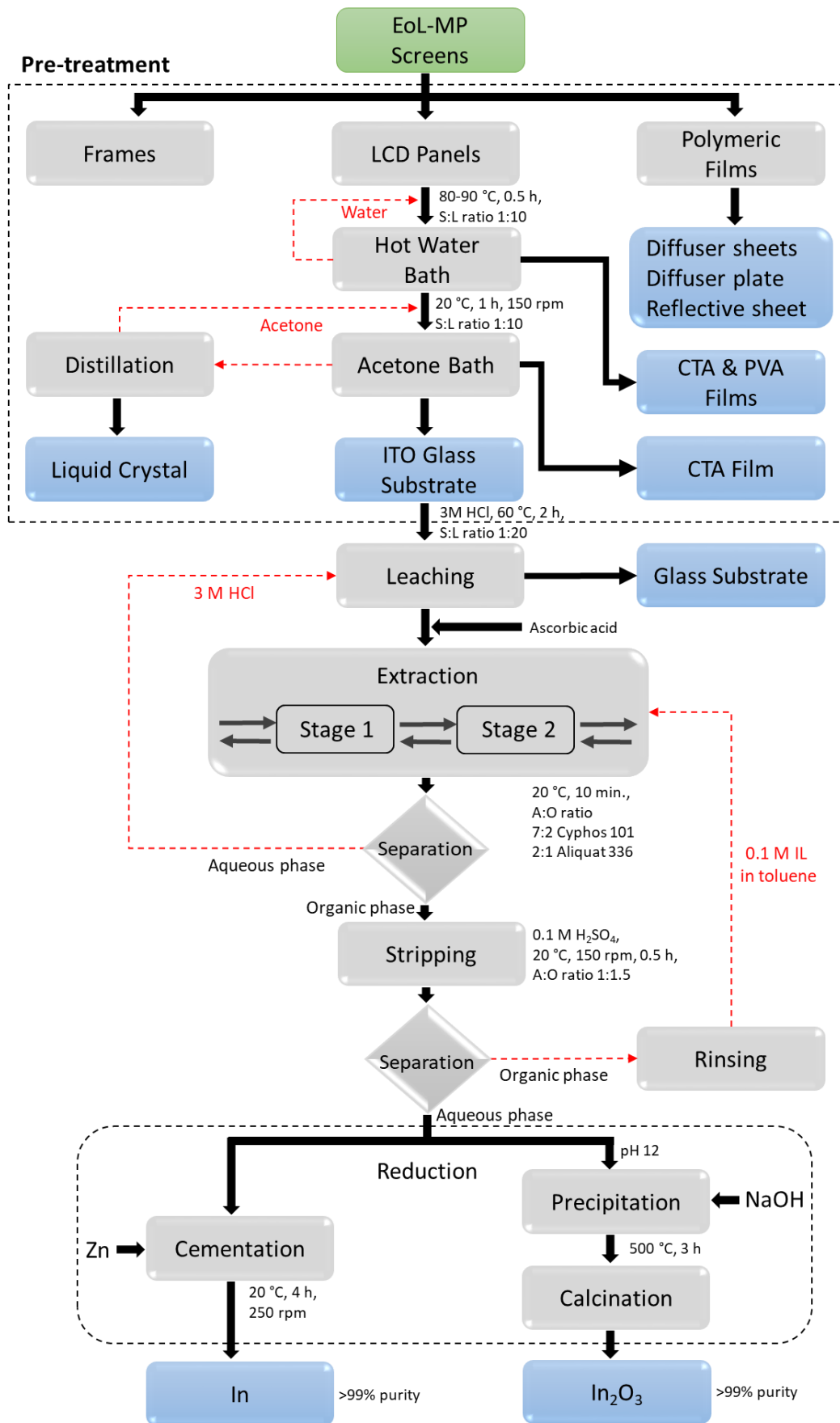


Figure 6.31: Flowsheet for Process Developed for Total Indium Recovery from EoL-MP screens.

6.4 Summary

In this chapter a hydrometallurgical process has been developed, which involves a leaching, extraction, stripping and reduction step, using, separately, two ionic liquids, Cyphos 101 and Aliquat 336, for the recovery of indium from waste LCDs derived from EoL-MPs. The process developed initially using a Model Test System (a simulated solution of indium) was optimised at each process stage before application on real as-received waste fractions. Due to the relatively low indium concentration in the waste LCDs, a pre-treatment step was deemed necessary. The process was developed and optimised to separate the polymeric films attached to the LCD panels, to enable access to an enriched indium source embedded in the glass substrate, and at the same to recover other non-target materials for recycle and reuse.

EoL-MP screens can be manually separated from mobile phones, where frames, polymeric films and LCD panels are easily dismantled. This first separation results in the recovery of diffuser sheets and plates. Further treatment of the LCD panels with a two-step immersion in a hot bath of water (80-90 °C, 0.5 h, S:L=1:10), followed by an acetone bath (20 °C, 1 h, S:L=1:10, 150 rpm) can effectively separate the polarisers (CTA and PVA films) attached on the LCD panels. The final product of the pre-treatment is an ITO glass substrate rich in indium, enriching the indium concentration nearly 50 times compare to the dismantled as-received LCD panels.

Indium leaching by three mineral acids (HCl, H₂SO₄, and HNO₃) showed that hydrochloric and sulphuric acids were the most suitable, leaching nearly 100% of indium under optimal conditions (60 °C, 2 h, 3 M, S:L=1:20 for both acids). Due to the affinity of the ILs used in the next step of extraction for HCl, hydrochloric was selected as the leaching reagent. Direct leaching on *untreated powder LCD panels* showed an indium concentration of 0.7 mg/L, with several contaminants including Cu, Al, Fe, and Zn. Leach liquor, under optimal conditions, obtained from *pre-treated powder LCD panels*, showed complete indium leaching with a concentration of 33.2 mg/L. In addition, it was found that the pre-treated LCD panels using strips, as *pre-treated strip LCD panels*, did not need a second shredding process (as LCD panels go through a first cutting of 1x1 cm², followed by a milling, to obtain LCD powder of ≤150 μm), allowing direct leaching of the *pre-treated strip LCD panels*, which reduces the energy consumption of the process.

The extraction process was carried out separately using the ionic liquids, Cyphos 101 and Aliquat 336, as extractants. Different organic solvents were studied for dilution with toluene proving to be the most effective. The extraction mechanism of the two ILs in chlorinated medium showed a one-to-one indium to IL molecule complex. The evaluated thermodynamic parameters suggest the

process to be spontaneous and endothermic. Several metals present in LCD panels were simultaneously extracted, with Al and Fe being the main undesirable metals, whilst other metals present were lower than 5% of the total metal extracted. The addition of ascorbic acid after leaching, however reduced Fe^{3+} to Fe^{2+} , which, in the reduced form is not extracted by the ILs, increasing the representation of indium in the extraction from 51% to 69%. Based on McCabe-Thiele diagrams, a two counter-current extraction was performed with A:O ratios of 7:2 and 2:1 for Cyphos 101 and Aliquat 336, respectively. The results showed an indium extraction of 100% using Cyphos 101 and 96% with Aliquat 336. Aluminium was not extracted by the ILs, separating In, Fe and Al in one step.

Finally, indium stripping from the organic phase was performed using the optimal acid concentration of 0.1 M H_2SO_4 , $V(\text{H}_2\text{SO}_4)/V(\text{IL})$ ratio of 1.5:1, 150 rpm, for 30 minutes. Indium was recovered as the metal via cementation by adding zinc at 20 °C, 4 h and 250 rpm (adding 2 times the amount of zinc required stoichiometrically), and as the oxide via precipitation by adding NaOH at pH 12, followed by a calcination at 500 °C for 3 h. The ILs, Cyphos 101 and Aliquat 336 were able to be recycled and reused five times, showing no sign of losing extraction capability. Based on these results, two indium recovery processes are proposed, with both achieving an overall efficiency >90%. The hydrometallurgical processes developed could easily be applied to any EoL waste LCD and thin film streams for the recovery of the target metal indium.

In summary a whole material and indium recovery process, from LCD panels derived from EoL-MPs, is proposed for the first time.

7 Recovery of Rare-earth Elements from EoL Mobile Phone Speakers Using Ionic Liquids

7.1 Introduction

Rare earth elements (REEs) are a group of 17 chemically similar metallic elements (15 lanthanides, plus scandium and yttrium). REEs are often categorised into two sub-groups as light rare earth elements (LREEs, from La to Eu) and heavy rare earth elements (HREEs, from Gd to Lu, including Y). REEs are not rare in nature as their crustal abundance (169.1 ppm) is higher than base metals such as zinc (70 ppm), copper (60 ppm), nickel (84 ppm), and lead (14 ppm), for example [198, 262]. In general, LREEs (137.8 ppm) are more abundant than HREEs (31.3 ppm). Therefore, REEs are not *rare* as its name suggests, rather the word *rare* comes from the fact that REEs are not commonly concentrated as economic ore deposits, though the viable deposits are distributed across the world in relatively low concentrations [262, 263]. According to the United States Geological Survey, the worldwide REEs reserve estimation in 2021 was 120 million tonnes and China, Vietnam, Russia, and Brazil have 36.7%, 18.3%, 17.5% and 17.5% of these reserves, respectively. China has led the world production of REEs for decades, accounting for more than 90% of global production and supply during the past decade [263].

REEs are becoming increasingly important in the transition to a green and low-carbon economy. This is due to their essential role in photovoltaic panels, wind turbines, permanent magnets, lamp phosphors, rechargeable NiMH batteries, catalysts, and other applications [16, 27, 55, 264, 265]. REEs have also been used for military purposes (missile guiding systems by lasers, reconnaissance satellites, smart bombs, joint direct attack munition, etc.) and even in the agricultural sector (fertilisers, feeding additives to enhance growing and fattening of farming animals, etc.) [262]. In mobile phones, numerous components (e.g. loudspeakers, touchscreens, vibrators, and electronics) are manufactured using REEs [266]. In fact, coloured touchscreens, which have become one of the most distinctive feature in any current mobile phone, were only possible due to the luminescent and electromagnetic properties of REEs [267]. According to Kingsnorth, the demand for REEs could increase by 7–8% annually [268], whilst Dutta et al. predicted an annual growth rate of 5% by 2020 [269]. Furthermore, it was estimated that the demand for neodymium (Nd) and dysprosium (Dy) will increase 700% and 2600% by 2035 compared to the production of 2010 [270]. An increase in the demand for these REEs will also raise their prices. For instance, the cost of a tonne of neodymium

oxide was US\$ 15.7 thousand in 2018 and it is expected to increase up to US\$ 77.5 thousand in 2025 [271].

The substantial consumption of REEs and the monopoly of their production have created serious deficit problems such as the REEs dispute in 2010-2013, where China reduced the REE export quota by nearly 40%, triggering a global spike in REEs prices and creating instability and shortage, exposing the potential influence of the criticality of certain materials [55, 78]. The European Commission (EC) has reported a list of critical raw material since 2011, with an update every four years, in which REEs have been highlighted as the most critical raw materials, with the highest supply risk of all listed raw materials [16, 78, 225]. Similarly, the U.S. Department of Energy (DOE) has reported a list of critical elements, where five REEs (neodymium, europium, terbium, dysprosium and yttrium) were catalogued as the most critical elements [272]. REEs have also been categorised as critical or of the importance in several other studies and organisations [16, 55, 78, 79, 225]. Therefore, their importance is undeniable for the future of society. Hoogerstraete et al. reported that there are three possibilities of maintaining the supply of REEs [273]. Firstly, reopening abandoned rare-earth mines or opening new ones; however, it would require considerable time. Furthermore, the extraction of REEs from ores involves the use of toxic acids and can lead to the accumulation of radioactive waste due to REEs often being found in deposits rich in radioisotopes of thorium and uranium [262, 274]. Secondly, substitution of the most critical rare earths by less expensive rare earths or by d-group metals (elements that have a partially filled d orbital). Although some REEs could be substituted, any substituent is likely to be less effective and will probably require a redesign of the product. Thirdly, recycling REEs from waste electronic and electrical equipment (WEEE, also known as e-waste) [273]. Among these three alternatives, recycling REEs from e-waste is the most promising solution due to recycling being less polluting compared to extraction in primary ore production, smaller amount of chemicals are needed, lower energy consumption, and the process can diminish the dependency of REEs mining countries [275]. The recycling of REEs, however, remains very low, at between 1% and 5% [27, 262]. Although, initial steps have been made, and various technologies been introduced for REEs recovery, there are still several challenges to be overcome such as complicated logistics, extraction efficiency, selectivity, and process economics and feasibility [276]. The development of novel alternative recycling processes for REEs is therefore of crucial importance to mitigate the risk of shortages in the future.

Conventional methods such as pyrometallurgical and hydrometallurgical processes have been used in the recovery of metals from WEEE; however, many of these processes have constraints associated with their operation including being energy intensive, incurring high operational costs, and the liberation of toxic gases to the atmosphere, etc. for pyrometallurgical process [12, 104], whilst

hydrometallurgical processes consume a substantial amount of toxic, corrosive and flammable reagents, and can generate a large volume of wastewater that has to be further treated [12, 91, 104]. Despite the constraints associated with hydrometallurgical processes, they are preferred over pyrometallurgical methods because of their milder conditions, lower energy consumption, capital cost, and environmental impact. The key in the development of a recovery process is the combination of novel extraction approaches with conventional methods. In the search for new leaching/extraction reagents, ionic liquids (ILs) are highlighted as an efficient and more environment-friendly extractant [27, 264, 277]. Ionic liquids are solvents with remarkable properties; wide liquid range (from room temperature to above 300 °C), negligible vapour pressure (they do not produce hazardous vapours in contrast to many conventional organic solvents), excellent thermal, chemical and electrochemical stability, high ignition points, relatively low viscosity, and high recyclability [104, 105, 107]. Due to these outstanding properties, ILs are also known as the new green chemical revolution. ILs have been successfully utilised for metal extraction and separation of REEs from e-waste, especially from NdFeB magnets [265, 273, 277] and lamp phosphor waste [278-280], showing that ILs can be suitable for greener recycling processes of REEs. In those studies, less reagents were used compared to traditional processes, high extraction rates for REEs were achieved, and the ILs, in their majority, were recycled for further extractions.

The work described in this chapter therefore is focussed on the development of processes to recover REEs from as-received e-waste derived from EoL Mobile Phone speakers that combines the use of ionic liquids in two hydrometallurgical processes that offer a green and more sustainable alternative to conventional leaching and extraction processes.

7.2 Methodology

7.2.1 Materials

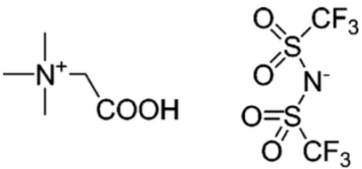
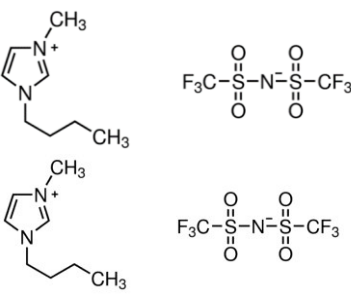
7.2.1.1 Chemicals and Reagents

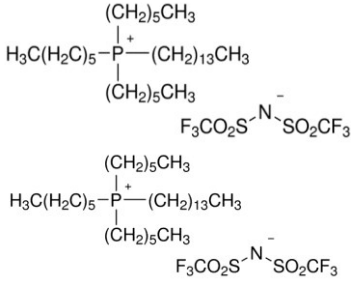
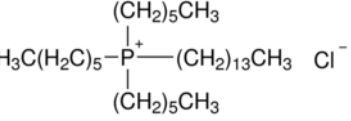
All chemicals were of reagent grade and obtained from either Sigma-Aldrich (USA), VWR (USA) and Fisher Scientific (USA), Alfa Aesar (USA), Fluorochem (UK) and Agar scientific (UK). Unless stated otherwise all chemicals and reactive were used as received.

7.2.1.2 Ionic Liquids (ILs)

Based on the literature review, four potential ionic liquids were selected for trialling the extraction of REEs from EoL MP components, namely: *betaine bis(trifluoromethylsulfonyl)imide* ([Hbet][Tf₂N]) was selected as the main IL for this study due to its ability to solubilise metal oxides [107, 281], other ILs included *1-butyl-3-methylimidazolium bis(trifluoromethylsulfonyl)imide* ([Bmim][Tf₂N]), *trihexyl(tetradecyl)phosphonium bis(trifluoromethylsulfonyl)amide* ([P_{6,6,6,14}][Tf₂N]), and *trihexyl(tetradecyl)phosphonium chloride* also known as *Cyphos 101* ([P_{6,6,6,14}][Cl]). Table 5.1 shows the properties and characteristics of these ILs. All the ILs were purchased and used as received, except for [Hbet][Tf₂N], which was synthesised.

Table 7.1: Properties, characterisation and structure of the ionic liquids used in this study.

Ionic liquid	Properties & characterisation	Structure
[Hbet][Tf ₂ N]	<p>Appearance: white powder in dry form; colourless, viscous liquid in fluid form</p> <p>Upper Critical Solvent Temperature (UCST) 55°C</p> <p>M_w: 398.33 g/mol</p> <p>Density: 1.727 g/cm³ (20°C), 1.541 g/cm³ (60 °C)</p> <p>Flash point: 60°C</p> <p>FTIR: 3292 (OH), 2998 (CH), 1768 and 1758 (C=O), 1721 (COO), 1495 (CH₂), 1477 (OH), 1423 (COOH), 1348 and 1138 (νSO₂), 1178 (CN), 1049 (νSNS), 928 (OH), 793 (νCS), 741 (δCF₃), 669 (δSNS), 607 (δSO₂)</p> <p>TGA-DSC: Onset decomposition temperature: 350 °C. Residue: <1 wt.% at 700 °C</p>	
[Bmim][Tf ₂ N]	<p>Appearance: colourless, viscous liquid</p> <p>M_w: 419.36 g/mol</p> <p>Density: 1.44 g/cm³ (20°C)</p> <p>Flash point: >200 °C</p> <p>FTIR: 2957 (CH₃), 2927 and 2856 (CH₂), 1467 (CCH₃), 1350, 1332 and 1137 (νSO₂), 1225, 1189, and 1058 (νSNS), 788 (νCS), 740 (δCF₃), 652, 617 (νSO₂)</p> <p>TGA-DSC: Onset decomposition temperature: 420 °C. Residue: 1 wt.% at 700 °C</p>	

[P _{6,6,6,14}][Tf ₂ N]	<p>Appearance: colourless, viscous liquid M_w: 764.00 g/mol Density: 1.07 g/cm³ (20°C) Flash point: 52 °C FTIR: 1574 (C=C), 1468 (CH₃), 1349 and 1332 (νSO₂), 1226 and 1185 (νCN), 1136 (νCH₂), 1055 (νSNS), 845 (δCH), 740 (δCF₃), 653 (νSNS), 602 (δSO₂) TGA-DSC: Onset decomposition temperature: 410 °C. Residue: 3 wt.% at 700 °C</p>	
Cyphos 101 [P _{6,6,6,14}][Cl]	<p>Appearance: colourless, viscous liquid M_w: 519.3 g/mol Density: 0.895 g/cm³ (20°C) Flash point: 118 °C FTIR: 2954 (νCH₃), 2920 and 2952 (νCH₂), 1465 and 1377 (δCH₃), 1458/1111/1003 (νP-C), 1415 (δCH₂), 988 (δC-H), 812 (νC-C), 719 (δP-C) TGA-DSC: Onset decomposition temperature: 370 °C. Residue: <1 wt.% at 700 °C</p>	

Molecular weight (MW), densities and flash point values were obtained from Sigma Aldrich, chemicalbook and PubChem. FTIR vibrations were obtained experimentally and compared with reference FTIR patterns in this study symbol; i) ν: stretching, ii) δ: bending, iii) ρ: rocking, iv) ω: wagging and v) τ: twisting. TGA-DSC information were obtained experimentally.

7.2.1.2.1 Synthesis of betaine bis(trifluoromethylsulfonyl)imide ([Hbet][Tf₂N])

[Hbet][Tf₂N] was synthesised using an equimolar metathesis reaction based on the reaction specified by Nockemann et al. [107]. In this reaction, 26.7 g (0.174 mol) of betaine hydrochloride ([Hbet]Cl) and 50.0 g (0.174 mol) of lithium bis(trifluoromethylsulfonyl)imide salt (Li[Tf₂N]) were mixed together, and the mixture was dissolved in 50 mL of (reverse osmosis) RO water, stirred at 600 rpm at room temperature (20 ± 2 °C) for one hour. Two immiscible layers were obtained with the ionic liquid in the lower layer and an aqueous phase in the upper layer. The IL was separated and washed with cold RO water several times until no trace of chloride was detected in the water effluent using the silver nitrate test. The IL was allowed to stand in a fridge for three hours until frozen, and then dried in a vacuum dryer for two days. [Hbet][Tf₂N] appears as a white solid which was ground before use to increase the ease of handling during experiments. Due to the hydrophobicity of [Hbet][Tf₂N], it was kept in a nitrogen atmosphere bag. A distinctive characteristic of [Hbet][Tf₂N] is that it is hydrophilic under alkaline conditions and at temperatures above 55 °C, but otherwise is hydrophobic. This temperature is regarded as the upper critical solvent temperature (UCST) [107]. Above the UCST, a one-phase-system is formed, and a two-phase system is re-established by lowering the solution temperature to below the UCST.

7.2.1.3 Rare-earth oxides (REOs)

Rare-earth elements (REEs) are a collection of 17 elements consisting of the lanthanides, yttrium, and scandium, which were divided into three subgroups; light REEs (LREEs), medium REEs (MREEs), and heavy REEs (HREEs) as listed in Table 7.2. Rare-earth oxides (REOs) are used as the source of REEs in this work. The oxide form was selected for the study of the leaching/extraction performance of [Hbet][Tf₂N] since the IL can dissolve metal oxides [107]. The oxides of La₂O₃, CeO₂, Pr₂O₃ and Nd₂O₃ were chosen to represent the LREEs, Eu₂O₃ and Gd₂O₃ to represent MREEs, and Yb₂O₃, Y₂O₃ and Tb₄O₇ as HREEs for testing the performance of the IL. Table 7.2 includes details on the REOs used in this study and some of their physical and chemical characteristics.

Table 7.2: REOs utilised in this study and their physical and chemical properties

Rare earth metal oxide	REE Group	Chemical Formula	Molecular Weight [g/mol]	Appearance
Lanthanum (III)	Light	La ₂ O ₃	325.81	white
Cerium (IV)	Light	CeO ₂	172.11	pale yellow
Praseodymium (III)	Light	Pr ₂ O ₃	329.81	light green
Neodymium (III)	Light	Nd ₂ O ₃	336.48	pale blue
Europium (III)	Medium	Eu ₂ O ₃	351.93	white
Gadolinium (III)	Medium	Gd ₂ O ₃	362.50	white
Terbium (III, IV)	Heavy	Tb ₄ O ₇	365.85	black
Ytterbium (III)	Heavy	Yb ₂ O ₃	394.08	white
Yttrium (III)	Heavy	Y ₂ O ₃	225.81	white

Each REO was used to test its solubility in the ILs, and mixes of REOs were tested to determine the selectivity of an IL for an REO.

7.2.1.4 Model Test System

A Model Test System was prepared using a mix of the oxides of neodymium and praseodymium as these metals represent the REEs that are most abundant in speakers and cameras, as determined in the characterisation studies reported in Chapter 3.

7.2.1.5 Speakers from EoL Mobile Phones

Whilst speakers and cameras are rich in REEs, for the purposes of investigating the recovery of REEs from real samples in this work, with a greater sample size of speakers available compared to cameras, speakers from the three generations of EoL mobile phones (feature, multimedia, and smartphones) were used. Detailed characterisation of these components from each generation of phone, (with each generation being made up of five mobile phones), was made and reported in Chapter 3. The component fractions of the speakers and cameras following dismantling are shown in Figure 7.1. A total sample of 21 mobile phones were used in the study to provide a more representative sample as the elemental composition varies between different phone manufacturers, production date and supply chain. The speakers were dismantled manually, demagnetised, shredded by cryomilling, using processes described in Section 3.2.2, Chapter 3. The final product was a powder of $\leq 150 \mu\text{m}$ (Figure 7.1). Due to the small amount of sample obtained from each speaker, the powder samples of each mobile phone were mixed, to provide a more representative sample.

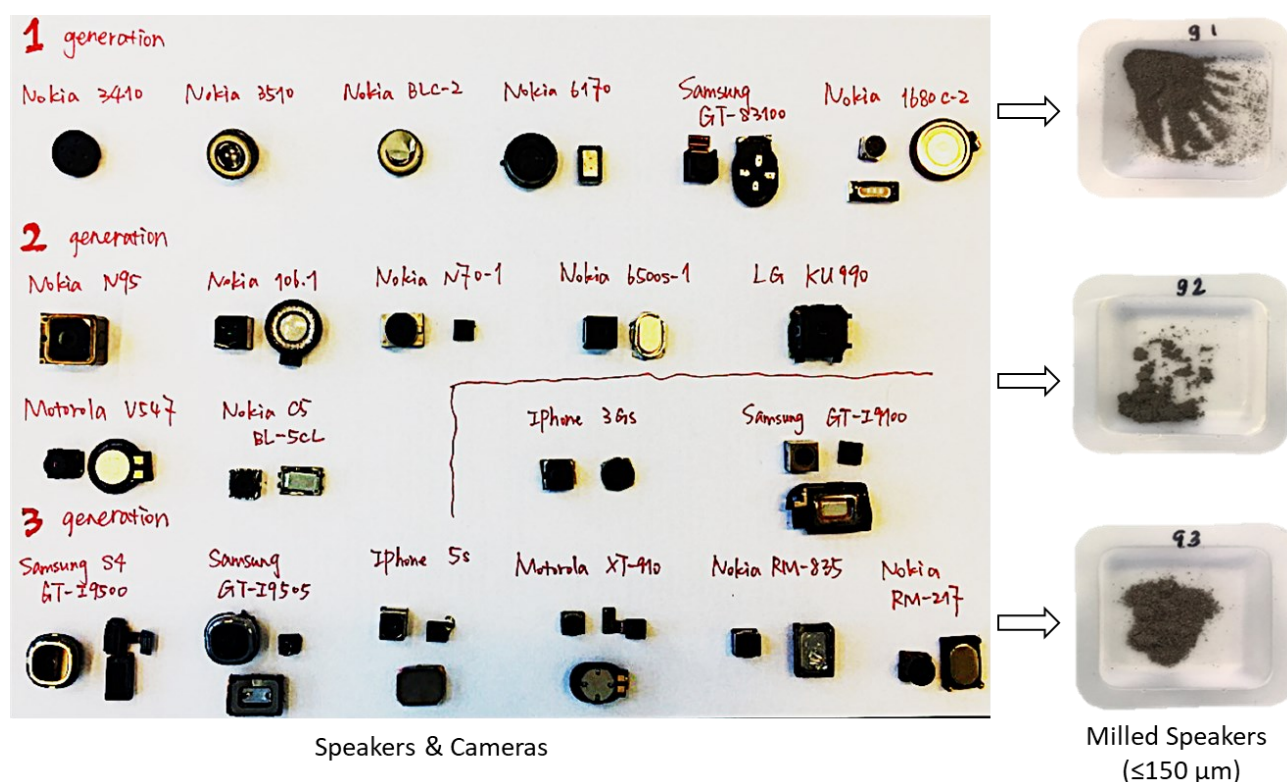


Figure 7.1: Speakers and cameras from EoL mobile phones utilised in the recovery of REEs. Generation 1: feature phones, generation 2: multimedia phones, and generation 3: smartphones.

7.2.2 Analytical Techniques for Characterisation

The analytical techniques used for characterisation of materials in this study are described in Chapter 3. Figure 7.2 summarises the analytical methods applied, and the measures used to determine the effectiveness of the proposed process steps of *Solubility testing*, *Leaching/Extraction*, *Elution and Recyclability*, *Recovery of REEs*, and *Liquid-Liquid Extraction* on the recovery of rare earth elements from simulated solutions and from real samples from EoL-MPs speakers.

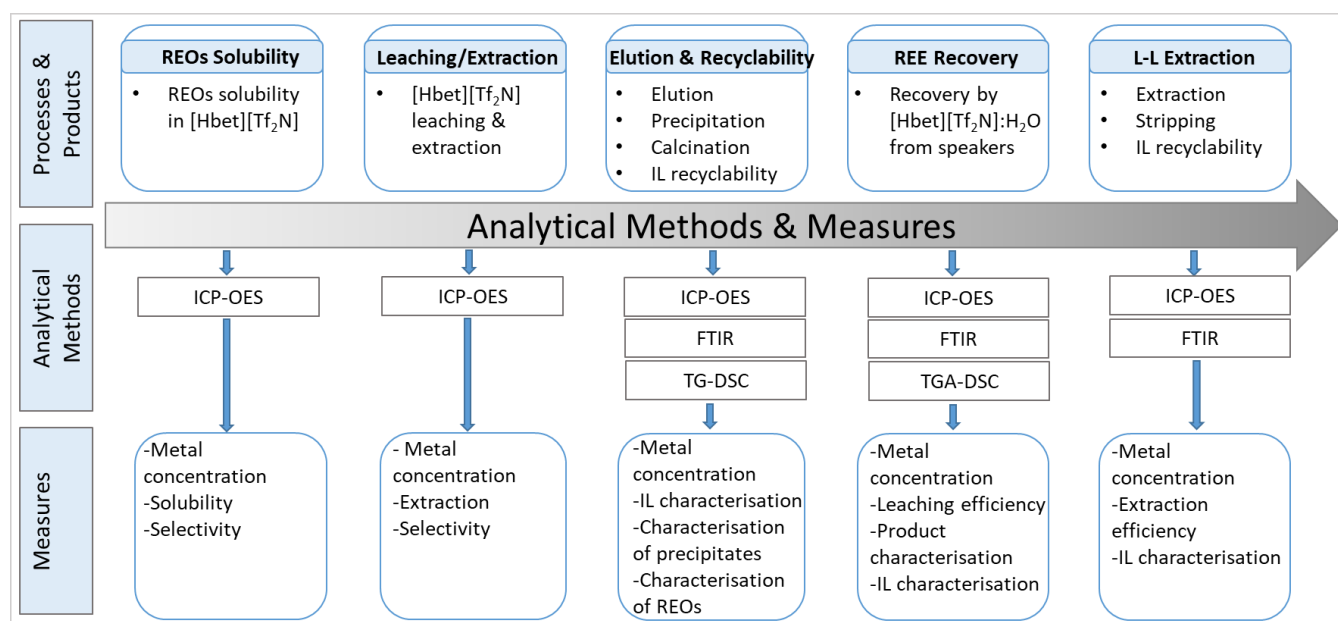


Figure 7.2: Analytical methods and Measures Used to Determine the Effectiveness of the Extraction and Recovery Methods Proposed.

7.2.3 Experimental Procedure

To investigate the potential for recovery of REEs from waste speakers derived from EoL mobile phones, a five-step approach is followed: (i) solubility testing of [Hbet][Tf₂N] for the target metals, using REOs as the representative source of REEs, (ii) determination of the optimised conditions for REOs leaching, (iii) pre-treatment of the as-received speakers from EoL-MPs for REEs recovery trials, and (iv) application of the optimised conditions for REEs extraction and recovery of pre-treated real samples. In addition, an alternative recovery method is studied using ILs as extractants but without pre-treatment. An overview of the experimental procedure followed is set out in Figure 7.3.

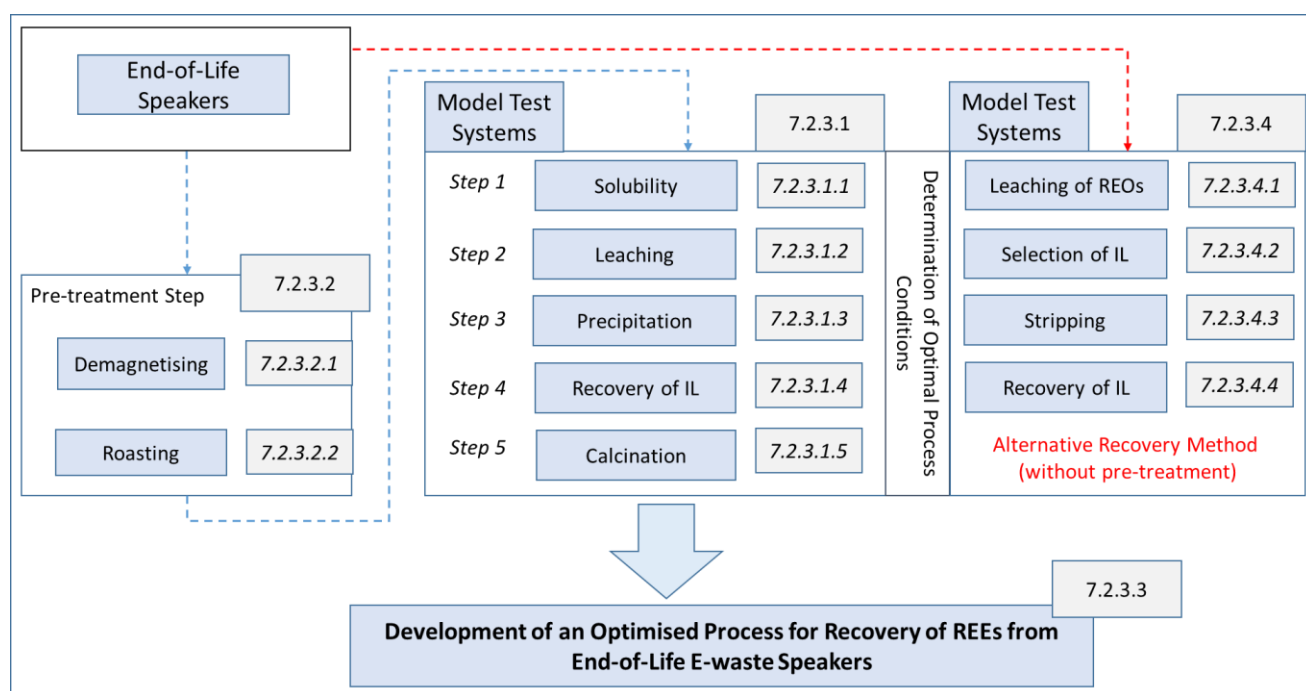


Figure 7.3: Overview of Experimental Procedure.

7.2.3.1 Determination of Optimised Conditions for REEs Extraction and Recovery using A Model Test System

7.2.3.1.1 Solubility of rare-earth oxides

To determine the solubility of REOs in [Hbet][Tf₂N], each REO was tested separately, to ensure there were no other interactions between different elements which may interfere with the solubility of the target REO. The [Hbet][Tf₂N]:H₂O ratio was set as 1:1 for all the solubility tests, using 1 g of [Hbet][Tf₂N] and 1 mL of RO water at 57 °C (above the UCST). In the solubility test, 0.01 g of REO was continuously added to the [Hbet][Tf₂N]:H₂O system until residues were observed at the bottom of the test tube. The final concentration of the rare earth element was confirmed by ICP-OES. Once the solubility was determined, each REO was added in excess (10 wt.%) to study the effect of time (1, 2.5, 5, 7.5, 10, 15, 20, 30, and 60 minutes) on the solubility in the IL:water system (1:1 [Hbet][Tf₂N]:H₂O, 57 °C, 250 rpm). The influence of temperature on the selectivity of [Hbet][Tf₂N]: H₂O system towards REOs was studied by mixing 1 g of [Hbet][Tf₂N] and 1 ml of RO water with 0.02g of each REO (Table 7.2), and varying the temperatures from 57 °C to 85 °C. The use of [Hbet][Tf₂N] as a separation process of light REEs from heavy REEs has been suggested based on a previous work done in Professor Grimes' group by N. Schaeffer [281]. The current research builds on this work with the inclusion of more REOs and medium REEs. In each experiment, the REO:[Hbet][Tf₂N]:H₂O mixtures, after reaction, were hot-filtered through 0.45 µm cellulose nitrate filter papers and the residue was washed with 8 mL hot RO water (60 °C) to remove any residual IL. The REEs are mostly present in the aqueous phase [265], but to ensure a total leaching of REOs, 5 mL of 1 M HCl containing 0.1 M betaine hydrochloride was added and mixed at 100 rpm for 4 h. Betaine hydrochloride was added to minimise the loss of the water-soluble betaine cation from the IL to the aqueous phase. The final solution was then placed in a refrigerated room at 3 °C for 2 h to ensure the separation of the [Hbet][Tf₂N]:H₂O system into a biphasic phase, and the metal concentration was determined in the aqueous phase by ICP-OES. Each experiment was carried out in triplicates.

7.2.3.1.2 Leaching

The leaching tests were carried out using the [Hbet][Tf₂N]:H₂O system on the oxides of the three most abundant metals found in speakers, namely neodymium, praseodymium and iron. The tests were performed on (i) each oxide individually; (ii) as a binary mixture of the two rare-earth oxides, and (iii) as a ternary mixture of the two rare-earth oxides and iron oxide.

Individual oxides: Experiments were carried out separately for Nd₂O₃ and Pr₂O₃ by varying the reaction time, [Hbet][Tf₂N]:H₂O ratio and the temperature. The experiments were carried out in glass

vials, sealed using a plastic screw cap to avoid water evaporation. Table 7.3 shows the different experimental conditions tested.

A suite of tests to investigate the influence of time and [Hbet][Tf₂N]:H₂O ratio, was set up to be carried out simultaneously. Each experiment was carried out by immersing the glass vials, containing the oxide and the IL with a magnetic stirrer (250 rpm) to assist the mixing, in a water bath for temperature control and placed on heating plate. Water was selected as the heating medium because the working temperature was up to 85 °C. Based on the solubility testing reported in Section 7.2.3.1.1 (solubility of 0.16 g REO/g [Hbet][Tf₂N]:H₂O for Nd₂O₃ and Pr₂O₃), with nearly 80% of the maximum solubility, the weight of each oxide, chosen to ensure that all available oxide would be solubilised/extracted in the experiments, was 0.13 g. After each experiment, the samples were then placed in a centrifuge at 3500 rpm for 10 minutes to precipitate the undissolved REOs; no residual oxide remained confirming that all the REO was solubilised/extracted. The vials were then placed in a refrigerated room at 3 °C for 2 h to ensure the separation of the [Hbet][Tf₂N]:H₂O system into a biphasic phase. The metal content in the aqueous phase was determined by ICP-OES, and the concentration in the IL was calculated from mass balance. Experiments were carried out in triplicate and analytical measurements were carried out in triplicate on each sample.

Table 7.3: Experimental parameters for leaching/extraction by [Hbet][Tf₂N]:H₂O system.

Time (min.)	[Hbet][Tf ₂ N]:H ₂ O ratio	Temperature (°C)
1, 3, 5, 7.5, 10, 15, 20, 30	1:0.5, 1:1, 1:2, 1:3	60
1, 3, 5, 7.5, 10, 15, 20, 30	1:0.5, 1:1, 1:2, 1:3	60
15	1:1	57, 65, 75, 85

The third most abundant metal in speakers, after neodymium and praseodymium, is iron, so its behaviour alone and its interaction with Nd and Pr (in a ternary system, described below) in the [Hbet][Tf₂N]:H₂O system was studied. Initial experiments to determine the effect of time (1-60 min.), temperature (57, 65, 75, and 85 °C), and [Hbet][Tf₂N]:H₂O ratio (1:0.5, 1:1, 1:2, 1:3, and 1:5) were carried out by mixing 0.2 g of Fe₂O₃ with 2 g of [Hbet][Tf₂N] and 2 mL of H₂O, (with the exception of trials investigating the impact of changes in the the [Hbet][Tf₂N]:H₂O ratio). The experimental procedure set out for the oxides of Nd and Pr separately, described above was followed.

Binary Mixture of Oxides: The selectivity of the [Hbet][Tf₂N]:H₂O system for the REOs in the presence of the other oxide was conducted using binary mixtures (Nd₂O₃ and Pr₂O₃) by varying the mass ratio of Nd₂O₃:Pr₂O₃ for 1:5, 1:2, 1:1, 2:1 and 5:1. Each experiment was carried out in sealed glass

vials with a [Hbet][Tf₂N]:H₂O ratio of 1:1 (2 g:2 mL), 60 °C, 500 rpm for 30 min. The amount of REOs used was 80% of the maximum solubility of [Hbet][Tf₂N]:H₂O system observed in Section 7.2.3.1.1. After each experiment, the samples were then placed in a centrifuge at 3500 rpm for 10 minutes to precipitate the undissolved REOs. The vials were then placed in a refrigerated room at 3 °C for 2 h to ensure the separation of the [Hbet][Tf₂N]:H₂O system into a biphasic phase. The metal content in the aqueous phase was determined by ICP-OES, whilst the concentration in the organic phase was calculated by mass balance. Experiments were carried out in triplicate and analytical measurements were carried out in triplicate on each sample.

Ternary Mixture of Oxides: The selectivity of [Hbet][Tf₂N]:H₂O system for the oxides in a ternary metal oxide mixture (Fe₂O₃, Nd₂O₃ and Pr₂O₃) was conducted at a fixed mass ratio of Nd₂O₃:Pr₂O₃=1:1 and varying the mass ratio of Fe₂O₃. The mass ratios used of Nd₂O₃:Pr₂O₃:Fe₂O₃ were 1:1:1, 1:1:2, 1:1:3, 1:1:4, and 1:1:5. The amount of Nd₂O₃ and Pr₂O₃ used was 0.1 g each, whereas Fe₂O₃ was 0.1g, 0.2g, 0.3g, 0.4g, and 0.5g. The experiments were conducted in sealed glass vials at 60 °C, 500 rpm and 30 min. After each experiment, the samples were then placed in a centrifuge at 3500 rpm for 10 minutes to precipitate the undissolved metal oxides. The vials were then placed in a refrigerator room at 3 °C for 2 h to ensure the separation of the [Hbet][Tf₂N]:H₂O system into a biphasic phase. The metal content in the aqueous phase was determined by ICP-OES. The determination of metals in the organic phase, as the metal was added in excess, was made by taking out 1 mL of the loaded IL (after centrifugation) and adding 5 mL of 1 M HCl containing 0.1 M betaine hydrochloride (stirring at 100 rpm for 4 h) to strip the metals from the IL. The metal concentration was then determined by ICP-OES. The leaching efficiency was calculated by:

$$\%L = \frac{(C_{aq} \cdot V_{aq} + C_{IL} \cdot V_{IL})}{m_{REE,oxides}} \cdot 100 \quad \text{Eq. 7.1}$$

where C_{IL} and C_{aq} are the equilibrium concentration (mg/L) of the target in the IL (organic) and the aqueous phase, respectively, V_{IL} and V_{aq} the volume (L) of the IL and aqueous phase, respectively, and $m_{REE,oxides}$ represents the mass of REE metal in the oxide metals added (mg).

7.2.3.1.3 Precipitation

After leaching of Nd₂O₃ in [Hbet][Tf₂N]:H₂O system (1:1 ratio, 60 °C, 500 rpm, and 30 min), the solution was cooled to 3 °C for 2 h for separation of phases and the aqueous phase was removed from the organic phase. Neodymium was stripped from the aqueous phase with nearly stoichiometric amounts of pure oxalic acid powder (5% of excess). The solution was mixed at room temperature

(20 ± 2 °C) at 250 rpm for 30 min. After the precipitation, a white precipitate was observed, and the sample was centrifuged at 3500 rpm for 10 minutes to separate completely the precipitate. Whilst centrifugation was not needed in the process, it was used to permit separation of the precipitate for analysis for metal concentration by ICP-OES to ensure precipitation was complete. The aqueous phase, containing the precipitate, was filtered and the residue was washed twice with RO water and then with ethanol.

7.2.3.1.4 Calcination

The resulting solid powder from precipitation, REE oxalate (>99 wt.%), was put into a crucible and calcined at 900 °C for 2 h to obtain the REOs. Preliminary studies were carried out with neodymium, where after precipitation a white powder formed, and followed by calcination the powder turned light blue-purple colour characteristic of Nd_2O_3 . The same procedure was carried out when speaker powder was utilised.

7.2.3.1.5 Recovery of IL ([Hbet][Tf₂N])

The recyclability of [Hbet][Tf₂N] was trialled by carrying out five continuous cycles of leaching/extraction using neodymium oxide. In each cycle, 0.14 g Nd_2O_3 was put in contact with the [Hbet][Tf₂N]:H₂O system with a ratio 1:1, at 60 °C, 500 rpm for 30 min. After leaching, the samples were placed in a centrifuge at 3500 rpm for 10 minutes to precipitate any undissolved Nd_2O_3 , followed by cooling at 3 °C for 2 h to ensure the separation of the [Hbet][Tf₂N]:H₂O system into a biphasic phase. The phases were separated by careful extraction of the phase using a pipette. In the aqueous phase, oxalic acid was added to precipitate the neodymium. The organic phase ([Hbet][Tf₂N]) was rinsed with a 0.1 M oxalic acid solution to precipitate any residual metal ions in the organic phase, and then washed with a 0.1 M HCl solution to ensure complete removal of any impurities. Following the stripping and washing steps, the [Hbet][Tf₂N] was dried in an oven at 90 °C for 10 h. This procedure was repeated five times.

7.2.3.2 Pre-treatment of As-Received Waste Speakers from EoL-MPs for REEs Recovery

Pre-treatment of as-received waste speakers from EoL-MPs before investigating the potential for recovery of REEs involved a demagnetisation step followed by roasting to convert the REE metals to the corresponding oxide. These methods are now described.

7.2.3.2.1 Demagnetisation

After dismantling the speakers from EoL mobile phones (Figure 7.1), the speakers were placed in a muffle furnace at 350 °C for 1 h, to ensure complete demagnetisation. The speakers were then cryomilled in liquid nitrogen (freezing the samples up to – 196 °C) for 15 min at 150 rpm in a closed system, using a cryomill (Retsch Cryomill, Germany), until a powder with a particle size $\leq 150 \mu\text{m}$ was obtained (Figure 7.1).

7.2.3.2.2 Roasting

The milled powder was then roasted to convert the REEs present in the speakers to their oxides, to facilitate their extraction into the [Hbet][Tf₂N]:H₂O system. The roasting temperature was determined using thermogravimetric analysis (STA-1500 Series, Austria), where a sample (~12 mg) of speaker powder was placed in an alumina crucible holder and was heated to 1000 °C (at 10 °C/min) under air flow (50 mL/min). Using the data from the TGA analysis, the roasting temperature was chosen, and the powdered speaker fraction was placed in a ceramic crucible in a muffle furnace at 950 °C for 5 h to ensure complete conversion of the metals to the metal oxides.

7.2.3.3 Application of the Optimised Conditions for REEs Extraction and Recovery from E-Waste Components

The conditions optimised for the recovery of rare earth metal oxides using the three-step leaching, precipitation and calcination process was trialled on the REOs obtained from pre-treatment of the speakers. Powdered oxide samples (30 mg) were placed in glass vials (10 mL) with a fixed amount of [Hbet][Tf₂N] (3 g) together with a magnetic stirrer to ensure complete mixing. A [Hbet][Tf₂N]:H₂O ratio of 1:1 was used in all leaching experiments, and leaching was carried out in a water bath at 60 °C, 500rpm for 1 h. The glass vials were sealed using a plastic screw cap to avoid the liberation of vapour. After leaching, the samples were placed in a centrifuge at 3500 rpm for 10 minutes to precipitate the residue, followed by cooling at 3 °C for 2 h to ensure the separation of the [Hbet][Tf₂N]:H₂O system into a biphasic phase. The metal content in the aqueous and organic phases was determined as described in Section 7.2.3.1.2, and the extraction efficiency calculated using Eq. 7.1. To determine the concentration of REE in the speakers, an *aqua regia* digestion method described in section 3.2.3.1 of Chapter 3 was used.

7.2.3.4 Determination of Optimised Conditions for REEs Extraction and Recovery using A Model Test System: Alternative Recovery Method

Using a Model Test System an alternative method for recovery of REEs without a pre-treatment step was investigated.

7.2.3.4.1 Leaching of REOs

To determine the most suitable acid for leaching REEs from speakers, each REO was dissolved separately in HCl, HNO₃, and H₂SO₄. In each experiment, 0.1 g of the REO (Table 7.2) was placed in a glass beaker into which was added 40 mL of 1 M of acid. The leaching was carried out at room temperature (20±2 °C) for 1 h. The final concentration of the leached REE was determined by ICP-OES. The results showed that HCl was the most efficient leachant and was therefore used for the leaching of powdered speaker without a pre-treatment step.

7.2.3.4.2 Selection of ILs

To select the most effective IL for liquid-liquid extraction, a neodymium solution in hydrochloric acid medium was placed in contact separately with three different ILs, namely: ([Bmim][Tf₂N], [P_{6,6,6,14}][Tf₂N] and Cyphos 101 [P_{6,6,6,14}][Cl]) (Table 5.1), with an organic to aqueous ratio of 1:1 (2 mL each), and the mixture was magnetically agitated at 500 rpm for 1 h. The influence of hydrochloric acid concentration, temperature, and time was studied under the different experimental conditions listed in Table 7.4. In each experiment, only one parameter at a time was changed while keeping all others constant. After each experiment, the solution was centrifuged at 3500 rpm for 10 minutes. Analyses for determination of the rare earth element and other metal concentrations was performed by ICP-OES by taking 1 mL of sample diluted in 4 mL of 1 M HCl. All the experiments and measurements were done in triplicate and the results averaged. The extraction was obtained by:

$$\%E = \frac{(C_i - C_f)_{(aq)} \cdot V_{IL}}{(C_i \cdot V_i)_{(aq)} \cdot V_{(aq)}} \cdot 100 \quad \text{Eq. 7.2}$$

where C_i and C_f represent the initial and final metal concentration (mg/L) in the aqueous phase, respectively, and V_{IL} and $V_{(aq)}$ are the IL and aqueous volume (L), respectively.

Table 7.4: Experimental parameters for determination of optimal extraction conditions.

Acid concentration (M)	Temperature (°C)	Time (min.)
0.5, 1.0, 2.0, 3.0	20	60
1.0	20, 40, 60, 80	10, 20, 30, 60, 90, 120, 270
1.0	20	60

7.2.3.4.3 Stripping

A neodymium solution in 1 M HCl was used as aqueous phase for extraction with a [Bmim][Tf₂N] (the IL selected). After extraction, separation of the phases was assisted by centrifugation at 3500 rpm for 10 minutes. The phases were separated, and the organic phase was put in contact with 1 M HCl solution with a volume ratio of 1:1 at 500 rpm for 30 min. After stripping, the solution was centrifuged at 3500 rpm for a further 10 min to ensure complete phase separation. The two phases were separated by careful extraction of the phase using a pipette, and the organic phase was washed three times with 0.1 M HCl for the next extraction, whilst solid oxalic acid was added to the stripping solution. The precipitated powder was filtered washed twice with RO water and then with ethanol. The resulting solid, was put into a crucible and calcined at 950 °C during 4 h to obtain neodymium oxide.

7.2.3.4.4 Recovery of IL

The recyclability of [Bmim][Tf₂N] was tested by carrying out five continuous cycles of extraction using neodymium oxide solution as the source of REEs. In the recovery of the IL, 5 mL of IL was mixed with 5 mL of the neodymium solution under optimised extraction conditions (1 M HCl, 20 °C and 1 h). After the extraction, stripping was achieved by contacting the IL with a 1 M HCl solution with an organic to aqueous ratio of 1:1, at room temperature (20±2 °C), 250 rpm, and 30 minutes. The IL was then washed 3 times with a solution of 0.1M HCl to strip any residue left and reused in the next cycle.

7.2.3.5 Summary

The four-step approach to investigate the development of an optimised process for recovery of REEs from waste speakers derived from EoL-MPs using ionic liquids is elaborated further in Figure 7.4 in terms of the process steps, the conditions tested, and the component fractions involved. An alternative recovery method, without pre-treatment, involving a two-stage process of liquid-liquid extraction using different ILs following by stripping was also studied.

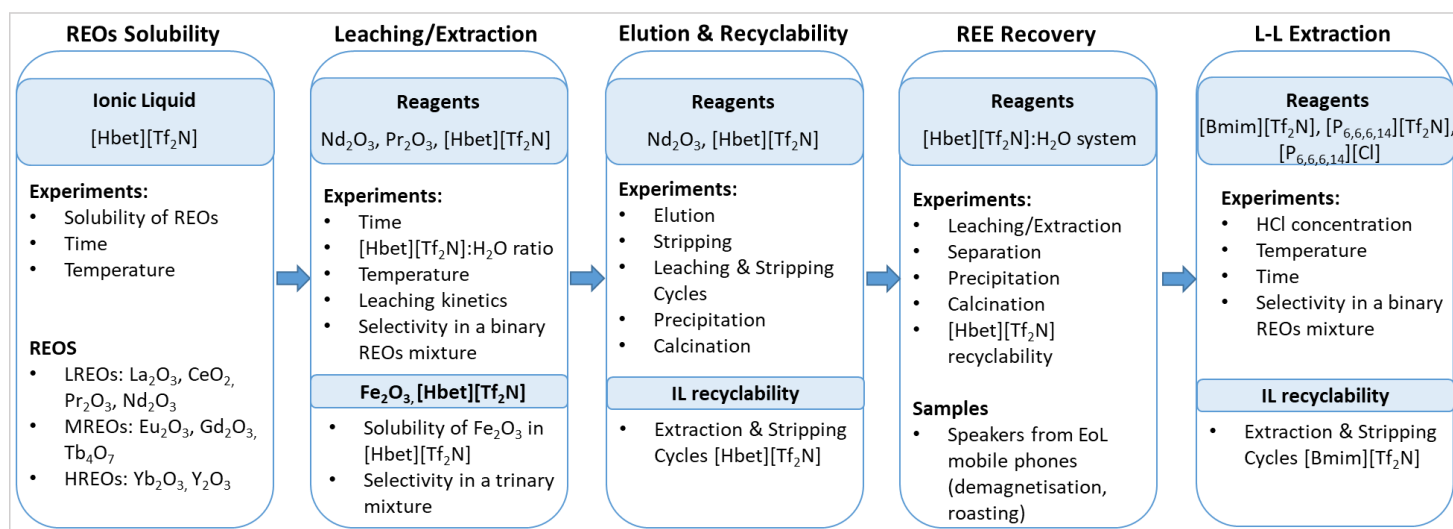


Figure 7.4: Overview of the experimental procedure applied in the development of an optimized process for rare earth elements recovery.

7.3 Results and Discussion

Detailed characterisation of metals present in speakers and cameras from three generations of EoL-MPs was carried out and the results presented in Chapter 3. The extent of REEs concentration and distribution in speakers and cameras are illustrated in Figure 7.5 and Figure 7.6 respectively. Among the REEs (Figure 7.5), neodymium and praseodymium are the most abundant, with erbium also being significant in cameras. It can be clearly seen in Figure 7.6 that REEs represents the major metals composition in speakers and cameras with 90.5% and 51.1%, respectively. With the predominance of these valuable and critical metals present in considerable proportions in these components of the mobile phone, the focus of this work is to develop an optimised method using ionic liquids for the recovery of target REE metals, from e-waste using speakers from EoL-MPs as a test case. As Nd and Pr represent more than 90% of the total REEs composition in speakers and more than 70% in cameras, these two REEs are studied in detail and the optimised conditions are trialled on speakers as the sample size of cameras was limited.

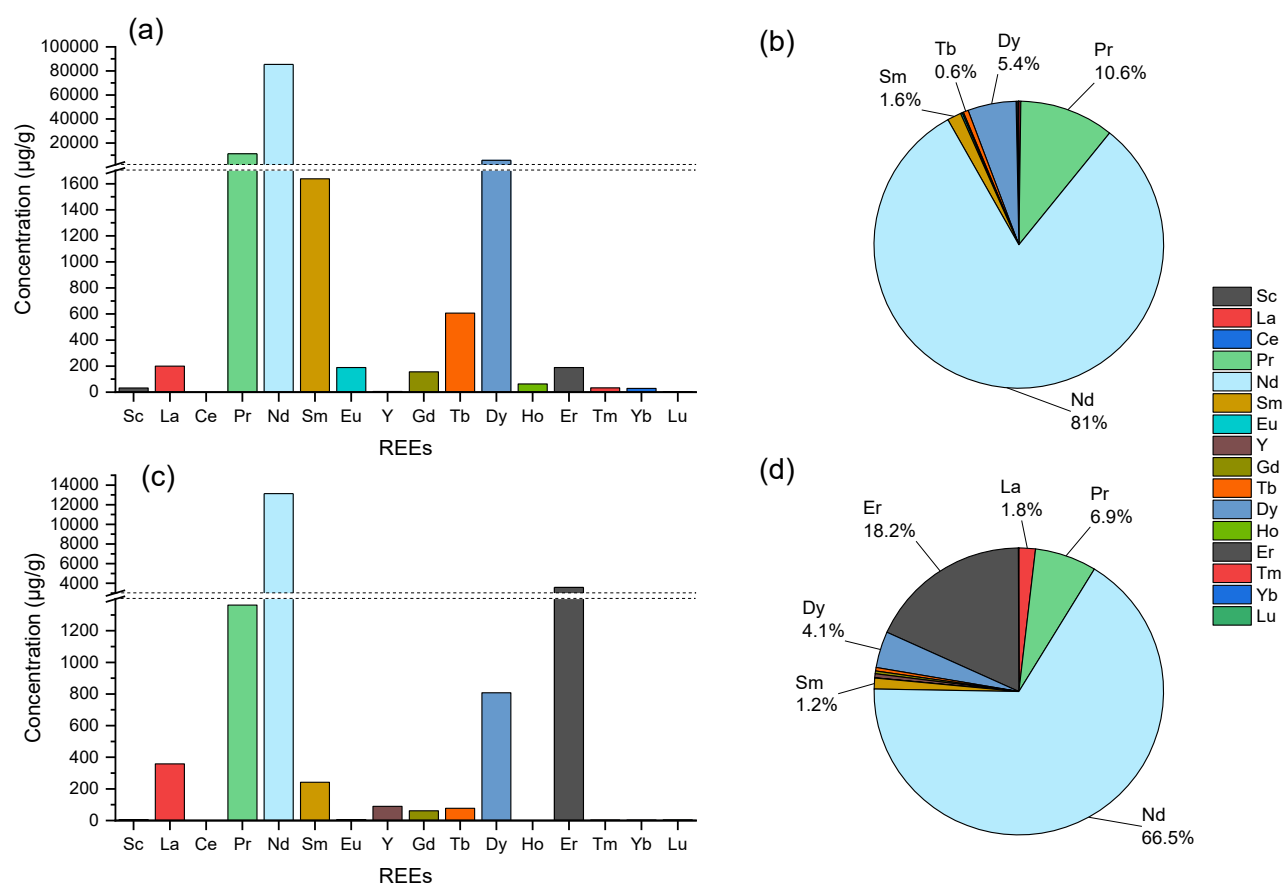


Figure 7.5: REEs concentration and distribution in speakers (a) and (b), and in cameras (c) and (d) of EoL-MPs.

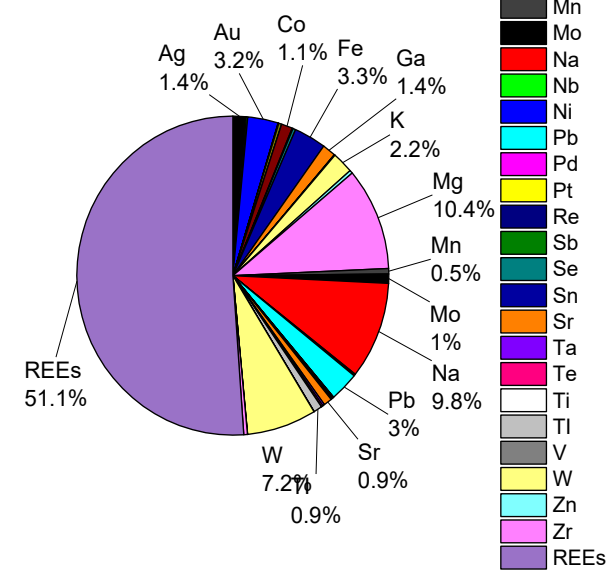
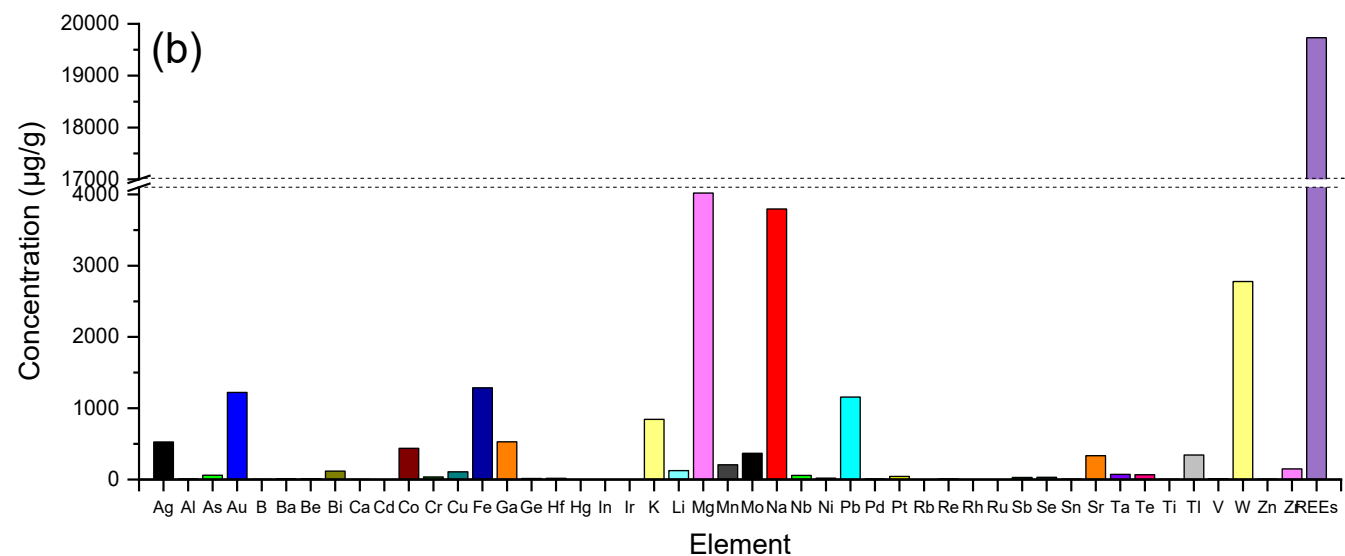
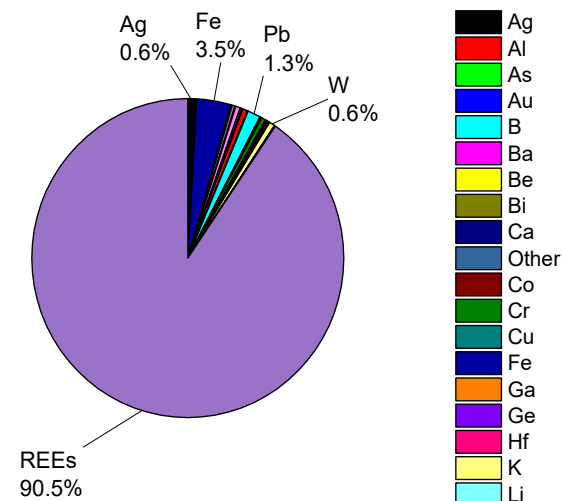
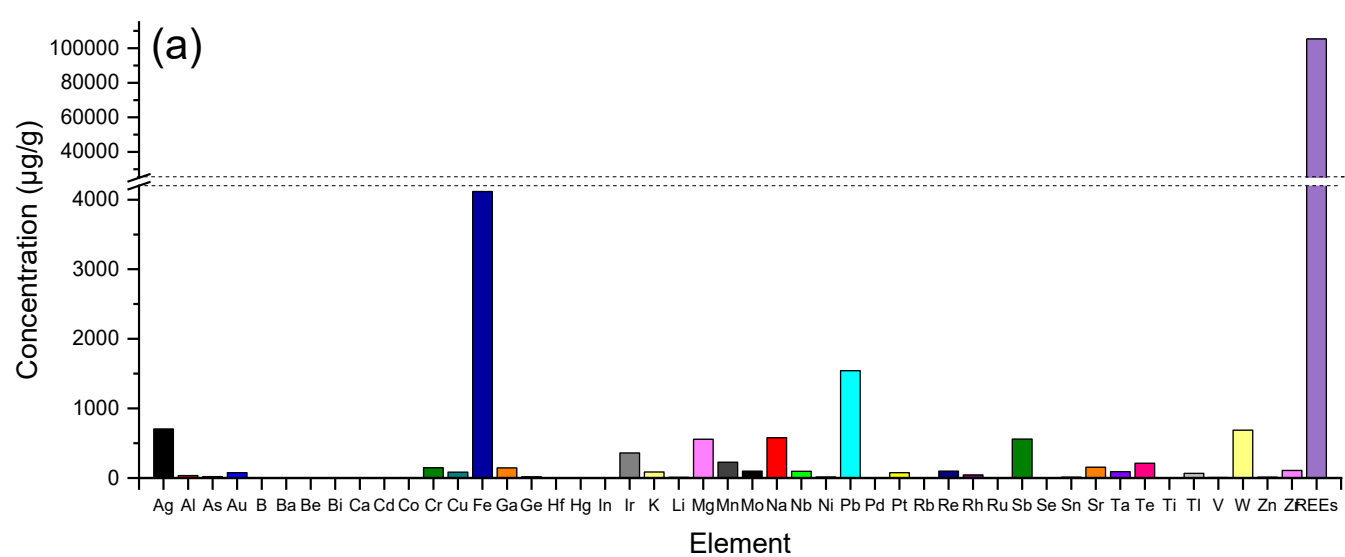


Figure 7.6: Total metal concentration and distribution; (a) speakers and (b) cameras.

7.3.1 Optimised Conditions of [Hbet][Tf₂N] for REEs Extraction and Recovery Using a Model Test System

To determine the optimised conditions for leaching, extraction and recovery of REEs using ionic liquids, a Model Test System was deployed and the behaviour of rare earth metal oxides in the [Hbet][Tf₂N]:H₂O system, alone, under various conditions of temperature, time, and ratio of [Hbet][Tf₂N]:H₂O, was studied. Due to the significant concentrations of certain metals present in speakers and cameras, the study was extended to include an investigation of the impact on leaching of the REOs from binary and ternary mixtures of oxides. The results of these investigations are now described.

7.3.1.1 Solubility of REOs in [Hbet][Tf₂N]-H₂O system

The effect of time on the solubility of a range of REOs in a 1:1 [Hbet][Tf₂N]:H₂O system at 57 °C was investigated and the results are shown in Figure 7.7. In all the cases, an equilibrium is reached within 15 minutes, with, in most cases, 10 minutes being sufficient for 95% equilibrium to be reached. The [Hbet][Tf₂N]-H₂O system showed good solubility for oxides of lanthanum (La₂O₃), praseodymium (Pr₂O₃), neodymium (Nd₂O₃), europium (Eu₂O₃), and gadolinium oxide (Gd₂O₃), reaching a solubility of approximately 0.161 g REO/g [Hbet][Tf₂N]-H₂O. Yttrium oxide (Y₂O₃) showed limited solubility of 0.05 g REO/g [Hbet][Tf₂N]-H₂O, whereas cerium oxide (CeO₂), terbium oxide (Tb₄O₇), and ytterbium oxide (Yb₂O₃) showed no signs of dissolution, being almost negligible for Yb₂O₃ (at 0.01 g REO/g [Hbet][Tf₂N]-H₂O). The solubility of REOs in the [Hbet][Tf₂N]-H₂O system is due to the ability of betaine bis(trifluoromethylsulfonyl)imide, present as the cation in the IL, to dissolve metal oxides. The metal oxides react with the carboxylic acid group of the ionic liquid to form carboxylate complexes and water [107]. In Figure 7.7b, the results show that although the medium REOs (Eu₂O₃ and Gd₂O₃) reached the same equilibrium as the light REOs, they were the slowest, suggesting a preference and faster kinetics for light REOs. The solubility of REOs shows a clear trend: light and medium REOs (except cerium oxide) are dissolved in [Hbet][Tf₂N]-H₂O system, whereas heavy REOs have zero or very low solubilities. Thus, leaching by [Hbet][Tf₂N]-H₂O system can be utilised for the separation of light and heavy REOs.

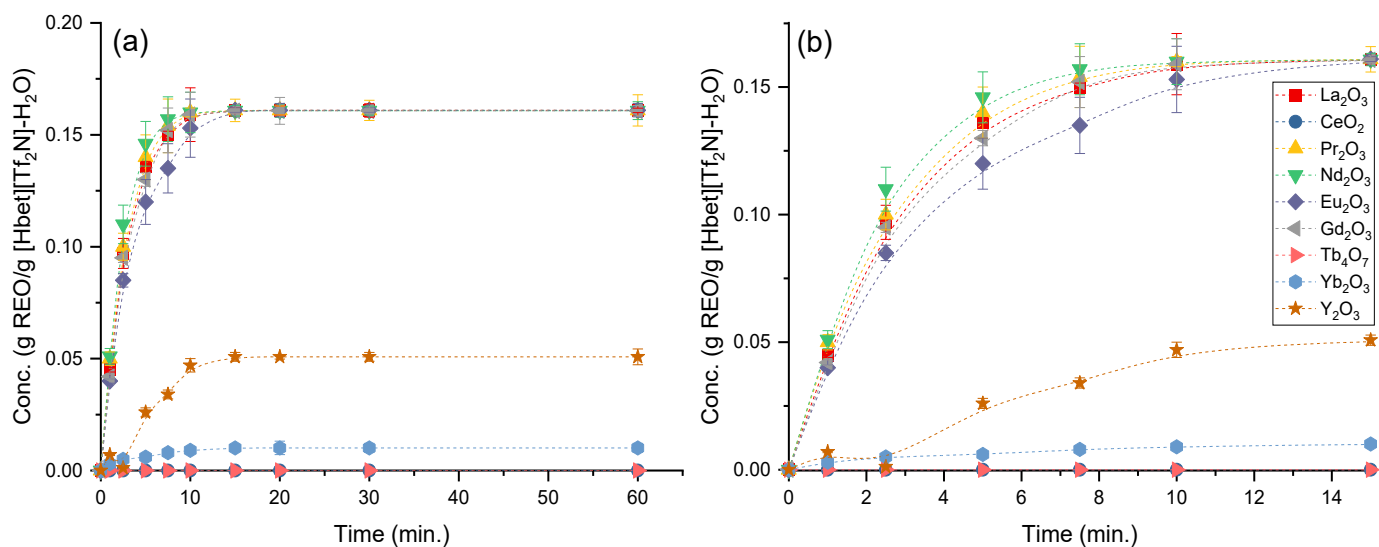


Figure 7.7: Solubility of REOs in 1:1 [Hbet][Tf₂N]:H₂O system with respect to time; (a) Effect of time over the duration studied, (b) shown in more detail in the range up to 15 mins.

The effect of the temperature, in the range of 57-85 °C, on the solubility of REOs and the IL's selectivity for the oxide is presented in Figure 7.8. The general trend observed is that at higher temperatures, the solubilities of REOs in [Hbet][Tf₂N]-H₂O system increase, but the solubilities increase at different rates. Light and medium REOs such as La₂O₃, Nd₂O₃, Eu₂O₃, and Gd₂O₃ show a similar increase of approximately 5-10%. These REOs also showed the highest solubilities in Figure 7.7. The exception to this finding is the zero solubility of CeO₂, which was under the detection limit of the equipment, suggesting very low or zero leaching. This behaviour could be attributed to its non-trivalent oxidation state, in which CeO₂ has a stable +4 oxidation state [107]. On the other hand, heavy REOs (Tb₄O₇ and Yb₂O₃) have very low solubilities at 57 °C, with Tb₄O₇ showing negligible increase in solubility as the temperature rises. Although the leaching of Tb₄O₇ was very poor, it was detected by the equipment, showing a slightly better leaching than CeO₂, due most likely to the fact that Tb is one of only a few rare earth elements that has dual oxidation states of +3 and +4, and its marginal solubility attributed to its oxidation state being closer to the trivalent state. Yttrium oxide (Y₂O₃) and ytterbium oxide (Yb₂O₃) were the only REOs that presented a marked rise in their solubility with an increase of temperature. Y₂O₃ increased its solubility by almost two-fold, from 4.9 mg/g [Hbet][Tf₂N]-H₂O at 57 °C to 8.8 mg/g [Hbet][Tf₂N]-H₂O at 85 °C, whereas the solubility of Yb₂O₃ was increased five-fold, from 0.8 mg/g to 4.3 mg/g [Hbet][Tf₂N]-H₂O, from 57 °C to 85 °C, respectively. The variation in solubilities of REOs at different temperatures followed a similar path to that depicted in Figure 7.7 (for time) confirming the preference of the IL system ([Hbet][Tf₂N]-H₂O) for light and medium REOs over heavy REOs. For separation of REOs therefore, lower temperatures are preferable as at these temperatures

there is higher selectivity between the LREOs from HREOs. Figure 7.8 provides detailed illustration of the selectivity of [Hbet][Tf₂N]-H₂O system for the REOs as the experiment was carried out by mixing the same amounts of each REO. In a complex mixture of different REOs, it is observed that the IL favours the leaching of light REOs rather than heavy REOs. Due to this selectivity, the REOs were divided into three regions of selectivity, namely: favourable (concentrations ≥ 9 mg REO/g [Hbet][Tf₂N]-H₂O or extraction $\geq 60\%$), partially favourable (concentrations between 1 and 9 mg REO/g [Hbet][Tf₂N]-H₂O or extraction between 5% and 60%), and unfavourable (concentrations ≤ 1 mg REO/g [Hbet][Tf₂N]-H₂O or extraction $< 5\%$). The upper and lower partial favourability categories were considered because of the large range in concentration and extraction. It is noted that the temperature increases the favourability of some REOs in the IL leaching, which is particularly noticeable with Y₂O₃ and Yb₂O₃. Interpretation of these results and their categorisation is useful for determining the applicability of [Hbet][Tf₂N]-H₂O system in the recovery and separation of REOs from a mixture light and heavy rare-earth oxides.

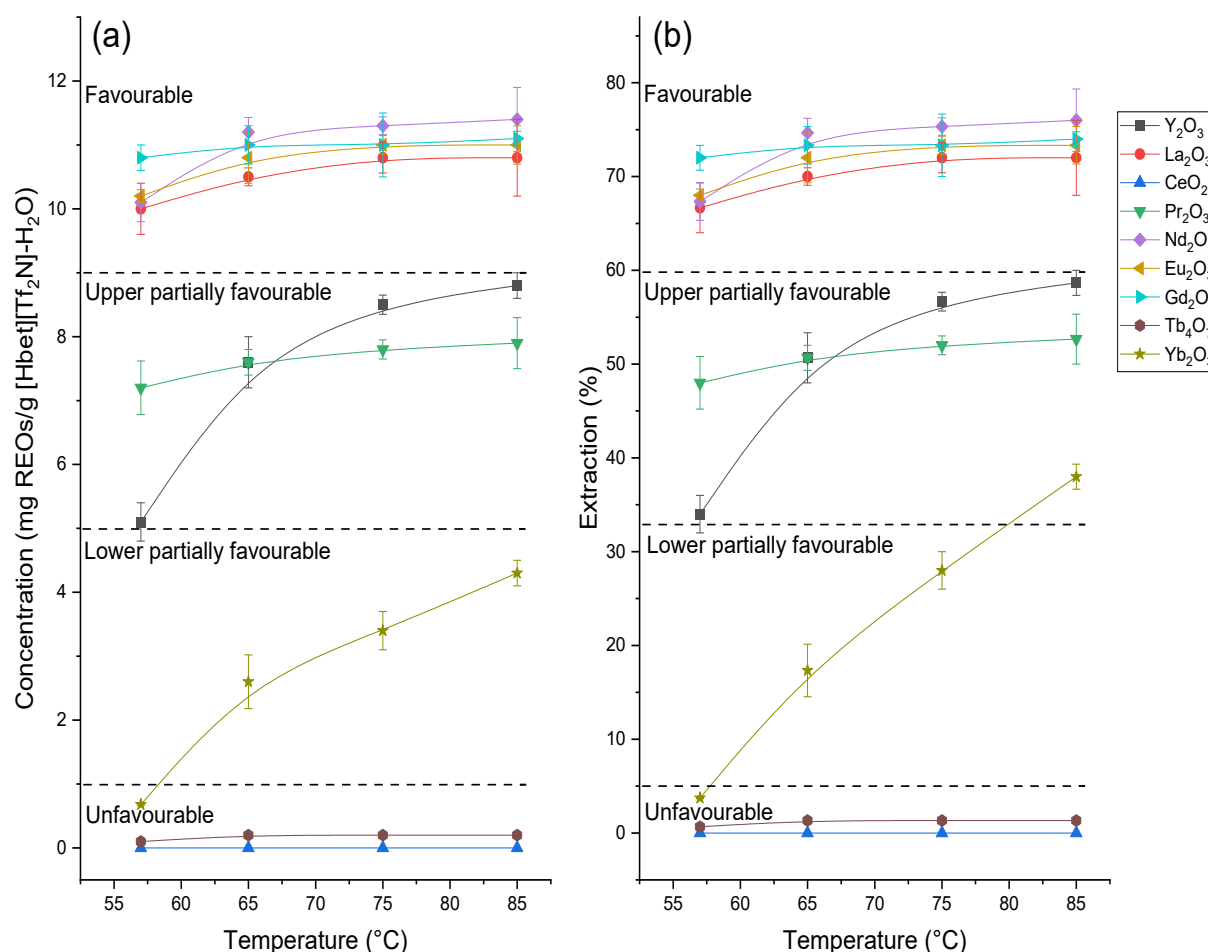


Figure 7.8: Effect of the temperature on REOs solubilities in [Hbet][Tf₂N]:H₂O (1:1) system; (a) extraction concentration, (b) extraction efficiency.

In summary, the solubility values of REOs in this study are in agreement with those reported by Schaeffer et al. [281]. There were two key aspects reported on their study which require comment related to the current work – (i) the effect of time and temperature on the leaching behaviour of a selection of REOs in the [Hbet][Tf₂N]:H₂O system, and (ii) the ability the [Hbet][Tf₂N]:H₂O system to separate light from heavy REOs. Schaeffer et al. studied the effect of time and temperature on the leaching of La₂O₃, Nd₂O₃, Eu₂O₃, Gd₂O₃, Y₂O₃ and Yb₂O₃ in 1:1 [Hbet][Tf₂N]:H₂O system, finding that the solubility of La₂O₃, Nd₂O₃, Eu₂O₃, Gd₂O₃ was 0.16 g RE/g [Hbet][Tf₂N], whereas the Y₂O₃ and Yb₂O₃ increased their solubilities with the temperature, reaching nearly 0.10-0.11 g RE/g [Hbet][Tf₂N] at 95 °C. The increase in dissolution rate with increase in temperature reported, is observed in the current work, and furthermore the observations on the ability for [Hbet][Tf₂N] to effectively separate the light and heavy rare earth oxides, is also confirmed. The current research study extended the investigation to consider nine REOs rather than the earlier reported six, which provides, as well as endorsement of the earlier findings, a more comprehensive summary of the behaviour across a wider range of oxides. The ability of [Hbet][Tf₂N] to dissolve metal oxides was first reported by Nockemann et al., who synthesised for the first time Hbet][Tf₂N] – referred to as a ‘*task-specific*’ ionic liquid [107]. They not only reported that the lanthanides oxides are dissolved in [Hbet][Tf₂N]- H₂O system, but also UO₃, PbO, ZnO, CdO, HgO, CuO, Ag₂O, NiO, PdO, and MnO. The leaching of those metal oxides is due to the ability of the carboxylic acid group of the ionic liquid to react, forming carboxylate complexes, whilst the addition of water to the [Hbet][Tf₂N] facilitates the dissolution of the metal oxide in the IL [106, 107]. A further study reported by the same group determined that a stoichiometric amount of metal oxide M_xO_y is present if for every mole of M_xO_y the amount of [Hbet][Tf₂N] equals x times the oxidation state of the metal [106]. This suggests that for any molecule of RE₂O₃ dissolved, six molecules of [Hbet][Tf₂N] are needed. The final solubility of, for instance, Nd₂O₃, is 0.161 g/g IL, and using the molecular mass of neodymium oxide (333.48 g/mol) and [Hbet][Tf₂N] (398.33 g/mol), the value of the solubility can be expressed as 1 mole Nd₂O₃/5.3 mol [Hbet][Tf₂N], which is nearly 6 moles of IL per mole of REO. The other REOS which presented similar solubility to neodymium oxide have similar molecular masses, consequently the stoichiometric value of 6 molecules of IL per mole of REO is approximately the same, corroborating the findings of Nockemann et al.

7.3.1.2 Effect of the [Hbet][Tf₂N]:H₂O ratio

The effect of the [Hbet][Tf₂N]:H₂O ratio from 1:0.5 to 1:3 on the solubility and metal distribution of Nd₂O₃ and Pr₂O₃ in the organic phase ([Hbet][Tf₂N]) and aqueous phase (H₂O) is shown in Figure 7.9. The first observation is that in all cases, a limit equilibrium of 1.61 g REO/g [Hbet][Tf₂N]:H₂O is achieved, which is in good agreement with the maximum solubility of these REOs in the IL-water system illustrated in Figure 7.7. The dissolution rates rise with an increase in water content (Figure 7.9a and Figure 7.9c); where water assists in breaking the hydrogen bonding within the [Hbet][Tf₂N], which lowers the viscosity of the [Hbet][Tf₂N]:H₂O system, favouring the mobility of the carboxylic acid-bearing betaine cation, and consequently, increasing the dissolution kinetics. The addition of water does not increase the solubility of REOs in the IL which was expected since the extraction mechanism involves the coordination via the carboxylic acid function of the cation, but the water simply facilitates the extraction by lowering the viscosity of the IL.

The characteristic colours of the Nd₂O₃ (light pink-purple) and Pr₂O₃ (light green) observed in the organic and aqueous phases, although with different intensities indicated the presence of rare-earth ions in both phases. It was necessary, therefore to determine metal distribution between the organic and aqueous phases (Figure 7.9b and Figure 7.9d). The solutions (57 °C), after extraction, were placed in a refrigerated room at 3 °C for 2 h to ensure the separation of the [Hbet][Tf₂N]:H₂O system into a biphasic phase, and the concentration of REOs was determined in the aqueous phase by ICP, whereas the concentration in the organic phase was calculated by mass balance (as all the REO was dissolved). Figure 7.9b and Figure 7.9d show that decreasing the [Hbet][Tf₂N]:H₂O ratio, the solubilised REOs in the [Hbet][Tf₂N]-H₂O system remain preferentially in the aqueous phase in both cases. In the case of Nd₂O₃, an increase in water in the system reduces the amount of neodymium in the aqueous phase by approximately 5%. On the other hand, increasing the water content in the Pr₂O₃-[Hbet][Tf₂N]-H₂O system favours the presence of praseodymium in the aqueous phase. It is important to note that REOs are insoluble in water due to most metal oxides possessing a hydrophilic surface (tested in water confirmed them to be insoluble). The presence of Nd and Pr in both the aqueous phase and organic phase can be due to various factors such as partial solubility of the IL and water, diffusion of soluble rare-earth compounds (after reaction) from the IL phase to the aqueous phase product of a high gradient of concentration, the decrease of the UCST with REO loadings [107, 281].

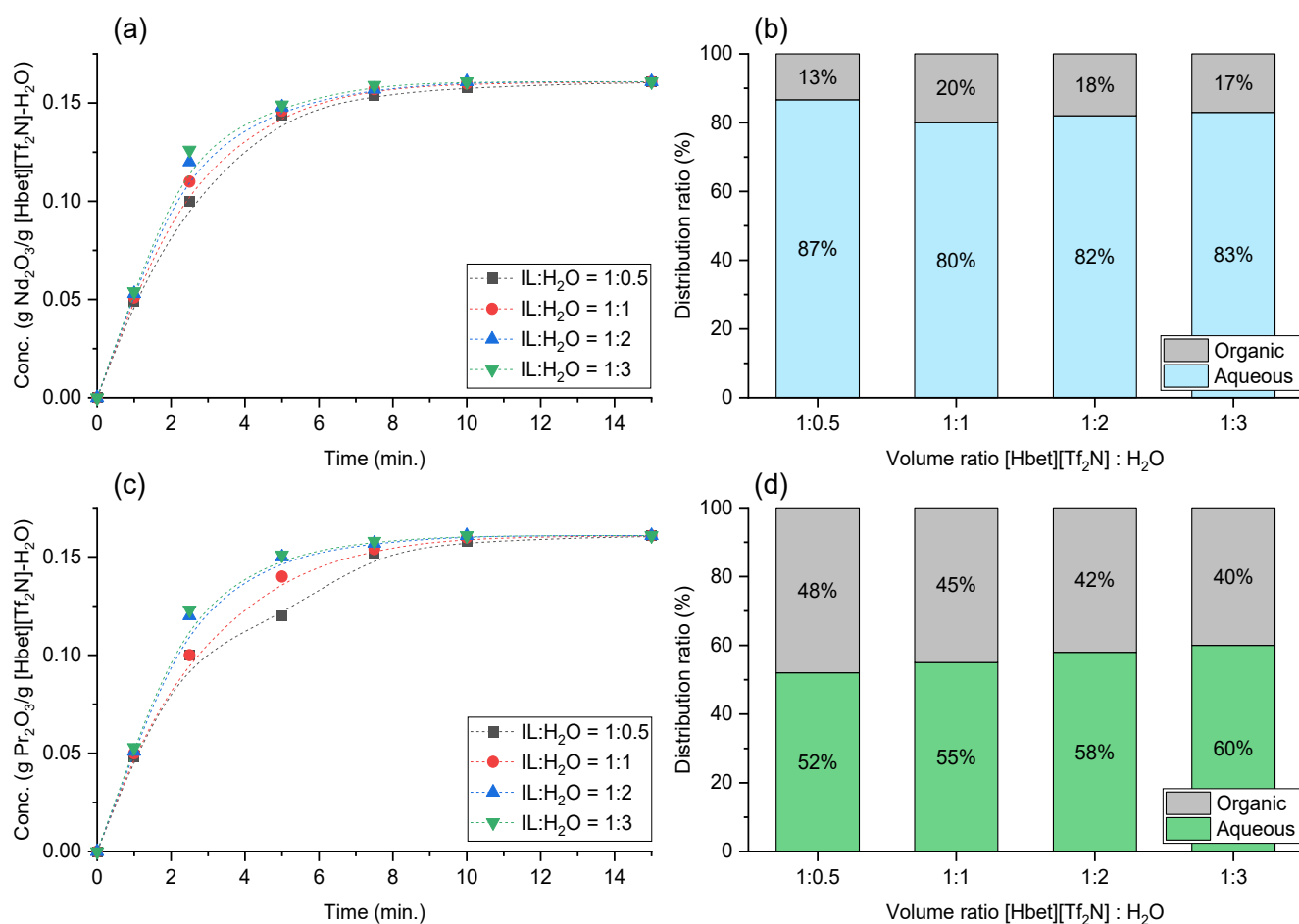


Figure 7.9: Effect of the IL:H₂O ratio in the solubility and metal distribution of Nd₂O₃ (a) and (b), and Pr₂O₃ (c) and (d).

The presence of Nd and Pr in both phases (aqueous and organic), i.e. low distribution ratio ($[M]_{aq}/[M]_{org}$), is not desirable because further separation/stripping processes will be needed for recovery of the rare-earth metal. To increase the distribution of the Nd and Pr towards the aqueous phase, two metal salts; sodium nitrate (NaNO₃) and sodium chloride (NaCl) were studied. Salt anions were selected since salt cations cannot form complexes with the RE ions. Figure 7.10 shows the influence of NaNO₃ and NaCl on the ratio distribution of Nd and Pr between the two phases. In both cases, the addition of a salt anion increases the distribution of the rare-earth ions in the aqueous phase by approximately 3 and 10 times for Nd and Pr, respectively. Water-soluble salt anions such as NaNO₃ and NaCl can form complexes with the metal ions in the aqueous phase and consequently increase the affinity of the metal ions for the aqueous phase [265]. The presence of NaNO₃ or NaCl does not interfere in the leaching/extraction process with the [Hbet][Tf₂N]:H₂O system, which can be added as the aqueous phase (1M) or added after leaching as a solid powder.

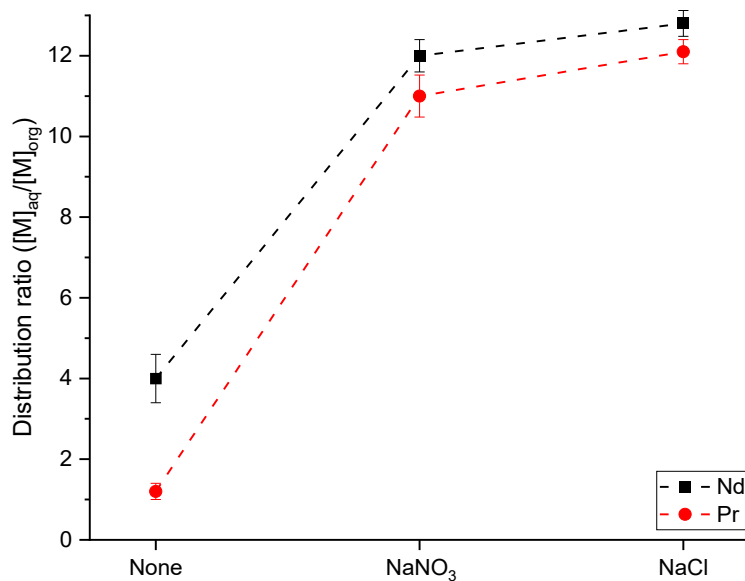


Figure 7.10: Influence of metal salts (1 M) on the distribution ratio of Nd and Pr ions in the 1:1 [Hbet][Tf₂N]:H₂O system.

7.3.1.3 Effect of the temperature

The effect of the temperature on the solubility of Nd₂O₃ and Pr₂O₃ is shown in Figure 7.11. It can be seen that an increase in temperature does not increase the solubility of the REOs in the [Hbet][Tf₂N]-H₂O mixture, with a limit equilibrium reached at 1.61 g REO/g [Hbet][Tf₂N]-H₂O, the same as reported previously in Figure 7.7. This was expected since the solubility limit in the IL is capped by the ability of the [Hbet][Tf₂N]-H₂O system to form stoichiometric metal carboxylate complexes and water. Using the experimental solubility, the stoichiometric metal complex was calculated, suggesting an interaction of one molecule of REOs per five/six molecules of [Hbet][Tf₂N] (1:5.2 for Nd₂O₃-[Hbet][Tf₂N], and 1:5.1 for Pr₂O₃-[Hbet][Tf₂N]). From Figure 7.11b) and Figure 7.11d), show the effect of temperature in more detail over the time period of the first 10 minutes, it can be seen that although the temperature does not affect the solubility, it does increase the rate of dissolution. This is because a rise of the temperature induces a decrease in the viscosity of the [Hbet][Tf₂N]-H₂O mixture, favouring the mass transfer, consistent with a more efficient mixing and a general increase in the kinetics [156].

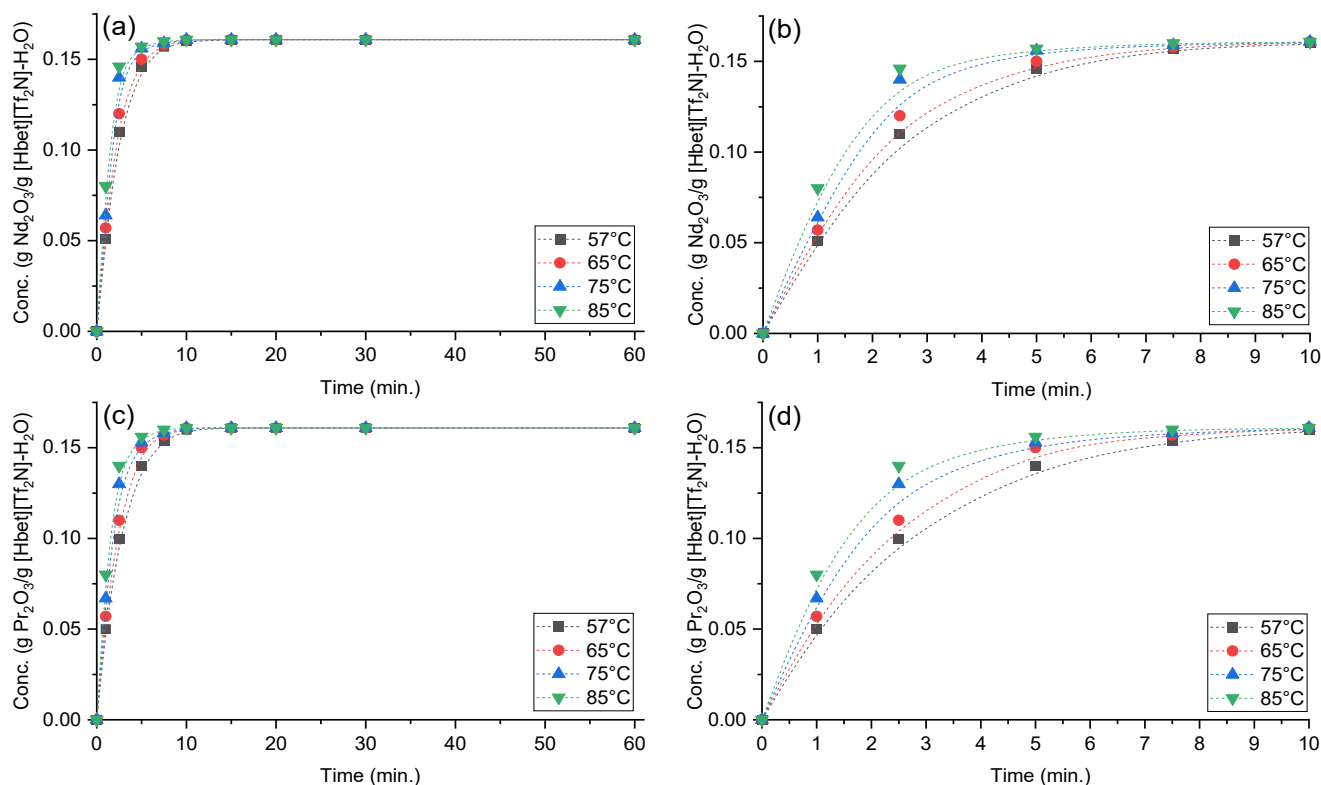


Figure 7.11: Effect of the temperature in the solubility of Nd₂O₃ (a) and (b), and Pr₂O₃ (c) and (d).

7.3.1.4 Kinetics of REOs extraction

To study the kinetics of dissolution of Nd₂O₃ and Pr₂O₃ leaching, the shrinking core model (SCM) is used. SCM model describes the dissolution or reaction of solid particles, which are consumed by a reagent. The amount of material being consumed in these solid particles is “shrinking”. The solid reacted is considered as a non-porous material with a spherical or cylindrical shape, which is surrounded by a fluid which mass transfer occurs between the solid and the bulk of the fluid [91, 176, 187]. According to this model, the following steps are understood to occur in succession during the dissolution: transport of the reactant through the solution to the surface of the solid, reaction on the surface between the reactant and the solid, and formation of the products on the surface layer of the reaction zone and their transport from the interface into the bulk of solution [91, 187]. The step with the greatest resistance is considered the rate-controlling step. In this kinetic study, both spherical and cylindrical shapes were considered. The kinetic equations to describe the process can be described as [91]:

- 1 Film diffusion control dense constant size small particles – all geometries

$$X = K_c t \quad \text{Eq. 7.3}$$

- 2 Film diffusion control dense shrinking spheres

$$1 - (1 - X)^{2/3} = K_c t \quad \text{Eq. 7.4}$$

- 3 Chemical reaction control dense constant size cylindrical particles model

$$1 - (1 - X)^{1/2} = K_c t \quad \text{Eq. 7.5}$$

- 4 Chemical reaction control dense constant size or shrinking spheres

$$1 - (1 - X)^{1/3} = K_c t \quad \text{Eq. 7.6}$$

- 5 Ash diffusion control dense constant size-spherical particles

$$1 - 3(1 - X)^{2/3} + 2(1 - X) = K_c t \quad \text{Eq. 7.7}$$

where, K_c is the reaction rate constant (min^{-1}), t = time (min), and X = metal leaching rate (% leaching).

Figure 7.12 and Figure 7.13 show the model fit using the shrinking core equations for Nd_2O_3 and Pr_2O_3 , respectively. The coefficient of determination R^2 value was adopted to compare the goodness of fit. Normally, a larger R^2 value indicates a better precision fit. Comparing the R^2 values, it was found that in both cases the data fitted best ($R^2 \geq 0.9501$) with the ash diffusion control dense constant size-spherical particles. This result suggests that the kinetics are governed by the diffusion mechanism. This result is plausible due to the fast dissolution rate found, where less than 15 minutes, and in most cases within 10 minutes, were sufficient for reaching equilibrium, suggesting that the reaction is unlikely to be the slowest step in the leaching process. Furthermore, as observed in the detailed range plots of the influence of water (Figure 7.9b) and temperature (Figure 7.11b) on the solubility, the solubility rate increases as the viscosity decreases, supporting that favouring the diffusion mechanism increases the extraction rate.

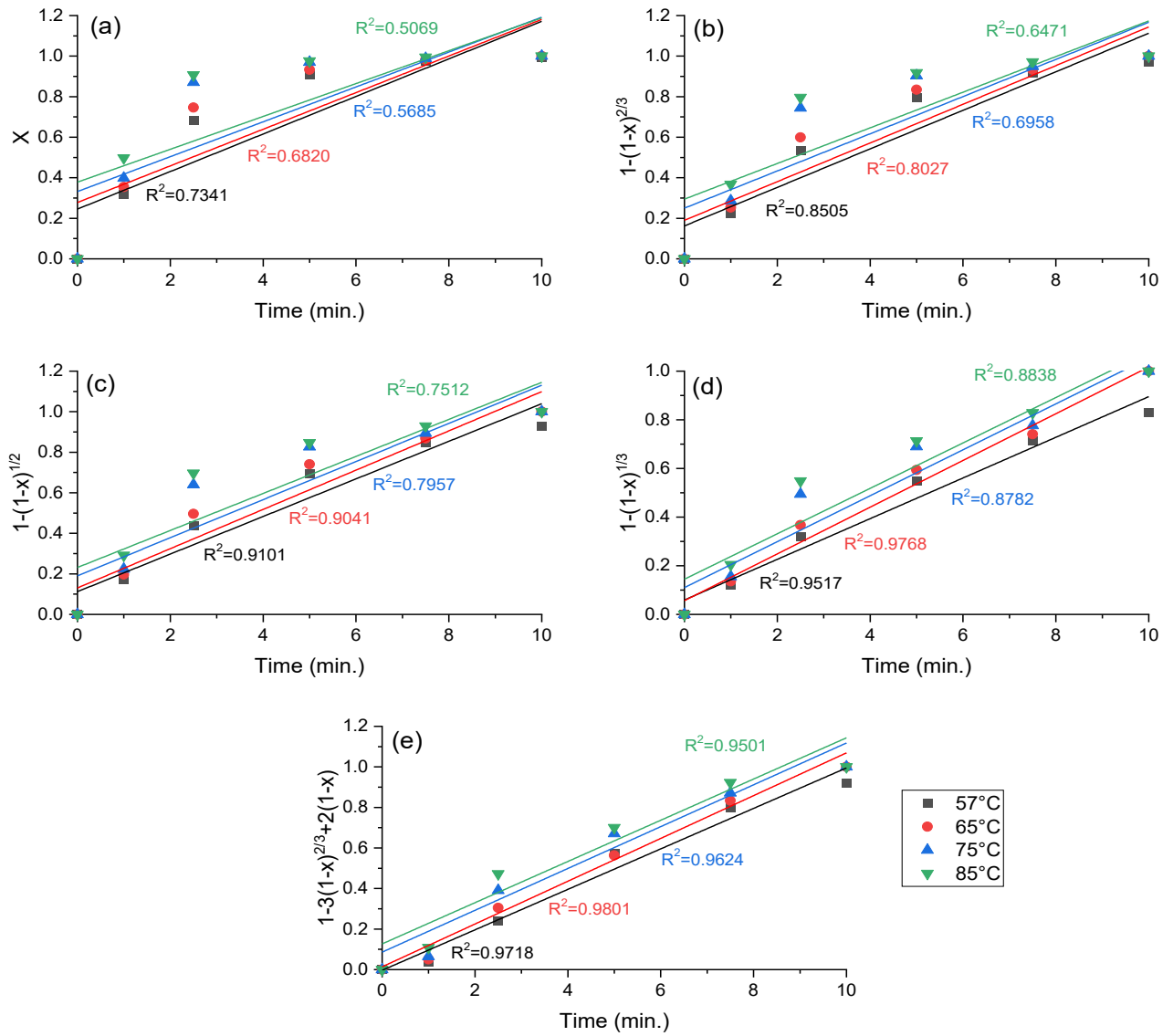


Figure 7.12: Model fitting for leaching kinetics of Nd_2O_3 by $[\text{Hbet}][\text{Tf}_2\text{N}]:\text{H}_2\text{O}$ (1:1); a) Film diffusion control dense constant size small particles – all geometries, b) Film diffusion control dense shrinking spheres, c) Chemical reaction control dense constant size cylindrical particles, d) Chemical reaction control dense constant size and e) Ash diffusion control dense constant size-spherical particles.

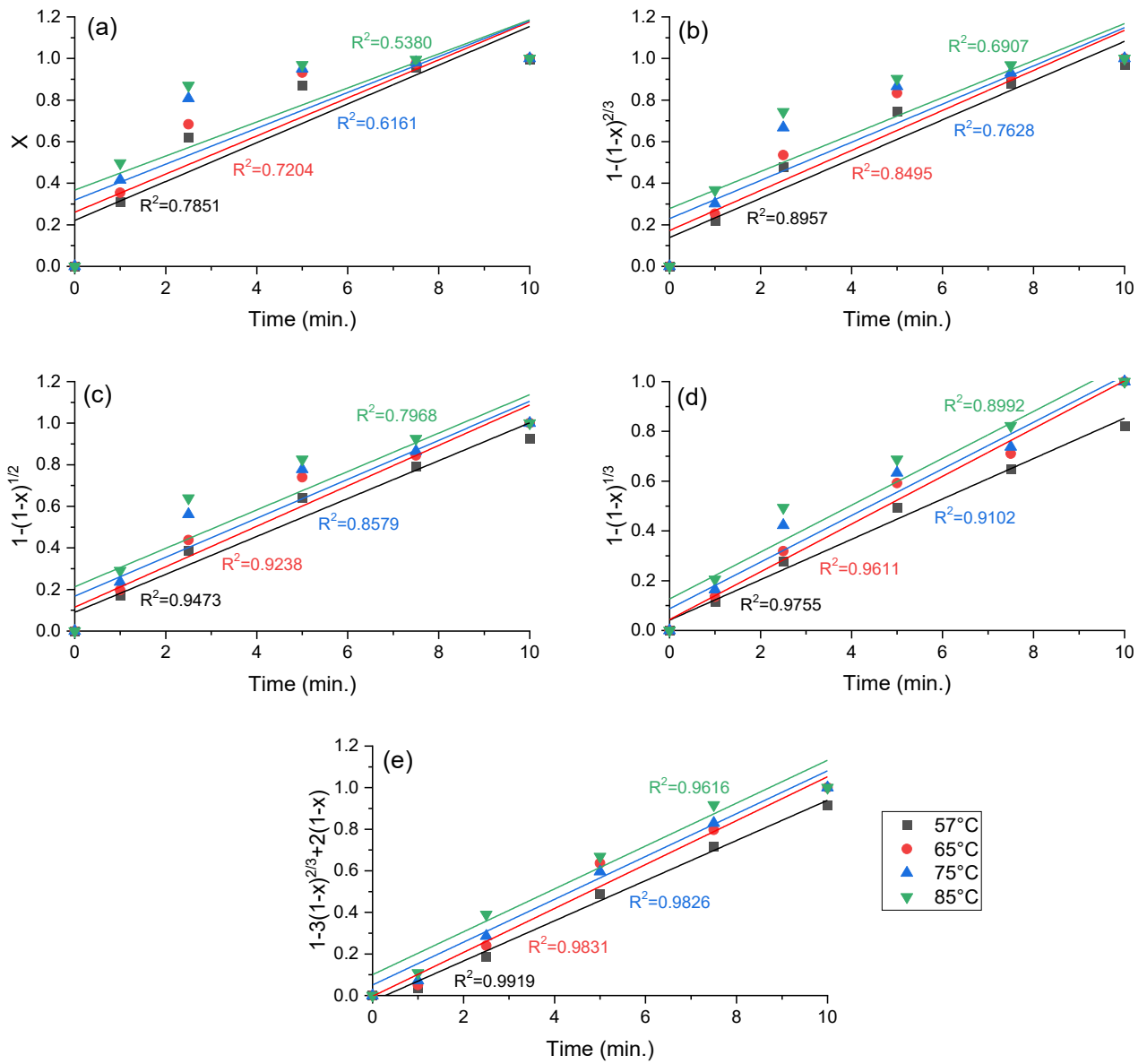


Figure 7.13: Model fitting for leaching kinetics of Pr_2O_3 by $[\text{Hbet}][\text{Tf}_2\text{N}]:\text{H}_2\text{O}$ (1:1); a) Film diffusion control dense constant size small particles – all geometries, b) Film diffusion control dense shrinking spheres, c) Chemical reaction control dense constant size cylindrical particles, d) Chemical reaction control dense constant size and e) Ash diffusion control dense constant size-spherical particles.

The leaching of Nd and Pr by [Hbet][Tf₂N]-H₂O is found to be governed by the ash diffusion control dense constant size-spherical particles as for both it presented the highest resistance in the SCM (the highest R² values). The slope of the linear fit of this model represents the apparent rate constant k_c , and the values for each oxide increasing with temperature are summarised in Table 7.5; consistent with the observations in Figure 7.11, as the temperature increased, so did the dissolution rate. This relationship between the leaching rate (K_c) and the temperature can be described by the Arrhenius equation:

$$K_c = Ae^{-E_a/RT} \quad \text{Eq. 7.8}$$

where k_c is the rate constant (min⁻¹), A is the frequency factor (min⁻¹), E_a is the activation energy of reaction (J/mol), R refers to the universal gas constant (8.3145 J/mol·K), and T is the temperature (K).

The Arrhenius plot was obtained by using the apparent rate constant k_c from Table 7.5, and the results are shown in Figure 7.14 for Nd₂O₃ and Pr₂O₃. The lineal regression with an R²=0.9739 for Nd₂O₃ and R²=0.9952 for Pr₂O₃ show that the leaching process fits well with the controlling diffusion model. Using the Arrhenius equation, the activation energy for Nd₂O₃ and Pr₂O₃ leaching was calculated to be 4.67 KJ/mol and 6.01 KJ/mol, respectively, in the temperature range of 57 °C and 85 °C. The magnitude of activation energy suggests that the process is indeed controlled by diffusion since high activation energies (≥ 30-40 kJ/mol) generally indicate that the chemical reaction is the rate limiting step, whilst lower activation energies are associated with transport-controlled reactions [111, 177]. Lower activation energy generally leads to higher speed rate, which is in good agreement with the rate constant from Table 7.5, where K_c values for Nd₂O₃ (lower E_a) are consistently greater than the K_c values for Pr₂O₃. In both cases, as expected, the higher the temperature, the higher the rate constant.

Table 7.5: Linear fitting parameters of ash diffusion control dense constant size-spherical particles model.

	K_c (min ⁻¹)				E_a (KJ/mol)
	57 °C	65 °C	75 °C	85 °C	
Nd ₂ O ₃	8.36x10 ⁻²	9.44x10 ⁻²	9.57x10 ⁻²	9.60x10 ⁻²	4.67
Pr ₂ O ₃	8.11x10 ⁻²	9.37x10 ⁻²	9.42x10 ⁻²	9.58x10 ⁻²	6.01

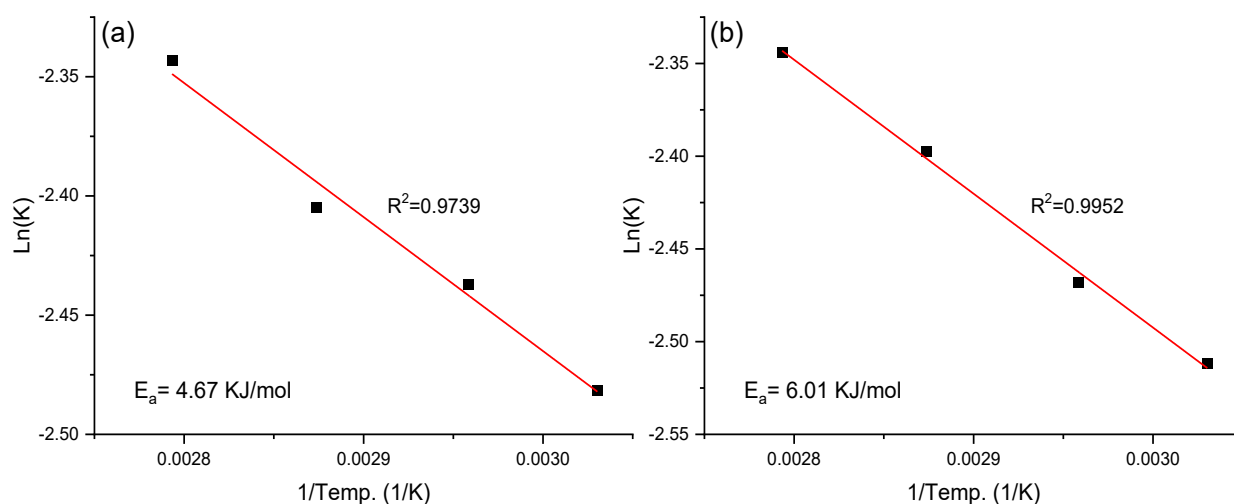


Figure 7.14: Arrhenius plot for REOs leaching (a) Nd_2O_3 and (b) Pr_2O_3 .

7.3.1.5 [Hbet][Tf₂N] selectivity of a binary REOs mixture

Neodymium and praseodymium are the major REEs present in speakers and cameras of EoL-MPs, so an important factor in investigating their extraction and recovery using the ionic liquid [Hbet][Tf₂N]-H₂O, is study of their behaviour in the presence of one another. Thus, the REOs selectivity in a binary REOs mixture (Nd_2O_3 and Pr_2O_3) was investigated. Figure 7.15 shows the selectivity of [Hbet][Tf₂N]-H₂O for the two oxides in a binary mixture of REOs presented in a combination of different Nd_2O_3 : Pr_2O_3 mass ratios from 1:5 to 5:1. It can be seen from Figure 7.15 that the IL has a marked tendency towards Nd_2O_3 , in comparison to Pr_2O_3 . This is evident especially in the case of 1:1 of Nd_2O_3 : Pr_2O_3 , where the concentration of Nd in [Hbet][Tf₂N]-H₂O system is 70% higher than the Pr concentration in the same IL system. As the ratio of Nd_2O_3 : Pr_2O_3 is increased to 1:2, although twice as much Pr_2O_3 is present compared to Nd_2O_3 , their concentrations in the IL are similar (at nearly 40 mg/g). With the ratio reversed to Nd_2O_3 : Pr_2O_3 =2:1, the concentration of Nd is nearly 3 times that of Pr. For the ratios of Nd_2O_3 : Pr_2O_3 as 1:5 and 5:1, the tendency was similar, favouring the extraction of Nd_2O_3 . Thus, only for the case in which the mass of Pr_2O_3 was twice the mass of Nd_2O_3 , [Hbet][Tf₂N] selected both elements equally. The selectivity of Nd_2O_3 over Pr_2O_3 by the [Hbet][Tf₂N]-H₂O mixture is approximately 1.5-2.0. In Table 7.5, it is shown that the activation energy of Nd_2O_3 (4.67 KJ/mol) is lower than the activation energy of Pr_2O_3 (6.01 KJ/mol), and consequently the rate of reaction is faster as indicated by the higher rate constants observed. This implies that when both REOs are present, the IL will interact more easily and faster with Nd_2O_3 , favouring its extraction over the extraction of Pr_2O_3 . This marked tendency is also observed with the extraction efficiency, with more Nd_2O_3 being extracted than Pr_2O_3 in all the cases, except in the Nd_2O_3 : Pr_2O_3 ratio of 1:5, where Pr_2O_3 it is in much greater

abundance than Nd_2O_3 . The sum of both REO concentrations is nearly constant (85 ± 4 mg/g IL) in the whole range studied, suggesting that the IL reached equilibrium.

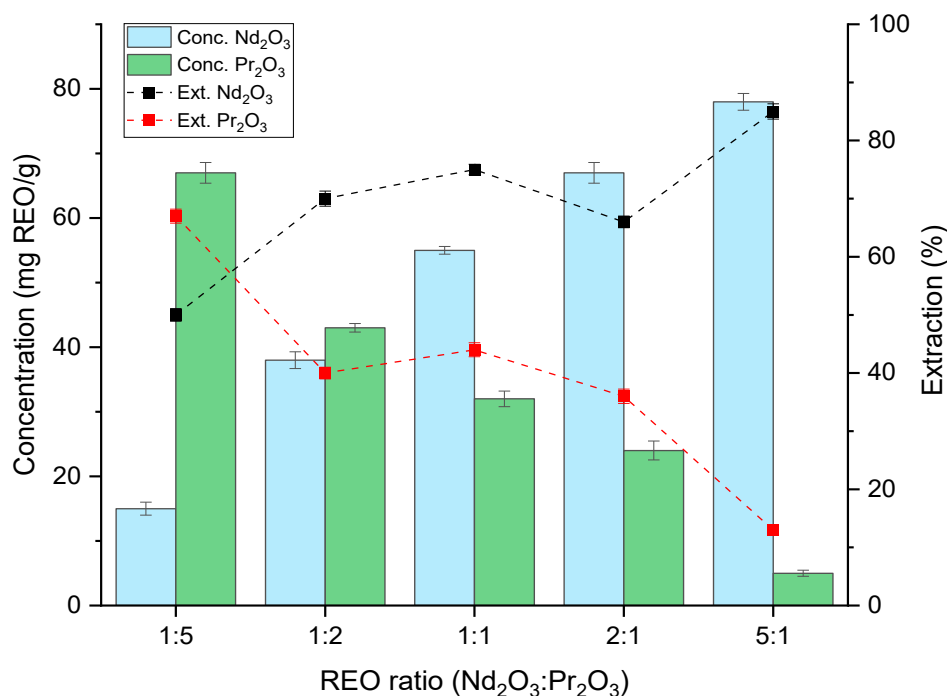


Figure 7.15: Effect of the Nd_2O_3 : Pr_2O_3 ratio on the leaching by $[\text{Hbet}][\text{Tf}_2\text{N}]:\text{H}_2\text{O}$ (1:1) system.

7.3.1.6 Solubility of Fe_2O_3 in $[\text{Hbet}][\text{Tf}_2\text{N}]$ and selectivity in a Nd_2O_3 - Pr_2O_3 - Fe_2O_3 mixture

In electronics (speakers and cameras) of EoL-MPs, copper and iron are the most abundant metals, which could impact REEs recovery. Copper is found mainly in the PCB of these electronic devices, so removal of the PCB component eliminates most of the copper in the system. The iron in cameras is also mainly in the PCB. Nevertheless, iron in speakers, as observed in Figure 7.6, is an intrinsic metal in the system present as NdFeB magnets. Iron and REEs, especially neodymium and praseodymium, are used in speakers for their magnetic properties [27]. Therefore, iron cannot be separated from neodymium by physical means. Due to this, the solubility of Fe_2O_3 in $[\text{Hbet}][\text{Tf}_2\text{N}]$ and the selectivity of the IL for Fe_2O_3 alone was first studied, and separately, a ternary Fe-Nd-Pr mixture was investigated to determine the impact, if any, of the presence of Fe_2O_3 on the solubility of the REOs in the IL and on the selectivity of the IL for them. Figure 7.16a shows the effect of the temperature on the solubility of Fe_2O_3 over time, whereas Figure 7.16b shows the effect of changing the $[\text{Hbet}][\text{Tf}_2\text{N}]:\text{H}_2\text{O}$ ratio on the concentration and the distribution in the organic phase (IL) and the aqueous phase (H_2O). It can be seen in Figure 7.16a that the leaching of iron oxide increases as the

temperature rises, reaching an equilibrium within 30 minutes, but the concentration of Fe_2O_3 in the $[\text{Hbet}][\text{Tf}_2\text{N}]:\text{H}_2\text{O}$ system is negligible, reaching a maximum of nearly $0.05 \text{ g Fe}_2\text{O}_3/\text{g} [\text{Hbet}][\text{Tf}_2\text{N}]:\text{H}_2\text{O}$ at 85°C . The effect of the $[\text{Hbet}][\text{Tf}_2\text{N}]:\text{H}_2\text{O}$ ratio on iron oxide (Figure 7.16b) shows that when the water content increases, iron oxide leaching also increases, likely due to the water decreasing the viscosity of the IL and favouring mass transfer although the leaching still remains low. An interesting observation is that decreasing the $[\text{Hbet}][\text{Tf}_2\text{N}]:\text{H}_2\text{O}$ ratio, i.e. adding more water to the $[\text{Hbet}][\text{Tf}_2\text{N}]:\text{H}_2\text{O}$ system, results in an increase of Fe_2O_3 present in the IL after cooling and separation. This is likely due to the hydrophilic surface of iron oxide, which is repelled from the aqueous phase and as the amount of water increases, so does the extent of repulsion, increasing the amount of Fe_2O_3 in the hydrophobic IL. From these results, it can be inferred that in a mixture of iron oxide and REOs, Fe_2O_3 will not interfere in the separation and recovery of Nd_2O_3 and Pr_2O_3 .

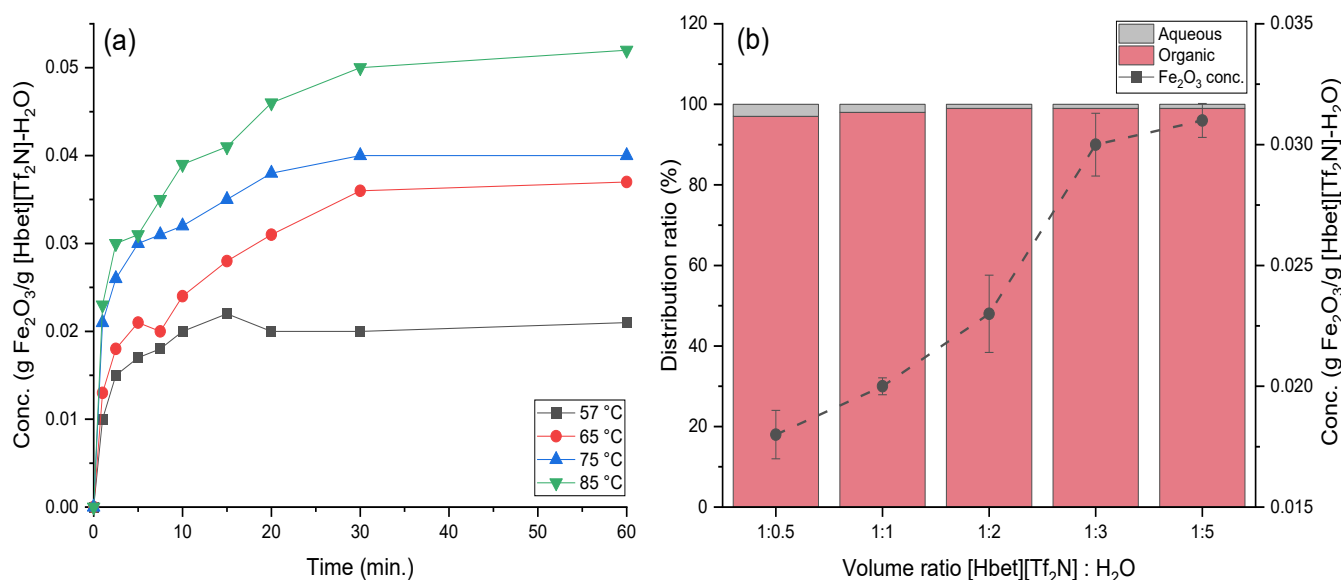


Figure 7.16: Solubility of Fe_2O_3 over (a) temperature, and (b) $\text{IL}:\text{H}_2\text{O}$ ratio.

To corroborate the low leaching and poor selectivity of iron oxide by the $[\text{Hbet}][\text{Tf}_2\text{N}]:\text{H}_2\text{O}$ system, a mixture of Nd_2O_3 , Pr_2O_3 and Fe_2O_3 with different ratios of iron oxide was further studied. In this experiment, the $\text{Nd}_2\text{O}_3:\text{Pr}_2\text{O}_3$ ratio was maintained at 1:1, and the ratio of iron oxide with respect to the REOs was varied from 1:1:1 to 1:1:5 ($\text{Nd}_2\text{O}_3:\text{Pr}_2\text{O}_3:\text{Fe}_2\text{O}_3$), as shown in Figure 7.17. Increasing the ratio of iron oxide, whilst keeping the $\text{Nd}_2\text{O}_3:\text{Pr}_2\text{O}_3$ ratio at 1:1, shows that leaching of Fe_2O_3 increases slightly from 1.8 to 3.1 mg $\text{Fe}_2\text{O}_3/\text{g}$ at 1:1:1 and 1:1:5 $\text{Nd}_2\text{O}_3:\text{Pr}_2\text{O}_3:\text{Fe}_2\text{O}_3$ ratios, respectively. This increase in the concentration of iron oxide is however very low as the extraction increases only

0.4%. In the case of Nd_2O_3 and Pr_2O_3 , Figure 7.17 confirms the results found in Figure 7.15, with the concentration and extraction levels for Nd_2O_3 and Pr_2O_3 at $\text{Nd}_2\text{O}_3:\text{Pr}_2\text{O}_3=1:1$, remaining almost constant and favouring the Nd_2O_3 leaching. The addition of Fe_2O_3 therefore did not impact the concentration and extraction of Nd_2O_3 and Pr_2O_3 , suggesting that even when the amount of iron oxide present is five times higher than Nd_2O_3 and Pr_2O_3 , it does not affect the extraction of the REOs. This is in good agreement with the extraction of iron oxide in $[\text{Hbet}][\text{Tf}_2\text{N}]:\text{H}_2\text{O}$ system without the presence of other metals, confirming the consistently poor leaching of Fe_2O_3 in $[\text{Hbet}][\text{Tf}_2\text{N}]$. These results show that iron oxide presents very poor solubility in the $[\text{Hbet}][\text{Tf}_2\text{N}]:\text{H}_2\text{O}$ system, alone and in the presence of REOs. This is very encouraging and confirms that separation and recovery of neodymium and praseodymium oxides from speakers can be achieved without the need for additional separation step to remove iron oxide.

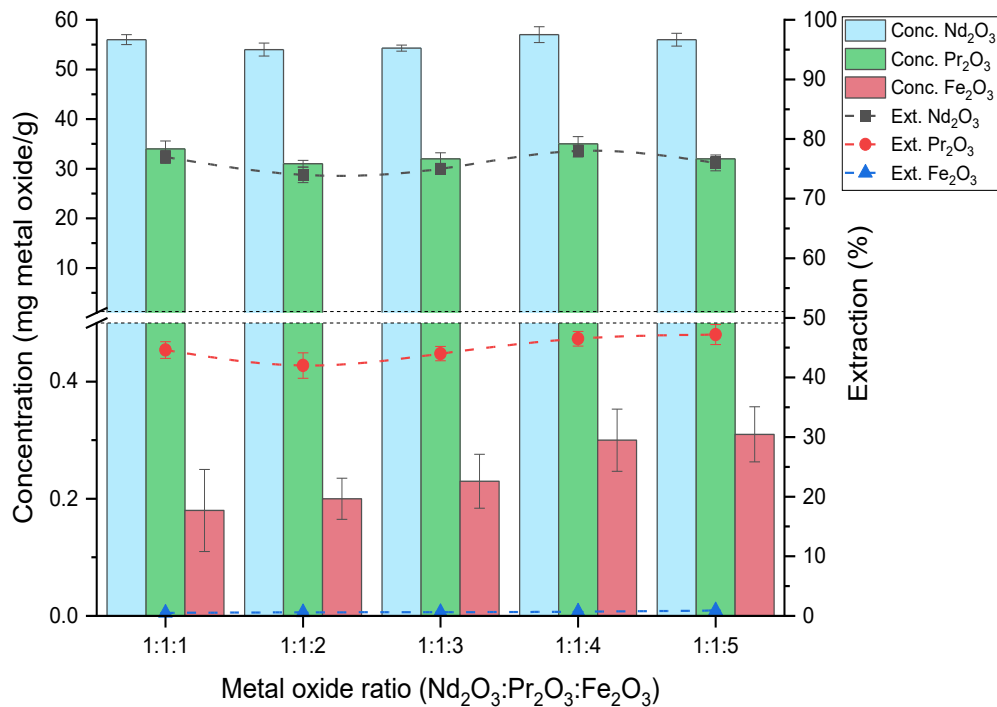
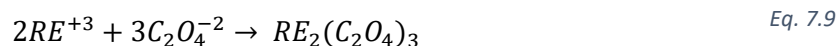


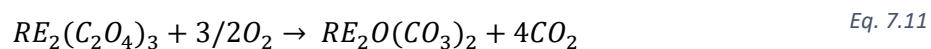
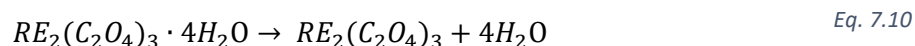
Figure 7.17: Effect of the $\text{Nd}_2\text{O}_3:\text{Pr}_2\text{O}_3:\text{Fe}_2\text{O}_3$ ratio on the leaching by $[\text{Hbet}][\text{Tf}_2\text{N}]:\text{H}_2\text{O}$ (1:1) system.

7.3.1.7 Precipitation

The recovery of REEs was carried out by precipitation using oxalic acid as precipitant from the aqueous phase to obtain rare-earth oxalates. The selection of oxalic acid was due to an efficient one-step recovery process, low-cost reagent, relatively low toxicity, and facile conversion of RE oxalates to REOs by calcination. The reaction between REE and oxalic acid ($C_2H_2O_4$) is:



Based on Eq. 7.9, the theoretical amount of oxalate that is required is $C_2H_2O_4$: REE=3:2. Preliminary tests in this work showed that adding the stoichiometric values of oxalic acid, recovery was incomplete (98% of precipitation), so to achieve complete recovery, oxalic acid was added with a 5% of excess. The precipitation was complete (with $\geq 99.5\%$) at room temperature (20 ± 2 °C), 250 rpm and 15 minutes (although 10 minutes was sufficient for precipitation, 15 minutes was selected to ensure full precipitation). Experiments were carried out using neodymium and after precipitation, neodymium oxalate ($Nd_2(C_2O_4)_3$) was collected and characterised by TG-DSC analysis (Figure 7.18). The analysis indicates that there is an initial mass loss of 11% between 90 °C and 380 °C, with a peak in DSC at 133.8 °C. This first decomposition corresponds to the dehydration of the hydrated oxalate and its mass loss suggests the dehydration of 4 molecules of water (theoretical loss of 4 molecules of water is 11.5%). A second mass loss of 23.6% occurs in the temperature range of 380-510°C, with a second peak in the DSC curve at 422.1 °C. This mass change in the second step of decomposition corresponds to the transformation of $Nd_2(C_2O_4)_3$ to $Nd_2O_3(CO_3)_2$, which is an unstable compound [282]. This is confirmed by the weight loss of 23.6%, which is accordance with the expected theoretical value of 23.2%. The final decomposition occurs between 510 °C and 950 °C, with a mass loss of 11.8%, which is characterised by a peak in the DSC curve at 580.4 °C. This decomposition is consistent with the conversion of the intermediate compound $Nd_2O_3(CO_3)_2$ into Nd_2O_3 ; being close to the theoretically calculated. The last stage of the neodymium oxalate decomposition can be divided into two stages as indicated in the DSC with T_{pk3} and T_{pk4} with 5.1% and 6.7% mass loss, respectively. This suggests the conversion of $Nd_2O_3(CO_3)_2$ to Nd_2O_3 involves more than one step and would need further analysis to confirm this observation. Based on the TG-DSC decomposition of neodymium oxalate to neodymium oxide, the general decomposition process of RE oxalates can be described as follows:



It is noted that the DSC curve does not appear as distinct plateaus but shows some background noise around the peaks which indicate that the process steps observed may not represent complete separation of intermediate fractions during the heating process. The data in Figure 7.18 confirm that the conversion of $\text{Nd}_2\text{O}_3(\text{CO}_3)_3$ to Nd_2O_3 can be achieved from a temperature of 800 °C. At 950 °C, the mass difference between 800 °C and 950 °C is just -1%, suggesting that a temperature of 800 °C can be used for calcination of neodymium oxalate. Therefore, to ensure the calcination of the rare-earth oxalates is complete a temperature of 900 °C for 90 minutes was selected.

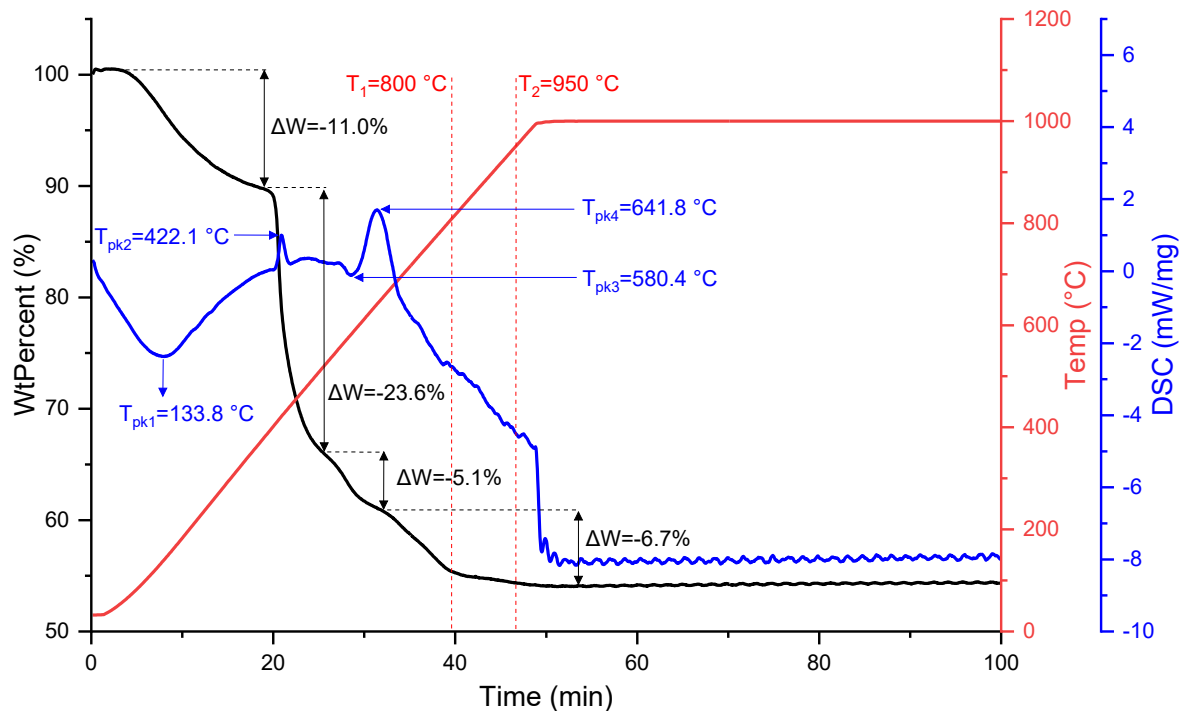


Figure 7.18: TG-DSC curves of REEs oxalates at a heating rate of 20 °C/mi in air.

In summary, the oxalate precipitation after leaching/extraction was observed to be very efficient, with just a 5% excess of the stoichiometric value needed of oxalic acid. Due to the mild conditions and fast kinetics, oxalic acid has been widely used for the precipitation of REEs [265, 273, 277, 278, 282]. Usually, stoichiometric amounts of oxalic acid are sufficient to obtain 100% stripping. Tian et al. studied the effect of oxalic acid dosage and pH value in the precipitation of Nd and Fe from NdFeB magnets leach solution by HCl [282]. They found that, in presence of iron, the precipitation of Nd increases with the increase in oxalic acid dosage, reaching a saturation at the stoichiometric value, precipitating 90% of the Nd. Further oxalic acid did not increase the Nd precipitation but decreased the purity of the precipitate since high doses of oxalic acid can accelerate the precipitation process, where impurities are unable to diffuse and so become trapped in the precipitate. The effect the pH

was similar; where a high pH value also increases the amount of product precipitated and accelerates the precipitation process, but a low purity product is obtained. The study suggests that the precipitation of REEs by oxalic acid is preferred over the precipitation of iron. After precipitation, calcination is also widely used to produce REOs, usually between 800 °C and 950 °C [265, 277, 282]. In this study, the calcination was carried out at 950 °C for 1.5 h, which is the usual temperature for complete calcination of rare-earth oxalates. The time of calcination varies from 1 h to 15 h; however, in this study 1.5 h was used as it was deemed enough time for complete oxidation of the RE oxalates to REOs.

7.3.1.8 Elution and Recovery of the [Hbet][Tf₂N]

Metals in the organic phase ([Hbet][Tf₂N]) can be stripped by extracting the IL in acidified aqueous solution, usually with a dilute acid. The metal complex of protonated betaine bis(trifluoromethylsulfonyl)imide is decomposed, and the betaine bis(trifluoromethylsulfonyl)imide is regenerated, whilst the metal ion is transferred to the aqueous phase [107]. Preliminary studies in the current research showed that of the three mineral acids (HCl, HNO₃, and H₂SO₄), hydrochloric acid is the best stripping agent for REEs. The stripping was carried out by a 0.5 M HCl in 0.1 M betaine chloride solution with an organic to aqueous ratio of 1:1, at room temperature (20±2 °C), 250 rpm for 30 minutes. Betaine was introduced in the stripping solution for two reasons: firstly, it acts as an extractant due to it can form complex with metal ions such as lanthanides, and secondly, the addition of betaine introduces cations of [Hbet]⁺ to the IL phase, replacing/substituting the betaine that might have been lost in the extraction and separation process. To study the stripping and the potential to reuse the IL, five cycles of leaching and stripping were carried out and the efficiency of leaching of Nd₂O₃ determined as shown in Figure 7.19. Although the leaching and stripping of Nd were slightly affected over five consecutive cycles, leaching and extraction efficiencies of ≥95% were achieved for each of the five cycles, suggesting that [Hbet][Tf₂N] can be successfully reused without any major loss in efficiency. The overall efficiency for the combined process shows a slight downward trend throughout the cycles, decreasing from 98% in the first cycle to 90% in the fifth cycle. This slight decrease is attributed to the IL leaching efficiency, which was decreases slowly through the cycles, but the stripping efficiency remains practically complete in all the cases (≥95%).

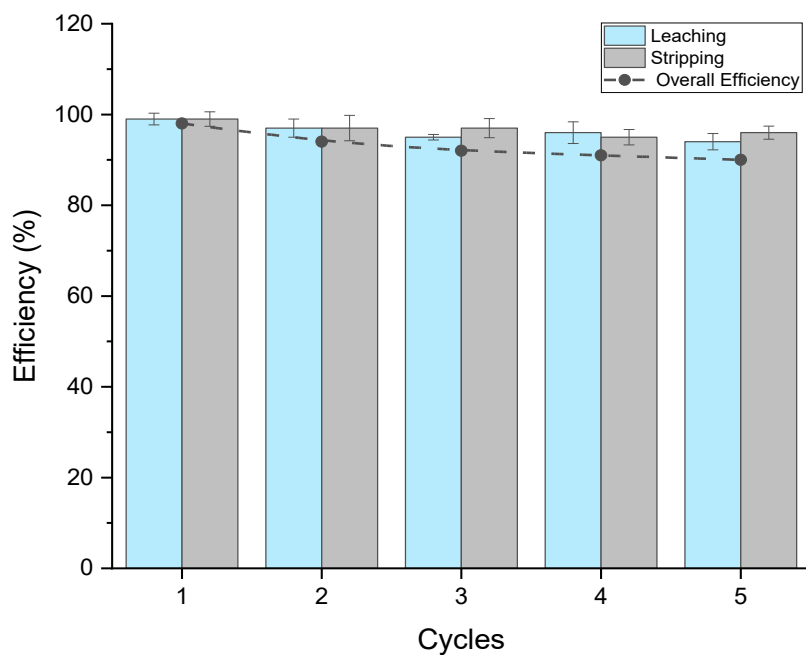


Figure 7.19: Nd_2O_3 leaching, stripping, and $[\text{Hbet}][\text{Tf}_2\text{N}]$ reusability over five cycles.

To corroborate that the IL ($[\text{Hbet}][\text{Tf}_2\text{N}]$) is not affected through the reuse process, FTIR analysis was used to record any changes in the structure of the organic extractant over the five cycles, and the spectra are shown in Figure 7.20. All spectra for the reused $[\text{Hbet}][\text{Tf}_2\text{N}]$ show peaks characteristics of the $[\text{Hbet}][\text{Tf}_2\text{N}]$ at 1769 cm^{-1} , attributed to the stretching vibration of C=O in COOH group, 1470 cm^{-1} associated with C-H bonds (CH_2), whereas the zone between $1000\text{-}1400\text{ cm}^{-1}$ is assigned to be vibration of $[\text{Tf}_2\text{N}]$ since the peaks at 1330 cm^{-1} and 1170 cm^{-1} are associated with S=O (SO_2) and C-F (CF_3) stretch bonds, respectively. The FTIRs after leaching and stripping over 5 cycles do not show any noticeable difference, confirming that $[\text{Hbet}][\text{Tf}_2\text{N}]$ can be reused at least five times without changes to the IL structure and loss in its leaching efficiency.

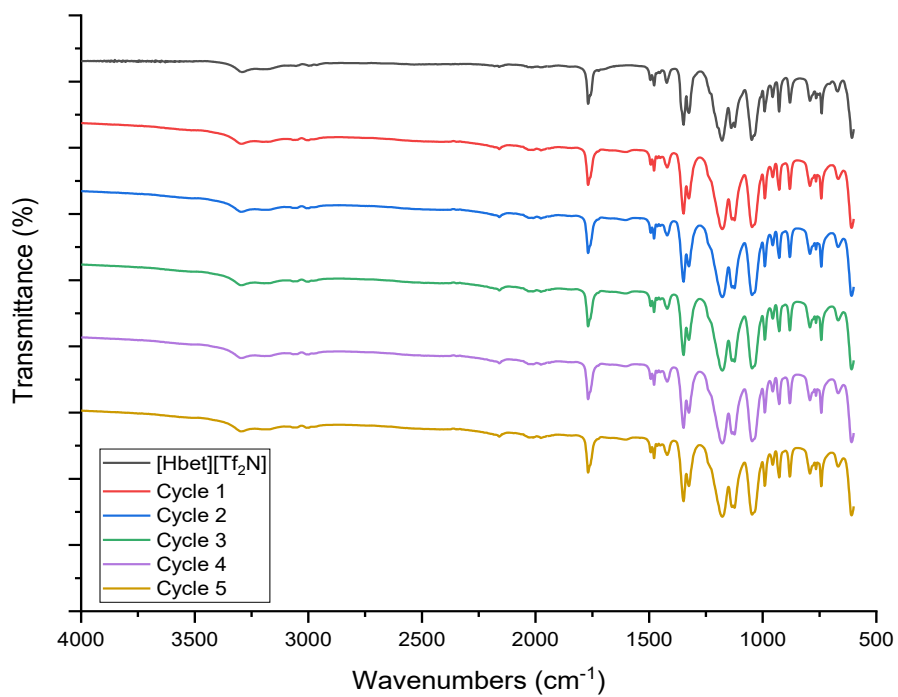


Figure 7.20: FTIR spectra of [Hbet][Tf₂N] over five cycles.

7.3.2 Pre-treatment of As-received Speakers from EoL-MPs

Pre-treatment of as-received speakers from EoL-MPs involving a demagnetisation and roasting step was studied to convert the REE metals to the corresponding oxide; a form that is suitable as feedstock for leaching using the [Hbet][Tf₂N]:H₂O system, and the results are now described.

7.3.2.1 Demagnetisation

Speakers from EoL mobile phones (Figure 7.1), after dismantling, were demagnetised in a muffle furnace at 350 °C for 1 h. This temperature was selected as it is 30 °C above the Curie temperature of neodymium magnets (~320 °C). The Curie temperature is the temperature above which certain materials lose their permanent magnetic properties. Furthermore, it has been reported that complete demagnetisation of NdFeB magnets can be achieved in 30 minutes at 350 °C [274, 283].

7.3.2.2 Roasting

After demagnetisation, the powder was roasted to convert the elements, mainly REEs, into their oxides, to enhance the leaching and selectivity of neodymium and praseodymium oxides in the [Hbet][Tf₂N]:H₂O system. Thermogravimetric analysis of the demagnetised speaker powder was utilised to determine the oxidation temperature and time to achieve this. Figure 7.21 shows the TG-DSC analysis of speaker powder, and two significant features are observed: a decrease in the mass of 20.1% from 250 °C to 500 °C, associated with the volatilization and decomposition of the organic material present (as reported in section 3.3.3.3, Chapter 3), followed by a mass gain of 10.2% in the range of 550-950 °C, which is associated with the oxidation of the metals present. The maximum mass gain was reached at 950 °C after approximately 50 minutes, being practically linear with the mass change after that time (with a small gain of less than 1%). This suggests that 1 h at 950 °C would be sufficient for roasting. The sample size tested, however, is small and conditions ideal for roasting (with a closed environment, constant air flow, and homogenous distribution of the powder in the crucible, etc.), so it was presumed that a longer time is required for 'non-ideal' conditions. Thus, roasting of the speaker powder was carried out at 950 °C for 5 h to assure full conversion to metal oxides. The samples treated at the roasting conditions selected were weighed before and after roasting, and a similar total mass loss of nearly 10% was observed.

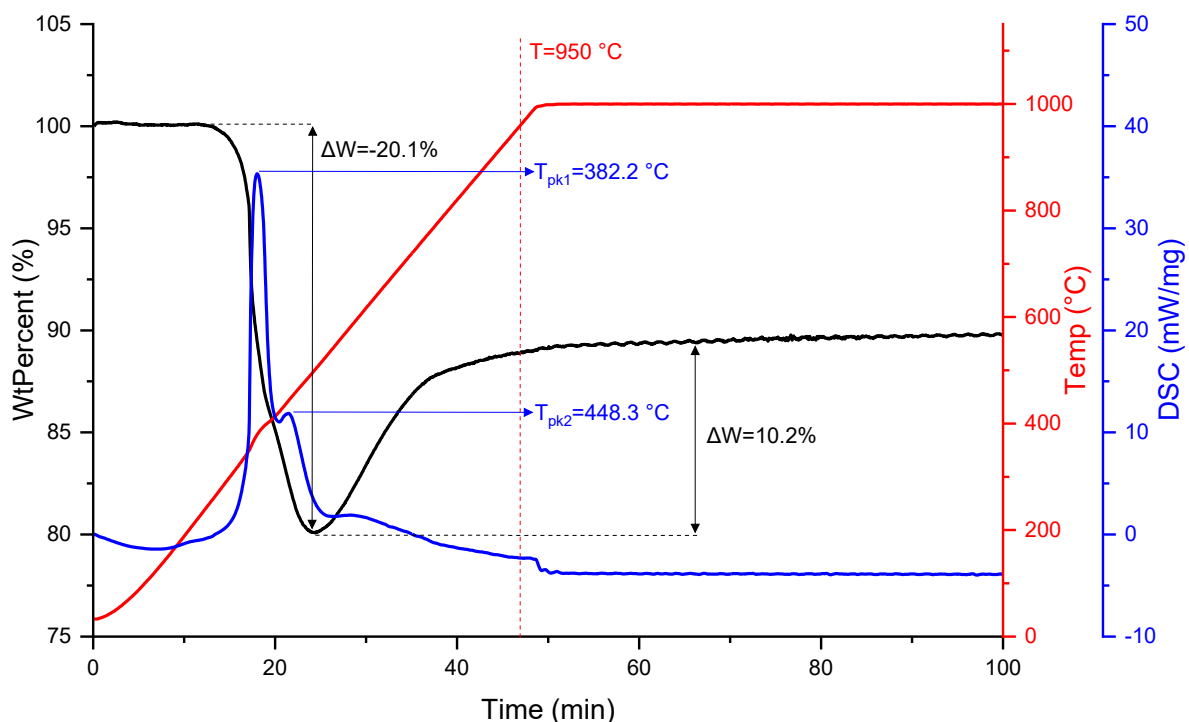


Figure 7.21: TG-DSC curves of speaker powder at a heating rate of 20 °C/min in air.

In summary, rare-earth metals in speakers and in general in WEEE are mostly present as compounds and alloys, requiring a pre-treatment step to oxidise the metals making them suitable for leaching with [Hbet][Tf₂N] for their recovery. In the recovery of REEs from NdFeB magnets, demagnetisation and roasting are usually carried out as pre-treatment before shredding and/or milling [265, 274, 277, 283]. The demagnetisation is essentially used to facilitate the handling of the magnets and facilitate the subsequent grinding step. Moreover, as the shredding equipment comprises metals without demagnetisation the metals would be difficult to separate and there would consequently be high mass loss of valuable materials in the process. The demagnetisation in this study was carried out at 350 °C, a temperature that is above the Curie temperature of neodymium magnets (approx. 320 °C), for 1 h. While it has been reported that complete demagnetisation of NdFeB magnets can be achieved in 30 minutes at 350 °C [274, 283], the longer time used in this study was to ensure complete demagnetization of the magnets. In the case of REEs recovery from [Hbet][Tf₂N], roasting was applied to convert the elements present in the speakers into their oxides, enhancing the selectivity of the [Hbet][Tf₂N] towards Nd₂O₃, Pr₂O₃ and other REOs in the subsequent leaching process. Roasting was carried out at 950 °C (as determined by TG-DSC analysis) for 5 h to ensure full conversion to the metal oxides. Roasting of speakers showed an initial mass loss of approximately 20 wt.% which was attributed to degradation of the organic matter, followed by a mass gain of nearly 10

wt.%. Hoogerstraete et al. studied the roasting of different NdFeB magnets particles sizes (<80 μm and <400 μm), observing that mass gain was low until a temperature of 300 °C, followed by a significant increase in oxidation, reaching full oxidation at 800 °C for the <80 μm powders and at 950 °C for the <400 μm powder in 6 h [273]. They reported mass gains of 23.6 wt.% and 24.2 wt.% for the <400 μm powder and <80 μm powder, respectively. It was also reported that lower roasting temperature (650 °C for the <80 μm powder) can also achieve complete oxidation, at the expense of a longer heating time (20 h). Other authors reported the roasting of magnets at similar temperatures, such as 900 °C and 8 h [274], and 950 °C for 15 h [265, 277], with mass gains between 27.4% to 34.5%. In those studies, only mass gains were observed, however, in this work a mass loss was also observed. The main difference between the reported studies, which used pure NdFeB magnets, and the current work is that the speakers used in this study were dismantled from EoL mobile phones and used whole, without further separation of the magnet from the other components. To provide a direct comparison therefore, further work on the speaker after, following separation of the magnet from the whole speaker, is recommended.

7.3.3 REEs recovery from EoL-MP speakers by [Hbet][Tf₂N]:H₂O system

Speakers from EoL-MPs were manually separated, demagnetised at 350 °C for 1 h, ball-cryomilled in liquid nitrogen (freezing the samples up to – 196 °C) at 150 rpm for 15 minutes in a closed system. The final product, a powder of ≤150 μm, was roasted at 950 °C for 5 h to convert the elements present into their oxides. The leaching process was carried out by adding the roasted speaker powder to the 1:1 [Hbet][Tf₂N]:H₂O system (sample/IL ratio of 10 mg/g), at 60 °C (above the cloud point temperature to ensure the formation of a homogenous phase), 250 rpm for 30 minutes. The water added in the [Hbet][Tf₂N]:H₂O system was a 1 M sodium nitrate (NaNO₃) solution, which was added to enhance the metal distribution towards the aqueous phase. The solution was then cooled to room temperature (20±2 °C) for phase separation, obtaining a biphasic system - the organic phase (lower layer) and the aqueous phase (upper layer) - and centrifuged to precipitate any remaining residue. Figure 7.22 shows the metal distribution after leaching/extraction between the organic phase, the aqueous phase, and the residue. Light REOs (Nd₂O₃ and Pr₂O₃) were almost completely leached (≥95%), followed by Sm₂O₃ with 87%. The heavy REOs, as expected, showed low leaching efficiency, approximately 24% for Dy₂O₃ and 1.5% for Tb₄O₇. Iron oxide also showed negligible leaching, being left in the residue, together with the un-leached HREOs (Dy₂O₃ and Tb₄O₇). The organic phase showed minor concentrations of elements, with the REEs being mainly found in the aqueous phase. As Nd and Pr represent 83 wt.% of the total metal content in speakers, the efficiency of their leaching/extraction process is promising. After the extraction and cooling, the aqueous phase is separated from the organic phase, and oxalic acid was added with a 5% stoichiometric excess to precipitate the rare-earth oxalate. This procedure was carried out at room temperature (20±2 °C), 250 rpm for 15 minutes, and the resulting rare-earth oxalate was roasted at 950 °C for 5 h in an oven to obtain REOs (Nd₂O₃ and Pr₂O₃). Unfortunately, because of time and sample constraints, there was limited product sufficient only to carry an *aqua regia* digestion which confirmed ≥98% of purity, but insufficient product to characterise the structural and morphological properties by XRD and SEM-EDS. The organic phase was rinsed, as described in section 7.3.1.8, and was available for further leaching/extraction.

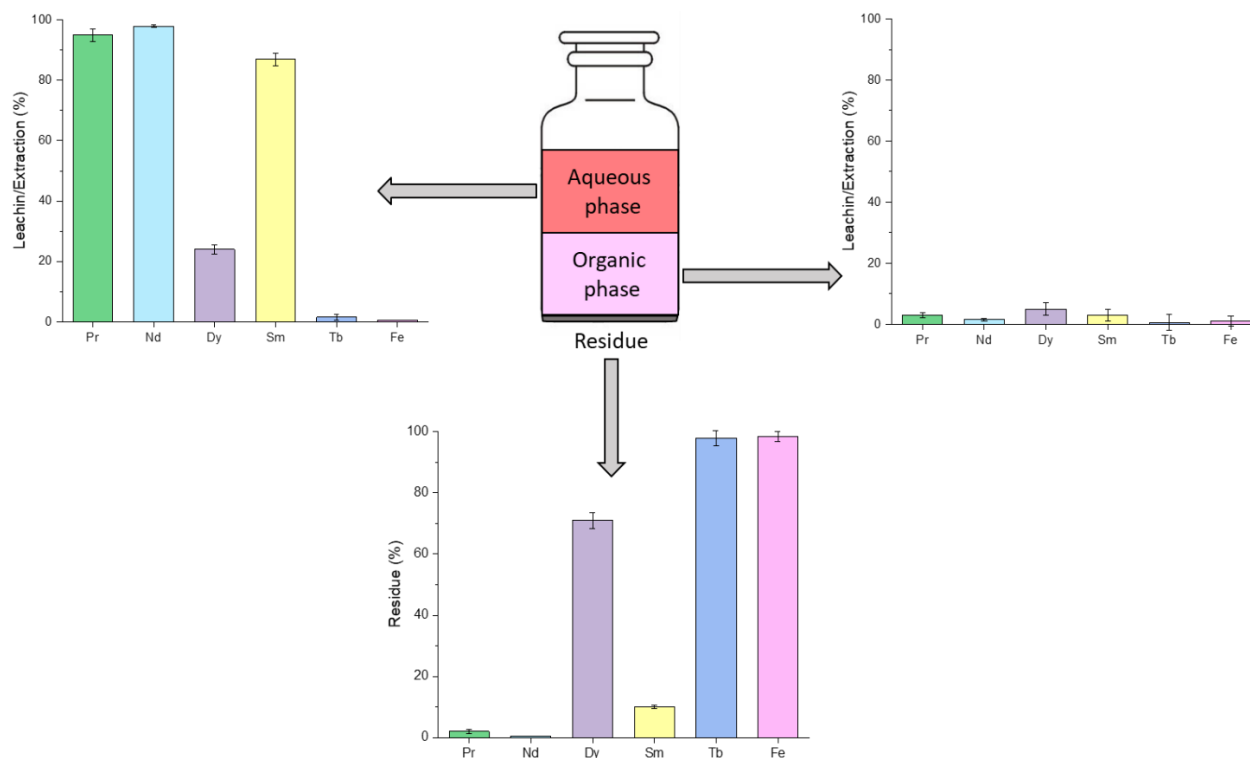


Figure 7.22: Metal distribution after [Hbet][Tf₂N]:H₂O system leaching/extraction.

7.3.3.1 Discussion

Dupont and Binnemans extracted and separated Nd, Dy, Co, and Fe from NdFeB magnets using [Hbet][Tf₂N] [265]. They found that the separation of iron from the REEs and Co ions was quite efficient, where Nd, Dy and Co ions were present in the aqueous phase and Fe in the organic phase. Iron was present in the organic phase due to the strong iron-betaine complexes formed, causing the iron to stay in the ionic liquid. In this study, however, the iron is found, unreacted, in the residue (Figure 7.22). Previous studies in the current work, where mixtures of Fe₂O₃, Nd₂O₃ and Pr₂O₃ were tested, even with higher amounts of iron oxide present in the mixture, the solubility of iron in the [Hbet][Tf₂N]-H₂O system was found to be negligible. Furthermore, since the amount of iron present in the speaker is 25 times lower than the amount of REEs, the probability of leaching would be further decreased. The difference may arise because in Dupont and Binnemans' work on the NdFeB magnets, the leaching was carried out by 1:1 [Hbet][Tf₂N]-H₂O at a higher temperature of 80 °C and with much longer reaction times between 8 h and 72 h. The higher temperature and longer reaction time can increase the iron oxide leaching. This is plausible as even after 72 h of reaction, the iron oxide leached was nearly 20% [265], showing slow kinetics, whilst in this study, after 0.5 h, little iron was dissolved.

In the current research sodium nitrate was used to increase the separation of the REEs distribution, favouring their presence in the aqueous phase. The addition of metal salts in [Hbet][Tf₂N] was studied extensively by Dupont et al. [284], who reported that the addition of metal salts in biphasic IL/water systems can significantly change the performance of the IL. For instance, it was reported that the solubility of [Hbet][Tf₂N] in water (up to 14 wt.% [107, 284]) can be drastically reduced by adding chloride and sodium salts, decreasing up to <5 wt.% by 1 M MgCl₂ and Na₂SO₄. This effect is called '*salting-out*' as the IL decreases its presence in the aqueous phase. As opposite, other salts can do the opposite, increasing the solubility in water ('*salting-in*' process). This is interesting because, each time leaching of the 1:1 [Hbet][Tf₂N]-H₂O system occurs, approximately 14 wt.% of the IL can be lost in the aqueous phase. Moreover, in the stripping or IL washing process, a further 14 wt.% of the IL can be lost. They reported that the addition of 1 M NaNO₃ favoured the salting-out of [Hbet][Tf₂N], reducing its loss in the aqueous phase by 5 wt%. Thus, the addition of NaNO₃ in the [Hbet][Tf₂N]-H₂O system not only increases the REE distribution in the aqueous phase, but also decreases the IL loss in it. Furthermore, according to the Hofmeister series, Tf₂N⁻ cannot be displaced by salt anions such as NO₃⁻, therefore no regeneration or cleaning of the IL is necessary since [Hbet][Tf₂N] does not undergo anion exchange [265, 284]. In a neodymium recycling from NdFeB magnets process by 1:1 [Hbet][Tf₂N]-H₂O system, Na₂SO₄ was added in the stripping stage as a salting-out agent to regenerate the IL as it was reported that at 3 M Na₂SO₄, only 0.15 wt.% of the IL is present in the aqueous phase, permitting almost a full recovery of the IL [265]. The use of salting-out agents can considerably reduce the loss of [Hbet][Tf₂N] in the aqueous phase, making the process more efficient.

The recycling of [Hbet][Tf₂N] was carried by mixing [Hbet][Tf₂N] with 0.1 M oxalic acid in a 0.1 M HCl solution to precipitate any residual metal present in the organic phase and to ensure the extraction of any impurity not removed after the oxalic acid solution. Nevertheless, after stripping, the IL can be regenerated without any further treatment. Huang et al. reused [Hbet][Tf₂N] in the extraction of zinc from zinc-cobalt slag up to three times without any washing or rinsing process [110]. It is noted that in that study, the Zn-loaded [Hbet][Tf₂N] was stripped with 0.5 M oxalic acid, which stripped the zinc and other minor impurities. The authors also reported that, after stripping, the concentration of metal ions in the regenerated [Hbet][Tf₂N] was negligible, and the FTIR of the regenerated ionic liquid was identical to that of the original ionic liquid. In the recovery of Nd and Dy from NdFeB magnets, it was reported that in the stripping step of the recovery process, the IL can automatically be regenerated and no further regeneration or cleaning of the ionic liquid was necessary [265]. In another work of Dupont and Binnemans in the recovery of Y₂O₃:Eu₃⁺ from lamp phosphor waste using [Hbet][Tf₂N], the stripping step was achieved by two methods; (i) by putting the loaded IL

in contact with 1M HCl, and (ii) by directly precipitating the REEs from the IL using pure (solid) oxalic acid. It was found that the second method was more efficient and rapid [278]. They used a stoichiometric amount of oxalic acid (for both yttrium and europium), stripping completely the rare-earth oxalates at 70 °C for 10 minutes. It was noted that an increase in the stripping temperature played a key role since pure oxalic acid was added to the viscous loaded IL, and increasing the temperature lowered the IL viscosity and improved the diffusion of the oxalic acid in the IL. It is argued that the presence of the Tf_2N^- ion in the IL, which is the most difficult anion to displace from the ionic liquid, and hence no anion exchange reactions will occur for $[\text{Hbet}][\text{Tf}_2\text{N}]$, removes the need to regenerate or clean the IL prior to recycling as the IL maintains its leaching/extraction properties through its reusability [265, 278, 280, 284]. Although these studies suggest that $[\text{Hbet}][\text{Tf}_2\text{N}]$ can be reused without any further treatment, a washing/rinsing step will be necessary at some point of the process to remove any metal ions accumulated during the cycles, which can be achieved by using slightly acid solutions. As previously discussed, the addition of a salting-out agent can be beneficial in the washing/rinsing step as it will avoid the loss of the IL through the process.

Another interesting observation made by Dupont and Binnemans, although it was not applied in their work, was the utilisation of microwave heating instead of a traditional heating source [265]. They pointed out that ILs can be heated in a very energy-efficient way by microwave irradiation, which does not interfere with the chemical dissolution process. In fact, elsewhere Dupont and Binnemans showed that $[\text{Hbet}][\text{Tf}_2\text{N}]$ can be heated to 100 °C in less than 15 s at 100 W, whereas water and toluene reached a temperature of nearly 65 °C and 30 °C, respectively [278]. Furthermore, as ILs consist entirely of ions, very high adsorption of microwave radiation can be achieved [285]. Thus, microwave heating can reduce the energy consumption of the process, which is beneficial from an economical and industrial perspective.

7.3.4 Proposed hydrometallurgical process for REOs recovery from EoL speakers

The six-step process of demagnetising, commutation, roasting, leaching, oxalate precipitation, and calcination developed and optimised for recovery of rare earth oxide from EoL-MP speakers is shown in Figure 7.23. The overall REEs recovery efficiency was $\geq 90\%$, recovering neodymium and praseodymium oxides. The whole process was repeated for a second cycle to confirm the recyclability of the IL and the process efficiency with an overall efficiency of $\geq 90\%$ was successfully achieved. All the experiments were carried out on a laboratory scale with excellent results, which can now be applied on a larger scale. An additional step is proposed to reuse the stripping solution (0.5 M HCl+0.1 M betaine) since the IL has only trace elements; this step is essentially to rinse and wash the IL. The recycling process is relatively easy to handle in a laboratory scale; the likely cost implications in the scaled-up process would lie in the energy consumption required in the heating processes (roasting and calcination), which could impact the economic viability of the process but with the recovery of the critical rare earth oxides from which pure RE metal can be recovered, any costs could likely be offset. The process is developed for recovery of REEs from EoL-MP speakers but can be applied to the recovery of rare earth elements from different types of magnets.

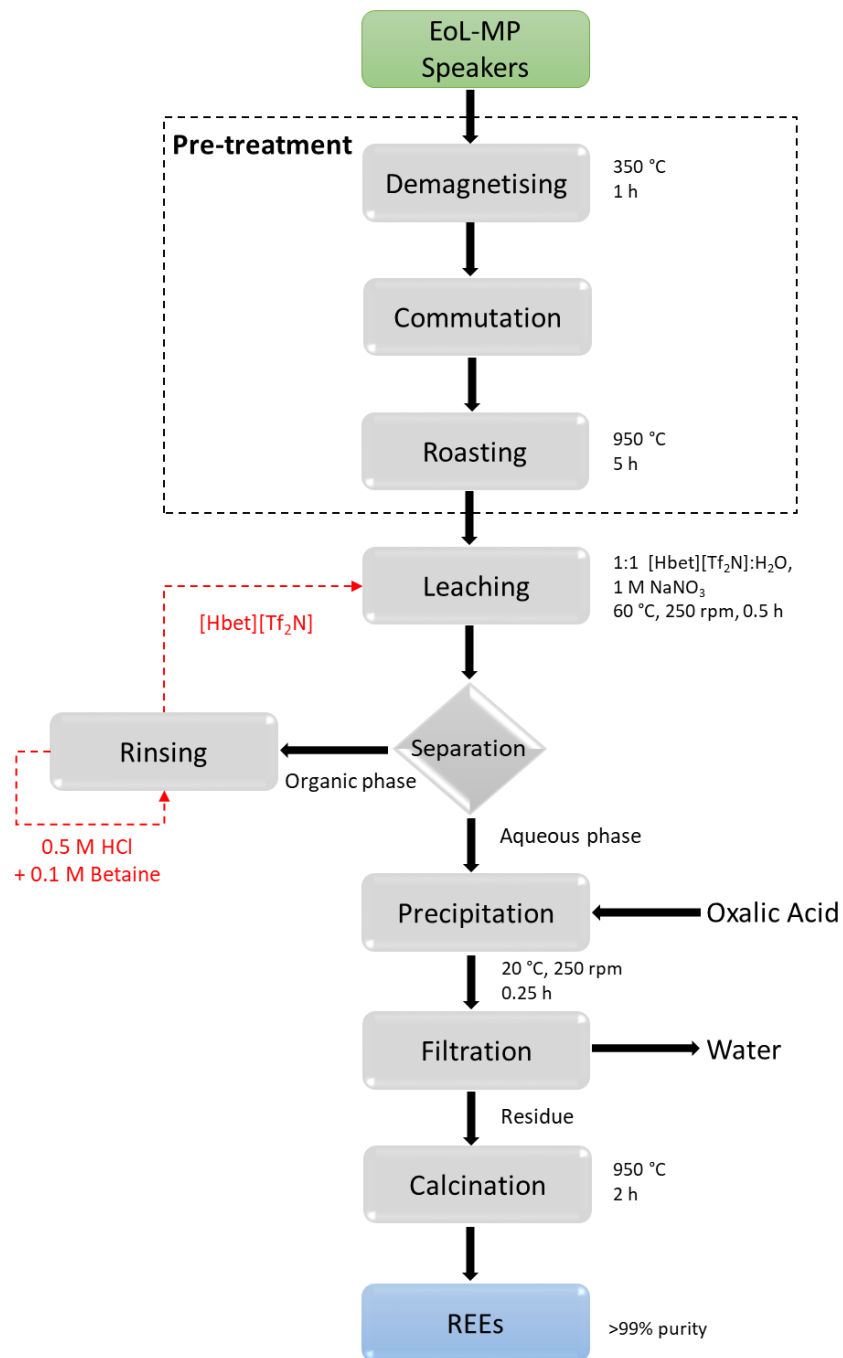


Figure 7.23: Flow chart of the recycling of rare-earth elements from EoL mobile phones speakers.

7.3.5 Optimised Conditions for REEs Extraction and Recovery Using a Model Test System: *Alternative Recovery Method*

An alternative method that involves the leaching, extraction and stripping of REEs directly without the need for a pre-treatment step is proposed, using a Model Test System. The results are now described. Although preliminary trialling of this process on as-received samples was carried out but because of time constraints it was not possible to refine the process and validate the findings for reporting here.

7.3.5.1 Selection and Leaching of the IL ([Bmim][Tf₂N], [P_{6,6,6,14}][Tf₂N] and [P_{6,6,6,14}][Cl])

In cameras and speakers, REEs are mostly present as compounds or alloys, and can be leached using a mineral acid (HCl, HNO₃, and H₂SO₄); in this work it was found that of the three acids, hydrochloric acid was the best leaching agent for REEs. Once in solution, different solvents can be used for REE extraction. In this study, three ILs were studied as potential extractants: ([Bmim][Tf₂N]), ([P_{6,6,6,14}][Tf₂N]), and Cyphos 101 ([P_{6,6,6,14}][Cl]) (Table 5.1), and the Model Test System selected for investigation was neodymium, identified as the most abundant REE in cameras and speakers shown in Figure 7.5. The effect of HCl concentration, temperature, and time on the neodymium extraction by the three ILs was determined, and the results are presented in Figure 7.24. The effect of the hydrochloric acid concentration on Nd extraction by the ILs (Figure 7.24a) shows an increase in HCl concentration (from 0.1 M to 3 M) leads to a slight increase in extraction (of approximately 5%) for both [P_{6,6,6,14}][Tf₂N] and [P_{6,6,6,14}][Cl], but a more pronounced increase (of 10%) in the range of 0.1-3 M HCl) for [Bmim][Tf₂N]. The greatest impact of HCl concentration on Nd extraction in the three ILs is observed in the range from 0.5 M to 1 M HCl, being relatively stable for all ILs above this acid concentration. This result confirms that only a relatively low concentration of HCl is required for Nd extraction; 1 M HCl was selected for further experiments. A further benefit is that the Nd leached in 1 M HCl, can be used directly for extraction, which minimises the use of reagents. The effect of temperature on Nd extraction (Figure 7.24b) shows that temperature, in the range of 20-80 °C, does not affect the Nd extraction, being practically unaltered. This result was surprising as an increase in temperature generally allows greater mass transfer because the viscosity of the IL decreases; this would be particularly noticeable for the IL, [P_{6,6,6,14}][Cl], as its viscosity is considerably higher than that of either [Bmim][Tf₂N] or [P_{6,6,6,14}][Tf₂N]. The chosen temperature for extraction was therefore set as 20 °C, as this reduces the energy consumption of the process. In terms of the effect on the extraction time, it is observed in Figure 7.24c that within the first 10 minutes of reaction, Nd extraction efficiencies reached 40.4, 35.4, and 36.7% for [Bmim][Tf₂N] and [P_{6,6,6,14}][Tf₂N] and [P_{6,6,6,14}][Cl], respectively. As the reaction continues, the extraction increases until reaching an equilibrium within

60 minutes for the three ILs. Therefore, 1 M HCl, 20 °C and 1 h were determined as the optimal parameters for the extraction of neodymium.

Under conditions of the varying conditions investigated for HCl concentration, temperature and time, the Nd extraction followed the same trend in all cases: [Bmim][Tf₂N] > [P_{6,6,6,14}][Tf₂N] > [P_{6,6,6,14}][Cl], with [Bmim][Tf₂N] proving to be the best IL for Nd extraction. The higher extraction efficiency of [Bmim][Tf₂N] compared to [P_{6,6,6,14}][Tf₂N] is explained by analysing the ionic cation, as both ILs share the same anion ([Tf₂N]⁻). The [Bmim] (C₈H₁₅N₂⁺) has a shorter organic chain than [P_{6,6,6,14}], which implies lower hydrophobicity, which is beneficial because the cation can more easily enter the aqueous phase, increasing the mass transfer and consequently the extraction. In the case [P_{6,6,6,14}][Cl], its lower extraction compared to [P_{6,6,6,14}][Tf₂N] is explained by the difference in the anion as they have they have the same cation; where the bonding of [P_{6,6,6,14}] with [Cl] is stronger than with [Tf₂N], because of the more electronegative anion (Cl⁻), making it more difficult to dissociate and to form REE complexes. The much higher viscosity of [P_{6,6,6,14}][Cl] than [Bmim][Tf₂N] is an indication of the stronger cation-anion bonding of [P_{6,6,6,14}][Cl]. In the case of the higher extraction efficiency of [Bmim][Tf₂N] compared to [P_{6,6,6,14}][Cl], a mixture of both features, lower hydrophobicity and lower cation-anion energy bonding can be the responsible.

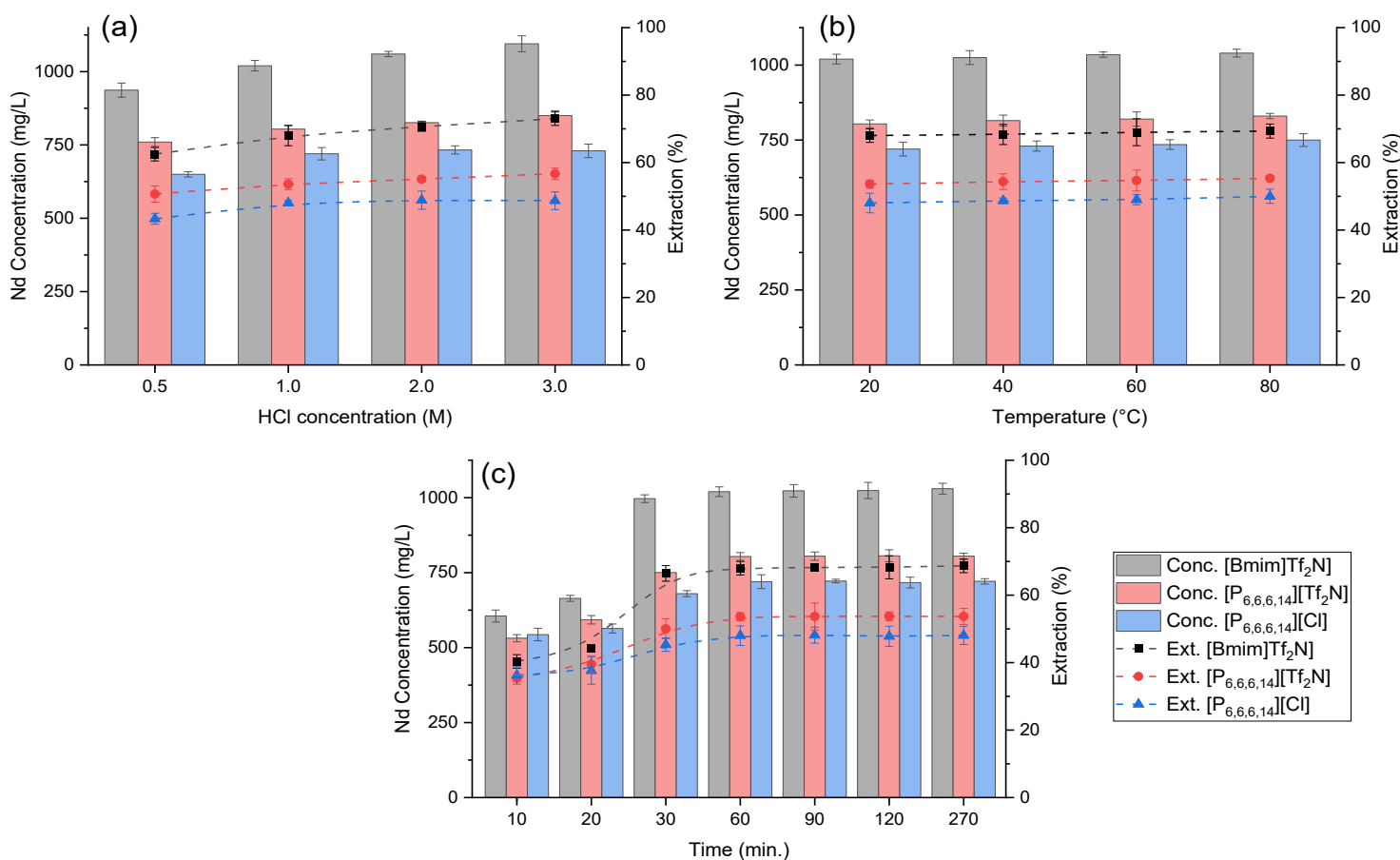


Figure 7.24: Effect of the ILs ([Bmim][Tf₂N], [P_{6,6,6,14}][Tf₂N] and [P_{6,6,6,14}][Cl]) in the extraction of Nd in hydrochloric solution in function of (a) HCl concentration, (b) temperature, and (c) time.

As praseodymium is the second most abundant REE in speakers and third most abundant in cameras, the extraction selectivity of the ILs for Pr is also of the great interest. Figure 7.25 illustrates the selectivity of [Bmim][Tf₂N], [P_{6,6,6,14}][Tf₂N] and [P_{6,6,6,14}][Cl] in a binary Nd-Pr mixture with different Nd:Pr mass ratios. The general trend observed is like that obtained with [Hbet][Tf₂N] (Figure 7.15), showing a clear tendency of higher selectivity towards neodymium by the three ILs. This higher selectivity towards Nd was specifically seen in the 1:1 mass ratio as the concentration of Nd present was substantially higher than Pr, particularly with [P_{6,6,6,14}][Tf₂N]. In the Nd:Pr=1:2, [P_{6,6,6,14}][Tf₂N] and [P_{6,6,6,14}][Cl] extracted nearly the same amount of Nd and Pr, even when the concentration of Pr was two times higher than the Nd concentration in solution, whereas the Nd extraction by [Bmim][Tf₂N] was nearly two-thirds of the Pr extraction. In all the cases, [Bmim][Tf₂N] performed as the best IL, extracting the highest amount of Nd and Pr, followed in order by [P_{6,6,6,14}][Tf₂N] and finally [P_{6,6,6,14}][Cl].

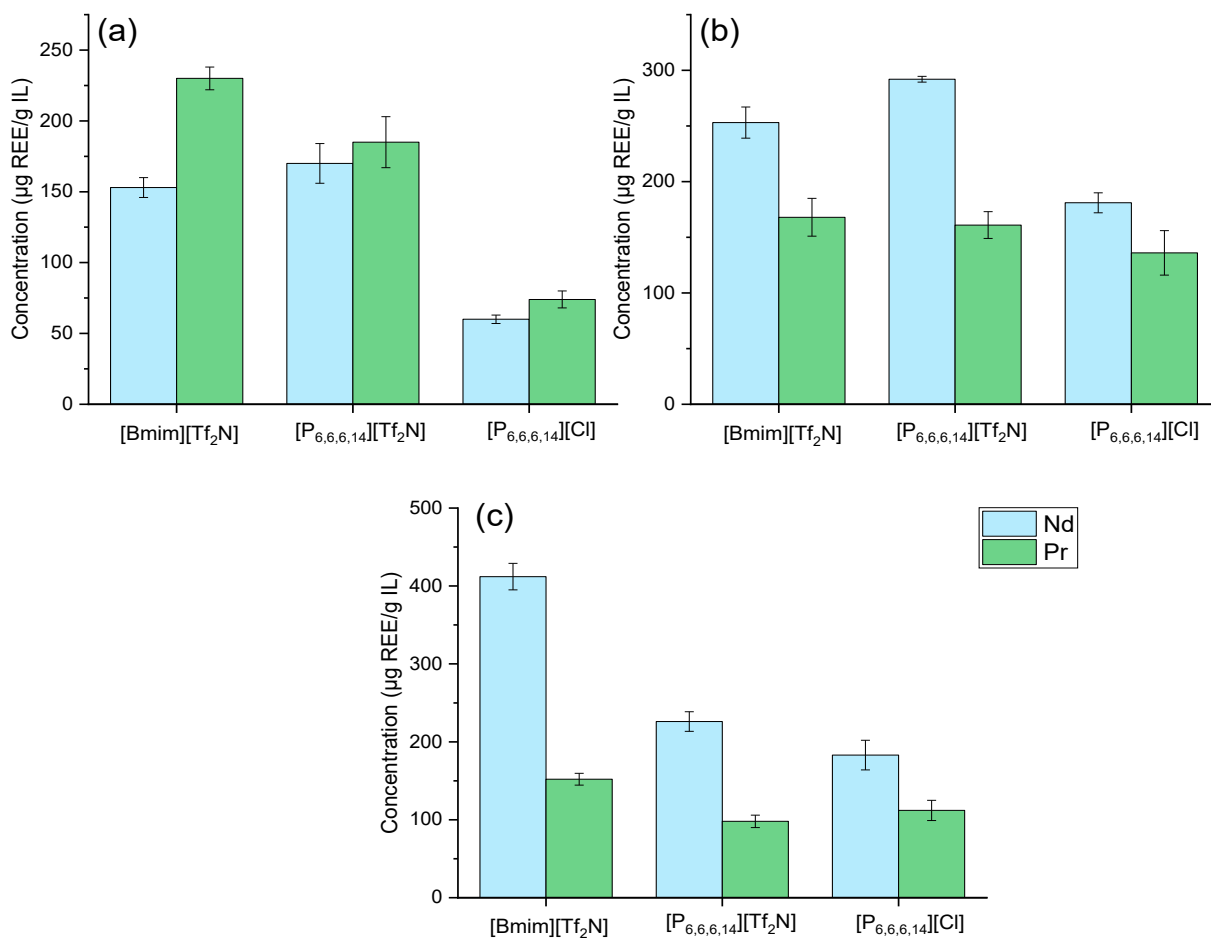


Figure 7.25: Effect of the Nd:Pr ratio on the leaching by [Bmim][Tf₂N], [P_{6,6,6,14}][Tf₂N] and [P_{6,6,6,14}][Cl] with ratios of; (a) Nd:Pr=1:2, (b) Nd:Pr=1:1, and (c) Nd:Pr=2:1.

7.3.5.2 Stripping and Recovery of Selected IL for Recycle

Of three ILs studied for extraction, [Bmim][Tf₂N] is confirmed as the best extractant for REEs. Consequently, it was therefore selected for further studies of stripping and recovery of the IL for recycle and reuse. The stripping was carried out by a 1 M HCl solution with an organic to aqueous ratio of 1:1, at room temperature (20±2 °C), 250 rpm, and 30 minutes. It is worth noting that a 0.5 M HCl solution was observed to strip approximately 85% of the REEs, suggesting that a higher acidity was needed to strip REEs from the loaded IL. In this study, earlier experiments showed that the stripping efficiency improved as the acidity increased, and complete stripping was achieved at 1 M HCl. The extraction and stripping efficiencies as well as the reusability of [Bmim][Tf₂N] was studied by comparing the saturation concentration of Nd³⁺ over five cycles of extraction and stripping, as shown in Figure 7.26. The neodymium extraction was approximately 80-85%; however, it is not an indication of low extraction efficiency, it was because the solution was highly concentrated with neodymium,

reaching the saturation of the IL. Nevertheless, the relevant information of Figure 7.26 is that the IL was only marginally affected over five consecutive cycles, suggesting that [Bmim][Tf₂N] can be successfully reused without any major loss in its extraction efficiency. Furthermore, the stripping was complete in all the cases ($\geq 99\%$), indicating that no residual neodymium is left in the IL. The overall efficiency, presented a downward trend throughout the cycles, decreasing from 97% in the first cycle to 91% in the fifth cycle. It is noteworthy to mention that the overall efficiency is the result of the ponderation between the extraction efficiency and the stripping efficiency, consequently, it is expected that as the extraction efficiency was lower than 90%, the overall efficiency cannot be higher than 90%. Nevertheless, the overall efficiency was calculated as the ponderation of the variation percentage of the extraction efficiency (<5) multiplied by the stripping efficiency. Thus, although the extraction was on average approximately 83%, as it was relatively constant through the cycles (slight percentage change), suggesting that the extraction capacity did not change substantially.

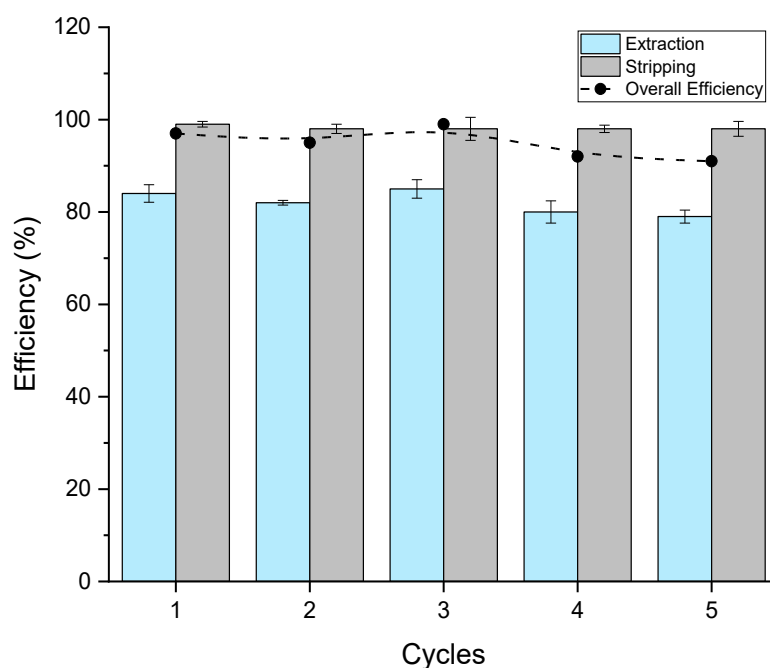


Figure 7.26: Neodymium (Nd^{+3}) extraction, stripping, and [Bmim][Tf₂N] reusability over five cycles.

To corroborate that [Bmim][Tf₂N] was not affected through the reuse process, FTIR was utilised to record any changes in the structure of the organic extractant over the five cycles, as shown in Figure 7.27. The FTIR spectrum shows the characteristic peaks of [Bmim] at 1750 cm⁻¹, 1480 cm⁻¹ and 1185 cm⁻¹, representing the C=C, -CH₃, and -N groups, respectively. In addition, the characteristic peaks of [Tf₂N] are found at 1350 cm⁻¹ and 1140 cm⁻¹, associated with =O (SO₂) and C-F (CF₃) stretch bonds, respectively. The FTIRs after leaching and stripping over 5 cycles did not show any noticeable difference, suggesting that [Bmim][Tf₂N] can be reused successfully at least five times without changes in their structure and loss in its leaching efficiency.

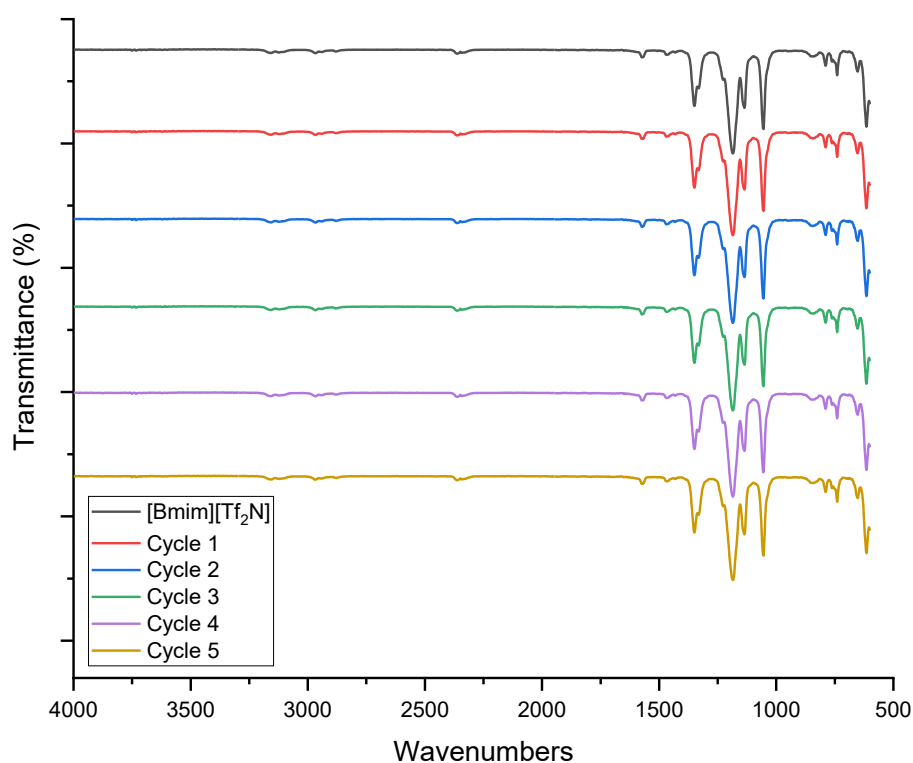


Figure 7.27: FTIR spectra of [Bmim][Tf₂N] over five cycles.

7.3.5.3 Proposed hydrometallurgical process for REEs recovery from EoL speakers;
Alternative Method

An alternative method that involves the leaching, extraction and stripping of REEs directly without the need for a pre-treatment step is proposed in Figure 7.28. It is important to note this proposed process was carried out using a Model Test System only with promising results. A great advantage of this process is the non-need of a pre-treatment, which can reduce considerable the energy consumption. The demagnetisation step maybe be needed for the handling of the real sample.

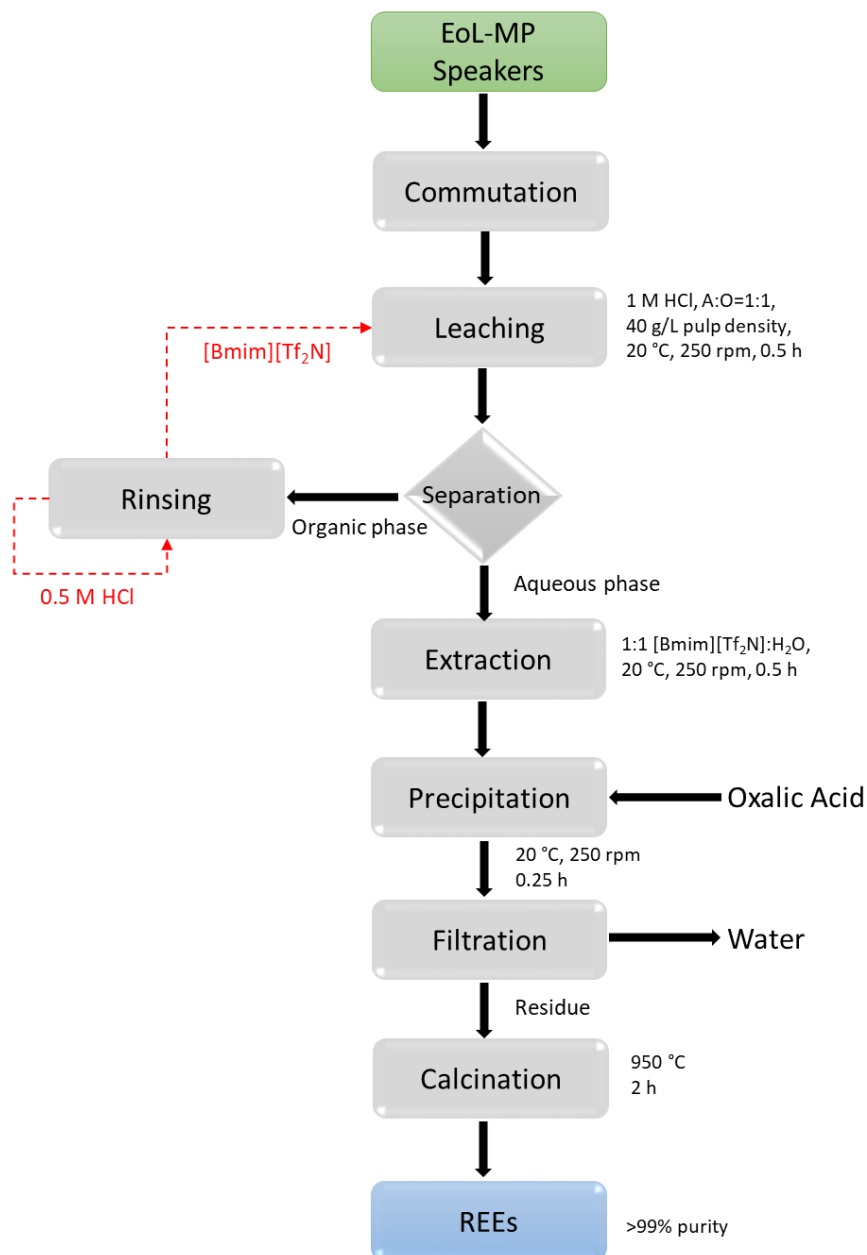


Figure 7.28: A proposed flow chart for the recovery of rare-earth elements from EoL mobile phone speakers using the Alternative method.

7.3.5.4 Discussion

This liquid-liquid extraction method was studied as an alternative to the more energy intensive hydrometallurgical method developed and optimised using the [Hbet][Tf₂N]-H₂O IL system. Although the extraction method was used only with Model Test System based on a synthetic solution, it has potential to be applied to the recovery of REEs from speakers. Although a preliminary trial on as-received samples was attempted it was not possible to validate the findings sufficient to report here. Riaño and Binnemans reported an extraction and separation process for neodymium and dysprosium from used NdFeB magnets by [P_{6,6,6,14}][NO₃] [277]. They also studied the leaching of magnets using nitric acid applying two different methods: direct leaching of magnets and leaching of roasted magnets. They found that leaching of roasted magnets was more efficient, leaching up to four times more than by direct leaching of the magnets. Furthermore, it allowed the production of iron-free leachates rich in REEs that can be directly employed in a solvent extraction process. The leaching process, however, could last for periods from 72 h up to 6 weeks. Kurami et al. reported that REEs can be leached completely by 0.5 M HCl at 95 °C, 100 g/L pulp density, 500 rpm for 5 h from spent wind turbine magnet blocks [286]. They also used roasting magnets as it facilitates the leaching process. Other studies have also reported high leaching efficiencies of NdFeB magnets after roasting compared to untreated magnets [274, 287]. Thus, roasting might be difficult to avoid for efficient recovery of REEs. Nevertheless, even using roasting as a pre-treatment for magnets recycling, it has still lower environmental impact than REEs mining [277].

7.4 Summary

In this study, an investigation of REEs recovery, especially neodymium and praseodymium, has been presented by the utilisation of the [Hbet][Tf₂N]-H₂O system and applied for the first time to the recovery of Nd and Pr from EoL mobile phone speakers. The special thermomorphic property of the [Hbet][Tf₂N]-H₂O system which causes the mixture to be homogeneous during leaching (temperature above the cloud point temperature) and biphasic when cooling back down to room temperature was exploited for the development of a novel method to recover REEs. The solubility of REOs was studied first, finding that [Hbet][Tf₂N]-H₂O system can leach/extract efficiently light REOs at 57 °C, 250 rpm, and 15 min, reaching an equilibrium of 0.161 g REO/g [Hbet][Tf₂N]-H₂O for La₂O₃, Pr₂O₃, Nd₂O₃, Eu₂O₃, and Gd₂O₃. The leaching/extraction method employs the interaction of 6 molecules of [Hbet][Tf₂N] per molecule of REO. Other REOs such as Y₂O₃, CeO₂, Tb₄O₇, and Yb₂O₃ showed a low to negligible solubility. This property has the potential to be used in the separation of light REOs from heavy REOs.

The determination of optimal leaching/extraction parameters was studied in simulated systems. Parameters that affect the leaching capability of the [Hbet][Tf₂N]-H₂O system such as time, water content, temperature, in a binary mixture (Nd₂O₃-Pr₂O₃), and ternary system (Nd₂O₃-Pr₂O₃-Fe₂O₃) were investigated. It was found that the IL has a strong selectivity for neodymium oxide over other metal oxides, with iron oxide remaining largely unreacted, which is beneficial for the separation of these metals. The optimal leaching/extraction parameters were 60 °C, 250 rpm, and 30 min. The kinetics studies indicated that the REOs leaching process by [Hbet][Tf₂N]-H₂O is governed by diffusion.

In the recovery of REEs from speakers, pre-treatment involves demagnetisation and roasting as necessary steps and crucial for the handling and conversion of REEs into REOs to permit their full recovery. The formation of a biphasic system after leaching induces metal separation, where REEs go predominantly into the aqueous phase. The addition of 1 M NaNO₃ not only benefits the separation of the rare-earth metals into the aqueous phase, but also act as a *salting-out* reagent, decreasing the IL loss in the aqueous phase. The REEs in the leached solution (aqueous phase) are precipitated with oxalic acid and the REE oxalate is further calcined at 950 °C for 2 h, to obtain the REOs as final product. The organic phase ([Hbet][Tf₂N]) is washed with a 0.1 M betaine in 0.5 M HCl solution, being regenerated for further processes. The [Hbet][Tf₂N] is capable being recycled in the process up to five consecutive times, showing no evidence of losing extraction efficiency. Thus, a closed-loop recycling process is developed, offering high selectivity for REEs, utilising mild conditions, permitting the reuse of the IL, and generating little waste. This promising green process can also be used for other similar e-waste such as NdFeB magnets, wind turbine magnets, among others. Considering that REEs are critical materials in high demand, recycling REEs from e-waste, particularly from NdFeB magnets (as

they are highly concentrated), could help to close the gap between their supply and demand, and the proposed process for rare-earth recycling provides a sustainable and efficient approach. Although further work is needed, the prospects of implementing the IL system using [Hbet][Tf₂N] on an industrial scale as a low-energy, sustainable and cost-effective process for REEs recovery is positive.

An alternative extraction process not yet tested fully on as-received real samples, was developed for the extraction of REEs from hydrochloric acid medium using three different ILs as extractants [Bmim][Tf₂N], [P_{6,6,6,14}][Tf₂N] and [P_{6,6,6,14}][Cl]. It was found that of the three ILs, [Bmim][Tf₂N] performed best under all conditions studied, and the optimised extraction conditions of 1 M HCl, 20 °C and 1 h were established. Stripping can be achieved by contacting the IL with 1 M HCl, and the recovery of REEs can be completed by precipitation using oxalic acid in the stripped solution to finally obtain REOs by calcination. Again, the IL [Bmim][Tf₂N] was shown to be able to be recycled at least five times without losing its extraction properties. Although the recovery of REEs from speakers was not tested using this method it offers promise as an efficient, cost-effective, and environmentally friendly process that does not require pre-treatment; one which is less energy intensive and conserves the use of reagents.

8 Conclusions and Recommendations

8.1 Conclusions

8.1.1 Motivation for the Research

WEEE is one of the fastest growing solid waste streams worldwide and presents serious health and environmental issues if not treated properly. Globally, approximately 17% of the WEEE is formally treated and the majority is discarded into landfill or exported to low-income countries, leading to serious impacts on human health and the environment as well as extensive loss of strategic metals. The dramatic increase in the consumption of raw materials over recent decades to meet consumer demand has led to an imbalance in the supply and demand and a potential threat to continued supply of critical metals. WEEE is a resource-rich source with many of the metals embedded in its composition listed as critical by the European Commission. To protect the environment and human health, reduce the scarcity and vulnerability of natural resources, conserve energy and reduce carbon footprint, the development of processes that extract these critical metals from WEEE is becoming an imperative.

8.1.2 Research Outcomes

The aim of this research is to develop methods to extract key value strategic materials from Waste Electrical and Electronic Equipment (WEEE) using End-of-Life mobile phones as a case study example, for conversion to products of commercial value and to minimise the environmental impact of waste through the safe reuse of resources contained in WEEE. To achieve this the following key specific objectives were set:

- Conduct a comprehensive characterisation of EoL mobile phone components to determine the metal and non-metal fractions.
- Identify task-specific ionic liquids as potential extractants that can selectively solubilise target metals.
- Develop optimised methods for recovery of target metals present in the key components of EoL mobile phones using Model Test Systems.
- Develop, where appropriate, optimised pre-treatment methods to facilitate ionic liquid extraction of the target metal from real samples.
- Apply the optimised processes to sample pre-treatment and recovery of target metals from real samples of as-received e-waste, as pure materials, and fractions of commercial value.

- Demonstrate the successful reuse of ionic liquids and reagents through multiple cycles to conserve reagent use and minimise energy consumption.

The research outcomes include the development of novel, efficient and integrated recycling processes using ionic liquids as extractant reagents to recover metal value from as-received EoL mobile phones: copper from PCBs, gold from PCBs, ICs and CPUs, indium from LCD screens, and REEs from speakers.

The key conclusions from this research are:

- Full characterisation of the metallic and non-metallic fractions within a mobile phone confirms the presence of up to 71 elements of the periodic table.
- Most of the elements in EoL mobile phones are found in higher concentrations than in their natural ores, confirming WEEE as a significant potential secondary resource for strategic and critical metals.
- [Bmim]BF₄ is the task specific IL for pre-treatment of as-received EoL-MP PCBs.
- [Bmim]HSO₄ is the task specific IL for selective extraction of **copper** from this waste stream, while Cyphos 101([P_{6,6,6,14}][Cl]) alone, and separately impregnated in Amberlite™ XAD-7 resins, is the task-specific IL for selective extraction of **gold** from this waste stream and from pre-treated as-received EoL Computer, ICs, and CPUs.
- Cyphos 101 ([P_{6,6,6,14}][Cl]) and Aliquat 336 are the task-specific ILs for selective extraction of **indium** from pre-treated EoL MP LCD screens.
- [Hbet][Tf₂N]-H₂O is the task specific IL system for selective extraction of **REOs** from pre-treated EoL-MP speakers.
- [Bmim][Tf₂N] is the task specific IL for selective extraction of **REEs**, without pre-treatment.
- Development and use of model test systems ahead of trialling on real waste streams allowed the refinement of process parameters for optimal recovery.
- Strategic and critical metals (with purities of 98-99%) are recovered from as-received EoL-MP components using ionic liquids for conversion to products of commercial value.
- Ionic liquids used as extractants can be recycled multiple times without impacting their integrity as extractants and their extraction efficiency.
- The proposed recovery processes can be applied to other sources of e-waste.

In summary the contribution to knowledge of this research lies in the recovery of strategic and critical metals from multigenerational mobile phones using novel extraction processes using ionic liquids developed in this work that minimise reagent use and energy consumption. The research therefore demonstrates the potential to unlock value from this e-waste stream that can be exploited in other WEEE streams, as a step towards balancing the criticality of supply and demand of metals that are under threat.

8.2 Recommendations for Future Work

The work in this thesis shows that ionic liquids can be effectively used in the extraction and recovery of metals from WEEE as a secondary source. For each proposed hydrometallurgical process, further optimisations and recommendations are suggested:

- Given the successful recovery of copper reported in Chapter 4 from EoL-MP PCBs using a combination of extraction and electrolysis, a larger electrowinning cell should be designed, and the optimal conditions of reagent use refined.
- In chapter 5, the focus was on the recovery of gold however, in a two-stage leaching process, the final solution was rich in palladium and as a critical metal a method should be developed for its recovery. The stripping of copper to permit access to the gold was achieved with one nitric acid leach but the addition of a second leach may be beneficial and worth exploring. In terms of scaling up the process, consideration should be given to the use of an alternative medium to *aqua regia* because of its corrosive properties and control of toxic fumes that can be released.
- The successful recovery of indium reported in Chapter 6, suggests that this process should be trialled on a larger scale. Detailed characterisation of different LCD panels as a source of indium would be useful to optimise recovery from mixed streams of LCD panels. Based on literature review, LCD panels from TVs, handsets, mobile phones, etc. are similar in components and composition, showing a real potential for indium recovery. Therefore, it is highly recommended to apply the indium recovery process on larger scale with LCD TVs, as TVs are the main EoL of indium. Furthermore, the benefits of recovering the glass substrate and separately the liquid crystal, for commercial value is worth investigating.
- The successful recovery of REEs (neodymium and praseodymium) from EoL-MP speakers in the form of REOs reported in Chapter 7 requires the process to be scaled up, and the process conditions optimised at that level. The second method involving liquid-liquid extraction using

[Bmim][Tf₂N] successfully recovered REOs but has not been applied to recovery from real samples. A next step would be to trial on real samples as results suggest this it is likely not to need a pre-treatment step.

- Consideration should be given to the value of the metal recovered and the potential for conversion to products of greater commercial value.
- Whilst preliminary techno-economic assessments have been carried out during the period of the research that show promise for each of the developed processes, full and detailed techno-economic assessments should be performed to confirm the viability of the processes developed in the context of the value of the strategic and critical metals recovered.
- Consideration should be given to dynamic substance flow analysis for each of the metals recovered (copper, gold, indium, and REEs), to identify potential paths and mechanisms to decrease losses and to identify the key EoL products for metal recovering.

References

1. Kuehr, R., *1 - Global e-waste initiatives*, in *Waste Electrical and Electronic Equipment (WEEE) Handbook*. 2012, Woodhead Publishing. p. 3-16.
2. Islam, M.T., Abdullah, A.B., Shahir, S.A., Kalam, M.A., Masjuki, H.H., Shumon, R., and Rashid, M.H., *A public survey on knowledge, awareness, attitude and willingness to pay for WEEE management: Case study in Bangladesh*. *Journal of Cleaner Production*, 2016. **137**: p. 728-740.
3. Huisman, J., *6 - Eco-efficiency evaluation of WEEE take-back systems*, in *Waste Electrical and Electronic Equipment (WEEE) Handbook*. 2012, Woodhead Publishing. p. 93-119.
4. Charles, R.G., Douglas, P., Hallin, I.L., Matthews, I., and Liversage, G., *An investigation of trends in precious metal and copper content of RAM modules in WEEE: Implications for long term recycling potential*. *Waste Management*.
5. Forti, V., Balde, C.P., Kuehr, R., and Bel, G., *The Global E-waste Monitor 2020: Quantities, flows and the circular economy potential*. 2020: Bonn, Geneva and Rotterdam. p. 120.
6. Tsydenova, O. and Bengtsson, M., *Chemical hazards associated with treatment of waste electrical and electronic equipment*. *Waste Management*, 2011. **31**(1): p. 45-58.
7. Charles, R.G., Douglas, P., Hallin, I.L., Matthews, I., and Liversage, G., *An investigation of trends in precious metal and copper content of RAM modules in WEEE: Implications for long term recycling potential*. *Waste Management*, 2017. **60**(Supplement C): p. 505-520.
8. Tansel, B., *From electronic consumer products to e-wastes: Global outlook, waste quantities, recycling challenges*. *Environment International*, 2017. **98**(Supplement C): p. 35-45.
9. Needhidasan, S., Samuel, M., and Chidambaram, R., *Electronic waste - an emerging threat to the environment of urban India*. *Journal of environmental health science & engineering*, 2014. **12**(1): p. 36-36.
10. Perkins, D.N., Brune Drisse, M.-N., Nxele, T., and Sly, P.D., *E-Waste: A Global Hazard*. *Annals of Global Health*, 2014. **80**(4): p. 286-295.
11. Maes, T. and Preston-Whyte, F., *E-waste it wisely: lessons from Africa*. *SN Applied Sciences*, 2022. **4**(3): p. 72.
12. Kaya, M., *Recovery of metals and nonmetals from electronic waste by physical and chemical recycling processes*. *Waste Management*, 2016. **57**(Supplement C): p. 64-90.
13. Işıldar, A., Rene, E.R., van Hullebusch, E.D., and Lens, P.N.L., *Electronic waste as a secondary source of critical metals: Management and recovery technologies*. *Resources, Conservation and Recycling*, 2017. **135**: p. 296-312.
14. Powell-Turner, J., Antill, P.D., and Fisher, R.E., *The United Kingdom Ministry of Defence and the European Union's electrical and electronic equipment directives*. *Resources Policy*, 2016. **49**(Supplement C): p. 422-432.
15. *Directive 2012/19/EU*, in *Official Journal of the European Union*. 2012.
16. Europejska, K., *Study on the review of the list of critical raw materials*. 2017. p. 93.
17. Gian Andrea Blengini, C.E.L., Umberto Eynard, Cristina Torres de Matos, Dominic Wittmer, Konstantinos Georgitzikis, Claudiu Pavel, Samuel Carrara, Lucia Mancini, Manuela Unguru, Darina Blagoeva, Fabrice Mathieux, David Pennington. , *Study on the EU's list of Critical Raw Materials (2020)*. 2020, European Commission
18. Caballero, B.M., de Marco, I., Adrados, A., López-Urionabarrenechea, A., Solar, J., and Gastelu, N., *Possibilities and limits of pyrolysis for recycling plastic rich waste streams rejected from phones recycling plants*. *Waste Management*, 2016. **57**: p. 226-234.
19. Tuncuk, A., Stazi, V., Akcil, A., Yazici, E.Y., and Devenci, H., *Aqueous metal recovery techniques from e-scrap: Hydrometallurgy in recycling*. *Minerals Engineering*, 2012. **25**(1): p. 28-37.
20. Cayumil, R., Khanna, R., Rajarao, R., Mukherjee, P.S., and Sahajwalla, V., *Concentration of precious metals during their recovery from electronic waste*. *Waste Management*, 2016. **57**(Supplement C): p. 121-130.

21. Diaz, L.A., Lister, T.E., Parkman, J.A., and Clark, G.G., *Comprehensive process for the recovery of value and critical materials from electronic waste*. Journal of Cleaner Production, 2016. **125**: p. 236-244.
22. Vats, M.C. and Singh, S.K., *Assessment of gold and silver in assorted mobile phone printed circuit boards (PCBs): Original article*. Waste Management, 2015. **45**: p. 280-288.
23. Petter, P.M.H., Veit, H.M., and Bernardes, A.M., *Evaluation of gold and silver leaching from printed circuit board of cellphones*. Waste Management, 2014. **34**(2): p. 475-482.
24. Grimes, S., Donaldson, J., and Cebrian, G., *Report on the Environmental Benefits of Recycling*. 2008, Bureau International du Recyclage: Brussels. p. 51pp.
25. Grimes, S., Donaldson, J., and Grimes, J., *Environmental Benefits of Recycling – 2016 edition*. 2016, Bureau International du Recyclage Brussels. p. 56pp.
26. Zhang, S., Ding, Y., Liu, B., and Chang, C.-c., *Supply and demand of some critical metals and present status of their recycling in WEEE*. Waste Management, 2017. **65**: p. 113-127.
27. Binnemans, K., Jones, P.T., Blanpain, B., Van Gerven, T., Yang, Y., Walton, A., and Buchert, M., *Recycling of rare earths: a critical review*. Journal of Cleaner Production, 2013. **51**: p. 1-22.
28. Vaccari, M., Zambetti, F., Bates, M., Tudor, T., and Ambaye, T., *Application of an Integrated Assessment Scheme for Sustainable Waste Management of Electrical and Electronic Equipment: The Case of Ghana*. Sustainability, 2020. **12**(8).
29. Parajuly, K., Habib, K., and Liu, G., *Waste electrical and electronic equipment (WEEE) in Denmark: Flows, quantities and management*. Resources, Conservation and Recycling, 2017. **123**(Supplement C): p. 85-92.
30. Union, E., *Directive 2002/96/EC of the European Parliament and of the Council*. 2003.
31. Union, E., *Directive 2012/19/EU of the European Parliament and of the Council*. 2012.
32. Shittu, O.S., Williams, I.D., and Shaw, P.J., *Global E-waste management: Can WEEE make a difference? A review of e-waste trends, legislation, contemporary issues and future challenges*. Waste Management, 2021. **120**: p. 549-563.
33. Baldé, C.P., Wang, F., Kuehr, R., Huisman, J., *The global e-waste monitor – 2014, United Nations. University, IAS – SCYCLE, Bonn, Germany*. 2015.
34. Menikpura, S.N.M., Santo, A., and Hotta, Y., *Assessing the climate co-benefits from Waste Electrical and Electronic Equipment (WEEE) recycling in Japan*. Journal of Cleaner Production, 2014. **74**(Supplement C): p. 183-190.
35. Robinson, B.H., *E-waste: An assessment of global production and environmental impacts*. Science of The Total Environment, 2009. **408**(2): p. 183-191.
36. (UNEP), B.c. *Basel convention mobile phone partnership initiative*. 2012 [cited 2018 15/03].
37. Sarath, P., Bonda, S., Mohanty, S., and Nayak, S.K., *Mobile phone waste management and recycling: Views and trends*. Waste Management, 2015. **46**: p. 536-545.
38. Tan, Q., Dong, Q., Liu, L., Song, Q., Liang, Y., and Li, J., *Potential recycling availability and capacity assessment on typical metals in waste mobile phones: A current research study in China*. Journal of Cleaner Production, 2017. **148**: p. 509-517.
39. Statista. *Mobile Phones*. 2018 [cited 2018 15/03]; Available from: <https://www.statista.com/>.
40. Diouf, B., Poda, R., and Osei, R., *Recycling mobile phone batteries for lighting*. Renewable Energy, 2015. **78**: p. 509-515.
41. Velmurugan, M.S., *Sustainable perspectives on energy consumption, EMRF, environment, health and accident risks associated with the use of mobile phones*. Renewable and Sustainable Energy Reviews, 2017. **67**: p. 192-206.
42. GSMA. *Environmental Impact of Mobile Communications Devices*. 2009 [cited 2018 13/03]; Available from: <https://www.gsma.com/publicpolicy/wp-content/uploads/2012/03/envirobmobiledevices.pdf>.
43. Berners-Lee, M., *How Bad Are Bananas? The carbon footprint of everything*. 2010: Profile Books.

44. Yu, J., Williams, E., and Ju, M., *Analysis of material and energy consumption of mobile phones in China*. Energy Policy, 2010. **38**(8): p. 4135-4141.
45. Dimitrakakis, E., Janz, A., Bilitewski, B., and Gidaracos, E., *Small WEEE: Determining recyclables and hazardous substances in plastics*. Journal of Hazardous Materials, 2009. **161**(2): p. 913-919.
46. Fontana, D., Pietrantonio, M., Pucciarmati, S., Rao, C., and Forte, F., *A comprehensive characterization of End-of-Life mobile phones for secondary material resources identification*. Waste Management, 2019. **99**: p. 22-30.
47. Kasper, A.C., Berselli, G.B.T., Freitas, B.D., Tenório, J.A.S., Bernardes, A.M., and Veit, H.M., *Printed wiring boards for mobile phones: Characterization and recycling of copper*. Waste Management, 2011. **31**(12): p. 2536-2545.
48. Hall, W.J. and Williams, P.T., *Separation and recovery of materials from scrap printed circuit boards*. Resources, Conservation and Recycling, 2008. **51**(3): p. 691-709.
49. Jun Park, Y. and Fray, D., *Recovery of High Purity Precious Metals from Printed Circuit Boards*. Journal of Hazardous Materials, 2009. **164**(2-3): p. 1152-1158.
50. Kumari, A., Jha, M.K., and Singh, R.P., *Recovery of metals from pyrolysed PCBs by hydrometallurgical techniques*. Hydrometallurgy, 2016. **165**: p. 97-105.
51. Hanafi, J., Jobiliong, E., Christiani, A., Soenarta, D.C., Kurniawan, J., and Irawan, J., *Material Recovery and Characterization of PCB from Electronic Waste*. Procedia - Social and Behavioral Sciences, 2012. **57**: p. 331-338.
52. Sepúlveda, A., Schluep, M., Renaud, F.G., Streicher, M., Kuehr, R., Hagelüken, C., and Gerecke, A.C., *A review of the environmental fate and effects of hazardous substances released from electrical and electronic equipments during recycling: Examples from China and India*. Environmental Impact Assessment Review, 2010. **30**(1): p. 28-41.
53. Foundation, T.E.M. *Towards a Circular Economy - Economic and Business Rationale for an Accelerated Transition*. 2021 [cited 2021 15/08]; Available from: <https://ellenmacarthurfoundation.org/>.
54. Micheline, G., Moraes, R.N., Cunha, R.N., Costa, J.M.H., and Ometto, A.R., *From Linear to Circular Economy: PSS Conducting the Transition*. Procedia CIRP, 2017. **64**(Supplement C): p. 2-6.
55. Gaustad, G., Krystofik, M., Bustamante, M., and Badami, K., *Circular economy strategies for mitigating critical material supply issues*. Resources, Conservation and Recycling, 2017.
56. de Jesus, A., Antunes, P., Santos, R., and Mendonça, S., *Eco-innovation in the transition to a circular economy: An analytical literature review*. Journal of Cleaner Production, 2017.
57. D.H. Meadows, D.L.M., J. Randers, W.W. Behrens, *The Limits to Growth*. 1972, New York: Chelsea Green Publishing Company.
58. Hey, C., *EU Environmental Policies: A short history of the policy strategies*. EU Environmental Policy Handbook: A Critical Analysis of EU Environmental Legislation. 2006, European Environmental Bureau, Brussels.
59. Kalmykova, Y., Sadagopan, M., and Rosado, L., *Circular economy – From review of theories and practices to development of implementation tools*. Resources, Conservation and Recycling, 2017. **135**: p. 190-201.
60. Sustainability, M., *Europe's circular-economy opportunity*. 2015.
61. Tukker, A., *Product services for a resource-efficient and circular economy – a review*. Journal of Cleaner Production, 2015. **97**(Supplement C): p. 76-91.
62. Government, U., *Circular Economy Package policy statement*, F.a.R.A.D. A statement issued jointly by the Department for Environment, the Department of Agriculture, Environment and Rural Affairs (DAERA), the Welsh Government and the Scottish Government., Editor. 2020.
63. Government, U., *Environment Act 2021*. 2021, The Stationery Office.

64. Sverdrup, H.U., Ragnarsdottir, K.V., and Koca, D., *An assessment of metal supply sustainability as an input to policy: security of supply extraction rates, stocks-in-use, recycling, and risk of scarcity*. Journal of Cleaner Production, 2017. **140**(Part 1): p. 359-372.
65. Blengini, G.A., Nuss, P., Dewulf, J., Nita, V., Peirò, L.T., Vidal-Legaz, B., Latunussa, C., Mancini, L., Blagoeva, D., Pennington, D., Pellegrini, M., Van Maercke, A., Solar, S., Grohol, M., and Ciupagea, C., *EU methodology for critical raw materials assessment: Policy needs and proposed solutions for incremental improvements*. Resources Policy, 2017. **53**: p. 12-19.
66. Stewart, R., *2 - EU legislation relating to electronic waste: the WEEE and RoHS Directives and the REACH regulations*, in *Waste Electrical and Electronic Equipment (WEEE) Handbook*. 2012, Woodhead Publishing. p. 17-52.
67. Council, T.E.P.a.t., *EPA5 Environmental Action Programme*. Official Journal of the European Union, 1993.
68. Council, T.E.P.a.t., *EPA7 Environment Action Programme* Official Journal of the European Union, 2013.
69. UK, G.o.t. *Legal definition of waste guidance*. 2012; Available from: <https://www.gov.uk/government/publications/legal-definition-of-waste-guidance>.
70. Council, T.E.P.a.t., *Directive 91/156/EEC*. Official Journal of the European Union, 1991.
71. Council, T.E.P.a.t., *Waste Framework Directive 2008/98/EC*. Official Journal of the European Union, 2008.
72. OECD. *Extended producer responsibility*. Available from: <http://www.oecd.org/env/tools-evaluation/extendedproducerresponsibility.htm>.
73. *Directive 2002/96/EC*, in *Official Journal of the European Union*. 2002.
74. Magalini, F. and Huisman, J. *Management of WEEE & Cost Models across the EU Could the EPR principle lead US to a better Environmental Policy?* in *Proceedings of the 2007 IEEE International Symposium on Electronics and the Environment*. 2007.
75. *Directive 2002/95/EC*, in *Official Journal of the European Union*. 2002.
76. Council, T.E.P.a.t., *Directive 2011/65/EU*. Official Journal of the European Union, 2011.
77. Council, T.E.P.a.t., *Directive (EU) 2015/863. Amending Annex II to Directive 2011/65/EU of the European Parliament and of the Council as regards the list of restricted substances*. Official Journal of the European Union, 2015.
78. Jin, Y., Kim, J., and Guillaume, B., *Review of critical material studies*. Resources, Conservation and Recycling, 2016. **113**: p. 77-87.
79. EASAC, *Priorities for critical materials for a circular economy*. 2016.
80. Matthias Bucher, D.S., Daniel Bleher, *Critical Metals for Future Sustainable Technologies and Their Recycling Potential*. United Nations Environment Programme & United Nations University, 2009.
81. Graedel, T.E., Harper, E.M., Nassar, N.T., Nuss, P., and Reck Barbara, K., *Criticality of metals and metalloids*. Proceedings of the National Academy of Sciences, 2015. **112**(14): p. 4257-4262.
82. European, C., Directorate-General for Internal Market, I.E., and Smes, *Study on the review of the list of critical raw materials : final report*. 2017: Publications Office.
83. Wang, L., Huang, X., Yu, Y., Zhao, L., Wang, C., Feng, Z., Cui, D., and Long, Z., *Towards cleaner production of rare earth elements from bastnaesite in China*. Journal of Cleaner Production, 2017. **165**: p. 231-242.
84. Fernandez, V., *Rare-earth elements market: A historical and financial perspective*. Resources Policy, 2017. **53**: p. 26-45.
85. Schaeffer, N., Grimes, S., and Cheeseman, C., *Use of extraction chromatography in the recycling of critical metals from thin film leach solutions*. Inorganica Chimica Acta, 2017. **457**: p. 53-58.
86. Yu, S. and Mitchell, T., *China merges 3 rare earths miners to strengthen dominance of sector*, in *Financial Times*. 2021.

87. Russell-Jones, L., *Western nations push back against China's rare earth dominance*, in *CITY A.M.* 2022.
88. Lahtela, V., Virolainen, S., Uwaoma, A., Kallioinen, M., Kärki, T., and Sainio, T., *Novel mechanical pre-treatment methods for effective indium recovery from end-of-life liquid-crystal display panels*. *Journal of Cleaner Production*, 2019. **230**: p. 580-591.
89. Qin, J., Ning, S., Fujita, T., Wei, Y., Zhang, S., and Lu, S., *Leaching of indium and tin from waste LCD by a time-efficient method assisted planetary high energy ball milling*. *Waste Management*, 2021. **120**: p. 193-201.
90. Pereira, E.B., Suliman, A.L., Tanabe, E.H., and Bertuol, D.A., *Recovery of indium from liquid crystal displays of discarded mobile phones using solvent extraction*. *Minerals Engineering*, 2018. **119**: p. 67-72.
91. Dutta, D., Panda, R., Kumari, A., Goel, S., and Jha, M.K., *Sustainable recycling process for metals recovery from used printed circuit boards (PCBs)*. *Sustainable Materials and Technologies*, 2018. **17**: p. e00066.
92. Yoo, J.-M., Jeong, J., Yoo, K., Lee, J.-c., and Kim, W., *Enrichment of the metallic components from waste printed circuit boards by a mechanical separation process using a stamp mill*. *Waste Management*, 2009. **29**(3): p. 1132-1137.
93. Cui, J. and Forssberg, E., *Mechanical recycling of waste electric and electronic equipment: a review*. *Journal of Hazardous Materials*, 2003. **99**(3): p. 243-263.
94. Jiang, P., Harney, M., Song, Y., Chen, B., Chen, Q., Chen, T., Lazarus, G., Dubois, L.H., and Korzenski, M.B., *Improving the End-of-Life for Electronic Materials via Sustainable Recycling Methods*. *Procedia Environmental Sciences*, 2012. **16**: p. 485-490.
95. Wu, J., Li, J., and Xu, Z., *Electrostatic Separation for Recovering Metals and Nonmetals from Waste Printed Circuit Board: Problems and Improvements*. *Environmental Science & Technology*, 2008. **42**(14): p. 5272-5276.
96. Ghosh, B., Ghosh, M.K., Parhi, P., Mukherjee, P.S., and Mishra, B.K., *Waste Printed Circuit Boards recycling: an extensive assessment of current status*. *Journal of Cleaner Production*, 2015. **94**: p. 5-19.
97. Tatarants, M., Yousef, S., Sidaraviciute, R., Denafas, G., and Bendikiene, R., *Characterization of waste printed circuit boards recycled using a dissolution approach and ultrasonic treatment at low temperatures*. *RSC Advances*, 2017. **7**(60): p. 37729-37738.
98. Zhou, Y. and Qiu, K., *A new technology for recycling materials from waste printed circuit boards*. *Journal of Hazardous Materials*, 2010. **175**(1): p. 823-828.
99. Ortuño, N., Moltó, J., Egea, S., Font, R., and Conesa, J.A., *Thermogravimetric study of the decomposition of printed circuit boards from mobile phones*. *Journal of Analytical and Applied Pyrolysis*, 2013. **103**: p. 189-200.
100. Shah, K., Gupta, K., and Sengupta, B., *Reclamation of copper from spent ammoniacal Printed Circuit Board (PCB) etch solutions*. *Journal of Environmental Chemical Engineering*, 2018. **6**(2): p. 2874-2880.
101. Zhu, N., Xiang, Y., Zhang, T., Wu, P., Dang, Z., Li, P., and Wu, J., *Bioleaching of metal concentrates of waste printed circuit boards by mixed culture of acidophilic bacteria*. *Journal of Hazardous Materials*, 2011. **192**(2): p. 614-619.
102. Li, K. and Xu, Z., *A review of current progress of supercritical fluid technologies for e-waste treatment*. *Journal of Cleaner Production*, 2019. **227**: p. 794-809.
103. Zhang, L. and Xu, Z., *A review of current progress of recycling technologies for metals from waste electrical and electronic equipment*. *Journal of Cleaner Production*, 2016. **127**: p. 19-36.
104. Chauhan, G., Jadhao, P.R., Pant, K.K., and Nigam, K.D.P., *Novel technologies and conventional processes for recovery of metals from waste electrical and electronic equipment: Challenges & opportunities – A review*. *Journal of Environmental Chemical Engineering*, 2018. **6**(1): p. 1288-1304.

105. Zhang, D.-j., Dong, L., Li, Y.-t., Wu, Y., Ma, Y.-x., and Yang, B., *Copper leaching from waste printed circuit boards using typical acidic ionic liquids recovery of e-wastes' surplus value*. Waste Management, 2018. **78**: p. 191-197.
106. Nockemann, P., Thijs, B., Parac-Vogt, T.N., Van Hecke, K., Van Meervelt, L., Tinant, B., Hartenbach, I., Schleid, T., Ngan, V.T., Nguyen, M.T., and Binnemans, K., *Carboxyl-Functionalized Task-Specific Ionic Liquids for Solubilizing Metal Oxides*. Inorganic Chemistry, 2008. **47**(21): p. 9987-9999.
107. Nockemann, P., Thijs, B., Pittois, S., Thoen, J., Glorieux, C., Van Hecke, K., Van Meervelt, L., Kirchner, B., and Binnemans, K., *Task-Specific Ionic Liquid for Solubilizing Metal Oxides*. The Journal of Physical Chemistry B, 2006. **110**(42): p. 20978-20992.
108. Greer, A.J., Jacquemin, J., and Hardacre, C., *Industrial Applications of Ionic Liquids*. Molecules, 2020. **25**(21).
109. Schaeffer, N., *RECOVERY OF VALUE FROM WASTE ELECTRICAL AND ELECTRONIC EQUIPMENT USING IONIC LIQUIDS*, in *Civil and Environmental Engineering*. 2017, Imperial College London.
110. Huang, Y., Duan, Z., Bai, N., Wang, H., Cao, Y., Song, X., Peng, W., and Zhu, X., *Highly selective dissolution and synchronous extraction of zinc from zinc-cobalt slag by an ionic liquid [Hbet][Tf2N]-H2O system: A novel method for separating zinc and cobalt*. Journal of Cleaner Production, 2021. **315**: p. 128301.
111. He, J., Yang, J., Tariq, S.M., Duan, C., and Zhao, Y., *Comparative investigation on copper leaching efficiency from waste mobile phones using various types of ionic liquids*. Journal of Cleaner Production, 2020. **256**: p. 120368.
112. Kim, B.-K., Lee, E.J., Kang, Y., and Lee, J.-J., *Application of ionic liquids for metal dissolution and extraction*. Journal of Industrial and Engineering Chemistry, 2018. **61**: p. 388-397.
113. Abbott, A.P., Frisch, G., Hartley, J., and Ryder, K.S., *Processing of metals and metal oxides using ionic liquids*. Green Chemistry, 2011. **13**(3): p. 471-481.
114. Nancarrow, P., Al-Othman, A., Mital, D.K., and Döpking, S., *Comprehensive analysis and correlation of ionic liquid conductivity data for energy applications*. Energy, 2021. **220**: p. 119761.
115. Cho, C.-W., Pham, T.P.T., Zhao, Y., Stolte, S., and Yun, Y.-S., *Review of the toxic effects of ionic liquids*. Science of The Total Environment, 2021. **786**: p. 147309.
116. Hartmann, D.O. and Pereira, C.S., *Chapter 13 - Toxicity of Ionic Liquids: Past, Present, and Future*, in *Ionic Liquids in Lipid Processing and Analysis*, X. Xu, Z. Guo, and L.-Z. Cheong, Editors. 2016, AOCS Press. p. 403-421.
117. Fukaya, Y. and Ohno, H., *Hydrophobic and polar ionic liquids*. Physical Chemistry Chemical Physics, 2013. **15**(11): p. 4066-4072.
118. Wandschneider, A., Lehmann, J.K., and Heintz, A., *Surface Tension and Density of Pure Ionic Liquids and Some Binary Mixtures with 1-Propanol and 1-Butanol*. Journal of Chemical & Engineering Data, 2008. **53**(2): p. 596-599.
119. Silvester, D.S. and Compton, R.G., *Electrochemistry in Room Temperature Ionic Liquids: A Review and Some Possible Applications*. Zeitschrift für Physikalische Chemie, 2006. **220**(10): p. 1247-1274.
120. Couling, D.J., Bernot, R.J., Docherty, K.M., Dixon, J.K., and Maginn, E.J., *Assessing the factors responsible for ionic liquid toxicity to aquatic organisms via quantitative structure-property relationship modeling*. Green Chemistry, 2006. **8**(1): p. 82-90.
121. Kagimoto, J., Taguchi, S., Fukumoto, K., and Ohno, H., *Hydrophobic and low-density amino acid ionic liquids*. Journal of Molecular Liquids, 2010. **153**(2): p. 133-138.
122. Singh, T. and Kumar, A., *Thermodynamics of dilute aqueous solutions of imidazolium based ionic liquids*. The Journal of Chemical Thermodynamics, 2011. **43**(6): p. 958-965.
123. Liu, W., Zhao, T., Zhang, Y., Wang, H., and Yu, M., *The Physical Properties of Aqueous Solutions of the Ionic Liquid [BMIM][BF4]*. Journal of Solution Chemistry, 2006. **35**(10): p. 1337-1346.

124. Earle, M.J., Esperança, J.M.S.S., Gilea, M.A., Canongia Lopes, J.N., Rebelo, L.P.N., Magee, J.W., Seddon, K.R., and Widgren, J.A., *The distillation and volatility of ionic liquids*. *Nature*, 2006. **439**(7078): p. 831-834.
125. Kosmulski, M., Gustafsson, J., and Rosenholm, J.B., *Thermal stability of low temperature ionic liquids revisited*. *Thermochimica Acta*, 2004. **412**(1): p. 47-53.
126. Köddermann, T., Paschek, D., and Ludwig, R., *Ionic Liquids: Dissecting the Enthalpies of Vaporization*. *ChemPhysChem*, 2008. **9**(4): p. 549-555.
127. Ngo, H.L., LeCompte, K., Hargens, L., and McEwen, A.B., *Thermal properties of imidazolium ionic liquids*. *Thermochimica Acta*, 2000. **357-358**: p. 97-102.
128. Fox, D.M., Awad, W.H., Gilman, J.W., Maupin, P.H., De Long, H.C., and Trulove, P.C., *Flammability, thermal stability, and phase change characteristics of several trialkylimidazolium salts*. *Green Chemistry*, 2003. **5**(6): p. 724-727.
129. Smiglak, M., Reichert, W.M., Holbrey, J.D., Wilkes, J.S., Sun, L., Thrasher, J.S., Kirichenko, K., Singh, S., Katritzky, A.R., and Rogers, R.D., *Combustible ionic liquids by design: is laboratory safety another ionic liquid myth?* *Chemical Communications*, 2006(24): p. 2554-2556.
130. Schaeffer, N., Passos, H., Billard, I., Papaiconomou, N., and Coutinho, J.A.P., *Recovery of metals from waste electrical and electronic equipment (WEEE) using unconventional solvents based on ionic liquids*. *Critical Reviews in Environmental Science and Technology*, 2018. **48**(13-15): p. 859-922.
131. Janssen, C.H.C., Macías-Ruvalcaba, N.A., Aguilar-Martínez, M., and Kobrak, M.N., *Metal extraction to ionic liquids: the relationship between structure, mechanism and application*. *International Reviews in Physical Chemistry*, 2015. **34**(4): p. 591-622.
132. Vanessa Forti, C.P.B., Ruediger Kuehr, Garam Bel, *The Global E-waste Monitor 2020; Quantities, flows, and the circular economy potential*. 2020.
133. Li, B., Yang, J., Lu, B., and Song, X., *Estimation of retired mobile phones generation in China: A comparative study on methodology*. *Waste Management*, 2015. **35**: p. 247-254.
134. Statista, *Production of cell phones by month in China 2019-2020*. 2021, Statista Research Department.
135. Tan, Q., Duan, H., Liu, L., Yang, J., and Li, J., *Rethinking residential consumers' behavior in discarding obsolete mobile phones in China*. *Journal of Cleaner Production*, 2018. **195**: p. 1228-1236.
136. He, P., Wang, C., and Zuo, L., *The present and future availability of high-tech minerals in waste mobile phones: Evidence from China*. *Journal of Cleaner Production*, 2018. **192**: p. 940-949.
137. Holgersson, S., Steenari, B.-M., Björkman, M., and Cullbrand, K., *Analysis of the metal content of small-size Waste Electric and Electronic Equipment (WEEE) printed circuit boards—part 1: Internet routers, mobile phones and smartphones*. *Resources, Conservation and Recycling*, 2018. **133**: p. 300-308.
138. Chen, M. and Ma, L.Q., *Comparison of Three Aqua Regia Digestion Methods for Twenty Florida Soils*. *Soil Science Society of America Journal*, 2001. **65**(2): p. 491-499.
139. Chand, V. and Prasad, S., *ICP-OES assessment of heavy metal contamination in tropical marine sediments: A comparative study of two digestion techniques*. *Microchemical Journal*, 2013. **111**: p. 53-61.
140. *CH&N Analysis*. [cited 2020 15/04]; Available from: <http://medacltd.com/services-view/chn-analysis/>.
141. Agency, E.P., *Method 5050: Bomb Preparation Method for Solid Waste, part of Test Methods for Evaluating Solid Waste, Physical/Chemical Methods*. 1994.
142. Ueberschaar, M., Schlummer, M., Jalalpoor, D., Kaup, N., and Rotter, S.V., *Potential and Recycling Strategies for LCD Panels from WEEE*. *Recycling*, 2017. **2**(1).
143. Palmieri, R., Bonifazi, G., and Serranti, S., *Recycling-oriented characterization of plastic frames and printed circuit boards from mobile phones by electronic and chemical imaging*. *Waste Management*, 2014. **34**(11): p. 2120-2130.

144. Duan, C.L., Diao, Z.J., Zhao, Y.M., and Huang, W., *Liberation of valuable materials in waste printed circuit boards by high-voltage electrical pulses*. Minerals Engineering, 2015. **70**: p. 170-177.
145. Ogunniyi, I.O., Vermaak, M.K.G., and Groot, D.R., *Chemical composition and liberation characterization of printed circuit board comminution fines for beneficiation investigations*. Waste Management, 2009. **29**(7): p. 2140-2146.
146. Zhao, C., Zhang, X., Ding, J., and Zhu, Y., *Study on recovery of valuable metals from waste mobile phone PCB particles using liquid-solid fluidization technique*. Chemical Engineering Journal, 2017. **311**: p. 217-226.
147. Directive, E., *Directive 2011/65/EU of the European Parliament and of the Council of 8 June 2011, on the restriction of the use of certain hazardous substances in electrical and electronic equipment (recast)*. Official Journal of the European Communities, 2011.
148. Singh, N., Duan, H., Ogunseitan, O.A., Li, J., and Tang, Y., *Toxicity trends in E-Waste: A comparative analysis of metals in discarded mobile phones*. Journal of Hazardous Materials, 2019. **380**: p. 120898.
149. Rocchetti, L., Amato, A., Fonti, V., Ubaldini, S., De Michelis, I., Kopacek, B., Vegliò, F., and Beolchini, F., *Cross-current leaching of indium from end-of-life LCD panels*. Waste Management, 2015. **42**: p. 180-187.
150. Silveira, A.V.M., Fuchs, M.S., Pinheiro, D.K., Tanabe, E.H., and Bertuol, D.A., *Recovery of indium from LCD screens of discarded cell phones*. Waste Management, 2015. **45**: p. 334-342.
151. Savvilotidou, V., Hahladakis, J.N., and Gidakos, E., *Determination of toxic metals in discarded Liquid Crystal Displays (LCDs)*. Resources, Conservation and Recycling, 2014. **92**: p. 108-115.
152. Zhang, K., Wu, Y., Wang, W., Li, B., Zhang, Y., and Zuo, T., *Recycling indium from waste LCDs: A review*. Resources, Conservation and Recycling, 2015. **104**: p. 276-290.
153. Park, H.S. and Kim, Y.J., *A novel process of extracting precious metals from waste printed circuit boards: Utilization of gold concentrate as a fluxing material*. Journal of Hazardous Materials, 2019. **365**: p. 659-664.
154. Zhang, Y., Chen, M., Tan, Q., Wang, B., and Chen, S., *Recovery of copper from WPCBs using slurry electrolysis with ionic liquid [BSO₃Hpy]-H₂SO₄*. Hydrometallurgy, 2018. **175**: p. 150-154.
155. Yang, D., Chu, Y., Wang, J., Chen, M., Shu, J., Xiu, F., Xu, Z., Sun, S., and Chen, S., *Completely separating metals and nonmetals from waste printed circuit boards by slurry electrolysis*. Separation and Purification Technology, 2018. **205**: p. 302-307.
156. Dhiman, S. and Gupta, B., *Cyphos IL 104 assisted extraction of indium and recycling of indium, tin and zinc from discarded LCD screen*. Separation and Purification Technology, 2020. **237**: p. 116407.
157. Zeng, X., Yang, C., Chiang, J.F., and Li, J., *Innovating e-waste management: From macroscopic to microscopic scales*. Science of The Total Environment, 2017. **575**: p. 1-5.
158. Xiu, F.-R., Qi, Y., and Zhang, F.-S., *Leaching of Au, Ag, and Pd from waste printed circuit boards of mobile phone by iodide lixiviant after supercritical water pre-treatment*. Waste Management, 2015. **41**: p. 134-141.
159. Jeon, S., Tabelin, C.B., Park, I., Nagata, Y., Ito, M., and Hiroyoshi, N., *Ammonium thiosulfate extraction of gold from printed circuit boards (PCBs) of end-of-life mobile phones and its recovery from pregnant leach solution by cementation*. Hydrometallurgy, 2020. **191**: p. 105214.
160. Tarantili, P.A., Mitsakaki, A.N., and Petoussi, M.A., *Processing and properties of engineering plastics recycled from waste electrical and electronic equipment (WEEE)*. Polymer Degradation and Stability, 2010. **95**(3): p. 405-410.
161. Yu, D., Duan, H., Song, Q., Liu, Y., Li, Y., Li, J., Shen, W., Luo, J., and Wang, J., *Characterization of brominated flame retardants from e-waste components in China*. Waste Management, 2017. **68**: p. 498-507.

162. Qiu, R., Lin, M., Ruan, J., Fu, Y., Hu, J., Deng, M., Tang, Y., and Qiu, R., *Recovering full metallic resources from waste printed circuit boards: A refined review*. Journal of Cleaner Production, 2020. **244**: p. 118690.
163. Wang, R. and Xu, Z., *Pyrolysis characteristics and pyrolysis products separation for recycling organic materials from waste liquid crystal display panels*. Journal of Hazardous Materials, 2016. **302**: p. 45-56.
164. GOV, U. *Digest of UK Energy Statistics (DUKES): calorific values*. 2018 [cited 2019 21/03]; Available from: <https://www.gov.uk/government/statistics/dukes-calorific-values>.
165. Li, J., Chen, F., Yang, L., Jiang, L., and Dan, Y., *FTIR analysis on aging characteristics of ABS/PC blend under UV-irradiation in air*. Spectrochimica Acta Part A: Molecular and Biomolecular Spectroscopy, 2017. **184**: p. 361-367.
166. Kasper, A.C., Bernardes, A.M., and Veit, H.M., *Characterization and recovery of polymers from mobile phone scrap*. Waste Management & Research, 2011. **29**(7): p. 714-726.
167. Ma, E. and Xu, Z., *Technological process and optimum design of organic materials vacuum pyrolysis and indium chlorinated separation from waste liquid crystal display panels*. Journal of Hazardous Materials, 2013. **263**: p. 610-617.
168. Chien, Y.-C., Liang, C.-P., and Shih, P.-H., *Emission of polycyclic aromatic hydrocarbons from the pyrolysis of liquid crystal wastes*. Journal of Hazardous Materials, 2009. **170**(2): p. 910-914.
169. Ebrahimi, M. and Cheshme Ghasabani, N., *Forecasting OPEC crude oil production using a variant Multicyclic Hubbert Model*. Journal of Petroleum Science and Engineering, 2015. **133**(Supplement C): p. 818-823.
170. D., S.H.a.K., *A short description of the WORLD 6.0 model and an outline of elements of the standard parameterization*. SIMRESS. 2016.
171. Wang, R. and Xu, Z., *Recycling of non-metallic fractions from waste electrical and electronic equipment (WEEE): A review*. Waste Management, 2014. **34**(8): p. 1455-1469.
172. Barontini, F., Marsanich, K., Petarca, L., and Cozzani, V., *Thermal Degradation and Decomposition Products of Electronic Boards Containing BFRs*. Industrial & Engineering Chemistry Research, 2005. **44**(12): p. 4186-4199.
173. Lateef, H., Grimes, S.M., Morton, R., and Mehta, L., *Extraction of components of composite materials: ionic liquids in the extraction of flame retardants from plastics*. Journal of Chemical Technology & Biotechnology, 2008. **83**(4): p. 541-545.
174. Baldé, C.P., Forti, V., Gray, V., Kuehr, R., and Stegmann, P., *The global e-waste monitor 2017: Quantities, flows and resources*. 2017: United Nations University, International Telecommunication Union, and Resources.
175. Wang, H., Zhang, G., Hao, J., He, Y., Zhang, T., and Yang, X., *Morphology, mineralogy and separation characteristics of nonmetallic fractions from waste printed circuit boards*. Journal of Cleaner Production, 2018. **170**: p. 1501-1507.
176. Chen, M., Huang, J., Ogunseitan, O.A., Zhu, N., and Wang, Y.-m., *Comparative study on copper leaching from waste printed circuit boards by typical ionic liquid acids*. Waste Management, 2015. **41**: p. 142-147.
177. Huang, J., Chen, M., Chen, H., Chen, S., and Sun, Q., *Leaching behavior of copper from waste printed circuit boards with Brønsted acidic ionic liquid*. Waste Management, 2014. **34**(2): p. 483-488.
178. Group, I.C.S. *Copper Market Forecast 2021*. 2021 [27th Jan 2022]; Available from: <https://www.icsg.org/index.php/component/jdownloads/viewdownload/113/2458>.
179. Watari, T., Nansai, K., and Nakajima, K., *Review of critical metal dynamics to 2050 for 48 elements*. Resources, Conservation and Recycling, 2020. **155**: p. 104669.
180. Schipper, B.W., Lin, H.-C., Meloni, M.A., Wansleeben, K., Heijungs, R., and van der Voet, E., *Estimating global copper demand until 2100 with regression and stock dynamics*. Resources, Conservation and Recycling, 2018. **132**: p. 28-36.

181. Kuipers, K.J.J., van Oers, L.F.C.M., Verboon, M., and van der Voet, E., *Assessing environmental implications associated with global copper demand and supply scenarios from 2010 to 2050*. Global Environmental Change, 2018. **49**: p. 106-115.
182. Zeng, X., Li, J., Xie, H., and Liu, L., *A novel dismantling process of waste printed circuit boards using water-soluble ionic liquid*. Chemosphere, 2013. **93**(7): p. 1288-1294.
183. Li, F., Chen, M., Shu, J., Shirvani, M., Li, Y., Sun, Z., Sun, S., Xu, Z., Fu, K., and Chen, S., *Copper and gold recovery from CPU sockets by one-step slurry electrolysis*. Journal of Cleaner Production, 2019. **213**: p. 673-679.
184. Zhang, S., Li, Y., Wang, R., Xu, Z., Wang, B., Chen, S., and Chen, M., *Superfine copper powders recycled from concentrated metal scraps of waste printed circuit boards by slurry electrolysis*. Journal of Cleaner Production, 2017. **152**: p. 1-6.
185. Chaudhary, A.J., Dando, S.O.V., and Grimes, S.M., *Removal of tin from dilute solutions*. Journal of Chemical Technology & Biotechnology, 2001. **76**(1): p. 47-52.
186. Kilicarslan, A., Saridede, M.N., Stopic, S., and Friedrich, B., *Use of ionic liquid in leaching process of brass wastes for copper and zinc recovery*. International Journal of Minerals, Metallurgy, and Materials, 2014. **21**(2): p. 138-143.
187. Habbache, N., Alane, N., Djerad, S., and Tifouti, L., *Leaching of copper oxide with different acid solutions*. Chemical Engineering Journal, 2009. **152**(2): p. 503-508.
188. Kaya, M., *Electronic Waste and Printed Circuit Board Recycling Technologies*. 1 ed. 2019: Springer International Publishing.
189. Yang, C., Li, J., Tan, Q., Liu, L., and Dong, Q., *Green Process of Metal Recycling: Coprocessing Waste Printed Circuit Boards and Spent Tin Stripping Solution*. ACS Sustainable Chemistry & Engineering, 2017. **5**(4): p. 3524-3534.
190. Zhu, P., Chen, Y., Wang, L.y., and Zhou, M., *A new technology for recycling solder from waste printed circuit boards using ionic liquid*. Waste Management & Research, 2012. **30**(11): p. 1222-1226.
191. Hannula, P.-M., Khalid, M.K., Janas, D., Yliniemi, K., and Lundström, M., *Energy efficient copper electrowinning and direct deposition on carbon nanotube film from industrial wastewaters*. Journal of Cleaner Production, 2019. **207**: p. 1033-1039.
192. O'Keefe, T.J., *Techniques for evaluating electrolytes for metal recovery*. Journal of Electroanalytical Chemistry and Interfacial Electrochemistry, 1984. **168**(1): p. 131-146.
193. Chu, Y., Chen, M., Chen, S., Wang, B., Fu, K., and Chen, H., *Micro-copper powders recovered from waste printed circuit boards by electrolysis*. Hydrometallurgy, 2015. **156**: p. 152-157.
194. Gorgievski, M., Božić, D., Stanković, V., and Bogdanović, G., *Copper electrowinning from acid mine drainage: A case study from the closed mine "Cerovo"*. Journal of Hazardous Materials, 2009. **170**(2): p. 716-721.
195. Peng, C., Liu, Y., Bi, J., Xu, H., and Ahmed, A.-S., *Recovery of copper and water from copper-electroplating wastewater by the combination process of electrolysis and electrodialysis*. Journal of Hazardous Materials, 2011. **189**(3): p. 814-820.
196. Munoz, M., Domínguez, C.M., de Pedro, Z.M., Quintanilla, A., Casas, J.A., and Rodriguez, J.J., *Ionic liquids breakdown by Fenton oxidation*. Catalysis Today, 2015. **240**: p. 16-21.
197. Ilyas, S., Srivastava, R.R., and Kim, H., *Gold recovery from secondary waste of PCBs by electro-Cl₂ leaching in brine solution and solvo-chemical separation with tri-butyl phosphate*. Journal of Cleaner Production, 2021. **295**: p. 126389.
198. U.S. Geological Survey. 2021 [cited 2021; Available from: <https://www.usgs.gov/>].
199. Bigum, M., Brogaard, L., and Christensen, T.H., *Metal recovery from high-grade WEEE: A life cycle assessment*. Journal of Hazardous Materials, 2012. **207-208**(Supplement C): p. 8-14.
200. Kim, E.-y., Kim, M.-s., Lee, J.-c., and Pandey, B.D., *Selective recovery of gold from waste mobile phone PCBs by hydrometallurgical process*. Journal of Hazardous Materials, 2011. **198**: p. 206-215.

201. Rao, M.D., Singh, K.K., Morrison, C.A., and Love, J.B., *Challenges and opportunities in the recovery of gold from electronic waste*. RSC Advances, 2020. **10**(8): p. 4300-4309.
202. Lee, C.-H., Tang, L.-W., and Popuri, S.R., *A study on the recycling of scrap integrated circuits by leaching*. Waste Management & Research, 2010. **29**(7): p. 677-685.
203. Cyganowski, P., Garbera, K., Leśniewicz, A., Wolska, J., Pohl, P., and Jermakowicz-Bartkowiak, D., *The recovery of gold from the aqua regia leachate of electronic parts using a core-shell type anion exchange resin*. Journal of Saudi Chemical Society, 2017. **21**(6): p. 741-750.
204. Ha, V.H., Lee, J.-c., Jeong, J., Hai, H.T., and Jha, M.K., *Thiosulfate leaching of gold from waste mobile phones*. Journal of Hazardous Materials, 2010. **178**(1): p. 1115-1119.
205. Lira, M.A., Navarro, R., Saucedo, I., Martinez, M., and Guibal, E., *Influence of the textural characteristics of the support on Au(III) sorption from HCl solutions using Cyphos IL101-impregnated Amberlite resins*. Chemical Engineering Journal, 2016. **302**: p. 426-436.
206. Navarro, R., Saucedo, I., Gonzalez, C., and Guibal, E., *Amberlite XAD-7 impregnated with Cyphos IL-101 (tetraalkylphosphonium ionic liquid) for Pd(II) recovery from HCl solutions*. Chemical Engineering Journal, 2012. **185-186**: p. 226-235.
207. Masilela, M. and Ndlovu, S., *Extraction of Ag and Au from chloride electronic waste leach solutions using ionic liquids*. Journal of Environmental Chemical Engineering, 2019. **7**(1): p. 102810.
208. Tang, Y., Bao, S., Zhang, Y., and Liang, L., *Effect of support properties on preparation process and adsorption performances of solvent impregnated resins*. Reactive and Functional Polymers, 2017. **113**: p. 50-57.
209. Navarro, R., Saucedo, I., Lira, M.A., and Guibal, E., *Gold(III) Recovery From HCl Solutions using Amberlite XAD-7 Impregnated with an Ionic Liquid (Cyphos IL-101)*. Separation Science and Technology, 2010. **45**(12-13): p. 1950-1962.
210. Domínguez, J.R., González, T., Palo, P., and Cuerda-Correa, E.M., *Removal of common pharmaceuticals present in surface waters by Amberlite XAD-7 acrylic-ester-resin: Influence of pH and presence of other drugs*. Desalination, 2011. **269**(1): p. 231-238.
211. Wilson, A.M., Bailey, P.J., Tasker, P.A., Turkington, J.R., Grant, R.A., and Love, J.B., *Solvent extraction: the coordination chemistry behind extractive metallurgy*. Chemical Society Reviews, 2014. **43**(1): p. 123-134.
212. Arias, A., Saucedo, I., Navarro, R., Gallardo, V., Martinez, M., and Guibal, E., *Cadmium(II) recovery from hydrochloric acid solutions using Amberlite XAD-7 impregnated with a tetraalkyl phosphonium ionic liquid*. Reactive and Functional Polymers, 2011. **71**(11): p. 1059-1070.
213. Campos, K., Vincent, T., Bunio, P., Trochimczuk, A., and Guibal, E., *Gold Recovery from HCl Solutions using Cyphos IL-101 (a Quaternary Phosphonium Ionic Liquid) Immobilized in Biopolymer Capsules*. Solvent Extraction and Ion Exchange, 2008. **26**(5): p. 570-601.
214. Rao, M.D., Singh, K.K., Morrison, C.A., and Love, J.B., *Optimization of process parameters for the selective leaching of copper, nickel and isolation of gold from obsolete mobile phone PCBs*. Cleaner Engineering and Technology, 2021. **4**: p. 100180.
215. Deferm, C., Van de Voorde, M., Luyten, J., Oosterhof, H., Franssaer, J., and Binnemans, K., *Purification of indium by solvent extraction with undiluted ionic liquids*. Green Chemistry, 2016. **18**(14): p. 4116-4127.
216. Mohammadzadeh, M., Bagheri, H., and Ghader, S., *Study on extraction and separation of Ni and Zn using [bmim][PF6] IL as selective extractant from nitric acid solution obtained from zinc plant residue leaching*. Arabian Journal of Chemistry, 2020. **13**(6): p. 5821-5831.
217. Alguacil, F.J., Alcaraz, L., Largo, O.R., and López, F.A., *Transport of Au(III) from HCl Medium across a Liquid Membrane Using R3NH+Cl-/Toluene Immobilized on a Microporous Hydrophobic Support: Optimization and Modelling*. Membranes, 2020. **10**(12).
218. Dahri, M.K., Kooh, M.R.R., and Lim, L.B.L., *Application of Casuarina equisetifolia needle for the removal of methylene blue and malachite green dyes from aqueous solution*. Alexandria Engineering Journal, 2015. **54**(4): p. 1253-1263.

219. Deng, Z., Oraby, E.A., and Eksteen, J.J., *Gold recovery from cyanide-starved glycine solutions in the presence of Cu using a molecularly imprinted resin (IXOS-AuC)*. Hydrometallurgy, 2020. **196**: p. 105425.
220. Zhao, Y., Yue, Q., Li, Q., Xu, X., Yang, Z., Wang, X., Gao, B., and Yu, H., *Characterization of red mud granular adsorbent (RMGA) and its performance on phosphate removal from aqueous solution*. Chemical Engineering Journal, 2012. **193-194**: p. 161-168.
221. Laatikainen, M. and Paatero, E., *Gold recovery from chloride solutions with XAD-7: Competitive adsorption of Fe(III) and Te(IV)*. Hydrometallurgy, 2005. **79**(3): p. 154-171.
222. Behnamfard, A., Salarirad, M.M., and Veglio, F., *Process development for recovery of copper and precious metals from waste printed circuit boards with emphasize on palladium and gold leaching and precipitation*. Waste Management, 2013. **33**(11): p. 2354-2363.
223. Alguacil, F.J., Adeva, P., and Alonso, M., *Processing of residual gold (III) solutions via ion exchange*. Gold Bulletin, 2005. **38**(1): p. 9-13.
224. Zhao Jingyue, F.B., *Synthesis of gold nanoparticles via chemical reduction methods*, in *Nanocon*. 2015, IME Institute of Process Metallurgy and Metal Recycling, RWTH Aachen University, Aachen, Germany.
225. Schrijvers, D., Hool, A., Blengini, G.A., Chen, W.-Q., Dewulf, J., Eggert, R., van Ellen, L., Gauss, R., Goddin, J., Habib, K., Hagelüken, C., Hirohata, A., Hofmann-Amttenbrink, M., Kosmol, J., Le Gleuher, M., Grohol, M., Ku, A., Lee, M.-H., Liu, G., Nansai, K., Nuss, P., Peck, D., Reller, A., Sonnemann, G., Tercero, L., Thorenz, A., and Wäger, P.A., *A review of methods and data to determine raw material criticality*. Resources, Conservation and Recycling, 2020. **155**: p. 104617.
226. Swain, B., Lee, C.G., and Hong, H.S., *Value Recovery from Waste Liquid Crystal Display Glass Cullet through Leaching: Understanding the Correlation between Indium Leaching Behavior and Cullet Piece Size*. Metals, 2018. **8**(4).
227. Fan, Y., Liu, Y., Niu, L., Zhang, W., and Zhang, T.-a., *Efficient extraction and separation of indium from waste indium–tin oxide (ITO) targets by enhanced ammonium bisulfate leaching*. Separation and Purification Technology, 2021. **269**: p. 118766.
228. Izhar, S., Yoshida, H., Nishio, E., Utsumi, Y., and Kakimori, N., *Removal and recovery attempt of liquid crystal from waste LCD panels using subcritical water*. Waste Management, 2019. **92**: p. 15-20.
229. Alfantazi, A.M. and Moskalyk, R.R., *Processing of indium: a review*. Minerals Engineering, 2003. **16**(8): p. 687-694.
230. Martin Lokanc, R.E., and Michael Redlinger, *The Availability of Indium: The Present, Medium Term, and Long Term*, in *National Renewable Energy Lab. (NREL)*. 2015.
231. Ciacci, L., Werner, T.T., Vassura, I., and Passarini, F., *Backlighting the European Indium Recycling Potentials*. Corporate Governance: Social Responsibility & Social Impact eJournal, 2019.
232. Graedel, T.E., Allwood, J., Birat, J.-P., Buchert, M., Hagelüken, C., Reck, B.K., Sibley, S.F., Sonnemann, G., United Nations Environment, P., and Working Group on the Global Metal, F., *Recycling rates of metals : a status report*. 2011.
233. Wang, R. and Xu, Z., *Pyrolysis mechanism for recycle renewable resource from polarizing film of waste liquid crystal display panels*. Journal of Hazardous Materials, 2014. **278**: p. 311-319.
234. Cao, Y., Li, F., Li, G., Huang, J., Zhu, H., and He, W., *Leaching and purification of indium from waste liquid crystal display panel after hydrothermal pretreatment: Optimum conditions determination and kinetic analysis*. Waste Management, 2020. **102**: p. 635-644.
235. Deferm, C., Onghena, B., Vander Hoogerstraete, T., Banerjee, D., Luyten, J., Oosterhof, H., Fransaer, J., and Binnemans, K., *Speciation of indium(iii) chloro complexes in the solvent extraction process from chloride aqueous solutions to ionic liquids*. Dalton Transactions, 2017. **46**(13): p. 4412-4421.

236. Nayak, S. and Devi, N., *Studies on the solvent extraction of indium (III) from aqueous chloride medium using Cyphos IL 104*. Materials Today: Proceedings, 2020. **30**: p. 258-261.
237. Cui, J., Zhu, N., Li, Y., Luo, D., Wu, P., and Dang, Z., *Rapid and green process for valuable materials recovery from waste liquid crystal displays*. Resources, Conservation and Recycling, 2020. **153**: p. 104544.
238. Jowkar, M.J., Bahaloo-Horeh, N., Mousavi, S.M., and Pourhossein, F., *Bioleaching of indium from discarded liquid crystal displays*. Journal of Cleaner Production, 2018. **180**: p. 417-429.
239. Chen, W.-S., Wang, Y.-C., and Chiu, K.-L., *The separation and recovery of indium, gallium, and zinc from spent GZO(IGZO) targets*. Journal of Environmental Chemical Engineering, 2017. **5**(1): p. 381-390.
240. Gupta, B., Mudhar, N., and Singh, I., *Separations and recovery of indium and gallium using bis(2,4,4-trimethylpentyl)phosphinic acid (Cyanex 272)*. Separation and Purification Technology, 2007. **57**(2): p. 294-303.
241. Virolainen, S., Ibana, D., and Paatero, E., *Recovery of indium from indium tin oxide by solvent extraction*. Hydrometallurgy, 2011. **107**(1): p. 56-61.
242. Kang, H.N., Lee, J.-Y., and Kim, J.-Y., *Recovery of indium from etching waste by solvent extraction and electrolytic refining*. Hydrometallurgy, 2011. **110**(1): p. 120-127.
243. Fan, S., Jia, Q., Song, N., Su, R., and Liao, W., *Synergistic extraction study of indium from chloride medium by mixtures of sec-nonylphenoxy acetic acid and trialkyl amine*. Separation and Purification Technology, 2010. **75**(1): p. 76-80.
244. Lupi, C. and Pilone, D., *In(III) hydrometallurgical recovery from secondary materials by solvent extraction*. Journal of Environmental Chemical Engineering, 2014. **2**(1): p. 100-104.
245. Drzazga, M., Palmowski, A., Benke, G., Ciszewski, M., and Leszczyńska-Sejda, K., *Recovery of germanium and indium from leaching solution of germanium dross using solvent extraction with TOA, TBP and D2EHPA*. Hydrometallurgy, 2021. **202**: p. 105605.
246. Jian, D., Guo, X., Li, X., Deng, Z., Wei, C., Li, M., and Fan, G., *Extraction of indium with N,N-di(1-methylheptyl)acetamide, di(1-methylheptyl)methyl phosphate, and tributylphosphate by solvent extraction in hydrochloric acid solution*. Minerals Engineering, 2020. **156**: p. 106510.
247. Kumari, A., Sinha, M.K., Sahu, S.K., and Pandey, B.D., *Solvent Extraction and Separation of Trivalent Lanthanides Using Cyphos IL 104, a Novel Phosphonium Ionic Liquid as Extractant*. Solvent Extraction and Ion Exchange, 2016. **34**(5): p. 469-484.
248. Van Roosendaal, S., Regadío, M., Roosen, J., and Binnemans, K., *Selective recovery of indium from iron-rich solutions using an Aliquat 336 iodide supported ionic liquid phase (SILP)*. Separation and Purification Technology, 2019. **212**: p. 843-853.
249. Zhao, K., Liu, Z., Wang, Y., and Jiang, H., *Study on recycling process for EOL liquid crystal display panel*. International Journal of Precision Engineering and Manufacturing, 2013. **14**(6): p. 1043-1047.
250. Zhang, L., Wu, B., Chen, Y., and Xu, Z., *Treatment of liquid crystals and recycling indium for stripping product gained by mechanical stripping process from waste liquid crystal display panels*. Journal of Cleaner Production, 2017. **162**: p. 1472-1481.
251. Houssaine Moutiy, E., Tran, L.-H., Mueller, K.K., Coudert, L., and Blais, J.-F., *Optimized indium solubilization from LCD panels using H2SO4 leaching*. Waste Management, 2020. **114**: p. 53-61.
252. Chinnam, R.K., Ujaczki, É., and O'Donoghue, L., *Leaching indium from discarded LCD glass: A rapid and environmentally friendly process*. Journal of Cleaner Production, 2020. **277**: p. 122868.
253. Song, Q., Zhang, L., and Xu, Z., *Indium recovery from In-Sn-Cu-Al mixed system of waste liquid crystal display panels via acid leaching and two-step electrodeposition*. Journal of Hazardous Materials, 2020. **381**: p. 120973.

254. Grimes, S.M., Yasri, N.G., and Chaudhary, A.J., *Recovery of critical metals from dilute leach solutions – Separation of indium from tin and lead*. *Inorganica Chimica Acta*, 2017. **461**: p. 161-166.
255. You, H., Yang, Y., Li, X., Zhang, K., Wang, X., Zhu, M., and Hsiao, B.S., *Low pressure high flux thin film nanofibrous composite membranes prepared by electrospraying technique combined with solution treatment*. *Journal of Membrane Science*, 2012. **394-395**: p. 241-247.
256. López-Yáñez, A., Alonso, A., Vengoechea-Pimienta, A., and Ramírez-Muñoz, J., *Indium and tin recovery from waste LCD panels using citrate as a complexing agent*. *Waste Management*, 2019. **96**: p. 181-189.
257. Zhang, K., Li, B., Wu, Y., Wang, W., Li, R., Zhang, Y.-N., and Zuo, T., *Recycling of indium from waste LCD: A promising non-crushing leaching with the aid of ultrasonic wave*. *Waste Management*, 2017. **64**: p. 236-243.
258. Swain, B., Mishra, C., Hong, H.S., and Cho, S.-S., *Beneficiation and recovery of indium from liquid-crystal-display glass by hydrometallurgy*. *Waste Management*, 2016. **57**: p. 207-214.
259. Fontana, D., Forte, F., De Carolis, R., and Grosso, M., *Materials recovery from waste liquid crystal displays: A focus on indium*. *Waste Management*, 2015. **45**: p. 325-333.
260. Luo, D., Zhu, N., Li, Y., Cui, J., Wu, P., and Wang, J., *Simultaneous leaching and extraction of indium from waste LCDs with acidic ionic liquids*. *Hydrometallurgy*, 2019. **189**: p. 105146.
261. Chou, W.-S., Shen, Y.-H., Yang, S.-J., Hsiao, T.-C., and Huang, L.-F., *Recovery of indium from the etching solution of indium tin oxide by solvent extraction*. *Environmental Progress & Sustainable Energy*, 2016. **35**(3): p. 758-763.
262. Dushyantha, N., Batapola, N., Ilankoon, I.M.S.K., Rohitha, S., Premasiri, R., Abeyasinghe, B., Ratnayake, N., and Dissanayake, K., *The story of rare earth elements (REEs): Occurrences, global distribution, genesis, geology, mineralogy and global production*. *Ore Geology Reviews*, 2020. **122**: p. 103521.
263. Van Gosen, B.S., Verplanck, P.L., Seal, R.R., Long, K.R., and Gambogi, J., *Rare-earth elements*, in *Professional Paper*, K.J. Schulz, et al., Editors. 2017: Reston, VA. p. 44.
264. Judge, W.D. and Azimi, G., *Recent progress in impurity removal during rare earth element processing: A review*. *Hydrometallurgy*, 2020. **196**: p. 105435.
265. Dupont, D. and Binnemans, K., *Recycling of rare earths from NdFeB magnets using a combined leaching/extraction system based on the acidity and thermomorphism of the ionic liquid [Hbet][Tf2N]*. *Green Chemistry*, 2015. **17**(4): p. 2150-2163.
266. Cucchiella, F., D'Adamo, I., Lenny Koh, S.C., and Rosa, P., *Recycling of WEEEs: An economic assessment of present and future e-waste streams*. *Renewable and Sustainable Energy Reviews*, 2015. **51**: p. 263-272.
267. Gupta, C.K. and Krishnamurthy, N., *Extractive metallurgy of rare earths*. *International Materials Reviews*, 1992. **37**(1): p. 197-248.
268. Kingsnorth, D.J., *Rare earths: The China conundrum*, in *12th International Rare Earths Conference*. 2016: Hong Kong p. 8–10.
269. Dutta, T., Kim, K.-H., Uchimiya, M., Kwon, E.E., Jeon, B.-H., Deep, A., and Yun, S.-T., *Global demand for rare earth resources and strategies for green mining*. *Environmental Research*, 2016. **150**: p. 182-190.
270. Alonso, E., Sherman, A.M., Wallington, T.J., Everson, M.P., Field, F.R., Roth, R., and Kirchain, R.E., *Evaluating Rare Earth Element Availability: A Case with Revolutionary Demand from Clean Technologies*. *Environmental Science & Technology*, 2012. **46**(6): p. 3406-3414.
271. Department, S.R., *Forecast of rare earth oxide neodymium oxide price globally 2009-2030*
- 2021, M. Garside
272. (DOE), U.S.D.o.E., *Critical materials strategy*. 2011, U.S. Department of Energy (DOE).
273. Vander Hoogerstraete, T., Blanpain, B., Van Gerven, T., and Binnemans, K., *From NdFeB magnets towards the rare-earth oxides: a recycling process consuming only oxalic acid*. *RSC Advances*, 2014. **4**(109): p. 64099-64111.

274. Reisdörfer, G., Bertuol, D., and Tanabe, E.H., *Recovery of neodymium from the magnets of hard disk drives using organic acids*. Minerals Engineering, 2019. **143**: p. 105938.
275. Mancheri, N.A., Sprecher, B., Bailey, G., Ge, J., and Tukker, A., *Effect of Chinese policies on rare earth supply chain resilience*. Resources, Conservation and Recycling, 2019. **142**: p. 101-112.
276. Peelman, S., Kooijman, D., Sietsma, J., and Yang, Y., *Hydrometallurgical Recovery of Rare Earth Elements from Mine Tailings and WEEE*. Journal of Sustainable Metallurgy, 2018. **4**(3): p. 367-377.
277. Riaño, S. and Binnemans, K., *Extraction and separation of neodymium and dysprosium from used NdFeB magnets: an application of ionic liquids in solvent extraction towards the recycling of magnets*. Green Chemistry, 2015. **17**(5): p. 2931-2942.
278. Dupont, D. and Binnemans, K., *Rare-earth recycling using a functionalized ionic liquid for the selective dissolution and revalorization of Y₂O₃:Eu³⁺ from lamp phosphor waste*. Green Chemistry, 2015. **17**(2): p. 856-868.
279. Yang, F., Kubota, F., Baba, Y., Kamiya, N., and Goto, M., *Selective extraction and recovery of rare earth metals from phosphor powders in waste fluorescent lamps using an ionic liquid system*. Journal of Hazardous Materials, 2013. **254-255**: p. 79-88.
280. Schaeffer, N., Feng, X., Grimes, S., and Cheeseman, C., *Recovery of an yttrium europium oxide phosphor from waste fluorescent tubes using a Brønsted acidic ionic liquid, 1-methylimidazolium hydrogen sulfate*. Journal of Chemical Technology & Biotechnology, 2017. **92**(10): p. 2731-2738.
281. Schaeffer, N., Grimes, S., and Cheeseman, C., *Interactions between trivalent rare earth oxides and mixed [Hbet][Tf2N]:H₂O systems in the development of a one-step process for the separation of light from heavy rare earth elements*. Inorganica Chimica Acta, 2016. **439**: p. 55-60.
282. Tian, Y., Liu, Z., and Zhang, G., *Recovering REEs from NdFeB wastes with high purity and efficiency by leaching and selective precipitation process with modified agents*. Journal of Rare Earths, 2019. **37**(2): p. 205-210.
283. Yadav, K.K., Anitha, M., Singh, D.K., and Kain, V., *NdFeB magnet recycling: Dysprosium recovery by non-dispersive solvent extraction employing hollow fibre membrane contactor*. Separation and Purification Technology, 2018. **194**: p. 265-271.
284. Dupont, D., Depuydt, D., and Binnemans, K., *Overview of the Effect of Salts on Biphasic Ionic Liquid/Water Solvent Extraction Systems: Anion Exchange, Mutual Solubility, and Thermomorphic Properties*. The Journal of Physical Chemistry B, 2015. **119**(22): p. 6747-6757.
285. Hoffmann, J., Nüchter, M., Ondruschka, B., and Wasserscheid, P., *Ionic liquids and their heating behaviour during microwave irradiation – a state of the art report and challenge to assessment*. Green Chemistry, 2003. **5**(3): p. 296-299.
286. Kumari, A., Sinha, M.K., Pramanik, S., and Sahu, S.K., *Recovery of rare earths from spent NdFeB magnets of wind turbine: Leaching and kinetic aspects*. Waste Management, 2018. **75**: p. 486-498.
287. Liu, F., Porvali, A., Wang, J., Wang, H., Peng, C., Wilson, B.P., and Lundström, M., *Recovery and separation of rare earths and boron from spent Nd-Fe-B magnets*. Minerals Engineering, 2020. **145**: p. 106097.

Appendix: Supplementary Information of Chapters

Chapter 4

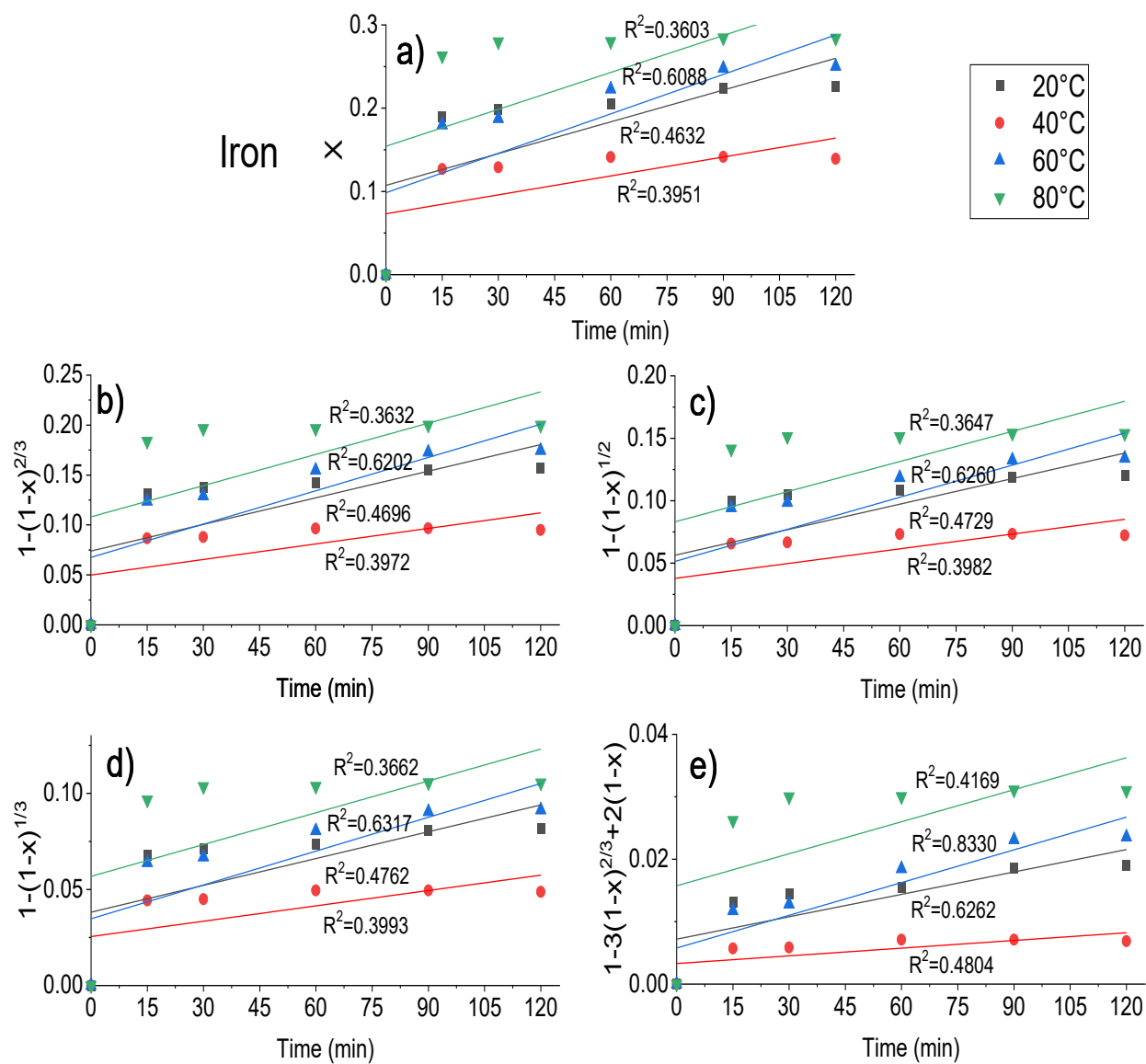


Figure A.1: Model fitting for leaching kinetics of iron from WPCBs by [Bmim]HSO₄.

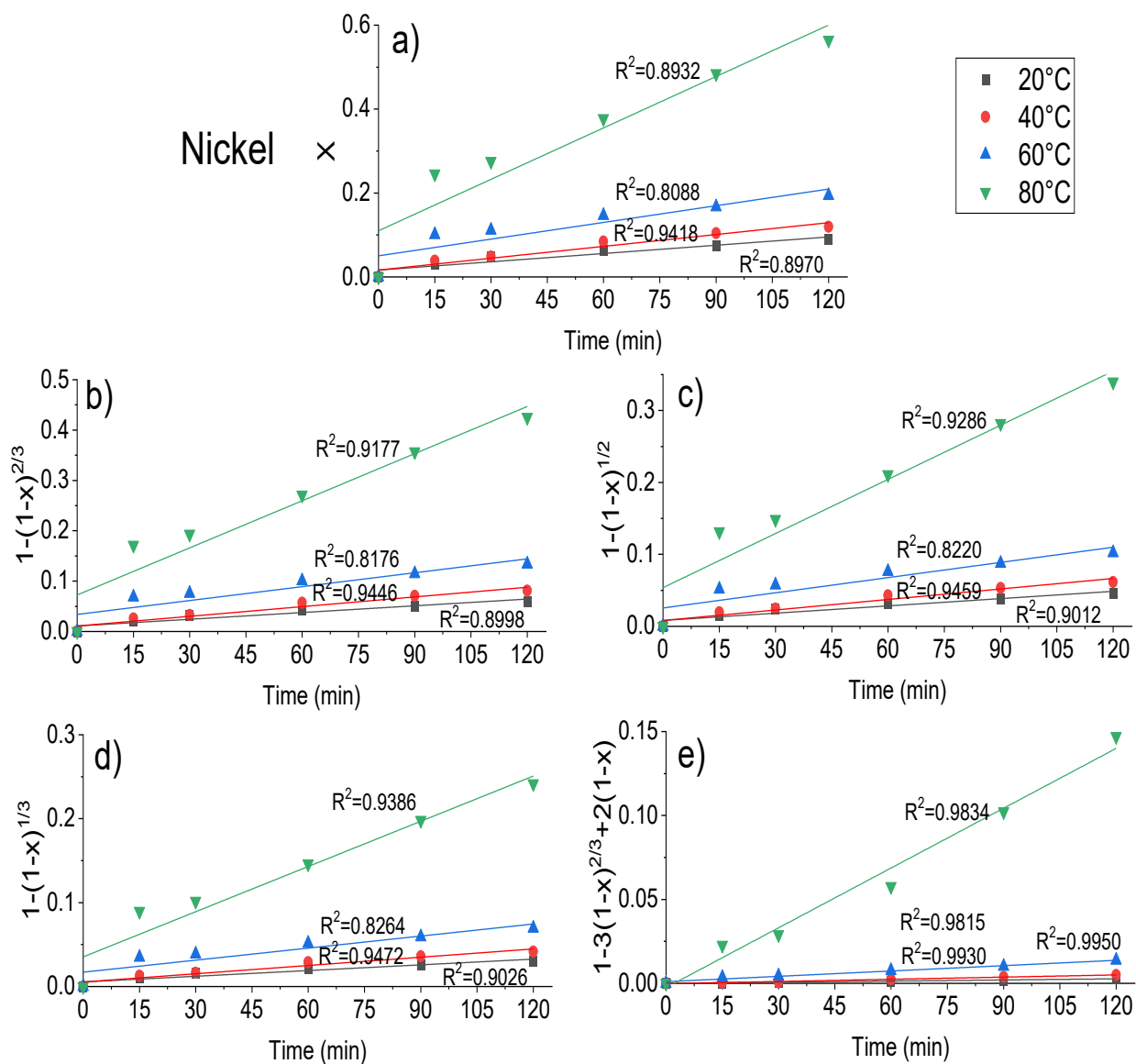


Figure A.2: Model fitting for leaching kinetics of nickel from WPCBs by [Bmim]HSO₄.

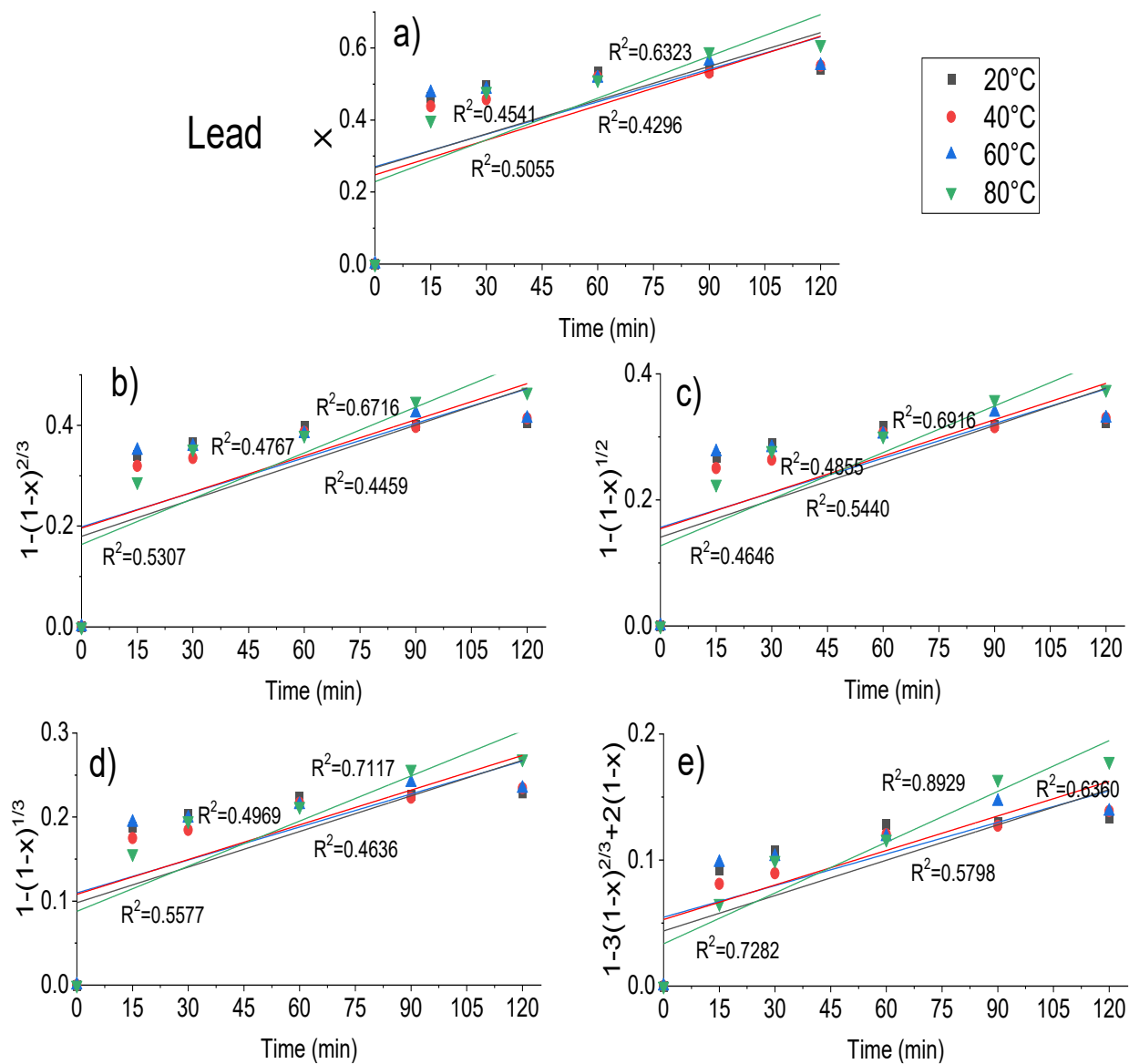


Figure A.3: Model fitting for leaching kinetics of lead from WPCBs by $[Bmim]HSO_4$.

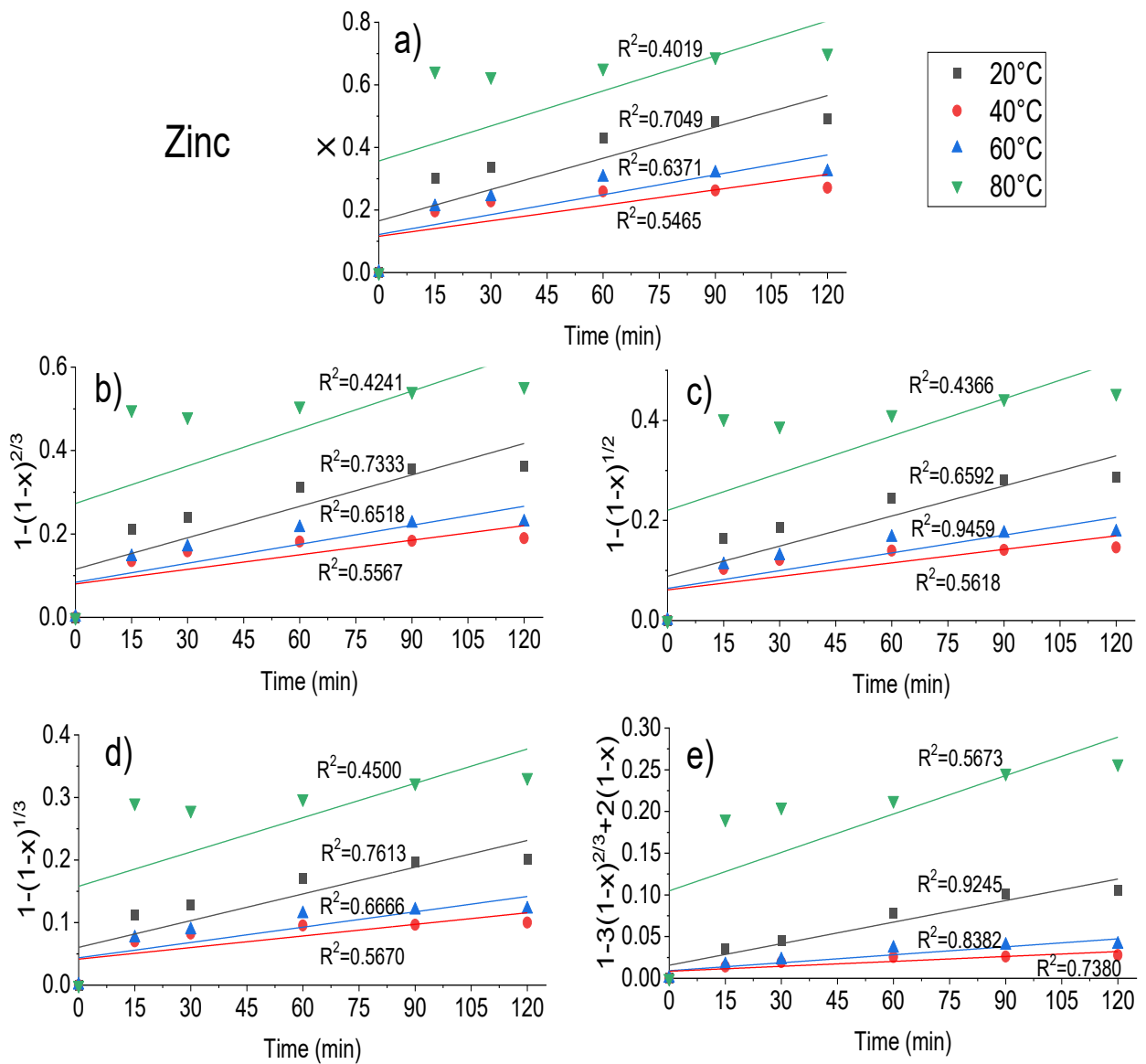


Figure A.4: Model fitting for leaching kinetics of lead from WPCBs by [Bmim]HSO₄.

Chapter 5

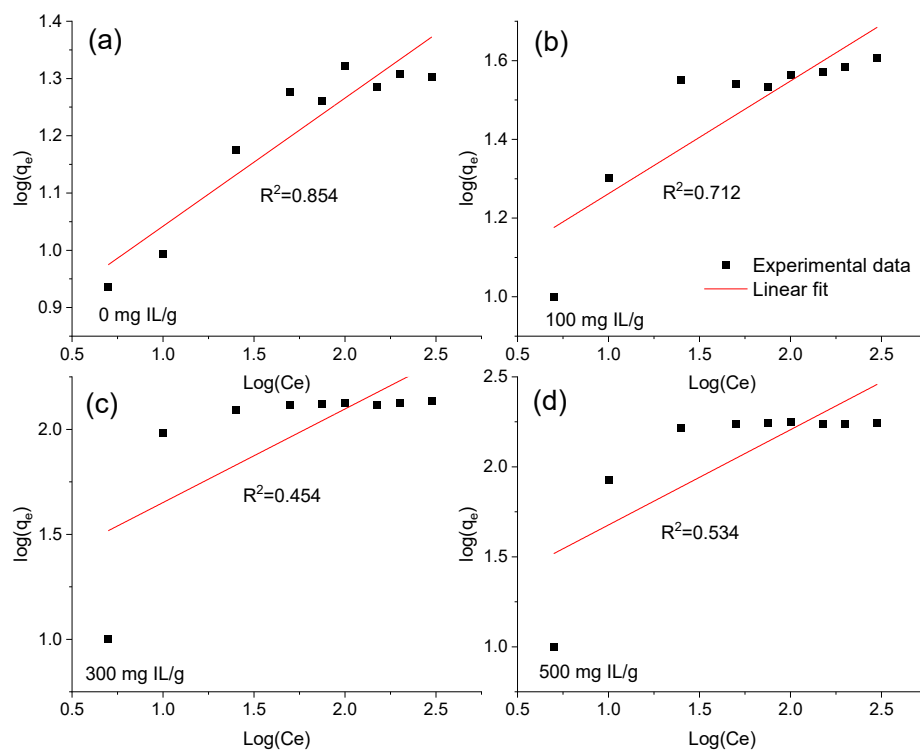


Figure A.5: Linear fit of the Freundlich model at different Au(III) equilibrium concentrations.

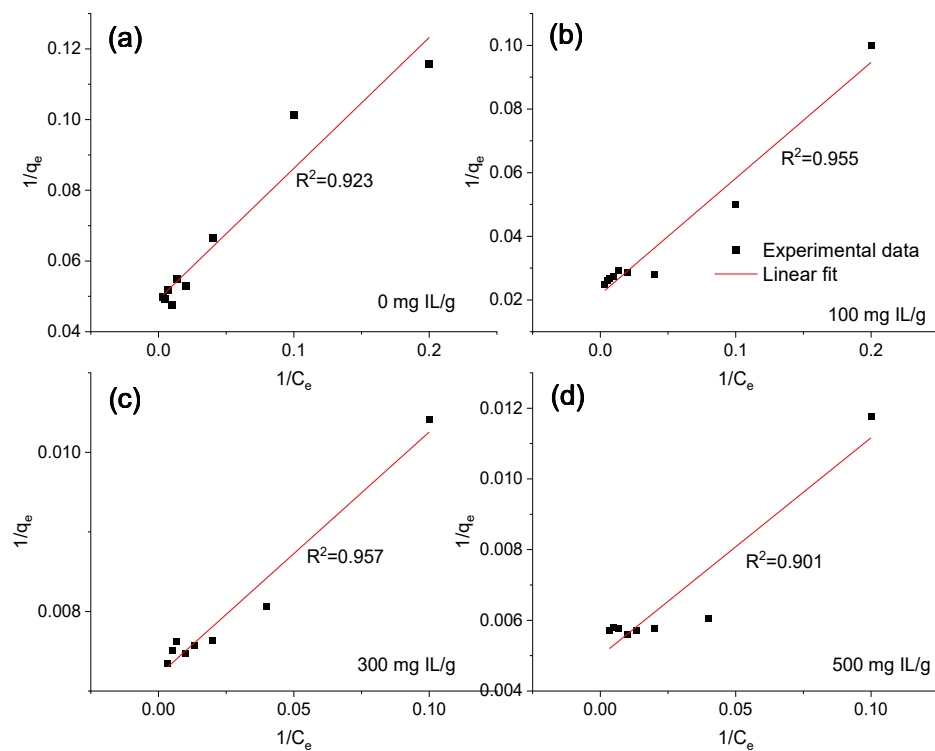


Figure A.6: Linear fit of the Langmuir model at different Au(III) equilibrium concentrations.

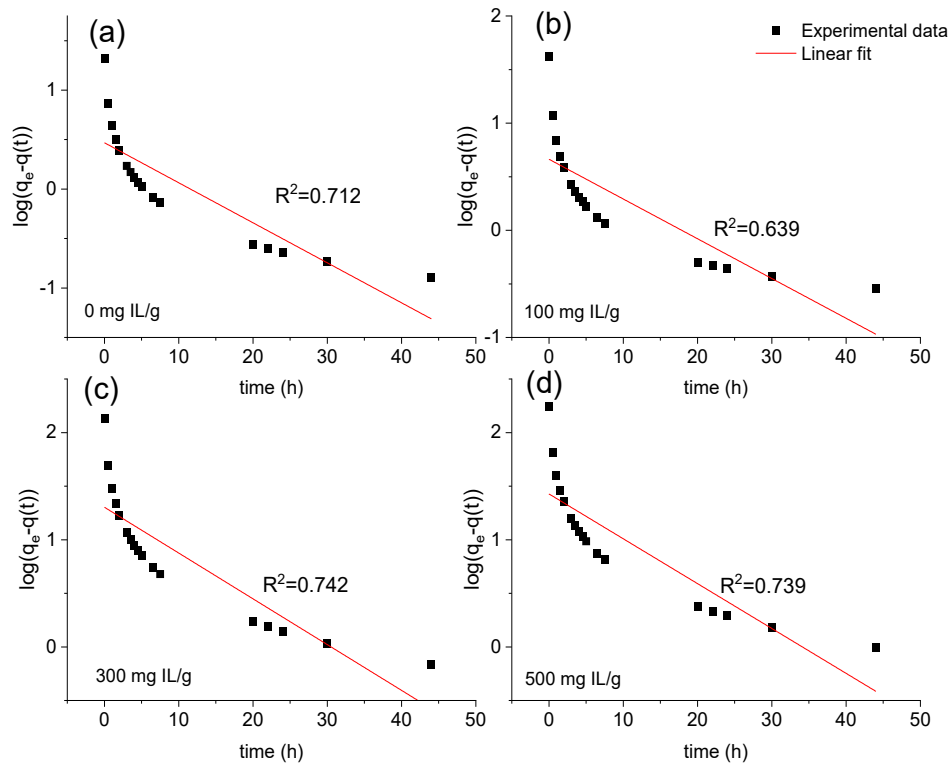


Figure A.7: Linear fit of the pseudo-first order model.

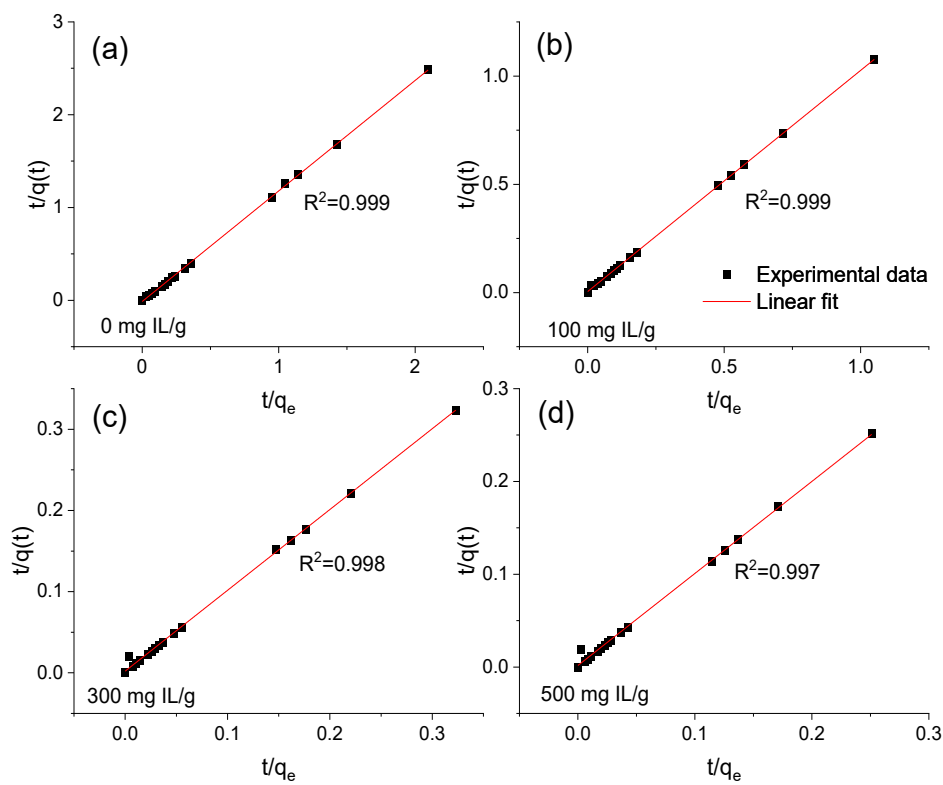


Figure A.8: Linear fit of the pseudo-second order model.

Chapter 6

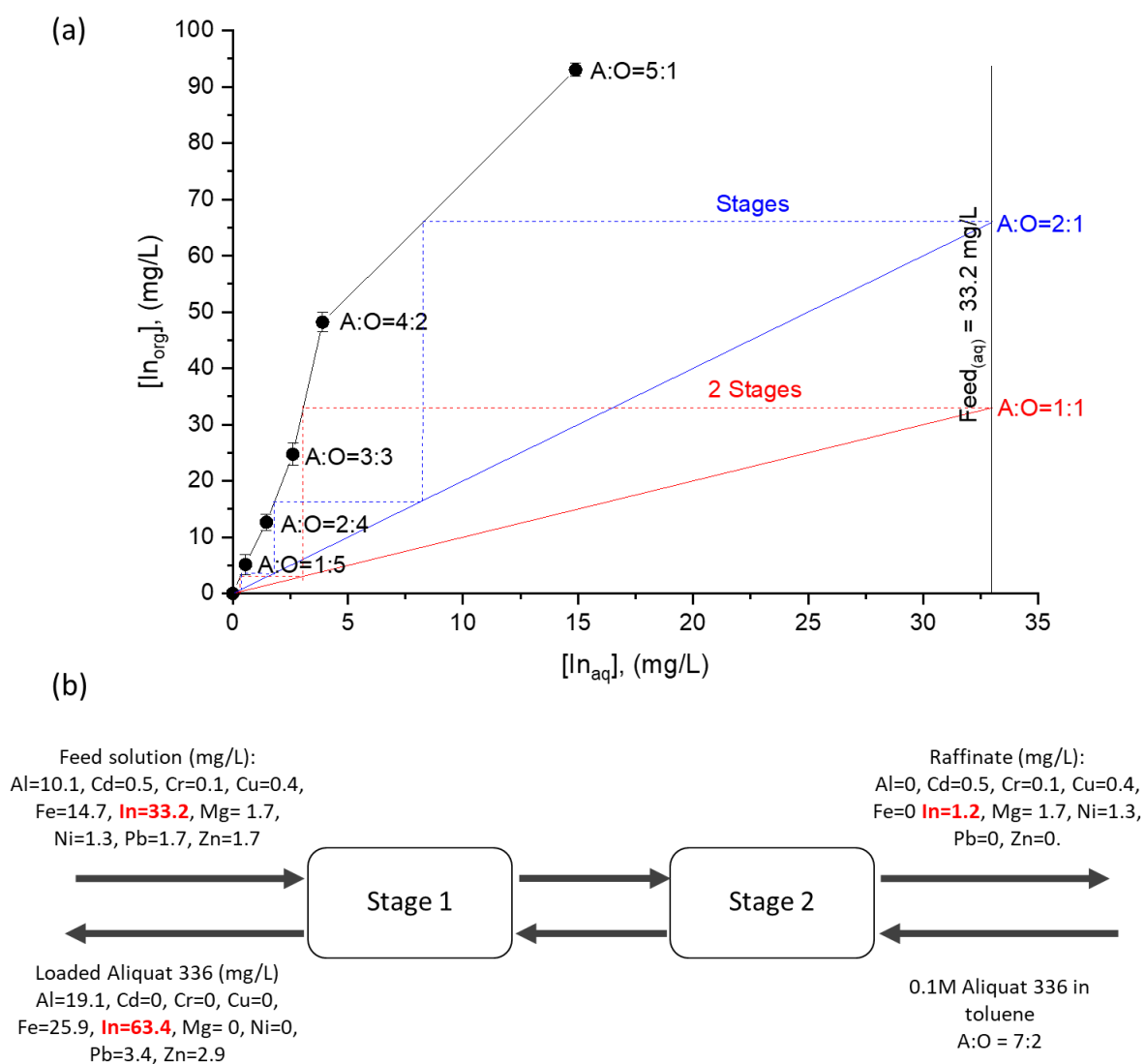


Figure A.9: Indium extraction by Cyphos 101 without ascorbic acid; (a) McCabe-Thiele plot for In, and (b) Counter-current on the extraction of In from LCD panels leached in hydrochloric medium.

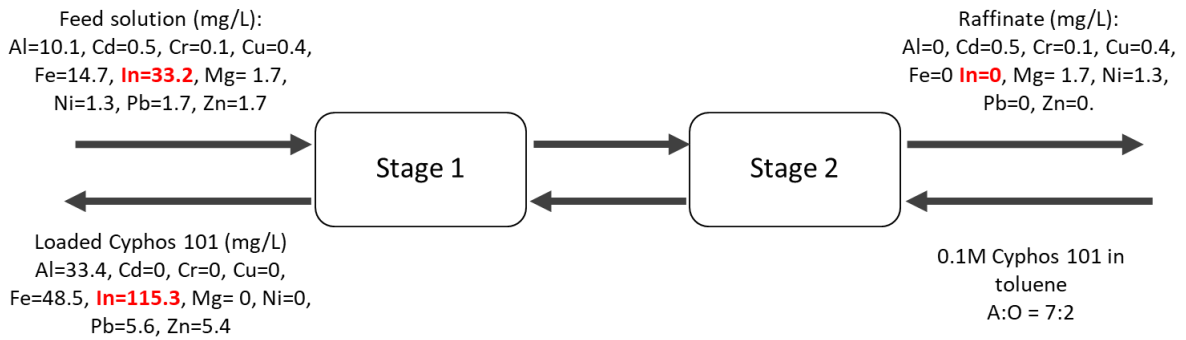
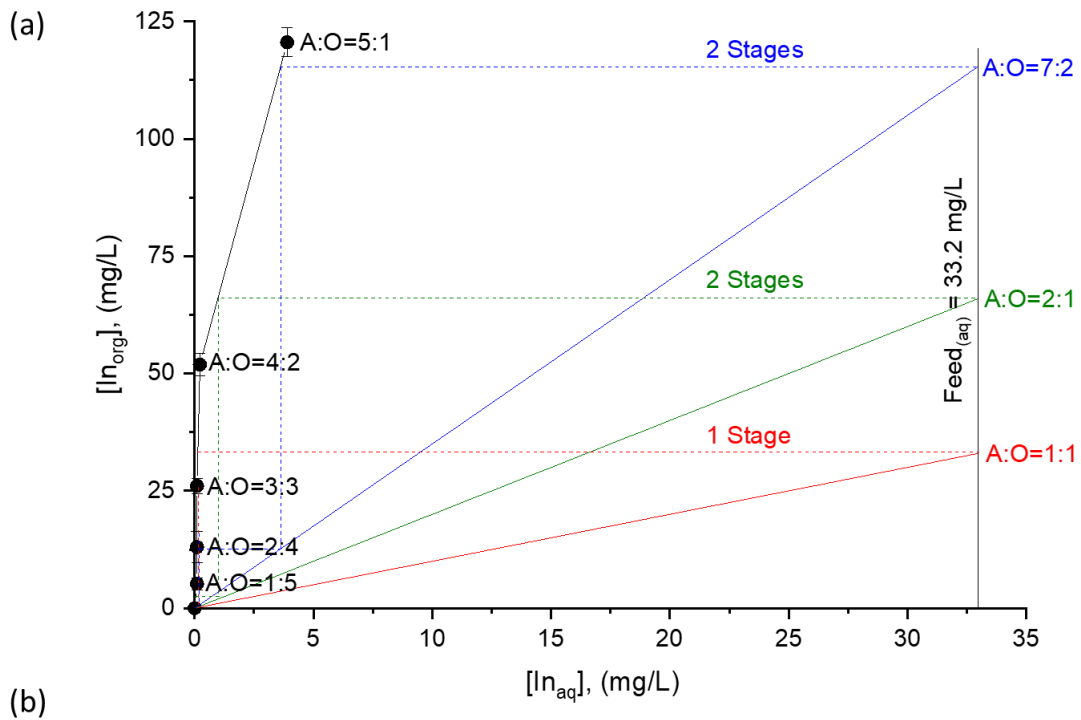


Figure A.10: Indium extraction by Aliquat 336 101 without ascorbic acid; (a) McCabe-Thiele plot for In, and (b) Counter-current on the extraction of In from LCD panels leached in hydrochloric medium.